Advanced strategies for the seismic assessment of existing RC moment-frame buildings: appraisal of modelling assumptions and development of parsimonious PBEE-based methods

26 June 2024

Doctor of Philosophy in Risk and Environmental, Territorial and Building Development	**POLITECNICO DI BARI**	**06**
Coordinator: Prof. Michele Mossa		2018
XXXI CYCLE – Curriculum: ICAR/09 – Structural Engineering		
DICATECh Department of Civil, Environmental, Land, Building Engineering and Chemistry		
	SERGIO RUGGIERI	
	Advanced strategies for the seismic assessment of existing RC moment-frame buildings: appraisal of modelling assumptions and development of parsimonious PBEE-based methods of analysis	

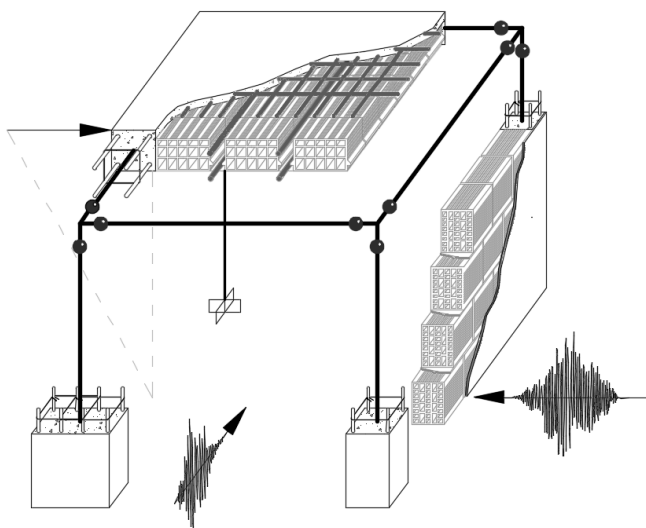Supervisors:

Prof. Eng. Giuseppina Uva
Prof. Eng. Domenico Raffaele
Prof. Eng. Francesco Porco
Department DICATECh - Polytechnic University of Bari

Prof. Eng. Dimitrios Vamvatsikos
Institute of Steel Structures - National Technical
Institute of Athens

EXTENDED ABSTRACT

The issue of seismic assessment of existing RC buildings has been extensively studied in the last few years and the international reference framework, both with regard to the scientific research and the development of technical codes, is very wide. Nevertheless, there are still a lot of challenging questions about the definition of reliable numerical models and methods of analysis, which are strongly affected by many uncertainty sources (knowledge of structural details, material properties, seismic input; accuracy and reliability of capacity models and discretization strategies). The management of these issues, especially in view of practice-oriented applications, requires the availability of effective strategies, so to allow a probabilistic assessment approach that can be relatively accessible in terms of implementation hurdle the computational time.

After an extensive background about the approaches to vulnerability assessment proposed by recent scientific literature and technical codes, the dissertation discusses the critical aspects related to some assumptions commonly adopted in the seismic modelling of existing RC buildings, with the aim of proposing proper sanitization strategies, which can be particularly useful in view of practical applications. As a first issue, the influence on the global response of alternative modelling assumptions for secondary structural elements such as slabs is investigated. The usual hypothesis of rigid floor is assessed by performing a sensitivity analysis based on several parameters, which are particularly significant for the structural response evaluation. Then, based on the results of the analyses, a numerical procedure for modelling the floor system is proposed, defining an orthotropic equivalent shell element capable to simulate the in-plan stiffness of the floor. The methodology actually increases the computational efforts, but has the significant advantage of avoiding aprioristic assumptions about the floor stiffness. An application of the method to the numerical modelling of existing RC buildings is then proposed, by appraising the variation of results in comparison with alternative models for considering in-plan stiffness (namely, equivalent strut models). Lastly, the application possibilities of the proposed procedure are appraised, by presenting a number of examples. As an additional effect, the presence of

infill panels is considered, in the perspective of retrofit solutions. More specifically, the possibility of increasing the capacity to horizontal actions by reinforcing the infilled frames or by introducing additional RC shear walls on the building perimeter is appraised.

The second issue addressed in the dissertation is the definition of the most effective methodology to be used for identifying the structural response both in the elastic and inelastic field. After a review of the nonlinear methods of analysis provided by the scientific literature, both static and dynamic, the dissertation presents some applications of the pushover method, which is by far the most popular choice of practitioners. Firstly, an application of conventional pushover analysis is performed on a set of ideal buildings, with the aim of appraising the role of the control node position. Anyway, as highlighted by current technical laws (Italian building code and Eurocode 8), nonlinear static procedure cannot be always applied in its conventional formulation. In particular, some limitations arise in the presence of structural irregularities or in the cases where higher modes have a strong influence. With the aim to bridge these gaps, a solution can be represented by non-conventional methods as multimodal or adaptive pushover analysis. With regard to this question, a simplified multimodal pushover procedure is proposed in the dissertation. The main advantage of the proposal is represented by the easiness of application, thanks to the adoption of a single load profile in the computation, which is moreover an approach very familiar to practitioners. For assessing the reliability of the procedure, it is tested on a real case study characterized by relevant dynamic irregularity and a consistent inhomogeneity of in-situ materials.

The final part of the dissertation is devoted to the possibility of extensively bringing the concepts at the base of Performance Based Earthquake Engineering (PBEE) to a wider audience of users, considering that this method has a high scientific relevance for the assessment of existing RC buildings. Generally, the application of PBEE needs a specialist knowledge about probability theories and about nonlinear modelling and analysis, which are skills not always common among practitioners. With the aim of reducing these obstacles, a methodology of nonlinear dynamic analysis is proposed,

which consists in an application of the multi-stripe analysis on numerical models implemented through a commercial software. In particular, the new procedure, called Few Stripe Analysis (FSA), is applied on a sample of 15 existing RC school buildings (located in the province of Foggia, Southern Italy) and the results, in terms of damage states, are compared with the ones obtained from SPO2FRAG software, an user-friendly tool able to compute the fragility curves starting from pushover curves.

Finally, a new simplified modelling procedure for estimating the global response of existing RC buildings is presented. It is able to produce 3D reduced-order models (characterized by very few degrees of freedom) starting from the geometrical and mechanical features of the case study. The main advantage of the present approach is to account for the effects predictable with MDoF models, but with low analysis time and computational efforts, with elevate convergence capacity, typical of the SDoF models. The performance of this simplified numerical modelling procedure has been tested by the application on the previously mentioned sample of school buildings and comparing the results, in terms of structural response, damage states and confidence levels, with the ones previously obtained from the application of FSA. The relevance and perspective impact of the research work here presented should be seen in the wider field of the vulnerability analysis of the building stock at the regional scale, which is a crucial issue for the scientific community and for the civil society. Governments and administrations are invested with the difficult task of providing mitigation strategies for the seismic risk for a very wide and inhomogeneous portfolio of buildings and the economic resources are often very limited. Therefore, the development of methods for estimating the vulnerability with limited data has been a subject of intense research activity. The framework that is depicted in the dissertation can provide a tool potentially very impactful, since it could allow, by the exploitation of the 3D Reduced Order Models combined with FSA, to overcome the well-known limitations of empirical vulnerability approaches in favor of mechanical based methods managed in a full probabilistic framework.

Key words: Existing RC buildings; Seismic Assessment; Numerical Modelling; PBEE; Few Stripe Analysis; 3D Reduced-Order Models

SOMMARIO ESTESO

Il problema della verifica di vulnerabilità sismica di edifici esistenti in calcestruzzo armato è stato oggetto negli ultimi anni di studi approfonditi, che hanno favorito lo sviluppo di un quadro di riferimento internazionale sul tema molto ampio, sia dal punto di vista della ricerca scientifica che da quello delle normative tecniche vigenti. Tuttavia, sono ancora molte le questioni irrisolte a riguardo di temi come la modellazione numerica e i metodi di analisi sismica, fasi fortemente influenzate da continue fonti di incertezza (conoscenza dei dettagli geometrici e strutturali, proprietà dei materiali, input sismico, accuratezza e affidabilità di modelli di capacità e strategie di discretizzazione). Ai fini di una valutazione affidabile delle prestazioni sismiche, tali problematiche richiedono lo sviluppo di strategie di modellazione e analisi innovative ed efficaci, soprattutto da un punto di vista di una accurata valutazione probabilistica e con uno sguardo attento alla pratica progettuale, dove la facilità di implementazione e i tempi di calcolo assumono un'importanza prioritaria.

Dopo un'estesa ricerca bibliografica degli approcci proposti e utilizzati per effettuare verifiche di vulnerabilità sismica di edifici esistenti in calcestruzzo armato, proposti dalla letteratura scientifica e dalle normative tecniche vigenti, nella tesi sono stati discussi inizialmente alcuni aspetti critici di modellazione, relativi alle consuete ipotesi semplificative adottate. Nella fattispecie, l'influenza dell'ipotesi di piano rigido, con riferimento agli elementi strutturali secondari come il solaio, è stata analizzata, con l'obiettivo di proporre un'idonea strategia efficiente di modellazione per una pratica applicazione, rivolta a ricercatori e professionisti. Ciò stante, un'analisi iniziale di sensibilità è stata condotta, investigando quali parametri influenzano significativamente la risposta sismica globale della tipologia di edifici in oggetto. Sulla base dei risultati ottenuti, una nuova procedura numerica di modellazione dell'impalcato è stata proposta, atta a definire una piastra ortotropa equivalente capace di simulare la reale rigidezza nel piano, per azioni orizzontali. La metodologia adottata, nonostante incrementi lo sforzo computazionale dell'analisi, ha il vantaggio di evitare le assunzioni aprioristiche sulla rigidezza dell'impalcato. Al fine di validare quanto proposto, il metodo è stato applicato ad

un edificio esistente in calcestruzzo armato, valutando i risultati e comparandoli con altre metodologie proposte dalla letteratura scientifica per considerare il comportamento nel piano dell'impalcato, come quella a puntoni equivalenti. Infine, è stata valutata la possibilità di applicare la procedura nei casi in cui si considera l'influenza delle tamponature esterne e successivamente, in una prospettiva di miglioramento o adeguamento sismico dell'edificio. In quest'ultimi casi, la prestazione dell'edificio alle azioni orizzontali è stata migliorata, mediante l'uso di tamponature rinforzate e mediante l'inserimento di pareti in calcestruzzo armato sul perimetro dell'edificio.

Per quanto riguarda la fase di analisi sismica, stabilire quale sia la metodologia più efficace per identificare la risposta strutturale in campo elastico e inelastico assume una grande importanza, considerando soprattutto la vasta casistica di procedure proposte dalla letteratura scientifica e dalle normative tecniche vigenti. A valle di un'estesa valutazione di quest'ultime, con particolare attenzione ai metodi di analisi non lineari, sia statici che dinamici, la dissertazione presenta alcune applicazioni di analisi statiche non lineari, metodo che rappresenta la prima scelta da parte dei professionisti. Inizialmente, un'applicazione di analisi statica non lineare convenzionale è stata condotta su un campione di edifici esistenti ideali in calcestruzzo armato, con l'obiettivo di verificare il ruolo del nodo di controllo. Tuttavia, come già evidenziato dalle normative tecniche vigenti (Normativa Tecnica Italiana e Eurocodice 8), le procedure di analisi statica non lineare non possono essere sempre applicate, a causa di alcune limitazioni dovute alle caratteristiche dell'edificio analizzato, come le irregolarità e la forte influenza dei modi superiori. Con l'obiettivo di proporre una strategia che possa colmare i limiti sopraelencati, una possibile soluzione è rappresentata dai metodi non convenzionali come le analisi statiche non lineari multimodali o adattive. A questo proposito, una procedura semplificata di analisi statica non lineare multimodale è stata proposta. La peculiarità di tale metodologia è dovuta ad un algoritmo capace di fornire un singolo profilo di carico, facilmente implementabile nelle stesse modalità di un'analisi convenzionale. Al fine di verificare l'efficienza del metodo, quest'ultimo è stato applicato ad un edificio esistente in calcestruzzo armato, caratterizzato da irregolarità dinamiche e da elevata inomogeneità dei materiali in situ.

Nella parte finale della tesi, è stata analizzata la possibilità di implementare i concetti alla base del Performance Based Earthquake Engineering (PBEE), metodo di elevata rilevanza scientifica, per applicazioni pratiche nella verifica di vulnerabilità sismica di edifici in calcestruzzo armato. Generalmente, l'applicazione del PBEE richiede conoscenze specifiche circa le teorie della probabilità e competenze specialistiche nel campo della modellazione e analisi non lineare, qualità non sempre comuni tra i professionisti. Con l'obiettivo di ridurre i sopramenzionati ostacoli, una metodologia di analisi dinamica non lineare è stata proposta, consistente in un'applicazione del metodo "multi stripe analysis" su modelli numerici redatti con programmi di calcolo commerciali. Nella fattispecie, la nuova procedura, chiamata "Few Stripe Analysis" (FSA) è stata applicata e testata su un campione di 15 edifici scolastici esistenti in calcestruzzo armato (nella provincia di Foggia, Sud Italia) e i risultati ottenuti, in termini di stato di danno e curve di fragilità, sono stati confrontati con quelli ottenuti utilizzando il programma di calcolo SPO2FRAG. Quest'ultimo consente di calcolare curve di fragilità, partendo da curve di capacità ottenute da analisi statiche non lineari.

Infine, una nuova procedura di modellazione per valutare la risposta sismica globale di edifici in calcestruzzo armato è stata proposta. In particolare, la metodologia consente di produrre modelli 3D ad ordine ridotto (caratterizzati da pochi gradi di libertà), partendo dalle caratteristiche geometriche e meccaniche di un edificio esistente. Il vantaggio principale del presente approccio è quello di cogliere molti degli effetti predicibili con un MDoF, ma con bassi tempi di calcolo e analisi e elevata capacità di convergenza, caratteristiche tipiche dei modelli SDoF. L'efficienza di questi modelli semplificati è stata testata sul campione di edifici esistenti sopramenzionato e i risultati, in termini di risposta strutturale, stato di danno e livello di confidenza, sono stati confrontati con quelli ottenuti precedentemente dall'applicazione della metodologia FSA. La rilevanza e l'impatto futuro del lavoro di ricerca presentato può essere valutato in una prospettiva più ampia e relativa ad un'analisi di vulnerabilità del patrimonio costruito a scala territoriale, che risulta essere attualmente un aspetto critico sia per la comunità scientifica che per le autorità governative. Infatti quest'ultime hanno il difficile compito di proporre strategie di mitigazione del rischio sismico per un ampio e disomogeneo

patrimonio strutturale, ma con risorse economiche spesso molto limitate. Pertanto, lo sviluppo di metodologie per la stima della vulnerabilità basata su dati limitati è un tema soggetto ad intense attività di ricerca. Le proposte presentate nella tesi possono fornire un potenziale strumento di analisi di grande utilità, in quanto potrebbero consentire, attraverso l'uso dei modelli 3D ad ordine ridotto combinati con la metodologia FSA, di superare le ben note limitazioni mostrate dagli approcci empirici, a favore di metodi meccanici, utilizzati in un quadro completo di analisi probabilistica.

Parole chiave: Existing RC buildings; Seismic Assessment; Numerical Modelling; PBEE; Few Stripe Analysis; 3D Reduced-Order Models

INDEX

1. Introduction

1.1 Motivations

The seismic vulnerability of existing buildings is one of central issues on which the scientific community has focused its attention in the last few years, exploiting the experience matured after the effects of the last earthquakes events, especially in the Mediterranean area. The necessity of a systematic evaluation of the safety level of the existing buildings is strictly related, firstly, to the nature of the seismic events, which are unpredictable phenomena characterized by significant uncertainty both in their intensity and recurrence and secondly, to the nature of the existing building stock. With this regard, a lot of existing buildings were designed by using old technical codes, which did not take into account the effects due to the seismic actions, besides not considering the modern design philosophy based on the concepts of capacity design. Despite the consistent presence of masonry buildings within historical centres, there is a widespread presence of reinforced concrete (RC) structures characterized by a potential high vulnerability to seismic actions. For example, in Italy, Istat Census Data (Istat, 2011) show that more than 50% of the RC building stock was built in early after World War II, before the first seismic code was issued, and almost 85% of RC structures was built before the 1991, when the seismic hazard was considered only in a little part of the territory. Furthermore, it should be considered that the quality of structural materials used in these buildings was often inadequate to actual code prescriptions (low materials' quality and strength, poor execution quality) and this aspect, associated to the lack of durability of old concrete, to the decay of the strength due to environmental conditions, leads to a low performance towards seismic actions. This evidence is highlighted by the observation about the damage suffered by existing buildings during recent earthquakes, as reported by many documents. Looking at the most recent events, it is worth mentioning the reports about the Molise Earthquake, in 2002 (Augenti et al., 2004, Maffei and Bazzurro 2004, Decanini et al., 2004), Aquila Earthquake, in 2009 (Dolce et al., 2015, Dolce et al., 2017, Giordano et al, 2009, Salvatore et al., 2009, Verderame et al., 2009, Bursi et al., 2009, Augenti and Parisi, 2010, Ceci et al.,

2010, Toniolo and Colombo, 2012, Verderame et al., 2011a, Ricci et al.,2011), Emilia-Romagna Earthquake, 2012 (Savoia et al., 2017, Liberatore et al., 2013), Centre Italy Earthquake, in 2016 (Santarsiero et al. 2016, Masi et al., 2017).

In view of the seismic risk mitigation of the built environment, the role of the scientific community is to support governments and local administrations in the decision making and in the development of plans for the disaster prevention and emergency management. In addition, the research community should also provide guidelines useful for practitioners, who represent the main actors involved in the process of seismic assessment of existing buildings, in order to promote a conscious and correct "way to do". To this aim, a solution can be represented by the proposal of methodologies and instruments easy to use and cheap from point of view of the computational efforts and time analysis. Another key point, in this sense, is the promotion of a greater awareness about the role of the practitioner as a "modeller", by providing a reference framework for rationally evaluating the significance of the hypotheses assumed and their possible effects on the final results. In this dissertation, the first part is devoted to the discussion and management strategy of some critical issues about the phases of modelling and analysis of existing RC buildings are discussed. In particular, the focus is on the effects induced by some simplified hypotheses that practitioners usually adopt, in order to discern common errors and shift towards a more critical approach.

The second part is focused on the definition of effective, simplified methods of analysis and modelling, with the aim to open up the framework of Performance Based Earthquake Engineering (PBEE) more effectively to practitioners and also in view of the possibility of performing fragility analyses at the regional scale according to a consistent mechanical probabilistic approach.

1.2 Objectives

This research work is aimed investigating several aspects about the seismic assessment of existing RC buildings. In particular, the interest is focused on the problems that can be encountered by practitioners in the process of the vulnerability analysis of existing buildings. The general objective is to propose methods and procedures

that provide, on the one hand, solutions to ambiguous situations in which the analyst is forced to assume subjective decisions and, on the other hand, allow a simplification of some phases of the assessment path, which are based on a forefront approach like the PBEE.

In the modelling phase and the subsequent evaluation of the structural response, practitioners are usually engaged in the definition of a finite element (FE) model that should be realistic as much as possible and able to predict the global response both in the elastic and inelastic field. Generally, in order to simplify the modelling phase, simplifying hypotheses about secondary and non-structural elements are assumed. The dissertation investigates the possibility to take into account the elements usually neglected in FE models, such as the slab, which is often considered as a rigid diaphragm. In particular, it is assessed how the structural response changes when the floor system is explicitly considered in the numerical model by proposing a simplified numerical procedure, compared with other ones from the scientific literature. Effects are evaluated in terms of variation of the capacity curve, considering also the contribution of non-structural elements such as infill panels and, in a perspective of retrofit solutions, the addition of RC walls or reinforced infill panels.

The second issue that is faced is related to the variability of the parameters involved in the knowledge phase of an existing building. Geometrical and mechanical parameters are defined on the base of the results of in-situ investigations and accurate surveys. Building codes provide some prescriptions in this sense, but in many cases, there is still a large margin of discretion about the values to assume in the FE model. In addition, depending by the method of analysis applied and by the input parameters, the results of the structural FE analysis can lead to appreciable differences in the results. In order to understand how the structural response can change, the above-mentioned problems are then discussed in the dissertation from the deterministic approach point of view, by evaluating the possible variation of the capacity curves and modifying the assumption about the in-situ materials and the typology of nonlinear static (NLS) analyses (by considering conventional and non-conventional methods).

Finally, the dissertation deals with the possibility to apply the concepts of PBEE, which is actually the forefront approach for the assessment of existing RC buildings, in a form that is parsimonious but still effective and, at the same time, operational and accessible also to practitioners, who still encounter too many difficulties in its application. Thanks to the availability of a sample of 15 existing RC school buildings, located in the Province of Foggia, Southern Italy, it has been possible to investigate, firstly, the structural response by using nonlinear dynamic (NLD) analyses in a probabilistic framework, with a special attention to the practitioners' needs (reduced time of analysis and computational efforts). Furthermore, the possibility of defining suitable simplified models to estimate the global response of the case studies is assessed. With this regard, it is worth noting that when adopting a simplified model, some effects are inevitably lost, both in the mechanisms of individual components and the accuracy of the structural behaviour, as shown by a full FE model. On the other hand, there is an unquestionable advantage in practical applications: using simplified models based only on the knowledge of the geometrical and mechanical information, practitioners can provide quantitative measures of performance, damages and losses for an existing RC building (o for a sample of buildings) with fully compatible times and costs.

1.3 Outline and organization of the thesis

In the first part of Chapter 2, a section about the recurring features of existing RC buildings, according to the observation of the Italian building stock, is presented, highlighting the main sources of irregularity and variability that influence the global structural behaviour. Then, the problem of vulnerability analysis of existing RC buildings is discussed, with reference to the methods provided by the most recent scientific literature. In particular, the focus is on the different methodologies developed for studying the seismic vulnerability at different observation scales, starting from the regional scale up to the level of detailed analysis of single buildings. With regard to the regional scale, it is important to distinguish two approaches for the analysis: empirical and analytical/mechanical methods. Considering the objectives of the thesis, the focus is then shifted on the full assessment of a single existing RC building, for which technical codes

provide some procedures that allow of following a well-defined path for computing the current safety level of the case study. With this regard, the deterministic and probabilistic assessment approaches are presented, highlighting the advantages and disadvantages from the practitioners' point of view.

In Chapter 3, an extensive discussion about the modelling methods of existing buildings is treated, considering the necessity to have FE models investigable in both elastic and inelastic fields. To this aim, firstly, the scientific literature about the NL modelling of structural elements is reported, discussing the different approaches that can be adopted to model the non-linearity and the behaviour to cyclic loadings. Then, the influence of secondary structural elements, such as the slab and of non-structural elements, such as infill panels, is discussed, appraising the variation that the explicit modelling of these components introduce in the results of FE analysis in terms of global response. Regarding the modelling of the floor system, a numerical simplified procedure is proposed, in order to simulate the slab through an equivalent orthotropic shell. The new element, calibrated on the base of a sensitivity analysis on the most significant parameters, can be used in the numerical model regardless of any aprioristic assumption about the hypothesis of rigid behaviour of the floor. Furthermore, the effect of the explicit modelling of floor deformability is evaluated in the presence of non-structural elements, such as infill panels, in the FE model. The same analysis is performed when a retrofit solution is designed, by appraising the effects on the case study. In particular, two practical applications are proposed, also accounting for the reduction of the horizontal displacement, obtained through an increment of effective stiffness: presence of reinforced infill (with reinforced plaster) and presence of RC walls added at the building perimeter.

In Chapter 4, an extensive discussion about the methods of seismic analysis for existing RC buildings is presented. With this regard, it is well-established that non-linear (NL) analyses are necessary in order to characterize the global structural behaviour of an existing RC building both in the elastic and inelastic fields. The main methods of seismic analysis, also proposed by technical laws, are the NLS analysis, or pushover, and NLD analysis. The scientific literature proposes several methodologies for

each of the two types, with the objective of considering the peculiarities that characterize, on the one hand, the seismic hazard and, on the other hand, the modelling and the analysis of the building.

With regard to NLS analyses, conventional and non-conventional methods are described. Subsequently, an evaluation of conventional pushover method is investigated, assuming a sample of 92 ideal existing RC frame buildings and studying the influence of the control node position. Concerning the non-conventional NLS methods, a multimodal pushover analysis procedure is thence proposed, which can be very useful for practical application. The method is applied to a real case study, which is an irregular existing RC school building characterized by a large dispersion of the mechanical properties of the in-situ concrete strength. Investigating the seismic response of the building through some analysis methods, the efficiency of the proposed multimodal pushover analysis procedure has been assessed, also accounting for several scenarios about the in-situ mechanical parameters. At the end of the Chapter, the most important methods of NLD analysis are then discussed, with specific reference to the input of analysis (records selection, number and scaling option) and the several methodologies of NLD analysis, developed by scientific literature.

In the first part of Chapter 5, the simplified methodologies proposed in the scientific literature for simplifying the operations of modelling and analysis in the field of existing RC buildings are presented. These models are usually aimed at reducing the time and computational efforts of NL analyses, but mainly in view of research applications. Starting from this base, in the following part of the Chapter, a new procedure of analysis is proposed, with the objective of applying the concepts at the base of the PBEE to the assessment of existing RC building, in a form suitable for the use by practitioners. With this regard, the main concern of practitioners is to spend little time for the analysis and to use commercial software with a low computational effort. Hence, the proposal is an application of the Multi Stripe Analysis (MSA) method, a very powerful approach of NLD analysis, able to investigate the full structural response of a building both in the elastic and inelastic fields. The novel procedure is based on the execution of few stripe analyses (FSA) on FE models, which can easily be performed

by using commercial software. In order to test and validate the procedure, it is applied on a sample of 15 real existing RC school buildings located in the province of Foggia (Southern Italy), for which a full knowledge of the geometrical features and mechanical parameters was available. For each building, the application of the procedure provides the structural response and the damage state at the different limit states (LSs), allowing the computation of the fragility curves. In order to assess the efficiency of the procedure, the results are compared with those obtained by the SPO2FRAG software, an user-friendly tool able to compute the damage states of buildings in a practical way.

The final part of the Chapter illustrates the definition, application and validation of a new procedure for making simplified models able to predict the global response or existing RC buildings, by using the concept of 3D reduced-order model. The proposed procedure provides the possibility of creating a FE model starting from the available information about the building, such as geometrical and mechanical features of structural elements. The 3D reduced-order model allows of performing a lot of NLD analyses and thence adequately characterize the structural response. Being able to substitute the full numerical model in the global assessment, the proposed modelling approach is particularly effective to meet the needs of practitioners (such as the reduction of computational time and efforts). The proposed novel 3D reduced-order modelling is applied to the sample of RC school buildings previously mentioned, preforming the seismic assessment and computing the structural response, the damage states and determining the confidence levels. Finally, in order to assess the effectivity of the proposal, the obtained results are compared with those obtained by applying the FSA on the full FE models.

2. Vulnerability analysis of existing RC buildings

2.1 Overview

In the last few years, the assessment of RC existing buildings has been a central issue in the interest of scientific and technical community, considering the relevance of damages caused to the building stock during recent seismic events. One of the main reasons is the presence of lot of buildings designed according to old code and characterized by significant limitations in their structural response. In order to verify the acceptability of the seismic performance of an existing RC building, practitioners need to carry out several phases, which finally allows to determine the safety level and to design a retrofit solution. The scientific literature provides a lot of methodologies for estimating and quantifying the vulnerability of RC buildings. This can be obtained through empirical or analytical procedures, as discussed in this Chapter. From the practical point of view, practitioners can refer to current technical codes that provide information about the assessment process of existing buildings, through the regulation of a logic path, which consists in the phases of knowledge of the structure, modelling, analysis and assessment of the safety level. Anyway, the approaches proposed by the technical codes, which are adopted in different countries, are different. Assessment procedures can be mainly distinguished in deterministic approach, such as the one implemented in Eurocode 8 (2005) and probabilistic approach, which is adopted in the FEMA 356 (2000) and FEMA P695 (2009). With this regard, a presentation about the two methods is proposed, highlighting the differences from the scientific and practical point of view.

2.2 Critical issues in the design approaches according to old technical codes

The problem of the seismic risk represents a relevant issue in the countries in which the seismic hazard is medium-high, such as Italy, Greece, Turkey and in the Mediterranean area. As reported in (Manfredi et al., 2007), in the last century we have had 120.000 losses in terms of human lives and, in the last 25 years, 145.000 billion euros have been spent for repairing post-seismic damages and rebuilding new substitute buildings. Especially in Italy, cities are characterized by historical centres made of

masonry buildings, while surrounding areas and suburbs are rather constituted by RC buildings, characterized by a significant fragility due to the old age of the structures and the unsatisfactory design approaches adopted at the time of construction. With regard to the age, it is interesting to analyse figure 2.1 that shows a classification of the age of about 85% of existing RC buildings in Italy, as reported in the ISTAT Census of 2001 (ISTAT, 2001).
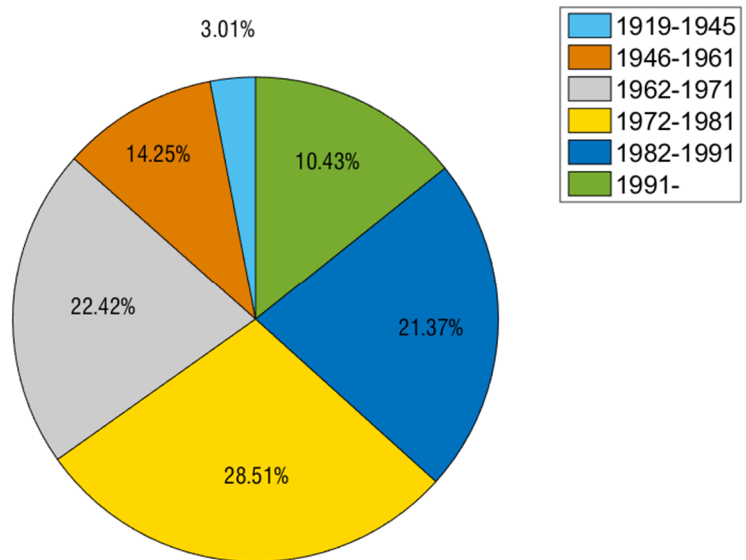

Fig. 2.1 – Age of the Italian buildings up to 1991, as shown in (ISTAT, 2001)

The pie chart shows that the major part of Italian buildings was built starting after Second World War, with a trend that quickly increases up to the end of the last Century. This situation was due to the great development of the building industry during the post-war reconstruction, boosted by the big economic boom occurred in the '70s. With regard to the design features, the existing RC building stock is generally characterized by structures designed according to old technical laws, which often did not take into account seismic actions and by the use of construction materials of low quality. It is even possible to find cases in which there are design mistakes, also according to the prescriptions of technical laws, poor maintenance and visible decay phenomena. A summary of the above-mentioned problems is reported in figure 2.2, showing the

causes of vulnerability in existing RC buildings, such as reported in a RELUIS report, in 2007. Generally, common critical issues characterize the existing RC buildings, which have been object of investigations by the scientific community. Typically, the design of existing RC buildings ignored the rules of the "conceptual design" and this circumstance has led to summarize these critical issues as in the following list:

- Irregularity in-plan;
- Irregularity in-elevation;
- Poor mechanical properties of concrete (design mistakes and degradation);
- Poor details about longitudinal and shear reinforcement;
- Poor details about beam columns joints.

devi specificare le criticità: "armature longitudinali" non è di per se una criticità.
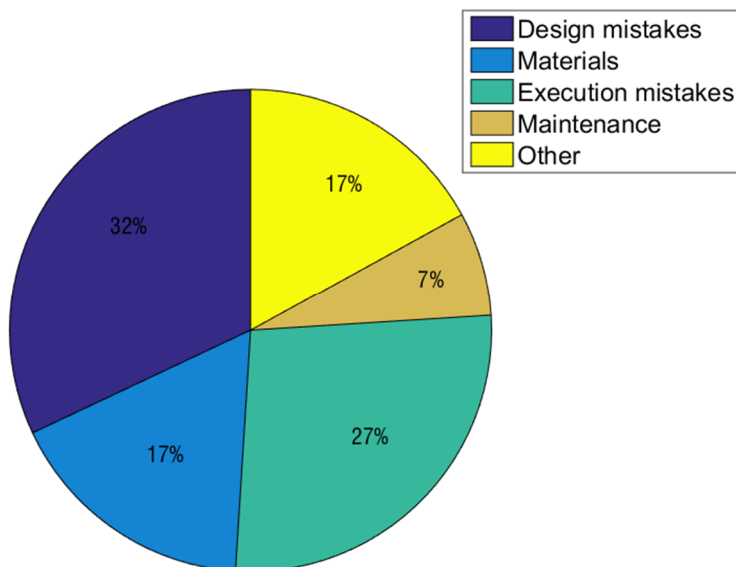

Fig. 2.2 – Causes of vulnerability of existing RC buildings

2.2.1 Irregularities in-plan and in-elevation

Concerning the irregularity in-plan, many existing buildings are characterized by a shape that does not account at all for the concept of "regularity". The trend, in

fact, was to design buildings mainly based on functional considerations. For example, a lot of existing RC school buildings have a very irregular shape, in order to accommodate as much classrooms as possible. Generally, we can say that a building is regular in-plan if designed following the criteria provided by the Eurocode 8 (EC8):

- Building structure must be symmetric along two orthogonal axes;
- In-plan configuration must be compact. Limited re-entrances are allowed, in order to do not influence in-plan stiffness;
- In-plan stiffness must be enough with respect to vertical one. In this regard, in-plan shapes as L, C, H, I, X must be carefully analysed, in order to assess the validity of the rigid floor assumption;
- The ratio between maximum and minimum dimensions of building must be lower than 4;
- For each level and analysis direction, the eccentricity e_0 and the torsional radius r must respect the following prescription:

  - $e_0 \leq 0.3\, r_x$;

  - $r_x \geq J_s$

  where r_x is the square root of the ratio between the torsional stiffness and the lateral stiffness in Y direction and J_s is the radius of gyration of the storey mass.

Irregularities in-plan provide a torsional behaviour of the building, due to a different position of the centre of the mass (CM) and the centre of the stiffness (CS), which is symptom of irregular distribution of mass, strength and stiffness (figure 2.3). In particular, this torsional behaviour is enhanced by the seismic action, which is an inertial force and then acts on the CM, generating an in-plane torque with CS. More distant are CM and CS, more consistent is the torsional effect. This latter effect causes an increase of the seismic demand in some parts of the building and, in particular, an increment of the stresses in the external and internal structural elements. If not accurately designed, they can suffer of brittle mechanism collapse (ductility reduction). Clearly, when some structural elements enter in the inelastic field, we can have some

effects, among which the change of CS and centre of strength (CV) positions, with subsequent variation of the previous equilibria.
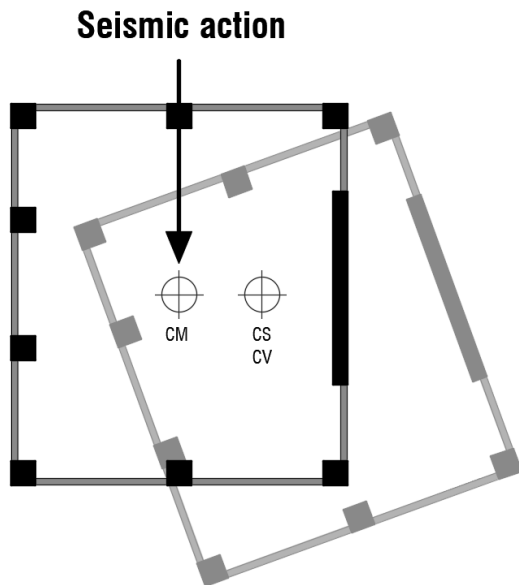
Seismic action

Fig. 2.3 – Torsional behaviour of RC buildings due to irregularity in-plan

Several studies about these and other effects, both in the elastic and inelastic field, are available in the scientific literature (Rutenberg, 2002, De Stefano and Pintucchi, 2008, Varadharajan et al., 2013, Anagnostopoulos et al. 2015). The first works about the study of torsional behaviour of buildings were conducted on single-storey asymmetric buildings. Among these, in (Dutta and Das 2002a and Dutta and Das 2002b) the strength degradation effects on an asymmetric one-storey building are studied by analysing the bidirectional response (with a bidirectional input) of a numerical model. The results of the analyses showed that unidirectional loading can underestimate the real response. Furthermore, the authors observed that the seismic demand in terms of displacement and ductility was greater when stiffness deterioration was taken into account, considering both sides of building considered. In (De Stefano and Pintucchi, 2002), a single-storey model was analysed in order to investigate the inelastic interaction between bidirectional loading and axial forces on structural elements. In particular, they found that, neglecting the previous interaction, the torsional response was

overestimated, due to the floor rotation in the inelastic field. In (Tso and Myslimaj 2003; Myslimaj and Tso 2005), authors investigated the correlation between strength and stiffness on a 1-storey model subjected to bidirectional actions. In particular, they assessed how to balance the strength and stiffness distributions, providing some criteria for locating the CV and CS in order to reduce the torsional behaviour. In addition, they showed that when one element reaches the yielding, a greater torque is generated due to the redistribution of the action towards other elastic structural elements. In (Pettinga et al., 2005), authors analysed the behaviour of a single-storey model under unidirectional and bidirectional earthquake excitation through a sensitivity analysis and assessed the influence of some parameters (hysteretic behaviour, P-Delta effects, seismic intensity, ductility) on the residual deformations of structural elements. They concluded that in the systems with low torsional restraints (Paulay, 1998), the buildings had an improvement in terms of residual displacement and residual rotational behaviour. In (Peruš and Fajfar, 2005), a general discussion about several problems is presented, with regard to the torsional behaviour of a 1-storey building in the elastic and inelastic field (in the cases of mass-eccentricity, strength eccentricity and stiffness eccentricity). In particular, they evaluated the behaviour change from the elastic to inelastic field, concluding that the response in the two configurations were similar. Furthermore, the excursion in the inelastic field provided a reduction of torsional effects, in favour of a translational behaviour. All systems investigated by the authors presented the same behaviour. In (Aziminejad and Moghadam, 2010), the performance of 1-storey building designed with irregular configuration was investigated in order to optimize the position of CV, CS and CM, based on the plasticity occurrence. Based on the damage observed, they provided criteria for establishing the best position of CV and CS.

Focusing on researches about multi-storey buildings, Paulay (Paulay, 2001, Paulay, 2002) redefined the criteria for designing the dual wall-frame systems. In particular, their most important deduction was the independence between the yield displacement and strength. The authors estimated that the stiffness was proportional to the nominal strength: if the value of the strength is fixed, automatically stiffness is determined. This result was also confirmed by Tso and Myslimaj (Myslimaj and Tso

2005), as previously mentioned, and subsequently by (Sommer and Bachmann, 2005), who defined design criteria from a practical point of view. After checking the interdependence between strength and stiffness, as shown in figure 2.4, they provided some prescriptions for a reliable design. Based on their study about a multi-storey model with RC walls, the authors suggested how to locate the CV with respect to CS and CM in order to have a uniform distribution of the ductility demand, based on the location of steel reinforcement in RC walls.
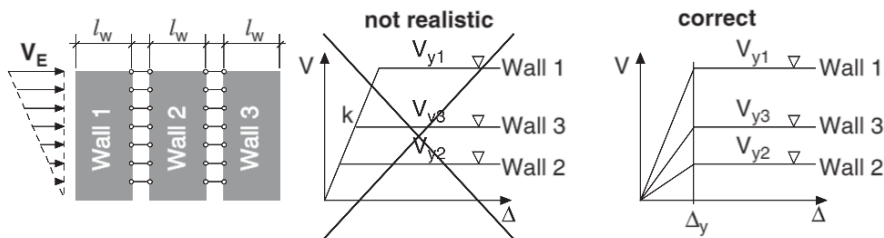

Fig. 2.4 – Force-displacement relationship, based on the interdependence between strength and stiffness, assuming independence from yield displacement (Sommer and Bachmann, 2005)

In (De Stefano et al., 2002), a 6-storey frame building was studied by assessing the code-design prescriptions. In particular, they found that their model had an excessive ductility demand due to a wrong location of the over-strength. They concluded that the prescriptions of the code were not able to provide a good torsional behaviour to the building because they were calibrated on a single-storey model. To confirm this, in (De la Colina, 2003), a sensitivity analysis was performed on a 5-storey building with eccentric stiffness, under bidirectional actions. They analysed the problem considering the ductility demand and identified practical cases in which eccentricity should be considered in the design. In (Anagnostopoulos et al., 2010), the authors demonstrated that the inelastic response of an asymmetric multi-storey building could be predicted with simplified models having a dynamic behaviour close to the original building, in terms of the first three natural periods, as soon as in terms of total strength. In the field of laboratory tests, it is worth mentioning the investigation performed in the SPEAR project (2005), where a full-scale 3-storey building was investigated by

pseudo-dynamic tests by using a bidirectional excitation (Mola et al., 2004). They assessed that the global behaviour of the building was underestimated by using conventional NLS analysis, due to contribution of the higher modes related to torsion, and, more in general, that some effects, such as the soft storey at second floor, was unpredictable using NLS analysis. In addition, in the works about the torsional behaviour of RC buildings with irregularity in-plan highlight the necessity to investigate the structural inelastic response through non-conventional NLS procedures calibrated on experimental or numerical results based on NLD analysis. Some aspects and scientific literature about this topic will be presented in the next section.

With regard to the irregularity in-elevation, several existing buildings are characterized by the presence of parts with different heights, sometimes related to unregulated building activities in which storeys were added in order to accommodate the functional needs of the users. Also in this case, EC8 provides some prescriptions, summarized below:

- Each structural vertical element must extend along the whole height of building, from foundation to the top storey;
- The mass of each storey must be constant or can change without abrupt variation;
- The stiffness of each storey must be constant or can change without abrupt variation;
- Re-entrances of each storey must be less than 20% of dimension considered;
- In the case of re-entrance that does not exceed the 15% of the total height of the building, it cannot be greater than the 50% of the correspondent in-plan dimension;
- In the case of asymmetric re-entrances, their sum on all storeys, in one direction, must be not greater than the 30% of the correspondent in-plan dimension.

Irregularity in-elevation can represent a critical issue mainly because it induces an increment of the plastic demand at particular points of the building that do not respect the rules of "hierarchy strength" design. Generally, this problem consist in an

irregular distribution of stiffness, strength and masses, causing an increment of the inter-storey drifts (θ_i) at some levels of the building and, consequently, an increment of structural and non-structural damage.

The scientific literature provides several studies about the irregularities in-elevation, and a lot of researchers have developed sensitivity analyses for understanding the parameters that influence the question. In (De Stefano and Pintucchi, 2008), an extensive state of art can be found. In (Magliulo et al, 2002), some case studies characterized by irregular distribution of mass, stiffness and strength are analysed. The authors assessed the code prescriptions about this topic, comparing the performance of the investigated structures with the ones obtained from regular cases with analogous configuration. The results suggested that criteria provided by international codes were not able to identify all the effects about the irregularity buildings. In (Magliulo and Ramasco, 2008), the irregularity in-elevation, in terms of strength, is investigated in the case of high ductility classes, according to EC8 definition. The results of the analyses performed on a 5-storey model showed that the performance was largely verified at safety LSs, but the regularity thresholds, assessed with the most important international code prescriptions, were different. In (Magliulo et. al, 2012), a study about the in-elevation irregular distribution of overstrength, among structural elements, is presented through the performance of NLS and NLD analyses on regular and irregular buildings designed with EC8 prescriptions. The authors suggested of improving the code provisions about the strength irregularity, which can be checked only at the end of the assessment, to difference of other properties as geometry, mass and stiffness. This induced to revise the behaviour factor (q) in practical application, at the end of the assessment. In (Romão et al., 2004) the influence of the axial force's variation in the columns on the global behaviour of RC buildings is studied. In particular, three case studies were investigated, which were characterized by different in-elevation irregularities. The comparison of the results with the ones obtained from ideal regular building showed that the axial force's variation only influences the lateral deformability, but not the ductility demand. In (Tena-Colunga, 2004), two irregular one-bay buildings, designed according to the Mexican code, were investigated in the weak direction by NLD

analyses. Based on the results showing that the performance of the building was very low, they provided suggestions for introducing penalty factors in the code prescriptions. In (Fragiadakis et al., 2005), the authors analyse the strength and stiffness of a steel frame structure with irregularities in-elevation, highlighting the variation of the effects according to the different the kind of irregularity, its location and the intensity of seismic excitation. In (De Stefano et al., 2005), a sensitivity analysis about the P-Delta effects for RC buildings designed according to EC8 and having irregularity in-elevation is presented. The results, in terms of fragility curves, suggested the relevance of the above effects, which can vary the structural performance estimation. In (Sarkar et al., 2010), a new "regularity index" for computing the fundamental period T of the structure is proposed. The procedure was assessed on an extensive sample of buildings with different kinds of irregularities. In the field of experimental tests, Reinhorn et al. preformed experimental tests on a 3-storey steel building in which there were irregularities in-elevation (Reinhorn et al., 2005). The observation about the structural damages induced the authors to suggest some techniques for designing this kind of structures, besides proposing a new numerical model able to simulate the steel connections.

2.2.2 Assessment of structural materials and compliance criteria

Concerning to the features of the concrete used in the existing RC buildings, it is well-known that it is often characterized by a low quality of the mechanical properties because of several factors, such as the limited knowledge about the techniques of mix design, the low accurateness of the concrete casting phase, the lack of acceptance controls (as imposed by present codes). In addition, the mechanical features of in-situ concrete, such as the strength, are usually strongly modified by degradation phenomena occurring during the life cycle of the building because of particular environmental conditions (Collepardi, 1992). The main consequence is a change of the structural response, with the reduction of the performance under seismic actions. For a correct evaluation of the structural response of existing RC buildings, it is necessary to characterize the properties of in-situ concrete, such as the compressive strength (f'_{cm}), the concrete elastic modulus (E_c), the yielding and ultimate strains (ε_{cy} and ε_{cu}). To this

aim, a detailed investigation plane should be prepared, in which the necessary in-situ investigations to be performed on the structural elements of the case study are defined. The most effective way for characterizing the mechanical parameters of the concrete is represented by destructive tests (DTs), which consist in the extraction of concrete specimens from the structural elements that will be analysed in laboratory (drilling core test). With this regard, it is important to specify that the operations that allows to measure the value f'$_{cm}$ of in-situ concrete strength are affected by practical events that can alter the results, such as the dimensions of the core, the presence of reinforcement bars in the specimen, the disturbance induced by the drilling phase and so on. In order to consider the influence of these elements, the scientific literature provide some formulations, such as the one by Masi (Masi, 2005):

$$\cdot_{cis,j} = \left(C_{H/_D} C_{dia} C_a C_d \right) f_{car,j} \qquad (2.1)$$

in which the in-situ compressive strength of the specimen (f$_{cis,j}$) is provided by the compressive strength of the core (f$_{car,j}$) modified by the coefficients C$_{H/D}$, which depends from the specimen's dimension; C$_{dia}$, which is a function of the specimen's diameter; C$_a$, which depends from the reinforcement embedded in the specimen and C$_d$, which depends from the disturbance degree during the drilling phase. Considering that in an existing RC building the number of DTs should be reduced as much as possible in order to limit damage, the previous investigations can be integrated by non-destructive tests (NDTs), which provide the values of some mechanical parameters that must be calibrated with the result of DTs. Table 2.1 summarizes the typologies of DTs and NDTs for assessing concrete compressive strength. The execution modalities of the tests will not be here described, but the discussion will be rather focused on the data that can be derived by investigation plans, considering that the definition of the values of the parameters that characterize in-situ concrete of existing RC buildings, which of course assumes a crucial role in the safety assessment, depends on the number of tests performed. A first crucial aspect is the choice of the representative structural elements to be investigated, that depends on the sensitivity and experience of the practitioner, should be performed in the lowest invasive way and consider the local

conditions for executing the tests (for example isolated elements). Clearly, the investigation should cover all the typologies of structural elements (beams, columns, slabs, beam-column joints …).

Tab. 2.1 – NDTs and DTs about in-situ concrete

CONCRETE tests	
NDTs	DTs
Ultrasonic test	Drilling core
Rebound hammer test	Pull-out test
Windsor Probe Test	Pull-off test
Georadar scanning	
Ultrasonic tomographic test	

The number of in-situ tests depends from the accurateness degree that practitioners want to achieve, according to the EC8 prescriptions (as discussed in the next Section). Even DTs represent the most significant measure, the minimum number required by EC8 is quite low, since they can cause damage on the structure. Precious additional information can be provided by NDTs, which are faster, easier, induce a very limited damage on the structure and can extensively performed on the whole structure. One of the main practical problem is represented by the dispersion of the values provided by the tests for the mechanical parameters. To this scope, technical codes suggest to evaluate the dispersion degree of the mechanical parameters through the computation of the Relative Standard Deviation (RSD), which is a dimensionless coefficient that, according to the American Code (FEMA 356, 2000), should not be greater than 14%. EC8 defines RSD as a coefficient of variation (CoV). Numerically, RSD is provided by the ratio between the standard deviation and the mean value of the parameter measured on the sample investigated, expressed in percentage. On the base of the number of analysis performed, the design values of the materials are properly reduced, which can be strongly penalizing for the analysis results. In order to improve the accuracy and quality of the information and to avoid excessive penalizations of materials' strength, the number of DTs and NDTs can be increased, but this also increases the costs. Usually, the dispersion of the materials' parameters depends by several factors, such as

mistakes in the concrete casting phase, different concrete suppliers (Giannini et al., 2014), errors in the concrete design and the well-known problem of the ineffective compaction during the casting phase. The scientific literature about these topics is widely extended and includes many studies in which real data of in-situ concrete mechanical parameters sourced from existing RC buildings have been gathered and processed, estimating the dispersion and trying to limit the abovementioned problems. In (Masi et al., 2014), a large database of 1500 DTs on 300 RC public buildings in Basilicata Region is presented. This database has been processed in order to provide statistic distributions of data, according to the period of construction. Finally, some indications about the evaluation of the concrete strength mean are provided, in order to avoid possible mistakes in the subsequent analyses. In (Masi, 2005) the widely used formulation about the determination of f'$_{cm}$, reported in eq. 2.1, was proposed. About the same topic, in (Fiore et al., 2013) the authors performed a wide investigation about the dispersion of data collected by in situ diagnostics of the existing concrete by processing and analysing the results of DTs performed on seven existing RC school buildings in the province of Foggia. In particular, it was observed that the values of RSD were higher than the threshold indicated by FEMA documents. An extensive analysis was also performed on one of the buildings, by processing and correlating additional results provided by NDTs (ultrasonic and rebound hammer tests), which showed to be homogeneous and consistent and allowed of improving the estimation of the RSD (that resulted to be lower). In (Cristofaro et al., 2015), an extensive investigation was performed on a large sample of existing RC buildings in Toscana Region. In particular, the authors investigated a database of 1000 DTs and NDTs regarding a portfolio of buildings dated back from 50' to 70', founding RSD values of about 50%. Using these latter data collected, other authors showed the effect of the variability of the in-situ concrete mechanical parameters in the seismic analyses. In fact, in (De Stefano et al., 2012 and De Stefano et al., 2013) authors showed the weight of the variability of the concrete features in the structural elements of existing buildings, in the computation of the seismic performance. In fact, this can cause problems about in-plan or in-elevation irregularity. Furthermore, other researchers investigated some aspects about the variability

of mechanical parameters of in-situ concrete in existing buildings (Masi and Chiauzzi, 2013, Pucinotti, 2013, Vona and Nigro, 2013, Quagliarini et al., 2016, Masi et al, 2016).

Another crucial issue is the execution of the compressive tests on in-situ concrete specimen, since the measured values can be influenced by various factors, such as the confinement effect, the aspect ratio of specimen, the presence of embedded reinforcements, and so on. In order to obtain reliable design value, the f'_{cm} values provided by laboratory tests should be properly corrected. In the scientific literature, there are some research studies about this topic, in which the quantification of degradation and damage due to concrete core sampling is investigated. In (Uva et al., 2014), a procedure for assessing the reliability of in situ concrete tests and improving the estimation of the compressive strength is proposed. This procedure was based on the determination of a coefficient called C_{DD}, which estimates the decrement of in-situ-concrete strength in drilled cores as a function of the concrete compaction degree, in order to account for the effects due to the alterations induced by extraction and the preparation of samples in the concrete strength evaluation. The same authors, in (Porco et al., 2014), have proposed an improvement of the procedure by correlating the results of DTs, NDTs and data documenting the compressive strength tested during the construction phases.

The problems about the characterization of in-situ materials of existing RC buildings regard also the type of reinforcement and its arrangement in the structural elements. Regarding the type of steel employed in the structural elements, especially in Italy, the major part of existing RC buildings was characterized by the use of smooth bars. In this case, the main problem is the well-known phenomenon of bond-slip between concrete and steel, which increases the deformations of the building and reduces its capacity in terms of strength, ductility and cyclic behaviour. For avoiding the bond-slip effect, the Italian building code (NTC, 2008) proposes a formulation based on the equilibrium of tangential forces developed on the contact surface between the concrete and a longitudinal bar subjected to tensile force. The formulation allows of computing the anchorage length (l_{anc}), such as reported below:

$$l_{anc} = d \frac{\sigma_s}{4\tau_{ad}} \qquad (2.2)$$

where d is the diameter of the bar and τ_{ad} and σ_s are defined in the code depending on the properties of the materials used. Furthermore, in order to assess the seismic performance of existing RC buildings, it is necessary to investigate the mechanical properties of in-situ steel bars, such as in-situ tensile strength (f'_{ym}), elastic modulus (E_s), following a suitable investigation plan. As for concrete, steel is investigated through destructive in-situ tests (DTs), which consist in the extraction of steel specimens from structural elements, which will be analysed in laboratory. In addition, NDTs are useful for determining the position of the bars. Table 2.2 summarizes some typologies of DTs and NDTs about in-situ steel. In this work, the execution modalities of the tests will not described.

Tab. 2.2 – NDTs and DTs about in-situ steel

STEEL tests	
NDTs	DTs
Pacometric test	Tensile test
	Bending test

The characterization of in-situ steel is generally easier than concrete. Generally, according to old codes, about 3-4 steel classes were usually adopted in the existing buildings. Each class corresponded to ruled mechanical parameters. In (Verderame et al., 2001) the mechanical properties of steel bars extracted from a sample of existing RC buildings (built in 60') were investigated and organized into a database. The authors identified 3 class of steel, called Aq. 42, Aq. 50 and Aq. 60, where the number indicates the design value f'_{ym}. They demonstrated that the factors that influence most the mechanical parameters of steel are the bars' diameters, the yielding tension (f'_{ym}), the ultimate tension and the percentage stretching of bars (due to tensile tests) up to the collapse for 10 different bars' diameters. In conclusion, authors assessed the correspondence between the mechanical parameters of the in-situ steel class and the ones of the steel designed according to the classification above. This study was improved in (Verderame et al., 2011b), where after the 70', the steel adopted for reinforcing the concrete was substituted with new typologies, called FeB22k and FeB32k. Processing

the database through statistical distributions (Gaussian and Lognormal), the authors provided statistical information about the features of in-situ steel, useful in order to support the practitioners in the characterization of the steel mechanical parameters. The behaviour of the structural elements with smooth steel bars has been investigated by some researchers by using laboratory tests. In particular, in (Cosenza and Prota, 2006), an experimental program about the structural elements of existing RC buildings with smooth bars and inadequate stirrups spacing is presented. Varying some geometrical parameters, such as the diameters of bars and the value of the stirrups spacing, authors established the limits for avoiding the buckling phenomena highlighted in the monotonic compressive tests. In addition, authors compared the experimental results with the ones obtained by theoretical formulations. Based on the previous work, in (Prota et al., 2009), a study of the cyclic behaviour of RC structural elements with smooth bars is presented through other experimental tests. Authors conducted experimental tests on some specimens and compared the results obtained with the ones computable by using the most common numerical models provided by scientific literature (Giuffrè and Pinto, 1970, Menegotto and Pinto, 1973, Monti and Nuti, 1992). In (Melo et al., 2015), the results of experimental tests on an extensive sample of specimens (about 30) is presented. In particular, using monotonic and cyclic pull-out tests, the authors propose an empirical formulation that takes into account the bond-slip effect (discussed in Melo et al., 2011) and compare it with similar models in scientific literature.

2.2.3 Design criteria for brittle mechanisms: shear and beam-column joints

Another issue is related to the shear reinforcement. In RC buildings designed only for vertical loads, the original design procedure was based on the use of shear reinforcements constituted by smooth stirrups with a very large spacing. Clearly, the presence of seismic action increases the stress in the end sections of columns and beams, and existing shear reinforcements turn out to be insufficient. The immediate effect, often manifested in several buildings after earthquakes events, is the development of cyclic damage, spalling of concrete cover and, buckling of longitudinal bars.

Of course, these effects occur near to the beam-column joints. In newly designed buildings, the occurrence of these mechanisms in the structural elements is inhibited through the adoptions of specific structural detailing, as suggested by the actual design methodologies that impose the increase of stirrups in the end parts of structural elements, called critical zones. In fact, shear mechanisms are considered to be brittle (or better, significantly less ductile than flexural mechanisms), and determine a significant and rapid strength decay of the structural capacity and performance. It is worth mentioning the mechanisms due to the degradation of the shear strength with cycling loading (Biskinis et al., 2004), such as:

- The reduction of the interlocking effect along diagonals, due to the change of smoothness of the ground parts;
- The degradation of dowel action, with accumulation of inelastic strain in the bars;
- The development of flexural cracks and the subsequent reduction of shear resistance contribution in the compressed zone;
- The reduction of the aggregate interlocking effect along diagonal cracks, due to the increase of the inelastic strain in the stirrups and the bond slippage;
- The softening of concrete in the diagonals subjected to compression, caused by the transverse tensile strain.

EC8 provides a formulation for computing the cyclic shear strength, proposed in (Biskinis et al., 2004):

$$V_R = \frac{1}{\gamma_{el}} \left[\frac{h-x}{2L_V} min(N; 0.55A_c f_c) + \left(1 - 0.5min\left(5; \mu_\Delta^{pl}\right)\right) \left[0.16max(0.5; 100\rho_{tot})\left(1 - 0.16min\left(5; \frac{L_V}{h}\right)\right)\sqrt{f_c}A_c + V_w\right]\right] \quad (2.3)$$

where γ_{el} is a factor depending on the typology of the element (primary or secondary), h is the depth of the transversal section, x is the height of the neutral axis, N is the axial force, Ac is the area of the transversal section, ρ_{tot} is the longitudinal reinforcement ratio, V_w is the contribution of transverse reinforcement to the shear resistance and μ_Δ^{pl} is a term that expresses the ductility of the member. The Italian Code

(NTC08) provides another formulation, in which the shear capacity (V_{Rd}) is the minimum between the compression shear strength (associated to the formation of compression struts) and the tensile shear strength (associated to the strength of shear reinforcements), as displayed in figure 2.5:

Compression shear strength:

$$V_{Rcd} = f'_{cd}\alpha_c b_w 0.9d \frac{(cotg\ \alpha + cotg\ \theta)}{(1 + cotg^2\ \theta)} \tag{2.4}$$

Tensile shear strength:

$$V_{Rsd} = f_{yd}(A_{sw}/s)0.9d(cotg\ \alpha + cotg\ \theta)\ sin\ \alpha \tag{2.5}$$

where f'$_{cd}$ is equal to 0.5 f$_c$; α_c is a coefficient dependent from the axial stress, b$_w$ is the length of the shorter section's side; d is the height of the section less the height of the cover; cotgα is the inclination of transversal reinforcements; cotgθ represents the inclination of the diagonal concrete struts; A$_{sw}$ is area of the transversal reinforcements and s is the stirrups spacing. As mentioned, the shear strength is given by:

$$V_{Rd} = \min(V_{Rsd}, V_{Rcd}) \tag{2.6}$$
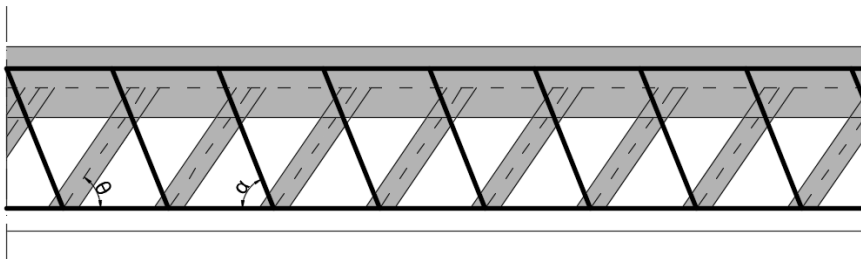
Fig. 2.5 – Strut model for computing the shear capacity in a RC structural element

The scientific literature and technical codes provide a lot of methodologies for assessing the shear capacity of structural elements, useful also for practical applications (De Luca and Verderame, 2013). For example, in (Priestley et al., 1994), the shear behaviour of columns, coupled with the flexural one, is investigated. Using the results of experimental tests, authors provided predictive equations for characterizing the shear behaviour on the base of some contributions, as the concrete mechanisms (e.g. the

cracking), the axial load mechanism and the truss mechanism. In other research studies, the problem has been faced basing on the results of laboratory tests (Ritter, 1899, Sezen and Moehle, 2004, Biskinis et al., 2004, Elwood and Moehle, 2005, Sezen and Moehle, 2006, Mwafy and Elnashai, 2008). Based on the tests results, a lot of authors have proposed numerical models (Ceresa et al., 2007 and the references wherein, Ceresa et al, 2009, Mergos and Kappos, 2008, Sezen, 2008), which takes into account the above cited mechanisms and the cyclic and hysteretic behaviour.

To conclude this brief overview about the main issues regarding existing RC buildings, it is necessary to spend some words on beam-column joints. Existing RC buildings are characterized by the absence of specific attention about reinforcements in beam-column joints, and therefore these are subjected to brittle failure mechanisms under earthquakes, compromising the entire structural performance. Generally, from the capacity design point of view, the constructive details in the beam-column joints should account for an adapt disposition of horizontal reinforcement, which come from the longitudinal bars of the beams and vertical reinforcement, which come from the longitudinal bars of the columns. In addition, in order to ensure the role of the beam-column joints, which must be able to transfer the shear action from beams to columns, a functional reinforcement should be made according to a diagonal path of the load. To this scope, additional stirrups should be added to longitudinal bars. In the case of existing RC buildings, the absence of transversal reinforcements in the joints' panels induces the activation of a concrete strut that generates diagonal cracking and loss of strength, stiffness and deformation capacity. When approaching this question, the differences between internal and external joints should be properly considered, accounting for the confinement effect of the adjoining structural elements and the presence of axial stress. In order to assess the strength capacity of beam-column joints, EC8 provides formulations for computing the maximum shear action in the joint panel, which represent the shear demand, both in internal and external joints:

For interior joints:

$$V_{jhd} = \gamma_{Rd} * (A_{s1} + A_{s2}) * f_{yd} - V_C \qquad (2.7)$$

For external joints:

$$V_{jhd} = \gamma_{Rd} * A_{s1} * f_{yd} - V_C \qquad (2.8)$$

where A_{s1} and A_{s2} are the top and bottom areas of reinforcements in the beam; V_C is the shear force in the column, derived from seismic analysis and γ_{Rd} is the over-strength factor. In addition, the EC8 provide a formulation for computing the compressive capacity of the diagonal strut, which shall be compared with the tensile strength of the joint in order to avoid diagonal cracking:

$$V_{jhd} \leq \eta f_{cd} \sqrt{1 - \frac{v_d}{\eta}} \; b_j h_{jc} \qquad (2.9)$$

where η is a factor that depends on the joint's position (external or internal); v_d is the normalised axial force in the column; b_j is the width of the joint and h_{jc} is the distance between the external locations of the longitudinal bars in the column. Furthermore, EC8 allows to assess the shear reinforcement, in order to avoid the achievement of the concrete tensile strength (f_{ctd}), which means diagonal cracking:

$$\frac{A_{sh} f_{ywd}}{b_j h_{jw}} \geq \frac{\left(V_{jhd} \; h_{jc}/b_j\right)^2}{f_{ctd} + v_d f_{cd}} - f_{ctd} \qquad (2.10)$$

where A_{sh} is the total area of the horizontal stirrups in the joint; f_{ywd} is the yielding strength of the steel and h_{jw} is the distance between the external locations of the longitudinal bars in the beam. For existing RC buildings, NTC08 provides a formula for computing the maximum diagonal tensile and compressive strength of the external joints and comparing them with threshold limits:

Maximum diagonal tensile strength:

$$\sigma_{nt} = \left| \frac{N}{2 A_g} - \sqrt{\left(\frac{N}{2 A_g}\right)^2 + \left(\frac{V_n}{A_g}\right)^2} \right| \leq 0.3\sqrt{f_c} \qquad (2.11)$$

Maximum diagonal compressive strength:

$$\sigma_{nt} = \frac{N}{2 A_g} + \sqrt{\left(\frac{N}{2 A_g}\right)^2 + \left(\frac{V_n}{A_g}\right)^2} \leq 0.5 f_c \qquad (2.12)$$

where N is the axial stress in the upper column; V_n is the shear stress acting on the joint (considering the shear in the upper column and the tensile stress in the top longitudinal bars); A_g is the area of the horizontal section of the joint and f_c, expressed

in MPa, is the compressive strength of the concrete. The above-mentioned formulation evaluates the shear strength of the joint through the equilibrium of the principal stresses, according to the Mohr's circle, as shown in figure 2.6, that is to say, by referring to the average stresses acting on the joint's panel.
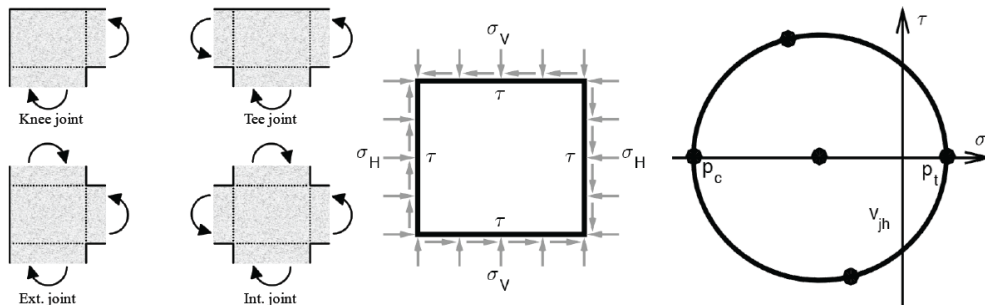
Fig. 2.6 – Evaluation of joint's shear strength through Mohr's circle (Gentile, 2017)

In the scientific literature, there are some research works about this topic, which are usually based on laboratory tests. In (Priestley, 1997), a discussion about the assessment of existing buildings is presented, where the author reports some simplified formulas for checking the shear strength of beam-column joints, both internal and external, based on available test data. In (Pampanin et al., 2002), an experimental laboratory campaign performed on typical Italian beam-column joints (reproduced in a 2/3 scale) subjected to seismic actions is presented. Based on the results obtained for 3 types of beam-column joints (knee-joints, tee-joints and cruciform joints), the authors have derived a trend of the degradation behaviour of the specimens with no shear reinforcements and adequate anchorage. Subsequently, in (Pampanin et al., 2003), a simplified numerical model that simulates the results of the mentioned experimental tests is proposed. (Masi et al., 2013) have studied the cyclic behaviour of external beam-column joints on 26 specimens, evaluating the role of the axial load and the type of failure occurred. In (De Risi et al., 2016 and Ricci et al., 2016), 2 specimens of beam-

column joints are investigated, considering plain and deformed bars. The authors compared their results, in terms of shear strength, with the main formulations provided by scientific literature. Furthermore, they assessed the condition in which the failure mechanisms in the joints were represented by the cracking of the concrete or by the rotation of beams or columns.

2.3 Vulnerability analysis at the regional scale

Earthquakes are among the most destructive natural disasters, which can cause severe physical losses in terms of human lives, damage on buildings, infrastructures and lifelines, disruption of economic activity. Therefore, considering the intrinsic randomness of the hazardous event, the engineering approach for limiting losses is trying to predict the behaviour of elements at risk, that is to say to propose predictive vulnerability models, in order to mitigate risk and adopt effective disaster prevention policies. To this scope, the scientific community has been intensely working for supporting governments in the management of risk mitigation strategies, also from an economic perspective. The main problem, in fact, is that available public funds are often limited, which means that a primary objective is the optimization of economic resources. In the field of vulnerability analysis of existing buildings, the above-mentioned issues require the development of models for predicting the expected losses in terms of repair costs or disruption of regular activities, accounting for the specific features of the local building stock (Calvi et al. 2006). In the framework of regional scale analysis, a vulnerability analysis means that it is provided a quantitative measure of damage. It can intuitively be expressed through the probability of occurrence of a given damage level, conditioned by a seismic intensity measured for example as the peak ground acceleration (PGA). This definition should not be confused with fragility idea. It is worth reminding that, as reported in (Porter, 2018), the vulnerability is not fragility, because the vulnerability measures the losses while the fragility measures the probability. On the other hand, the vulnerability functions usually implied the losses as function of the environmental excitation. It is evident that regional scale methodologies, for being able to estimate which buildings are more vulnerable for seismic actions within a very large

portfolio, must be simplified. Once that the more vulnerable buildings are identified, the focus can be shifted on the vulnerability assessment of the single buildings, applying the procedures prescribed by technical codes (as described in detail in the next Section). In the following paragraphs, the most important simplified methods adopted for the regional scale analyses in the scientific literature will be described, with reference to the two main types of vulnerability methods - empirical and analytical/mechanical approaches – and their combination into hybrid methods.

2.3.1 Empirical approaches

In empirical methods, the prediction of the damage state is performed by processing damages observed after earthquake events. The main advantage of these methods is the reliability of the damage estimated, which can be applied to buildings with similar features. On the other hand, they can be developed only if post-earthquakes data are available and, strictly speaking, cannot be extended to different typological or constructive classes. Moreover, the heterogeneity of data should be properly calibrated for obtaining results about homogenous classes of buildings. As reported in (Del Gaudio, 2015 and Calvi et al., 2006), the different existing empirical methods can be summarized as follow:

- Damage Probability Matrices;
- Empiric vulnerability functions;
- Vulnerability Index;
- Screening methods.

Damage probability matrices are based on the definition, in a discrete form, of the conditioned probability of obtaining a certain structural or non-structural damage level due to a ground motion intensity (Calvi et al., 2006). The first proposal is present in (Whitman et al., 1973), where this concept is developed through a classification of the structural typologies and information about the costs of repair and retrofit. In (Braga et al. 1982), based on the Irpinia Earthquake, authors define a damage probability ma-

trix with 3 vulnerability classes, related to different structural systems, linked to a seismic intensity measure provided by MSK scale. Later, in (Di Pasquale et al., 2005), the seismic intensity measure has been replaced by MCS scale and, moreover, the number of vulnerability classes has been increased. A similar application is presented in (Dolce et al., 2003), where authors have adopted the seismic intensity and vulnerability classes proposed in EMS-98 scale (Grünthal, 1998). As shown in figure 2.7., EMS98 provides 6 vulnerability classes and, for each class, a classification of the damage level. The method of the damage probability matrix is characterized by some drawbacks, such as the presence of purely qualitative descriptions of buildings and the incomplete correlation between each damage state with each seismic intensity. Furthermore, the method does not allow of accounting for the different typologies of buildings, which means that the sample of building investigable is limited.

Damage Level	Damage Grade				
Intensity	1	2	3	4	5
V					
VI	Few				
VII		Few			
VIII		Many	Few		
IX			Many	Few	
X				Many	Few
XI					Many
XII					Most

Fig. 2.7 – Example of damage model for a vulnerability class according to EMS-98 scale (Calvi et al., 2006)

With regard to empiric vulnerability functions, the method consists in the derivation, from observational data, of continuous functions, that relate the seismic intensity to the expected damage level. The vulnerability curve is obtained by fitting the data evaluated as shown for the damage probability matrix method (figure 2.8). Finally, data are classified in vulnerability classes related to damage states. In Sabetta et al. (1998),

vulnerability curves are derived by using as seismic intensity the PGA and the Arias Intensity, applied on the data available at that time for Italian earthquake. About 50.000 building were involved in the computation and the authors concluded providing a mean damage index, expressed as the weighted average of the frequency of each damage level for each building typology. In (Rossetto and Elnashai, 2003), the authors have provided vulnerability curves for homogenous classes of existing RC buildings, as shown in figure 2.8, exploiting available data about the damage state of European RC buildings observed after different earthquakes. The seismic intensity parameter used is strictly related to the spectral acceleration of the fundamental period (S_a(T)) and results show a good estimation of the capacity, justifying the efficiency of the choice. In (Rota et al, 2008), typological fragility are provided on the base of the damage data recorded on 150.000 Italian buildings after the seismic events occurred in the last years.
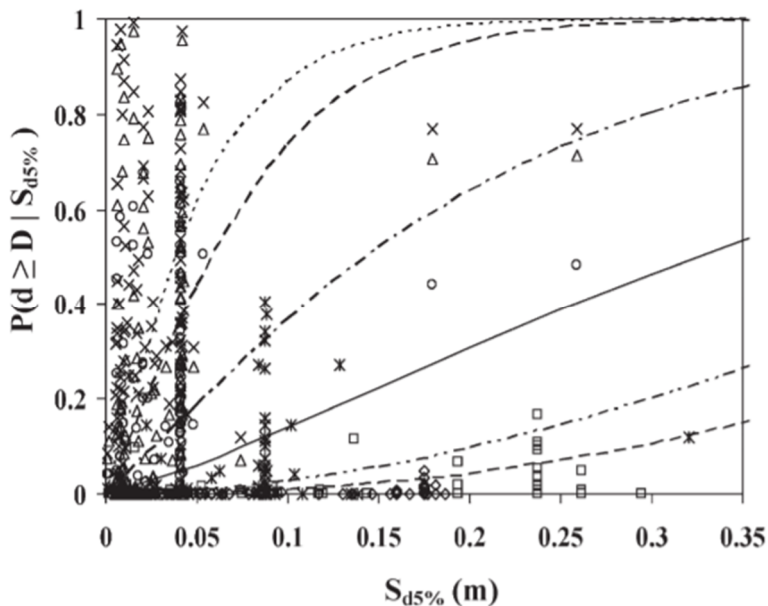
Fig. 2.8 – Example of vulnerability curves obtained by fitting observational data (Rossetto and Elnashai, 2003)

In (Del Gaudio et al., 2015), a database of almost 8000 RC buildings surveyed after the Aquila Earthquake is analysed. The buildings were classified in terms of PGA demand and morpho-typological features, such as the number of storeys and presence

of non-structural elements. The final output were the fragility curve at each LS, for the classes produced and the damage probability matrices were estimated, mainly highlighting the strong influence of infills in the above computations.

Concerning to the vulnerability index method, it is an indirect approach that correlates surveyed data about damages with the seismic action. More precisely, the method provides a vulnerability index that takes into account the seismic response of the building by means of some influencing parameters, such as in-plan shape, foundation, structural and non-structural elements, mechanical and geometrical materials properties. The first proposal of this method was made by (Benedetti and Petrini, 1984), who assumed a vulnerability index according to the following relationship:

$$I_v = \sum_{i=1}^{11} K_i \, W_i$$

(2.13)

In the sum, there are 11 vulnerability parameters, evaluated by compiling a specific form. The parameters are identified with coefficients K_i, identified with a score related to some classes (from A to D) and these coefficients are weighted by W_i. By using the vulnerability index, it is possible to define vulnerability functions, such as shown in figure 2.9. Other applications of the method can be retrieved in the literature, such as (Faccioli et al., 1999, Mouroux and Le Brun, 2006).
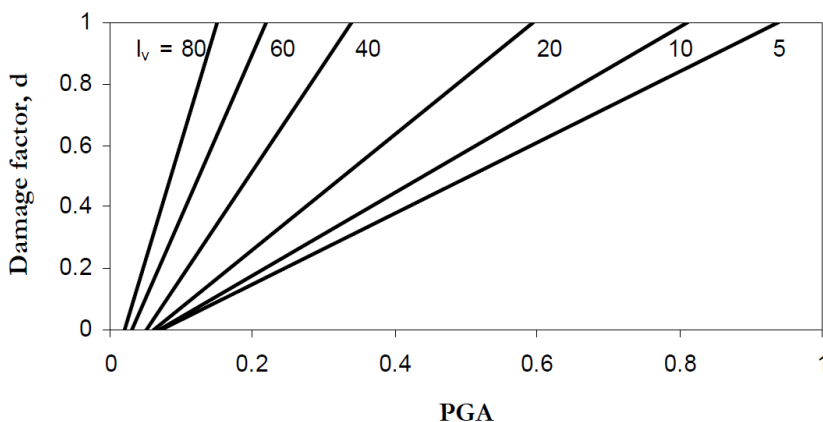
Fig. 2.9 – Example of vulnerability functions computed using different values of the vulnerability index (Guagenti and Petrini, 1989).

For example, in (Uva et al., 2015), a modified algorithm has been proposed and tested within the ANTEUS project, where using the data of almost 5.000 buildings in the Province of Foggia, South Italy, a vulnerability classification was provided through GIS maps. The vulnerability index method has the undisputed merit of considering the building stock features. Still, the application as eq. 2.13 needs expert judgements, which are usually subjective.

Screening methods allow of estimating the vulnerability of a building through the rapid computation of the seismic performance. The first application of this method was a Japanese model applied to existing RC buildings (JBDPA, 1990). In particular, the method provides the following formulation for computing the performance index I_s:

$$I_S = E_o S_D T \tag{2.14}$$

where E_o represents the structural performance, computable through the definition of ultimate strength and ductility; S_D is a sub-index that depends on the design of building and T is a sub-index dependent from the deterioration of the building. Once that I_s has been estimated, it is compared with the judgement index I_{S0} that depends on the safety degree of the building. There are many other research works that report the application of screening methods and the development of indexes, such as the priority index (Hassan and Sozen, 1997); the capacity index (Yakut, 2004) or the seismic safety screening method (Ozdemir et al., 2005). Despite the application of the screening method s can provide good estimation of the seismic performance, which can be compared with the seismic action, the approach requires the application to one building per time, and therefore still involves a big effort for performing the assessment at the regional scale,

2.3.2 Mechanical/Analytical approaches

In mechanical/analytical methods, the vulnerability assessment is performed through the direct derivation of the relationship between seismic intensity and damage state/losses by using the results of analyses on numerical models, which simulate a building or a class of buildings. This means that the model is able to take into account

the dynamic properties of the building simulated, besides the uncertainty in the capacity. The main advantage is given by the possibility of explicitly considering the variability of the building features within a homogeneous class and to introduce additional aspects in the model, such as the presence of non-structural elements. Furthermore, unlike empirical methods, seismic hazard can be simulated through seismic hazard maps, which are expressed in terms of $S_a(T)$ rather than using macro-seismic intensity. However, for a realistic evaluation of the vulnerability, the numerical models must be varied using a lot of input data, increasing much the computational efforts compared with empirical methods. On the other hand, these methodologies can be used for supporting the simulation of damage probability matrices (hybrid methods). One of the most important analytical method for estimating the vulnerability at a regional scale is the HAZUS methodology (Hazard in United States, FEMA, 2001), developed by the Federal Emergency Management Agency (FEMA). The main objective of the method is to estimate the losses of civil infrastructures due to natural disasters and a specific module for buildings subjected to earthquakes is included. The method allows of computing the buildings' capacity and fragility, which represent the input for the computation of losses. Regarding the computation of capacity, a parametrization about 36 building typologies is established and the method provides the parameters for computing capacity curves for them, based on the yield and ultimate capacity. Figure 2.10 shows the concept of HAZUS capacity curve, where the yield capacity depends from design strength (accounting lateral one), material strength and technical code requirements, while the ultimate capacity depends from the maximum strength. Once that the capacity curve is defined, the method provides LS threshold, based on the NLD analyses previously performed on all building typologies and the related performance points. The comparison with the seismic demand is performed in the acceleration-displacement (ADRS) plane, in which the elastic spectrum for a 5% damping and the capacity spectrum are plotted, as shown in figure 2.11.
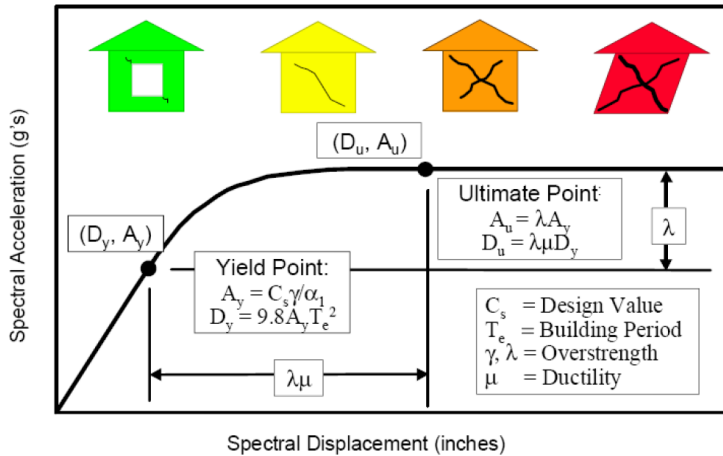
Fig. 2.10 – Definition of the buildings capacity curve in terms of yielding and ultimate points (FEMA, 2001)
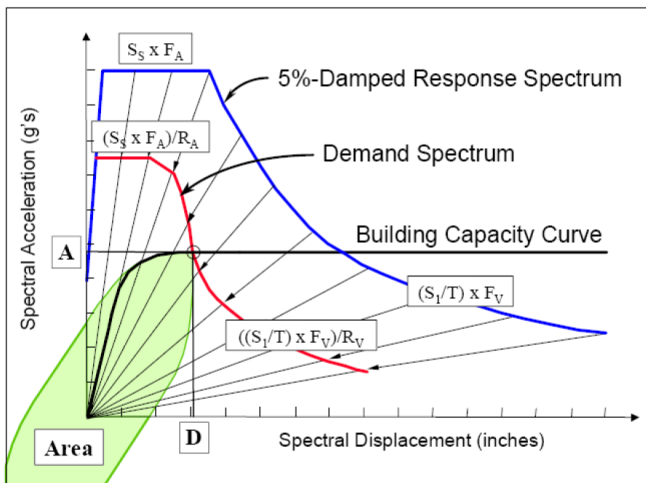
Fig. 2.11 – Comparison between capacity and demand, through capacity spectrum method (FEMA, 2001)

Furthermore, HAZUS allows of computing fragility curves for each LS, accounting both for structural and non-structural elements. For each LS, the threshold is computed in terms of displacement through the following equation:

$$S_d = S_{d,ds}\, \varepsilon_{ds} \tag{2.14}$$

where $S_{d,ds}$ is the median spectral displacement for the LS and ε_{ds} is the lognormal random variable, dependent from median and standard deviation values. In particular, the median value is computed as the average of θ_is of the building, which correspond to the displacement of capacity curve related to the LS threshold; while the standard deviation, which rules the slope of fragility curve, accounts for the dispersion of seismic demand and capacity (further details will be provided in the next paragraphs). Figure 2.12 depicts an example of fragility curve for a set of suggested LSs (Slight, Moderate, Extensive and Complete). One of the limitations of the method regards the computation of dispersion, which is entrusted to the expert judgements of the user. This means that, for the same case study, it is possible to have a high variability of fragility and capacity curves.
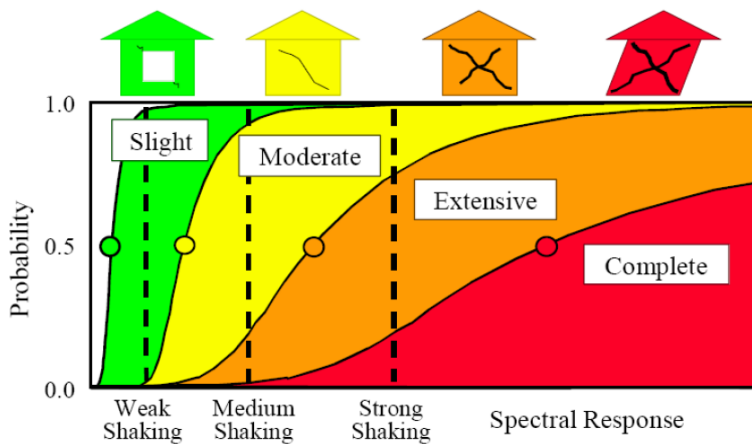
Fig. 2.12 – Fragility curves for the LSs suggested in HAZUS (FEMA, 2001)

In the scientific literature, several mechanical approaches for estimating the vulnerability of buildings, with complex or simplified methodologies, are present. In some cases, the proposed methods are aimed at estimating both the capacity and the fragility of classes of buildings and finally are able to define the losses. For example, in (Singhal and Kiremidjian, 1996) authors present vulnerability curves for RC frames of different height, by varying the mechanical properties of concrete and steel. Using NLD

analyses and some earthquake records selected via a Monte Carlo simulation, the conditioned probability of violating several given LSs for the case studies is provided. The results of the analysis are expressed in terms of vulnerability curves for all the building classes investigated, obtained by fitting all the points derived by the numerical analyses (figure 2.13). Finally, the authors have developed the damage probability matrices using, as seismic intensity, a modified Mercalli scale.
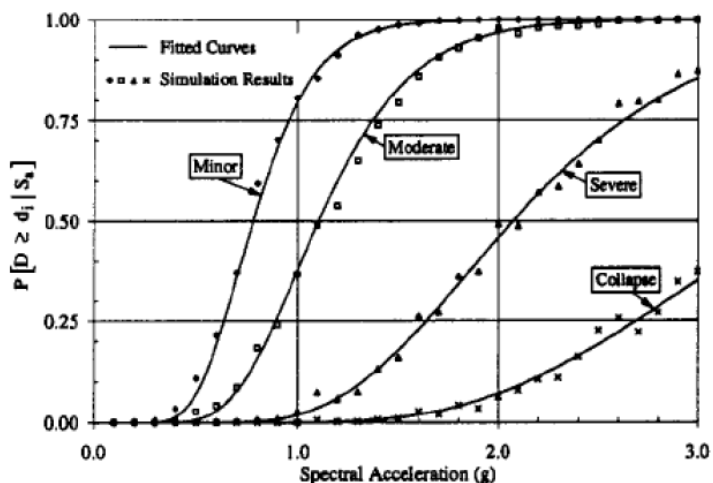
Fig. 2.13 – Vulnerability curves for a class of RC buildings investigated in (Singhal and Kiremidjian, 1996)

A similar approach has been developed by Masi in (Masi, 2003) for characterizing the vulnerability of some classes of existing RC buildings generated through a simulated design, taking into account different configurations and non-structural elements. The numerical models are excited with artificial accelerograms through NLD analyses and based on the results each building class is assigned to an EMS-98 vulnerability class.

In (Cosenza et al., 2005), a procedure for evaluating the capacity of building classes is proposed, in which the elements of the class are generated by a simulated design procedure and then categorized according to the construction age and the number of storeys. By varying the geometrical and mechanical parameters of the models, the authors have defined the possibility to have a number of pre-defined mechanisms

equal to 3*N (N=number of storeys), which are computed through the evaluation of the seismic capacity, expressed in terms of a base-shear coefficient (ratio between base shear and total weight) versus the global drift. Global drift depends from the considered mechanism, as displayed in figure 2.14. For each building, all the possible mechanisms are computed and the one having the lowest value of the base shear coefficient is assumed to represent the failure mechanism of the building. At the end of the work, authors have investigated the influence of the parameters involved through a response surface method.
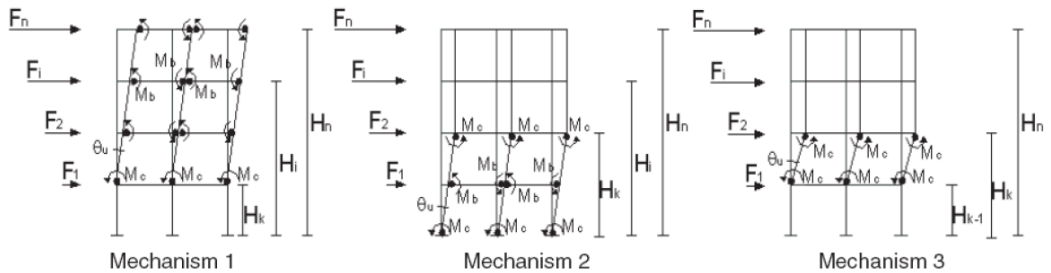
Fig. 2.14 – Collapse mechanisms proposed in (Cosenza et al., 2005)

In (Rossetto and Elnashai, 2005), the authors derive vulnerability curves for ideal sample of buildings, by considering the uncertainty of mechanical parameters of materials and the uncertainty of the seismic demand (through the use of a lot of accelerograms). Using an adaptive pushover procedure, authors estimated the performance points for each LS, through the Capacity Spectrum method and generated the vulnerability curves, through the response surface method. After they compared the results obtained from numerical simulation with ones estimated from observational data.

In (Crowley et al., 2004), a displacement based earthquake loss assessment (DBELA) procedure is proposed, based on the evaluation of building classes' vulnerability through a displacement based method, following the road mapped in former works (Calvi, 1999). The capacity of the building is computed in terms of displacement on an equivalent single degree of freedom (SDoF) system. Then, the capacity is compared with the seismic demand, expressed in terms of displacement response spec-

trum. The DBELA procedure, finally, establishes a relationship between the displacement capacity and the height of building (directly related with the T), accounting for both structural and non-structural elements. Using the methodology, the authors have developed a probabilistic framework for vulnerability analysis in which the influence of the uncertainty due to geometrical and mechanical parameters and that related to seismic demand are accounted for. The result is a joint probability density function that expresses a relationship between the displacement capacity and the period T.

In (Borzi et al., 2008), a mechanical approach known as Simplified Pushover-Based Earthquake Loss Assessment (SP-BELA) is developed, which is able to estimate the capacity curves of a class of buildings through simplified NLS analysis. In particular, through a mechanical procedure it is possible to determine the base shear capacity. By randomly varying geometrical and mechanical features, the authors define representative structures that are loaded with an inverse triangular distribution of forces. Using a method similar to the one proposed in (Cosenza et al., 2005), the possible collapse mechanisms are estimated, such as beam-sway or column-sway (figure 2.15). After defining the LS threshold in terms of element chord rotation, the capacity curve is computed and, subsequently, it is compared with the seismic displacement demand, which is a function of PGA.
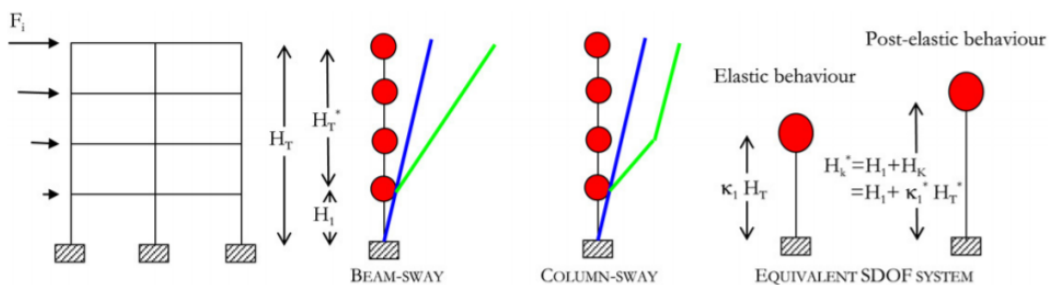
Fig. 2.15 – The procedure for evaluating the collapse mechanisms proposed in SP-BELA (Borzi et al., 2008)

In (Del Gaudio et al., 2015), a simplified procedure for assessing the vulnerability to regional scale, known as PushOver in Shear Type models (POST), is presented. The numerical models are developed through a simulated design under gravity loads,

assuming the shear-type hypotheses. The novelty of the method consists in the consideration of the contribution of infill panels, to which the damage state is assigned according to the EMS-98 scale. The classes of buildings are generated varying few parameters, according to the observational data in Campania region and the results obtained are compared with those obtained by other methods proposed in the scientific literature, accounting for the empirical and hybrid (Rota et al., 2008, Giovinazzi, 2005).

In (Del Vecchio et al., 2018 and Gentile, 2017), a procedure called simple lateral mechanism analysis (SLaMA) is presented, which provides the estimation of the probable global capacity through a NLS analysis performed by hand. The novelty of the procedure is the possibility to derive the global capacity from the local capacity of the elements of the building, such as structural elements and beam-column joints. The procedure is developed for many structural RC systems, such as moment-frame, dual system (figure 2.16) and infilled frame system. The possible effect of global irregularity, such as torsion, is also taken into account.
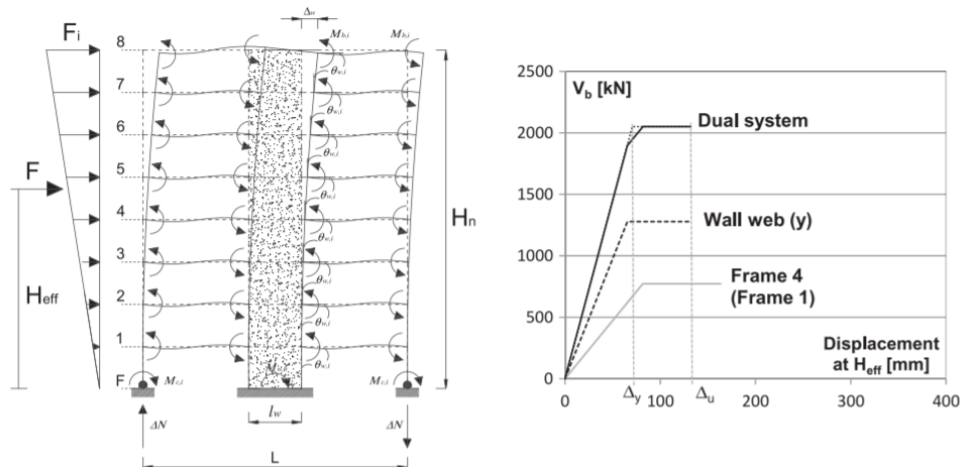
Fig. 2.16 – SLaMA procedure applied to a dual-system example (Del Vecchio et al., 2018)

2.4 Code-based approaches for the assessment of existing RC buildings

In the last decades, the procedures prescribed by technical codes for assessing the seismic performance of existing buildings have been continuously and rapidly evolved, thanks to the improvement of scientific and technical knowledge. Furthermore,

this process has been also a consequence of the changes in the constructive systems and the experiences gained from past earthquakes in terms of building damages and seismic hazard.

In particular, the codes have developed paths for driving the practitioners in the assessment of existing buildings, through the proposal of several phases. Generally, as for the new buildings design procedures, the assessment can be made through performance-based approaches, where the aim is to define the real seismic response of the building study (and the possible losses), in order to establish the safety level of the building and to design the possible retrofit solution. We want to specify that, the word "performance" is related to the exposure to natural hazards, for identifying the building state after the seismic event. This concept can be summarized as level of damage expected on the building, due to a certain loading. The main problem of these procedures is the presence of a lot of uncertainty sources, due both to the seismic action and to the nature of the structural system (uncertainty in the mechanical and geometrical parameters, in the model and methods of analysis …). However, the procedures presented in the previous sections, which allow of deriving a priority scale for the analysed buildings, are very useful for public institutions in order to allocate available funds, which shall be focused on the most vulnerable buildings. After the preliminary selection operated, the buildings identified must be analysed in detail. To this scope, a detailed vulnerability assessment procedure has to be defined, according to the following scheme:

- Complete knowledge of the structural system in terms of geometry, vertical loads and mechanical properties of materials and their conservation state;
- Definition of the target performance levels, according to the seismic hazard of the site;
- Structural analysis of the existing building, through an accurate NL numerical modelling in which both the existing vertical loads and the seismic action are simulated ;
- Comparison of the structural performance with the target one and assessment of the safety level;

42

- If the safety level is not sufficient, design of the retrofit solution and assessment of the building in the new configuration.

All the most recent technical codes around the world provide a procedure similar to the one just sketched, generally known as Performance-Based Design, with some differences in the format and operational procedures. The performance-based design applied to existing buildings was firstly developed in a deterministic form, as provided in the EC8. Subsequently, the approach was re-edited by following PBEE concepts (Cornell and Krawinkler, 2000 and Cornell et al., 2002), in order to take into account the probabilistic nature of the problem. The rigours methodology of PBEE, adopted in FEMA P695 (2009), was written in (Jalayer and Cornell, 2003) in a simplified form, which is particularly user-friendly for practitioners, which provided a way for evaluating the structural performance through a load resistance factor design (or demand capacity factor design).

The scope of the next Sections is to describe the features of the deterministic and probabilistic assessment procedures, highlighting the most important aspects, differences, advantages and disadvantages from practitioners' point of view. For the deterministic approach, the scheme provided by EC8 will be followed, with some additional notes about the real operational applications in assessment process. For the probabilistic approach, the steps of the procedure will be described with a reference to the already cited PEER report (Jalayer and Cornell, 2003).

2.4.1 The deterministic approach of Eurocode 8

The methodology proposed in EC8 for existing RC buildings (Design of structures for earthquake resistance - Part 3: Assessment and retrofitting of buildings EN 1998:3: 2005) is focused on the definition of the structural performance for three LSs: Damage Limit State (DLS); Significant Damage or Life Safety Limit State (LSLS) and Near Collapse Limit State (NCLS). The first one is related to the serviceability concept whereas the others are ultimate LSs, which actually incorporate the concepts of robustness and resilience. The word LS is a synonymous of performance target level,

which means that to each LS a seismic demand defined in probabilistic terms is associated. In particular, for each LS, it is possible to define an elastic spectrum (damping for RC structures is assumed as 5%), which expresses the probability of exceeding a certain seismic intensity measure in a certain time. To each LS, a return period (T_r) is associated. For ordinary RC buildings this is equal to 2475 years for NCLS (probability of exceedance of 2% in 50 years), 475 years for LSLS (probability of exceedance of 10% in 50 years) and 225 years for DLS (probability of exceedance of 20% in 50 years). Clearly, the seismic demand varies based on the type of building, depending on the importance, exposure and site's features (type of ground and geographical position).

A crucial phase of the assessment, then, is the characterization of the structural system through an extensive phase of preliminary knowledge. With this regard, the first step is the historical analysis that includes the retrieval of original design drawings, information about foundations, ground conditions, dimensions and cross-sectional properties of building elements, properties of materials, constructive details. The documentation collected is useful for a providing a first vision of the structural system. In fact, the subsequent step shall be a complete survey of the building, in which the data gathered will be compared with the observed ones. If historical data are insufficient, it is necessary to "simulate" the design of the building at the construction time. To this scope, the prescriptions of the coeval technical codes or manuals written by expert engineers can be adopted. The building is accordingly modelled by considering geometry, materials, details and vertical loads of the construction time and analysed, obtaining the stresses state of all structural elements.

Simulated design is useful for having a general framework about the structural behaviour and it is propaedeutic for the phase of in-situ investigations, which is ruled by EC8 depending on the desired knowledge level (KL) about the building information. In fact, EC8 proposes 3 classes of KL; limited (KL1), normal (KL2) and full (KL3). For each class, the EC8 suggests qualitative and quantitative criteria in terms of minimum requirements to achieve, regarding the geometry, details and materials and the kind of analysis to use (table 2.3). For each KL, the achievement of a level of in-situ investigation, in terms of percentage of structural elements to be investigated, is required. This

level is defined as "limited" for KL1, "extended" for KL2 and "comprehensive" for KL3 (Table 2.4). For each Knowledge Level, EC8 provides a confidence factor (CF), which is a safety factor that should be applied for reducing the mechanical properties of in-situ materials. The role of CF is to take into account the uncertainties related to the knowledge of the building system, known as epistemic uncertainties. The knowledge state, also if comprehensive, regards only a part of all elements, which constitute the structural system. The incomplete knowledge of the system has the consequence of penalizing some mechanisms, such as shear. Hence, the most practical way for considering the intrinsic uncertainties is the use of a fixed factor. Regarding in-situ investigations, practitioners have to draw up a plan of in-situ tests, including DTs and NDTs on structural and non-structural elements, as mentioned in tables 2.1 and 2.2.

The next phase is the definition of a realistic numerical model that takes into account the information collected during the knowledge path. In particular, the numerical model should be realized considering the NL mechanical and geometrical features of the structural elements, besides the loads acting on the building, with the aim to investigate the structural behaviour in both elastic and inelastic fields. As reported in table 2.3, for KL1 it is possible to use only linear methods of analysis (lateral force analysis method or linear static analysis; modal response spectrum analysis), by assuming $q \leq 1.5$ in the response spectrum. The use of linear analyses is allowed only in the cases in which the ratio ductility demand/capacity is uniform for the structural system. In other words, if the ductile behaviour of structural elements is not sufficiently investigated, it is preferred to assume a numerical model that provides conservative results, considering only the linear properties of the elements. It is clear that, for an effective assessment of the building capacity, it is necessary the use of NL analyses. Regarding NL modelling of existing RC building, more details are given in the Chapter 3. Generally, the NL modelling of RC elements should take into account the yield and ultimate capacity, both for ductile and brittle mechanisms. By taking into account the geometry, loads and mechanical parameters of materials, suitable capacity models are defined in order to carry out the safety verifications for each structural element, based on the LS chosen and the acting seismic action.

Tab. 2.3 – Knowledge levels and methods of analysis (EC8 – part 3)

Knowledge Level	Geometry	Details	Materials	Analysis	CF
KL1		Simulated design in accordance with relevant practice and from limited in-situ inspection	Default values in accordance with standards of the time of construction and from limited in-situ testing	Static analysis or Modal response spectrum analysis	CF=1.35
KL2	From original outline construction drawings with simple visual survey of from full survey	From incomplete original detailed construction drawings with limited in-situ inspection or from extended in-situ inspection	From original design specification with limited in-situ testing or from extended in-situ testing	All	CF=1.2
KL3		From original detailed construction drawings with limited in-situ inspection or from comprehensive in-situ inspection	From original test reports with limited in-situ testing or from comprehensive in-situ testing	All	CF=1.00

Tab. 2.4 – Minimum requirements for each level of in-situ inspection and testing (EC8 – part 3)

	Inspection (of details)	Testing (of materials)
	For each type of primary element (beam, column, wall)	
Level of inspection and testing	Percentage of elements that are checked for details	Material samples per floor
Limited	20	1
Extended	50	2
Comprehensive	80	3

As method of analysis, the choice is between NLS analysis (or pushover) and NLD analysis (for which more details are given in the Chapter 4). It is worth of remembering that, before performing a seismic analysis, practitioners must assess the capacity of the building to resist to vertical loads. In the case in which this verification is not satisfied, seismic assessment is useless. Generally, NLD analysis provides results more accurate than other methods, thanks to the greater accuracy in simulating the seismic action. Nevertheless, NLD analysis is rarely used in ordinary engineering applications, because presents many difficulties, such as the selection of representative design accelerograms, the choice of constitutive laws able to consistently reproduce the post-elastic and hysteretic behaviour of the structure. Moreover, there is a relevant computational effort and the possibility of misinterpreting the results. In practical applications, NLS analysis has gained increasing importance, considering its good capacity to reproduce the response of building (even if only in under specific conditions), trying to represent the envelope of the dynamic response. The result of the NLS analysis is the capacity curve, usually depicted on the plane base shear (V_b) – roof displacement (δ_R). Once that the structural behaviour is defined, it is possible to perform the comparison with the seismic demand through local and global verifications. In other words, for the building and its structural elements, the practitioner should assess the safety level, expressed like capacity/demand ratio (CRD). Concerning to the local verifications, each structural element should be assessed for ductile and brittle mechanisms. For the first ones, the formulas proposed by the codes are expressed in terms of deformation, by evaluating the chord rotation capacity at the end section of the elements and comparing it with the chord rotation demand. The chord rotation is defined as the angle between the chord that connects the end section of the element to the section having a zero bending moment null and the axis of the same element. In this way, each element is ideally constituted by 2 cantilevers identified by the shear span L_s (figure 2.17, left). The shear span is defined as:

$$L_s = \frac{M}{V} \tag{2.15}$$

where M and V are the bending moment and the shear demand, respectively. L_s is assumed equal as 0,5 L.

For columns (figure 2.17, centre), the demand in terms of rotation (θ) is evaluated as the difference between the nodal rotation θ_1 and the drift at the end of the shear span length θ_2:

$$\theta = \theta_1 - \theta_2 \qquad (2.16)$$

For beams (figure 2.17, right), the chord rotation is defined as the nodal rotation of the end section of the considered element. In order to define the rotation for different LS, the acceptance criteria are fixed as follow:

- DLS: $\theta = \theta_y$;
- LSLS: $\theta = \frac{3}{4}\,\theta_u$;
- NCLS: $\theta = \theta_u$.

where θ_y is the chord rotation at yielding, while θ_u is the ultimate chord rotation.
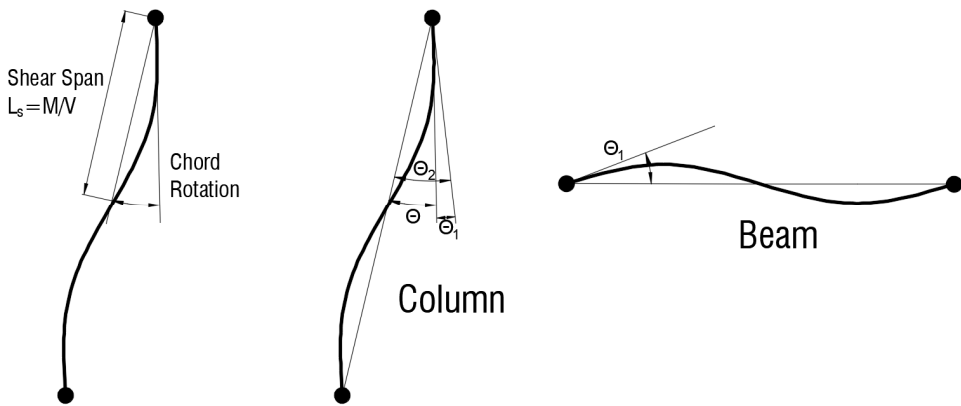
Fig. 2.17 – Chord rotation with reference for beams and columns and indications for θ_1 and θ_2.

For brittle mechanisms, the safety verifications are provided in terms of strength. In particular, for the LSs considered, the comparison is made between the acting shear stress and the shear strength, as reported in eq. 2.3.

Regarding the global assessment, EC8 proposes a method called "N2 Method", which is a "Displacement Based" methodology (Fajfar and Fishinger, 1989, Fajfar and Gasperic, 1996, Fajfar, 2000). The name of the method derives from two distinctive

features. The letter "N" indicates that the method is NL, whereas "2" refers to the use of two different computational models of the structure: a multi degrees of freedom (MDoF) model, on which a pushover numerical analysis is performed, and an "equivalent" SDoF model, which is derived by the previous one trough proper manipulations. The steps of N2 method are summarized as follow:

- Definition of the numerical MDoF model for the case study and of the elastic pseudo-acceleration spectrum at the considered LS, for a fixed value of damping. Execution of the NLS analysis and derivation of the capacity curve;

- The capacity curve obtained for the MDoF system is scaled in order to represent the response of an SDoF system having an equivalent mass

$$m^* = \{\Phi\}^T[M] = \sum m_i \Phi_i \qquad (2.17)$$

  by applying the modal participation factor:

$$\{\Gamma\} = \frac{\sum m_i \phi_i}{\sum m_i \phi_i^2} \qquad (2.18)$$

  where [M] is the diagonal matrix of the storey masses; $\{\Phi\}$ is a proper displacement shape vector of fundamental vibration mode (normalized with respect to the δ_R, displacement monitored at the performance point or control node). In particular, both δ_R and V_b values are scaled for Γ, as indicated in the following relationships:

$$d^* = \frac{\delta_R}{\Gamma} \qquad (2.19)$$

$$F_b^* = \frac{V_b}{\Gamma} \qquad (2.20)$$

  where d* and F$_b$* indicate, respectively, the top displacement and the base shear of the equivalent SDoF system. It is worth observing that all the described procedure is based on the assumption of a time-independent displacement shape.

- After determining the capacity curve of the SDoF system, it is transformed into a simplified bilinear capacity curve characterized by a yield and an ultimate point. To this scope, EC8 suggests that the yielding force F$_y$* represents the ultimate strength of the system, which is the V$_b$ corresponding to

the first plastic mechanism occurrence. Subsequently, the linear elastic branch is defined based on an equal area criterion, as shown in Figure 2.18.
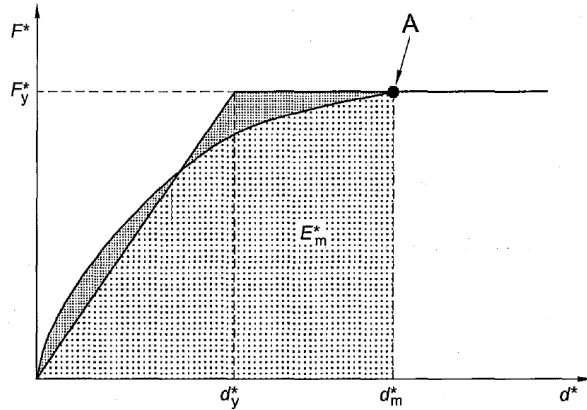
Fig. 2.18 – Bi-linearization of the capacity curve of the equivalent SDoF system (EC8)

From the curve obtained, it is possible to estimate the elastic period of the SDOF system, called T*, as follow:

$$k^* = \frac{F_y^*}{d_y^*} \qquad (2.21)$$

$$T^* = 2\pi\sqrt{m^*/k^*} \qquad (2.22)$$

where F_y^* is the yielding base shear, d_y^* is the yielding displacement, k^* is the elastic stiffness of the SDoF system.

- The final capacity curve obtained at the previous step can be directly compared with the seismic demand evaluated for the SDoF system through the elastic spectrum. In particular, the elastic spectrum can be expressed in the ADRS plane ("Acceleration - Displacement Response Spectrum"), in order to graphically compare the seismic demand and the capacity curve. The relationship governing the ADRS spectrum format is:

$$S_a = \frac{F_b}{\Gamma m^*} \qquad (2.23)$$

Actually, the seismic demand should be referred to the inelastic spectrum, in order to consider the inelastic features of the structural system. This can be obtained by scaling the elastic design spectrum by a reduction factor

R_μ, which expresses the overall structural ductility. R_μ is calculated as follows:

$$R_\mu = \frac{S_{ae}}{S_{ay}}$$ (2.24)

where S_{ae} is the value of elastic spectral acceleration for the period T* and S_{ay} is the spectral acceleration corresponding to yield force as well as acceleration capacity. EC8 provides several mathematical relationships that relate the reduction factor R_μ, the ductility μ and the period T*, depending on the structural type:

$$R_\mu = (\mu - 1)\frac{T}{T_c} + 1 \text{ for T < Tc}$$ (2.25)

$$R_\mu = \mu \text{ for T > Tc}$$ (2.26)

Both in eq. 2.25 and 2.26, the inelastic seismic demand in terms of displacement and acceleration corresponds to the intersection point of the capacity curve with the spectrum demand, which has ductility μ (figure 2.19). By using eq. 2.19, the displacement demand of the SDoF system can be transformed into the displacement demand of the MDoF, known as "target displacement". Based on this value, the structural performance can be investigated comparing seismic demand with capacity at the different LS.
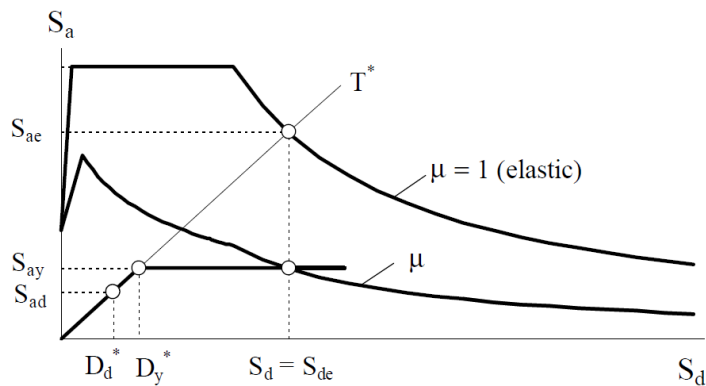
Fig. 2.19 – Comparison between capacity and demand in the ADRS plane (Fajfar, 2000)

Following the procedure above described and considering the limits of pushover procedure, the capacity curve must be defined correctly, in order to do not distort the subsequently verification. The N2 method has been extended for in-plan irregular building by amplifying the effect of NLS analysis through a "torsional amplification" or a "corrective eccentricities", as suggested in several methods provided in the scientific literature (Fajfar et al., 2005).

Once that the CDR values are assessed both for local and global behaviour, the practitioner can indicate the structural interventions to be performed. The retrofitted building must be assessed after the interventions, verifying that the CDR is greater than the one found for the original building and, of course, greater than the unit.

2.4.2 Probabilistic approach: Performance Based Earthquake Engineering

The very nature of the seismic assessment of existing RC building, both on the seismic demand side and the structural capacity side, has led to develop the concepts of performance-based design in probabilistic terms. Generally, this kind of approach is aimed to define the performance of the building by providing the probability that the system behaves in a certain way under seismic events of different intensity. Thanks to a study promoted by the Pacific Earthquake Engineering Researcher (PEER) centre, a new approach known as PBEE was developed. The PBEE paradigm was developed firstly by Cornell and Krawinkler (Cornell and Krawinkler, 2000 and Cornell et al., 2002), and subsequent revisited by other authors (Porter, 2003, Moehle and Deierlein 2004, Yang et al, 2009). This approach is able to provide quantitative measures for assessing the performance of a building system subject to earthquake excitation. The final goal of the method is to provide the probabilistic distribution of the output metrics that describe the actual performance of the building in terms easily understandable by stakeholders, such as direct or indirect losses, downtime and casualties. The general mathematical formulation of the method is an application of the total probability theorem, as indicated below:

$$\lambda(DV, D) = \int_{DM} \int_{EDP} \int_{IM} G(DV|DM, D) * dG(DM|EDP, D) * \qquad (2.27)$$
$$dG(EDP|IM, D) * d\lambda(IM, D)$$

where in the formulation, given D as a parameter that accounts for the prelimi-
nary knowledge of the building and the geographic site, λ indicates the Mean annual
frequency (MAF) of exceeding a certain level of the decision variable DV chosen for
expressing the losses. λ is calculated as a function of a set of variables representing
the damage measure (DM), the severity of an event or intensity measure (IM), the build-
ing response to the event expressed by a representative engineering demand parameter
(EDP). The general expression $G(X|Y)$ is the conditioned complementary cumulative
distribution function of a variable X, at a fixed value of Y, and $dG()$ is its derivative.

Generally, this approach allows of performing the assessment procedure
through the development of 4 steps (figure 2.20): seismic hazard analysis; response
analysis; damage analysis and loss analysis, in which all variables are independent.
The above-mentioned steps of the PBEE approach will be briefly discussed. Subse-
quently, the same approach will be described as proposed in (Jalayer and Cornell,
2003), where through some hypotheses, the methodology is provided in form of "Load
and Resistance Factor Design", more suitable for practitioners.
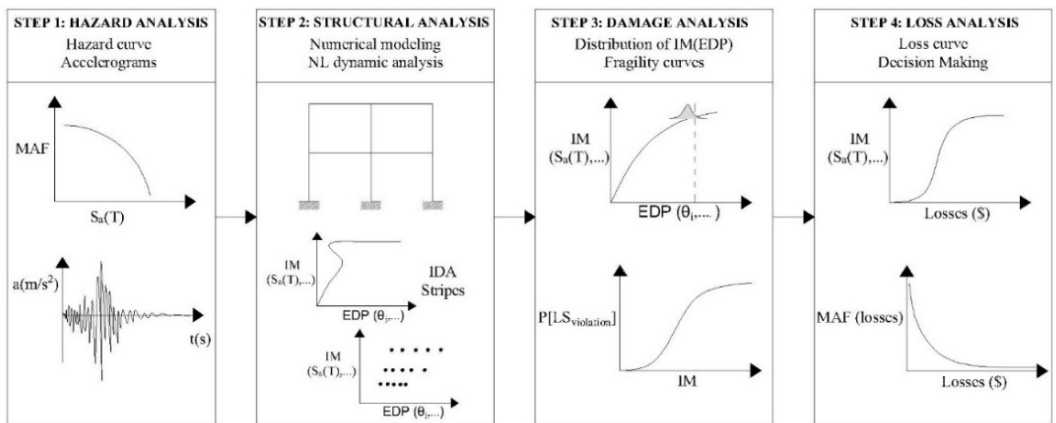
Fig. 2.20 – Steps and numerical outputs of PBEE

Hazard analysis consists in the description of the earthquake hazard in a prob-
abilistic manner. In particular, the aim is to define the probability of exceeding different
earthquakes levels, represented by a parameter of the ground motion intensity (IM) in
a given site. To this scope, it is necessary to define the hazard curve that describes the

variation of the selected IM versus the MAF. It is important to clarify that the MAF of exceeding and the probability of exceedance, in this kind of problems, are numerically the same. As shown in (Vamvatsikos and Ascheim, 2016), the hazard curve can be evaluated through the definition of the seismic hazard surface, which is a 3D graph that summarize the MAF of exceeding an IM level (usually $S_a(T)$) on a full range of Ts. As depicted in figure 2.21, by vertically cutting the hazard surface, a hazard curve can be obtained for a selected value of the T, while by horizontally cutting the hazard surface, the result is provided in term of response spectrum (or rather, uniform hazard spectrum, where each point has an equal MAF of exceed).
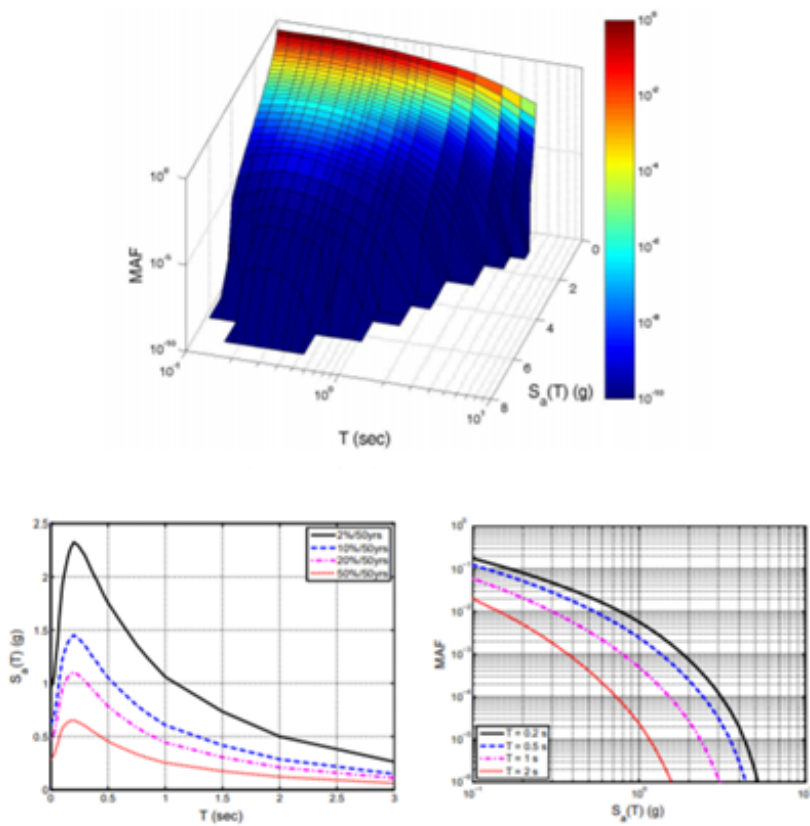
Fig. 2.21 – Hazard surface defined for the IM like $S_a(T)$, with generation of uniform hazard spectrum and hazard curve, for different ground motion levels (Vamvatsikos and Ascheim, 2016)

By fixing a value of IM and its dispersion, which are functions of the LS and the EDP value associated, from the hazard curve related to the analysed building, it is possible to compute the MAF for a LS (λ_{LS}), through the following equation:

$$\lambda_{LS} = \frac{1}{T_R} e^{(\frac{1}{2}\beta_{RTR})^2}$$
(2.28)

where T_R is the return period and β_{RTR} is the record-to-record dispersion, defined as follow:

$$\beta_{RTR} = \frac{lnS_{84\%} - lnS_{16\%}}{2}$$
(2.29)

where $S_{84\%}$ and $S_{16\%}$ are the 84 and 16% fractiles of the seismic intensity.

The final goal of the probabilistic seismic hazard analysis (PSHA) is extensively described in (Baker, 2008a). The phases of PSHA can be summarized as follows (figure 2.22):

- Identification of all seismic sources able to produce damaging ground motions;
- Outline the distribution of earthquakes' magnitudes;
- Definition of the distribution of earthquakes' distances (source to site);
- Definition of the distribution of the ground motion intensity, through the definition of functions of magnitude, distance and epsilon;
- Using the total probability theorem, identification and combination of the uncertainties related to the earthquake size, location and ground motion intensity.

Once that the seismic hazard is defined, it is necessary to choose a consistent seismic input for predicting the effects on the structure, that is to say, to select a set of accelerograms that are consistent with the seismic hazard of the building site. In order to evaluate the structural response for different IM levels, these signals should be scaled or changed. More details about the number, the selection and the scaling of accelerograms are given in the Chapter 4.
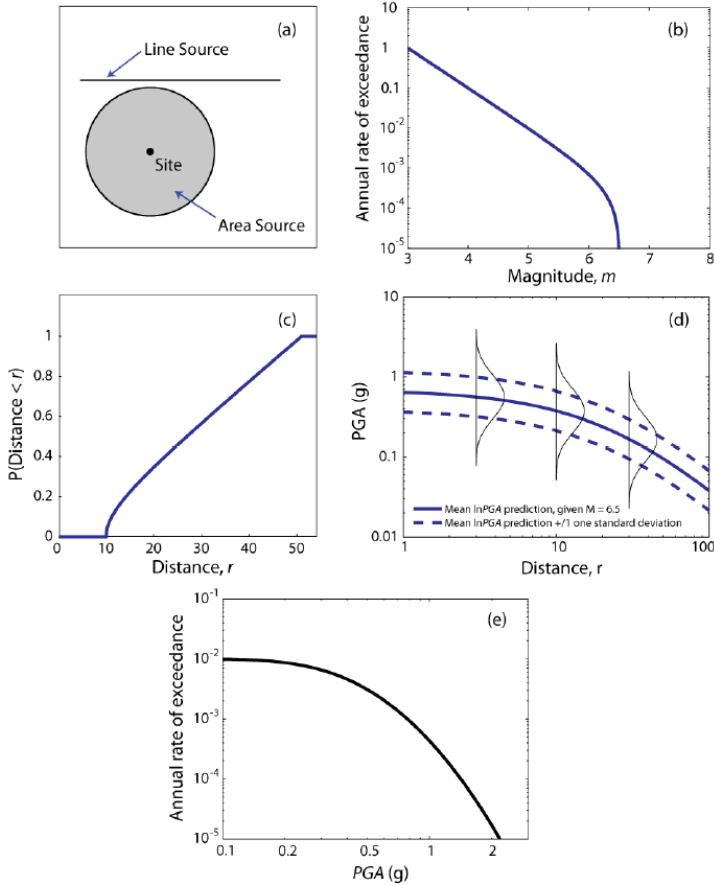
Fig. 2.22 – Steps of PSHA (Baker, 2008a)

Regarding the structural analysis, the response of the analysed building should be investigated in a probabilistic manner, for different levels of seismic hazard. In particular, a NL numerical model should be developed by taking into account uncertainties, such as the ones related to mass, stiffness, strength, damping and so on. In FEMA P-695 (2009), uncertainties, expressed in terms of total dispersion β_{TOT}, are estimated as the square-root-sum-of-squares (SRSS) of four individual dispersion contributions:

$$\beta_{TOT} = \sqrt{\beta_{RTR}^2 + \beta_{DR}^2 + \beta_{TD}^2 + \beta_{MDL}^2}$$

(2.30)

where β_{RTR} is related to the seismic demand; β_{DR} is the uncertainty related to design requirements; β_{TD} is the uncertainty in test data and β_{MDL} introduces the uncertainty due to structural modelling, related to the knowledge of the structural system. For studying the structural response at different seismic intensity levels, it is necessary to monitor an EDP able to provide information about local and global behaviour in terms of strength and deformations. For the local behaviour of RC buildings, the parameters to be monitored are the strength of structural elements (such as the axial or shear force) and the deformations of structural element (such as the plastic deformation - chord rotation). For the global behaviour, the most important parameter in terms of deformation is the maximum θ_i, useful also for considering the non-structural elements response. In addition, in terms of strength, the V_b or the floor acceleration can be monitored. After the choice of the EDP and IM parameters to monitor, NL dynamic analyses are performed on the numerical model by using the selected ground motions, with the aim to investigate the structural behaviour both in elastic and inelastic fields. In particular, it is interesting to define the seismic intensity when global instability (or global collapse) occurs, situation that corresponds to an infinite displacement increment under little increment of the seismic input. Some researchers developed methodologies able to provide a complete structural response, such as the incremental dynamic analysis (IDA) (Vamvatsikos and Cornell, 2002) or MSA (Jalayer and Cornell, 2009). The final goal of the structural analysis is to determine the probability distribution (Gaussian, lognormal…) of the structural response for each IM level. The result is the probability density function, which depends from the number of EDP-IM bins.

The results of the numerical analyses, in terms of probability distribution of the IMs associated to the given EDP, represent the base for the damage analysis, which expresses the physical damage of the structural system or of its components. In the practice, the damage state is represented by fragility curves. As reported in (Bakalis and Vamvatsikos, 2018), a fragility curve is a probability function of violating a certain LS, given a certain IM level. Mathematically, it is estimated through cumulate distribution functions. Being a function of IM, it can be expressed as below:

$$F_{LS}(IM) = P(LS \text{ violated}|IM) \tag{2.31}$$

which means that with the fragility curve we estimate the probability that the demand is greater than capacity, for a given IM. In other words, eq. 2.31 can be re-written as:

$$F_{LS}(IM) = P(IM > IM_C) \qquad (2.32)$$

$$F_{LS}(IM) = P(EDP > EDP_C | IM) \qquad (2.33)$$

where IM_c is the capacitive IM that corresponds to the capacitive EDP (EDP_C), defined for the LS selected. In addition, the role of fragility curves is to provide a unique definition of the damage state, by taking into account the uncertainty sources present in the problem (Porter, 2018). Despite a single EDP value is assumed for a LS, it should be observed that the uncertainty is different from element to element. In fact, uncertainties in the damage are firstly due to the uncertainty in the characterization of geometry and materials (that propagates in the damage computation) and secondly to the uncertainty in the loading of structural elements, which varies from an element to another one. In order to account for uncertainties, each fragility curve is represented by a shape characterized by a median value of the IM and an associated dispersion (standard deviation of the log-data). The latter, as defined in eq. 2.30, rules the slope of the fragility (figure 2.23). Starting from the serviceable LSs until ultimate ones, the fragility curves are shifted to right, with greater values of IM.
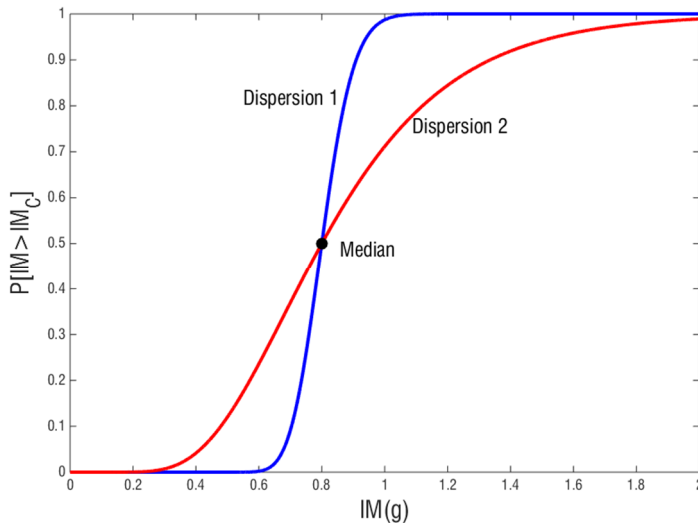
Fig. 2.23 – Fragility curves with same median and different dispersion

The last step of the PBEE is the loss analysis, in which the data obtained from the previous steps, in particular from the damage analysis, are converted into DVs. The goal of the approach is to provide DVs directly usable for the decision-makers. The losses can be summarized with the 3-d: deaths, dollars and downtime. The loss analysis allows to compute the probability of exceeding a certain loss, expressed in terms of DV, for a given LS. For each kind of loss, it is possible to provide a loss curve, which is the combination of the conditioned probability indicated in eq. 2.27 (figure 2.24). As for fragility curves, it is possible to define loss curves with reference to groups of elements in the structural system, considering the different incidence of some elements for different typologies of losses. From the application of the PBEE paradigm to existing RC buildings, it is possible to understand in probabilistic terms which factor has a higher influence on earthquake repair costs and, subsequently, to establish which retrofit strategy provides the lower retrofit cost together with the lower possibility to have future losses.
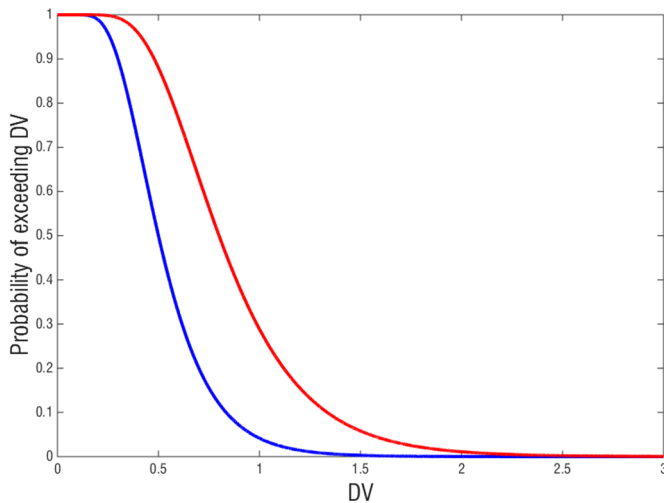
Fig. 2.24 – Loss curves for different LS

AS already mentioned, the PBEE approach was reformulated by (Jalayer and Cornell, 2003) in order to provide a method adapt for practitioners in terms of load resistance factor design. In particular, through some simplifying hypotheses, a closed

form of MAF of exceeding a LS, able to provide an approximate estimation of the collapse probability, was proposed. The first simplified hypothesis consists in the approximation of the seismic hazard curve of the site with another one depending from the S_a region of the analysed building (S_a is the selected IM), for the LS investigated. To this scope, an exponential formulation was proposed, where the MAF of the LS (λ_{LS}) is a function of λ_{Sa} defined as:

$$\lambda_{sa}(x) = k_0 * x^{-k} \tag{2.34}$$

where k_0 and k are parameters that define the new hazard curve shape and x is the value of S_a, or any other IM. Eq. 2.34 can be displayed in figure 2.25.
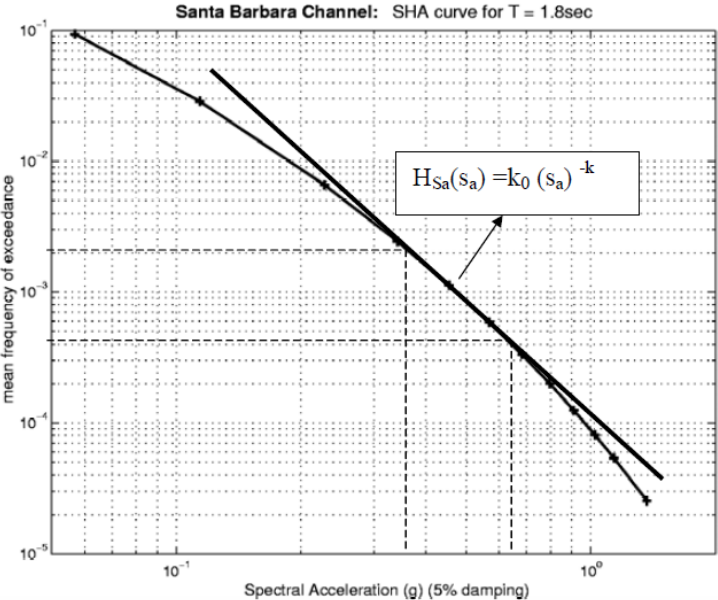
Fig. 2.25 – Approximation of the Hazard curve (Jalayer, 2003)

The second simplified hypothesis concerns the probabilistic demand model. The input of the structural analysis is represented by a set of accelerograms chosen with certain criteria. Considering the application of IDAs on the numerical model, the accelerograms have to be scaled using the $S_a(T_1)$, where T_1 is the first period of the

structure (in Jalayer and Cornell, 2003, T_1 was equal to T). For a given $S_a(T_1)$, the structural response has a certain variability. This means that, assuming as unique uncertainty the β_{RTR} and neglecting others uncertainty sources, the demand variability is represented by the dispersion of the spectra of the set of accelerograms, in the neighbourhood of the $S_a(T_1)$ value. Under these assumptions, the demand can be expressed in probabilistic terms, as follow:

$$D = \eta_{DM|Sa}(x) * \varepsilon \qquad (2.35)$$

where $\eta_{DM|Sa}(x)$ is the variation law of the median demand, conditioned by the variation of the S_a and ε is an aleatory variable, which represents the variation of structural response for a given x. Within this framework, the authors assumed that the ε has a lognormal distribution, with unitary median and dispersion constant and dependent from the demand dispersion. The latter can be expressed as follow:

$$\eta_\varepsilon = e^{median(ln(\varepsilon))} = 1 \qquad (2.36)$$

$$\sigma_{ln(\varepsilon)} = \beta_{DM|Sa} \qquad (2.37)$$

Furthermore, the $\eta_{DM|Sa}(x)$ was defined with a linear relationship on logarithmic plane with the value of IM imposed (x), such as the S_a:

$$\eta_{DM|Sa}(x) = \alpha * x^\beta \qquad (2.38)$$

where α and β are coefficients obtained by linear regression in the logarithmic plane of the median demand value. By substituting eq. 2.38 in 2.35, the result is the well-known power-law approximation (Cornell, 2002):

$$D = \alpha * x^\beta * \varepsilon \qquad (2.39)$$

Based on the above considerations for the demand, the third simplified hypothesis regards the distribution of the structural capacity that is assumed as a lognormal function with median η_C and dispersion β_{RC} (only aleatory uncertainties are considered). The approximate demand and capacity probabilistic models are depicted in figure 2.26. Based on the above-mentioned hypotheses, it is possible to define the drift hazard (λ_{DM}), which is the MAF of exceeding of a given demand conditioned by the IM selected for the building. Knowing that the demand is represented by a lognormal distribution, in

which the parameters median and dispersion have some properties, the λ_{DM} can be expressed as:

$$\lambda_{DM} = \lambda_{Sa} * e^{\frac{k^2}{2b^2}\beta_{DM|Sa}^2} \qquad (2.40)$$

where k is defined in eq. 2.34 and b is the β defined in eq. 2.39. In simple words, the MAF of exceeding a given demand is equal to the seismic hazard evaluated for a certain value of S_a, multiplied for a coefficient that takes into account the dispersion of the demand.
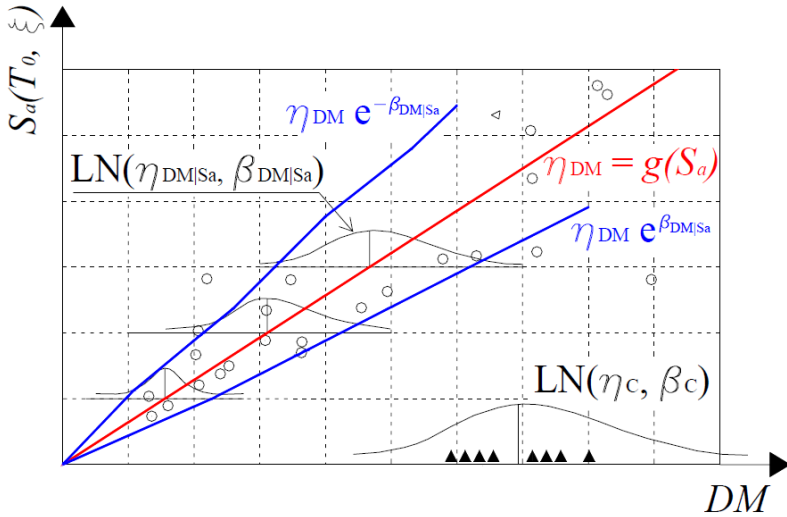
Fig. 2.26 – Approximate demand and capacity probabilistic models (Jalayer and Cornell, 2003)

Hence, the MAF of exceeding a LS, in the hypothesis that the structural capacity has a lognormal distribution, can be written as:

$$\lambda_{LS} = \lambda_{Sa} * e^{\frac{k^2}{2b^2}\beta_{DM|Sa}^2} * e^{\frac{k^2}{2b^2}\beta_{RC}^2} \qquad (2.41)$$

where a coefficient that takes into account the capacity dispersion is included. In order to carry out the assessment of existing buildings in a way feasible for practitioners, the authors have proposed a closed form of eq. 2.41, with the aim to define a performance target: in other words, the building performance is assessed if the MAF of exceeding a certain LS is lower than a fixed value P_0. This means that eq. 2.41 is rewritten as:

$$\lambda_{LS} = \lambda_{Sa} * e^{\frac{k^2}{2b^2}\beta_{DM|Sa}^2} * e^{\frac{k^2}{2b^2}\beta_{RC}^2} \leq P_0 \tag{2.42}$$

Substituting eqs. 2.34 and 2.38 in eq. 2.42, the latter becomes:

$$k_0 * \left(\frac{\eta_c}{\alpha}\right)^{-\frac{k}{b}} * e^{\frac{k^2}{2b^2}\beta_{DM|Sa}^2} * e^{\frac{k^2}{2b^2}\beta_{RC}^2} \leq P_0 \tag{2.43}$$

and pooling η_c, the result is:

$$\eta_c * e^{-\frac{k^2}{2b^2}\beta_{DM|Sa}^2} * e^{-\frac{k^2}{2b^2}\beta_{RC}^2} \geq \alpha \left(\frac{P_0}{k_0}\right)^{-\frac{b}{k}} \tag{2.44}$$

The term at the right member in the eq. 2.44 is proportional to the spectral acceleration and then assumes the meaning of a median value of demand, which corresponds to the IM with a MAF of exceeding of the LS, directly related to P_0. Bringing the terms of the demand's dispersion to the right member of the above equation, the general expression in terms of capacity/demand becomes:

$$\eta_c * e^{-\frac{k^2}{2b^2}\beta_{RC}^2} \geq \eta_{DM|Sa} * e^{\frac{k^2}{2b^2}\beta_{DM|Sa}^2} \tag{2.45}$$

where $\eta_{DM|Sa}$ and $\beta_{DM|Sa}$ must be expressed in function of the requirement P_0. To this aim, eq. 2.45 can be rewritten as:

$$\eta_c * e^{-\frac{k^2}{2b^2}\beta_{RC}^2} \geq \eta_{DM|Sa^{P_0}} * e^{\frac{k^2}{2b^2}\beta_{DM|Sa^{P_0}}^2} \tag{2.46}$$

Factorizing the capacity and the demand through the following equations:

$$\varphi = e^{-\frac{k^2}{2b^2}\beta_{RC}^2} \tag{2.47}$$

$$\gamma = e^{\frac{k^2}{2b^2}\beta_{DM|Sa}^2} \tag{2.48}$$

eq. 2.46 become:

$$\gamma * D^{P_0} \leq C * \varphi \tag{2.49}$$

where C is the median capacity and D is median demand, which takes into account the target P_0.

In order to consider the epistemic uncertainties of the problem, which cannot be avoided, the procedure concludes estimating the confidence interval related to the achievement of the performance required for the LS investigated. With this regard, it is possible to perform some analyses, guaranteeing a certain confidence level. In particular, considering the epistemic uncertainties, eq. 2.41 can be integrated with the terms

β_{UC} and β_{UD}, which are the dispersions due to the epistemic uncertainties, respectively in the capacity and demand. If we call the aleatory uncertainties as β_{RC} and β_{RD} (which before were called as $\beta_{DM|Sa}$) respectively for capacity and demand, eq. 2.41 can be rewritten as:

$$\lambda_{LS}^{*} = \lambda_{Sa} * e^{\frac{k^2}{2b^2}(\beta_{RD}^2+\beta_{UD}^2)} * e^{\frac{k^2}{2b^2}(\beta_{RC}^2+\beta_{UC}^2)} \qquad (2.50)$$

In this view, also the λ_{LS} is a variable, and can be represented by a lognormal distribution with a median λ_{LS}^{*} and a dispersion $\beta_{\lambda LS}$. The first one is defined in the eq. 2.50, while the dispersion is:

$$\beta_{\lambda_{LS}} = \sqrt{\left(\frac{k^2}{b^2}\right) * (\beta_{UD}^2 + \beta_{UC}^2)} \qquad (2.51)$$

The variability of the variable λ_{LS} can be associated to a confidence interval around the λ_{LS}^{*}, which can be defined as:

$$\lambda_{LS}^{X} = \lambda_{LS}^{*} * e^{K_x * \beta_{\lambda_{LS}}} \qquad (2.52)$$

where λ_{LS}^{X} is the MAF of exceeding a given LS and associated to a confidence level, K_x is the normal standard variable with probability x of not being exceeded. Through some mathematical manipulations of the above-written equations, λ_{LS}^{X} is obtained according to the following equation:

$$\lambda_{LS}^{X} = \lambda_{Sa} * e^{\frac{k^2}{2b^2}(\beta_{RD}^2+\beta_{UD}^2)} * e^{K_x * \beta_{\lambda_{LS}}} \qquad (2.53)$$

Eq. 2.53 is similar to eq. 2.41 and, in terms of demand capacity factor design, the MAF of exceeding a given LS associated to a confidence level should be compared with a value P_0:

$$\lambda_{LS}^{X} \le P_0 \qquad (2.54)$$

Following a similar procedure, including the factorization of capacity and demand, which this time considers aleatory and epistemic uncertainties (γ_{TOT} and φ_{TOT}, which are the product of epistemic and aleatory dispersion for demand and capacity), it is possible to define a "confidence factor" (which is from the one defined in the approach of EC8) called λ_X and defined as:

$$\lambda_X = e^{-\beta_{TOT}\left(K_X - \frac{k}{2b}\beta_{TOT}\right)} \qquad (2.55)$$

where β_{TOT}, just defined in eq. 2.28, takes into account all uncertainties.

The admissible condition, analogues to eq. 2.49 can be defined as:

$$\lambda_X \geq \frac{\eta_{DM|Sa^{P_0}}\gamma_{TOT}}{\eta_C\varphi_{TOT}} \tag{2.56}$$

By using eq. 2.56, it is possible to check that the ratio between the factorized demand and capacity is lower than a given confidence factor, which is function of the desired confidence level (CL). In this way, the fractiles of the MAF for satisfying the target performance, dependent from the given LS, are defined. To this purpose, FEMA code suggests adopting a high CL, such as 90-95%. With lower CLs, analyses show that the building could not satisfy the target performance. The main advantage of this approach, besides to be practitioner-friendly, is that it allows to perform a low number of NLD analyses with a seismic input related to the seismic hazard of the site. With this regard, the authors of the method assumed as P_0 value the mutual value of the return period (T_r), for each LS to assess.

2.4.3 On the side of practitioners: comparison between the two approaches

The approaches for performing the vulnerability assessment of existing RC buildings described in the previous section are characterized by some advantages and limitations, especially for the practitioners. As already specified, the deterministic approach is ruled by EC8 code, while the deterministic approach, with the related simplifications, is ruled in FEMA guidelines. Starting from the names attributed to the approaches, it is easy to understand that the first approach is developed in deterministic terms, while the second one is proposed as an improvement of the previous based on the probabilistic nature of the problem and driven by the limitations pointed out by some practical applications and research works about the topic.

The deterministic approach does not provide the actual safety level of the structure expressed in terms of probability of exceedance for a given LS. In fact, only the seismic hazard is defined in probabilistic terms, associating a fixed level of probability of exceeding to the seismic intensity, whereas the other sources of uncertainty, such as the aleatory ones that strongly affect the demand, are neglected. In addition, many

other input parameters are a source of uncertainty, but their management is usually demanded to the personal experience of the practitioner, as summarized below:

- Rational and univocal choice of a criterion for identifying the LS thresholds, especially in the case of ultimate LS, for which the global damage can be very different for each case study;
- Incomplete knowledge about those parts of the structure that cannot be completely analysed through in-situ investigation;
- Choice of the modelling criteria and methods of analysis;
- Definition of the capacity models for the structural elements.

Concerning the criteria for defining the LS thresholds, the code suggests an θ_i equal to 0.5% for the DLS. The code does not provide indications for the ultimate LS, instead, different damage levels can be assumed for the same building, for the same LS. Just to make an example, for defining the LSLS of a building, all the following criteria can be adopted, and none of them is rebuttable:

- First structural element reaches a chord rotation equal to ¾ θ_u;
- First column reaches a chord rotation equal to ¾ θ_u;
- A certain percentage of structural element reach a chord rotation equal to ¾ θ_u;
- Point of pushover curve at 85% of the maximum V_b (15% of softening);
- Point of pushover curve at 80% of the maximum V_b (20% of softening);

A lot of uncertainty sources arise during the knowledge path of the existing structure, since in many cases the original documentation of the building is incomplete. The mechanical and geometrical characterization of the structural elements is a crucial part of this phase, considering that it is impossible to systematically investigate all building's parts. Clearly, an incorrect evaluation of in-situ materials can significantly affect the results. The scientific literature about this topic is extensive, as discussed in some works (Uva et al., 2013, Fiore et al., 2013) that have analysed and evaluated the sensitivity of the results obtained by in-situ investigation on real RC structures, through

DTs and NDTs. As previously mentioned, the EC8 approach tries to incorporate these epistemic uncertainties in the CF, relating it to the amount of information collected (table 2.3 and 2.4). About this topic, some researchers (Franchin et al., 2010, Jalayer et al. 2010) have demonstrated that the use of partial factors on the structural capacity in existing buildings can provide subjective results on the same case study. Firstly, on a same building, in-situ tests can be subjectively performed on different structural elements, introducing epistemic uncertainties about the structural detailing and concrete and steel mean strengths. In addition, the use of a fixed partial factor, whose value has been calibrated on a set of numerical investigation, could not be suitable for all existing structures and could be inaccurate with respect to the continuous variation of the mechanical properties of materials (strength/stiffness deterioration). Additional uncertainties sources are related to the modelling method adopted by the analyst, which can use a fiber or a plastic hinges model and can consider or not the contribution of non-structural elements and secondary elements or can select different types of hysteretic behaviour. In addition, the results are strictly depended from the analysis method, such as the choice of NLS or NLD analysis, with particular reference to the seismic input and dynamic properties of the numerical model. A rational assessment procedure of existing buildings should account for all the mentioned uncertainties and, at the same time, incorporate all factors, which are in play in the path for computing the safety level.

Differently from a deterministic approach, which is strongly based on the "expert opinion" of the analyst in each phase, the PBEE approach has many advantages and provides numeric outputs based on the hazard level adopted, in terms of fragility and expected losses that are very useful in practical applications. On the other hand, the application PBEE presents several difficulties for practitioners (Gunay and Mosalam, 2013), mainly caused by the probabilistic nature of the approach and the necessity of developing several analysis phases.

A first problem is the choice of a set of accelerograms composed by a sufficient number of records, in order to be representative of the real seismic hazard from a probabilistic point of view. There is not a simple and univocal rule for driving practitioners in this choice. In the last few years, some research works have focused this problem,

developing tools for selecting the signals consistently with the code spectrum (Iervolino et al. 2009) or with the conditional mean spectrum (Baker, 2011). Difficulties grow when real accelerograms suitable for the case study are not available and it is necessary to perform a preliminary selection and a subsequent scaling, using a certain value of IM (Iervolino and Cornell, 2005, Bayer and Bommer, 2007, Hancock et al., 2008).

Regarding the phase of structural analysis, the main problem is due to the limited time usually available by practitioners. This induces to reduce as much as possible the efforts for performing NL analyses on the numerical model. The most popular commercial software used for structural analysis focus on the availability of attractive and friendly graphical user interfaces but are not optimized and effective for NL analyses, even static ones, in which they result to be time-consuming and require a lot of storage memory. Within these computer environments, performing IDA or MSA on a numerical NL model for a lot of records becomes a true nightmare. Clearly, things can only get worse when PBEE methodology is to be applied, since it is necessary to fix an EDP value for each LS to investigate. The a-priori knowledge of these threshold values, especially for the ultimate LSs, typically requires a preliminary NLS analysis that provides the global collapse of the structural system. Further considerations can be provided, thinking that in deterministic and probabilistic approaches, the fixed value of T_r for a LS come from seismic hazard studies, based on social-economic evaluations, while different meaning has a collapse probability of a structure that takes into account the probabilistic distribution of demand and capacity. In addition, the LSs should be most differentiated, considering that structural elements do not assume the same importance in the evaluation of safety level of a structure.

3. Seismic modelling of existing RC buildings

3.1 Overview

In the vulnerability assessment of existing RC buildings, the modelling phase assumes a key role in the evaluation of the structural behaviour. In particular, based on the kind and the features that characterize the FE model, the analyst is able to predict with more or less accurateness the structural response of structure, under vertical and seismic loads. Once that the building features are known, in terms of knowledge of geometrical and mechanical parameters, the use of practitioners is to make just one FE model in an user-friendly software, with the claim of capturing the linear and NL structural behaviour, from both global and local mechanisms points of view. This trend is clearly wrong for several reasons. For example, to consider or not the non-structural elements, such as the infill panels, can strongly change the dynamic behaviour shown by the FE model, in terms of periods and participating mass (M[%]) and consequently, the results of simple pushover analysis can be very different. Furthermore, the assumptions at the base of the numerical model, usually based on the experience and sensibility of the analyst, can produce subjective results, which can be different in the modelling of the same case study, performed by different practitioners. Finally, also the modelling typology used influences the result, such as the adoption of certain numerical elements, numerical integration laws, capacity models for the NL behaviour and so on. Generally, the scientific literature shows that, for investigating the structural behaviour, one should adopt several FE models with different features for the same case. In this view, the result provided by each numerical model should highlight the weight of each single aspect investigated. This confirm the philosophy at the base of engineering problems, where on the same numerical model, one has to change one variable per time. In this Chapter, the author is going to investigate the global behaviour of existing RC buildings, considering in the modelling the influence of some elements usually neglected or subjected to numerical hypotheses, which constitutes the structural system. In particular, the focus is on secondary elements, as the slab and non-structural elements, as the infill panels. After a briefly description of the scientific literature about the modelling of principal, secondary and non-structural elements, a numerical procedure

is proposed, able to simulate the floor system behaviour in existing RC buildings under horizontal actions, with its in-plan deformability and comparable with other methods proposed by scientific literature (Porco et al., 2017 and Ruggieri et al, 2018a). Subsequently, with the aim to consider the influence of the modelling elements involved in the FE model of the building investigated, the global behaviour of some case studies is analysed, in which both floor system and infill panels are modelled. Finally, in a perspective of retrofit solutions, the influence on the global structural behaviour of reinforced infill panels and added RC walls is evaluated (Ruggieri et al., 2017 and Ruggieri et al., 2018b).

3.2 Nonlinear models for structural materials and elements

Before speaking about the modelling of RC structural elements, one should know the properties of the concrete and the steel. The importance of this topic has been evident since the first studies about the RC structures, where some researchers tried to define specific relationships for characterizing firstly the linear and NL behaviours of concrete and steel and after, a unique behaviour for simulating the mix of them. The trend was of loading specimens of both materials considered (compression for concrete and tension for steel) and, based on the results obtained, to define empirical stress-strain relationship. As well-know, after a certain loading (monotonic or cyclic), the concrete exhibited a post-elastic behaviour with softening and brittle collapse, while the steel exhibited a post-elastic behaviour with hardening and ductile collapse. The scientific literature about the topic is extensive and the author is going to report just the most significant works. Concerning to the concrete, the first tests campaigns were described in (Hognestad et al., 1955, Sturman et al., 1965), where the stresses distribution of section subjected to axial and bending force were identified, concluding that the first cracking of concrete is delayed when the above stresses are coupled. In (Popovics, 1970) after an extensive comparison among experimental tests, authors provided a constitutive law influenced by the load ratio, number of cycles and magnitude of the stress. In (Kent and Park, 1971) a couple of constitutive laws were proposed, considering and not the confinement (modified Kent and Park constitutive law). This latter study was fundamental for the development of the stress-block law. The most used

constitutive law for concrete is the one proposed by Mander (Mander et al., 1988), as shown in figure 3.1, which provides formulations that account for the effects of the axial and bending loads, with and without confinement and considering other micro-mechanics effects studied until this work. Generally, the experimental tests about concrete need of interpretation, due to the strongly dependence from the size of the specimens and the boundary conditions of tests. With this regard, the parameters that should drive the researchers are the total cracking energy or the cracking energy post-peak.
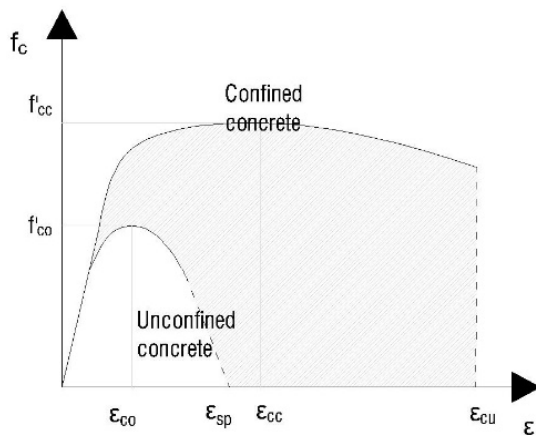
Fig. 3.1 – Constitutive law proposed by Mander

Regarding to the steel used in RC elements, the nature of the material, which is isotropic, allow of predicting the linear, NL and cyclic behaviour through experimental, which provide results with lower dispersion. In fact, in a lot of works (Aktan et al., 1973, Kent and Park, 1973) the backbone of the stress-strain law is composed by four parts, as an elastic region, a yielding plateau, a strain hardening region and a final strain softening part. Some researchers proposed simplified constitutive laws for the steel. The most used constitutive law is the one proposed in (Menegotto and Pinto, 1973), as shown in figure 3.2, with the proposal of a cyclic law, which took into account the well-known Bauschinger phenomenon, useful for describing the cyclic behaviour. Other important law is the one proposed in (King et al., 1988), where the authors well captured

the first three parts of the generic constitutive law and proposed limits for the strain, based on tests about cycle fatigue loads. The technical codes assume the constitutive laws proposed in the scientific literature and provide to practitioners simplified diagrams. For example, EC8, like NTC08, proposed 3 simplified models for the concrete, such as the stress-block, parabola-rectangle or bi-linear (figure 3.3) and 2 simplified models for the steel, such as the elasto-plastic perfect and elasto-plastic with strain hardening (figure 3.4).
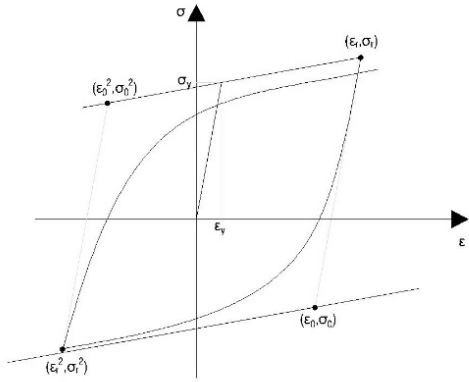
Fig. 3.2 – Constitutive law and cyclic behaviour proposed by Mengotto-Pinto
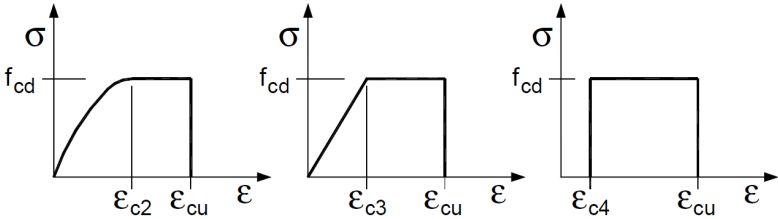
Fig. 3.3 – Simplified constitutive laws for concrete (NTC08)
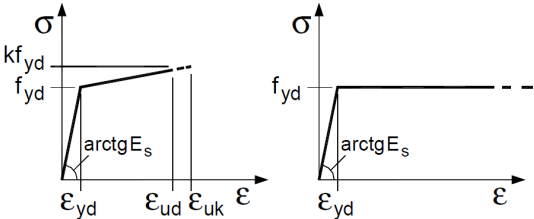
Fig. 3.4 – Simplified constitutive laws for steel (NTC08)

In this specific case, the code provides the way for computing each parameter shown in figures 3.3 and 3.4, with fixed values for the strains and formulations for evaluating the stresses, based on the values of design yielding cylindrical strength of steel (f_{yd}) and design ultimate cylindrical strength of concrete (f_{cd}), in the cases of new buildings.

The inhomogeneity of the RC and the assumptions about the materials in RC sections, lead to match the 2 behaviours, with mutual interaction of concrete and steel. With this regard, making some simplified hypotheses, such as the plan section conservation, the perfect bond between steel and concrete and the neglect of the tensile in the concrete, it is possible to define NL capacity model of RC sections. This latter computation is strictly related to the failure mechanisms of accounting in the model. For the structural elements as beams and columns, it is necessary to consider both flexural and the shear behaviours, which are defined based on the acting loads. Regarding to the flexure behaviour, literature and codes provide several representations, in terms of moment-curvature or moment-rotation (curvature is the rotation per unit length). Therefore, the rotation of a section can be calculated by integrating the curvatures along a certain length, computable with sectional equilibrium and congruence equations (more details are provided in the next Section). Concerning to the shear behaviour, some information about the shear strength have just been provided in the Chapter 2. Here, it is more interesting the interaction with the flexural behaviour. In fact, based on the geometry of the section, this latter can be limited by shear failure and overall, its cyclic degradation property. Figure 3.5 shows three possible behaviours of RC elements, considering flexural and shear failures. In the first case, the shear capacity, also with degradation, is higher than the flexural capacity. This means that the sections has a ductile behaviour and high capacity, which can manifests problems only in the cases in which some phenomena happen, such as the buckling or cover spalling. In the second case, the failure is coupled, because the element reach the yielding, but in the post-elastic part, the shear failure occur with degradation and loss of capacity. In the third case, the

shear failure occur in the elastic part of the element and the strength is strongly compromised. In the cases in which the axial loads are considered, as in the columns, the above classification is strongly influenced, considering the role of axial force in the definition of the moment-curvature law (depends form the moment-axial load diagram) and of the shear capacity.
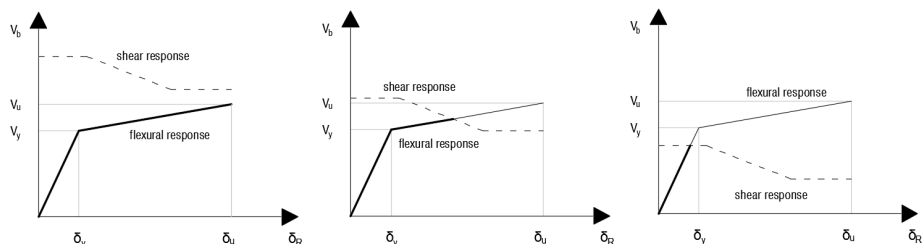
Fig. 3.5 – Collapse mechanisms of RC elements, accounting for flexural, shear-flexure and shear behaviours

Lastly, for completing the characterization of RC structures and their elements, besides to define the behaviour through a backbone, it is worth mentioning the hysteresis response that the members shown under cyclic loading. Generally, the NL behaviour of RC structures depends from the capacity to dissipate energy under strong-motions. A lot of researchers defined rules for computing the hysteresis models of RC members, as the kinematic, the Takeda (Takeda et al., 1970) or the Pivot (Dowell et al., 1998) models, with the aim of representing some phenomena, such as reloading, degradation, pinching and so on. For the technical codes, the hysteresis phenomenon is characterized by the viscous damping (really it is hysteretic), which has a value of 5% for RC buildings. Clearly, this value cannot represent the energy dissipated from all vibration modes and, for this reason, the best way for accounting an acceptable estimation of the hysteretic behaviour is the Rayleigh damping method (Chopra, 2012). It consists in the computation of the damping matrix from a linear combination of mass and stiffness matrices, through the adding of two coefficients, such as shown in figure 3.6. Basing on the frequency of each vibration mode, the method allow of computing the damping value.
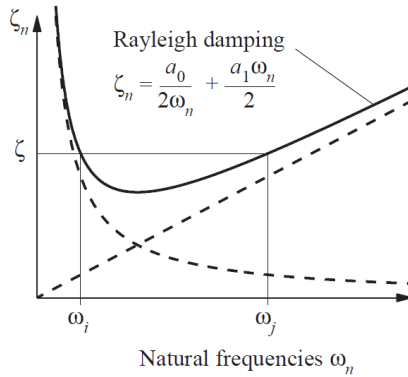
Fig. 3.6 – Rayleigh damping model (Chopra, 2012)

3.3 Nonlinear computational approaches

A numerical model that simulates the real behaviour of existing RC buildings is constituted by numerical elements that accounts the mechanical and geometrical parameters found in the knowledge path of the structure. In particular, the structural elements should exhibit their linear and NL behaviour in a seismic analysis, in order to predict both local and global behaviour of the building investigated. To this scope, RC beams and columns, which constitute the skeleton of the building, are usually modelled trough frame elements. Numerically, a frame is a three-dimensional (3D) element, which defines equilibrium, congruence and constitutive law equations between two consecutive nodes. Regarding to the linear properties of beams and columns, the numerical model should accounts the mass and the stiffness of the elements, which depend from the elastic properties of the materials constituent, such as the self-weight, the density, the elastic modulus, the dimension of the element section and so on. For defining the real behaviour of RC elements, it is necessary to simulate the NL behaviour of the elements. To this scope, the numerical model should account for the flexural and shear behaviour. Before explaining how to consider the nonlinearity in the RC elements, it is worth remembering that a numerical model, which simulate the behaviour of a building under seismic actions, manifests the first plastic deformations in the ends of the elements, near to the interface with the beam-column joint. This is due to the stress distribution of seismically-dominated frames. On the other hand, one can model the

nonlinearity of all the infinite sections that constitute an RC element, with the conse-
quence of improving the quality of the results but increasing the time and computational
efforts of the subsequent seismic analysis. This latter sentence, introduce the possibil-
ity that one has for modelling the nonlinearity of structural elements. Regarding to the
flexural behaviour, the plasticity can be modelled along the member or in the more
stressed sections, in the ways shown in figure 3.7.

| Finite element | Fiber sections | Finite lenght plastic hinge | Nonlinear spring hinge | Plastic hinge |
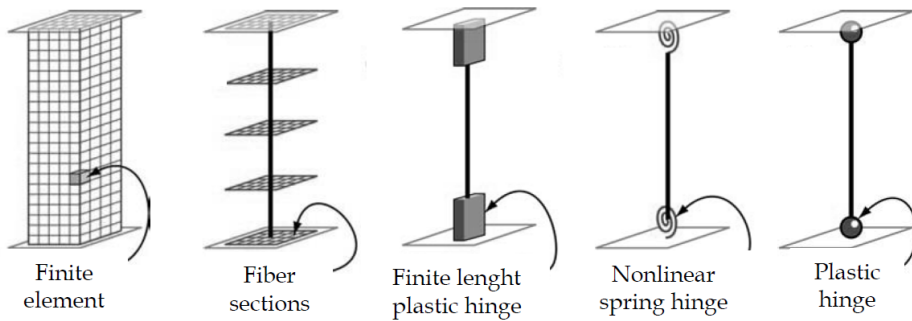
Fig. 3.7 – Modelling typologies for flexural behaviour, as provided in (Deierlein, 2010)

The most complex model is the one discretized in FEs, along its entire length.
Each FE takes into account the linear and NL properties of the material that simulates,
ensuring the balancing from the equilibrium, the congruence and the constitutive law
equations points of view. This kind of model is surely the most expansive, in terms of
time and computational efforts, but can provide a real simulation of the members, being
able to predict whatever effect. The second model is composed by fiber sections, which
provide a discretization of the RC member in significant sections, modelled on fibres.
To each fiber, a constitutive law is assigned, in order to simulate the NL behaviour of
materials. Numerically, all fibres should be integrated over the section, in order to obtain
the resultant, in terms of force and displacement. This kind of model is able to provide
stress and strain of each fiber, but is more sensitive to the element length, integration
method and constitutive laws assigned. The third model is a finite length hinge one,
which consider the plasticity concentrated in the end-sections of elements, through a
hinge zone with fixed length. The sections of the hinge zones are usually modelled
trough fibres, defined as abovementioned. This kind of model is strongly dependent

from the hinge zone length. The main advantage is the capacity to predict in realistic way the yielding and ultimate behaviour of the element, with information about the hinge rotation. The simplest models are the ones to concentrated plasticity, through the adoption of plastic hinges (in the fourth case it is used an inelastic spring), which are located in a section and they are defined through a moment-rotation model. As mentioned, this is strictly related to the plastic hinge length because the integration of the curvature is performed proper along this latter. For the models with fibres, the modelling is able to account directly some phenomena, such as the interaction between axial and moment forces, the strength degradation due to the buckling and interaction with shear behaviour. On the other hands, lumped plasticity models, besides to be more functional from the computational efforts point of view, included the above phenomena in a unique moment rotation-law, usually based on empirical experiences. In this case, one should determine the shape of the backbone, in terms of stress-strain, to whom assign the cyclic behaviour. The simplest moment-curvature representation is the bilinear one, which is characterized by yielding (M_y, Φ_y) and ultimate (M_u, Φ_u) points. Subsequently, the number of points can be increased, for accounting the results of experimental tests and some effects, such as the P-Δ effects, the confinement, the interaction between axial and bending forces and so on. Very used constitutive law for RC section is the a quadrilinear moment-curvature (or rotation) one, which represents the element behaviour with 4 damage levels: first cracking of concrete, yielding of longitudinal bars with hardening behaviour, softening simulating the strength degradation of the section and the residual moment, fixed at a certain percentage of the yielding moment. This kind of constitutive law is like the one adopted by FEMA-356 code, as shown in figure 3.8
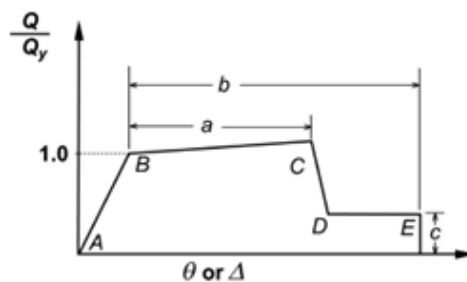
Fig. 3.8 – Constitutive law for plastic hinges, proposed in FEMA-356 code

Regarding the definition of the points of the backbone, a lot of researchers and technical codes proposed some empirical formulation for defining the values of moment-curvature relationship. EC8, such as the NTC08, proposed the following formulations for computing the chord rotation demand, in terms of yielding and ultimate rotation (θ_y and θ_u):

$$\theta_y = \frac{\Phi_y L_V}{3} + 0.0013\left(1 + 1.5\frac{h}{L_V}\right) + \frac{\Phi_y d_{bL} f_y}{8\sqrt{f_c}} \tag{3.1}$$

$$\theta_u = \frac{1}{\gamma_{el}} 0.016(0.30^\nu)\left[\frac{\max(0.01; \omega')}{\max(0.01; \omega)} f_c\right]^{0.225}\left(\frac{L_V}{h}\right)^{0.35} 25^{\left(\alpha\rho_{sx}\frac{f_{yw}}{f_c}\right)}(1.25^{100\rho_d}) \tag{3.2}$$

where Φ_y is the yielding curvature, L_v is the shear span, as defined in eq. 2.15, h is the height of the cross section, d_{bL} is the median diameter of longitudinal reinforcement, f_c and f_y are cylindrical compressive strength of the concrete and yielding strength of the steel reinforcement, γ_{el} is a coefficient equal to 1.5 for primary elements and 1.0 for secondary ones, ω and ω' are the mechanical ratio of tensile and compressive longitudinal reinforcement, ρ_{sx} is the ratio of transversal reinforcement in the load direction, f_{yw} is the cylindrical yielding strength of the transverse steel reinforcement, ρ_d is the ratio of diagonal reinforcement in each direction of load and α is the confinement efficacy coefficient. Alternatively, the θ_u can be computed using the following equations:

$$\theta_u = \frac{1}{\gamma_{el}} 0.0145(0.25^\nu)\left[\frac{\max(0.01; \omega')}{\max(0.01; \omega)} f_c\right]^{0.3} f_c^{0.2}\left(\frac{L_V}{h}\right)^{0.35} 25^{\left(\alpha\rho_{sx}\frac{f_{yw}}{f_c}\right)}(1.275^{100\rho_d}) \tag{3.3}$$

$$\theta_u = \frac{1}{\gamma_{el}}\left(\theta_y + (\Phi_u - \Phi_y)L_{pl}\left(1 - \frac{0.5L_{pl}}{L_V}\right)\right) \tag{3.4}$$

where the curvature Φ_y and Φ_y are involved and L_{pl} is the plastic hinge length, evaluated as follow:

$$L_{pl} = 0.1L_V + 0.17h + 0.24\frac{d_{bl}f_y}{\sqrt{f_c}} \tag{3.5}$$

while, for accounting also the cyclic behaviour, the L_{pl} can be computed as below reported:

$$L_{pl} = \frac{L_V}{30} + 0.2h + 0.11 \frac{d_{bl}f_y}{\sqrt{f_c}} \tag{3.6}$$

The scientific literature provides other semi-empirical methodologies for computing the θ_u and L_{pl}, as reported in (Verderame et al., 2010), in which the focus was the correction factor of applying, due to the presence of plain bars in existing RC structural elements. Regarding the θ_u, the formulations proposed in the EC8 are similar to the ones proposed in (Panagiotakos and Fardis, 2001), where an experimental tests campaign was conducted and an extensive database was produced. Subsequently, the same authors (Fardis, 2007) proposed an improvement of the previous formulation of θ_u, inserting the influence of the cross section height. Other formulation was proposed in (Rossetto, 2002, Haselton and Deierlain, 2007, Zhu et al., 2007). Comparable with the results obtained from the EC8 formulation is the one proposed by (Perus et al., 2006), where the authors proposed a method for predicting the chord demand rotation, through a multi-dimensional non-parametric regression (CAE method). Regarding to the L_{pl}, the scientific literature provides formulations based on the concept that this parameter should account the sum of three mechanisms, as the flexural, the shear and the slippage behaviours, as below reported:

$$L_{pl} = L_{pl,flex} + L_{pl,shear} + L_{pl,slip} \tag{3.7}$$

Besides the Fardis experiences, the most important formulation are the ones proposed by (Park et al., 1982) where $L_{pl} = 0.4h$, (Priestley and Park, 1987) where $L_{pl} = 0.08L_V + 6d_{bL}$ and (Paulay and Priestley, 1992) where $L_{pl} = 0.08L_V + 0.022d_{bL}f_y$.

Regarding the modelling of the shear behaviour, the most feasible way is represented from the assessment of maximum shear strength condition (as computable by using eqs. 2.3 and 2.6), especially evaluated in post-processing. This latter, which makes sense for buildings designed through capacity design philosophy, can be not adequate in the cases of existing buildings. This is due to the strongly interaction with flexural behaviour and axial loads. Generally, for accounting the shear behaviour, it is necessary to add in the numerical model an additional element. To this scope, the scientific literature proposed some numerical methods, which generally consists in the introduction of NL shear springs, disposed in series with the flexural ones, as shown in

figure 3.9. Generally, to the shear spring, a multilinear constitutive law is assigned, taking into account shear strength degradation and cyclic behaviour.
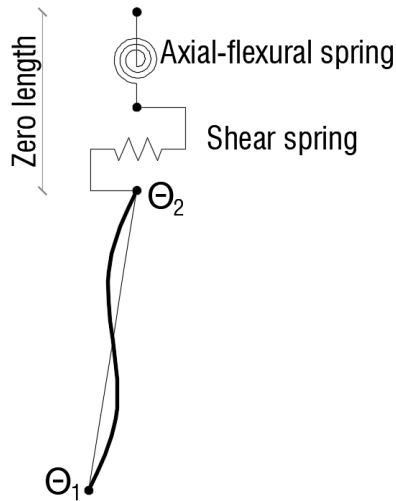
Fig. 3.9 – Modelling of the NL shear spring, in series with the axial-flexure one

For computing the parameters of the shear backbone, some authors adopted the well-known modified compression field theory (Vecchio and Collins, 1986). In particular, in (Pincheira et al., 1999) a model was proposed, able to simulate the monotonic and cyclic response, in which the authors accounted the degradation, in terms of strength and stiffness and they evaluated the increment of deformation demand. In (Lee and Elnashai, 2001), authors used the modified compression field theory for developing a hysteretic rule, accounting the axial load variation. In (Sezen and Chowdhury, 2009) the authors proposed a hysteretic rule, adding the bond-slip effect to the shear behaviour. Some authors developed shear strength models, based on empirical data. In (Pujol et al., 1999) a drift-capacity model was proposed for RC columns with high transverse reinforcement. In (Elwood, 2004), a model called "limit state material" was proposed. The model had a trilinear backbone constituted by some parameters for defining pinching and stiffness degradation (figure 3.10). In (Elwood and Mohele, 2005) an empirical drift capacity model was proposed, based on a database made by tests on existing RC elements. In (LeBorgne and Ghannoum, 2014), the model of Elwood was improved,

with the development of an algorithm able to estimate the shear degradation of RC elements, upgrading for each analysis step, the real state in terms of shear and flexural capacity.
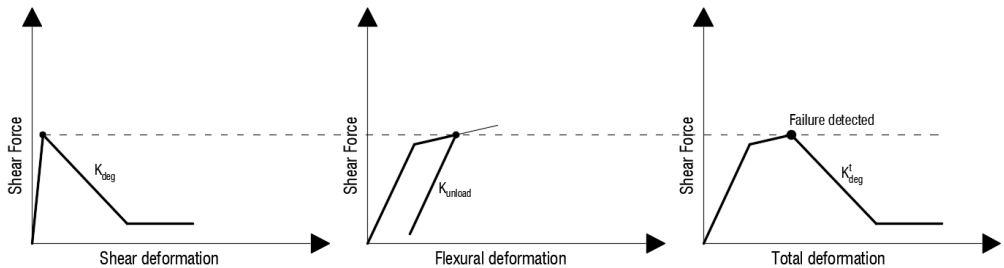
Fig. 3.10 – "Limit state material" model proposed by (Elwood, 2004)

In addition, in the assessment of existing RC buildings designed through old codes, particular importance assumes the beam-column joints modelling, which are usually the first element subjected to failure (brittle behaviour) under seismic events. The modelling of beam-column joints, should take into account the capacity of predicting the shear strain, due to the leakage of shear reinforcement and the rotation of the end sections of the convergent RC elements, due to the slippage of the longitudinal bars. Figure 3.11 shows some models proposed in the scientific literature.
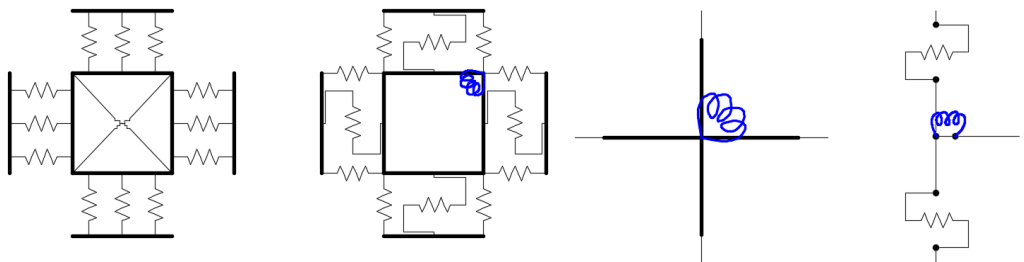
Fig. 3.11 – Modelling typologies for beam-column joints NL behaviour

The first model concerns to the multi-spring modelling approach, where the joint panel was linked to the beams and columns, through one or more springs, which accounted the NL behaviours to consider. It is the case shown in (Youssef and

Ghobarah, 2001), where the joint panel were modelled through four rigid elements enclosing the joint core, linked to the structural elements through NL springs. Each one was made, accounting for one particular behaviour. The second model was a macro-model, as suggested in (Lowes and Altoontash, 2003), where the joint panel were modelled through four rigid elements enclosing the joint core, a single rotational spring for accounting the shear behaviour and some springs linked with beams and columns, for simulating each effect to account for. It is worth mentioning that the above methods well estimate the realistic behaviour of the joints, but reach great computational efforts and time analysis. The third model was proposed in (Alath and Kunnat, 1995), which is called "scissor model", composed by a NL rotational spring, rigid linked between the beam and columns convergent in the joint. It is very simple to implement and in fact, it was adopted in other scientific works (Pampanin et al., 2003, Celik and Ellingwood, 2008). In (Park and Mosalam, 2013) the same model was adopted, including the shear deformability of the joint panel and bond slip of the beam. The last model is the one proposed in (Sharma et al., 2011), where the joint core was modelled through shear springs in the end parts of the column and a flexural spring in the end parts of beams. These latter two methods are not able to predict the kinematic of the joint panel, but they are computationally simple and able to predict the response observed in a lot of experimental campaigns. Regarding to the methods used for computing the shear and flexural capacity of the beam-column joints, the scientific literature provides several analytical methods, summarizable as modified compression field theory, strut and tie based model, semi-empirical approaches, and principal tensile stress based models (see chapter 2). The use of modified compression field theory (Vecchio and Collins, 1986), was adopted in few works, because it underestimated the shear strength in low-reinforced joints (Shin and LaFave 2004). Same consideration was observed about the strut and tie model that, despite gave good results for new design, it was characterized by conceptual limitations in the shear analysis of RC beam-column joints, because provided an estimation in terms of localized brittle failures (Park and Mosalam, 2012). Many formulations were developed through semi-empirical approaches, which were

based on statistical analyses. In (Kim and LaFave, 2007) a database of RC joint specimens were investigated, and the authors found that the shear behaviour changed from the kind of joint (interior, exterior, tee, knee). Based on the previous database, in (Kim et al., 2007) a sensitivity analysis was presented, in which the influence of some parameters were assessed, such as dimensions of beams and columns, geometry, mechanical parameters and amount of longitudinal and transversal reinforcement. In (Celik and Ellingwood, 2008) an evaluation of the maximum joint shear strength was performed, through some experimental tests, with the aim to correct the formulation proposed by the ASCE-SEI code. The same authors developed a capacity curve based on statistical evaluation, which depended from four parameters, as joint shear cracking, reinforcement yielding, beam and column capacity and residual joint strength. In (Hassan, 2011), author proposed an empirical model for considering the influence of the axial load in the failure. Furthermore, it was proposed a model for accounting the possibility to have a pull-out failure, due to short anchorage length of the longitudinal bars. Concerning to the principal stresses based model, the first approach was the one in (Paulay and Priestley, 1992), which proposed a formulation for determining the shear failure of unconfined joints, through the application of the above method. Subsequently, as just wrote in the Chapter 2, the method was adopted in some works (Priestley, 1997, Pampanin et al., 2003, Pampanin et al., 2002), where the value of the principal tensile stresses of the joint was suggested to be the 42% of the square root of the f_c. Important indications were provided about the capacity of the joints, provided for typology (figure 3.12). In (Park and Mosalam, 2012) the effects of the joint aspect ratio, longitudinal reinforcement of the beam and axial load on the column were investigated and the same authors proposed an approach for evaluating the shear strength and degradation effect, taking into account the beam yielding. In subsequent work (Park and Mosalam, 2013) the authors developed a multilinear capacity curve, dependent from the shear strain of the nodal panel and slip rotation at the interface with the beam.
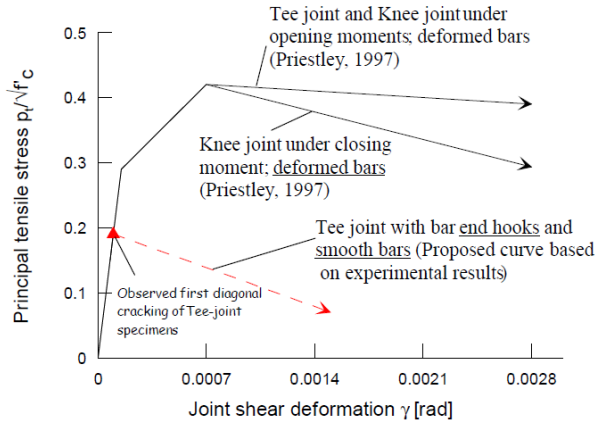
Fig. 3.12 – Capacity curves with strength degradation for exterior joints (Pampanin et al., 2003)

3.4 Floor systems: behaviour under seismic actions

As easily observable in RC new and existing, the structural elements described in the previous sections represent only the skeleton of the structural system. The structural behaviour depends from other components and a particular focus should be aimed on the secondary element, such as the slab. Herein, the complex constituted by the slabs and the beams, which compose the horizontal system of each floor, is called "floor system". In the evaluation of the performance of existing RC buildings, the floor system play a fundamental role for manifold reasons. First of all, the slab is a bi-dimensional system, orthogonally loaded from the gravity and vertical actions, such as permanent and live ones. Hence, the primary role of the slab is to transmit the vertical action to the beams and subsequently to columns and foundation. To this scope, the slab is usually designed aside to the structural elements, accounting the maximum effects provided by the vertical loads, combined as suggested from national and international technical codes. Related to this practical use, one should account for the possibility to have an excessive out of plane deformability of the slab, mainly due to the consideration of lower loads in the design, far from the actual prescriptions and, in some cases, mistakes in the design and the cast in place. Furthermore, from the seismic loads point of view, the role of the slab is to subdivide the horizontal actions among the vertical elements, proportionally to them stiffness. Generally, one can say that this

84

latter condition is possible if the slab, or rather the floor system, is infinitely rigid. It is worth noting that the above condition is not sufficient for defining a real stiffness condition. For this reason, the floor system is able to accomplish its function of transferring loads, if the in-plan deformability of the floor system is strongly lower than the one shown by the vertical elements. In other words, the rigid floor assumption can be assumed based on the comparison of the in-plan stiffness of the floor system with the shear and flexural stiffness of the vertical elements. Besides to the stiffness and deformability conditions, of elements, in the skill of transmitting the vertical and horizontal actions, a fundamental role assume the connection among the slab and the surrounding beams, in order to consider a unique floor system. A not perfect connection among the above elements provides a loss in the action transfer, with subsequent occurrence of local failures in the slab. For some kinds of slab, the connection problems regard the slab and columns, with the occurrence of shear failures as punching. A lot of researchers studied the problems about the connections among slab, beams and columns, developing numerical models based on experimental tests. In this section, the author is not going to speak about the connection problems, but the focus is on the global seismic response of existing RC buildings. To this scope, the first step is the identification of the slab typologies in the existing RC buildings. With this regard, the first distinction can be among the materials that constitute the slab systems. Broadly, the materials used in the slab can be steel, timber, RC and hallow clay blocks. In existing RC buildings, especially in the Italian cases, slab made with steel and timber are not present, considering that they are usually adopted as retrofit solutions or for reducing the self-weight in the over-elevation cases. The most adopted solutions are shown in figure 3.13. The first case is a ribbed slab with RC joists (cast in place or precast) alternate with hallow clay blocks (also called lightening blocks). Over these elements, there is a RC plate, herein called "top concrete slab", reinforced with a grid of longitudinal bars. The second case is constituted by hallow clay blocks, reinforced through longitudinal bars and linked among them through mortar composed by concrete and sand. From the mechanical point of view, these typologies of slab are classifiable as orthotropic

plate, which are three-dimensional body, constituted by a certain thickness (one dimension is smaller than other two ones), with a different behaviour in the two main horizontal directions.
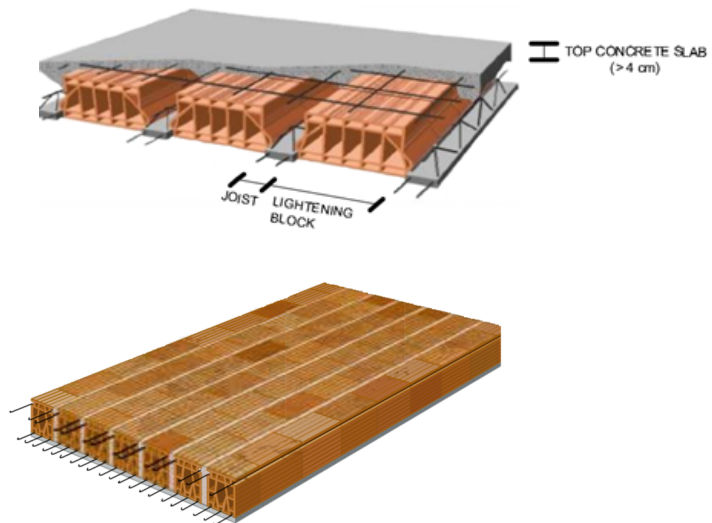
Fig. 3.13 – Typologies of slab present in Italian existing RC buildings

This means that, considering the in-plan behaviour, the elastic and tangential moduli of the plate are different in the two main directions and, subsequently, the shear and flexural stiffness have different value in the two direction. For some technical codes, this latter property is considered fundamental for defining the slab as rigid. In fact, based on the construction details of the slab, with regard of the in-plan stiffness and property to transfer the seismic actions, some codes as NTC08, assumes as "rigid" a slab with the following properties:

- Total thickness of the slab greater than 80 mm;
- Thickness of the top concrete slab, greater than 40 mm.

The above prescriptions do not take into account the interaction with the beams and then, with the columns. In fact, the behaviour of the floor system strongly depend

from several parameters, as suggested by the International codes and the scientific literature. With regard of prescriptions provided by International codes, each one gives some indication for defining the in-plan floor stiffness as rigid. Specifically, one can found qualitative and quantitative criteria, as highlighted in (Doudoumis and Athana-topoulou, 2001, Moeni and Rafezy, 2011). Regarding to qualitative criteria, EC8 defines that a floor system is rigid when buildings have in-plan irregular geometries (as re-cesses, re-entrances, large opening) or irregular distribution of mass or stiffness and when buildings are constituted by walls located on the perimeter. Furthermore, the same code provides another qualitative criterion related to in-plan displacement under horizontal actions. In particular, it is denoted that the floor must be modelled with its in-plan flexibility when the horizontal displacements exceed more than 10% of those ob-tained by model with rigid diaphragm. Even in (NZS 1170.5, 2004) is pointed out that the rigid-floor assumption is not valid when there are abrupt discontinuities, major var-iations in in-plan stiffness and major re-entrant corner in the floor. In the Greek code (Greek seismic code, 2000), it is suggested that the rigid-floor assumption is to avoid when the buildings analysed have a long shape in-plan (length to width ratio> 4), as well as they are constituted by long parts as L, H, U shapes. In these cases, an accurate analysis of lateral force distribution on vertical resistant elements must be carried out, taking into account the weak areas. Concerning to quantitative criteria, some codes focus on the value of the ratio between in-plan maximum and minimum displacements under horizontal actions, like shows in figure 3.14. In particular, specific limits for this parameter are provided. Herein, the previous ratio is called "in-plan displacements ra-tio" and it is indicated like λ, defined as follow:

$$\lambda = \frac{Y}{X} \tag{3.8}$$

where Y is the maximum in-plan displacement and X is the minimum in-plan displacement. The definition of λ is paramount, because it takes into account the influence of the significant parameters that govern the problem of the in-plan stiffness of the floor system.
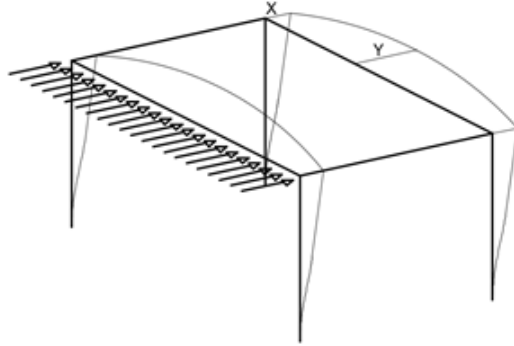
Fig. 3.14 – In-plan deformed shape of a simple structure, due to horizontal action

In figure 3.14 it is not depicted the possibility to have a torsional effect, due to the different distribution of mass and stiffness in the structure (CM is not coincident with CS), which provides different value of X on the two sides. In this case, the eq. 3.8 can be rewritten as:

$$\lambda = \frac{Y}{(X_1 + X_2)/2} \tag{3.9}$$

where X_1 and X_2 are the minimum in-plan displacements on the structure sides. Based on the evaluation of this parameter or other ones that depend from it, some International codes provide quantitative criteria. In (SEAOC, 1999) and (ASCE/SEI 7-16, 2016) is provided a β factor, defined as ratio between maximum lateral deformation of the diaphragm ($\Delta_{flexible}$) and average storey drift of the associated storey (Δ_{storey}). If the ratio is larger than 2, the diaphragm is flexible, vice versa it is rigid. Even in (IBC, 2009) is defined the same factor β, as soon as the previous code. In the Iranian Code (Iranian Code, 2007) another factor is defined, called λ, obtained by ratio between the maximum lateral deformation of the diaphragm along its length (Δ_{flex}) and the inter-storey drift evaluated on the considered storey and the immediately below one (Δ_{stor}). If this ratio is smaller than 0.5, the diaphragm is rigid, vice versa it is flexible. In FEMA P-58 the same factor of previous code is defined, but ascertaining the diaphragm as rigid when λ is larger than 2. When this value is included between 0.5 and 2, the diaphragm is defined as "stiff" and it should be modelled with its stiffness. The prescriptions of

abovementioned codes, take into account the influence of some parameters, which have been study from the scientific literature. Generally the codes can be low accurate in the estimation of the rigid floor limits, such as shown in (Moeni e Rafezy, 2011), which analysed the rigid floor assumption on buildings with irregular in-plan shape, evaluating results in terms of in-plan displacement ratio (therein called Deflect-Drift ratio) through all qualitative and quantitative criteria aforementioned. Authors tested the efficiency and accuracy of all indications available in the matter of floor deformability. In the recent years, the scientific community has strongly improved the background on RC buildings structural behaviour under horizontal action as seismic loads, evaluating the effects of flexible floor. Already from the more ancient studies, a lot of researchers show the highlights of this focus and with the growing of the computational tools, several applications have been carried out. Firstly, in (Goldberg, 1967) it was shown that the rigid floor assumption in RC buildings is less and less valid when the ratio between vertical elements stiffness and in-plan elements stiffness increases. In (Blume et al., 1961), dynamic behaviour of existing RC school buildings were analysed, did not focus on in-plan flexibility of floors but showed the possible structural damages under seismic actions, especially for the structures having RC walls. In (Saffarini and Qudaimat, 1999) several RC building models were analysed for comparing the differences between rigid floor and flexible-floor. A sensitivity analysis was carried out, through numerical models where some parameters were varied, such as number of stories, story height, slab typology, building-plan aspect ratio, regularity of building plan, openings in the slab, the sizes and spacing of columns and shear walls. They found that the assumption of rigid floor was accurate for buildings without shear walls, but it can cause errors for building systems with shear walls. This error was quantified through a stiffness factor R_i, which depended by the relative stiffness ratio. In the same work, it was ensured how in-plan irregularity, given by strong recesses and large opening in the slab, can cause the deformability of floor. In (Ju and Lin, 1999) the error committed using the rigid floor assumption was quantified, analysing several RC frames and walls buildings. They believed the above hypothesis was valid if the in-plan displacement was smaller than 20% of the same displacement obtained by deformable floor. When this difference exceeded

the 45%, the error in the stress distribution in the structural elements became significant, about 40%. The consequence of different stress distribution in the vertical elements, due to floor deformability, was the reduction of torsional coupling, which can be a positive aspect for RC buildings. In (Kunnath et al., 1991) the effect of deformable floor system on regular frame building with shear walls on the structure sides was studied, through a simplified model, which included elements modelled with inelastic behaviour. The authors showed that, using the two different hypotheses about the floor stiffness, the shear distribution among columns and shear walls changed. In this case, the design of buildings with shear walls was not conservative if one consider the rigid floor assumption, because in the inelastic field the internal frames needed larger strength and ductility demand. This evidence increased the possibility to have columns mechanisms. In (Dolce et al., 1994) the inelastic dynamic response of a large number of simple models, which simulate the floor system, were studied. On their cases studied, author analysed the variability of the ratio k_{floor}/k_{vert}, varying the elements stiffness. They obtained that, when the stiffness distribution of structural vertical elements was uniform, the flexibility of floor system was negligible, while when the structures had important re-entrances, the deformability effect was relevant. In (Tena-Colunga and Abrams, 1995) an existing building was monitored, measuring its response during the Loma Prieta Earthquake and adopting different strategies of modelling. In (Barron and Hueste, 2004) the influence of the in-plan floor deformability was evaluated on rectangular RC structures with different heights, aspect ratio and both RC shear walls and columns. The results in terms of θ_i, showed that with flexible floor, the displacements were higher in the frame close to the CM. In (Khajehdehi and Panahshahi, 2016) a FE approach was used for investigating the role of openings in the diaphragms. In particular, authors investigated three kinds of openings located at the centre of the slab, with three sizes (6, 14 and 25% of the area), showing the percentage error toward the same cases modelled using the rigid floor. Following, other authors studied aspects related to in-plan irregularity effects and dynamic parameters of buildings analysed (T, M[%]). Generally, a flexible floor system increase the T of the structure and the participation of the higher modes (Fleishman et al., 2001, Lee et al., 2007, Sadashiva et al., 2012). The

consequence of this latter effect can be the "modal shifting", with inversion of the modes, toward the situation with rigid diaphragm. In (De-La-Colina, 1999) the seismic response of one bay single-story structures, with in-plan irregularity and flexible diaphragm. The author considered the strength of elements independent from their stiffness and concluded that, increasing the natural T of a structure, the flexibility could be reduced. Same conclusion was observed, considering an increment of structural elements, in terms of yield capacity. In (Eivani et al., 2018) the seismic behaviour of asymmetric structures, in terms of different configuration of CM, CS and CV, with a flexible diaphragm was investigated, trough NLD analyses. The results showed that the rigid modes, obtained from a rigid floor assumption were reduced as well as the flexural deformations, expressed in terms of displacement and ductility demand. At the same time, the shear deformation were dominant. Another interesting conclusion was provided, in which the strength eccentricity is considered more influent than the stiffness eccentricity. In some works, the structural behaviour of existing RC buildings were analysed, varying the typology and constituent elements of slab. In particular, in (Tena-Colunga et al., 2015) the effects of different slab typologies and thicknesses on several type of buildings were studied. In (Pecce et al., 2017) a research of lightening elements role in the ribbed slab was carried out and authors, using elastic solid models of slabs, determined an equivalent slab thickness, made of a homogenous concrete layer. This was one of the few experimental studied about RC ribbed slab. The authors concluded that the effects of in-plan deformability cannot be neglected a priori, especially when the aim of analysis is the vulnerability assessment of existing RC buildings. From this point of view, the cases of major interest can be when the thickness of top concrete slab is smaller than 4 cm or when in a retrofit solution, in which the dimensions of vertical resistant elements are increased, the rigid floor assumption can be back out.

3.4.1 Numerical models

In order to analyse the real behaviour of the existing RC building and carry out the vulnerability assessment of ones through the procedures seen in the Chapter 2, paramount significance assume the numerical model and, overall, the initial assumptions at the base of its performance. Generally, practitioners have the work to decide

what structural elements involve in the numerical model, even considering the secondary ones. The result of the choice is a structural behaviour, which can be completely subjective and dependent from the sensibility and experience of the analyst. Then, one of the main usual initial hypothesis assumed by practitioners is the rigid floor one. In a FE model, to assume the floor system as rigid is synonymous of reducing the DoFs of the FE model and subsequently the computational efforts in the analyses. In a FE model, the rigid floor assumption lead to concentrate the storey mass in a unique node. As shown in figure 3.15, to use the rigid floor assumption means of inserting an internal constraint to each node of a floor, in which there is a node, called "master joint" that drives the motion of the other nodes, called "slave joints". Assuming the usual hypotheses of the axial inextensibility of the structural elements and negligible rotation around the horizontal axes (X and Y), all nodes can move together, under an horizontal action, proper as a rigid body, with possibility of translations decomposable in the two main direction (u_X and u_Y) and in-plan rotation (θ_Z) in the case of eccentricity.
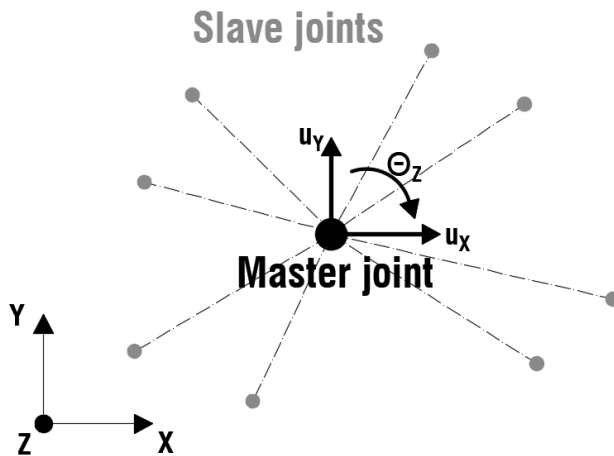
Fig. 3.15 – Concept of rigid floor assumption in a FE model

Just for concluding the definition of the rigid floor assumption, it is worth mentioning that the rigid floor assumption is not like the limit hypothesis of "shear-type", in which the floor is infinitely rigid than the vertical elements, in terms of axial, shear and flexural stiffness. In fact, a floor systems as the one shown in figure 3.13, is 4-5 times

more stiff than the vertical elements (in the cases of moment-resisting frames) and the hypothesis of shear-type is not appropriate, because this kind of system allows of having rotation between columns and beams. As just shown in the previous section, the rigid floor hypothesis could be incorrect in several cases, where the overall configuration of geometric and structural system (dimension of vertical elements, presence of holes of re-entrances in the slab,…) play a fundamental role in the force distribution and in the dynamic behaviour. To establish that the floor system is rigid or not, it is important in the prospective to carry out NL seismic analysis, where apply the inertial forces or displacements at each level. For example, in the case of NLS analysis, if the rigid floor assumption is assumed, the lateral force is applied in the CM of each storey and it drives the motion of other nodes. In the opposite case, for carrying out the NLS analysis, the previous force should be subdivided for all nodes of the floor, proportionally to the mass of them, with possible result of having different capacity curves.

Regarding to the modelling of the floor system, accounting for its stiffness, or rather its flexibility, both international codes and scientific literature provide several possibilities. The simplest model proposed was the "deep-beam" (figure 3.16). The model consists in a continuous beam characterized by a flexural stiffness equivalent to the in-plan stiffness of the floor, which account also the mass. The supports simulate the vertical elements and they are characterized by bearing springs, which account for flexural and shear behaviour. A distribute load on the continuous beam simulates the in-plan action, due to the seismic force. Following the eq. 3.8, the maximum displacement is provided by the deflection in the centre of each bays (Y) and the minimum displacement is the deflection of supports (X). This kind of model is suggested, as a-priori model for evaluating the status of the floor stiffness (EC8, Iranian code). Even several researchers used the deep beam for their analyses, such as in (Nakashima et al., 1982, Jain and Jennings, 1985, Jain, 1984, Aktan and Nelson, 1988, Kunnath et al., 1991, Dolce et al., 1994, Sadashiva et al., 2012).
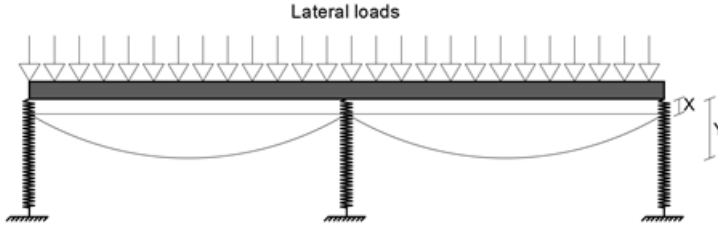
Fig. 3.16 – "deep beam" model

Another simplified model, but more refined than previous one, is the "strut model", showed in figure 3.17 (Petrini et al., 2007). In this 3D model, the floor system is schematized by two cross equivalent struts, which have dimensions of their section computed through the equivalence between the slab stiffness (K_{slab}) and equivalent strut stiffness (K_{strut}). Slab stiffness is defined as follow:

$$K_{slab} = \frac{1}{\frac{L'^3}{12\,J\,E_c} + \frac{L'}{A_s G_c}} \tag{3.10}$$

where L' is the slab dimension orthogonal to seismic action, J is the inertia moment of slab section, A_s is the shear area of section slab, E_c is the elastic modulus of slab material (it can be a bit different from E_c defined in the Chapter 2, considering that the slab as in figure 3.13 is composed by RC and hallow clay blocks) and G_c is the shear modulus of slab material. The struts are ruled by the following equation:

$$K_{strut} = \frac{E_s A_s}{L_s} \tag{3.11}$$

where E_s is the elastic modulus of strut material, L_s is the length of strut and A_s is the area of section strut. If K_{slab} is equivalent to K_{slab}, the A_s is the unique unknown term of the equation and it is:

$$A_s = \frac{L_s}{\left(\frac{L'^3}{12\,J\,E_c} + \frac{L'}{A_s G_c}\right) E_s} \tag{3.12}$$
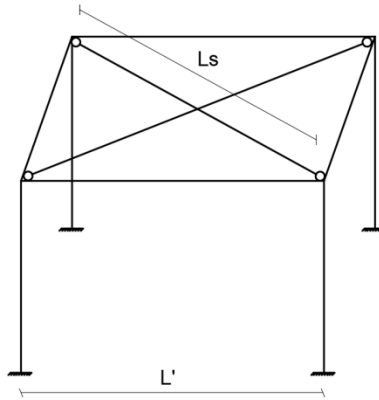
Fig. 3.17 – struts model

Subsequently, with the development of the FE software, some authors developed methodology for modelling the floor system through micro-models and macro-models. The first one is surely the most complex and wasteful, from the computational efforts point of view and it is made through solid FEs. This kind of model allow of modelling each element of the floor system, assigning to each element the proper geometrical and mechanical properties. Furthermore, it is the best approach for predicting the results of experimental tests, as shown in (Pecce et al., 2017). The second one is lower dispendious of the previous and it is constituted through shell elements. This kind of model is more usable in the FE model, also by practitioners, and it is able of accounting for the geometrical and mechanical properties with simplifications. Usually, it should be calibrated based on experimental tests or the behaviour showed by micro-models. Figure 3.18 shows a case of micro-model (Pecce et al., 2017) and a case of macro-model (Fleishman and Farrow, 2001). Generally, the main advantage to use micro or macro-models, rather than using simple methods such as the strut model, is due to the necessity of investigating the in-plan stress states of elements that constitute the floor system, under horizontal actions and the possibility of performing the effective verification of ones.
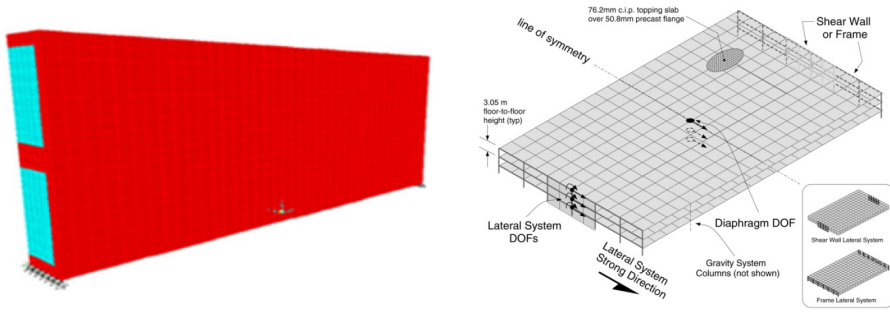
Fig. 3.18 – Examples of micro-model (Pecce et al., 2017) and macro-model (Fleishman and Farrow, 2001)

3.4.2 Proposal of a procedure based on an equivalent orthotropic shell

Based on the scientific literature and what about written in the previous sections, the effects of in-plan deformability cannot be neglected a-priori, especially when the aim of analysis is the vulnerability assessment of existing RC buildings. To this scope, a correct numerical model of floor system in RC buildings, which simulates the real structural response, should be composed by an in-plan element, which has the real in-plan stiffness of the floor system and it can behaves as rigid and deformable, depending by several boundary conditions. In addition, as showed in the previous section, floor system performance has a strong dependence by minimum and maximum in-plan displacements, caused by horizontal actions. The aim of this section is to propose a numerical procedure for calibrating a shell element to use in FE models, able to explore and simulate the effective in-plan deformability, in all possible configurations (rigid or not). In particular, due to the nature of the slab typology investigated (figure 3.13), an orthotropic material will characterize the shell element, which will have an equivalent thickness dependent from the numerical analyses. It is worth mentioning that the following analyses and models are based only on numerical procedures and evaluations made by the author and they are not based on experimental tests, due to their leakage in the scientific literature. For our scope, an accurate micro-model was developed, according to the constructive features of an usual RC ribbed slab in existing RC buildings. In particular, the slab micro-model made was constituted by RC joists, which have constant dimension (height of 20 cm, width of 10 cm, spaced of 50 cm) and the

lightening blocks contribute is neglected (despite it is an important aspect, as show in (Pecce et al., 2017). The thickness of top concrete slab can be varied from 5 cm to 1 cm, in order to emulate the possibility to have floor systems with a top concrete slab with null (SAP slab) or low thickness, as in some real cases of existing RC buildings. This latter condition can be caused by the presence in the floor system of hydraulic and electrical systems or human mistakes. Micro-model is based on a reference 3D solid model, which has dimension of 100x100 cm. It has been modelled using SAP2000 software (SAP2000 manual, 2018) as shown in figure 3.19. The 3D reference model has been implemented through solid elements, which take into account the bending and the shear deformation. The dimensions of solid elements has a thickness of 1 cm, in order to simulate the thickness of the top concrete slab with the right dimension. The in-plan dimensions of elements are in the order of centimetre, for avoiding locking problems. The mesh chosen is fixed, assuring a maximum scatter of 3% in results, respect to a fitter mesh or same model with square elements. Material of reference 3D model can be fixed according with the user necessity. In the cases analysed, mechanical parameters of concrete chosen are defined according to class C25/30, as classified in EC8. Cubic compressive strength (R_c) of 30 MPa, E_c is 31467 MPa, shear modulus (G_c) is 11315 MPa and Poisson's ratio (ν) is equal to 0.2. Based on the scope of the micro-model, which is the assessment of the in-plan displacements ratio and the global response under horizontal actions, the modelling is in the elastic field. In addition, the influence of the steel was neglected, considering its low influence in the in-plan deformed shape, due to the effective role of ensuring the flexural out of plane capacity, besides the low interest of investigating problems as failures, slippages or others.
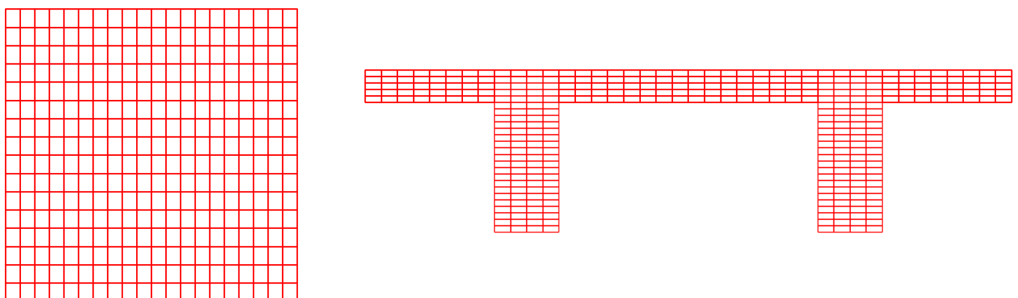
Fig. 3.19 – Reference 3D micro-model (100x100 cm), with top concrete slab of 5 cm

In order to investigate the parameters, which influence the problem of the in-plan deformability, the micro-model has been replied, in a new reference model, which is a one bay structure, with in-plan dimension of 300x600 cm and height of 300 cm. Edge beams, which have dimension fixed to 30x30 cm and same material of the slab, enclose the entire extension of slab and they are modelled through solid elements, meshed in accordance to the mesh dimension of slab elements. Once that the reference model is constituted, a first preliminary analysis has been carried out. In particular, a comparison with a similar frame model has been performed, in which the rigid floor assumption was imposed through an internal constraint. Figure 3.20 shows the reference models made with solid elements and frame elements. In the reference solid model, the total mass inserted is related to the slab self-weight, automatically computed from the software. In the frame model, after computing the same weight of the previous model, the mass is inserted through the application of a distributed load on a shell null linked to the storey nodes. Furthermore, despite the micro-model allow of computing the top concrete slab thickness variation, the following sensitivity analysis has been performed by using a fixed value of 4 cm. The choice is proper for testing the validity of the above prescription provided by NTC08, regarding to the constructive details about slab stiffness (the floor is rigid if the top concrete slab is $\geq$ of 4 cm).
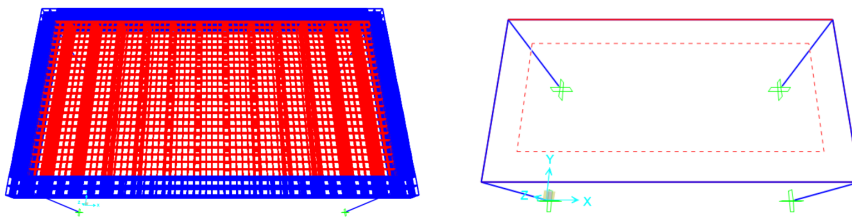
Fig. 3.20 – Reference models made with solid elements and frame elements

The parameters firstly varied, each one per time, were:
- Number of storeys: 1, 3 and 5;
- In-plan shape ratio: 1:2, 1:3 and 1:4 (with unitary length of 300 cm);
- Dimensions of vertical elements, as shown in table 3.1

Tab. 3.1 – Variation of vertical dimensions

Vertical element	Parallel direction (cm)	Orthogonal direction (cm)
Columns	30	30
	40	30
	50	30
	60	30
	90	30
	120	30
Walls	length of bay	20
	length of bay	30
	length of bay	40

For reducing the computational efforts of subsequent analysis, vertical resistant elements have been modelled with frame or shell elements. This latter case occurs in the cases of RC walls, where the shell elements have been meshed according to the solid beams mesh. It is worth mentioning that the numerical element used for modelling the RC walls is like "shell thick", which simulate the behaviour of a thick-plate. This kind of FE is based on the Mindlin-Reissner formulation in which it is included the transverse shearing deformation. Whether this is, the reason of using in the micro-models, different FEs from the solid ones is related to the sole necessity of modifying the vertical stiffness and thus, the relative stiffness among the floor system and the vertical elements. Furthermore, when models have more storeys, consecutive frame elements have been connected with a linear link, ensuring an equal displacement of the elements that converge in the node. It is worth specifying that the choices of the minimum dimensions of the reference model and the successive sensitivity analysis are in accordance to observation on real RC (residential and school) existing buildings (or part of them) in Italy. This will be highlight later in this section, with reference to the application of the numerical procedure developed on a real case study. In addition, the values of columns dimensions have been imposed, varying the ratio between the sides from 1:2 to 1:4, where this latter is the usual threshold for differentiating the vertical elements between columns and walls, according with EC8. Instead, regarding the walls, the di-

mensions have been chosen based on the usual values observable in existing RC buildings or looking to retrofit solutions. Coming back to the sensitivity analysis proposed, the first comparison has been performed in terms of modal parameters (T and M[%]) along the weak direction. Figure 3.21 shows two of the models made for the sensitivity analysis, such as the 3 storeys solid model and the 1 storey solid model with double in-plan shape of the reference model (1:4). The results are shown in figure 3.22a, 3.22b, 3.22c and 3.22d, where the blue bars represent the results for the solid model, while the yellow bars represents the result for the frame model. The headings in abscissa indicated the dimensions of columns and walls reported in table 3.1, with the specification for walls with the letter "W". Generally, the parametric analysis provides the following indications:

- As the structural vertical element dimensions increase, the floor become more flexible and Ts and M[%]s decrease, showing the importance that assume this parameter in the evaluation.
- For the reference model, the T of the solid model is higher than the one of the frame model. The M[%]s are comparable, but slightly higher in the case of rigid floor. In addition, it is evident that, when the vertical elements are constituted by walls, there is a big variation in terms of M[%], due to the occurrence of the modal shift phenomenon;
- As the number of storeys increase, the relative differences among Ts decreases, as soon as happens for the M[%]s. Furthermore, the M[%]s decrease in the models with more storeys, due to the influence of higher modes. For both Ts and M[%]s, the values of the solid models are slightly lower than the values obtained from the frame model, but the modal shift phenomenon does not occur, because the influence of the number of storeys increment is heavier of the vertical elements stiffness. The result of these evaluations is that the number of storeys increment, reduces the effect on the in-plan flexibility;
- Increasing the in-plan shape ratio from 1:2 to 1:4, the differences among Ts of the two models are greater than the ones in the reference model, due to

the more flexibility. For the M[%]s the results is same to the one obtained from the reference model.

In addition, the second aim of the sensitivity analysis has been to evaluate the in-plan displacement ratio of the models. To this scope, a horizontal action has been applied at each storey of the models, uniformly applied on the solid surface of edge beams. The value of the load is equal to 1 kN/m^2 is, which is arbitrary and irrelevant for the scope of the work, considering that the models are elastic. All results are depicted in figure 3.23, where the light blue bars represent the models with columns while the red bars represent the models with walls. The results, in terms of in-plan displacement ratio, show that the λ is always greater than 2, in the cases of walls. For the columns, the value of λ increases as their dimensions increase and just in one cases, exceed the limit imposed from the International codes.
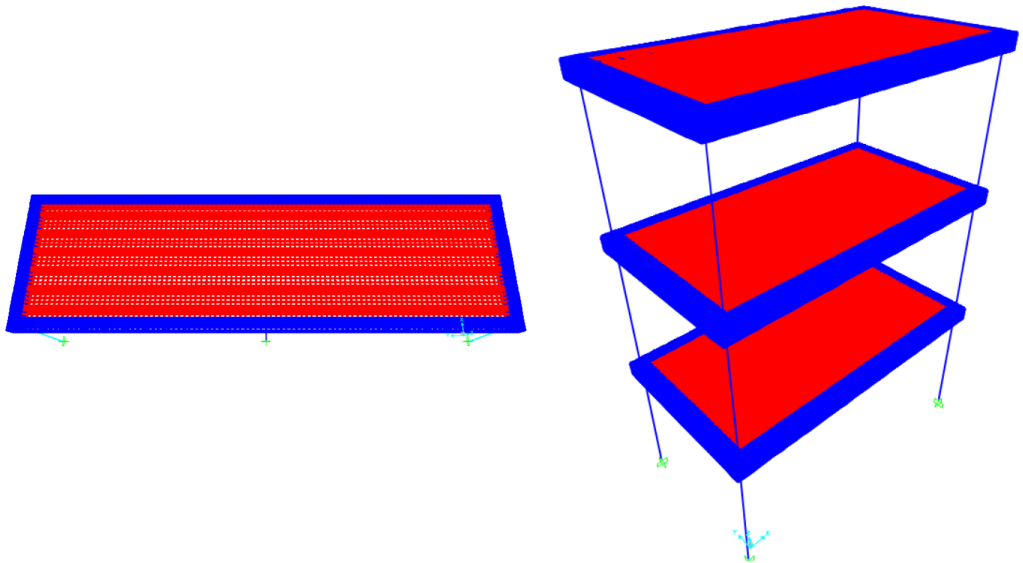
Fig. 3.21 – Solid models made for the sensitivity analysis
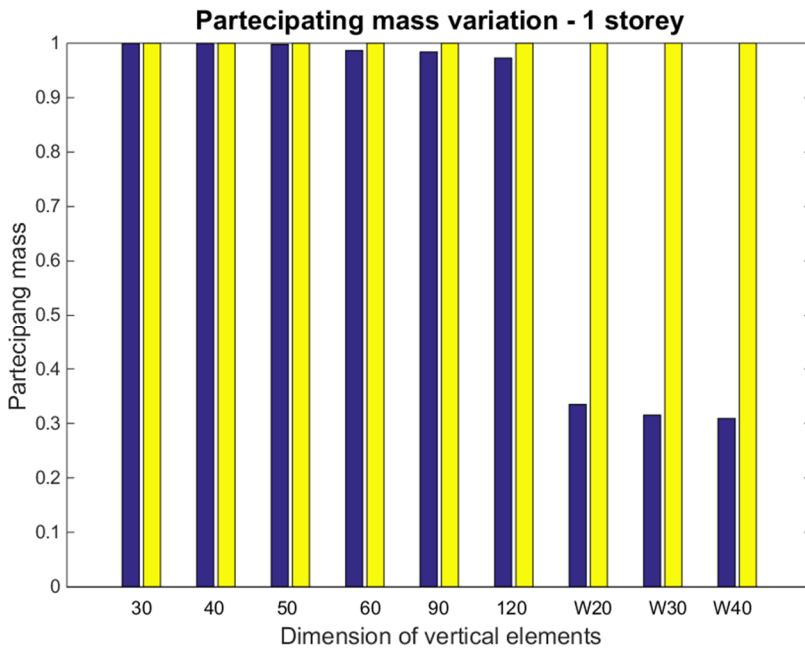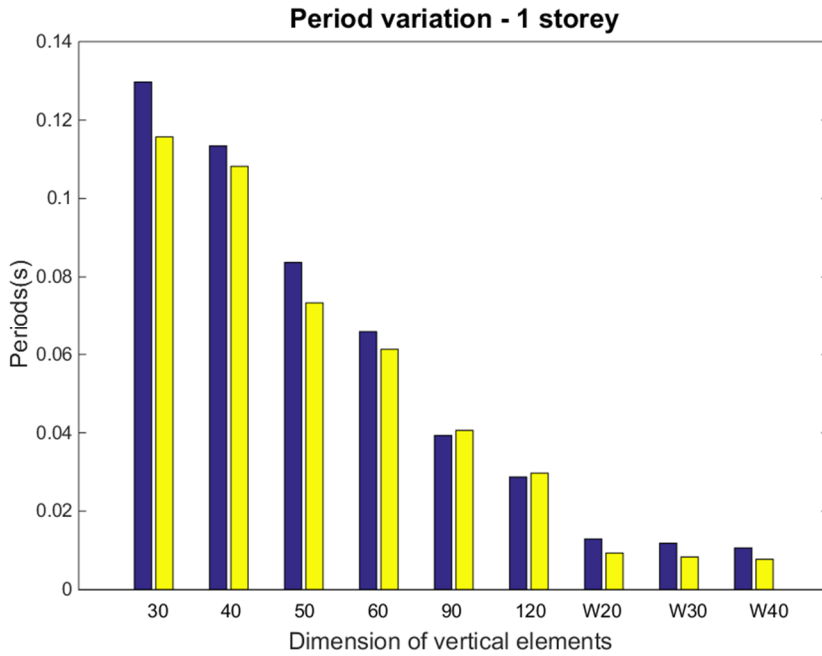
Fig. 3.22a – Comparisons in terms of T and M[%] for 1 storey models

Period variation - 3 storeys

Periods(s) vs Dimension of vertical elements

Partecipating mass variation - 3 storeys

Partecipang mass vs Dimension of vertical elements
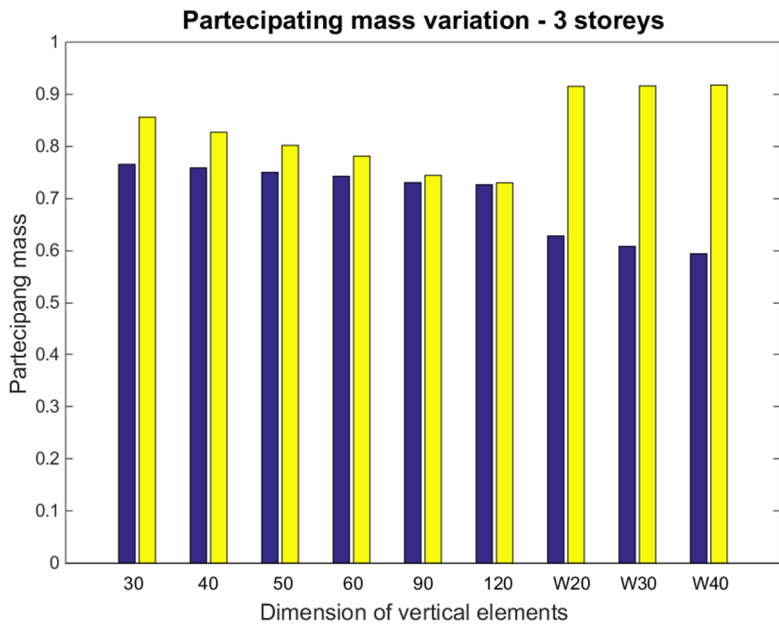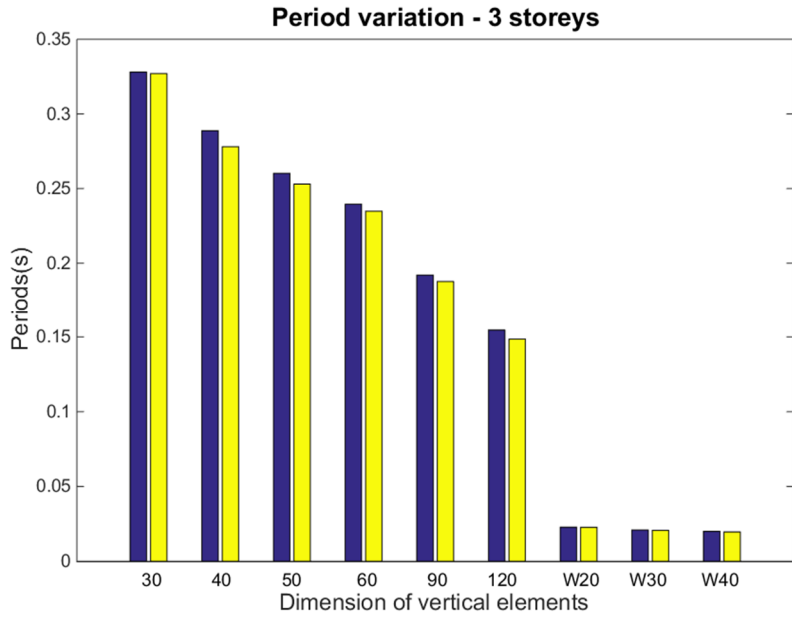
Fig. 3.22b – Comparisons in terms of T and M[%] for 3 storeys models

103
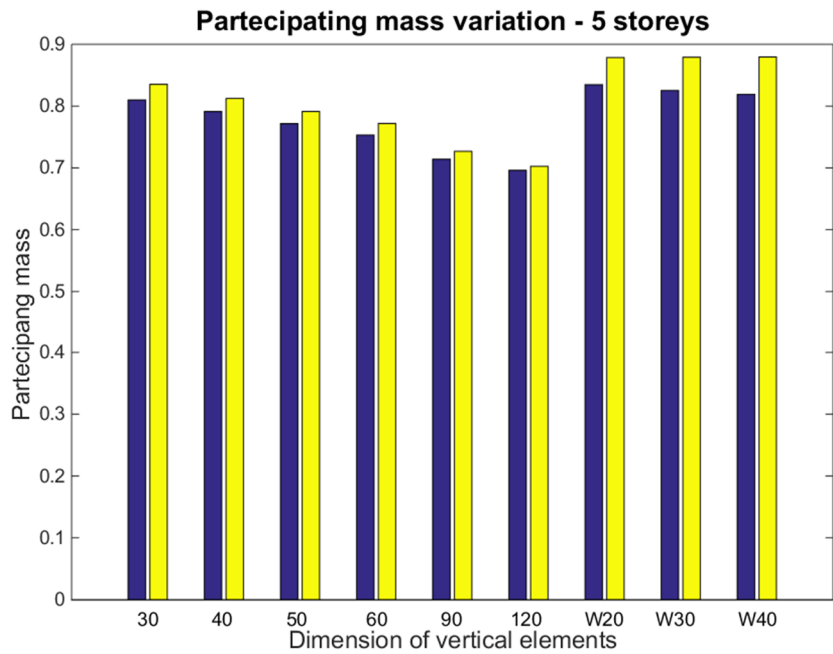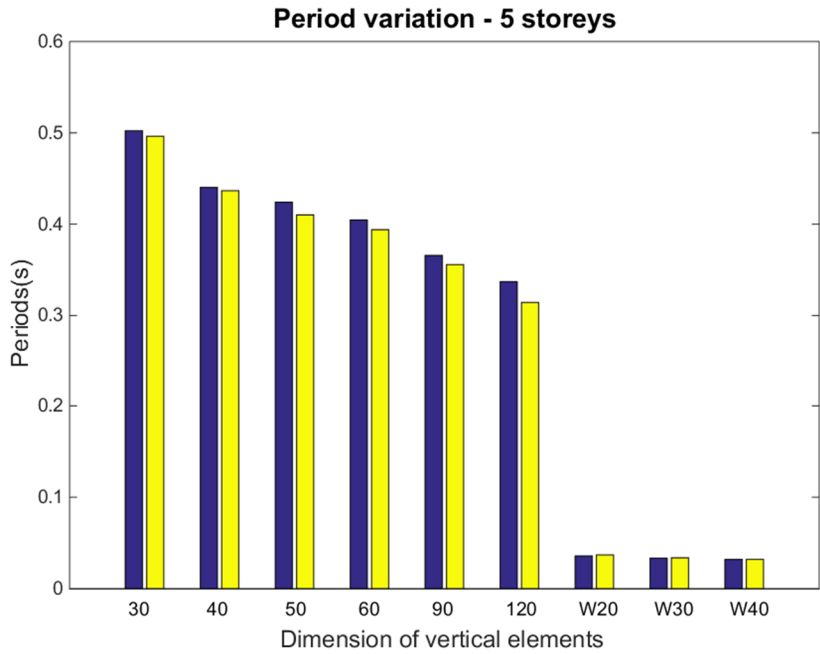
Fig. 3.22c – Comparisons in terms of T and M[%] for 5 storeys models
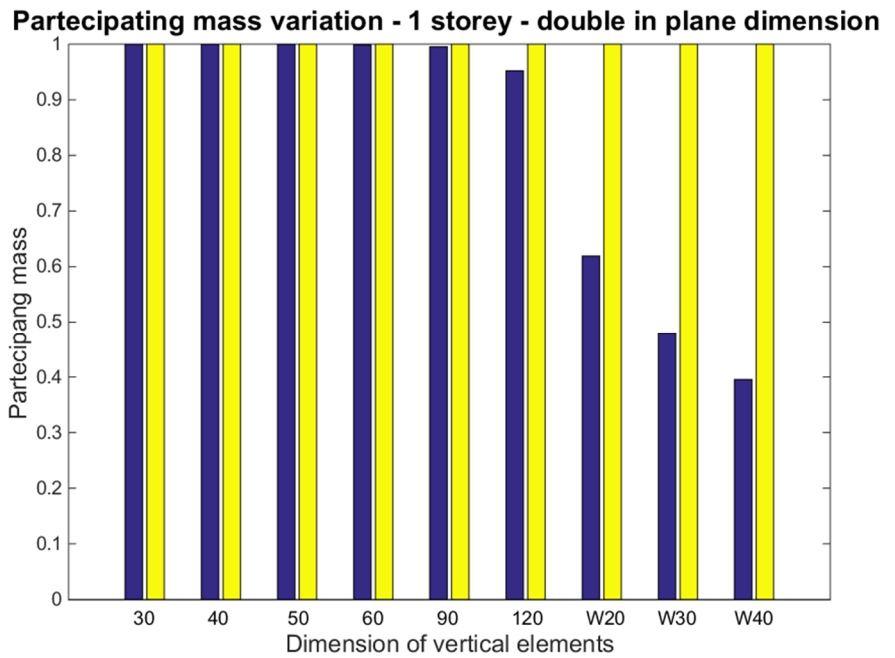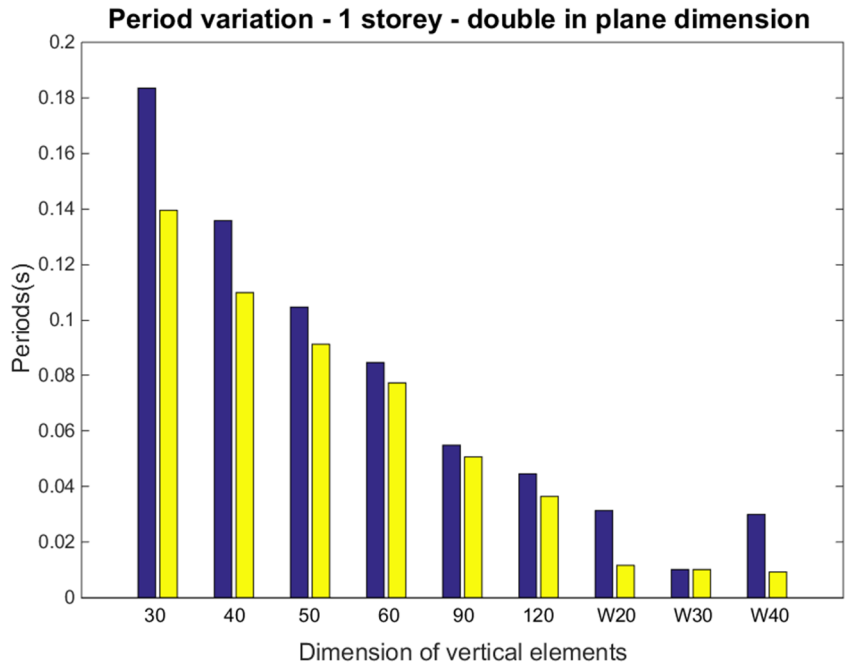
Fig. 3.22d – Comparisons in terms of T and M[%] for 1 storey models with in-plan shape ratio of 1:4
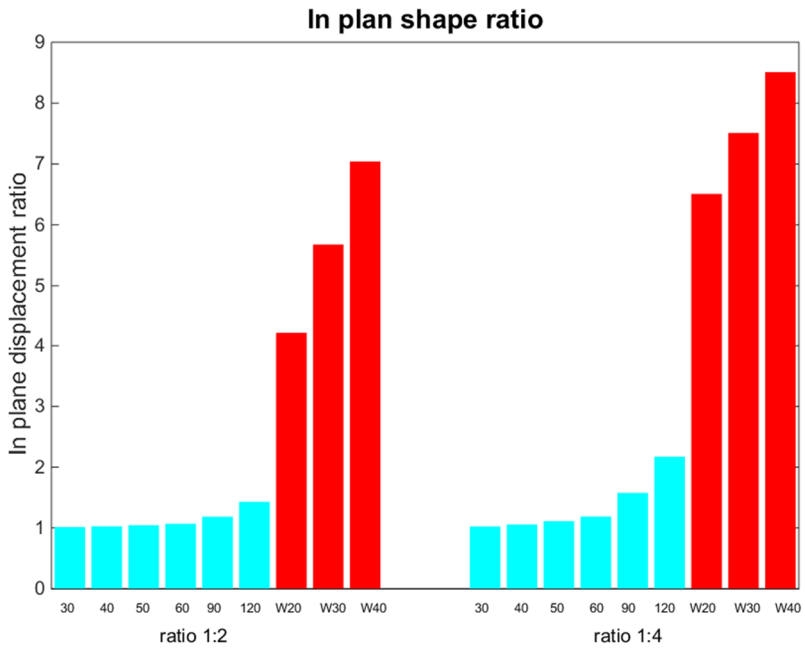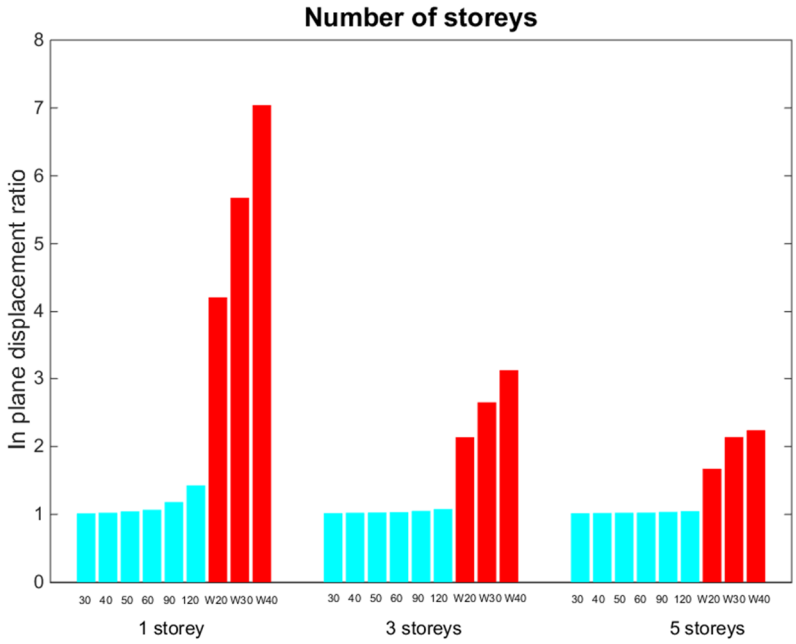
Fig. 3.22d – In-plan displacement ratio results, increasing the number of storeys and the in-plan shape ratio

For better investigating the behaviour of the floor system, a couple of real numerical applications have been carried out, using the technique of the solid models. The main aim of these applications was of assessing how the presence of the RC walls (perimetric and C-shape) can influence the deformability of the floors. We can already anticipate that the more interesting results have been provided in the configurations with one storey, as just demonstrated from the sensitivity analysis. The first numerical application is a structure with in-plan dimensions of 600 x 1200 cm and height of 300 cm. In particular, two bays in the short direction and one long bay in the long direction constitute the model, typical of existing RC building designed through old codes. Beams and columns have dimension of 30 x 30 cm. At the centre of the model, there is an opening, due to the presence of a C-shape wall, which simulate the presence of an elevator. The case investigated is depicted in figure 3.23, where the C-shape wall is simulated through shell elements (thick), meshed as the floor system. Regarding this case, a sensitivity analysis has been performed, varying the thickness of the wall (by using 20, 30 and 40 cm), keeping constant the opening dimension, and comparing the results, in terms of in-plan displacement ratio, with the ones obtained from the same geometrical model without the C-wall. This latter is the new reference model, only for the next evaluations (see figure 3.23).
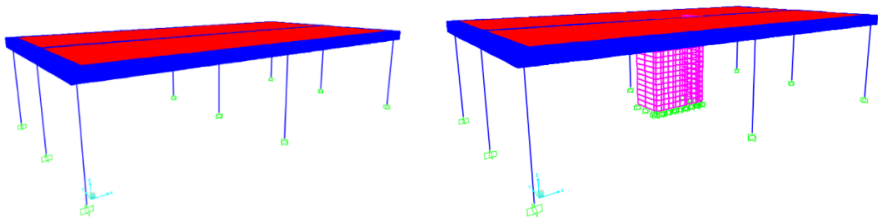
Fig. 3.23 – First numerical application with C-shape wall, which simulate an elevator

The second numerical application is similar to the first one, in terms of geometry of structure and elements, with involvement of perimetric walls on the short sides of model (to substitute the external central columns), as shown in figure 3.24. In this case, the thickness of walls is equal to 30 cm, while the sensitivity analysis has been performed varying lateral dimensions of the walls (130, 230, 330 and 430 cm). Even

in this case, the results, in terms of in-plan displacement ratio, were compared with the ones obtained from the same geometrical model without the perimetric wall.
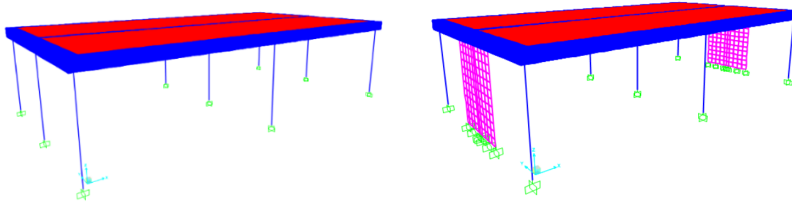
Fig. 3.24 – Second numerical application with perimetric shear walls

The evaluation of the in-plan displacement values, depicted in figure 3.25, confirmed that the problem of the floor flexibility cannot neglected in more case of existing RC buildings (in green the result of the new reference model and in brown the results of the sensitivity analyses). In fact, in the first case, the C-shape RC wall with constant opening in the floor, as the wall thickness increases, the floor becomes more flexible, exceeding the value of λ equal to 2 for ordinary values, as 30 cm. At the same way, in the second case, the addition of RC walls on the structure perimeter, provides the same effect, as the wall length increases, exceeding the value of λ equal to 2 for a dimension of a little more of 200 cm. It is worth mentioning that the sensitivity analyses performed on simplified models and numerical applications, do not characterized by torsion phenomena. With this regard, it has been not considered the possibility of having in-plan rotations, due to the kind of action applied and to the application of shear walls in symmetric way. This latter has been accounted for a perspective of retrofit solution, where the insertion of RC walls has the rule of regularizing the dynamic behaviour of building and of increasing the horizontal strength of it. This choice is usual among practitioners, for the simplicity in computation and in-situ application.
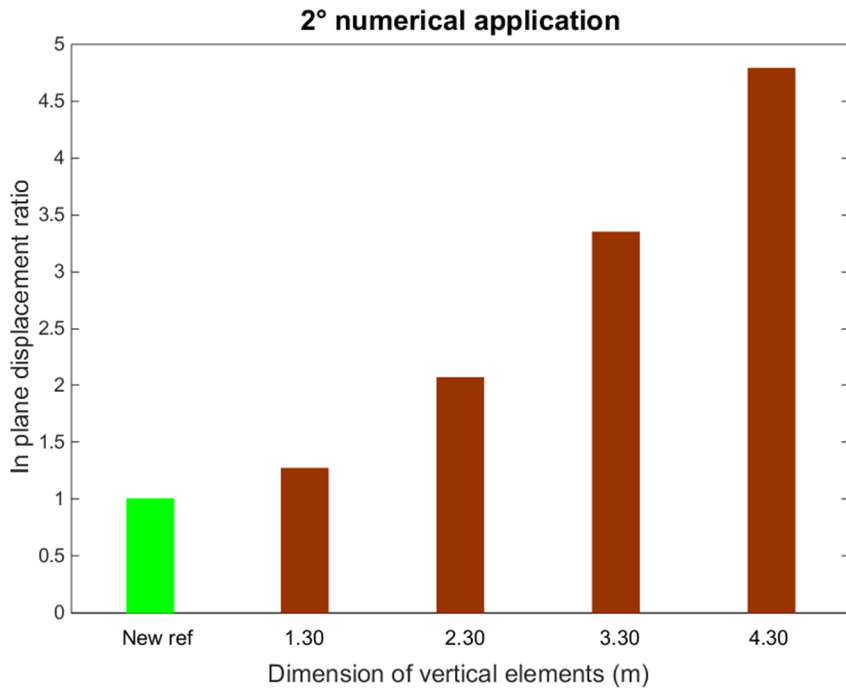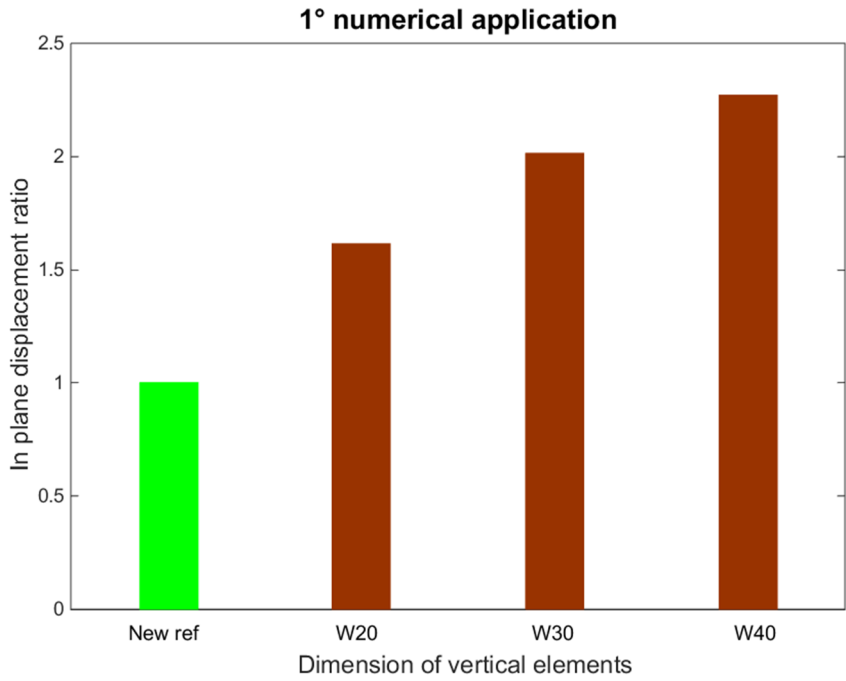
Fig. 3.25 – In-plan displacement ratio results for the two numerical applications

Once that the influence of some parameters has been assessed, as the dimension of vertical elements, the in-plan shape ratio and the number of storeys, the orthotropic nature of the slab typology investigated has been taken into account. In fact, another fundamental parameter in the estimation of the in-plan displacement ratio is the orientation of the joints of the slab. In particular, this parameter assumes relevance with regard of the loading direction. Hence, all models developed in the parametric analysis have been loaded (through the load above descripted), in both parallel and orthogonal directions, showing different effects in the in-plan deformability and in particular in the values of the in-plan displacement ratio. It is worth mentioning that in the first sensitive analysis, the load was parallel to the joists orientation and directed along the short direction of the simplified model. For studying the effects due to the variation of the joists orientation, the model has been modified, rotating of 90 degrees the solid elements (see figure 3.20 for the first configuration), as shown in figure 3.26, in order to always loading the model along the short direction.
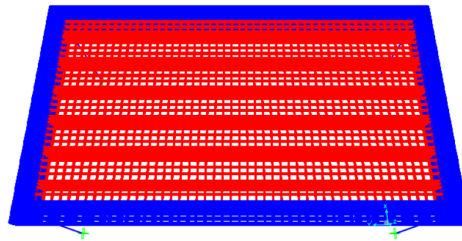
Fig. 3.26 – Solid model with variation of the joists orientation

The results of the sensitivity analysis showed that floor system is more flexible when the loads act perpendicularly of joists direction. In fact, in this case, the bending stiffness of joists has a little influence on in-plan displacement, while in the opposite case, the in-plan displacement ratio is smaller than the previous one, because the axial stiffness of joists participates to reduce the maximum in-plan displacement. This result can sounds strange, considering that one would expect that the stiffness of the floor joints (mostly axial) would increase the in-plan stiffness of the slab when the joints are perpendicular the direction of seismic loading of floor diaphragm. The reason of this

difference is mainly due to the absence in our model of lightening blocks. In fact, as shown in (Pecce et al., 2017), the influence of the lightening blocks provides results opposite to the ones here obtained. On the other hand, in our initial assumptions, it is neglected the lightening blocks influence. In addition, the usual methodology of design-ing of the slab elements does not provides the consideration of the hallow clay blocks. Lastly, as just mentioning, the scientific literature about the topic is not exhaustive, considering the absence of experimental tests on the particular floor system analysed, which is widespread just in some geographic areas, like Italy. Based on the results obtained from the sensitivity analyses, the next step of this work is to provide a fast method for practitioner, in order to simulate in the FE model the real behaviour the floor system, avoiding any initial hypotheses. In particular, the proposal is a numerical sim-plified procedure, able to provide an equivalent shell thickness of orthotropic material. With this regard, the equivalent shell should be a homogenous layer, with unitary thick-ness and faithful to the behaviour provided by the micro-model. Furthermore, the shell should be "thick", as well as able to simulate the behaviour of a thick-plate, following the Mindlin-Reissner formulation in which transverse shearing deformation is ac-counted (as assumed for the RC walls). With these goals, the idea consisted into reply all micro-models, developed for the above sensitivity analysis, as equivalent macro-models, obtained modelling the slab as shell and varying the shell thickness up to have the same results in terms of in-plan displacement ratio. In other words, in SAP2000 software, same applications have been modelled as macro-models, with same hori-zontal loads and boundary conditions. In particular, edge beams dimensions have been modelled through frame elements with fixed dimension of 30x30 cm (according to the dimensions used for the micro-models) and vertical element dimensions have been varied as in table 3.1. Shell elements have been meshed using square FE having di-mensions of 50 cm. Assigning to trial a value of shell thickness, it is gradually varied, in order to obtain the same in-plan displacement ratio of micro-models, with a maxi-mum error of 10% (in absolute value). This latter is retained a reasonable scatter, con-sidering efforts of the iterative numerical procedure. For generalizing the above purpose

and making it prone for the practitioners use, a new numerical procedure has been proposed, as following summarized and graphically outlined in flow chart in figure 3.27:

- For each "floor field", defined as the part of floor encloses among minimum 4 beams (two in one way and two in the other way) and below columns, a FE micro-model, using solid elements, is carried out;
- In each analysed model, loaded with a fixed horizontal action, the maximum and minimum in-plan displacements are detected and the ratio between them is computed (in this paper "in-plan displacement ratio");
- For each application, an equivalent FE macro model is carried out. In particular, beams and columns are modelled with frame elements, while slab is modelled with shell elements.
- Using in-plan displacement ratio, previously determined, shell thickness is calibrated. Assigning to trial a shell thickness value, the macro-model must have the same in-plan displacement ratio of micro-model;
- If the differences between solid and frame models is greater than 10%, the shell thickness assigned must be changes.

It is worth mentioning that the macro-models have been associated to a "floor field", where the author means an isolated part of the structure, enclosed in a minimum of four beams, two in one direction and two in the other one. Clearly, it is possible to have floor fields with more columns under the floor fields, which in the micro-model must be condensed in the four external columns and the all beams in the four external beams, accounting for the geometrical information for computing the in-plan displacement ratio. It can seem a simplification, but this concept is based on the observations about the existing RC buildings, where in a lot of case one can find a slab oriented just in one direction (the reference is to moment resisting frame buildings, with resistant elements oriented only in one direction). Then, it is justified the use of the in-plan displacement ratio, where the minimum in-plan displacement is strongly dependent by vertical elements stiffness, while maximum in-plan displacement is strongly dependent by in-plan elements stiffness. Furthermore, for the models with more levels, the value

of in-plan displacement ratio takes into account is the one at the first level, considering that on the upper storeys, this value is always lower.

```
┌─────────────────────────────────────────┐
│   To identify the floor field and to     │
│   carry out Micro-model, using solid      │
│                elements                   │
└─────────────────────────────────────────┘
                    │
                    ▼
┌─────────────────────────────────────────┐
│   To load the Micro-model with           │
│   horizontal actions (uniformely         │
│   distributed), in order to determine     │
│   the in-plane displacement ratio         │
└─────────────────────────────────────────┘
                    │
                    ▼
┌─────────────────────────────────────────┐
│   To perform an equivalent Macro-model   │
│   by using frame elements for simulating │
│   beams and columns and shell elements   │
│         for simulating slab              │
└─────────────────────────────────────────┘
                    │
                    ▼
┌─────────────────────────────────────────┐
│   To assign a trial slab thickness and    │◄──┐
│   to evalate the in-plane displacement    │   │
│   ratio obtained by linear analysis       │   │
└─────────────────────────────────────────┘   │
                    │                          │
                    ▼                      ┌──────┐
┌─────────────────────────────────────────┐│  NO  │
│   Is the difference, between in-plane    ││      │
│   displacement ratios restored, less     │┘──────┘
│             than 10%?                    │
└─────────────────────────────────────────┘
                    │
                ┌───────┐
                │  YES  │
                └───────┘
                    │
                    ▼
┌─────────────────────────────────────────┐
│        To analyze the next floor field    │
└─────────────────────────────────────────┘
```

Fig. 3.27 – Flowchart of the proposed numerical procedure

Using this methodology, for the cases performed in preliminary analysis, a summary of equivalent shell thickness is presented in the graphs in figure 3.28, which have in abscissa the "inertia moment of vertical elements" and in ordinate the thickness. The inertia moment of vertical element is the sum of inertia moments of each vertical structural element under the structure considered. The choice of this parameter is due to the strong importance of relative stiffness between vertical and horizontal elements. However, for what above written regarding to the floor fields, being sure that vertical elements under the floor field were usually designed based on the vertical loads, it is rather sure that, under a big floor field there is a total vertical inertia greater than the one under a little floor field, also with the same in-plan ratio. Each graph of figure 3.28 shows three curves, where each curve is representative of one value of in-plan shape ratio. Difference between graphs is due to loading direction, with regard to the orientation of the joists. Each graph has been defined considering both top concrete slab thickness and loading direction fixed. In particular, in the graphs, each star points out the value of equivalent shell for a model with dimension of vertical element shown in table 3.1. For clarity of image, the points of the models with columns of 40 cm and 50 cm are not depicted in the graphs. Furthermore, the figure takes into account the models with more levels, considering the possibility of using the value of in-plan displacement ratio obtained for the models with one storey in a conservative way, as abovementioned. For same model, a practitioner can enter into the two graphs with same inertia and obtains the equivalent shell thicknesses resultant. Whereas the thicknesses in output are different for the two directions, but in numerical model the slab must be only one, practitioner can assume the smallest shell thickness (usually the dimension obtained loading orthogonally to slab orientation) and change the elastic properties of material in the other direction. To this scope, one can follow the relationship below:

$$E_p = \frac{h_p}{h_o} E_o \qquad (3.13)$$

where "o" and "p" point respectively orthogonal and parallel. Using the equation 3.13, an orthotropic concrete material is defined. In particular, in direction where thickness is higher, a higher value of modulus E (and consequently G) is determined, maintaining the shell thickness constant (lower value).
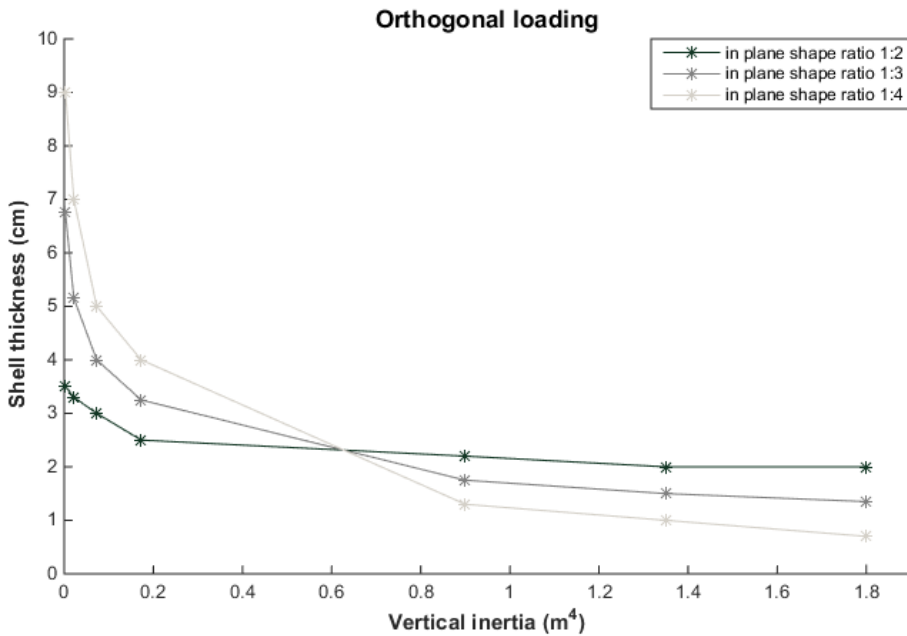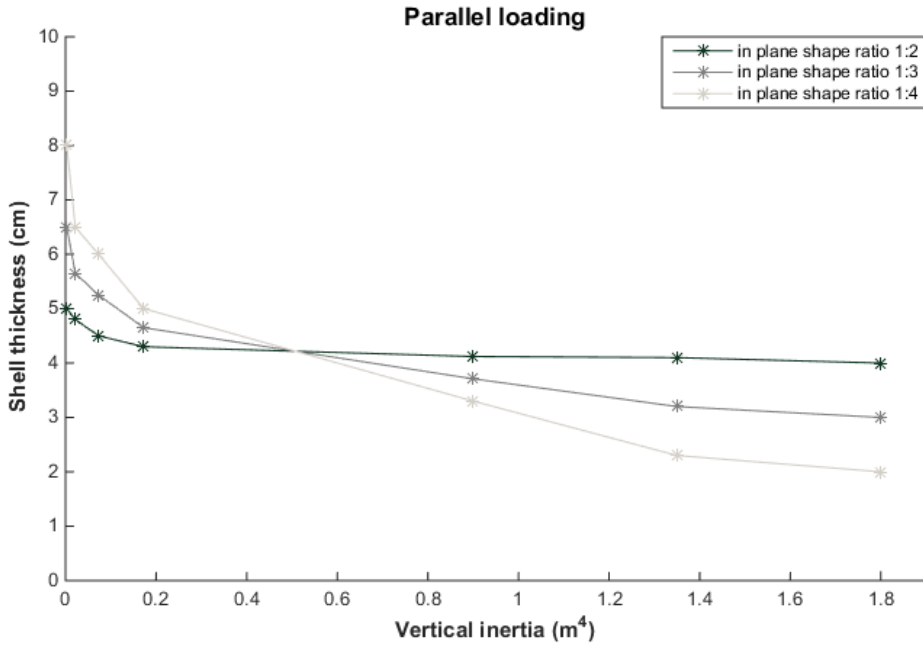
Fig. 3.28 – Graphs defined through preliminary analysis, to determine equivalent shell thickness (fixed top concrete slab produce equal to 4 cm; loading orthogonal and parallel).

The terms in eq. 3.13 are the parameters that describe the in-plan stiffness of slab and, in this way, the in-plan deformability of slab in both directions is insured, coherently to what obtained by FE micro-model results. Clearly, in some cases, the thickness of equivalent shell provided by fig. 3.28 can be lower than the real thickness of top concrete slab. For this method, which is a numerical method, this evidence can be acceptable because, as just widely shown, the value of shell thickness is strongly dependent by the dimension of vertical elements, according to FE micro-model results.

In order to verify the effectiveness of the new simplified procedure to define an equivalent shell thickness with orthotropic behaviour, summarized in the graphs in figure 3.28, an existing RC building has been analysed. The case study is an existing RC school building located in Castelluccio Valmaggiore (Province of Foggia, Puglia, Southern Italy), which has a plant inscribed in a rectangle of dimension 20.00x27.85 m, 3 floors above ground and a pitched roof with total height of 14.00 m. The structure, built in the 60s' in the absence of specific seismic codes, was designed considering only vertical loads and it is constituted by RC frames with beams and columns. The knowledge of the building is due to the investigation performed within an Agreement between "AdB Puglia" and "Polytechnic University of Bari", in which vulnerability analyses on some school buildings in the Province of Foggia were carried out, in order to develop guidelines for the vulnerability assessment of existing buildings (Mezzina et al., 2011). Dimensions of the structural elements, design loads and mechanical parameters of materials (determined through in-situ investigation on concrete elements and steel rebar's) are summarized in table 3.2, where B and H are the dimensions of beams and columns, G_1 and G_2 are the gravity permanent loads, Q is the live loads and Q_s is the snow load. The foundations are constituted by plinths connected by beams, while the orientation of elevation beams is in just one way. Staircase has been modelled considering its influence, in terms of masses, on competence beams. The slab typology of building is a RC ribbed slab, with constant joists dimensions (height 20 cm, width 10 cm, spaced 50 cm) and thickness of top concrete slab of 4 cm. The structural modelling of the case study has been performed by using the FE software SAP2000. Beams and columns have been modelled as one-dimensional frame elements, assuming fixed-

end restraints at the base of the columns. On each floor, horizontal joint forces of 1 kN (it is not important the value of the forces, because the analysis will be linear) have been applied in one direction (weak axis), in order to simulate a constant load profile over the height of building. The numerical model has been duplicated, in order to consider and not the rigid floor assumption. In fact, in one model, an internal rigid diaphragm constraint at each floor has been inserted, while in other model, through the procedure described, shell elements have been defined and inserted. Shell elements, which simulate the slab, have been meshed in square elements with dimension of 50 cm, coherently with shell mesh of macro-models. Frames, directly linked to shell, have been meshed coherently with slab mesh, for obtaining the correspondence of each joint. For calculating the thickness of equivalent slab, the first operation has been to determine the in-plan shape ratio of each floor field including among beams, as indicated in figure 3.29.
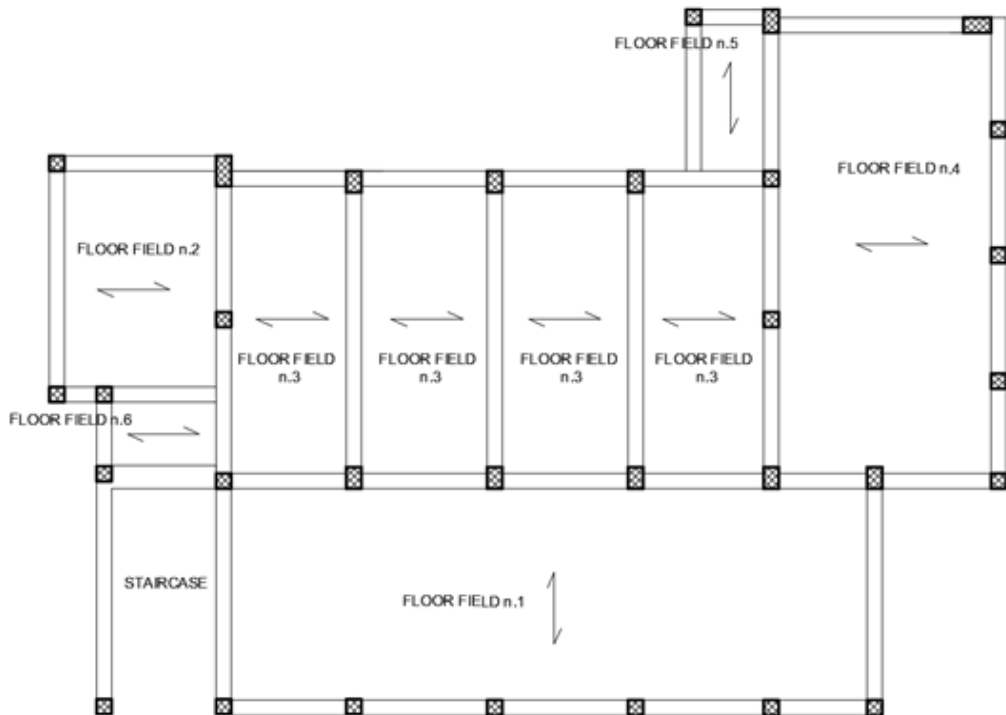
Fig. 3.29 – Floor configuration of the case study, with indication of each floor field

Tab. 3.2 – Dimension of the structural elements, design loads and mechanical parameters of materials

Level	Elements	B (mm)	H (mm)	Materials (MPa)	Loads (kN/m²)
Ground floor	Columns	500	500	f'_{cm}: 9,3 f'_{ym}: 430	$G_1 = 3.50$ $G_2 = 2.50$ $Q = 3.00$
		400	400		
		400	500		
		400	600		
	Beams	400	600		
		400	500		
		500	400		
First floor	Columns	400	400	f'_{cm}: 9,3 f'_{ym}: 430	$G_1 = 3.50$ $G_2 = 2.50$ $Q = 3.00$
		400	500		
		500	500		
	Beams	400	400		
		400	500		
		400	600		
		400	800		
Second floor	Columns	400	400	f'_{cm}: 9,3 f'_{ym}: 430	$G_1 = 3.00$ $G_2 = 2.00$ $Q = 0.50$ $Q_s = 0.80$
		400	500		
		500	500		
	Beams	400	800		
		400	500		

Considering that the floor fields identified regard the cases already analysed in preliminary analysis, it is possible to apply the procedure proposed using graphs in figure 3.28. Choosing the curve corresponding to in-plan shape ratio and considering the inertia of vertical elements under each floor part, two thicknesses of equivalent shell can be defined, for loading parallel and orthogonal to joists orientation. Subsequently, the thickness detected in the direction orthogonal to joists orientation has been assumed as equivalent shell thickness, while other thickness is used to define different elastic parameters of materials (E_c, G_c) in the other direction, according to eq. 3.13.

The results of the application of procedure is summarized in table 3.3. It is worth explaining the differences between floor fields that have the same in-plan shape ratio, also if the dimensions are different. For example, if one consider, in the case studied, the floor fields n.2 and n.6 (according to figure 3.29), they present two different areas, but a ratio between the sides is same and then, the ratio is 1:2. The variation of thickness and mechanical parameters of the 2 equivalent shell thickness (for the 2 floor field considered above) is due to value of vertical inertia (it is the sum of the inertia columns under the floor field considered) and the slab orientation.
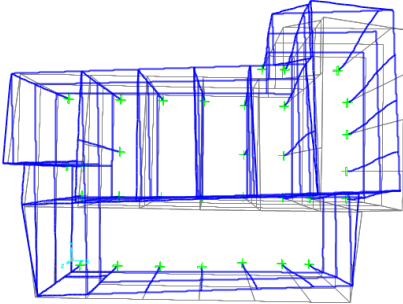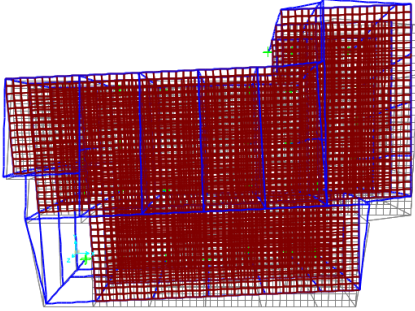
Tab. 3.3 – Values of thicknesses of floor fields and modified elastic parameters for defining the orthotropic shells

Floor field	In-plan shape ratio	Thicknesses (cm)	Elastic parameters (MPa)
1	1:3	Ortho = 4,3 Parallel = 5,4	E_p = 26967,6 G_p = 13219,4
2	1:2	Ortho = 3,9 Parallel = 5,0	E_p = 27531,0 G_p = 13495,6
3	1:2	Ortho = 4,2 Parallel = 5,3	E_p = 27098,4 G_p = 13283,5
4	1:2	Ortho = 3,0 Parallel = 4,5	E_p = 32211,3 G_p = 15789,9
5	1:2	Ortho = 3,2 Parallel = 4,6	E_p = 30869,2 G_p = 15131,9
6	1:2	Ortho = 3,2 Parallel = 4,6	E_p = 30869,2 G_p = 15131,9

Comparison between models defined, with rigid floor assumption and not, are showed in the table 3.4, in terms of modal parameters as T and $M[\%]_X$, $M[\%]_Y$ and $M[\%]_\theta$. The low differences (in the order of 10%) between models show that, in this case, rigid floor assumption is an appropriate hypothesis. Furthermore, even stress distribution over both vertical and horizontal structural elements is similar in both models. Clearly, using this shell element, the hypothesis of rigid floor can be avoid. The

comparison with rigid floor model has been done for demonstrating that the shell element can be used in each case.

Tab. 3.4 – Comparison between case study models with rigid floor assumption and not

Model with rigid floor assumption	Model with orthotropic shell
1st mode – T = 0.6754 s M[%]$_x$ =9.3%; M[%]$_x$ =52.1%; M[%]$_x$ =24.0%	1st mode – T = 0.6951 s M[%]$_x$ =3.0%; M[%]$_x$ =62.4; M[%]$_x$ =20.6%

In order to clarify the role of a possible retrofit solution effect on structural response, from the point of view of floor flexibility and considering the irregular dynamic behaviour of building investigated, it has been hypothesized to insert RC walls of 40 cm to the both small edges of the building, along the horizontal loading direction (weak direction). It is important to say that the addition of the two RC walls is one of possible retrofit solutions, which emphasize the behaviour of floor system. This choice is usual among practitioners, which have the aim to regularize the dynamic behaviour of existing structure and to increase the strength of the one. In addition, the addition of RC walls with irregular in-plan distribution does not make sense, such as only along one side, because it should be not a right retrofit solution. Even in this case, two FE models have been realized, considering and not the rigid floor assumption. RC walls have been modelled as shell elements, meshed coherently with slab and frame mesh, for obtaining the correspondence of each joint. The numerical element used for modelling the floor system is like "shell thick", the same used for modelling the floor system. This choice is coherent with the modelling way of the sensitivity analyses. In figure 3.30, the two models with RC walls added are showed. The variation of vertical element dimensions,

leads that the equivalent shell thickness in same floor part must be recalculated, following the same procedure abovementioned.
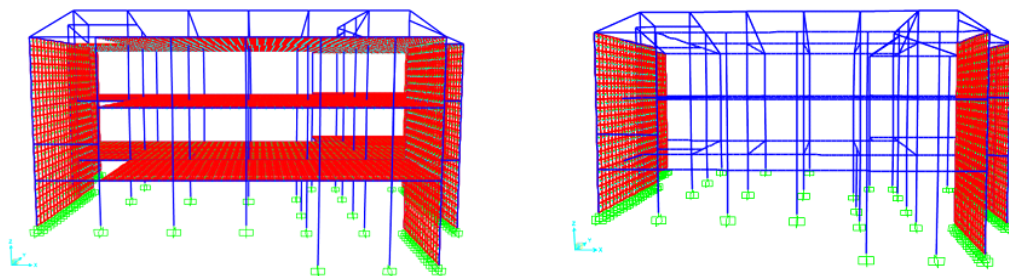
Fig. 3.30 – FE models with RC walls

In terms of modal analysis, the comparison of results presented in table 3.5 shows that, already from the fundamentals T, the difference are not negligible. In particular, the model with flexible floor has a first T higher than another one. In the same way to the previous models, the value of the fundamental vibration mode is shown. In this case, the inclusion of walls in the models cause the inversion of fundamental vibration mode direction (in long direction), which is above indicated as modal shifting phenomenon.

Tab. 3.5 – Comparison between models with RC walls, with rigid floor assumption and not

Model with rigid floor assumption	Model with orthotropic shell
1st mode – T = 0.4565 s $M[\%]_x$ =76.2%; $M[\%]_x$ =0.0%; $M[\%]_x$ =0.0%	1st mode – T = 0.5467 s $M[\%]_x$ =75.67%; $M[\%]_x$ =0.0; $M[\%]_x$ =0.0%

The main consequence of what shown in table. 3.5 is that the $S_a(T_1)$ can be very different, for the same building modelled through different initial hypotheses. In a practitioners perspective, for performing a linear response spectrum analysis or linear static analysis on a model as the our one, the flexible floor lead to have a first T greater, which correspond to a $S_a(T_1)$ shifted to right in the elastic spectrum. This observation can be evaluate differently, due to the case analysed. In fact, if the model has low period (compared to the plateau), the shifting of $S_a(T_1)$ can provide a seismic action greater than the one with rigid floor and the situation is conservative. On the other hand, if the model has high period (compared to the plateau), the shifting of $S_a(T_1)$ can provide a seismic action lower than the one with rigid floor and the situation is not conservative. For this latter case, structures with higher Ts can be the ones with more storeys and large mass or lower stiffness. For the cases with more storeys, as shown in the previous sensitivity analysis, the variation with the rigid floor model become minimum as the number of storeys increase and this means that the shifting is lower. For models with large mass or lower stiffness, the solution is not conservative, but the hypotheses of rigid floor could be initially assessed, always considering the general standards (in terms of geometrical, mechanical and vertical loading configuration) of these kinds of structures. Coming to talk about the case study, in figure 3.31 is shown the in-plan deformed shape of building with RC walls, with rigid floor and not, under the same loading condition. The results, in terms of structural behaviour, is strongly different, caused by the two different hypothesis made on floor system. In particular, the floor system in the model with slab made by shell elements, has a deformed shape at each level similar to the one obtained by a support beam under uniformly distributed load, usually called "arch effect". In addition, stress distribution on structural elements, derived by the same static analysis, is different between two models, as shown in table 3.6 where is reported the percentage differences in terms of V_b distribution between walls and columns, under rigid floor assumption and not. Supposedly, rigid floor assumption is not accurate in this case.
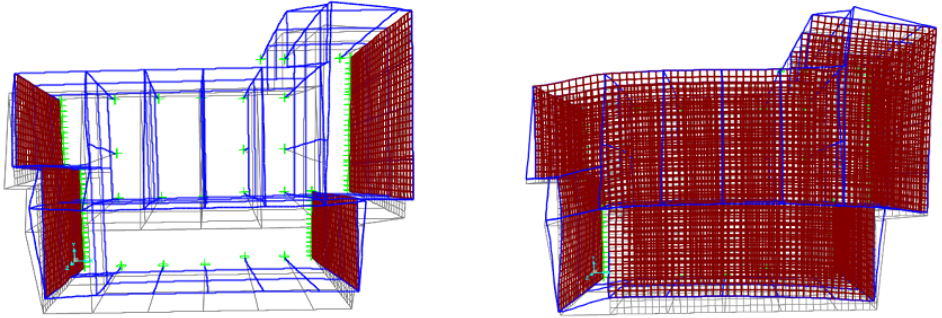
Fig. 3.31 – Comparison of in-plan deformed shape between models with RC walls, with rigid floor assumption and not

Tab. 3.6 – Stress states differences between models, expressed in terms of total base shear percentage

Model with rigid floor assumption		Model with flexible floor	
$V_{b,walls}$ (%)	$V_{b,frame}$ (%)	$V_{b,walls}$ (%)	$V_{b,frame}$ (%)
98	2	89	11

In order to verify the reliability of method proposed, same building with RC walls has been modelled using the "strut model". Since not all floor parts are square (necessary requirement for applying the strut model methodology), each one has been divided into square portions and, following the eqs. 3.10 and 3.11, the areas of struts were computed (similar for all levels). Assuming the struts as square, section dimension have been calculated through square root of areas founded, as written in 3.12. In table 3.7 are summarized the dimensions of struts section for all floor field, numerated as in figure 3.29. In figure 3.32, the building with slab modelled through struts on each floor is showed. The choice of performing a comparison of results obtained from the use of equivalent shell with those obtained by a model where slab is simulated with a more consolidate method like the "strut model", is due to the simplicity that this latter macro-modelling method hides. In fact, this kind of modelling has the ability to predict the real

global behaviour of structures, adding that the properties of the strut elements are simply computable.

Tab. 3.7 – Dimension of struts for each floor field

Floor field	Dimension of struts (cm)
1	35.34
2	37.54
3	45.23
4	55.85
5	35.62
6	10.76
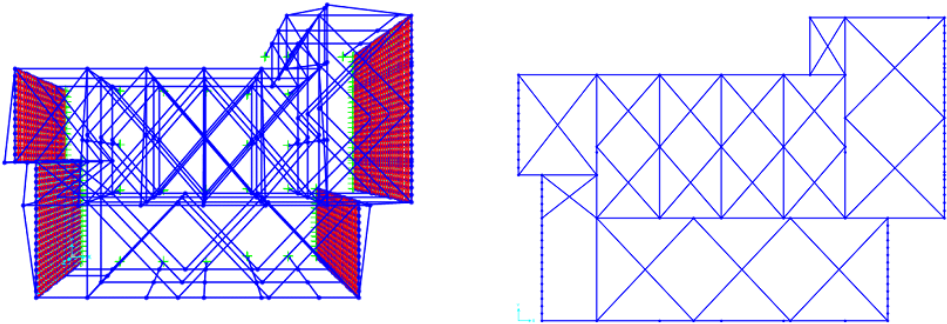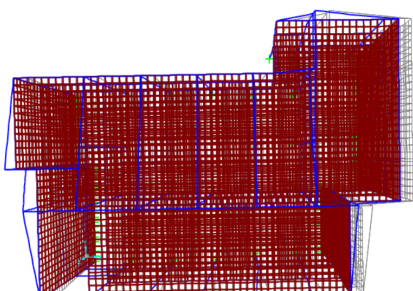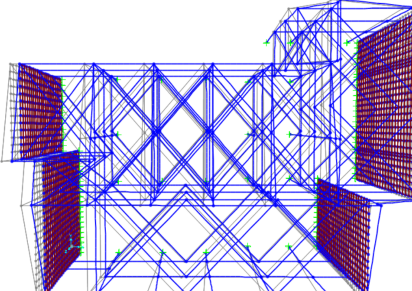
Fig. 3.32 – Building investigated with slab modelled through equivalent struts

Performing the same analysis on the model with slab simulated through struts, the results are shown in table 3.8 and 3.9, wherein is reported the comparison, respectively, of the V_b distribution in frame and RC walls and the modal parameters.

Tab. 3.9 – Stress states differences between models, expressed in terms of total base shear percentage

Model with orthotropic shell		Model with struts	
$V_{b,walls}$ (%)	$V_{b,frame}$ (%)	$V_{b,walls}$ (%)	$V_{b,frame}$ (%)
89	11	88	12

Model with orthotropic shell	Model with struts
1st mode – T = 0.5467 s M[%]$_x$ =75.67%; M[%]$_x$ =0.0; M[%]$_x$ =0.0%	1st mode – T = 0.5625 s M[%]$_x$ =76.18%; M[%]$_x$ =0.0; M[%]$_x$ =0.0%

As foreseeable, the models are similar (with percentage differences in order of 10%). In addition, the in-plan deformed shape of strut model is strongly similar to the one obtained by model with equivalent shell, as depicted in figure 3.33.
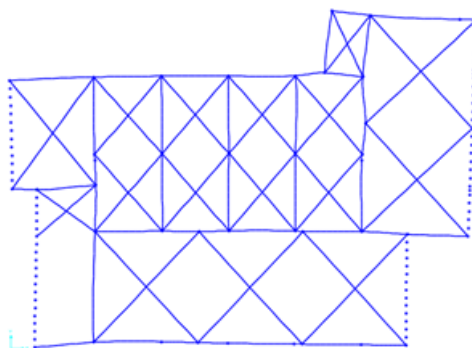
Fig. 3.33 – In-plan deformed shape of the strut model, under horizontal actions

It is worth mentioning that the difference between the model proposed and strut model is due to the possibility of displaying the distribution of in-plan stress states, which does not be provided by a model with struts. The main advantage of the equivalent shell of orthotropic material is that, by using a computational source that wants

125

low efforts, it is possible to carry out local and global assessment of top concrete slab and joists. Furthermore, also the stress distribution in the slab elements is greatly different from results obtained by model with rigid floor assumption. Figure 3.34 shows the in-plan stress states of a floor system of the case study. Near to the figure, it is provided a grey scale with both tensile state of light colour and compression states of dark colour. The values attached to the grey scale are based on the horizontal forces applied with values above provided. The in-plan stresses distribution shows the arch effect, in the case of retrofit solution with RC walls.
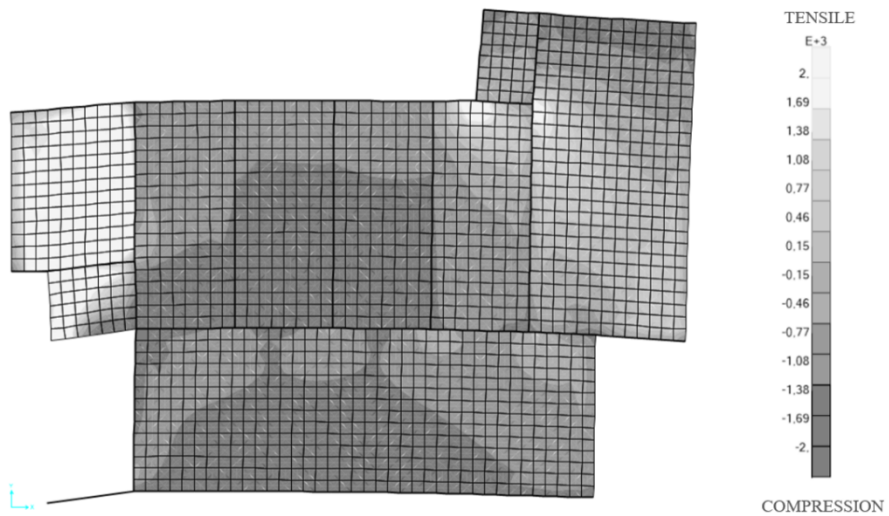
Fig. 3.34 – In-plan stresses distribution of building investigated under linear static analysis

For concluding, the numerical procedure presented allow of computing an equivalent shell of orthotropic material for a RC ribbed slab with lightening blocks, based on a sensitivity analysis performed on micro-models. The main advantaged of the proposal are the possibility to avoid of a-priori fixing hypothesis about the floor stiffness, maybe according to indication of International seismic code. The use of methodology, advantageous in the local and global assessment view, allow of computing a realistic deformed state of building under horizontal action, in elastic field. Generally, it can be used also in model with NL structural elements, in the case in which the aim of the analysis is to investigate the behaviour of structural element, overall when they are

subjected to retrofit solution. Here, it is usual to increase the dimension of vertical elements or their stiffness through reinforced material (as fiber-reinforced plastic). As shown in the case study investigated, the in-plan deformed shape obtained with a static linear analysis shows that the V_b distribution among vertical elements (columns and walls) results quite different. In the model with rigid floor assumption, V_b is almost completely assigned to RC walls while, in the model with equivalent shell, a larger part of V_b is assigned to frame system, as confirmed in the scientific literature. Lastly, a relevant advantage provided by the equivalent shell, compared to a more consolidate method for simulating the slab behaviour as "strut model", is the exactly characterization of the in-plan stress states of slab system, under horizontal actions, useful for the structural verification of elements that constitute the slab.

3.5 Infill panels: behaviour under seismic actions

The non-structural elements as the infill panels assume a fundamental role in the study of fragility and vulnerability of existing RC buildings. The observation after the earthquakes events showed that in RC buildings designed through old codes, the infill panels are usually "non-engineered", which means that they are linked with the surrounding frames, without presence of separation joints. This latter condition provides that masonry infills behave as structural elements, with an important and not negligible contribute to the seismic response of building. In particular, the masonry infills in existing RC buildings can induce a benefit, in terms of increasing of energy dissipation, stiffness and strength (Negro and Colombo, 1997, Kappos, 2000), with the result of reducing the horizontal displacement caused by seismic actions. On the other hand, the infill panels cause the increment of seismic demand, with consequent possibility of premature local collapse, induced also in the structural elements (without to forget the possible degradation of the bond-friction in the frame-infill contact length). In addition, in some cases, the infill panels can provide variation of global structural behaviour, such as the introduction of additional torsional actions of soft-storey mechanism in the cases of pilotis or short-column (Dolsek and Fajfar, 2001). With regard of these aspects, one should consider the effects after events, in which the structural behaviour of

a RC building can be strongly modified by a brittle failure of panels, which change the equilibria of the stresses in the building elements. That abovementioned suggests that the influence of infill panels cannot be neglect in a numerical model, which want to predict the global response of the building, despite this usually happen in a practice-oriented analysis. In addition, the numerical model should account the nonlinearity of infill panels, considering the progressive degradation of strength and stiffness during cyclic loads. Regarding to the dynamic performance of infilled frames, it is important to consider that, the failures of infilled frames occurs for frequent earthquakes, with low intensity. This causes that the infill panels are subjected to a larger acceleration then the one at the ground, phenomenon that is amplified, in terms of possibility of failure, for the low ductility and the low damping capacity. At the same time, the T of building reduces, with consequent variation of $S_a(T)$. Regarding to the code prescription, EC8 and NTC08 consider that masonry infill are non-structural elements and, for this reason, they do not contribute in the lateral resistance. In addition, the codes mention that in the case in which the infill panels contribute in the lateral resistance, they should be taken into account in the seismic analysis. This aspect anyway is not ruled, with definition of fixed threshold for estimating when the damage collapse at DLS starts. In the last 60 years, a lot of researcher investigated this problem, developing FE models based on the results of numerical investigation. The relevance of the infills is also due to the paramount value, in terms of economic and human lives losses after seismic events, to whom the existing RC buildings are subjected. It is worth mentioning that in this view, one should consider both in-plan and out of plane response of infill panel to seismic actions. The out of plane assessment needs of different characterization, such as shown in (Ricci et al., 2018 and reference therein), which is not focus of this thesis. The author is going to report information provided by most important works of scientific literature about the behaviour and in-plan response of infill panels (the literature is very extensive) and, in the next section, the numerical models proposed in the time. Concerning to the behaviour of infill panels and surrounding frame, the possible failure mechanisms of masonry panels can be subdivided in shear, flexural and compression ones, while for the concrete frames, it is possible to have flexural, axial, shear failures,

besides to beam-column joints failures. In details, in order to consider the coupling of masonry panel and surrounding frame, as reported in (El-Dakhakni et al., 2003, Asteris et al., 2011) the possible failure mechanisms due to horizontal actions have been summarized as follow. In particular, as shown in figure 3.35, it is possible to have the following possibilities:

- Diagonal compression failure, which is given by diagonal cracks in the centre of infill. This kind of failure is usually due to the geometric properties of infill, such as the slender;

- Diagonal cracking failure, which is identifiable through some cracks, along to the compression diagonal of infill panel. This kind of failure is usually due to weak frame or strong frame with weak infill of strong frame with strong infill and weak joints;

- Sliding shear failure, which is given by a horizontal sliding along the bed joints of infill. This kind of failure is usually due to the poor mechanical features of mortar presents in the joints;

- Corner crushing failure, which exhibits crushing at the corners of infill. This kind of failure is usually due to weak infill panel with strong elements in the frame and weak joints;

- Frame failure crushing, which is given from by the plastic hinges in the surrounding frame. This kind of failure is usually due to weak frame or frame with weak joints.

The above list is the result of some numerical investigations, in which researchers, varying mechanical and geometrical parameters of their tests, observed these occurrences. The first studies about infilled frames was proposed in (Polyakov, 1960), where after experimental tests on infilled steel frames, the author suggested that the panel worked as a diagonal braced. In (Holmes, 1961) almost 15 full scale and small scale tests were conducted, under rocking and shear loading on infilled steel frames. The author confirmed what proposed in the previous research and proposed a method for computing an equivalent dimension of the braced for numerical models. In (Stafford-

Smith, 1962) a set of three infilled frames was investigated and the author proposed a new method for computing the dimension of strut, which simulate the diagonal brace, accounting for the influence of the mortar and the panel stiffness. In (Mainstone, 1971) monotonic experiments on full scale tests of concrete infilled frames were performed and an empirical formulation for computing the dimension of the brace, dependent by relative stiffness between frame and infill panel and length of the diagonal brace was provided.
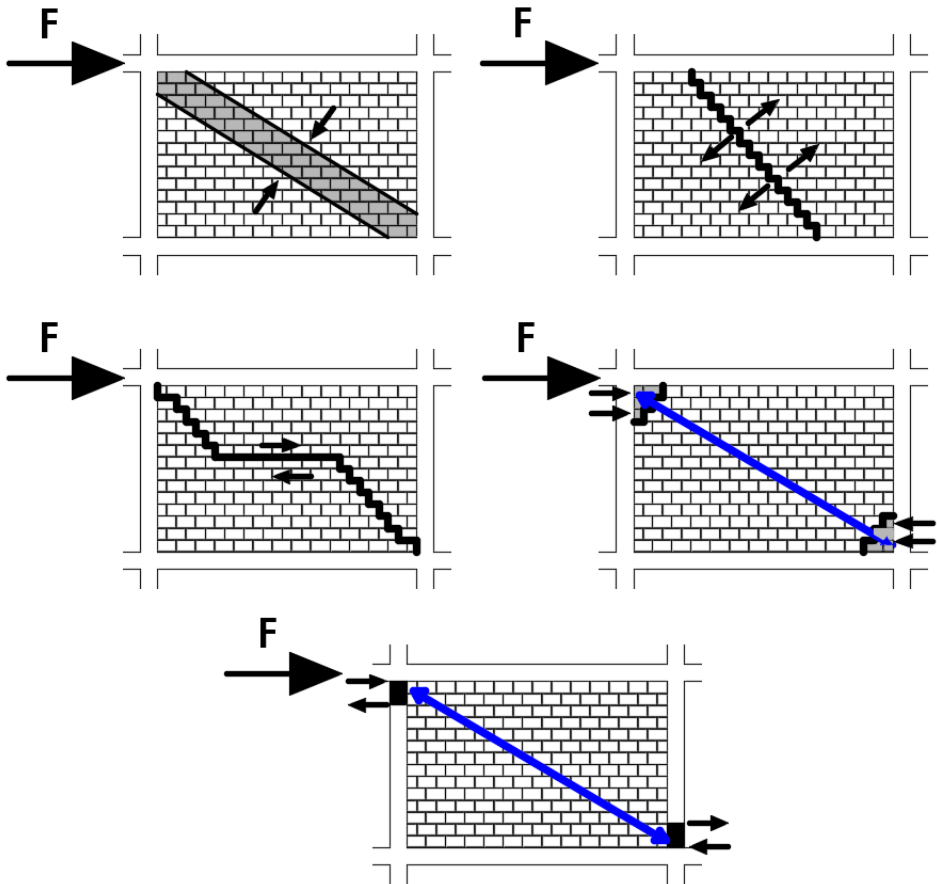
Fig. 3.35 – Possible failure mechanisms of infilled frames under seismic actions

In (Zarnic and Tomazevic, 1988), almost 30 specimens of bare and infilled frames were investigated through cyclic loads, accounting for the variation of materials

(clay and concrete blocks) and presence of openings. Comparing the bare and infilled frames, authors defined that the infilled one were characterized by greater strength and stiffness and lower ductility than the bare ones. In (Dave and Seah, 1989) authors collected experimental results of precedent researches, analysing the influence of several variables, as the stirrups in the columns, the mortar strength, the gap between panel and beam, the friction between panel and frame and the openings in the panel. Authors concluded considering that, infill panels gave extra stiffness and a major ultimate strength and they provided observation about the variables considered, from the stiffness and strength variation point of view. In (Crisafulli, 1997) the most common failure mechanisms were provided, due to his experimental tests data. In particular, author investigated the specimen through monotonic loads, assessing the stress states in the structural elements (e.g. columns of infilled frames had a bending moment almost six times greater than the same one in bare frames) and highlighted the behaviour of infill panels during the pushing, considering all elements. Finally, as shown in a subsequent work (Crisafulli et al., 2000), author provided the possible shear failures of infill panels and subsequently proposed a refined backbone curve with a hysteresis rule for cyclic loadings, all implemented on a numerical model. In (Kappos et al., 1998), 24 single storey RC frames (small scale) were investigated under cyclic loading, up to a displacement of 3% of drift. Authors varied several parameters, as the slender of the frame, the thickness of masonry panels, the external force in terms of axial loading and longitudinal reinforcement of columns. As result, it was provided a trilinear constitutive law, where the global shear response was computed as sum of the bare frame and the panel. This latter assumption, common in the research world, was better represented in the computation provided in (Gentile et al., 2018), where authors separated the contribution of the masonry panels from the RC frame, through equilibrium equations, at each instant, of the internal vertical forces. In (Fardis and Panagiotakos, 1997), based on the constitutive law previously developed (Panagiotakos and Fardis, 1994), authors performed sensitivity analyses using NLD analyses on a 4-storeys building, varying the infilled panels (bare, partially and fully infilled). Authors evaluated the dynamic behaviour of case study, before and after the panel cracking and considering the variation of

the properties of the panels, in which there were weak and strong infills. Comparing their results with code prescriptions, authors assessed several irregular configurations, with global and local responses. With regard of weak infills, in (Calvi and Bolognini, 2001), experimental tests on single storey specimens with weak infills were performed and the authors assessed that, inserting a little reinforcement, the seismic response of system had a great improvement. In (Dolsek and Fajfar, 2001) a study about the influence of the mechanical characteristics of infill panels on the seismic demand was proposed, with the aim of considering the infill panels in the N2 method. In particular, a new relationship was proposed, accounting for a typical force displacement law with degradation of infill panels, developed in (Dolsek and Fajfar, 2004), which will be reported in the next Section. Subsequently, the same authors (Dolsek and Fajfar, 2008a and Dolsek and Fajfar, 2008b) investigated a case study through deterministic and probabilistic approaches, in order to determine the influence of the masonry infills on the performance at several LSs. Regarding the probabilistic analysis, authors defined the failure probability, considering the uncertainties due to the properties of infill panels. The results of other experimental tests are reported in (De Risi et al., 2018, see reference therein), considering that the main aim of the tests are to calibrate a numerical model faithful to the real behaviour of infilled frames under seismic actions.

3.5.1 Numerical models

The seismic analysis of existing RC buildings, as just mentioned in the previous Section, should account the presence of infill panels, overall with regard of seismic performance for serviceability LS. For considering the infill panels in the FE models, one should insert numerical elements, able to account the properties of the masonry panels and to predict both local and global response of building and its parts. In this frame, the scientific literature provides several techniques for modelling the masonry panels, also considering the orthotropic nature of the material, due to the presence of two materials: brick and mortar. Generally, it is possible to distinguish three kinds of modelling (figure 3.36), basing on the accurateness level that one want to reach:

- Micro-models (micro-scale), in which brick and mortar joints are modelled as discrete FEs and the interface between the above elements are modelled as interface element. All numerical elements are modelled as NL, with assignment of NL stress-strain constitutive law;

- Simplified Micro-models (meso-scale), in which only the bricks are modelled as discrete FEs, while mortar joints and interface are considered as an unique interface model, among the bricks. All numerical models are modelled as NL, with assignment of NL stress-strain constitutive law;

- Macro-models (macro-scale), in which all elements are condensed in a unique numerical element that should account for all possible mechanisms. In particular, it is possible to have a homogenized model, wherein bricks, mortar and interface are condensed in an unique discrete FE or a strut model, which is an equivalent diagonal brace, to whom assign elastic and inelastic properties based on the observation of the seismic load path in the frame.
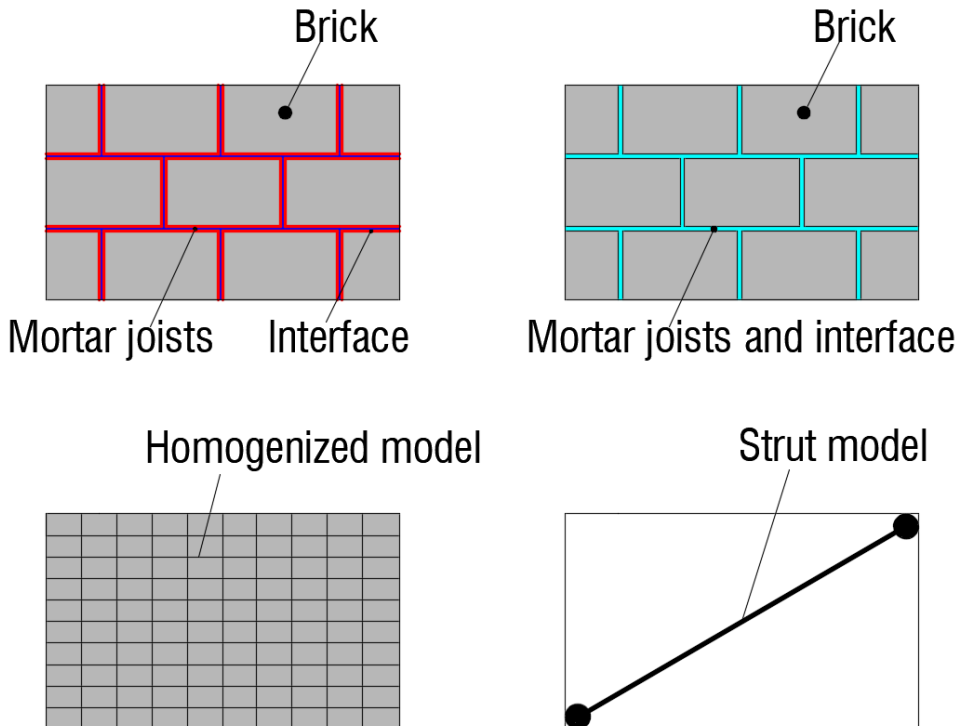
Fig. 3.36 – Modelling kinds for the masonry panels

The micro-models present a greater accurateness than the macro-models, but the computational efforts are elevated. In fact, in the practical application, the most used method is the macro-model with equivalent struts, due to its simplicity and versatility to simulate a lot of properties highlighted in the scientific literature. On the other hand, this kind of modelling presents some problems related to the elevated variability of the parameters for defining the linear and NL parameters (usually one can have no physical correspondence with the reality) and the kind of failure to account. In this section, the author is going to describe some features related to the infill modelling with struts, not reporting information about the micro-models, because not used in the practice. Regarding to the definition of equivalent struts, the necessary parameters for the modelling are summarized below, as provided in (Uva et al., 2012):

- The width of the strut (b_w);
- The constitutive relationship of the panel and hysteretic behaviour to cyclic loads;
- The number of struts used.

Concerning to the geometrical definition, the section of a strut is usually rectangular with sides composed by the transversal dimension of the panel and b_w. A lot of researchers provides in the scientific literature criteria for computing b_w. It is important to specify that the role b_w in a FE model is to provide a real prediction of the initial stiffness of the undamaged panel (elastic field). The most simple formulation of this quantity were provided in (Holmes, 1960), where $b_w = 0.33d$, in (Paulay and Priestley, 1992), where $b_w = 0.25d$ and (Penelis and Kappos, 1997) where $b_w = 0.20d$. In these latter formulations, d represents the length of the diagonal strut, measured between the opposite nodes of the frame. Some authors, for accounting the mechanical and geometrical parameters of the infill panel and the surrounding frame, provided formulations for defining b_w. In (Stafford Smith, 1966) author computed the b_w as function of the relative stiffness between frame and panel (λ), defines as:

$$\lambda = \sqrt[4]{\frac{E_w t_w sin2\theta}{4E_c I_c H_w}}$$

(3.14)

where E_w is the elastic modulus of masonry, E_c is the elastic modulus of concrete, t_w is the thickness of the panel, I_c is the moment of inertia of the column, H_w is the height of the panel and θ is the slope of the diagonal strut. Based on the λ, some formulation were proposed, such as in (Mainstone, 1971 and after adopted in Klingner and Bertero, 1976) where:

$$b_w = 0.175d(\lambda H_w)^{-0.4} \qquad (3.15)$$

In (Kadir, 1974) the parameter λ was subdivided in two parts, dependent from the columns and beams of the surrounding frame. In particular, the λ computed in eq. 3.14 was considered as λ_c (for the columns), while the λ_b (for the beams), was defined as:

$$b_w = \frac{\pi}{2}\left(\frac{1}{4\lambda_c^2} + \frac{1}{\lambda_b^2}\right) \qquad (3.16)$$

In (Dave and Seah, 1989) a similar formulation to the previous one was proposed:

$$b_w = \frac{2\pi}{3}\left(\frac{cos\theta}{\lambda_c} + \frac{sin\theta}{\lambda_b}\right) \qquad (3.17)$$

In (Bertoldi et al., 1993), authors provided a formulation for accounting the response of masonry panels under cyclic loads, as function of two parameters k_1 and k_2, which are dependent from the value of λ. In particular, the formulation was proposed in the following equation:

$$\frac{b_w}{d} = \frac{k_1}{\lambda H} + k_2 \qquad (3.18)$$

In (Flanagan and Bennet, 2001), the formulation of the strut area (A) was proposed, as function of an empirical constant C, which varied based on the in-plan drift displacement:

$$A = \frac{\pi t_w}{C\lambda cos\theta} \qquad (3.19)$$

In (Papia et al., 2003), in the formulation of b_w, a parameter for considering the effect of axial stiffness was inserted, in addition to the lateral one. In particular, the

formulation depended from two parameters, called β and c, empirically calibrated. A new definition of λ was proposed, called λ*. In particular:

$$b_w = d\frac{c}{z}(\lambda^*)^{-\beta} \tag{3.20}$$

$$\lambda^* = \frac{E_{w\theta}}{E_c}\frac{th}{A_c}\left(\frac{H^2}{L^2} + 0.25\frac{A_c}{A_b}\frac{L}{H}\right) \tag{3.21}$$

where $E_{w\theta}$ is the elastic modulus of masonry, diagonally compressed, A_c is the section area of the adjacent column and A_b is the section area of the upper beam.

Concerning to the constitutive laws for simulating the NL behaviour of struts and NL hysteretic behaviour, several models were provided in the scientific literature. The most important solutions were the constitutive law proposed in (Panagiotakos and Fardis, 1996), and in (Bertoldi et al., 1993), as sown in figure 3.37. The first one is suggested in the EC8 and is actually the more used from practitioners. The second one is more complete, from the simulated mechanisms point of view.
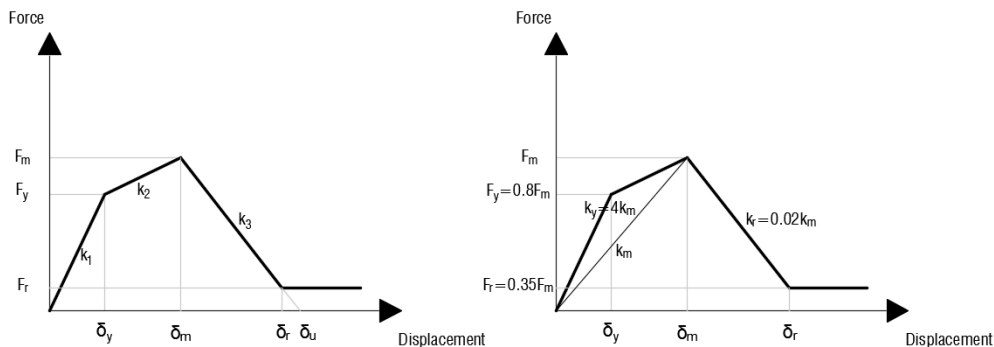
Fig. 3.37 – Constitutive law proposed by (Panagiotakos and Fardis, 1996) and (Bertoldi et al., 1993)

Four branches composed the force-displacement relationship proposed in (Panagiotakos and Fardis, 1996), where the first one represents the elastic stiffness and shear behaviour of un-cracked panel. The second branch represents the post-elastic response with a reduction of the stiffness, due to the detachment between frame and masonry panel. The third branch represents a softening behaviour of the panel and

the last one simulate a residual axial strength, with a horizontal segment with a constant force. Following the indications of the figure 3.36, the initial stiffness k_1 is computable as:

$$k_1 = \frac{G_w t_w L_w}{H_w} \tag{3.22}$$

where G_w is the tangential elastic modulus of the masonry and L_w is the length of the panel. The yielding force F_y is given by:

$$F_y = f_{tp} t_w L_w \tag{3.23}$$

where f_{tp} is the tensile strength of the panel, evaluated after a diagonal tests. The yielding displacement is given by:

$$\delta_y = \frac{F_y}{k_1} \tag{3.24}$$

The second branch has the following stiffness:

$$k_2 = \frac{E_m b_w t_w}{d} \tag{3.25}$$

which correspond to a maximum Force (F_m) and the related displacement:

$$F_m = 1.3 * F_y \tag{3.26}$$

$$\delta_m = \delta_y + \frac{F_m - F_y}{k_2} \tag{3.27}$$

Finally, the stiffness of softening branch (k_3), the residual force (F_r) and the ultimate displacement are given by the following assumptions:

$$0.005k_1 \leq k_3 \leq 0.1k_1 \tag{3.28}$$

$$0 \leq F_r \leq 0.1F_y \tag{3.29}$$

$$\delta_r = \delta_m + \frac{F_m - F_r}{k_3} \tag{3.30}$$

Concerning to the constitutive law proposed in (Bertoldi et al., 1993), it was a quadrilinear force-displacement relationship, similar to the previous model, where the most important parameters are the F_m and k_m (according to figure 3.37). In particular, the previous parameters are given by:

$$k_m = \frac{E_w b_w b_w}{d} cos^2\theta \tag{3.31}$$

$$F_m = (\sigma_w)_{min} t_w b_w cos\theta \tag{3.32}$$

where F_m is function of the four possible failure mechanisms, identified as σ_w. In particular, the occurrence considered are the crushing at the centre of panel (σ_{w1}), the crushing of the panel corners (σ_{w2}), the sliding of horizontal bed joints (σ_{w3}) and the diagonal tensile failure (σ_{w4}), computable as below:

$$\sigma_{w1} = \frac{1.16\,\sigma_{m0} tan\theta}{k_1 + k_2 \lambda H} \tag{3.33}$$

$$\sigma_{w2} = \frac{1.12\,\sigma_{m0} sin\theta cos\theta}{k_1 (\lambda H)^{-0.12} + k_2 (\lambda H)^{0.88}} \tag{3.34}$$

$$\sigma_{w3} = \frac{(1.2\,sin\theta + 0.45 cos\theta)u + 0.3\sigma_0}{\dfrac{k_1}{\lambda H} + k_2} \tag{3.35}$$

$$\sigma_{w4} = \frac{0.6\tau_{m0} + 0.3\sigma_0}{\dfrac{k_1}{\lambda H} + k_2} \tag{3.36}$$

where σ_{m0} is the compressive strength of masonry infill, τ_{m0} is the shear strength of the masonry infill, given by a diagonal compression test, u is a parameter that accounts for the sliding of the mortar joint and σ_0 is the mean of the normal stresses, which acts on the panel. Besides these two solutions, which are the most used, other authors calibrated the force-displacement behaviours (cyclic and mono-tonic). In (Paulay and Priestley, 1992) the force-displacement relationship of the strut was computed accounting for the mechanisms of diagonal tension cracking, bed joint sliding and diagonal compression, based on the axial force value. In (Saneinejad and Hobbs, 1995), a bilinear constitutive law was calibrated, as function of geometry of the frame, ductility and cracking and crushing loads. In particular, the maximum forces of the diagram parts were F_{cr} (cracking load) and F_{max} (crushing load), while the maximum displacement was δ_{cap} (function of ductility). In (Crisafulli, 1997) a trilinear stress-strain backbone was proposed, based on the variation of several parameters, among which the axial force. In (Dolsek and Fajfar, 2008a) a trilinear constative law was proposed,

accounting for an elastic part, hardening and post-capping branch with null residual strength (unique consistent difference with the model of Fardis), based on a previous work of (Zarnic and Gostic, 1997). In particular, the maximum shear strength of the infill panels was computed with the following equation:

$$F_{max} = 0.818 \frac{L_w t_w f_{tp}}{C_I} \left(1 + \sqrt{C_I^2 + 1} \right) \tag{3.37}$$

$$C_I = 1.925 \frac{L_w}{H_w} \tag{3.38}$$

Furthermore, they assumed the post-capping slope as 20% of the initial stiffness, a capping displacement as 0.2% of drift ratio and F_{cr} as 60% of the same value in the work of Zarnic and Gostic. An important aspect of this constitutive law is that, to difference of the previous laws, F_{max} is considered with its projection in the in the horizontal direction, because the aim of authors was to insert in the infill law, the masonry contribute in the horizontal displacement of the infilled frame. Regarding to the cyclic behaviour, one of the first proposal was provided in (Klingner and Bertero, 1976) that proposed a NL hysteretic response of the strut, accounting the strength degradation and deterioration for the initial stiffness reloading. In (Panagiotakos and Fardis, 1996) a hysteretic model was proposed, based on interstorey force-interstorey drift relationship. Using three empirical parameters calibrated, authors proposed a way for simulating the loading and unloading branches, with the above-described backbone. In (Crisafulli, 1997 and Crisafulli and Carr, 2007) a detailed cyclic model was proposed, able to account some failure mechanisms, such as strength and stiffness degradation, by observing a lot of cyclic experimental tests. In (Cavaleri et al., 2005 and Cavaleri and Di Trapani, 2014) a modification of the model of Bertero was proposed, where the cyclic behaviour was simulated through the Pivot model, accounting the pinching effect during the reloading. The branches of unloading and reloading were simulated as function of three parameters.

Concerning to the number of struts, the use of a single strut is useful for describing the global behaviour of the building investigated, but it is not able to account

the local interaction between the masonry panel and the structural elements of the surrounding frame. The major problem that a multiple struts model is able to solve, despite the increment of computational efforts, is a right computation of the stresses distribution between the frame and the masonry panel. This can totally modify the local behaviour of the frame, considering the cases in which the FE models are sensitive to the brittle shear mechanisms. Furthermore, by using a single strut model, it is not possible to predict failures in the beam-column joints. Generally, the force-displacement backbone of assigning to a multiple strut model, should be the same of the single strut one, but the b_w should be reduced, which means a subdivision of elastic stiffness in the number of struts employed. Lastly, a main parameter to estimate is the distance from the node to the position of the end part of the struts, which can be different among different modelling ways. One of the first proposal was provided in (Symakezis and Vratsanou, 1986), where the authors used five parallel struts with a result of accurate estimation of bending moment on the frame elements, after an analysis on the value of the contact length. In (Zarnic and Tomazevic, 1988), a single strut model was performed, but varying the slope of the strut, linked a beam-column joint with a point of the column, calibrated on the results of cyclic tests. In (Chrysostomou, 1991), in order to simulate the stiffness and strength degradation, author proposed a model with six diagonal strut, three for each direction (figure 3.38), where the external ones were positioned in a determined point of column, as function of a parameter, called α, directly dependent from the plastic hinge length. In (Saneinejad and Hobbs, 1995) a model with two struts was proposed, through the performance of a sensitivity analysis, in order to predict the influence of the limited ductility provided by masonry panel. In (Crisafulli, 1997 and Crisafulli and Carr, 2007), for accounting the axial and shear behaviour of the panel, a macro-model was proposed, constituted by a four nodes linked by two struts. Between them, a shear spring was located, where it was function of shear friction mechanism (figure 3.38). This latter was calibrated based on shear stress, axial loads and geometry of the infill panel. The area of the struts and the contact length (H_z) were computed as function of the axial strut displacement, in order to estimate the cracking of the masonry infill. In (El-Dakhakhni et al., 2003), a model with three non-parallel

struts was proposed, in order to predict the interaction between masonry panel and RC frame, accounting for the right distribution of bending moment and a possible corner crushing of the panel.
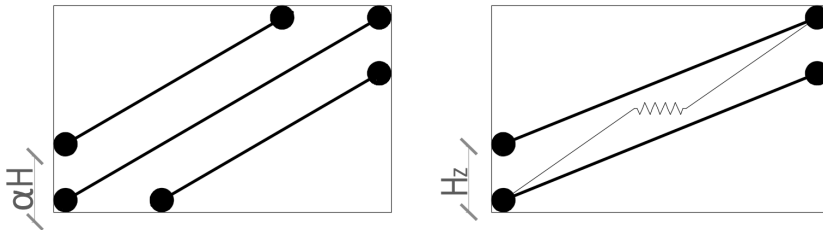
Fig. 3.38 – Multi struts model proposed in (Chrysostomou, 1991) and macro model proposed in (Crisafulli, 1997 and Crisafulli and Carr, 2007)

For concluding, it is worth mentioning that the above parameters could not be used as the analyst wants, because for each research work, a different behaviour of the infilled frames was observed, with the development of the features of numerical models, due to different mechanical and geometrical parameters of the specimens. In our context, the focus is aimed to the strong infills, which can provide others effects in the global behaviour, as will show in the next Section.

3.6 Interaction among principal, secondary and non-structural elements

In the vulnerability assessment of existing RC buildings, as just mentioned in the precedent Sections, the modelling phase assume a key role, especially based on the initial hypothesis about the FE model, which should predict the real response of the case study, under seismic actions. With this regard, the use of practitioners is to carry out an unique numerical model, which can account or not for the real behaviour of principal, secondary and non-structural elements, with the final goal of estimating the performance of the building at different LSs. In some cases, this can be a pretentious way to do, also considering that the usual initial hypotheses, able to reduce the computational efforts of the analyses, are not always conservative, such as explained for the floor deformability. On the other hand, a practice-oriented usage provide to perform the assessment procedure in a bit of time and in a conservative way, which is also the

philosophy of the technical codes. In fact, one has to think that the structural capacity of a building is given by the pushover curve with the lower CDR. In order to continue on this path, the scope of this Section is to try of defining how to change the global response of existing RC buildings, forgetting the usual hypotheses at the base of numerical models. To this scope, the author is going to account for all elements in some FE models, which simulate real existing RC buildings, evaluating the results due to the interaction among primary (beams and columns), secondary (slab) and non-structural elements (masonry panels). Before of analysing a real existing RC building, in order to become familiar with the above issues, a sensitivity analyses is necessary. Considering that the behaviour of buildings, by considering the influence of secondary structural elements, as slab, have just been presented in a precedent Sections, to follow it is presented a preliminary sensitivity analysis about the global behaviour of infilled frames. In addition, knowing that the flexibility of the floor system is strongly influenced from the stiffness of vertical elements, the aim is to understand what could be the influence of the infill panels on the floor flexibility. The idea was the same to the one presented in (Uva et al., 2012), in which after a presentation of the scientific literature about the macro-models of infilled frames, a sensitivity analysis was performed, considering the variation of the main parameters that influence the NL modelling of struts, as the value of b_w, constitutive law and number of struts. The results showed that, assuming different hypotheses about the above parameters, some intervals in terms of pushover curves results were obtained. The analysis was performed on a frame extracted from a real existing RC buildings, where the mechanical parameters of the masonry infill was known after laboratory tests, among which the results of diagonal compression tests. The value of the masonry infill mechanical parameters are reported in table 3.9 and they will be used for all applications that follow. The sensitivity analysis proposed consists in a series of 2D pushover analysis on regular RC infilled frames, in which a reference model has been replicated, varying the following parameters:

- Number of storeys: 2, 4 and 6;
- Number of bays: 1, 2 and 4.

Regarding to the reference model of the frame, it is a simple trilithon frame, with height of 300 cm and span of 600 cm, according to the common dimension of the Italian existing RC buildings bays. Beams and columns were predesigned with a capacity design philosophy. In particular, beams have section of 40 x 40 cm, with longitudinal reinforcement of 3Φ16 placed at top and bottom of section and transversal reinforcement made with stirrups of Φ6, with two braces. Columns have section of 40 x 40 cm, with longitudinal reinforcement of 4Φ16 per direction, placed in each sides of section and transversal reinforcement made with stirrups of Φ8, with two braces and one pin. Mechanical parameters of concrete chosen are defined according to class C25/30, as classified in EC8, with f_c equal to 24.9 MPa, E_c of 31467 MPa, G_c of 11315 MPa and ν of 0.2.

Tab. 3.9 – Mechanical parameters of infill panels

Floor field	Value (MPa)
Elastic modulus E_w	3080
Diagonal elastic modulus $E_{w\theta}$	1495
Shear modulus G_w	1233
Tensile strength f_{tp}	0.36
Compression strength σ_m	2.5

The numerical models have been made by using the FE software SAP2000, modelling beams and columns as frames, fixed at the ground with fix restraints and assuming the hypothesis of rigid floor through an internal constraint. The geometrical and mechanical nonlinearities were modelled through a lumped plasticity approach. In particular, at the section ends of elements plastic hinges have been placed, which are defined considering inelastic mechanisms of simple bending for the beams and a combination of axial stress-bending stress for the columns. In both cases, the plastic hinges have been defined according to FEMA 356 rules (figure 3.8). Brittle mechanisms have been not accounted, as shear and beam-column joints, because the main aim of the

analysis is to predict the global response of the models, avoiding local failures. Consistently with the previous affirmation, the masonry infills have been modelled through the employment of a single strut, linked between the opposite nodes. It is worth mentioning that, with the view of pushover analysis, the single strut was placed taking into account the pushing direction. Generally, an infilled frame model should be made by two cross struts, modelled with an half of the initial stiffness, for accounting that, the numerical elements for modelling the struts have the same behaviour for tensile and compressive actions. This kind of model is also the right way for the modal identification of the case study. On the other hand, to use a single strut, which will be only compressed, is the most adopted and practical way in the field of pushover analysis.

Concerning to the sensitivity analysis about infills, the parameters assumed are the following:

- Constitutive law: (Panagiotakos and Fardis, 1996) and (Bertoldi et al., 1993), as shown in figure 3.37;
- Value of b_w: (Mainstone, 1971), as reported in eq. 3.15 and (Dave and Seah, 1989) eq 3.17.

The choice of constitutive law is not very arguable, due to they are the most used in the practical and scientific applications. Regarding to the choice of b_w dimension, the above proposal have been selected because they were the smallest and largest values among the methodologies proposed by the scientific literature. In fact, assuming a thickness of panel t_w of 20 cm and using the geometrical and mechanical parameters above provided about frame and masonry infill, the values of the b_w are the ones in table 3.10 (in bold the value assumed).

Concerning to the numerical model of the strut, it has been modelled as truss element, which allows of having only compressive (or tensile) stresses and free from shear, torsional and flexural actions. The geometrical and mechanical nonlinearities of infills have been modelled through a lumped plasticity approach. In particular, in the central section of elements a plastic hinge has been placed, defined considering inelastic mechanisms of axial ductile deformation. In the sensitivity analysis, the openings

in the panels have been not considered. Some of the numerical models made are shown in figure 3.39, while the numerical results of pushover curves, performed with a triangular inverse load pattern, are shown in the graphs collected in figure 3.40a, 3.40b and 3.40c, including the bare frame curve. In the legend of figures 3.40, the bare frame curve is indicated as BF, the constitutive laws of (Panagiotakos and Fardis, 1996) and (Bertoldi et al., 1993) are respectively indicated as PF and B, the b_w of (Mainstone, 1971) and (Dave and Seah, 1989) are respectively indicated as M and DS.

Tab. 3.10 – Values of b_w from the scientific literature, for the reference model

Scientific literature	b_w value (cm)
Holmes, 1960	221.37
Paulay and Priestley, 1992	167.71
Penelis and Kappos, 1997	134.16
Mainstone, 1971 and Kinglier and Bertero, 1976 – eq. 3.15	**78.71**
Kadir, 1974 – eq. 3.16	239.26
Dawe and Seah, 1989 – eq. 3.17	**310.10**
Bertoldi, 1993 – eq. 3.18	201.56
Flanagan and Bennet, 2001 – eq. 3.19	262.38
Papia et al., 2003 – eq 3.20	239.33
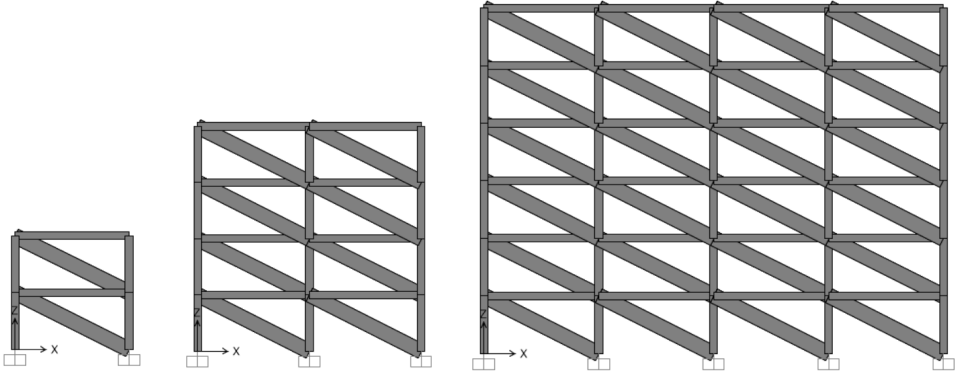
Fig. 3.39 – Some of the 2D infilled frames models performed in the sensitivity analysis

Figure 3.40a, 3.40b and 3.40c shows the possible structural response of the same cases, assuming different hypotheses about the infill modelling. In some cases, the results presented convergence problems, whit curves stopped after low analysis steps.
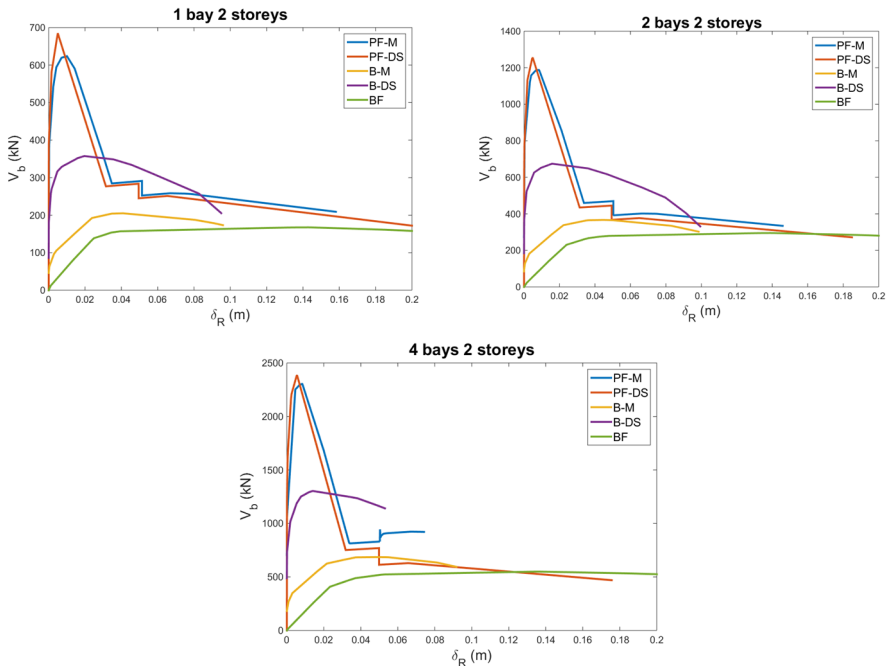
Fig. 3.40a – Results of sensitivity analysis for 2 storeys models
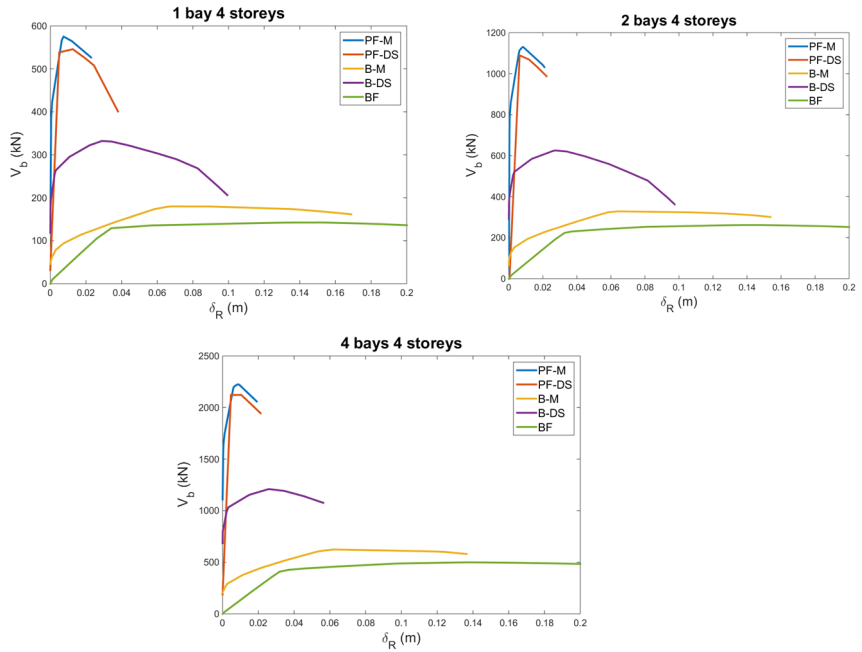
Fig. 3.40b – Results of sensitivity analysis for 4 storeys models
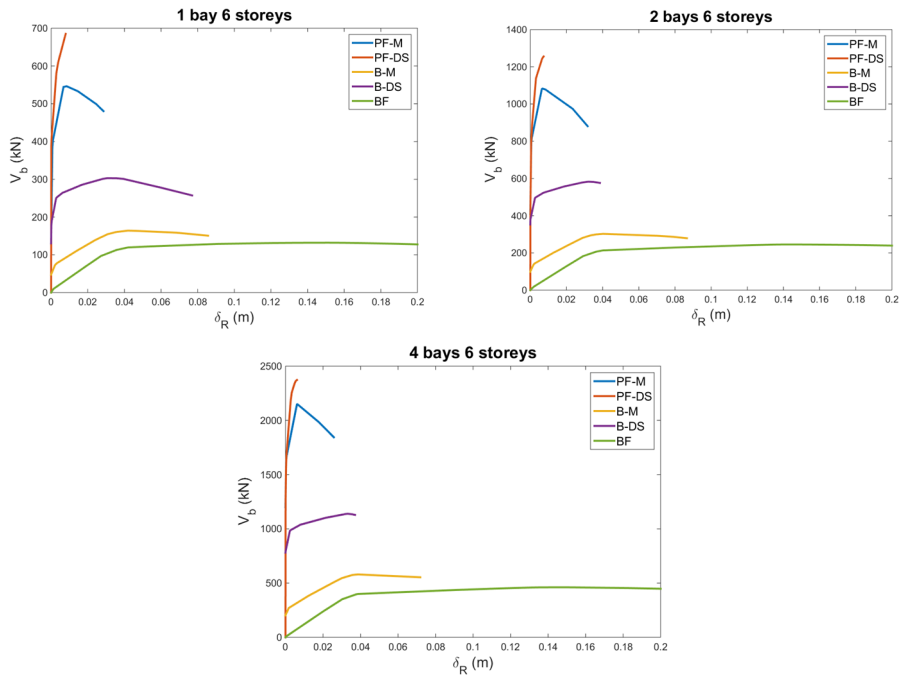
Fig. 3.40c – Results of sensitivity analysis for 6 storeys models

147

From the structural response point of view, the curves with constitutive law of Panagiotakos and Fardis, presented a strut with strong behaviour, with regard to the maximum shear strength. Furthermore, using this latter, the value of the b_w had negligible influence, considering a lower difference for the initial stiffness and a post-elastic behaviour comparable. The differences become more important when the number of storeys increase. In the other cases, using the constative law of Bertoldi et al., the strut manifested a weak behaviour, with regard of the maximum shear strength. In addition, the results showed important differences of shear, using different values of b_w. Lastly, as suggest by scientific literature, the curves trend to come back on the bare frame one, when the strut loses its capacity. Hence, the sensitivity analysis suggested of considering, in the analysis with flexible floor, a strut model modelled with a constitutive law of Panagiotakos and Fardis, independently from the relationship adopted for b_w, considering that the case studies that are going to be shown are low-rise buildings. Then, the b_w considered is the one of Mainstone, which is more common in the practical and scientific use.

In order to assess the interaction among principal, secondary and non-structural elements, a first application have been performed on two existing RC school buildings located in the city of Lesina, Province of Foggia, Puglia, Southern Italy. Both buildings, built between the 60s' and 70s, in the absence of specific seismic codes, was designed considering only vertical loads and neglecting constructive details able to cope the seismic action. They are constituted by RC frames with beams and columns and they have two storeys for a total height of 8.20 m. The first Building (E1) has an irregular in-plan shape, with significant re-entrances, inscribed in a rectangle of dimension 25.00 x 30.00 m, while the second Buildings (E2) has manly a regular in-plan shape, inscribed in a rectangle of dimension 26.00 x 9.50 m. The carpentries of both building are shown in figure 3.41. Dimensions of columns and beams, design loads and mechanical parameters of materials (determined through destructive and non-destructive in-situ investigation on concrete elements and steel rebar's), was performed within the abovementioned Agreement between "AdB Puglia" and "Polytechnic University of Bari" (Mezzina et al., 2011). In this case, geometrical, mechanical parameters

and loads surveyed on the two buildings are shown in the table 3.11, where B and H are the dimensions of beams and columns, G_1 and G_2 are the gravity permanent loads, Q is the live loads. The dimensions of beams and columns do not vary from the first to second level. In both cases, plinths connected by beams constitute the foundations and the orientation of elevation beams is usually in one way. The slab typology of buildings is a RC ribbed slab, with constant joists dimensions (height 20 cm, width 10 cm, and spaced 50 cm) and thickness of top concrete slab of 4 cm. Concerning to the definition of mechanical parameters of masonry infill panels, the values used are the ones in table 3.9. Assuming that the masonry typologies are same for the same geographic zone, the considered parameters simulate the results of investigation tests (in situ and in laboratory), which provided the constructive features, materials and dimensions of hallow clay blocks and mortars. In particular, the hallow clay masonry blocks are made with dimension 25 cm x 25 cm x 12 cm, while the mortar is constituted by Portland cement 325 and quarry sand.
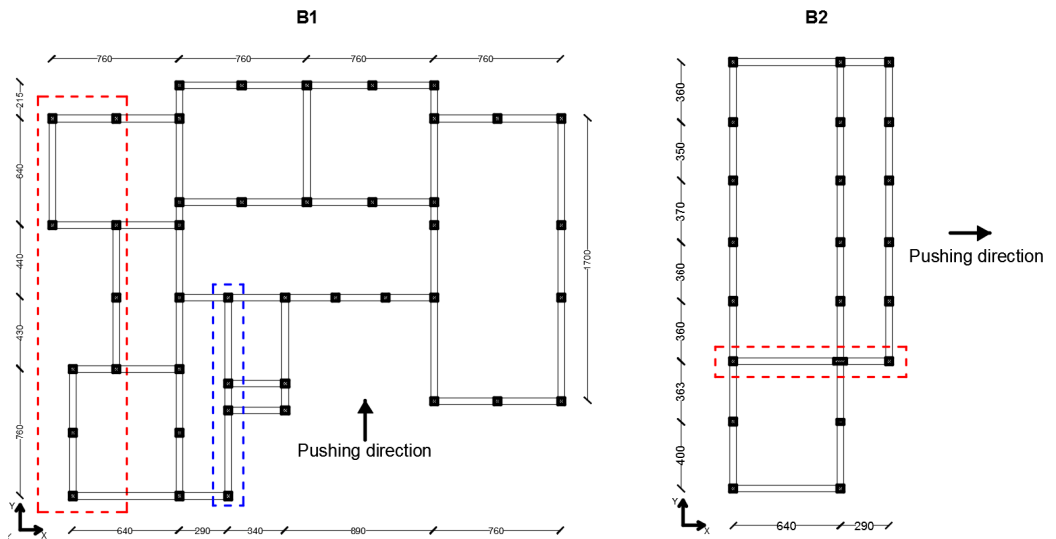
Fig. 3.41 – Carpentries of case studies E1 and E2

149

Tab. 3.11 – Dimension of the structural elements, design loads and mechanical parameters of materials

Case study	Elements	B (mm)	H (mm)	Materials (MPa)	Loads (kN/m²)
E1	Columns	500	400	f'_{cm}: 20	$G_1 = 3.50$
				f'_{ym}: 437	$G_2 = 2.50$
	Beams	400	600		$Q = 3.00$
E2	Columns	400	400		
		300	400	f'_{cm}: 24	$G_1 = 3.00$
		400	750	f'_{ym}: 450	$G_2 = 2.00$
	Beams	400	600		$Q = 3.00$
		400	900		

The structural modelling of the case studies have been performed by using the FE software SAP2000. Beams and columns have been modelled as one-dimensional frame elements, assuming fixed-end restraints at the base of the columns. FE models included the nonlinearity of materials and sections, simulated through a lumped plasticity approach. In particular, at the end sections of elements plastic hinges have been placed, defined considering inelastic mechanisms of simple bending for the beams and a combination of axial stress-bending stress for the columns. In both cases, the plastic hinges have been defined according FEMA 356 rules, as shown in figure 3.8. Brittle mechanisms have been not accounted, as shear and beam column joists, because the main aim of the analysis is to predict the global response of the models, avoiding local failures. Concerning the floor flexibility, the slab has been modelled considering and not the rigid floor hypothesis. In particular, in the case of deformability (FLEX), the floor has been simulated through the strut model, as ruled by eqs. 3.10, 3.11 and 3.12, while in the case of rigid floor (DIAPH), an internal constraint in each floor has been considered, concentrating the mass in the geometric centre of storeys. It is worth mentioning that these struts have been modelled as linear, does not taking into account the possibility of local failure in the slab and considering that the focus is on the global behaviour. For considering the presence of infill panels in the structure, the single strut method has been adopted, employing single equivalent struts on the external sides, parallel to the

pushing direction showed in figure 3.41 and able to simulate the real compressive stress under horizontal actions, following a diagonal path. The dimension and nonlinearity of the struts have been modelled as suggested by the previous sensitivity analysis. Based on the geometrical and mechanical parameters founded, for evaluating the influence of infill panels on the flexibility of floor system, the buildings have been modelled in the first phase as bare frame (BR), considering and not the rigid floor hypothesis. Subsequently, in the same models, the influence of infill panels have been taken into account (I). Finally, in order to exalt the strong behaviour of the infill panels and to evaluate the influence on the floor flexibility, a retrofit solution has been applied on the masonry, in order to obtain a system with infill reinforced panel (RP). Concerning to the retrofit method, as shown in (Fiore and Uva, 2013, Porco et al. 2014), one of the most common method adopted in the practice is the connection between the panel and the structural elements of the surrounding frame. In particular, this solution provides to reinforce the masonry panels through the insertion of strips of welded steel mesh combined with connecting tassels along the top and lateral edges or application of reinforced plaster on the whole panel. The main role of the methodology is to avoid the problems related to usual consequence of seismic events, in which the infill panels can be strongly damaged. This solution provides a way for preventing out-of-plane overturning of the panel and reducing undesired local effects at the end sections of columns. On the other hand, the methodology varies the infill contribution to the lateral strength, incrementing in-plan stiffness and strength, and consequently, provide an increment of the vertical stiffness. In order to take into account the retrofit solution, the constitutive law of the reinforced infill panels should be modified, increasing the mechanical parameters of struts, in terms of force and displacement, then in terms of elastic stiffness. For the masonry, as shown in (Calvi and Bolognini 2001) and as provided in NTC08, for the case of reinforced plaster, a correction factor is equal to 1.3, which should be applied to the original mechanical parameters. In this case, for predicting the structural behaviour and the interaction among elements in play, the constitutive laws of reinforced infill panels were modified with an artificial preliminary analysis. In particular, the elastic stiffness of each equivalent strut has been incremented until to the single panel

can be considered strong and, at the same time, it has been calibrated in a way that its crushing occur at the middle of panel for compression, before that the structural elements reached the global mechanism. In particular, for the E1, the elastic stiffness has been incremented of a factor equal to 2.2, while for the E2 the incremental factor is equal to 1.5. The results attended in NL field are shown in Figure 3.42, where the "option 1" shows the capacity curve of system reinforced while the "option 2" shows the structural behaviour of a system with infill disconnected by the frame (retrofit solution coincident with the result obtained by the analysis on the bare frame). Hence, considering each case aforementioned and them combination, 6 numerical models have been investigated. Figure 3.43 shows the numerical models of E1 and E2, with modelling of equivalent struts for simulating the floor and equivalent struts for simulating the infill panels.
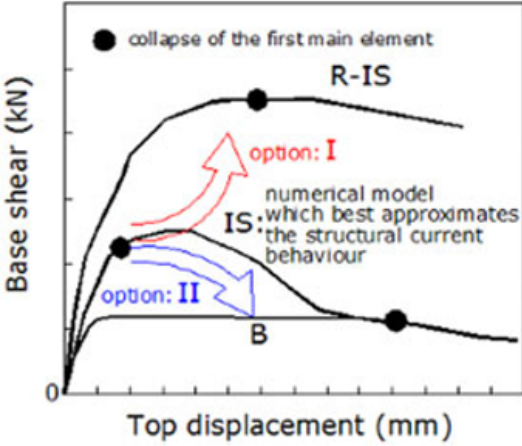
Fig. 3.42 – Global structural response obtained in correspondence of the different reinforcement options for the infill panels (as reported in Porco at al., 2014)
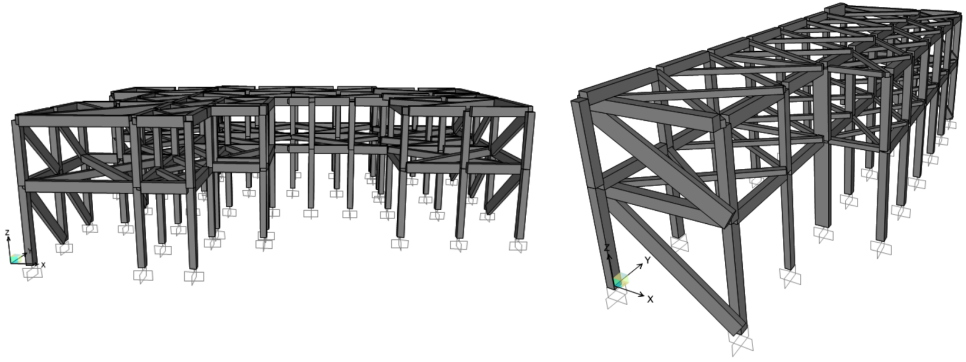
Fig. 3.43 – Numerical models of E1 and E2, accounting struts for simulating slab and infill panels.

Once that the models were made, NLS analyses have been performed on each model, according the pushing direction shown in figure 3.41. In particular, three load profiles have been adopted, as the unimodal, the triangular inverse and the uniform ones. For models with rigid floor assumption, the forces have been applied in the CM of each storey, while for the models with floor system modelled through struts, NLS analyses have been carried out, by applying at each node of storeys forces proportional to the nodal masses. The results of NLS analyses are shown in Figures 3.44a, 3.44b and 3.44c for E1 3.45a, 3.45b and 3.45c for E2, where the continuous lines represent the models with rigid floor (bare frame = blue, infilled frame = red, infilled plaster frame = green), while the dotted lines represent the same models without rigid floor assumption.
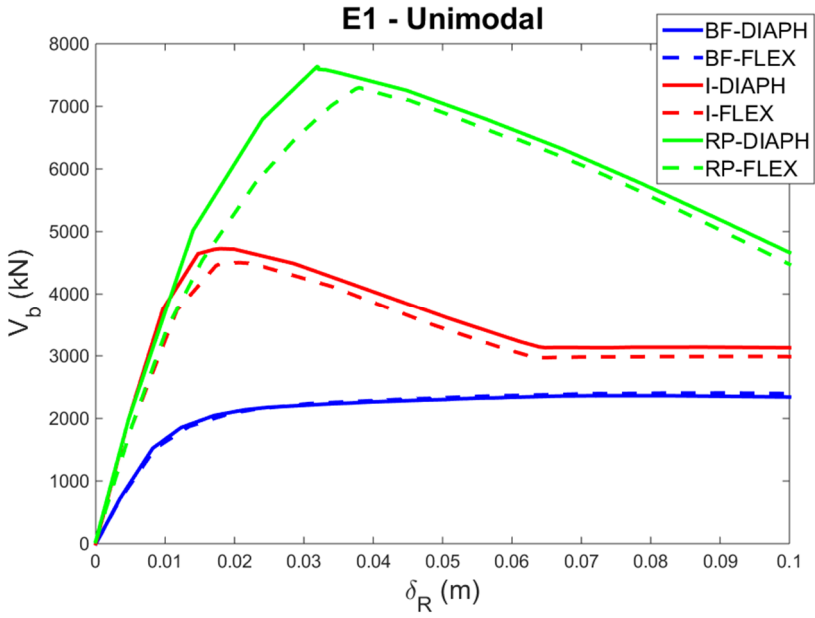
Fig. 3.44a – NLS analysis with unimodal load profile for E1
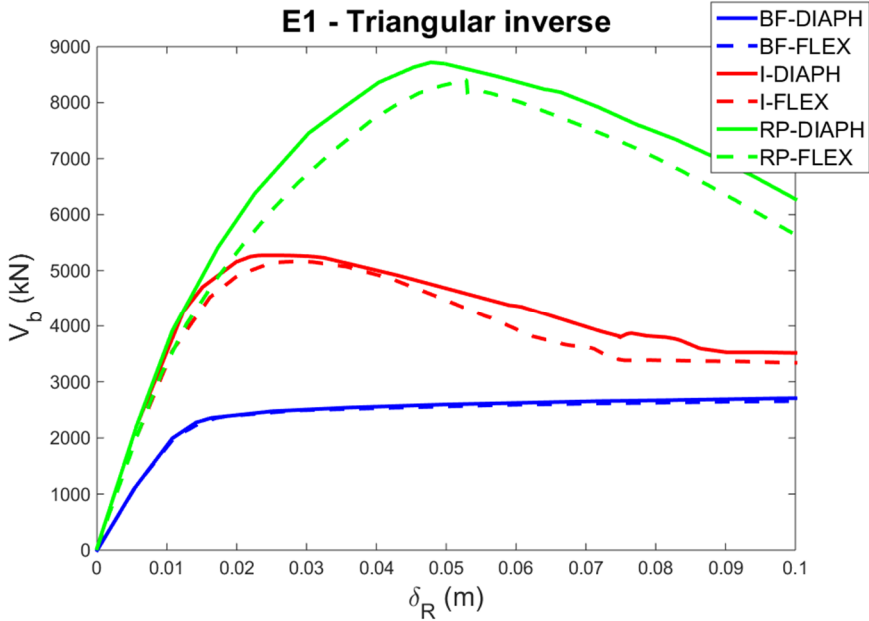
Fig. 3.44b – NLS analysis with triangular inverse load profile for E1

154
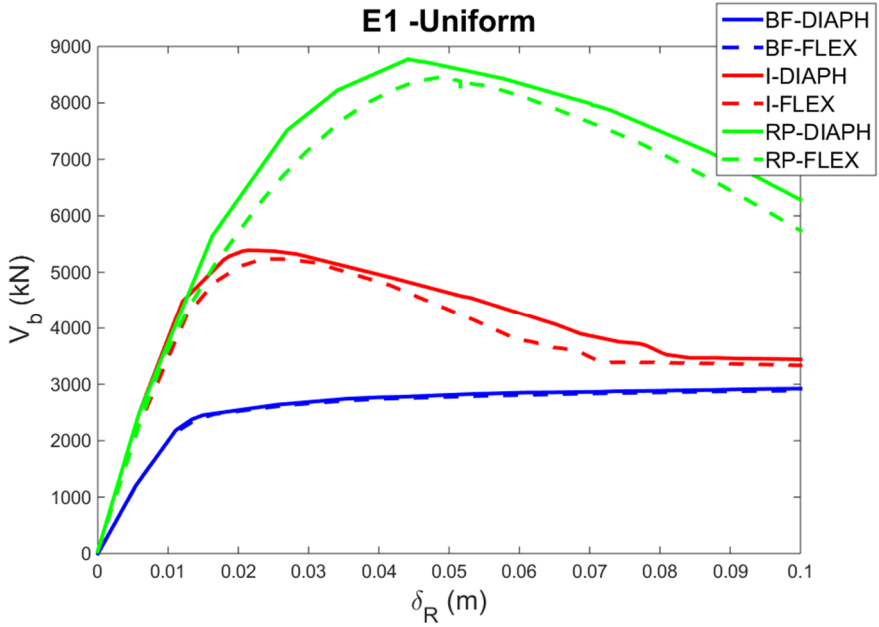
Fig. 3.44c – NLS analysis with uniform load profile for E1
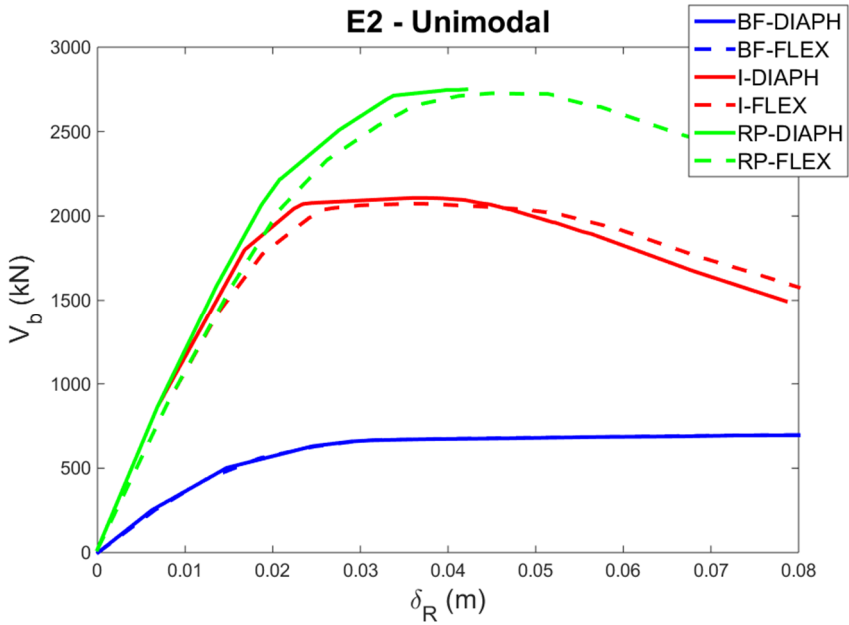
Fig. 3.45a – NLS analysis with unimodal load profile for E2
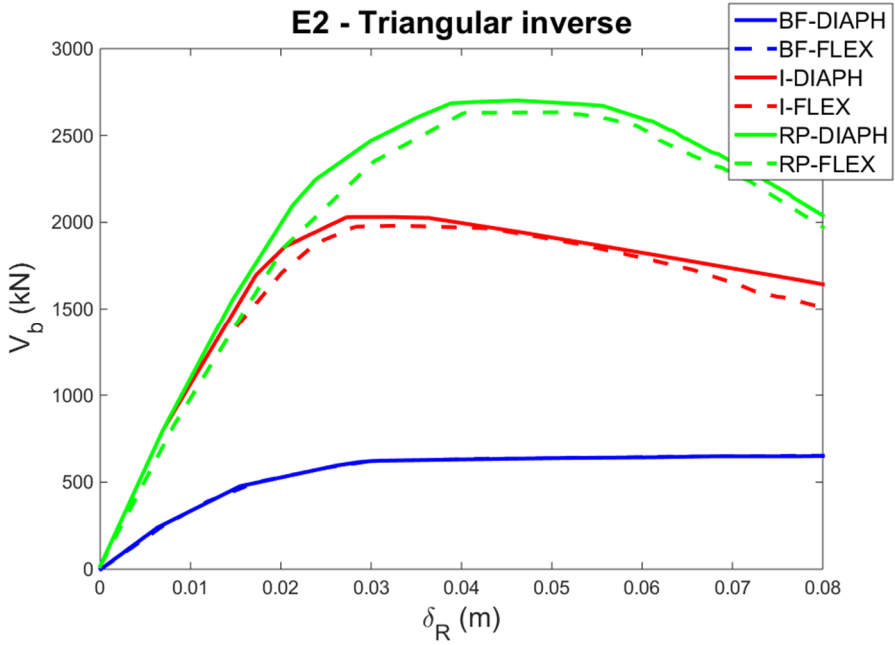
Fig. 3.45b – NLS analysis with triangular invers load profile for E2
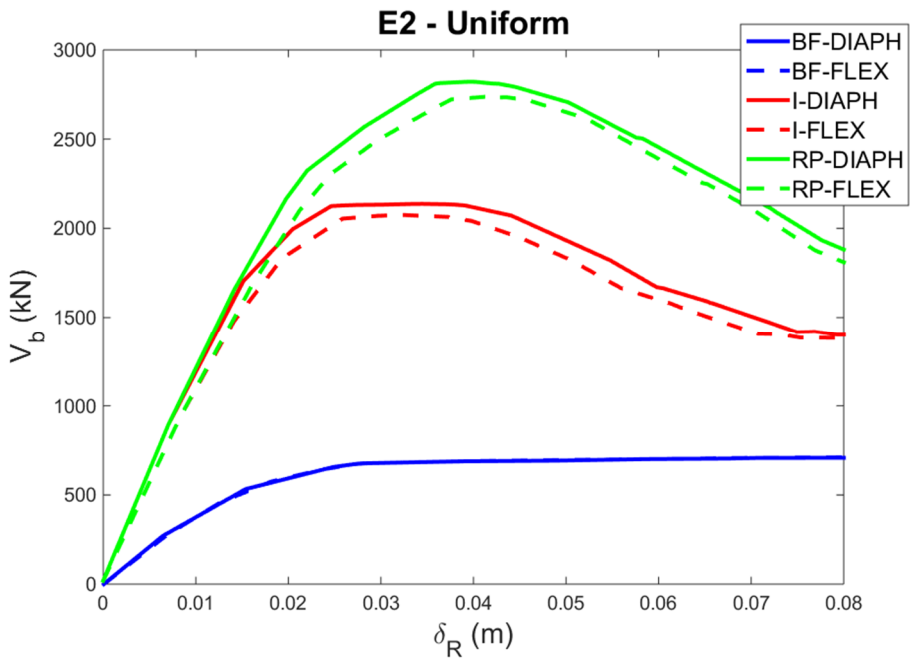
Fig. 3.45c – NLS analysis with uniform load profile for E2

The results of analyses show that, for each load pattern, the difference of global structural response between models with rigid and flexible floor increases, when the parameters of equivalent struts are greater. This means that infill panels provide a contribute, in terms of vertical stiffness, which emphasizes the flexibility of floor system. This contribute is accentuated for the cases of reinforced infill panels, where the distance between the rigid and flexible pushover curves are greater than the previous difference. The result of this difference between the curves, which is not very relevant, can be useful for better accounting the displacement related to the global mechanisms, for each LS. In particular, the difference between rigid e flexible models can be directly estimated, evaluating the formation of plastic hinges at certain values of displacement. In particular, with reference to figure 3.41, some significant 2D frame of the two buildings have been investigated, as soon as reported in figure 3.46a (E1) and 3.46b (E2) where, for values of roof drift equal to 1% (blue box) and 1,5% (red boxes), the plastic hinges formation is depicted. In particular, in the above figures, specific references to the LSs reached by each hinge are shown for the drift values considered and the rigid floor is represented with a thick line. The formation of plastic hinges in bare frame models is not reported, because the difference between rigid and flexible floor is negligible. Figures show what above deduced from the pushover curves, where the effects of infill panels and of the reinforced infill panels (with greater influence) on the floor system deformability, lead to a variation of structural response, with different V_b for a fixed displacement (and vice versa). In table 3.12, this evidence is shown, taking into account the global yielding roof displacement for each model (only for the curves obtained by triangular inverse load profile). Despite the difference among the pushover curves seems negligible, the V_b variation, at fixed displacement, reached values over 10% and this result is most apparent in the plastic hinges evolution, where the formation of ones happened in different way, also considering the different stresses distribution among vertical elements and the continuous variation of stiffness distribution among vertical elements.
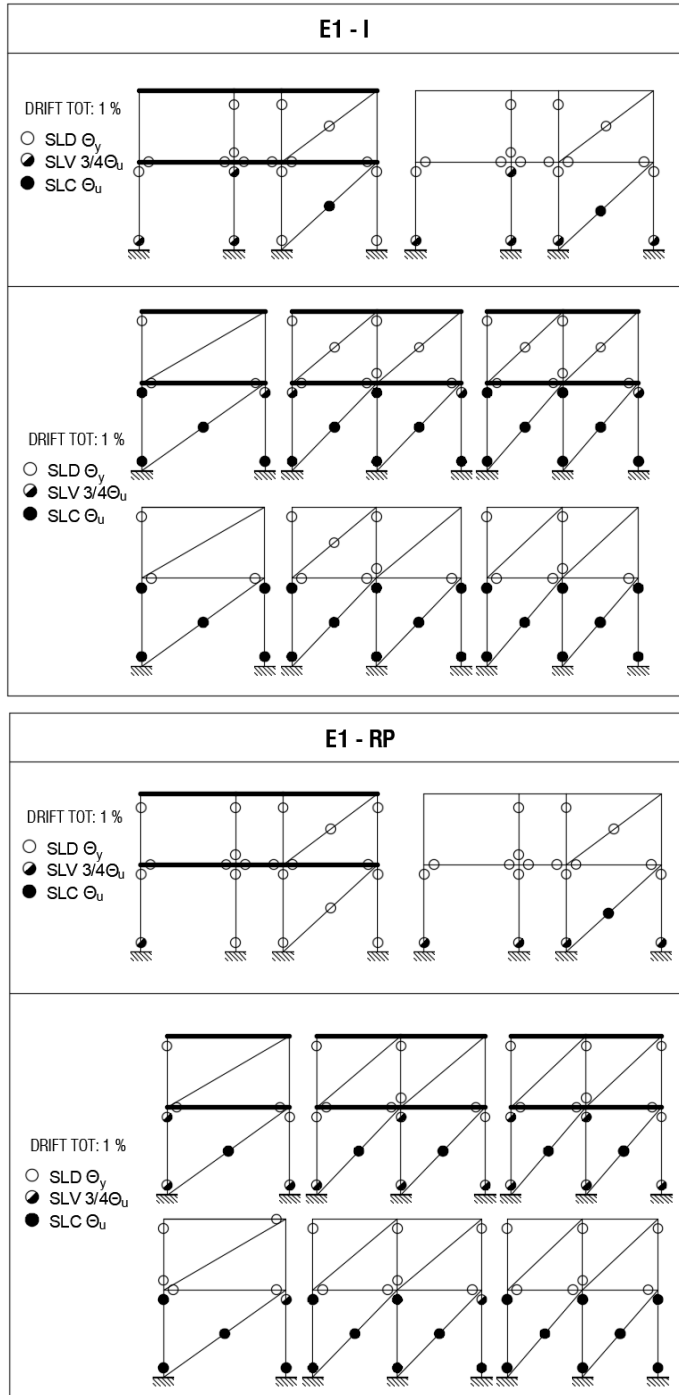
Fig. 3.46a – Occurrence of plastic hinges at fixed values of roof drift for E1

E2 - I

DRIFT TOT: 1.5 %
○ SLD Θ_y
◐ SLV $3/4\Theta_u$
● SLC Θ_u

E2 - RP

DRIFT TOT: 1.5 %
○ SLD Θ_y
◐ SLV $3/4\Theta_u$
● SLC Θ_u
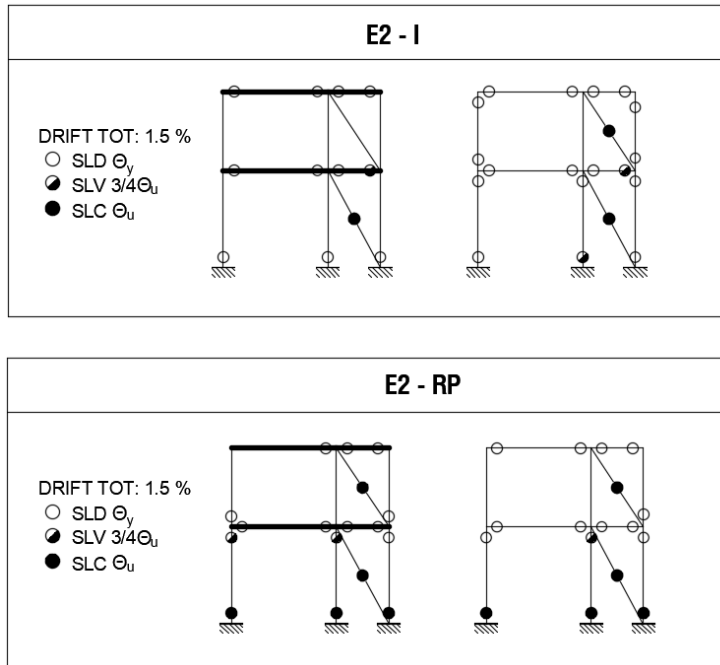
Fig. 3.46b – Occurrence of plastic hinges at fixed values of roof drift for E2

Tab. 3.12 – Percentage variation of base shear at global yielding displacement

Model	Displacement (m)	Base shear variation (%)
E1 – B	0,015	0,45
E1 – I	0,02	4,80
E1 – RP	0,04	6,70
E2 – B	0,017	0,55
E2 – I	0,02	8,15
E2 – RP	0,025	11,65

These evidences show that the effective deformability of floor system is an important factor in the evaluation of seismic capacity of RC buildings and the rigid floor assumption cannot be considered always a realistic hypothesis, especially in the retrofitting cases. In fact, the deformability of floor system can be strongly accentuated in

the seismic retrofitting cases, where the practical solutions provide to reduce the horizontal displacement through an increment of effective stiffness or strength (RC shear walls, damped braced or infill panels connected with the surrounding frame).

A second application about the topic treated in this Section has been proposed and, in particular, another case study has been investigated. In particular, a RC school building located in the city of Manfredonia, Province of Foggia, Puglia, Southern Italy has been analysed. The building, always studied within the abovementioned Agreement between AdB Puglia and Polytechnic University of Bari for the vulnerability analysis of school buildings in the Province of Foggia (Mezzina et al., 2011), was built between the 60s' and 70s in the absence of specific seismic codes and it was designed considering only vertical loads, using old design philosophy. The building (shown in Fig. 3.47, in which is shown a photo) is constituted by RC frames and is completed by infill masonry panels. The school is inscribed in a rectangle of dimensions about 22.00 x 36.00 m, with 2 storeys, for a total height of 6.80 m. No significant re-entrances and recesses are present, and the building can be classified as "regular" both in-plan and in elevation. All geometrical features of the structural elements and mechanical parameters of materials were extensively investigated, with a full KL. In particular, the properties of materials were determined through destructive and non-destructive in-situ investigations on concrete elements (drilled core test, rebound hammer test, ultrasonic test) and steel reinforcement (tensile test, bending test). The floor system is constituted by a RC ribbed slab, with constant joists dimensions (height 20 cm, width 10 cm, spacing 50 cm) and thickness of top concrete slab of 4 cm. The orientation of floor system, which substantially follows the short direction, is displayed in figure 3.47. Furthermore, the elevation beams are oriented in the two directions, favourable situation for the seismic actions. Isolated plinths constitutes the foundation system. All the significant geometrical and mechanical features of the case study are summarized in table 3.13. Regarding to the mechanical parameters of infill panels, the data used are the ones shown in table 3.9
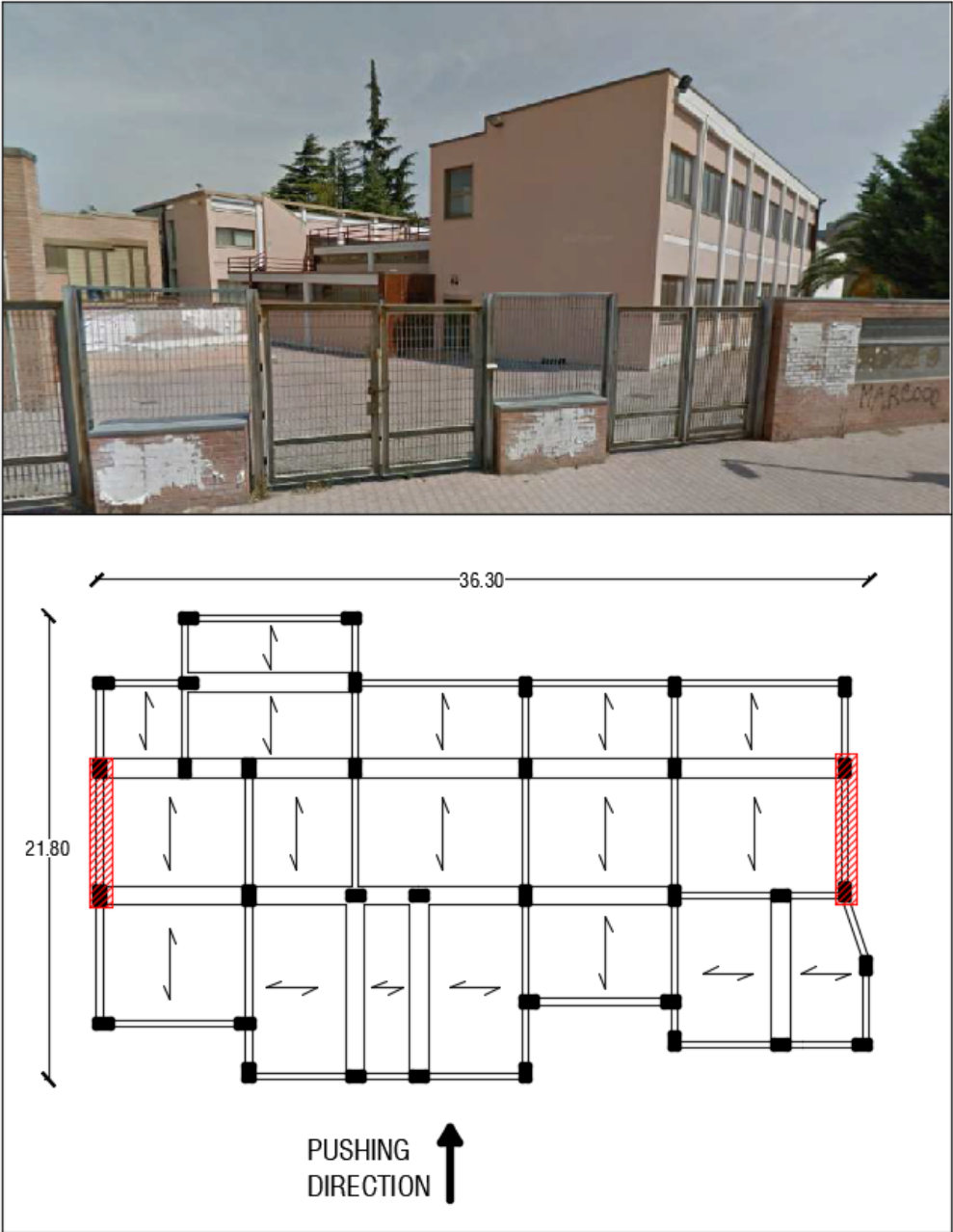
Fig. 3.47 – Carpentry and photo of case studies here investigated

Level	Elements	B (mm)	H (mm)	Materials (MPa)	Loads (kN/m^2)
Ground floor	Columns	300	650	f'_{cm}: 24.60	$G_1 = 3.60$
	Beams	300	700	f'_{ym}: 440	$G_2 = 2.40$
		900	300		$Q = 3.00$
First floor	Columns	300	650	f'_{cm}: 24.60	$G_1 = 3.60$
	Beams	300	700	f'_{ym}: 440	$G_2 = 2.00$
		900	300		$Q = 3.00$

Regarding to the numerical model, it has been implemented by using the FE software SAP2000. For the structural elements, beams and columns have been modelled through a lumped plasticity approach, by introducing proper plastic hinges located at the end sections of the elements. For beam elements, the inelastic mechanism assumed has been only that due to simple bending, by defining a NL moment-curvature relationship. For the columns, the moment-curvature relationship has been computed by evaluating the combination of axial and bending stresses. In all cases, the plastic hinges have been defined according to the constitutive law provided by FEMA 356, as shown in figure 3.8. Even in this case brittle shear mechanisms and possible nodes' failures have been neglected. The presence of infill panels has been considered by implementing simple equivalent struts in the FE models. For each panel of the external sides, parallel to the pushing direction as indicated in figure 3.47, one strut was employed, linking the opposite nodes of the surrounding frame. The dimension and nonlinearity of the struts have been modelled as done for the precedent application, using the b_w of eq. 3.15 and the constitutive law of Panagiotakos and Fardis. The focus of this application is to investigate the role of the floor flexibility in the global behaviour, taking into account the influence of the infill panels and a possible retrofit solution, through insertion of RC walls on a part of the sides of building (replacing the infill panels and united with the existing RC structural elements). In this case, the floor system has

been modelled in three different ways. The first one is the rigid floor, made through the insertion of internal constraint at each floor. This allows of concentrating the floor mass in the CM of storeys, ensuring the same displacement for each node. The second way reproduces the stiffness of floors by using equivalent struts. In particular, each floor field has been schematized by two equivalent diagonal struts, which connect the opposite nodes. The struts had a square section with dimension computed according eqs. 3.10, 3.11 and 3.12. Differently to the precedent application, the author tried to modelling the NL behaviour of the floor system. It is worth mentioning that the criterion used was the result of some evaluations and it was very simplified, because the strut model is usually adopted for elastic modelling. This can be acceptable also because the main aim of this work is to evaluate the global response and not the local ones. Hence, for simulating the NL behaviour, in each strut a plastic hinge has been placed in the central section, which took into account only the axial stress. This latter was defined using a constitutive law, which provides a perfect elastic-fragile behaviour, both in compression and tension, without ductility, according to the possible behaviour of an element not reinforced to shear. The maximum compression strength (F_c) depended from the area section of strut and strength class of concrete, while the maximum tensile strength (F_s) depended from the number of steel rebars in the equivalent area of strut, strength class of steel, diameter of steel rebar (Φ_s). The number of rebars (n_{eq}) in the equivalent struts have been evaluated considering an equivalence with the total reinforcement of the slab considered. The above criteria can be summarized in the following equations:

$$F_c = A_s * f'_{cm}$$
(3.39)

$$F_s = n_{eq} * f'_{ym} * \Phi_s$$
(3.40)

In the third model the floor system has been made, by using the equivalent orthotropic shell, according to the procedure developed in the previous section. The thicknesses of the shells have been evaluated for each floor field, through the proposed numerical procedure and, subsequently, the values of orthotropic material have been calibrated, considering the differences in deformability terms in the two direction (different joists orientation). For accounting the NL behaviour of equivalent shell, the floor has been modelled by using shell thick elements, modelled with a NL fiber approach.

The concrete constitutive law, which characterized each fiber, has been considered according to the Mander model, while for the steel rebar, an elastic-plastic law with hardening behaviour has been used. Shell elements have been meshed using square FE elements having dimensions of 50 cm. The 3 floor system typologies are depicted in figure 3.48. Concerning to the infill panels, the FE models have been duplicated, in order to investigate the cases with and without (bare frame) infill panels, for a total of 6 models. Subsequently, the numerical models with infill panels have been duplicated, for inserting the RC walls. The retrofit solution employed in this case, considered one of the most common adopted in the practical use for its design and phase of casting in place, consists in the addition of RC walls in a part of building perimeter. From the theoretical point of view, the RC walls are useful for reducing the lateral displacement under horizontal actions and, at the same time, for increasing the strength capacity of all structure. In addition, RC walls placed in symmetrical way on the sides of existing buildings can strongly regularize the dynamic behaviour, reducing the in-plan torsion phenomena. In our case, the additional RC walls were located on the short sides of building perimeter, according to the red filled boxes shown in figure 3.47. The RC walls, designed according to capacity design approach and inserted between the existing columns, had the following features: thickness of 20 cm, concrete class 25/30, two layers of steel rebar with diameter of 1.6 cm along the two directions, steel class B450C, concrete cover equal to 4 cm. Concerning to the numerical modelling, an analogous procedure to orthotropic shell was implemented (NL fibres on shell thick elements).

Rigid floor model	Struts model	Orthotropic equivalent shell model
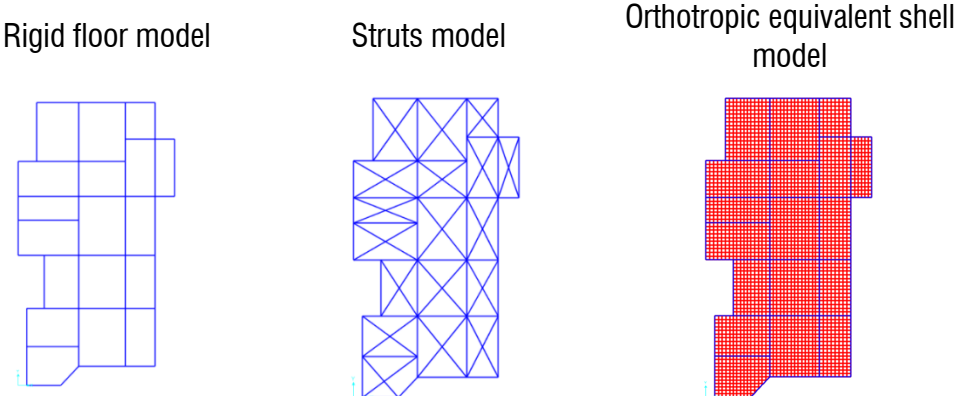
Fig. 3.48 – Floor systems employed in the FE models

The combination of the abovementioned hypotheses and proposals leads to have 9 FE models. For investigating the structural response of the FE models, each model has been investigated through NLS analyses only in the weak direction (according to figure 3.47), using a triangular inverse lateral load pattern. For models with rigid floor, the horizontal load has been applied in the CM of each storey, while in the floor systems modelled through struts and equivalent shell, the horizontal load has been divided among each node of storeys, using forces proportional to the nodal masses. Regarding to analyses on models with infilled panels, the equivalent struts have been placed in one direction, coherently with the pushing direction. The results of NLS analyses on the bare frame and infilled models, by using the three modelling methodologies for the floor system, are displayed in figure 3.49. Figure 3.49 shows that in bare frames cases, the trend of capacity curves is similar for all models with different floor system, while in the infilled frames cases, the models with flexible floor are more deformable than rigid one. For this reason, the pushover curves (the dashed and dotted lines) manifest a horizontal shifting to right of the curves peak point. This evidence was due to the "strong of infill panels" that influence the floor deformability, which increased the inertia of vertical system. Both graphs of the figure 3.49 show that the modelling, with struts and equivalent shell, provides same results. Furthermore, in this case, the differences between rigid and flexible floor are greater than the result obtained in the bare frame application, mainly due to the shape of this building, which has a rectangular extended in-plan shape. In addition, the pushover curves show that the models with flexible floors have an elastic stiffness lower than the one obtained by the rigid floor model. In particular, the difference is about 10% for bare frames models and about 20% for infilled frames model, with regard to the initial slope of pushover curve, assuming as reference the rigid floor model. This result is summarized in table 3.14, where the percentage difference of models are reported, in terms of δ_R, evaluated at maximum value of V_b and assuming as reference the rigid floor model.
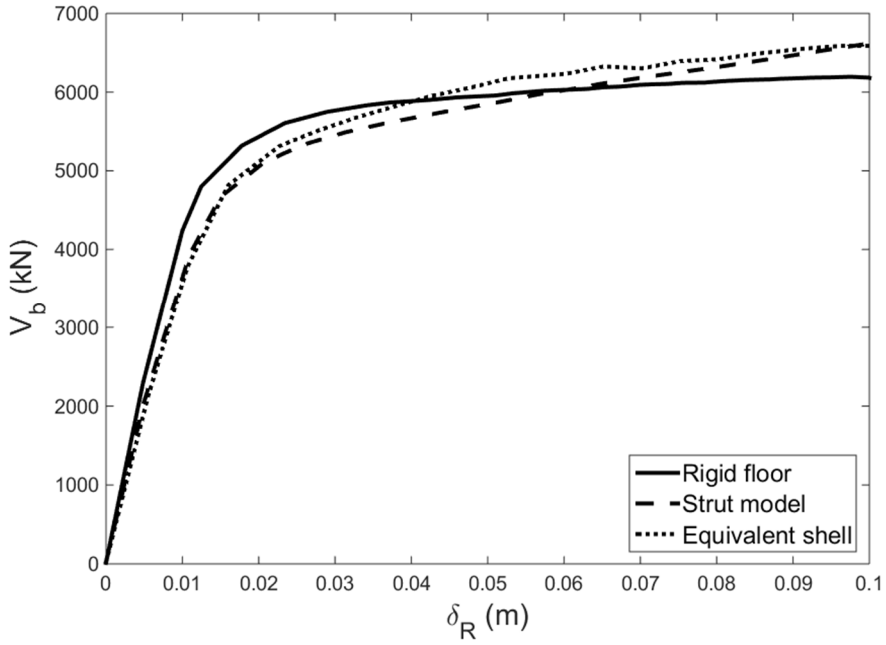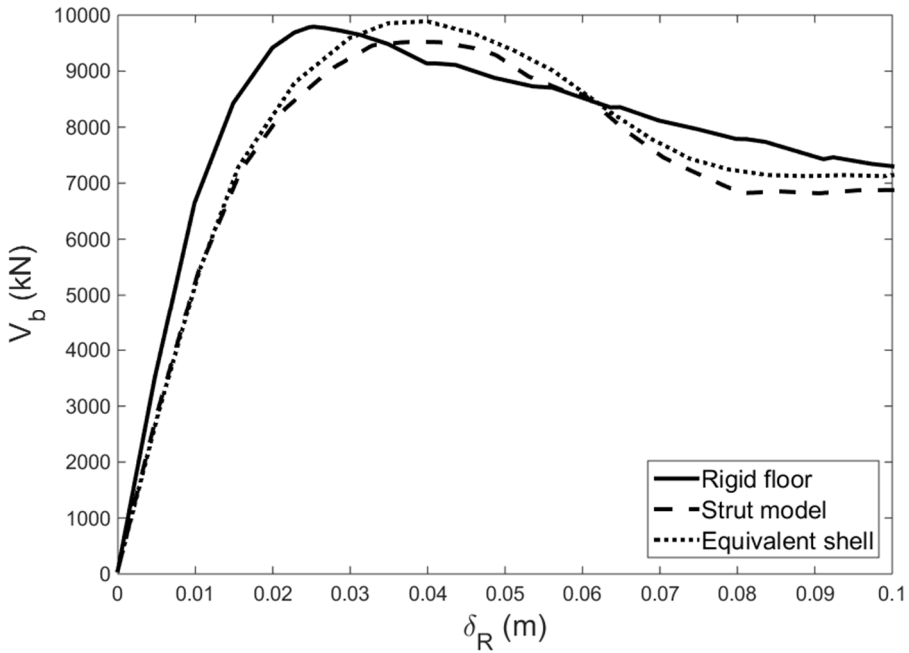
Fig. 3.49 – NLS analyses results for bare frame and infilled models

Tab. 3.14 – Percentage variation of roof displacement, at maximum value of base shear

Models compared	Bare frames – variation of δ_R (%)	Infilled frames – variation of δ_R (%)
Rigid floor – Strut model	3.85	34.19
Rigid floor – Equivalent shell	2.67	36.71

Regarding to the model with retrofit solution employed on the existing RC struc-ture, as explained above, two RC walls have been added on building perimeters, with a length of 4 meters for the entire height of structure. The results of NLS analyses, using the 3 typologies of floor systems, are shown in Fig. 3.50, while in table 3.15 are shown the V_b percentage differences, for a fixed displacement of 1 cm, assuming as reference the rigid floor model.
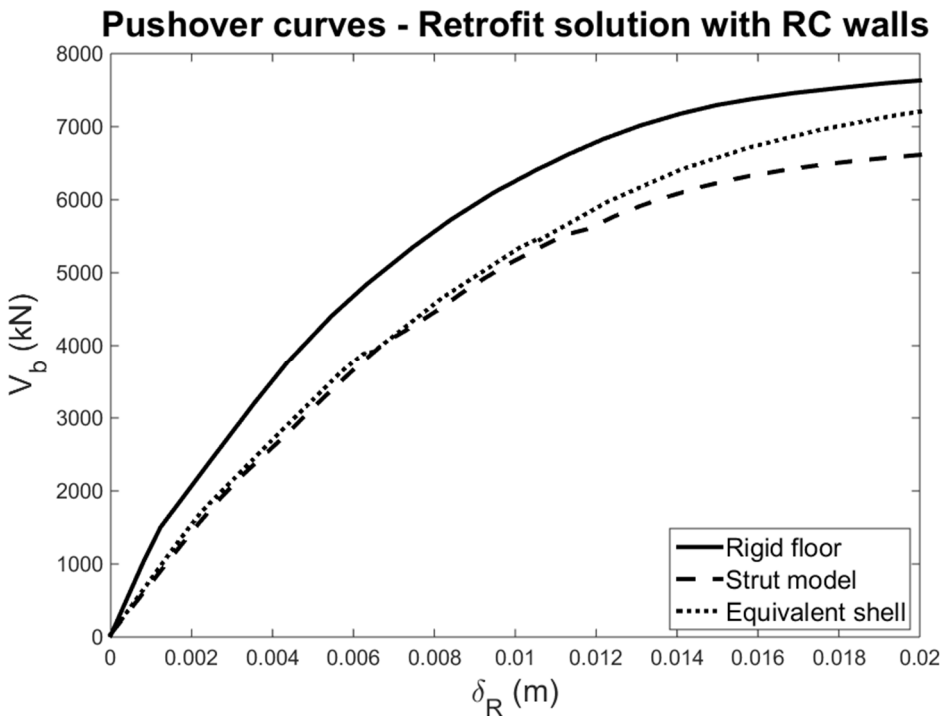
Fig. 3.50 – NLS analyses results for retrofitted with RC walls models

Tab. 3.14 – Percentage variation of roof displacement, at maximum value of base shear

Models compared	Model with RC walls – δ_R of 1 cm – variation of V_b (%)
Rigid floor – Strut model	17.10
Rigid floor – Equivalent shell	16.60

As shown for the infilled frame models, in the models with RC walls, the difference among capacity curves was strongly accentuated, with elastic stiffness different of about of 25%, assuming as reference the rigid floor model. The results obtained imply that FE models with different hypothesis about floor stiffness, presented a variation, in terms of V_b at a fixed δ_R, which is larger when the vertical elements are stronger. In addition, the evidences shown in figures 3.44 and 3.45, occurred also in this case (Figure 3.51), where increasing the stiffness of vertical elements, the differences among pushover curves with rigid and flexible floor increase. In the figure 3.51 is also note the differences, in terms of elastic stiffness that the retrofit solution provides to the stiffness. It can be interesting to observe the resultant in-plan deformed shapes of structural models, at fixed displacement. With this regard, the nodes of rigid floor models have an equal displacement in the pushing direction, while for the flexible floor models, an "arch effect" occurs. This effect is gradually increased when vertical elements are more important. In Figure 3.52, the in-plan deformed shapes are shown, for models with RC walls, at fixed displacement of 2 cm. The shape of the two models with flexible floor are similar. Generally, the results show how the hypothesis about floor system can play an important role, providing different results about the global response of existing RC buildings, with different evaluation of the vulnerability. Especially in the cases of strong masonry infills and in the cases of retrofit solution with increment of strength capacity, the rigid floor assumption should be assessed, also if consistent with the codes prescriptions and with regard of the stresses distribution in the structural elements. This latter consideration requests major in-situ investigations, with analysis of geometrical and mechanical parameters of masonry panels and RC slab.
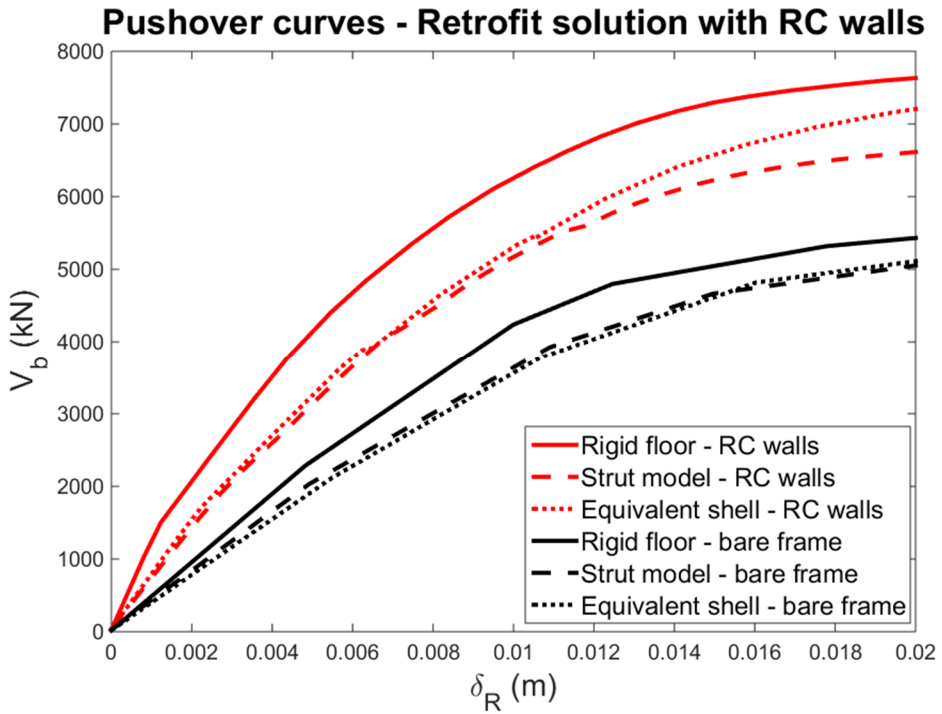
Fig. 3.51 – Difference of initial stiffness among bare frame and retrofitted models.

Rigid floor model   Struts model   Orthotropic equivalent shell model
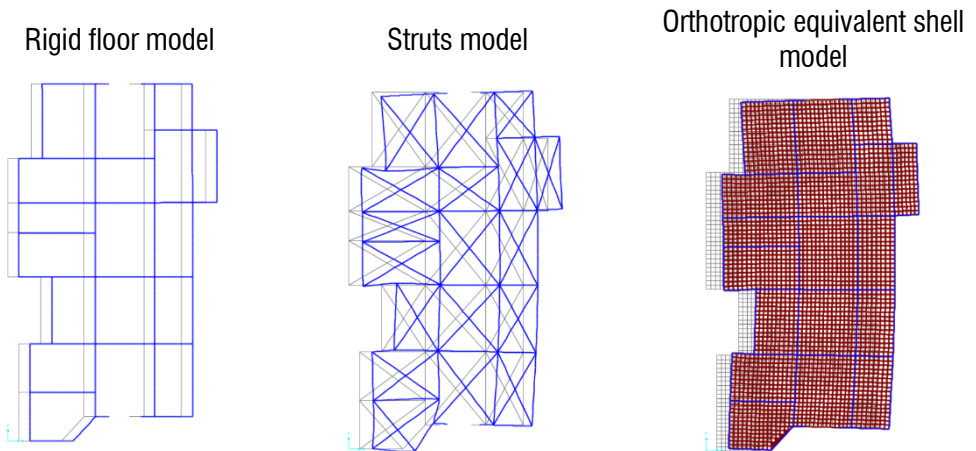
Fig. 3.52 – In-plan deformed shape of models with RC walls

4. Methods of seismic analysis of existing RC buildings

4.1 Overview

Within the context of vulnerability assessment process of existing RC buildings, one of the fundamental phase is the one of seismic analysis. The main aim of this phase is to predict the performances of the structure under seismic actions, with regard of global and local responses for several LSs. The core of the seismic analysis is the application of external forces, which simulate the seismic actions, to a numerical model that represents the building investigated. The result of the analysis should provide an information about the building behaviour under horizontal actions, which are definable in different modalities, due to the time and application methods. To this purpose, the first distinction is between static and dynamic actions, where the difference between them is related to the ratio between the application time of the action and the modal behaviour of the building. It is worth mentioning that both static and dynamic analysis can be linear and NL and the combination of these provide four methods of analysis, as suggested by all technical codes. On the other hand, for investigating the behaviour of existing RC buildings, it is strongly suggested from scientific literature to consider the geometric (P-Δ effects) and mechanical nonlinearities of all members, which exclude the linear methods of seismic analysis (useful in the design phase of new buildings). Generally, NLD analysis is rarely used in ordinary engineering applications because of its complexity and relevant computational efforts, but also due to the difficulty of choosing representative design accelerograms, consistently reproducing the post-elastic and hysteretic behaviour of the structure, besides to the difficulty of interpreting of the results. On the other hand, NLD analysis results are expected to be more accurate than other methods, due to the better simulation of the seismic action. In recent years, NLS analysis has gained increasing importance as an alternative NL method of analysis. It is proved that usually the resulting response well represents the envelope of all the possible dynamic responses and can so be used to replace a full NLD analysis. It can provide information about some important response characteristics that cannot be obtained from linear analyses and, at the same time, it is relatively easier than NLD

analysis. In this Chapter, the author is going to describe the main features of NLS and NLD analysis, from the technical codes and scientific literature point of views, with an eye to practitioners' use. After a widely presentation of the NLS and NLD analysis methodologies, a sensitivity analysis on a sample of ideal existing buildings is presented, on which conventional NLS analysis are performed, with focus on the role of the control node (or performance point) position (Uva et al., 2018). Subsequently an application of simplified non-conventional NLS analysis (multimodal), adapt to the use by practitioners, is proposed and applied on a particular real case of existing RC building (Porco et al., 2018).

4.2 Nonlinear static analysis

The NLS analysis, also called pushover analysis, is a seismic method of analysis that consists in the application to a structural system, subjected to gravity loads, of a load vector made by horizontal forces (F_0), which are directly related to the structural masses. In addition, in some cases it is possible to apply a vector of displacements, in a substitution of F_0. For carrying out the analysis, F_0, which simulate the seismic action applied to the storeys mass, is monotonically increased until to the structural collapse, by using an incremental factor α, whose value varies from 0 to a certain level. The structural behaviour is monitored in a node representative of the entire building (or of its part), called performance point or control node (CN), which is usually chosen in the CM of the last storey (it is not a fixed rule, but valid for the regular buildings). This procedure is gradually performed and, for each increment of the factor α, it is possible to monitor the displacement of CN (if CN is coincident with the CM of the last storey, the CN displacement is equal to the δ_R) and the total V_b, in order to define the capacity curve of building. For each instant, the resultant force of αF_0 is equal to V_b. Mathematically, the most common algorithms used for performing the pushover analysis works as "displacement-control", where, for each step, an incremental displacement of CN is fixed and the equilibrium among external and internal forces is performed, in order to obtain the value of V_b for that step. The NLS analysis should investigate the evolution of the structural response, accounting the NL behaviour of all structural elements. In particular, if the numerical model accounts for the nonlinearity through plastic hinges,

the capacity curve, as above defined, shows the evolution of the plasticity in the structural elements. As shown in figure 4.1, the capacity curve of the system depicted, assuming it as a ductile structure, modelled through plastic hinges made (does not accounting brittle mechanisms) and subjected to αF_0, is describable as summarized below:

- A first branch where the structural system is elastic and the forces applied provide elastic displacements, proportional to the global flexural stiffness of the building;
- Occurrence of the first plasticization in a structural element, which corresponds to the system yielding;
- Progressive formation of plastic hinges in the structural elements, with continue changes of flexural stiffness in the curve;
- Activation of a failure mechanism in the structure, due to the formation of a certain number of plastic hinges that does not allow the equilibrium of the forces in play.
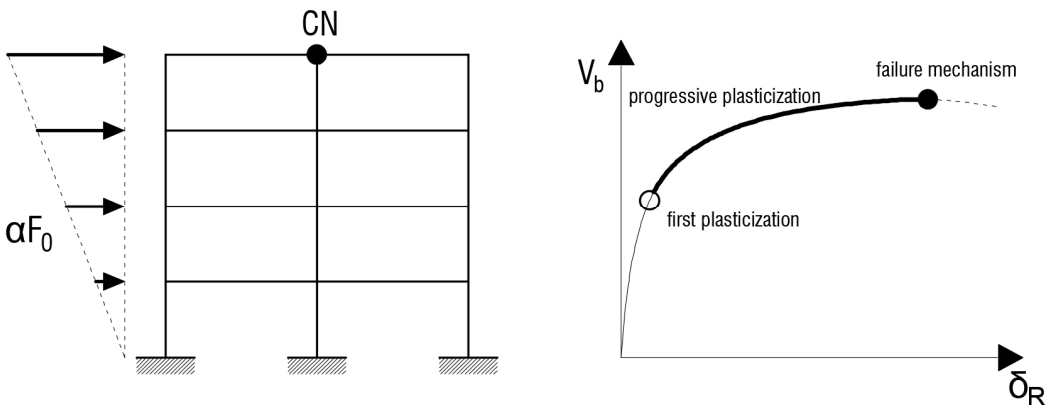
Fig. 4.1 – Capacity curve of a ductile system

Generally, the last branch can show a softening trend or a horizontal one, depending from the plastic hinges definition. As above specified, the capacity curve shown in figure 4.1 is related to a ductile structural system. When one accounts the brittle mechanisms, as the shear of structural elements or the beam-column joints behaviour, the capacity curve can be strongly different, with the occurrence of degradation

phenomena. In these cases, local or global failure mechanisms does not allow of exhibiting a post-elastic branch, because the capacity curve stops itself before. With this regard, it is possible to reduce or to eliminate in the analysis the elements that lose their stiffness, as in the sawtooth capacity curves. The capacity curve can be plotted also in others ways, accounting displacement parameters more significant with regard to the structural damage, such as the θ_i. Through the definition of the capacity curve, the NLS analysis allow of identifying the following parameters (Krawinkler and Seneviratna, 1998 and Kim and D'Amore, 1999):

- Evaluation of the overstrength ratio, defined as α_u / α_1, where α_u is the value of incremental factor to the failure mechanisms and α_1 is the value of incremental factor to the yielding;
- Estimation of the maximum seismic demand, in terms of strength, for the brittle mechanisms of structural elements;
- Estimation of the maximum seismic demand, in terms of deformation, for the flexural mechanisms of structural elements;
- Possibility of assessing the effective distribution of the inelastic demand, for building designed with q factor;
- Estimation of assessing the structural behaviour, after the strength or ductility losses in some structural elements;
- Evaluation of the irregularities in-plan and in elevation, which cause modifications in the dynamic response;
- Evaluation of θ_i, which is a significant damage parameter, also accounting for the possible discontinuities, in terms of strength or stiffness;
- Monitoring of the deformations, rotations, stresses, yielding, failures or collapses of the structural elements and the entire structure, in order to define the performance of the building for the LSs to investigate.

The role of capacity curve consists in the evaluation of the structural capacity towards the seismic demand, through some methodologies, which allow of comparing the response of an equivalent SDoF system with the response spectrum, in the ADRS

format. In particular, the assessment is performed through methodologies proposed by the technical codes as the well-known N2 method (see Chapter 2) or other ones, such as the capacity spectrum method (ASCE, 41-13) or the displacement-based assessment (Priestley, 1997 and NZSEE, 2017). The capacity curve is strongly dependent from the lateral load vector applied on the structure. Geometrically, a generic load pattern can be defined as follow:

$$\{F_0\} = \{\Psi\} * p(t) \tag{4.1}$$

where p(t) is a scalar that describe the amplitude of the force system in the time and Ψ is a vector that takes into account the force distribution and then, its shape. The value of Ψ can assume a value directly related to the main building properties, such as the first mode of vibration (unimodal pushover). It is worth mentioning that, based on the kind of load profile adopted, the pushover analysis can be divided in conventional or non-conventional. This classification can be addressed to two main limitation. Firstly, the assumption of an unimodal profile does not allow of taking into account the effects of higher modes, which can significantly influence the structural response in some situations (e.g., tall buildings, presence of structural irregularities in mass or stiffness,…). A second drawback concerns the assumption of time invariant load-profiles, which neglects the changes of the dynamic properties of the structure (Ts, shape of fundamental mode,…) due to the progressive plasticization of structural elements and consequent loss of stiffness. These two issues introduce the non-conventional pushover, which will be described subsequently.

4.2.1 Conventional methods

A conventional pushover accounts for a load pattern that has an invariant shape throughout the analysis. The typologies of load patterns used in conventional pushover analysis are summarized below:

- Unimodal load pattern, where the shape of the load vector is proportional to the first mode of the structure and the mass of the building storeys. The value of Ψ can be computed as:

$$\{\Psi\} = [M]\{\Phi_1\} \tag{4.2}$$

where M is the diagonal matrix of masses and Φ_1 is the eigenvector of the first mode of the structure.

- Inverse triangular load pattern, where the shape of the load vector is proportional to the mass and height of the building storeys. The value of ψ can be computed as

$$\{\Psi\} = [M]\{H\} \tag{4.3}$$

where H is the total height of the structure.

- Uniform load pattern, where the shape of the load vector is proportional to the mass of the building storeys. The value of ψ can be computed as

$$\{\Psi\} = [M]\{I\} \tag{4.4}$$

where I is the influence vector associated to the input direction of motion.

Generally, for regular buildings, the unimodal and inverse triangular load profiles can be same and provide the same results. The above vectors are characterized by several limitations, confirmed in several scientific publications. In particular, as shown in (Miranda, 1991, Krawinkler and Seneviratna, 1998, Gupta and Kunnath, 2000, Papanikolau et al., 2006), the use of conventional load profiles provides good results in the cases of low-rise buildings, in which the influence of higher modes is negligible. For high and irregular structures, the conventional load profiles cannot estimate the seismic behaviour, because the deformation profiles can have a different shape from the one of the above profiles. In addition, the conventional pushover analysis can be strongly disadvantageous in the behaviour estimation, because when the first plasticization occurs, the force distribution acts in the parts degraded with more influence. This lead to increase the damage in a localized part of the structure, which is the result of a time-invariant nature of the conventional load profile. The reliability of pushover analysis can be checked through the comparison between the capacity curve and the results obtained from time-history analysis. In (Mwafy and Elnashai, 2001), the results of pushover analysis through inverse triangular, multimodal and uniform invariant load patterns on several RC buildings were compared with the results of time history analyses. In particular, in figure 4.2 the results are shown for a high regular building. The

results of work showed that the triangular inverse and multimodal analysis provided same results, different from the one obtained by the uniform load profile. The main difference is that the uniform distribution provided a capacity curve with greater V_b and lower collapse δ_R than the one obtained from the triangular inverse (and multimodal) analysis. This is due to a resultant of uniform load profile, which is applied on a height lower than the application point of the resultant of the triangular inverse load profile. This provides major strength and a minor limit for a collapse LS. In this case, the uniform load pattern overestimated the response, as confirmed from the time history analysis, in terms of initial stiffness and V_b. On the other hand, the uniform load profile can be useful in the cases of pilotis, where the soft-storey mechanism can occur.
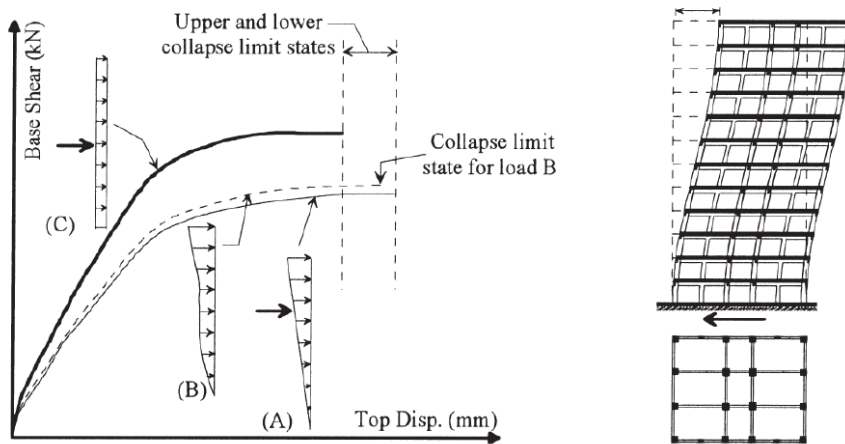
Fig. 4.2 – Comparison of capacity curves obtained from different load profiles (Mwafy and Elnashai, 2001)

Generally, this difference in the response, due to the different load profiles, suggest that the real behaviour of the building is in the middle of the responses. With this regard, the international codes, such as EC8 provides some criteria for performing the pushover analysis in conventional way. In particular, it suggests that the pushover analysis must be performed with two load profiles (taken from two groups that account for the differences in figure 4.2) and evaluate the response in conservative way, considering the more disadvantageous case. In addition, the same code fixes limitations about the dynamic properties of the buildings, suggesting two conditions to observe, like a

minimum M[%] of 75% and a T_1 lower than two seconds and $4T_c$ (where T_c is a point of the elastic spectrum) in the analysis direction. With these latter conditions, the code imposes that conventional pushover can be applied on regular buildings, with negligible influence of higher modes, also when the building go into the inelastic field. The limitation about the M[%] introduces (besides the weight of the higher modes) a focus on the torsional effects of the pushover analysis. It is worth mentioning that the NLS analysis was firstly developed on bi-dimensional (2D) numerical systems, representative of the 3D buildings. With this regard, the abovementioned load profiles were developed for accounting the behaviour of 2D frames, while in the practical applications the buildings are simulated through 3D numerical models. Clearly, with this kind of models, it is possible to simulate the real behaviour of building, taking into account also the real irregularities of buildings, as widely explained in the Section 2.2. In the cases of irregularities in-plan, as happens when the CM and CS are not coincident, pushing with the above profiles can cause the situation shown in figure 2.3, with wrong estimation of the global performance and structural element behaviour, different from the one shown by NLD analyses. At the same way, in the cases of irregularities in-elevation, the use of the conventional load profiles, can induce to apply the loads in a different way for each storey, with development of local mechanisms, which are not predictable by NLD analyses. From the torsional point of view, the unimodal load profile is better than the triangular inverse and uniform ones, because it is able to take into account the rotational inertia forces (numerically, the unimodal load profile turns out to be composed by a force and a couple in the CM). On the other hand, the results are not reliable if the fundamental mode in the direction considered has low M[%]. For accounting the torsional effects, besides to the M[%] limitation, the EC8 suggests to perform NLS analysis considering an equivalent eccentricity. In particular, the value of eccentricity, for each direction of pushing, is equal to 5% of perpendicular length of building, considered from the CM to right and left. Hence, EC8 imposes to practitioners of performing eight pushover per direction (two load profiles, two eccentricities, two verses) and of considering the more conservative result for the assessment. For concluding, the NLS analysis method is more accurate of a linear analysis (static or dynamic), but the static nature

of the forces applied does not allow of evaluating the real dynamic behaviour. Furthermore, the choice of two load profiles, such as suggested from EC8, could be not conservative, especially if the influence of higher modes in both elastic and inelastic fields is important.

4.2.2 Appraisal of the role of control node position by conventional nonlinear static analysis on a sample of building models

Concerning to conventional NLS analysis, the aim of this Section is to investigate the limits provided from the prescriptions suggested by EC8. In particular, remembering the problems about the 2D and 3D numerical models due to the torsional effects, the author is going to investigate the applicability of conventional NLS analysis, by using unimodal load profiles on 3D numerical models. In particular, according to EC8, an ideal sample of existing RC buildings with irregularity in-plan has been simulated. As summarized in the Chapter 2, the EC8 provides several indications for defining a building as irregular in-plan, but at the same time, the evaluation of modal parameters is propaedeutic for applying unimodal NLS analysis, with focus on the value of M[%], which should be greater than 75%. Furthermore, another aspect investigated is the definition of CN position, which is fundamental for the definition of capacity curve and then, the structural response. Generally, the choice of CN position, according to the EC8 prescriptions (and other codes), is usually assumed coincident with the CM of the last storey. For irregular buildings, the choice of CN coincident CM could provide results not conservative, with greater value of real building capacity, in terms of roof displacement at life safety limit state (δ_R, which here is called δ_{LS} with reference to the LSLS). This assumption is significant when, in order to verify the structural capacity with N2 method, the equivalent SDoF system is considered and the real variability of CM position is neglected, provided by the accidental loads. This means that in the computation of CDR, the results could lead to an overestimation of structural capacity. In addition, it is possible that the position of CM is not well-defined for irregular buildings or it is geometrically out of the plant, which is an evidence that can induce to wrong evaluate the global performance of the building. Hence, the scope of the work herein presented is the definition of a new formulation, able to provide the increment or decrement of δ_{LS}

of capacity curve for buildings with generic in plane shape, which have M[%] greater than the inferior limit for applying the conventional (unimodal in this case) pushover. The formulation allow of computing the capacity curve, by assuming whatever CN position on the last storey, starting from the usual assumption of CN coincident with CM and accounting for the variation of number of storeys. It is worth mentioning that, changing the CN position, the structural capacity is always the same, but the representation of the capacity curve can be different, with the above problems in the CDR computation. The methodology proposed can find an application also in the expeditious estimation of structural behaviour for several RC buildings of urban aggregates, which have irregular in-plan shape and different number of storeys. In this typology of analysis, the method can be useful for correcting fragility curves, providing the most unfavourable and conservative solution. Concerning to our case studies, the sample of buildings is constituted by several ideal RC buildings, made starting from a reference model (RM), which is a square frame system constituted by 4 RC beams with length of 5.00 m and 4 RC columns with height of 3.00 m. The modelling has been carried out using finite element (FE) software as SAP2000. Beams and columns have constant section with dimensions respectively of 40 x 50 cm and 40 x 40 cm. The RM has been in-plan replied, in order to obtain a starting model (SM) made with sixteen RM (4 RM in both directions), as shown in figure 4.3. Subsequently, the SM with storey has been replied in-elevation, in order to obtain buildings with 2,4,6,8 levels.
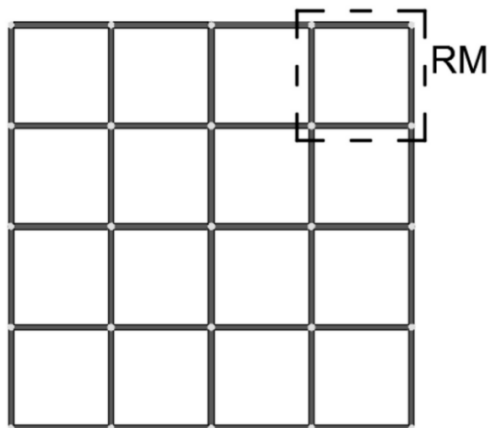
Fig. 4.3 – In-plan view of the starting model (SM), obtained by duplicating the reference model (RM)

In order to complete the description of RM, the amount of longitudinal and transversal bars have been inserted by hypothesizing that RM is a part of existing RC building designed through old technical rules, considering only gravity loads and with construction details that do not take into account seismic actions. The amount of longitudinal steel bars is indicated as the number n of bars having diameter ϕ (nϕ), whereas the amount of transversal steel bars isi indicated in terms of the ratio ϕ/s, expressed in cm (s = spacing of stirrups, ϕ = diameter of longitudinal and transversal bars). Using a simulate design, which has been carried out with the oldest Italian technical law (R.D.L 2229, 1939), in each beam have been inserted 4 ϕ16 as longitudinal steel bars and ϕ6/30 as transversal steel bars, in both top and bottom sides of end sections. While, in each column have been inserted 4 ϕ18 as longitudinal steel bars and ϕ6/20 as transversal steel bars along each side. In the cases analysed, the mechanical parameters of concrete have been defined according to the strength class C25/30, as classified in EC8. In particular, E_c is equal to 31467 MPa, G_c is equal to 11315 MPa and v is equal to 0,2. Mechanical parameters of steel rebar chosen have been defined according to strength class B450C as classified in EC8, with E_s equal to 210000 MPa. Dead (G) and Accidental (Q) loads has been applied on RM, according to EC0, paragraph 6.4.3.4. In particular, G_1 is equal to 3,5 kN/m^2 (considering that each floor is constituted by a ribbed slab with an height of 30 cm and a top concrete slab of 5 cm), G_2 is equal to 2,5 kN/m^2 (including the weight of non-structural elements as masonry infills, which is not modelled in case study) and Q is equal to 2 kN/m^2. Starting from SM, several buildings with different shapes have been defined, removing casually RM and obtaining all possible combinations of irregular in-plan structures. A summary framework of models analysed, with all in-plan shapes considered, is depicted in figure 4.4. In addition, considering that each model has been analysed with 2, 4, 6 and 8 levels, the sample is constituted by a total number of 92 FE models. Firstly, for each models, eigenvalues analyses have been carried out, by determining modal parameters as T, eigenvectors (Φ), coefficients of modal participation (Γ) and M[%]. This latter analysis has been able to provide indications on what models can be applied the NLS analysis, considering only ones with M[%] greater than of 75%, coherently with lower

limit provided by EC8 for carrying out a pushover. In order to consider a model with a proper shape in the analysis, this limitation must be always valid varying number of storeys.
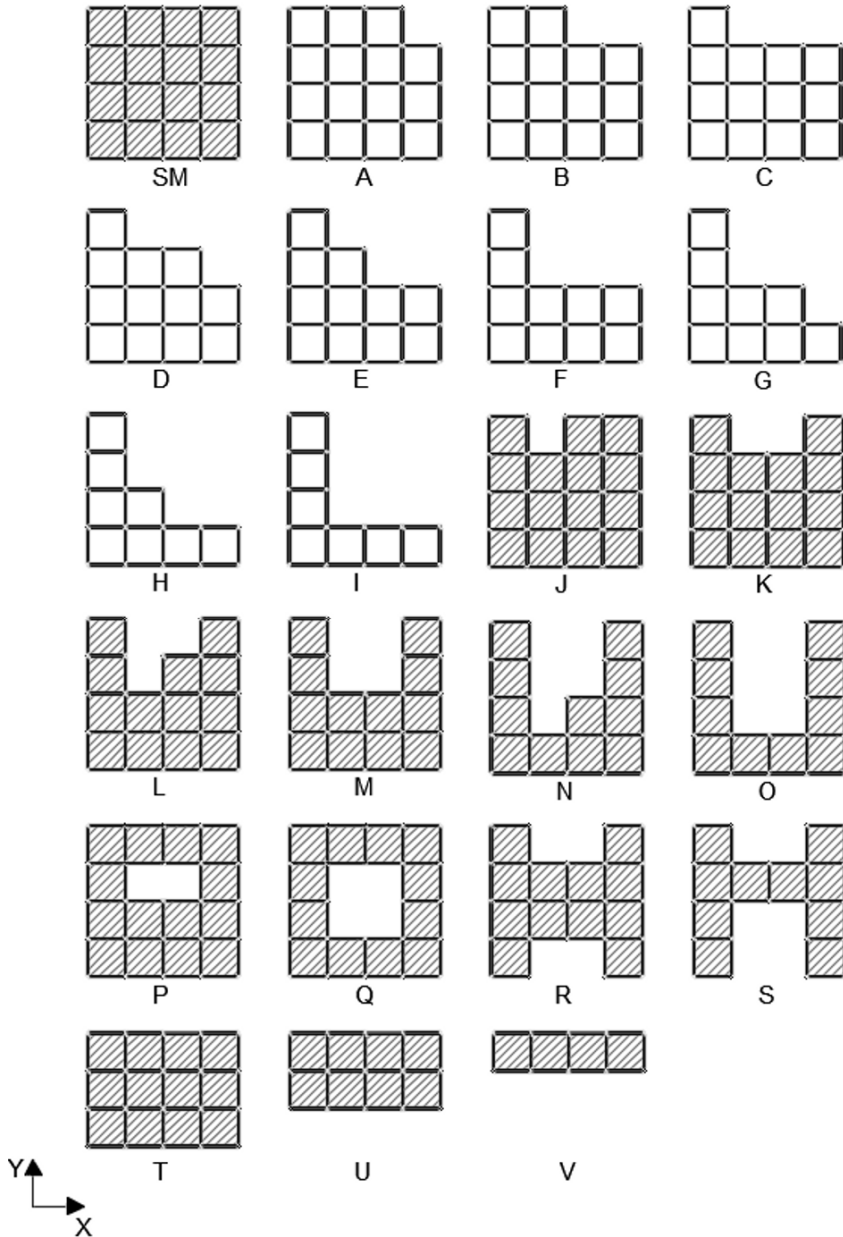
Fig. 4.4 – In plane shape of models analysed

It is worth mentioning that for this Section, where indicated, the major part of the figures are reported in Annex A. Here, only the figures for buildings with 2 storeys are reported. In the Annex A, one can find similar figures for the others buildings. Figure 4.5 and figures from A.1 to A3 (see Annex A) show histograms that summarize the M[%]s of fundamental modes of models, with specific indication about the inferior limit on the parameter investigated, accounting for the main directions (X and Y).
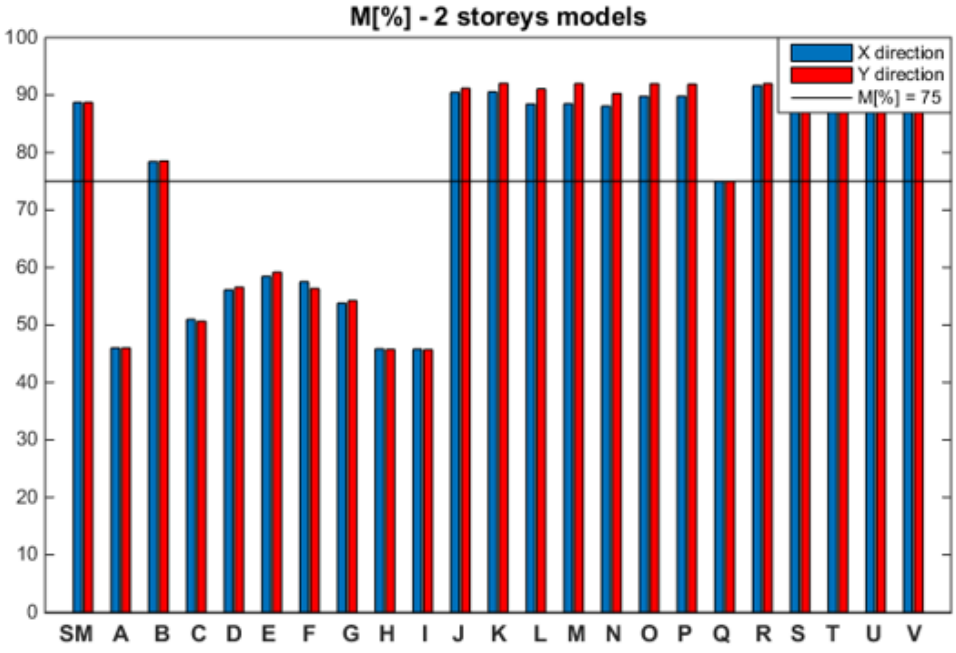
Fig. 4.5 – M[%]s of fundamental modes in both directions (X and Y) for models with 2 storeys.

The tag assignment of the buildings is causal and made according to the generation of the models. Based on the results obtained from the eigenvalue analyses, the models accounted for the pushover analyses are the ones indicated in figure 4.4 with fillings. The linear model have been made considering the hypothesis of rigid floor, through the introduction of an internal rigid diaphragm constraint at each floor. In addition, models have been embedded at the base. One could note that the models B and J have been not considered in the subsequent analyses (they are not filled in figure 4.4). In fact, the study has been performed for models in which, for each height (2, 4, 6 and

8 storeys), the M[%] is greater than 75% for the fundamental mode. Nevertheless, only some models of B and J typologies have M[%] greater than 75%, reason for which they are not significant for the investigation. Furthermore, just in this part of the analyses, one can note that models as M is irregular in-plan, according to the definition provided by EC8, but the conventional pushover is applicable, as highlighted in figures 4.5 and A.1-A.3. Before to perform the NLS unimodal analyses, in the FE models have been included the NL properties of materials and sections, simulated through a lumped plasticity approach. In particular, at end section of elements plastic hinges have been placed, which are defined considering inelastic mechanisms of simple bending for the beams and a combination of axial stress-bending stress for the columns. In both cases, the plastic hinges have been defined according to FEMA 356 rules, as shown in figure 3.8. For NLS analysis results, two hypotheses about collapse mechanisms have been supposed, as well as the brittle shear mechanisms are neglected (shear plastic hinges are not inserted) and the local mechanisms, as soft story, are not allowed. For respecting this latter condition, the simulated design has been calibrated more times, especially for the higher buildings. For each model, NLS analyses have been carried out, by using an unimodal load profile, assumption which results correct, because M[%] related to fundamental mode of vibration is greater than of 75%, according to EC8 – part 3, paragraph 4.4.4.2 and EC8 – part 1, paragraph 4.3.3.4.2. Analyses have been performed assuming CN coincident with geometrical CM of last storey, obtaining as result the capacity curves (or pushover curve) in terms of V_b - δ_R. The term δ_{LS} (then, the criterion for defining the achievement of the LSLS) has been defined as roof displacement due to the first achievement of $\frac{3}{4}\ \theta_u$ in one column. In figures 4.6 and from figure A.4 to figure A.6 (see Annex A) are shown the results of pushover curves in X direction (for simplicity, pushover curves in Y direction are not reported, because the treatment is similar in both directions), for each model selected above, varying the number of storeys. The curves in figures 4.6 and from figure A.4 to figure A.6 (see Annex A) are shown in a-dimensional terms, normalizing the V_b respect to the total seismic weight of the structure ($W_{building}$) and δ_{LS} respect to the total height of the building ($H_{building}$). It is

worth mentioning that the choice of LSLS threshold is not specified in anyone technical rule.
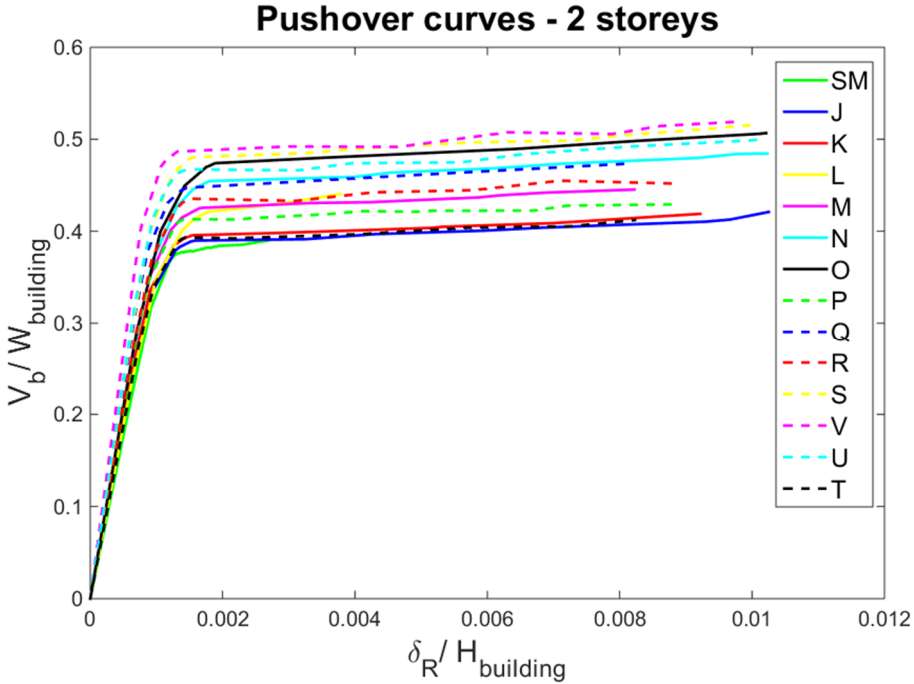
Fig. 4.6b – A-dimensional pushover curves of 4 and 2 storeys models selected, assuming CM =CN.

Therefore, the criterion chosen is in accordance with the crucial role that the vertical elements assume into global safety of building analysed. In fact, analysing the columns behaviour, it is possible calibrates the retrofit intervention. In the cases in which the LSLS is achieved by a horizontal structural element, one should do an evaluation case by case, with attention to the collapse mechanism typology (shear or flexural collapse). For the above reasons, the choice of LSLS threshold can be defined in different way, such as done in other works described in this Thesis. Once that the first NLS analyses have been performed, the position of CN has been varied on the models investigated. In particular, CN has been moved in a grid of points made on top storey plane. To this scope, the grid has been determined through the definition of a new reference system "α-β", centred in the origin of X-Y reference system, according to figure 4.3. Each CN is identified by using a normalization of X-Y values, as follow:

$$\alpha_i \frac{X_i}{X_{Tot}} \tag{4.5}$$

$$\beta_i \frac{Y_i}{Y_{Tot}} \tag{4.6}$$

where X_{TOT} and Y_{TOT} are the total lengths of SM, respectively in X and Y directions. In this way, the coordinates were dimensionless and both α and β are included between 0 and 1. In this new reference system, CM has coordinates α_{cm} and β_{cm}. In each model, CN has been positioned in 16 different positions obtained by varying α and β. The values that α and β assumed in the above positions are summarized below:

- α: 0; 0,5; 1; α_{cm};
- β: 0; 0,5; 1; β_{cm}

In figure 4.7 is shown the combination of α and β values, for 16 points where positioning CN. In some cases, the number of points of grid is reduced, because some of these can be both out of plane or coincident with other ones.
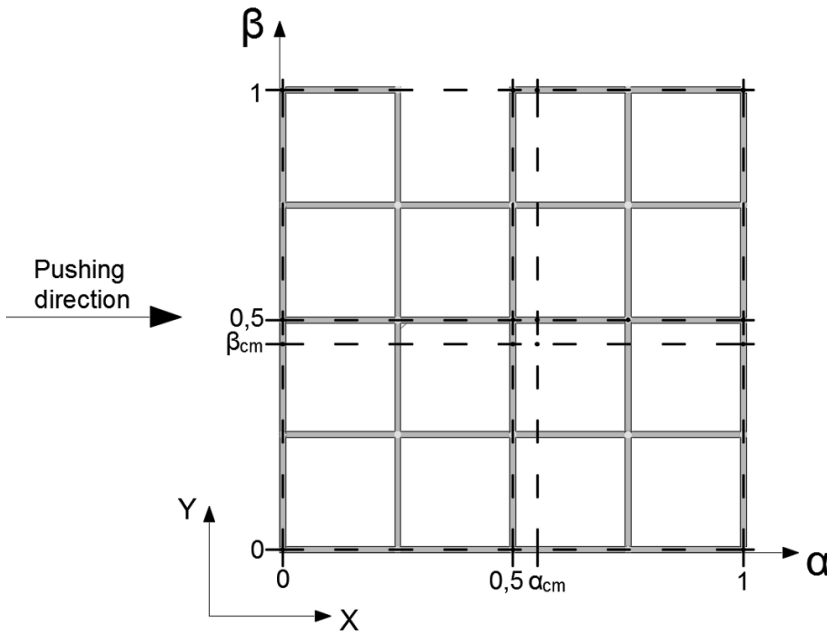
Fig. 4.7 – Grid points for model J, using the parametric approach to positioning CNs.

This parameterization takes into account the usually uncertainty related to the real position of CM, provided by the accidental loads. Clearly, to consider the CM in the corner of the building is not physically significant, but the procedural choice is focused on the identification of an extensive and complete trend of structural capacity plotting. Plotting the pushover curves varying the CN position, results has shown that in some cases, especially those with regular in plane shape, as in SM, T, U and V, all capacity curves are similar in terms of δ_{LS}. Same result has been obtained on Q and R models, which are in-plan symmetric in both direction. Furthermore, even the results of model P did not present high differences. For these models, maximum differences between $\delta_{LS,CM}$ (obtained by analysis with CN = CM) and δ_{LS} obtained by CN in other points of the grid ($\delta_{LS,i}$), are lower than 5%. Table 4.1 shows the percentage differences of what previous described, considering maximum and minimum $\delta_{LS,i}$. In the other models (J, K, M, N, O and S), which have generally irregular in-plan shape, there are consistent differences between $\delta_{LS,i}$ and $\delta_{LS,CM}$, which in some cases, reached values of 20%. Table 4.2 shows percentage differences in the previous models (in absolute value).
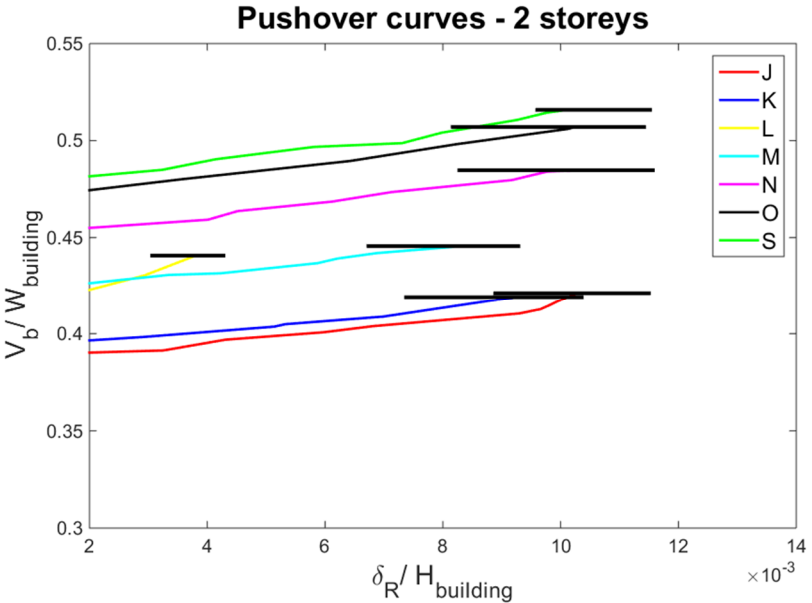
Fig. 4.8 – Zoom view of a-dimensional pushover curves of models selected and reported in tab. 4.2, considering the variation of δ_{LS} for each model to 2 storeys

Tab. 4.1 – Models with low differences of δ_{LS}

Model		$\delta_{LS,CM}$ (m)	Variation $\delta_{LS,imax} - \delta_{LS,CM}$ (%)	Variation $\delta_{LS,imin} - \delta_{LS,CM}$ (%)
SM	8 Storeys	0,0818	0,00	0,00
	6 Storeys	0,0726	0,00	0,00
	4 Storeys	0,0573	1,33	-2,89
	2 Storeys	0,0513	1,83	-1,83
T	8 Storeys	0,0875	0,00	0,00
	6 Storeys	0,0703	0,01	-0,79
	4 Storeys	0,0589	0,15	-3,31
	2 Storeys	0,0494	0,55	-0,37
U	8 Storeys	0,0906	0,00	-2,31
	6 Storeys	0,0741	0,15	-0,16
	4 Storeys	0,0665	0,01	-0,01
	2 Storeys	0,0511	0,14	-0,16
V	8 Storeys	0,0986	0,13	-1,04
	6 Storeys	0,0751	0,00	-0,68
	4 Storeys	0,0629	0,01	-0,01
	2 Storeys	0,0494	0,04	-0,04
P	8 Storeys	0,1091	1,37	-2,66
	6 Storeys	0,0866	0,92	-0,58
	4 Storeys	0,0712	0,42	-1,69
	2 Storeys	0,0621	2,42	-1,29
Q	8 Storeys	0,0897	0,54	-0,94
	6 Storeys	0,0732	3,71	-3,73
	4 Storeys	0,0573	0,00	-1,86
	2 Storeys	0,0489	0,03	-0,03
R	8 Storeys	0,0979	0,04	0,00
	6 Storeys	0,0762	2,02	0,00
	4 Storeys	0,0669	0,43	-0,43
	2 Storeys	0,0526	0,02	-0,02

Tab. 4.2 – Models with high differences of δ_{LS}

Model		$\delta_{LS,CM}$ (m)	Variation $\delta_{LS,imax} - \delta_{LS,CM}$ (%)	Variation $\delta_{LS,imin} - \delta_{LS,CM}$ (%)
J	8 Storeys	0,0838	8,37	-7,57
	6 Storeys	0,0775	10,92	-10,92
	4 Storeys	0,0707	12,98	-12,02
	2 Storeys	0,0615	13,21	-12,25
K	8 Storeys	0,0891	11,04	-7,33
	6 Storeys	0,0659	13,83	-10,86
	4 Storeys	0,0562	18,08	-12,29
	2 Storeys	0,0553	19,92	-12,48
L	8 Storeys	0,0717	11,80	-7,50
	6 Storeys	0,0521	14,33	-11,60
	4 Storeys	0,0356	17,96	-12,56
	2 Storeys	0,0226	18,96	-12,99
M	8 Storeys	0,0936	10,99	-6,78
	6 Storeys	0,0700	15,21	-11,10
	4 Storeys	0,0565	17,85	-12,74
	2 Storeys	0,0493	18,06	-12,89
N	8 Storeys	0,1092	13,01	-6,50
	6 Storeys	0,0953	15,01	-19,52
	4 Storeys	0,0775	17,66	-12,89
	2 Storeys	0,0613	19,06	-13,02
O	8 Storeys	0,0936	8,97	-9,69
	6 Storeys	0,0911	17,63	-10,93
	4 Storeys	0,0755	18,62	-11,60
	2 Storeys	0,0613	20,04	-11,78
S	8 Storeys	0,1001	3,60	-3,60
	6 Storeys	0,0877	8,36	-7,68
	4 Storeys	0,0744	10,62	-7,09
	2 Storeys	0,0605	13,50	-6,70

In figures 4.8 and from figure A.7 to A.9 (see Annex A) are reported the final parts of the curves in figure 4.6 and from figures A.4 to A.6 (see Annex A), showing the variability of results in terms of δ_{LS}, with the pushover curves, which can be shift in horizontal. Clearly, as just mentioned, the value of maximum V_b is constant for each capacity curve of same model and the structural capacity is the same, but the variation of CN change the plot of the response. This is a limitation of NLS analysis, because it strongly depends from the CN (differently from the NLD analysis). In addition, results of NLS analysis of all models showed that, in X direction, δ_{LS} is equal for each position on the line that connect the points with same α. This means that to 4 values of β correspond to 4 values of δ_{LS} in the 4 capacity curves, as showed in figure 4.7. The same observation can be made regarding analyses in Y direction, where δ_{LS} is equal for each position on the line that connect the points with same β. Results obtained by NLS analyses are plotted in particular graphs (figures 4.9 and from figure A.10 to A.12, see Annex A) in which, for a fixed number of storeys, in abscissa there is a position β, while in ordinate there is the ratio $\delta_{LS,i}/\delta_{LS,CM}$. As shows in this figure for model J, points are reported and, in order to define a general rule for identifying the results, a trend line are outlined. Assuming trend lines as linear, each one is plotted in the graphs, showing their trend of varying, when the number of storeys change. The regression factor R^2, in each case, is greater than 0.98, being R^2 the coefficient usually adopted for estimating the good fitting of the regression lines to the data. This result was expected, considering that, using an unimodal load profile for pushover analysis, the rotational component of loads provided a torsional effect. In figures 4.10 for model J and from figure A.13 to A.18 for other models (see Annex A), the 4 trend lines obtained for the cases analysed are plotted, varying the number of storeys. Same figure provides two main indications:

- Increasing the number of storeys, the slope (m) of the trend line decreases;
- The 4 trend lines are placed on the graph, according to a proper bundle of straight lines, with centre of rotation in a specified point: CM. The coordinates of the centre of rotation are: β_{CM} in abscissa and $\delta_{LS,i}/\delta_{LS,CM} = 1$ in ordinate.

The second indication can be expressed in a generic format, with the following relationship, where the unknown factor is only $\delta_{LS,i}$:

$$\frac{\delta_{LS,i}}{\delta_{LS,CM}} - 1 \ = m(\beta_i - \beta_{CM}) \tag{4.7}$$
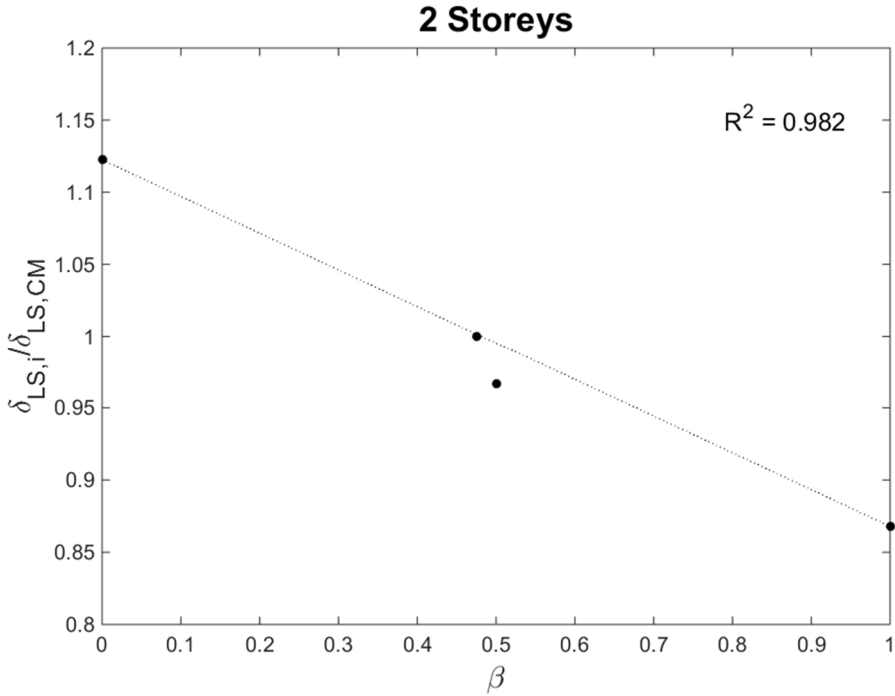
2 Storeys

Fig. 4.9 – Distribution of $\delta_{LS,i}/\delta_{LS,CM}$, varying β for 2-storeys models of J.

In eq. 4.7, firstly, the influence on formulation of X_{TOT} value must be assessed and secondly, the slope of the trend line (m) must be determined, considering all parameters that influence its value. To this purpose, the X_{TOT} value has been varied, in order to check that the in plane dimensions do not vary the formulation found. By retaining constant the building height and varying the length of beams at values of 6.00 m and 2.50 m, dimensions of RM have been changed. The new RMs have been replied, in order to obtain the same in-plan shapes of models previously analysed. All phases performed have been replied, assuming the position of CN in the grid of points defined above. The proof have been carried out randomly, investigating the variation of X_{TOT}, for

3 models as M, L and K. Results are shown in figures 4.11 and from figure A.18 to A.20 (see Annex A).
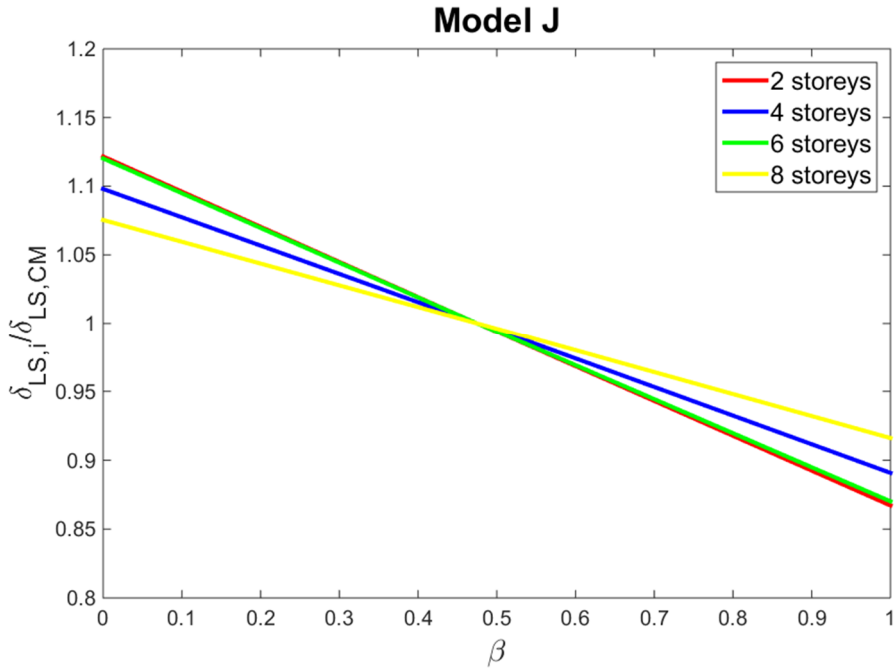
Fig. 4.10 – Distribution of $\delta_{LS,i}/\delta_{LS,CM}$, varying number of storeys, for models J

In eq. 4.7, In each graph the trend of the parameters $\delta_{LS,i\ MIN}/\delta_{LS,CM}$ and $\delta_{LS,i\ MAX}/\delta_{LS,CM}$ are depicted, assuming the 3 values of X_{TOT} for RM (X_{TOT} RM) and varying the number of storeys. The 3 lines are positioned similarly to a horizontal line, with maximum differences in the order of 5%, value which suggest that the variation of X_{TOT} do not change the trend showed in eq. 4.7. In order to provide a relationship able to estimate m for each model, a correlation between m and the number of storeys (n) has been evaluated. For this reason, a fitting curve has been carry out for each model and all have been inserted in a graph with in abscissa the value of n and in ordinate the value of m. Figure 4.12 shows all trend lines and, from these, a global linear trend has been determined as follow:

$$m = 0.35 \left(1 - \frac{n}{20}\right) \tag{4.8}$$
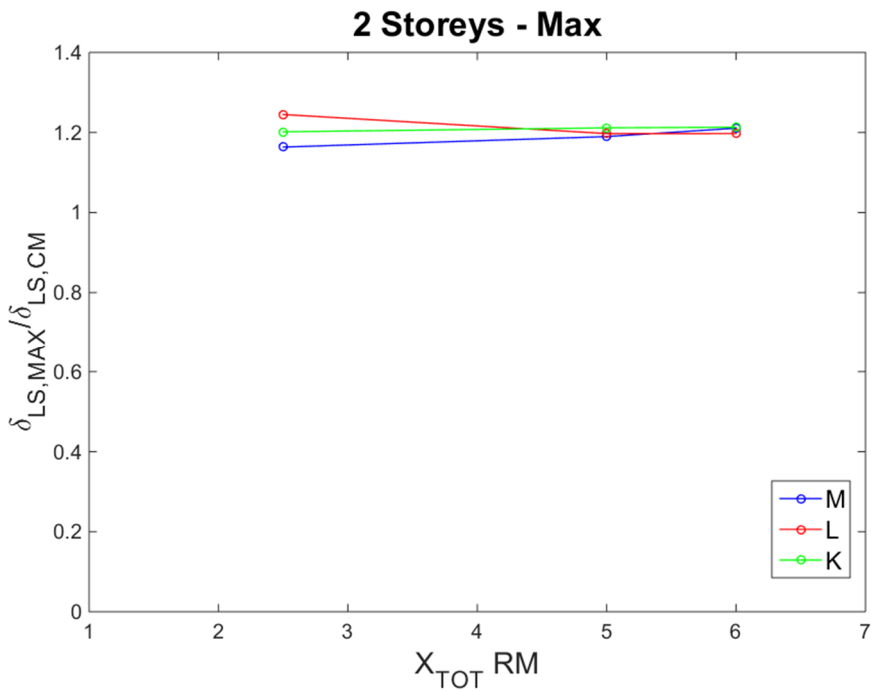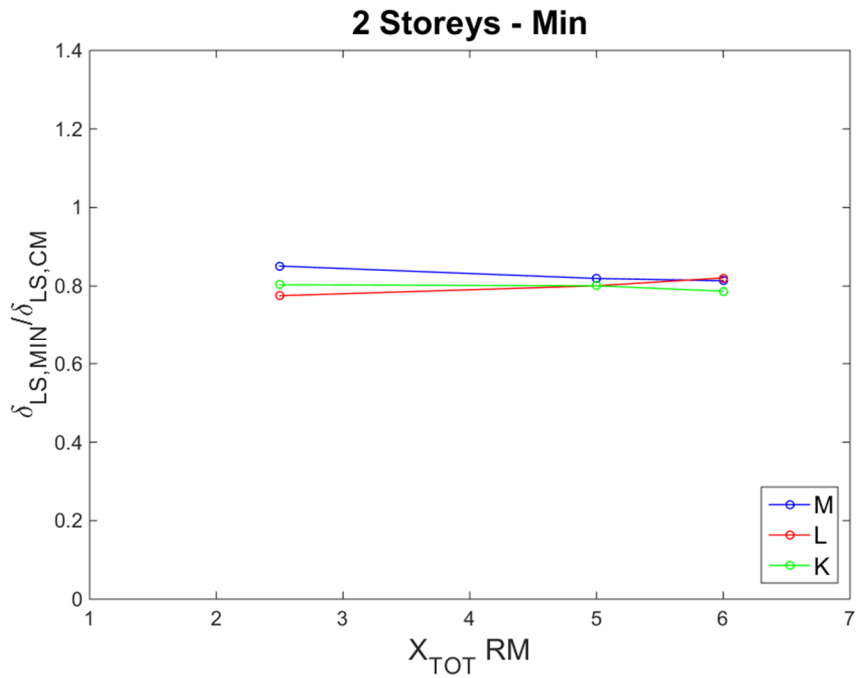
Fig. 4.11 –Trend of $\delta_{LS,i\ MIN}/\delta_{LS,CM}$ and $\delta_{LS,i\ MAX}/\delta_{LS,CM}$, varying X_{TOT} for models M,L and K, with 2 storeys.
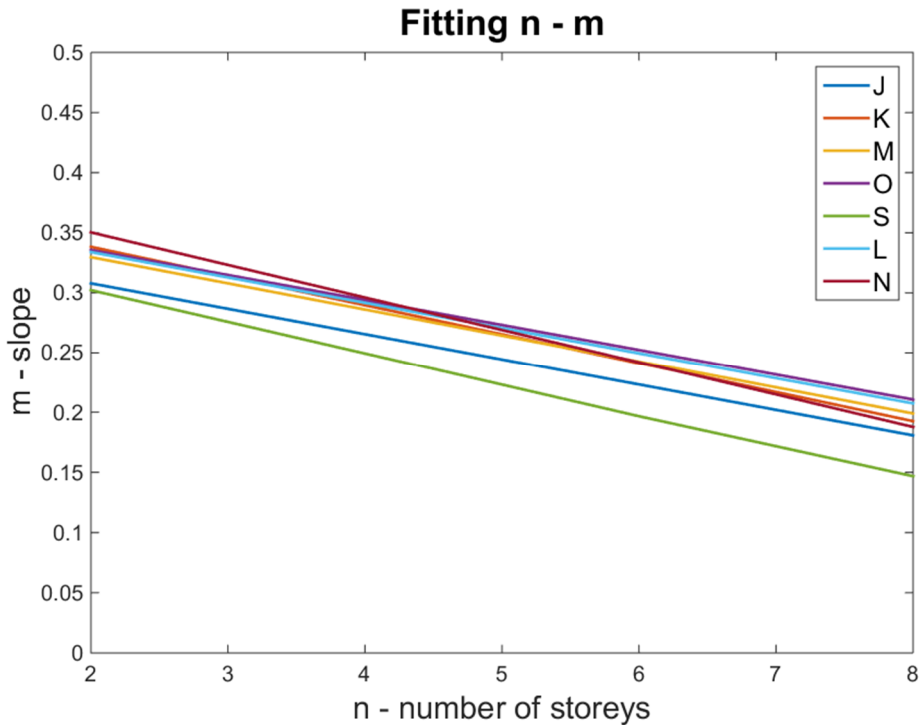
Fig. 4.12 - Trend lines for each model, consecutive to fitting m-n.

In order to validate the eq. 4.8 this latter one has been inserted in eq. 4.7 and for each model investigated the value of $\delta_{LS,i}$ has been analysed, comparing these results with the ones obtained by NLS analyses on numerical models (varying the position of CN). To follow, in tables 4.3 and from table A.1 to A.3 (see Annex A), the percentage differences, between $\delta_{LS,i}$ obtained by FE models and $\delta_{LS,i}$ obtained by eq. 4.8, are reported for each model. Results of comparison show that the percentage differences are in the order of 10–15%, with maximum variation, in very few cases, of about 20%. These values imply that the eq. 4.8 represent, with good accurateness, the real trend of m variation.

Tab. 4.3d – Results of methods validation; percentage differences between FE models and formulation in terms of δ_{LS}, for 2 storeys buildings

Model	β	$\delta_{LS,i}/\delta_{LS,CM}$ Model	$\delta_{LS,i}/\delta_{LS,CM}$ (eq.4.8)	Variation (%)
J	1	0,868	0,811	6,737
	0.5	0,995	0,991	0,198
	β_{CM}	1,000	1,000	0,000
	0	1,122	1,171	7,736
K	1	0,800	0,801	20,115
	0.5	0,963	0,970	4,441
	β_{CM}	1,000	1,000	0,000
	0	1,126	1,161	9,496
L	1	0,810	0,807	18,509
	0.5	0,980	0,987	2,602
	β_{CM}	1,000	1,000	0,000
	0	1,130	1,167	9,736
M	1	0,819	0,790	14,574
	0.5	0,974	0,970	2,203
	β_{CM}	1,000	1,000	0,000
	0	1,129	1,150	11,026
N	1	0,809	0,795	17,264
	0.5	0,971	0,975	3,317
	β_{CM}	1,000	1,000	0,000
	0	1,130	1,155	10,842
O	1	0,810	0,793	16,968
	0.5	0,970	0,973	3,370
	β_{CM}	1,000	1,000	0,000
	0	1,130	1,153	10,908
S	1	0,865	0,811	7,250
	0.5	0,921	0,991	15,442
	β_{CM}	1,000	1,000	0,000
	0	1,067	1,171	3,050

The results of all analyses performed, show the effects of NLS analysis on existing RC buildings with irregularity in-plan, varying the position of CN. In particular, a sample of 92 ideal buildings has been investigated, made according to predominant features of real existing buildings and with casual in-plan shape and number of storeys variables from 2 to 8. From the first analyses, 28 buildings of the sample have been considered, because dynamically regular (M[%]>75%). On these models, through the application of NLS unimodal analyses, a new formulation has been developed, able to describe how to change the plotting of capacity curve, with reference to LSLS, changing the position of CN. In particular, the formulation proposed, through a parametrization of the CN on the last storey of buildings, is able to provide the increment or decrement of δ_{LS}, starting from the value of $\delta_{LS,CM}$, by using the mathematical equation of a straight line. This evaluation takes into account the uncertainty related to the real position of CM, provided by the accidental loads, important datum in order to carry out the N2 method for assessing the performance of existing buildings.

4.2.3 Non-Conventional methods: multimodal and adaptive pushover

As just mentioned in the Section 4.2, NLS procedures, despite their effectiveness, have two main limitations (figure 4.13). Firstly, the assumption of an unimodal profile, which accounts for only the deformed shape of the fundamental vibration mode and it is not able to consider the effects of higher modes, with higher frequency. This latter can be significant in some situation, especially when the buildings are irregular. In particular, the higher modes can be important when the buildings present irregularities in-plan or in-elevation, or systems that hide irregular mass and stiffness distributions. In this case, the building can be defined as dynamic irregular, in the sense that the vibration modes are coupled, with lower M[%] in the main directions. The direct consequence of applying an unimodal pushover to an irregular building could be a wrong prediction of the structural response just in elastic field, with different elastic stiffness shown from the capacity curve. Consequently, the post elastic branch of capacity curve does not catch the real inelastic behaviour, considering the continuous evolution of the vibration modes. In addition, another effect is a wrong estimation of the

torsional effects of the structure, which can lead to the increment of the seismic demand for the storeys elements, especially for the ones on the building sides. This effect can increase the occurrence of brittle mechanisms in the structural elements. The torsional behaviour of the existing buildings, in both elastic and inelastic field is highlighted in several works available in the scientific literature (see Chapter 2, where is shown the explanation of the main parameters, which influence the problem). Clearly, these effects provide different results, in terms of assessment and definition of structural performance and safety level, such as shown in (Kreslin and Fajfar, 2012). In order to overcome this limitation, it is possible to use a load profile proportional to the storey shear distribution, computed by combining modal responses from a modal response spectrum analysis of the building. Another methodology, which was developed in several scientific works, is the multimodal pushover analysis.

1) Unimodal load profile vs.High influence of higher modes

2)Time invariant load profile vs. Continous variation of plasticization and dynamic properties

1) Multimodal
2) Adaptive
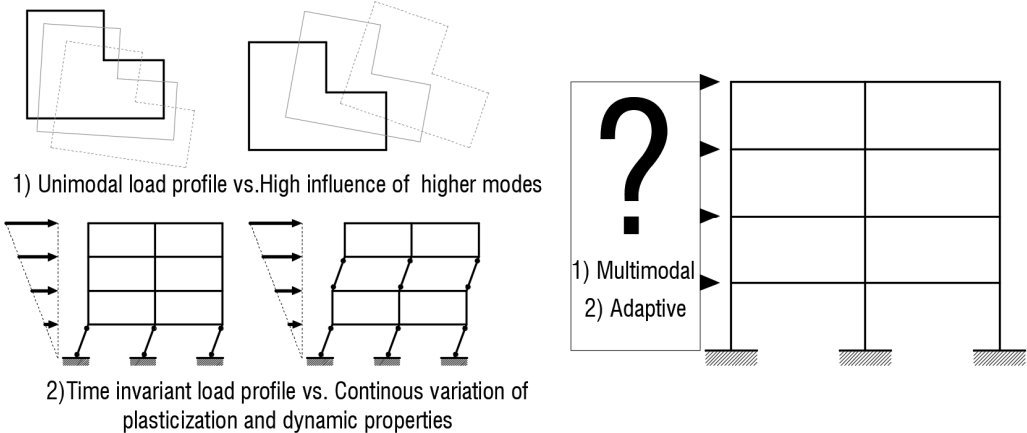
Fig. 4.13 – Drawbacks of conventional pushover analysis

The second issue related to conventional NLS analysis concerns the assumption of time invariant load profiles. Generally, when a building is stressed with a pushover analysis, in the post-elastic field progressive plasticization of structural elements occurs, even for regular buildings. This is due to a continuous redistribution of inertial forces that in turn is due to local losses of stiffness and damage of the structural elements. The assumption of a time invariant load profile lead to neglect the variations of the dynamic properties of the structure, as the fundamental frequencies, the shapes of

fundamental modes and the M[%]s and to provide a good estimation of the structural response until the end of the elastic field. In the inelastic field, the structural response can results not consistent with the ones observed from NLD analyses. In order to overcome the problem given by a time invariant load profile, technical codes suggest of performing adaptive pushover analysis. In the last 30 years, the scientific community employed for developing methodologies for estimating the structural response through non-conventional pushover analyses, as the multimodal and adaptive ones. Concerning to the multimodal pushover analysis, the first work in which was assessed the relevance of higher modes in NLS analysis, was (Paret et al., 1996), where authors performed unimodal pushover analyses proportional to the first three modes of two high RC buildings, one with strong columns and weak beams and another one with strong beams and weak columns. For identifying the critical mode for the buildings, authors proposed of computing a vulnerability index called "Modal Criticality Index" (MCI), computed relating the capacity curve with the response spectrum. The mode with the greater MCI was the critical one for the building, as the second mode for the case in figure 4.14.
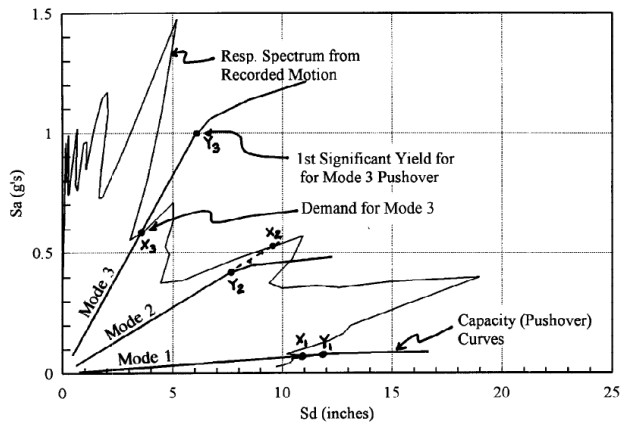
Fig. 4.14 – Graphic computation of MCI with critical vibration mode, which is the second one

Subsequently, other authors (Sasaki et al., 1998) presented a similar study to the previous one, in which they proposed to perform three different pushover analyses, with load profiles proportional to the first three main modes. The results of the research

work confirmed that, in some cases, the actual damage mechanisms were not associated to the first mode, according to the results obtained from NDL analyses. The most important procedures for performing multimodal analyses were proposed by Chopra, which published some works about this topic, proposed some solutions, and subsequently improved them. In particular, in (Chopra and Goel, 2002), authors proposed a procedure known as Modal Pushover Analysis (MPA). The aim of the authors was to develop a procedure based on the elastic theory of the dynamic of the structures, performing pushover analyses according to the elastic behaviour of the structure. Starting from it and assuming that the structures in the inelastic field have same initial stiffness, mass, damping and vibration modes, authors extended the procedure in the inelastic field. In particular, they uncoupled the vibration modes, defining the load profiles as in eq. 4.2 (see figure 4.15). The pushover analyses were performed until a target displacement, dependent from the vibration mode and from the damping of system, computed through the equivalence of the structure with the equivalent SDoF for that mode. After the performance of the pushover analyses, the MPA was performed, combining the response of the structure, through the elastic method combination, such as the complete quadratic combination (CQC) or SRSS. In the application of the methodology, authors found a good agreement with the results obtained from NLD analyses results and the ones provided by MPA. The main limitations of the method proposed were firstly, the study of the inelastic behaviour neglected the well-known phenomena that occur, such as the increment of plasticization and the variation of the vibration modes. In addition, the major critical issue was the combination of inelastic responses (e.g. in terms of deformation as θ_i), by using methodologies valid in the elastic field and without theoretical base. In fact, when the plasticization effects became significant, there is a continuous change of the structural stiffness, with variation of modal shapes and coupling of vibration modes, which are effects that cannot be neglected in a NL analysis. In a successive paper (Chopra and Goel, 2004), the same authors applied the aforementioned procedure for buildings asymmetric in-plan. Numerical analyses showed that the method was applicable both to spatial "torsionally-stiff" and "torsionally-flexi-

ble" systems, whereas the method lost its accuracy for "torsionally-similar-stiff" systems (i.e. systems for which torsional stiffness and flexible stiffness are comparable) because the vibration modes become strongly coupled.
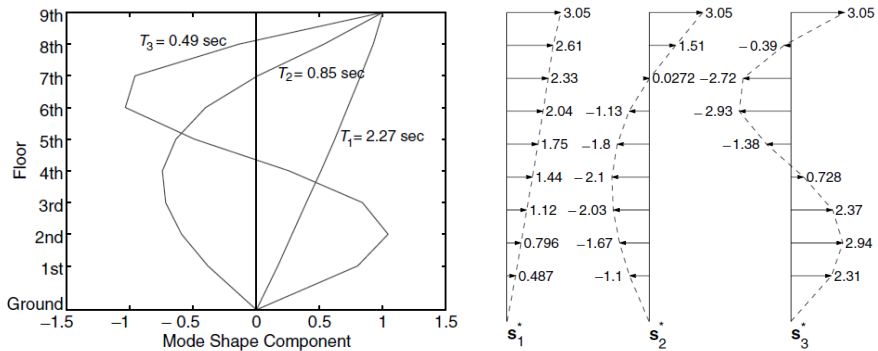
Fig. 4.15 – Application of MPA on a 9 storeys building, considering the first three vibration modes (Chopra and Goel, 2001)

In (Goel and Chopra, 2005), authors applied the MPA to an extensive set of case studies composed by more of 100 tall buildings. As a general result, they observed that the consideration of the higher modes in the analyses, especially in the cases of high buildings, were important for predicting the formation of mechanisms in the higher floors. In addition, in few cases, performing the pushover analysis proportional to the 3rd vibration mode, the phenomenon of reversal occurred, in which the formation of plastic hinges causes an inversion of the direction of the top floor displacement. In this case, the results of MPA showed the inapplicability of the method. The same researcher (Chopra et al., 2004) proposed a modified version of MPA, in which the inelastic response of buildings was derived from the combination of the inelastic response of the 1st mode and the elastic contributions of the responses provided by static analyses performed according to the higher modes. The main advantage of this method was to provide results comparable to MPA results, carrying out fewer NLS analyses and substantially decreasing the computational efforts. Contemporary to the works of Chopra and following the above idea, (Moghadam, 2002) formulated a pro-

cedure similar to MPA, proposing to use, in the elastic range, of a simplified combination of modes, through coefficients obtained by the modal participation factors of the considered modes. Other authors (Hernadez-Montes et al., 2004), proposed an energy-based formulation for predicting the structural response of buildings through NLS analyses. In particular, authors showed that in some cases, such as when occurs the case of "reversal", the capacity curve depicted by the usual performance point (δ_R - V_b) was not a good representation of the capacity of structure. In fact, one of the main problems of MPA was that, in the inelastic range, the growth of the δ_R had different trend of the other floors displacements, as instead happens in the elastic range. In order to show the real critical damage state of the building, preventing problems related to the choice of the performance point, the authors proposed an energetic procedure for the determination of the capacity curve. In particular, instead to plot the capacity curve as above indicated, the authors proposed to plot the capacity of the system, for each mode, in terms of V_b vs. the energy dissipated from the system during the analysis, through the definition of an energy-based displacement ($D_{e,n}$). This latter was defined as follow:

$$D_{e,n} = \frac{2E_n}{V_{b,n}} \tag{4.9}$$

where E_n is the energy dissipated from the system under the analysis and $V_{b,n}$ is the V_b, for the load profile related to the nth vibration mode. The energy dissipated is the area underlying the curve. In order to apply the energy-based approach also in the inelastic field, for each analysis step, the authors recorded the work done by $V_{b,n}$ on the system, in differential way, through the computation of dE_n, which is proportional to the differential displacement $dD_{e,n}$, as indicated in figure 4.16. The application of the procedures on a case study, showed how this procedure was able to reproduce the results obtained from the conventional pushover curve for the fundamental mode and the possible anomalies criticized in the previous works of Chopra, such as the application of the elastic combination rule (SRSS) in situation of strong plasticization. In (Kunnath, 2004), a multimodal procedure was proposed, based on the combination of two load profiles proportional to the sum and difference of the first two modes. The results of the procedure applied on two case studies (8 and 16 storeys buildings) showed that,

in the first case, the structural response, expressed in terms of θ_i, was overestimated for lower floors, while in the second case there was an overestimation for higher floors, based on the comparison with NLD analyses. In order to predict the structural response of buildings, the author conducted a subsequent campaign of numerical analyses for regular RC frame buildings and calibrated a procedure called Method of Modal Combination (MMC), in which the load profiles proportional to the first three modes were combined through modification factors "α_i". These latter coefficients depended by the seismic demands and elastic T of the mode considered.
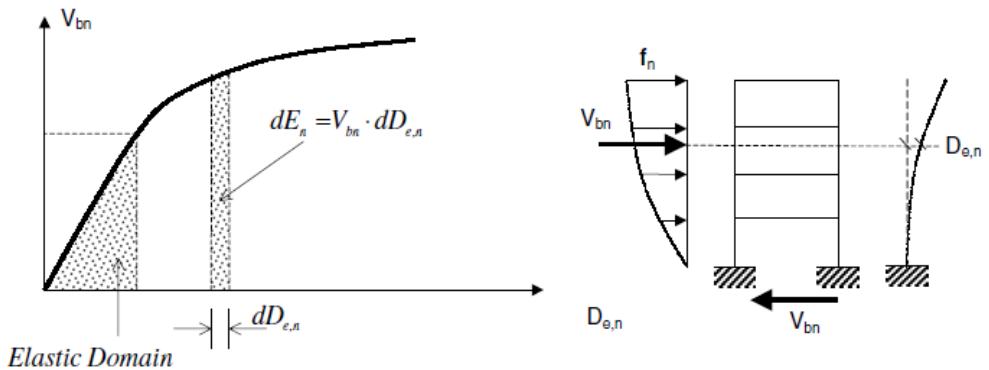
Fig. 4.16 – Definition of energy-based capacity curve, extended to inelastic domain (Hernandez-Montes et al., 2004)

In (Barros and Almeida, 2005), with the aim of simplifying the computational efforts of multimodal analysis previously proposed, authors accounted for the contribution of higher modes, through the proposal of a multimodal analysis procedure based on a single load profile. This was computed through the combination of the modes by using participation factors called α (different from the ones previously defined) for each vibration mode, obtained by the elastic response of the structure subjected to seismic action. They carried out pushover analyses on 3D models with different features (symmetrical structure, stiffness asymmetric structure, mass asymmetric structure) and the results were compared with NLD analysis and unimodal pushover results, in order to calibrate the load profile combination on simple structures. In (Poursha et al., 2009) a different approach to the problem was proposed, by leading consecutive pushover

analysis performed by pushing the structure to determined displacements, based on the modal properties of the structure. In particular, the analysis started with an inverse triangular or uniform load profile and then, according to the T of the first vibration mode of the structure. After, the load profile was updated to different consecutive displacements, established on the base of the target displacements. The update was performed by using standard coefficients estimated by the modal parameters of structures. The method, called consecutive modal pushover (CMP), allowed of changing the load profile, one time for rigid system, two times for deformable system. Furthermore, the results of the method were compared with MPA ones, showing that CMP provided more accurate values of interstorey drifts and plastic hinges rotations, especially at lower floors (according to the results of NLD analyses). In (Sucuoglu and Günay, 2011), a multimodal procedure was proposed, called generalized pushover analysis (GPA). In particular, the procedure provided generalized load profiles, computed as combination of modal components obtained from response spectrum analysis. The results of analyses were the peak seismic responses obtained from the envelope of N+1 pushover analyses, where N is the number of storeys of the building investigated. For each pushover step, the load profiles were maximized through a modal analysis, in order to reach the maximum damage parameter, in terms of θ_i. In (Surmeli and Yuksel, 2015) a variant of modal pushover analysis (VMPA) was proposed, based on an iterative process, able to modify the secant stiffness of the structural elements and then, able to account the dynamic behaviour variation. Using the equal displacement rule, for each analysis step, authors updated the moment-curvature law of structural elements through the computation of the secant stiffness on the ADRS plane, in order to consider the building behaviour in the inelastic field and to account for the plasticization. Changing the constitutive laws of structural element, the dynamic parameters changed, such as the vibration modes, which ruled the definition of the load profiles. The application of the method provided high accuracy with the results obtained from NLD analyses, with some problems related to the structural elements in the upper stories. Other recent research works should be mentioned about the multimodal pushover, such as the ones proposed by (Kaatsiz and Suculoglu, 2014, Ferraioli et al., 2016, Colajanni et al., 2017, Ferraioli,

2017). The lack of a unique method able to define a "correct" load profile for simulating the seismic actions and, at the same time, able to take into account the stiffness variation in the post-elastic range induced several researchers to consider the possibility of performing NLS analyses with an adaptive load profile. This latter must be continuously update, by considering the real damage state of the system and its structural elements. In the scientific literature, many adaptive pushover methods were proposed and developed. The first proposal of adaptive method was in (Bracci et al., 1997), where the authors developed a procedure valid for medium-low-rise buildings in which the load profile was updated when the stiffness variation become significant. The load pattern was update three times, as well as at the yielding, near to the collapse and at collapse. For each update, the capacity curve was compared with a range of seismic demand, depicted in the band in figure 4.17. Based on the position of the curves bundle, which was dependent from the dynamic parameters of the building, it was possible to understand the behaviour of the system under seismic action, with regard of the yielding and failure states.
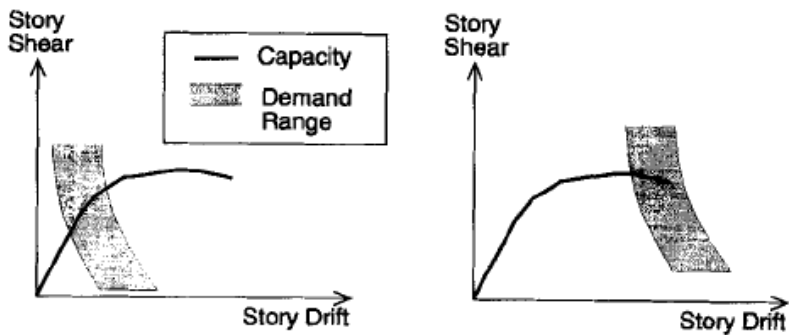
Fig. 4.17 – Comparison of structural capacity and seismic demand, after the load profile update (Bracci et al., 1997)

In (Gupta and Kunnath, 2000) a new procedure was proposed, which provided the execution of a certain number of pushover analyses, according to the number of significant vibration modes. The load profiles were function of the elastic spectrum of the site considered and the analysis was conducted in incremental form, in which the

modal shapes associated to the tangent stiffness matrix were calculated at the beginning of each load step. If at the end of a step, an element was yielded, the stiffness matrix was changed, accounting for the phenomenon. After evaluating the response parameters for each mode, they were combined through the SRSS modal combination rule. The authors applied the method to buildings with different heights, varying the strength and stiffness features of the case studies and evaluating the seismic demand parameters, such as V_b and θ_i. Concerning to their application, authors concluded affirming that, excluding the low-rise buildings, the higher modes must be considered in the analysis, such as done in their proposal. In (Elnashai, 2001), based on the procedure developed in (Bracci et al., 1997) a procedure was proposed, based on a single pushover analysis in which at each load step, the load profile was determined by combining the profiles corresponding to each vibration mode considered, through the SRSS combination rule. The author proposed two methods for updating the load profile, as the incremental and the total one. The total change of the load profile manifested instability problems. In the procedure, the structural element were investigated at each deformation level, varying the associated tangent stiffness matrix and inserting a parameter dependent from the response spectrum. In particular, the load profile was update through the factor $C_{Sa,I}$, computed as below:

$$
C_{Sa,i} = \frac{W_i \sqrt{\sum_{k=1}^{m} \left[\Phi_{ik} \Gamma_k \frac{S_{ak}}{\sum_{k=1}^{m} S_{ak}} \right]^2}}{\sum_{l=1}^{n} W_i \sqrt{\sum_{k=1}^{m} \left[\Phi_{ik} \Gamma_k \frac{S_{ak}}{\sum_{k=1}^{m} S_{ak}} \right]^2}}
$$

(4.10)

where k and l are counters, I is the number of storeys, j is the increment number, m is the number of modes, n is the storey considered, Φ is the mode shape vector, Γ is the coefficient of participating mass and S_a is the spectral acceleration. The method, which was an arbitrary extension of linear modal analysis, did not always provide accurate results, with respect to the response of NLD analysis. Based on the procedure of previous research, other authors proposed an algorithm that allowed the development of an adaptive pushover, able to account for the progressive stiffness deterioration and the effects caused by higher modes, as shown in (Antoniou and Pinho, 2004a).

The methodology, called Force Adaptive Pushover (FAP), was based on the previous work and had the aims of the accessible use, the identification of the critical regions where the strong inelastic deformations occur and the seismic demand for brittle elements and the good capacity of predicting the correct sequence of structural elements yielding, during the analysis. The steps of the procedure were similar to the ones shown in (Elnashai, 2001), where the scalar factor was called λ. The algorithm provided of updating the load profile in incremental or in total way, starting from an eigenvalue analysis of the structure. In particular, the modal load profiles proportional to the modes considered were determined by using the Lanczos algorithm and profiles were combined through SRSS or CQC combination rule. The methodology was developed on several stick-models, where authors recorded the load profile shape, at different levels of total drift, such as shown in figure 4.18

at 0% total drift   at 0.5% total drift   at 1.0% total drift   at 1.5% total drift
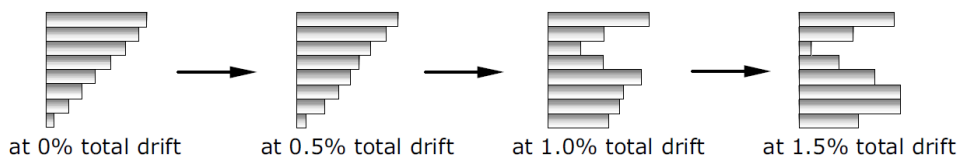
Fig. 4.18 – Update of the load profile, for different level of deformation (Antoniou and Pinho, 2004a)

The results of analyses showed that, despite the capacity curves in terms of V_b-δ_R were acceptable, for some response parameters as the total drift, the methodology did not provide a trend comparable with that calculated through NLD analyses. In order to improve the method, the same authors later developed an alternative procedure (Antoniou and Pinho, 2004b) called Displacement Adaptive Pushover (DAP), in which the innovation was represented by the use of a lateral displacement profile instead of a force profile. The methodology at the base of the procedure was analogous to the FAP, with greater results, in terms of total drift, as shown in figure 4.19. Generally, the new algorithm proved to be effective, thanks to the continuous update of the displacement profile shape, but suffered of a main limitations, consisting in the application of SRSS or CQC combination rules, which are valid for elastic systems, but scarcely indicated to NL systems. Other adaptive methods can be found in the literature, in which the

lateral load profile was updated at the occurrence of a defined number of plastic hinges. One of these (Raquena and Ayala, 2000) was based on the calculation of an equivalent vibration mode obtained by the SRSS combination of significant modes.
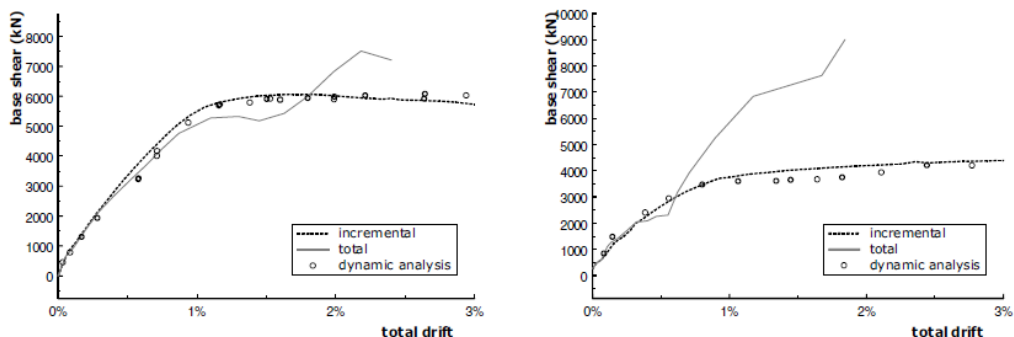
Fig. 4.19 – Comparison of DAP and FAP results of a case study (Antoniou and Pinho, 2004b)

Based on the experience of the scientific literature about non-conventional methods of NLS analysis, a general summary of the skills that a pushover methods should have, in order to predict the local and global structural responses, is below listed:

- An inelastic analysis should account for the influence of higher modes, especially for irregular and high buildings;
- An inelastic analysis should account for the variation of modal parameters in the post-elastic field, directly related to the occurrence of the plasticization or the variation of constitutive laws of materials;
- An inelastic analysis should account for the variation of damping level in the post-elastic field, for avoiding errors until 200% (number provided in Elnashai, 2001);
- An inelastic analysis should account for the real development of the structural elements yielding and failure;
- A pushover analysis should depend from the seismic demand, parameters easily considerable through the dependence of the load profile by the S_a (the most commonly used and directly related to the fundamental vibration modes);

206

- A pushover analysis should include in the analysis some features, often neglected in the pushover analysis, as the earthquake duration of the amplification effects;
- The load profile of a pushover analysis should adapt to the continuous local variation of stiffness and strength, with the aim of equilibrating the system.

Despite the non-conventional methodologies try to solve the above features, they are characterized by some limitations, especially from the practitioners point of view. Concerning the multimodal analysis, besides the well-explained problem about the time invariance of the load profile, the main problem for practitioners is the performance of a lot of pushover, especially for irregular buildings, modelled with a 3D FE model. While, for the regular buildings, the multimodal analysis can be useless, considering that the capacity curve should locate between the response of the inverse triangular and uniform profiles. In addition, for building extremely irregular, the multimodal procedures developed and described can provide structural response not enough precise. Regarding to adaptive methodologies, the concepts at the base of analysis is surely noble but, as shown in the scientific literature, they need algorithms usable with open source software (or low commercial software of high level). For concluding, the pushover analyses results are usually validated with NLD analyses, which strongly depend from several features of the set of accelerograms chosen (other information will be provided in the next Sections) and then, this represents an uncertainty source.

4.2.4 Proposal of an effective simplified multimodal approach: application to a case study

The choice of a proper methodology of seismic analysis, such as the NLS analysis, can lead to have not accurate results, despite its consistence with the prescriptions provided from the technical codes, as EC8. Especially for existing RC buildings, others factors can influence the response of analysis, as a reliable appraisal of the parameters involved in the structural modelling. It is evident that, for performing a correct assessment, the preliminary study of the building and the definition of the correct geometry, materials and loads are crucial for obtaining an effective FE model, able to

predict the real structural response in the elastic and inelastic field. In the Chapter 2, several information about the knowledge path have been provided, with specific reference to the in-situ investigations for determining the mechanical parameters of structural materials, as the concrete strength. As will show in the next Section, this latter parameter can be an uncertainty source, which can provide a structural response totally different from the real one. It is worth mentioning that the approach proposed and used in this application concern to a deterministic approach, which is friendly for practitioners. On the other hand, the scientific literature proposes approaches more refined, where the uncertainty sources, as the epistemic one, can be considered in probabilistic way, using some methodologies known as Monte Carlo simulation or first order second moment (these latter are not focus of this thesis). Here, the author is going to propose a methodology for accounting the uncertainty due to the irregularity of a building, through the application of a multimodal pushover analysis on a case study. The aim of the procedure is to estimate the building behaviour with a simple procedure, able to take into account for the dynamic irregularity of buildings, which means the irregularity in terms of modal parameters (T and M[%]).

The case study investigated is an existing RC school building located in Bovino, Province of Foggia, Puglia, Southern Italy. The building has a plant inscribed in a rectangle of dimension 24.90 m x 35.65 m, 3 floors above ground and a pitched roof with total height of 15.55 m, as shown in the picture in Figure 4.20. The structure, built in the 60s' in the absence of specific seismic codes, was designed considering only vertical loads and it is constituted by a RC frame with beams and columns. The floor systems were constituted by ribbed slabs for the first two floors and SAP slab at the 3rd floor. The case study is representative of the structural typology that constituted a school building stock in abovementioned geographic area. The dimensions of the structural elements are variable, according to the design loads, as summarized in table 4.4, which also reports the sectional parameters in terms of geometry (indicating with B and H respectively the height and the base of each section), longitudinal and transversal steel bars. In the table, the amount of longitudinal steel bars is indicated as the number n of bars, having diameter ϕ (nϕ), whereas the amount of transversal steel bars is

indicated in terms of the ratio φ/s expressed in cm (s = spacing of stirrups, φ = diameter of stirrups).

Fig. 4.20 – Picture of the existing RC school building investigated

In addition, there is specific reference to the longitudinal bars orientation, according to the global reference system of the building. It is also reported the amount of longitudinal steel bars in the middle (M) and in the End (E) sections of the beams. The foundations are constituted by plinths connected by beams, while the orientation of elevation beams is in just one way. Concerning to the in-situ materials, after some investigation about steel and concrete, the medium values founded are respectively, f'_{ym} equal to 401 MPa and f'_{cm} equal to 14.3 MPa. It is worth mentioning that the values of in-situ materials assumed will be modified in the next Section, considering that especially for the concrete, the f'_{cm} is characterized by elevate dispersion. With regard of knowledge path, the building was object of investigations, performed within the just mentioned Agreement between "AdB Puglia" and "Polytechnic University of Bari" (Mezzina et al., 2011). According to the prescription provided by EC8 and based on the amount of in-situ investigation performed related to the building dimensions, a complete process of knowledge on the case study was carried out. The knowledge level

achieved was a KL3, which allow of considering the mechanical parameters of materials as provided by the tests.

Tab. 4.4 – Dimension and geometry of structural elements

Level	Element	B (mm)	H (mm)	Longitudinal bars X	Longitudinal bars Y	Transversal bars
Ground floor	Columns	400	600	4 Φ18	4 Φ16	Φ6/20
		500	600	8 Φ18	4 Φ18	Φ6/18
		550	700	8 Φ18	4 Φ18	Φ6/18
		500	650	8 Φ18	4 Φ18	Φ6/18
	Beams	800	400	E: 3Φ18 M: 6Φ18		Φ8/15
		800	200	E: 4Φ16 M: 4Φ16		Φ8/20
		400	600	E: 3Φ16 M: 6Φ16		Φ8/15
First floor	Columns	400	600	4 Φ16	4 Φ16	Φ6/20
		400	400	4 Φ16	4 Φ16	Φ6/20
		400	650	4 Φ16	4 Φ16	Φ6/20
		500	650	8 Φ18	6 Φ18	Φ6/20
		350	400	4 Φ16	4 Φ16	Φ6/20
	Beams	800	200	E: 5Φ18 M: 8Φ18		Φ8/20
		400	800	E: 6Φ18 M: 6Φ18		Φ8/15
		400	600	E: 3Φ16 M: 3Φ16		Φ8/20
Second floor	Columns	400	400	4 Φ16	4 Φ16	Φ6/20
		400	600	4 Φ16	6 Φ16	Φ6/20
		350	400	4 Φ12	4 Φ12	Φ6/20
		350	500	4 Φ16	4 Φ16	Φ6/20
		300	300	4Φ12	4 Φ12	Φ6/20
	Beams	350	800	E: 5Φ16 M: 6Φ16		Φ8/20
		350	700	E: 3Φ18 M: 3Φ18		Φ8/20
		350	500	E: 2Φ16 M: 2Φ16		Φ8/20

In order to investigate the structural response of the building, this latter has been modelled by using the FE software SAP2000. Beams and columns have been

modelled as one dimensional frame elements, assuming fixed end restraints at the base of the columns. Dead loads have been applied to beams, according to the direction of the joists and the influence area. In particular, $G_1 = 2.50$ kN/m^2, $G_2 = 1.00$ kN/m^2 for all floors; $Q = 3.00$ kN/m^2 for the 1st and 2nd floor while $Q = 0.50$ kN/m^2 for the top floor, this latter established according to the value provided by Italian codes for a service floor. Thanks to the completeness of the available documentation, it has been possible to accurately reproduce the actual geometric configuration of structural elements. The pitched roof has been modelled by considering the mass consistently distributed on the supporting beams (a preliminary analysis has shown that there was no significant variation by assuming a complete model with the actual inclination of joists). The NL behaviour of the building has been modelled by a lumped plasticity approach, considering a Takeda behaviour for cyclic loads and neglecting P-Δ effect (because it did not influence the analysis results of this case study). In this case, the concrete cracking effect has been considered, through the reduction of E_c, considering that, in NL analysis, this effect may be considered when the plastic hinges overcome the yield limit. Regarding to the plastic hinges, they have been defined through the evaluation of the chord rotation demand and the corresponding capacity, for each section investigated, according to the formulation provided by EC8, as shown in eqs. 3.3 and 3.4. In particular, the plastic hinges have been placed at the ends of structural elements. It is worth remembering that the inelastic mechanisms considered for beams are only those due to simple bending, by defining a NL moment-rotation relationships. For the columns, the combination between axial and bending stresses has been considered, in order to define the NL moment-rotation relationships dependent from the variation of the axial stress. Based on the characteristics of the constructive elements of the floors, the hypothesis of infinite extensional stiffness has been assumed, by introducing an internal rigid constraint at each floor. E_c of concrete has been calculated according to NTC08 formulation, which depends by f'$_{cm}$, G_c has been calculated according to the well-known elastic formulation which links it with E_c and ν. In this work, the possible activation of brittle shear mechanisms in the structural elements has been neglected, even if a very low amount of transversal reinforcements was detected during the investigation

phases. This is a quite common situation for Italian RC frame buildings designed in the absence of anti-seismic standards. It is thence evident that brittle shear mechanisms can develop since the very first steps of the analysis, undermining the objectives of the research study. It was supposed that shear mechanisms would be anyway preliminarily prevented by means of proper intervention strategies. In order to investigate the possible differences in modelling methods and to include the influences of secondary structural elements (such as influence of slabs and joists) an additional numerical model has been implemented, replacing the previous one and introducing horizontal elastic elements in the first two floors. In particular, the presence of double joists or concrete bands have been simulated, as detected from the in-situ investigation. In figure 4.21 is shown the plan of the case study, with specific reference to the position of the elastic elements inserted, as abovementioned.
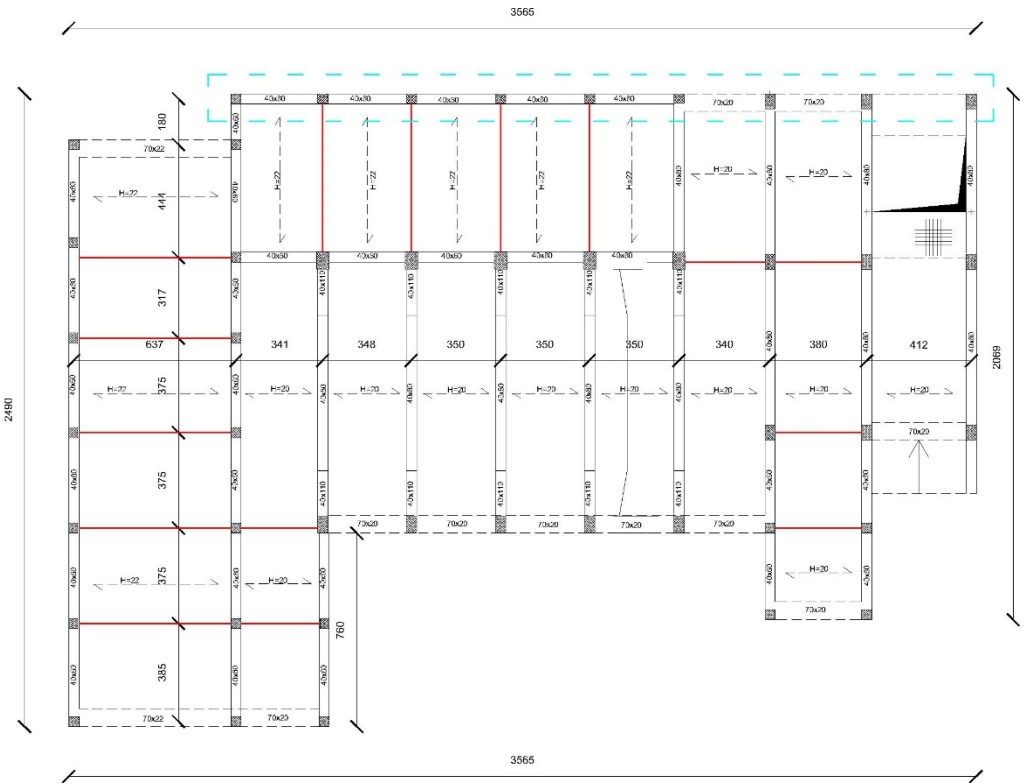
Fig. 4.21 – Carpentry of the case study. Red signs indicate double joists and concrete band

Being made from a different floor system, the 3rd level does not present additional contribution of double joists or concrete bands and, for this reasons, the elastic elements have been added only at the first two floors. Therefore, 2 numerical models have been made and, subsequently investigated. The model that account for the floor elements is called "complete model". Preliminary eigenvalue analyses has shown that the explicit modelling of floor elements (double joists or large concrete bands) did not provide significantly effects, considering a lower variation of mass and stiffness in the numerical model. However, all subsequent analyses have been performed with reference to the complete model, which is closer to the real structural configuration. After an eigenvalue analysis, the modal parameters of the model investigated have been shown in the table 4.5, with reference to the first 6 Ts and the related M[%]s.

Tab. 4.5 – Periods and participating masses of the building model

Mode	T (s)	M[%]$_x$ (%)	M[%]$_y$ (%)	M[%]$_\theta$ (%)
1	0.849	86.066	0.066	3.468
2	0.562	2.977	27.61	58.993
3	0.517	0.625	64.694	29.189
4	0.275	8.549	0.105	0.233
5	0.211	0.226	3.32	5.46
6	0.171	0.014	3.21	1.60

For assessing the structural behaviour of the building in the inelastic field, NLS analyses have been performed on all models, for the two main directions X and Y and taking into account the gravity loads before of pushing the structure with horizontal loads. Nevertheless, based on the eigenvalue analyses, it is important to highlight that in the X direction, the M[%] of the fundamental mode is always greater than 85% for all models, whereas in the Y direction it is comprised in the range 60-65%, which is a level not sufficient for using a unimodal profile. Therefore, the focus of the subsequent evaluations is going to be the structural response along Y direction and only the results obtained from NLS analysis in this direction are going to be shown. Concerning to the

choice of load profile, for each model, the pushover analyses have been carried out by using an unimodal (ULP) and a multimodal load profiles (MLP). For completeness, NLS analysis by using inverse triangular and constant load profiles have been performed, but they are not reported here, because not significant for the aim of the research. The procedure used for defining the MLP accounts for a weighted contribution of significant modal shapes, considering new participation factors calculated using the response of the structure, obtained by the linear response spectrum analysis above performed. The main advantages of the procedure adopted consists in the performance of a multimodal analysis, by using just a unique load profile (different from the MPA proposed by Chopra), which takes into account the higher modes contribute. As abovementioned, this is surely a benefit in terms of computational efforts, especially from the practitioners' point of view. The adopted procedure was firstly proposed in (Caliò et al., 2010) and, after few modifications, the steps of procedure are listed below:

1. The modal shapes $\{\Phi\}_n$ are evaluated from the eigenvalue analysis. For each mode, the modal participation factors are computed as:

$$\Gamma_n = \frac{\{\Phi\}_n^T[M]}{\{\Phi\}_n^T[M]\{\Phi\}_n}\{e\} \tag{4.11}$$

   being [M] the mass matrix of structure and $\{e\}$ the influence vector associated to the input direction of motion;

2. From the elastic response spectrum, through a response spectrum analysis, the modal displacements $\{D\}_n$ are determined.

3. For each mode, the maximum modal displacements are function of the spectral values:

$$\{u\}_n = \Gamma_n D_n \{\Phi\}_n \tag{4.12}$$

4. The maximum response $\{u\}_{max}$, in terms of displacements, is evaluated through the application of the CQC combination rule of vectors $\{u\}_n$.

5. The Modal decomposition of $\{u\}_{max}$ into the modal contributions of the each vibration mode is performed and the corresponding participation factors are calculated as:

$$z_n = \frac{\{\Phi\}_n^T[m]}{\{\Phi\}_n^T[m]\{\Phi\}_n}\{u\}_{max} \tag{4.13}$$

6. The NLS analysis is performed by using a MLP determined as the combination of the vibration modes of the structure, according to the participation factors obtained at step 5 and scaled with respect to floor masses (load profile normalized), as below reported

$$F_{0,i} = \sum_{n=1}^{j} \varphi_i z_n \tag{4.14}$$

where $F_{0,i}$ is the storey force of the MPL at the storey i, ϕ_i is the component of the eigenvector of the storey i for the mode n. After calculating the new participation factors z_n by eq. 4.13, only the modes having a M[%] higher than 1% are taken into account, since the remaining modes had a negligible influence on the computation of the load profile.

The above listed procedure has been applied to the FE model of the building, in order to obtain a MLP to be applied along Y direction. An observation about the procedure is related to the combination rule used. In particular, the CQC is a combination rule that takes into account the sign of the eigenvectors and the phasing of the modes and then, of their maximum effects. Avoiding to report the formulation of CQC, easily fundable on whatever technical code, the author believe that the use of this combination rule is better than the SRSS, because this latter is always additive, with regard of the higher modes. In addition, the author knows that the scientific literature provides other combination methods, accurate and useful for accounting the inelastic phenomena and what these latter imply. On the other hand, the CQC rule is the most easy and practical way for combining the modes, from the practitioners' point of view. Another key point is related to the MLP computation. In particular, the load pattern computed is composed by forces applied just in Y direction, in the centers of the mass of the storeys. In fact, the load vector does not take into account a bidirectional loading. In addition, in its computation, it is strongly influenced from the modes with higher M[%] in the Y direc-

tion, while the modes with high M[%] in the X direction are accounted with them influence in the direction considered, which is low. This way to proceed is consistent with the use of pushover analyses in the practical application. For assessing the efficiency of the procedure, the results obtained from the NLS analyses, have been compared with the ones obtained from other NL analyses. In particular, 3 IDAs (Vamvatsikos and Cornell, 2002) have been performed, by applying 3 different artificial design-consistent accelerograms automatically generated with SIMQKE software (Gasparini and Vanmarcke, 1976), with duration equal to 20 seconds and stationary part of duration equal to 10 seconds. In figure 4.22, the accelerograms used are shown, considering them spectrum-compatibility with the elastic acceleration spectrum of site of case study, at LSLS. For performing the IDAs, the accelerograms have been properly scaled in amplitude. The value of scale factor has been increased of 0.25 per time, starting from a low action up to strong acceleration that caused the structure collapse. The aim of the analysis is to reproduce the trend of structural response in Y direction, in order to compare it with the ones obtained from the multimodal and unimodal analyses. To this scope, each accelerogram was composed by just one component, which was applied (and after scaled) in the Y direction.
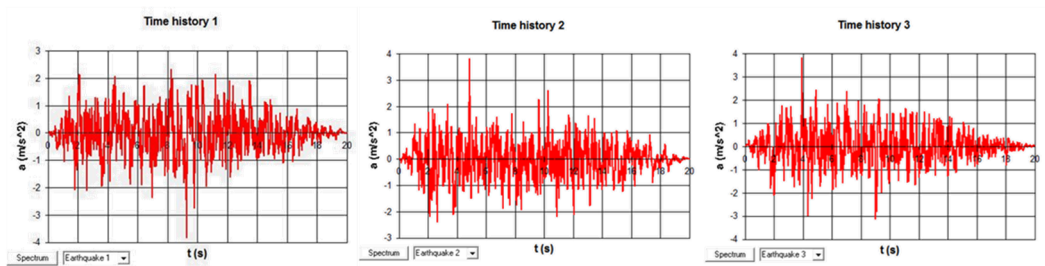
Fig. 4.22 – Artificial accelerograms used in the IDAs, simulated with SIMQKE software

It is worth mentioning that when one performs an IDA with one accelerogram (or group) on a building, as suggested by some works about this topic, it is necessary to apply the two horizontal components of the accelerogram (in some case, also the vertical component) and, subsequently, one should scale them up to the global instability. Furthermore, the IDA is suitable for investigating the linear and NL structural response, in a probabilistic way, considering some phenomena that a pushover analysis

cannot account for, such as reversal effect, higher mode effect in the elastic field, possibility to find median and dispersion of the structural behavior (major details will be provide in the Sections 4.3.2). In this work, author recognizes that the term IDA can be improper in this application, because here IDAs have been performed by using artificial accelerograms (not recommended in this kind of analysis), with 3 accelerograms composed by one component (not consistent from the probabilistic point of view). Hence, in this case, the performance of IDAs does not follow all concepts at the base of the original procedure, because the aim is to confirm if the multimodal procedure reproduces the trend of capacity curve (it should be done from the median of the results). On the other hand, the easier way for reproducing the behavior of a unidirectional pushover can be the performance of some IDAs by using spectrum-compatible accelerogram, applied in the same direction and plotted in the same plane of the pushover. In this way, the results of IDAs are coherent with the ones obtainable from a pushover analysis. The results of the analyses obtained by increasing the accelerogram amplitude have been depicted in the same graph of the NLS analyses, in the plane V_b-δ_R. With this regard, figure 4.23 shows the comparison among NLS analyses performed with ULP, MLP and IDAs results. The trend of IDA results come near the NLS analyses results obtained using MLP in both elastic and inelastic field for all models and this confirmed the validity of MLP calculated for estimating the real structural response. The comparison between the model can be summarized in table 4.6, where the percentage differences of V_b in two different cases, for two different values of roof drift (0.2% for the elastic range and 0.4% for the inelastic range) have been evaluated. The differences are reported in absolute value.

Tab. 4.6 - Percentage differences of base shear between MLP and ULP, at defined values of the roof drift

Roof drift (%)	$\Delta V_{b,(UPL-MPL)}$(%)
0.2	11.29
0.4	6.81
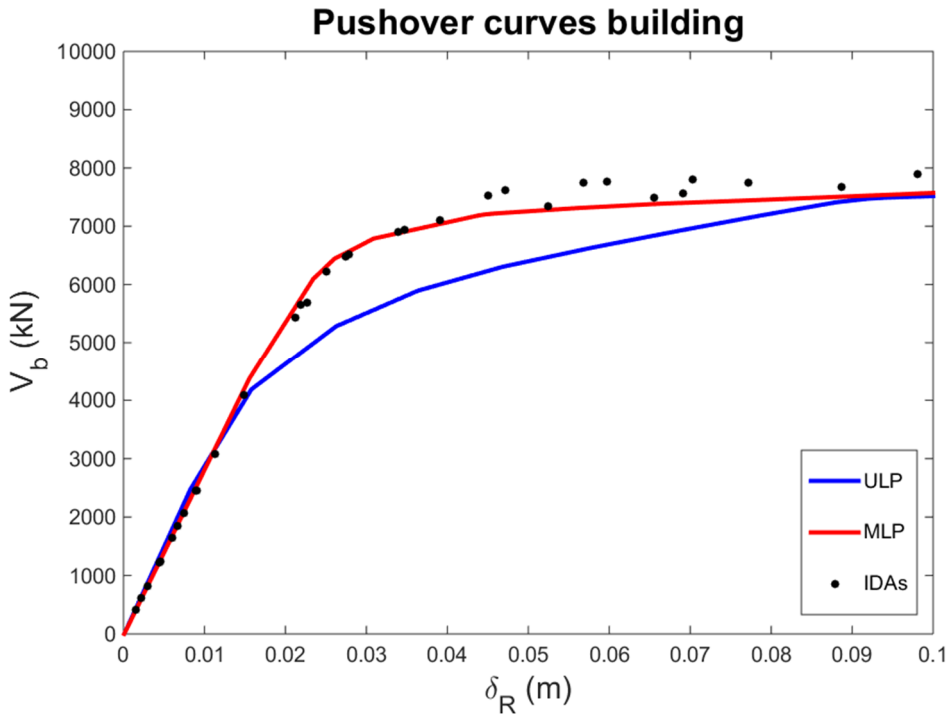
Fig. 4.23 – Comparison among NLS analyses with ULP and MLP and IDAs

From the results shown in figure 4.23 and table 4.6, one can observe how the capacity curves of the same model present differences, due to the load pattern employed in the pushover. This difference is more evident in the yielding zone, while the curves tend to rejoin in the post-elastic branch. The results makes physically sense, considering that using an ULP, we apply a system of force that account for torque. Then, in the elastic part, the torques cause this difference with a curve obtained by the MPL, which intrinsically consider the torsion contribute. After the yielding, the building loses the coupling of the modes and the effect of torque loses its power. Even the IDAs confirm the efficiency of the methodology. Clearly, the methodology has been tested on a case study. The procedure should be tried on other cases study, in order to discover what can be its limits and leakages.

4.2.5 Appraisal of the influence of compressive strength variation by means of nonlinear conventional and multimodal static analysis

In addition to the problem of irregularity in terms of modal parameters, as just mentioned in the previous Section, also the characterization of mechanical parameters of structural materials, as the concrete strength, can be represent a source of irregularity and uncertainty. Generally, in order to investigate the features of an existing building, one should perform a largest number of materials tests (DTs and NDTs). This practice has the aims of improving the accuracy and quality of information about the mechanical parameters of in-situ materials and the one of avoiding an excessive penalization of materials strength with consequent penalization of the CDR, according to the philosophy proposed by EC8. On the other hand, the immediate consequence is the disproportionate in the immediate release of costs of the assessment. In addition, besides being uncertainty source, the mechanical parameter of a building can represent also an irregularity source for the existing RC buildings, especially in the cases of different concrete strengths, distributed randomly among the structural elements. This can be mainly due to constructive technologies, which did not provide acceptance criteria for the cast in place concrete in the existing RC buildings built about 50 years ago. Assuming the number of in-situ tests that have not to exceed a certain cost, it is possible that the in-situ characterization of the materials of existing buildings can provide results very dispersed. This situation can lead to a subjective choice of the key features of in-situ materials, with possible wrong estimation of the structural behaviour of building. The case study investigated in the previous Section is proper characterized by this kind of problem. In particular, concerning to the investigation performed on the structural elements, in order to estimate the mechanical properties of steel, the investigation plan provided the execution of the widespread pacometric tests, with the performance of them in 18 structural elements and tensile and bending tests of reinforcement bars, at each floor, for a total number of 3 tests. The results revealed the presence of smooth bars of "Aq42" steel class, a mild steel with f'_{ym} equal to 401 MPa. With regard to the assessment of concrete mechanical properties, the extraction of 9 cylindrical cores was performed, which were subjected to laboratory compression tests. As shown by

scientific literature, the DTs on concrete specimens can be integrated with NDTs. There-fore, an investigation plan about mechanical parameters was drafted, wherein 28 NDTs, like ultrasonic tests were performed. Table 4.7 shows the results in terms of cubic strength (R_c) and, through a correction factor, the values of cylindrical strength (F_c) for each specimen. In addition, the table shows the dimensions of specimens (d and h) and the specific weight of the in-situ concrete (γ_c).

Tab. 4.7 – Results of compression tests on RC specimens

Core	d (mm)	h (mm)	F_c (MPa)	R_c (MPa)	γ_c (kg/m3)
C1	94.00	94.00	11.60	12.05	2131
C2	94.00	94.00	25.20	25.95	2290
C3	94.00	94.00	15.50	16.30	2253
C4	94.00	94.00	17.50	17.65	2242
C5	94.00	94.00	11.90	12.15	2281
C6	94.00	94.00	13.10	13.50	2154
C7	94.00	94.00	12.80	13.20	2096
C8	94.00	94.00	11.50	11.65	2134
C9	94.00	94.00	14.80	15.45	2263

The results of compression tests showed a relevant dispersion of the strength values and consequently the mean value could not be assumed as representative pa-rameter in view of the structural modelling. In particular, the difference between the maximum and the minimum values found for the compressive strength was equal to 14.3 MPa, with a RSD (as defined in section 2.2) equal to 0.29, whereas the threshold indicated by FEMA is 0.14. Even the performance of NDTs, which usually allow of un-derstanding the presence of different homogeneous strength classes of in-situ con-crete, confirmed the uncertainties related to characterization of these parameters. In order to understand how the in-situ materials influence the structural response, the numerical model shown in the previous Section has been duplicated to 3 FE models, which are characterized by different f'$_{cm}$. In particular, in each model, steel strength has

been assumed according to in-situ measured parameters (f'_{ym} = 401 MPa). Regarding to the concrete, a sensitivity analysis has been proposed, performed with regard to the concrete strength value. 3 possible values of f'_{cm} have been considered, as well as 10 MPa, 20 MPa and 30 MPa, based on the range of strength values provided by destructive tests. This choice clarifies that the purpose of this work is not determine the representative value of f'_{cm} for our existing RC structure. The purpose is to study several engineering scenarios related to the assessment of existing RC buildings, wherein the author want to show the possible structural responses, analysing a real case study and varying the in situ concrete strength in a certain range of values. For the 3 numerical models of investigating, through the performance of eigenvalue analyses, the natural vibration modes have been computed. Figure 4.24 reports the shape of the first 2 modes for the complete model, which has a value of f_{cm} = 10 MPa. Herein, this model has been assumed as the reference one for all subsequent comparisons, because it has an f'_{cm} nearest to the average of results obtained by compressive tests previously computed.
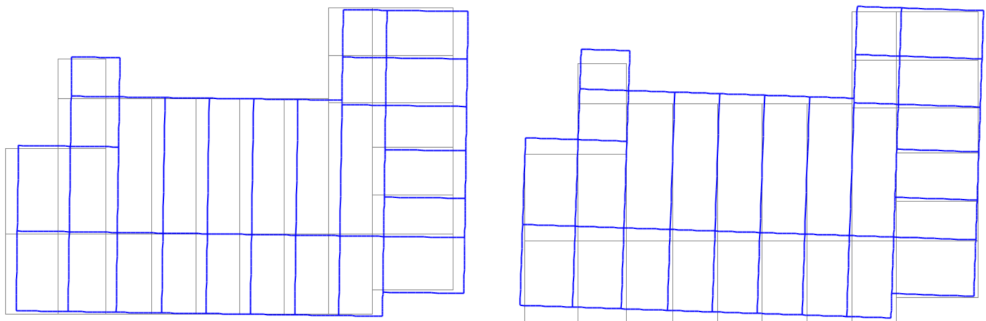
Fig. 4.24 – Shape of vibration modes in the two main directions, for the reference model

In table 4.8 are shown the first 6 Ts and the related M[%]s for the reference model, whereas in table 4.9 are shown the percentage variations of T and M[%] in the two main directions of the others two models, for which f'_{cm}=20 MPa and 30 MPa. Subsequently, a modal response spectrum analysis has been performed, according to the features of the building site. In particular, the seismic action has been defined through the definition of the elastic response spectrum calculated in the building site.

Tab. 4.8 – Periods and participating masses of reference model

Mode	T (s)	M[%]$_x$ (%)	M[%]$_y$ (%)	M[%]$_\theta$ (%)
1	0.876	87.123	0.031	3.458
2	0.573	1.940	33.326	59.909
3	0.542	0.629	59.037	28.125
4	0.284	8.643	0.073	0.233
5	0.216	0.145	3.415	5.641
6	0.179	0.00985	3.134	1.589

To this scope, a design nominal life (N_L) of 50 years and an usage class (U_C) III (to which a Coefficient of importance cu equal to 1.5 is associated) have been assumed, in order to determine the reference T_r for the seismic action at the LSLS. According to the seismic hazard map of Italy, the PGA of the building site, for an A-type of ground is equal to 0.2491/g, where g is the gravity acceleration. As suggested by EC8, the response spectrum analysis has been performed assuming a design spectrum, computed by using a q=1.5, which is the minimum value for RC building and the suggested value for existing buildings. Results in terms of stress distribution on the structural elements have been compared among the different FE models. In particular, in table 4.10 are shows the comparison, in terms of maximum percentage variation, of the bending moments, shear stress and normal stress among the reference model and the models with f'$_{cm}$= 20 MPa and 30 MPa.

Tab. 4.9 – Variations of periods and participating masses among the reference model and models having f$_{cm}$ equal to 20 and 30 MPa

Mode	f'$_{cm}$ = 20 MPa			f'$_{cm}$ = 30 MPa		
	ΔT(%)	ΔM[%]$_x$ (%)	ΔM[%]$_y$ (%)	ΔT(%)	ΔM[%]$_x$ (%)	ΔM[%]$_y$ (%)
1	-9.86	-0.01	0.00	-15.17	-0.02	0.00
2	-9.86	0.05	0.07	-15.18	0.10	0.11
3	-9.87	0.00	-0.05	-15.19	0.00	-0.07

Tab. 4.10 – Variations of stresses among the reference model and other ones

f'$_{cm}$ = 20 MPa			f'$_{cm}$ = 30 MPa		
ΔN$_{max}$ (%)	ΔT$_{max}$ (%)	ΔM$_{max}$ (%)	ΔN$_{max}$ (%)	ΔT$_{max}$ (%)	ΔM$_{max}$ (%)
7.11	1.62	11.63	10.36	2.60	16.99

The figure 4.25 shows the geometric configuration of the frame considered for computing the stress differences in table 4.10, which is indicated in figure 4.21, by a light blue dashed box. In the figure, it is possible to appreciate the dimensions of the structural elements in a vertical section of buildings, through an extruded view of the FE model.
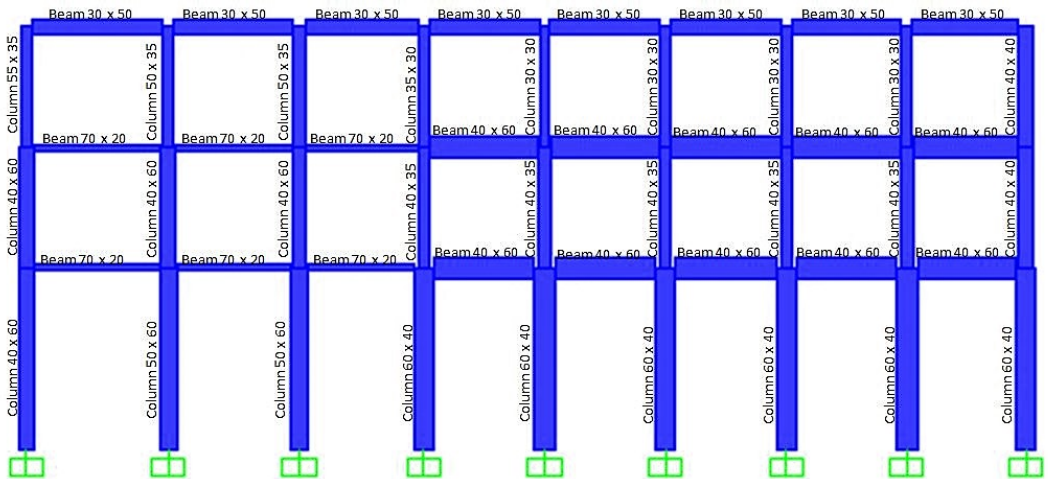
Fig. 4.25 – Geometric dimensions of a representative frame of the case study

The comparisons of modal parameters in table 4.9 (T and M[%]) shows that for the T, variation of f'$_{cm}$ provides differences about, respectively, 10 and 15%, which cannot be considered very high. In addition, the differences of M[%] among the models are negligible, which means that the shapes of vibration modes are the same. Concerning to the stress variation among models, table 4.10 shows that the differences are in the order of 10-15%, such as occurred for the modal parameters. These evidences

suggested that a wrong evaluation of the in situ concrete mechanical parameters, as f'$_{cm}$, could provide variation in the elastic field relatively low, for a case as the one investigated (low-rise building). Regarding to the NLS analysis, analogously with what done in the previous Section, the results are going to show only for Y direction, due to a M[%] in a range of 60-65%, value not sufficient for applying a ULP. Therefore, for the 3 models, the pushover analyses have been carried out by using a ULP and the MLP, computed according to the procedure before proposed, in order to obtain a MLP to be applied along Y direction. Clearly, for each model there are variations of the modal parameters, with consequent variation of the MLP shape. In figure 4.26, the MLP computed for the reference model, through the specified procedure, is shown, where in abscissa there is the normalized force, related to the weight of building storeys and in ordinate, there is the height of the building. In the figure, the MLP is compared with an inverse triangular load profile, normalized in the same way.
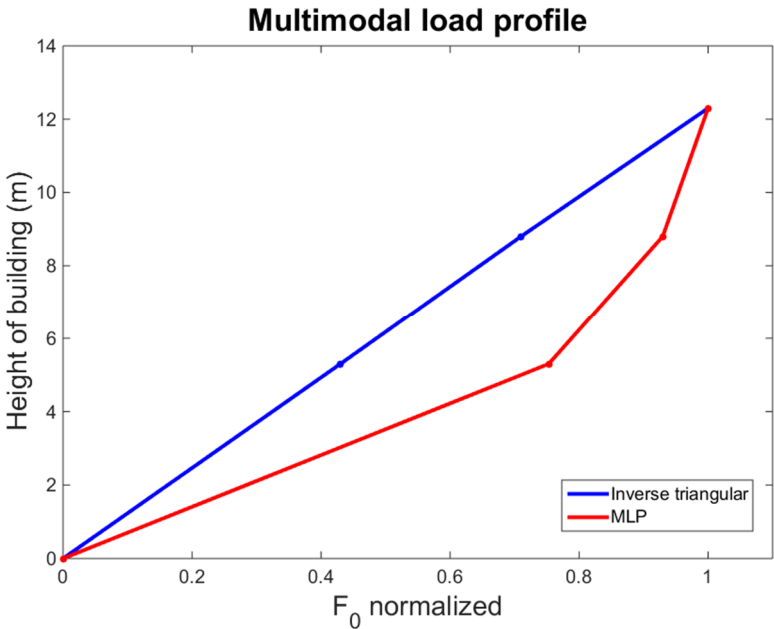
Fig. 4.26 – Comparison between multimodal and inverse triangular load profiles

Then, the MLP has been implemented in the FE models, in order to perform multimodal NLS analyses, besides to use the ULP for NLS unimodal analyses. For each

of the 3 models, varying the load profile shapes and the mechanical parameters of materials, capacity curves have been obtained and the these latter have been compared with the reference model, in order to appraise the differences among the related capacity curves. In addition, in order to assess the NLS analyses results, varying the assumption about in-situ material, IDAs have been carried out, according to the artificial accelerograms of figure 4.22 and performing the analyses in the analogous way (one component in Y direction and same scale factors). The results of the analyses have been plotted in the same graph of the NLS analyses, in the plane V_b-δ_R. With this regard, figure 4.27 shows the comparison among NLS analyses performed with ULP and MLP, applied on the 3 models (f'_{cm}= 10 MPa, 20 MPa and 30 MPa) and IDAs results.
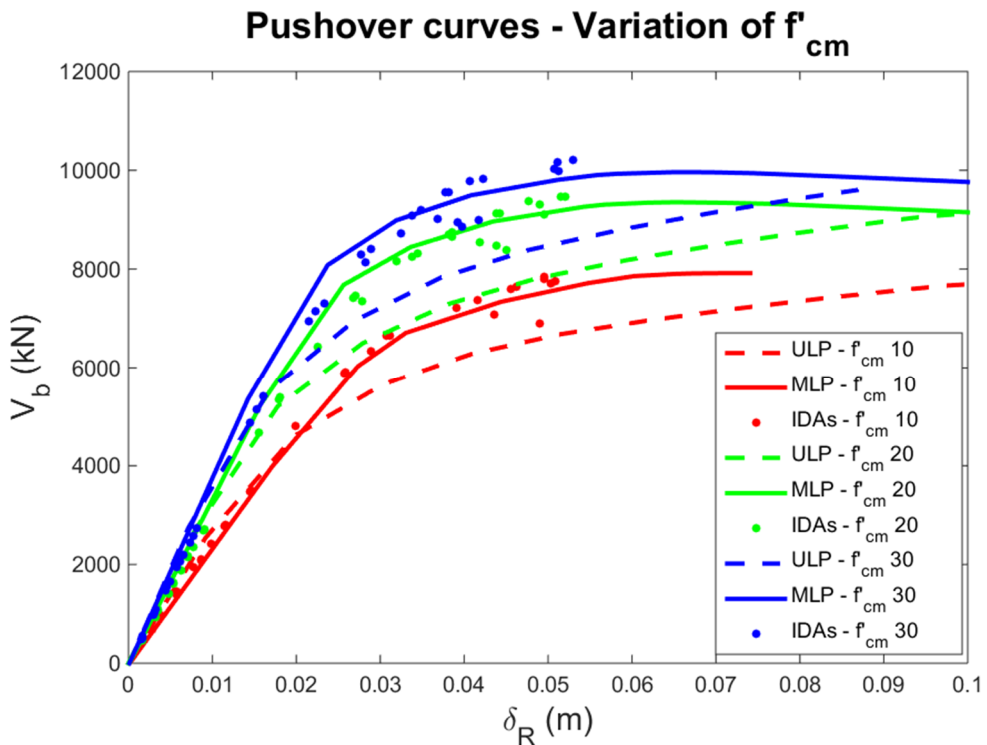
Fig. 4.27 – Comparison among NLS analyses and IDAs, varying the concrete strength

Also in these cases, the trend of IDA results come near the NLS analyses results obtained using MLP in both elastic and inelastic field for all models and this confirmed

the validity of MLP calculated for estimating the real structural response. The comparison is also summarized in table 4.9, in terms of percentage differences of V_b in the different cases, for two different values of roof drift (0.2% for the elastic range and 0.4% for the inelastic range). From the results, it is possible to appreciate the clear difference of the elastic stiffness with the variation of concrete from 10 MPa to 30 MPa. In addition, table 4.11 shows that the uncertainty of the building response in the inelastic field related to the variation of f'_{cm} (curves of different colors), which is greater than the one due to the approximation related to analysis method (curves and points of same color). This evidence, albeit limited to the case study examined and therefore not directly generalizable, clarifies the importance of the phase of in-situ investigation about mechanical parameters in the vulnerability assessment of RC buildings, phase that is often disregarded with respect to those of structural modeling and analysis.

Tab. 4.11 - Percentage differences of base shear among different models, at defined values of the roof drift, due to the variation of f_{cm} in all structural elements of the building

Roof drift (%)	$f_{cm} = 10$ MPa $\Delta V_{b,(UPL\text{-}MPL)}(\%)$	$f_{cm} = 30$ MPa $\Delta V_{b,(UPL\text{-}MPL)}(\%)$	f_{cm} 10 - f_{cm} 30 $\Delta V_{b,(UPL)}(\%)$
0.2	9.62	20.58	30.76
0.4	15.38	16.67	29.23

Additional analyses have been carried out, by considering the eventuality that concrete classes used in construction phases may be different from floor to floor, due to possible errors in execution (addition of water in the concrete mixture in order to improve the workability, inaccurate in-place concrete compaction, etc...). In particular, 3 scenarios have been considered, by varying the f'_{cm} in a single floor per time in the numerical model. This time NLS analyses have been performed in the Y direction only through MLP and the results are compared with the ones obtained from the IDAs analyses performed in the same way of the precedent one (by using the accelerograms in figure 4.22). In particular, the capacity curve, provided from MLP on the model with $f'_{cm}=30$MPa has been compared with the results provided by multimodal NLS analyses

and IDA by changing the f'$_{cm}$ of each floor, from 30 MPa to 10 MPa. In figure 4.28, the results of the analyses are shown.
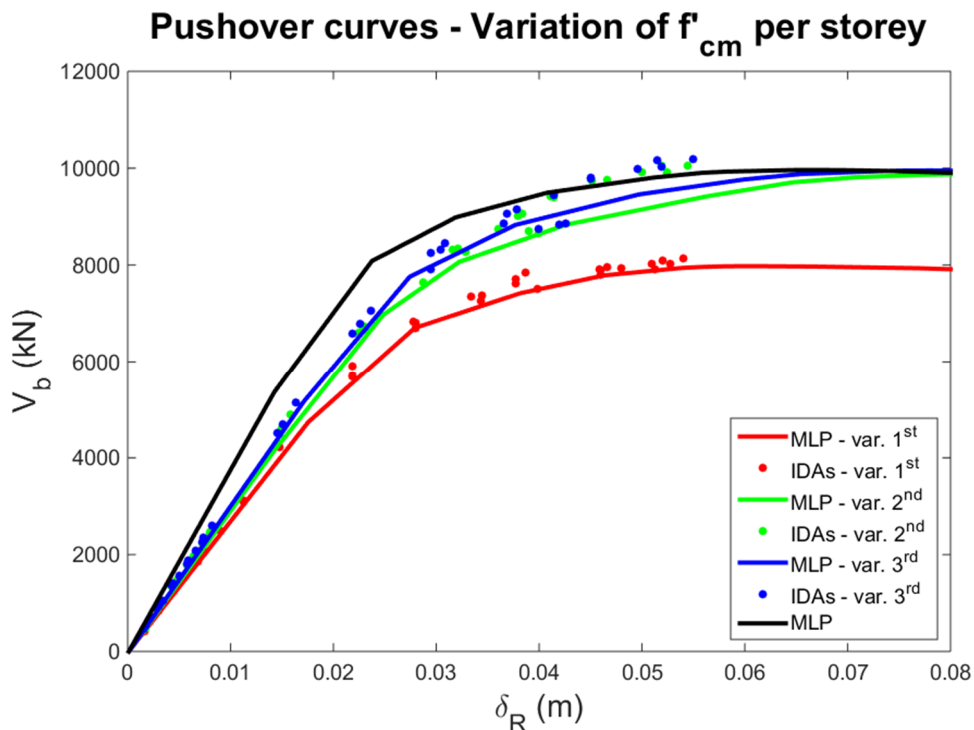
Fig. 4.28 – Comparison among NLS analyses and IDAs, varying in turn the concrete strength at each floor

Analogously to table 4.11, table 4.12 shows the percentage differences in terms of V_b at two different values of roof drift (0.2% - elastic range; 0.4% - inelastic range).

Tab. 4.12 - Percentage differences of base shear among different models, at defined values of the roof drift, due to the variation of f$_{cm}$ in turn of each storey of the building

Roof drift (%)	Variation 1st floor ΔV_b (%)	Variation 2nd floor ΔV_b (%)	Variation 3rd floor ΔV_b (%)
0.2	18.54	8.83	4.53
0.4	20.99	4.21	0.59

By varying the concrete strength at each floor, it has been observed that the results had little variations, except for the case of first level. The results summarized in table 4.12 and figure 4.28, show that the failure of the structure, neglecting brittle mechanisms and considering that in all analyses the system collapses for soft storey at the 1st level, is greatly accentuated decreasing the f'$_{cm}$ of the structural elements at the first level. To confirm the above results, in figure 4.29 are showed how plastic hinges are formed in one main frame, at 0.4% of roof drift. In particular, in the figure the formation of plastic hinges for that displacement value are depicted, with specific indication to plastic deformation.
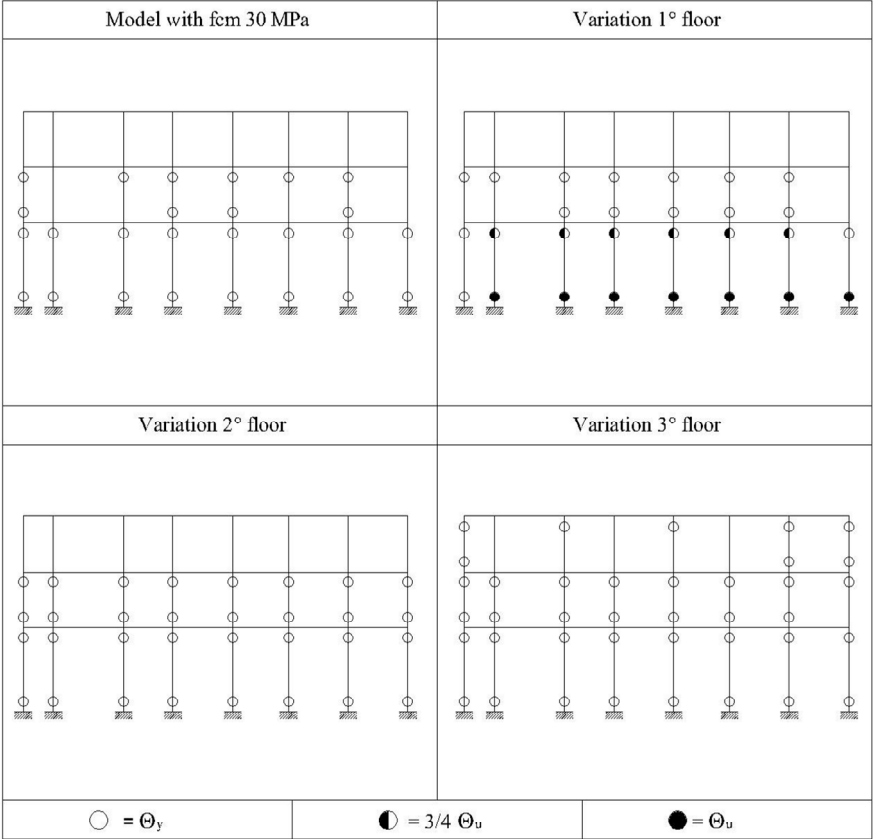
Fig. 4.29 – Formation of plastic hinges in one main frame at 0.4% of roof drift

In the case of material variation at the 1st floor, the building almost reached the collapse (ultimate rotation for the hinges at the base of first columns), differently from

the other cases, where the building is yet yielded, besides a different formation of plastic hinges. This evidence confirms the necessity to have specific rules about the distribution of in-situ investigation among the floors of the existing RC buildings.

4.3 Nonlinear dynamic analysis

The NLD analysis is a generic term for indicating an analysis able to compute the time dependent NL response of a structure, assuming as external input one or more acceleration waveforms. In particular, an analysis that provides the application of one acceleration time history on a structure can be defined as nonlinear time history (NLTH) analysis. The scientific community has always considered this kind of analysis as the most suitable method for simulating the seismic response of structures, considering the research of a faithful simulation of the real seismic excitation. In particular, the application of a ground motion to a building, leads to have a full time history response of the structure, accounting whatever interest quantity, such as displacements, stresses, section rotations and so on. Due to the typology of numerical model, which simulates the structure, the response can be linear or NL and, in this latter case, the geometrical and mechanical parameters of materials, section and structural elements should be accounted for, according to the nature of the building (for RC buildings, these features are widely described in the precedent Chapters). In addition, the numerical model should including the hysteretic behaviour, necessary for estimating the energy dissipation due to cyclic loads. Mathematically, a simple NLTH analysis is performable on a MDoF structure, through the resolution of a system of linear differential equations of second order. In particular, the system of equilibrium equations for a MDoF structure in motion, responds to the d'Alembert principle, which is writable as:

$$[M]\{\ddot{u}(t)\} + [C]\{\dot{u}(t)\} + [K]\{u(t)\} = \{S(t)\} \qquad (4.15)$$

where [M], [C] and [K] are, respectively, the matrices of mass, damping and stiffness of the structure, {S(t)} is the time dependent vector of the seismic loads, {ü(t)},{ù(t)} and {u(t)} are respectively the acceleration, velocity and displacement vectors to whom the system is subjected, due to the external forces. The above principle is characterized by elastic quantities, which can be extended to NL cases, in which it is solved for a FE model that accounts for geometrical and mechanical nonlinearities.

In both elastic and inelastic cases, for solving the equations system, the scientific literature provides some numerical procedures and techniques, which provide the direct integration (e.g. Newmark method). In particular, the system is integrated, using step-by-step procedures, does not transform the equation before the numerical integration. Despite the NLD analysis is considered the best method for performing a seismic analysis, its application hides several disadvantages, such as the time and the computational efforts of the analyses. Moreover, the aim of the method is not of analysing the structural response due to a single earthquake record, considering the high uncertainties related to the seismic demand and the structural capacity. Therefore, NLD analysis must be performed by using a seismic input characterized by a certain set of ground motion records, selected in a certain way, able to provide the most reliable structural capacity trend. In the next Section, information about the seismic input selection will be described, according to the scientific literature and the EC8 prescriptions, with insertion of critical observations from the practitioners' point of view.

4.3.1 Seismic input: number, selection and scaling

The choice of the set of accelerograms for the design or assessment purposes is a difficult task, due to the high uncertainty related to the nature of the seismic excitation. Concerning to the procedures involved for performing one of a series of NLD analysis, the set of accelerograms should respect the real seismic demand for a structure, according to the hazard of the building site. General information about the phase of seismic input determination for NLD analysis have been provided in Chapter 2, speaking about the probabilistic seismic hazard analysis (PSHA). Before speaking about the accelerograms, it is important to define briefly the characteristics of accelerograms that rule the ground motions and the influencing factors of them. In particular, the main characteristics of accelerograms are:

- Amplitude;
- Frequency;
- Duration.

Concerning to the amplitude, the main parameter for defining the ground motion severity is the PGA, which is the maximum value of acceleration in a time history record. On the other hand, the PGA parameter cannot define the potential damage of the earthquake and for this reason, by integrating the records, it is possible to compute the peak ground velocity (PGV) and the peak ground displacement (PGD), definable in the analogous way of the PGA. Generally, the PGA is strictly related to the dynamic forces induced by the seismic event on the structure and it is the best parameter for identifying the more destructive events, especially for low duration of the motion. On the other hand, it cannot always provide information about the damage of the structure, evidence shown on some structure, subjected to earthquakes with high values of PGA, which reported low damage. The PGV is a parameter useful for motion with intermediate frequency and for this reason, it is adapt for investigating the effects on structures sensitive to intermediate frequency, such as high and flexible buildings or bridges. On the other hand, it is low sensitive to motion with high frequency. The PGD is the best parameter for characterizing the motion with low frequency. On the other hand, it is provided by a double integration of the acceleration, which lead to have errors in its computation (problem that can be overcome through direct measurements).

Regarding to the frequency, this parameter describe how the amplitudes of the motion are distributed in the signal. It is indispensable for defining the dynamic response of the structure, considering that the effects of the motion on the structure are strictly related to the ratio between the frequency of the ground motion and the natural frequency of the building. Mathematically, the motion can be described as sum of simple harmonic functions, characterized by different frequencies, amplitudes and phases. Each function is computable through the Fourier transform. Hence, for defining how to vary the amplitude at the variation of the frequency, it is necessary to define the Fourier spectrum, which provides information about the predominant frequencies and amplitudes. Some measures, strictly related to the frequency can be extracted from the Fourier spectrum, as the predominant T, the band amplitude, the central frequency and the shape factor. However, this introduce the concept of response spectrum, which describes the maximum response of a SDoF system, for a particular input motion, at the

variation of the natural frequency. It is worth mentioning that the abovementioned spectra are different, because the first one describes the seismic motion while the second one describes the response.

Concerning to the duration, this parameter is related to the time request for releasing the energy accumulated along the rupture surface and then, depend from the seismic moment and from the magnitude. From the engineering point of view, despite the duration contains all accelerations recorded in the complete motion event, the relevant part is the strong motion one, definable with the duration T_d. This latter is defined as interval between the first and last exceeding of an acceleration threshold (e.g. 0.05g) or the interval between the instants in which the energy recorded is equal to 5% and 95%. In addition, the scientific literature provides other parameters for describing the seismic motion, which take into account the combination of the motion characteristics above defined, such as the Arias intensity, the root mean square acceleration and the spectrum intensity (Acevedo, 2003 and references therein). Regarding to the influence factors of accelerograms, it is worth considering the below list of parameters:

- Characteristics of sources,
- Path;
- Site effects.

Concerning to the characteristic of sources, earthquake events are caused by the release and propagation of energy due to the rupture of the earth's crust in a certain point. For characterizing the source of the event, the main parameter is the magnitude, which is the measure of the energy released in the earthquake. This is classified through magnitude scales, such as the Richter one, which rules the size of the earthquake. Other characteristic of sources are the rupture mechanisms, directivity and focal depth.

For identifying the path that the energy released runs, the main parameter to describe is the distance. It is measured form the point in which the rupture occurs to the building site. The definition of distance can be simply the hypocentral distance, which is the distance between the building site and the hypocentre. Clearly, with a major

distance, some path effects increase, such as the reduction of the amplitude. Another parameter for characterizing the path is the crustal structure.

Regarding to the site effects, the earthquake propagation is dependent from the material, which constitutes the soil layers. Clearly, a soil constituted by rock tends to attenuate the shaking, toward a soil constituted by clay, lime or sand. In addition, the event can be strongly influenced from the ground topography of the ground surface.

In order to define the seismic hazard of the building to assess, the magnitude and distance should be combined. With this regard, the attenuation relationships (or attenuation models) are defined, which are able to define the strong motion parameters as function of other ones that represent the earthquake on a site of interest. An attenuation relationship is usually based on empirical data, which includes almost the magnitude-distance bin. The aim of this step of PSHA is not to define the distribution of the magnitude and distance, but to predict the probability distribution of the ground motion intensities. As reported in (Baker, 2008a), the general formulation of the attenuation model is:

$$\ln IM = \overline{\ln IM}\,(M, R, \theta) + \sigma(M, R, \theta)\,\varepsilon \qquad (4.16)$$

where ln IM is the natural logarithm of the ground motion intensity measure (IM), which is the sum of median and standard deviation (σ) of the same ground motion intensities, dependent from the magnitude (M), distance (R) and other parameters (θ). ε is the standard random variable, which represents the variability observed in the ln IM definition. Once that the attenuation models are defined, it is possible to compute the probability of exceeding a certain IM level, given a magnitude-distance bin, through the application of the total probability theorem. The general equation of PSHA, able to compute the rates of exceeding a certain IM for the source considered ($\lambda(IM > x)$) is:

$$\lambda(IM > x) = \lambda(M_i > m_{min}) \int_{m_{min}}^{m_{max}} \int_{0}^{r_{max}} P(IM > x | m, r)\, f_{Mi}(m) f_{Ri}(r) dr dm \quad (4.17)$$

where M_i and R_i are the magnitude and distance for the ith source, $f_M(m)$ and $f_R(r)$ are the probability distribution factors of magnitude and distance. By using the equation 4.17, the result is the hazard curve, properly defined in the Chapter 2. Within this latter, the hazard curve is strictly related to the UHS, which is the target to consider,

for a certain LS and for describing the hazard of the site. Therefore, the choice of accelerograms to apply on a building in a certain site must be depend from the hazard of the building site. In this frame, the main features to define about the seismic input, at the base of the performance of a NLD analysis, are summarized below:

- Typologies of accelerograms;
- Selection methodologies of accelerograms;
- Scaling techniques;
- Number of accelerograms;

Concerning to the typologies of accelerograms, it is possible to use 3 kinds of records: artificial, synthetic and natural accelerograms (Bommer and Acevedo, 2004). The artificial accelerograms are unreal signal generated for matching the target spectrum (usually the code spectrum or the uniform hazard spectrum (UHS) in the building site, for a certain LS). In particular, with the total compatibility, the signal obtained are usually constituted by a high number of cycles, with the generation of records that reach an elevate energy dissipation from the structure. This can cause a conservative result of NLD analysis, which can be appropriate in design procedure, but not in the assessment. For generating artificial accelerograms, the scientific literature provides some software, such as the above used SIMQKE (Gasparini and Vanmarcke, 1976). The synthetic accelerograms are unreal signal generated by modelling, through deterministic or stochastic methods, some ground-motion characteristics, accounting for some influencing factors of signals. The use of the synthetic signals is due to particular scenarios, for example for simulating an unusual magnitude. Despite the scientific literature provides some methodologies for defining synthetic accelerograms (Boore, 2003, Cornell, 2004), their generation reaches many efforts and for this reason, they are rarely involved in the NLD analysis. The natural accelerograms are the ones recorded from the earthquakes really happened. In particular, this kind of records are the most reliable ones to use in the seismic analysis, considering that this signals take into account all ground-motion characteristics, besides to consider the influencing factors of accelerograms, all abovementioned. Despite these kinds of records represent the

real events, the main disadvantage is related to the difficult of matching the spectrum of signal with the target spectrum, also considering the large record variability for representing the real building site scenario.

Generally, the natural accelerograms are usually collected in on-line database, on which one can select a certain number of records, according to the target spectrum, by using appropriate criteria of selection and, in the case, manipulation. This introduce the aspects about the selection of accelerograms. About this topic, some researches focus in the choice of natural records, developing some tools for selecting the signals compatibly to the code spectrum as REXEL (Iervolino et al. 2010) or conditional mean spectrum (Baker, 2011). Generally, for the records selection, two macro-methodologies can be adopted:

- Selection in terms of seismological parameters;
- Selection in terms of spectral matching.

Regarding to the record selection in terms of seismological parameters, the procedure to perform is called disaggregation (or deaggregation), which is the inverse procedure of the hazard curve definition above explained. In particular, starting from the target spectrum, defined for a site with a certain kind of soil and for a structure with certain N_L and U_C, all for a given LS, the procedure consists in the determination of the several seismic sources contribute to the hazard scenario in the site.
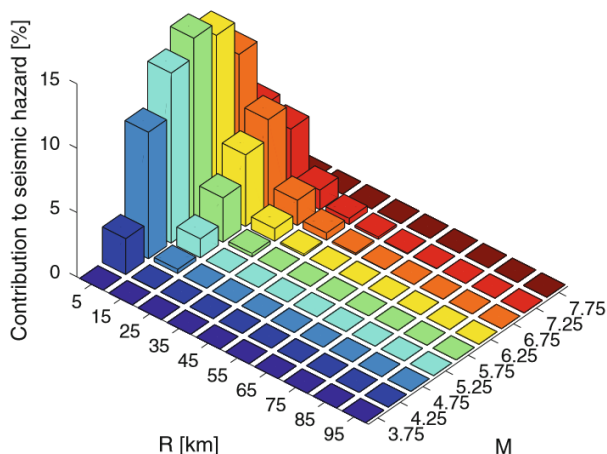
Fig. 4.30 – Example of disaggregation (Iervolino et al., 2010)

In other words, as shown in figure 4.30, for a disaggregation in terms of M and R, the process provides several records, where each record is defined by a M-R bin, which has certain probability of exceeding the in situ PGA. Obviously, this is not the sole procedure for selecting accelerogram, but one can perform the choice according to the abovementioned geophysical parameters, such as the expected faulting, duration and so on (see Bommer and Acevedo, 2004).

Regarding to the record selection in terms of spectral matching, the goal is to choose accelerograms in order to have the spectrum of the record close with the target one or with a part of it. With this regard, one should select a certain IM and to find a set of records that match the target spectrum, following this parameter, independently from M and R. The choice of the IM is not easy and it was object of several studies from the scientific community. In particular, the IM to select must be practical, efficient and sufficient (Luco and Cornell, 2007). Regarding to the practicality, the IM must be chosen according to the necessity to have a parameter directly related to the result of attenuation relationship results. This usually converge in the use of the PGA. On the other hand, the IM should be a parameter dependent from both hazard of the site and building to investigate, able to describe the seismic response of the structure. In the NLD analysis, the response of building through the choice of an EDP, which must be significant in terms of damage due to the application of seismic force. As in the pushover curve, the δ_R and θ_i are the most involved parameters for identifying the structural behaviour. Hence, a sufficient IM consists in a parameter that provide a structural response, in terms of EDP, conditioned by the same IM, which is independent from the ground motion characteristics as magnitude and distance. An efficient IM consists in a parameter that provide a structural response, in terms of EDP conditioned by the same IM, which is characterized by small dispersion. As shown by scientific literature, the most used parameter of IM for the records selection is the $S_a(T_1)$, obtained from the elastic target spectrum, 5% damped (Shome at al., 1998), which is also the most used approach provides in technical codes. The $S_a(T_1)$ is not always sufficient, such as in the case of soft-soil and near-source records. This problem occurs also when one scales the accelerograms with large scale factors. In addition, for structures with high influence of

higher modes, the T_1 is not significant in the power prediction and better results are provided by the spectral acceleration of the fundamental vibration mode. Another IM can be the PGA, which is a good parameter for estimating the non-structural response (Iervolino et al., 2008). A series of methods for selecting the IM is provided in (Kazantzi and Vamvatsikos, 2015), where it was carried out a comparison of IM selections for single and class of buildings. For example authors adopted for a class of buildings, an IM equal to $S_a(T=1s)$ for moderate to long period structures and $S_a(T_{1m})$ for a generic class of buildings, where T_{1m} is the median value of the Ts related to the first mode of all buildings considered. A valid approach for a single building, with the aim to obtain a sufficiency and efficiency of the IM, is the following (Bayer and Bommer, 2007):

$$S_{agm}(T_i) = \left[\prod_{i=1}^{n} S_a(T_i)\right]^{1/n} \tag{4.18}$$

where S_{agm} is the geometric mean of spectral acceleration values for the n Ts. This formulation can be used for combining both horizontal components of accelerograms and for a range of Ts defined on the base of the case study. This formulation introduces the concept of spectrum matching in a band of Ts. In fact, the S_{agm} can be computed assuming as bounds, values of Ts that are function of the first vibration mode (see references in Kazantzi and Vamvatsikos, 2015). About this topic, the EC8 suggests to match the records (the code does not provide limitation about the kind of accelerograms) with the code spectrum, with a limitation that the mean of the $S_a(T=0)$ must not be smaller than PGA*S, where S is the term that considers the soil class and the topography of the site. In addition, EC8 provides limitation about the matching with the target spectrum in a T range of interest (between $0.2T_1$ and $2T_1$,), where anyone record must be less than 90% of the code spectrum values. In each case abovementioned, the record selection phase can be very complicated for the practitioners. For this reason, a friendly method for the record selection can be the randomly selection, after the identification of the building site, in terms of PGA, according to a seismic hazard models. For example, the EFHER association (Giardini et al, 2013) provides a seismic hazard model of Europe, considering the PGA with 10% in 50 years exceedance

probability. In this model, a classification of hazard level was proposed, with a distinction among low (PGA=0.05g-0.15g), moderate (PGA=0.15g-0.25g) and high (PGA=0.25g-0.35g) hazard, basing on different PGA ranges. To each hazard level is attached a set of accelerograms and practitioners, based on the building site PGA, can select the records useful for NL dynamic analysis. In (Iervolino and Cornell, 2005) authors compared the structural response obtained from the application of a set of records chosen randomly and another one chosen according to the seismological parameters. The results showed that there was no evidences for preferring the above first or second set of records. Clearly, for matching the seismic hazard in the site investigated and the dynamic behaviour of building to analyse, it needs of scaling the records selected.

Regarding to the scaling phase, besides to matching the records with the spectrum, the utility of the scaling is also due to the necessity of investigating the structural response to different IM levels, such as occurs in the structural analysis phase of the PBEE. To this latter scope, the set of record can be scaled in a certain way, depending from the method of NLD analysis or can be substituted with another set of records (some authors do it, in order to do not vary the features of the accelerograms). In the practical application it is preferable to select one time the records and after to scale them, rather than changed the set of data for different IM levels. The most common way for scaling the accelerogram is the scaling in amplitude, using IM values as PGA (adapt for structures with low Ts), PGV (adapt for structures with moderate-high Ts), PGD (adapt for structures with high Ts) and $S_a(T_1)$. This latter is the most used approach suggested by technical codes, with the disadvantage of the sole dependence from the structural features, but not from the seismological parameters. For the methodologies, which provide the scaling in amplitude, it is worth mentioning that it can be performed by using other parameters, such as the Arias intensity, the root mean square acceleration and the spectrum intensity. Other methodologies for scaling the accelerograms can be the scaling in time, scaling by wavelets or Fourier transform and scaling through seismological parameters. The scaling in time consist in the variation of dura-

tion and frequency. This kind of scaling method is low used, considering a certain energy variation, besides to the loss of the ratio between duration and number of cycles. The scaling by wavelets or Fourier transform consists in the modification of the response spectrum through the addition of wavelets, in order to match the target spectrum. The scientific literature proposes some works with NLD analysis in which the accelerograms were modified in this way (Hancock et al., 2008) and some software perform this transformation, such as RSPMATCH (Abrahamson, 1998). Scaling with seismological parameters is low common and not preferred toward other methods, among the scientific community. Finally, a fundamental parameter for performing NLD analysis is the number of accelerograms. Generally, in the scientific literature, the number of accelerograms for NLD analysis is different among the research works. The advantage to use a lot of records is a consistent estimation of the structural response, with a low bias of the results (Hancock et al., 2008). On the other hand, in a practical application it is unthinkable of performing a large number of time-history analysis, considering the time, computational efforts and high restore space capacity reached. EC8 suggests the choice of a minimum of 3 accelerograms groups up to a maximum of 7 ones, where each group is composed by 2 horizontal components and 1 vertical component. Increasing the number of records adopted, the same code suggests of adopting the mean of structural response, rather than the maximum effects. In each case, for having acceptable results, the lower number of accelerograms to consider is equal to 11.

4.3.2 Recent alternative approaches for the seismic assessment based on nonlinear dynamic analysis

As just abovementioned, the scope of NLD analysis cannot be provide the structural response obtained from a single earthquake record, considering that both seismic demand and structural capacity are affected by uncertainty, such as indicated in eq. 2.30. The scientific literature provides some powerful methods able to accurately estimate the seismic demand for several intensities, in order to define the structural response for the objective LSs to investigate. This concept converges with the goal of

the PBEE, which wants to describe the performance of the building, in terms of probability of violating a given LS, in order to quantify the seismic fragility and vulnerability. It is worth mentioning that, for performing NLD analyses, each record should be applied on the structure with all components (2 horizontal and 1 vertical). On the other hand, some studies presented in scientific literature investigate the response of structure, analysing 2D FE models and applying just one component of the accelerogram. The main methodologies of NLD analysis to highlight are:

- Cloud analysis;
- Single stripe analysis;
- Multi stripe analysis (MSA);
- Incremental dynamic analysis (IDA).

The first two methods can be classified as narrow-range methods, which investigate the structural response in a limited band of IM levels, while the last two methods are wide-range methods, because they investigate the structural response over a large range of IM values. As understandable, the narrow-range methods reach the performance of low NLD analysis than the wide-range methods. On the other hand, the wide-range methods provide results more accurate than the ones obtained from the narrow-range methods. It is worth mentioning that the description of all methods is going to be pointed out to a practitioners' use, according to the definition of the load resistance factor design described in the Chapter 2 and with reference to the work in (Jalayer, 2003 and Jalayer and Cornell, 2009).

Concerning to the cloud analysis, the procedure consists to excite the structure by using a set of records with different values of IM, selected for the building. This means that, if the IM is the $S_a(T_1)$, the structural response obtained for a certain number of records is constituted by the same number of points with different $S_a(T_1)$. Therefore, the result of this series of NLTH is a cloud of points, plotted in the graph IM-EDP, from which define the trend of the seismic demand and structural response. From the cloud of points, the statistical parameters can be extracted, such as the $\eta_{DM|Sa}$ and $\beta_{DM|Sa}$ of the DM for a given level of S_a. These parameters are involved in the application of a

lognormal distribution model, which estimates the demand and the capacity through a linear regression on logarithmic plane (figure 2.26), as ruled by the formulations proposed in the Chapter 2. One of the main feature of this method is that the seismic input can be represented by a set of original records chosen in a certain way, such as using the seismological parameters as M and R, related to the building site. Then, the cloud analysis is adapt for a structure investigated through a set of unscaled records. For improving the estimation of the probability model features, the set of records can be chosen in order to cover a large range of IM levels. On the other hand, in order to investigate the structural response to more IM levels, without changing the set of accelerograms, one should scale the set of records. An example of cloud analysis on scaled and unscaled records was provided in (Jalayer, 2003), which applied this analysis method on a building and investigated the statistical parameters, for computing the factored demand for a given value of S_a. Author numerically demonstrated that the statistical parameters obtained from the cloud analysis underestimated the structural response (toward the results obtained from numerical integration), with a not good $\eta_{DM|Sa}$ value and lower $\beta_{DM|Sa}$ value. This result was due to the choice of a set of ground motion, which had difficult to represent the seismic demand related to a proper value of IM. In addition, author tried to scale the set of records with a scale factor equal to 2, in order to define the probabilistic model for a greater IM level (figure 4.31 shows this case, with representation of the regression line and its parameters). In this latter case, besides to have a greater value of $\beta_{DM|Sa}$ (which cannot be considered constant), the results of the probabilistic models showed a conservative estimation of the structural response, with a wrong estimation of the parameters that rule the regression line. Other application of the cloud analysis are available in (Mackie and Stojadinovic 2001, Padgett and DesRoches 2008), which used the method for applying the PBEE paradigm on bridges. Despite the real nature of the ground motion involved in the cloud analysis, for what abovementioned, the methodology presents some limitations. Firstly, assuming an unscaled set of records, the statistical parameters computed are valid for a certain range of structural response, conditioned by an IM. This means that, with the increment of the IM level, the $\eta_{DM|Sa}$ and $\beta_{DM|Sa}$ (overall) change, with right estimation of

the structural response in a sole band of intensity levels. In addition, the method cannot provide the good estimation of the local mechanisms in the post-elastic field, especially when they changing rapidly. Finally, if one uses a set of records that provides global instability of the FE model, the adoption of a constant $\beta_{DM|Sa}$ could be not reliable (a solution of this problem was proposed in (Miano et al., 2018)).
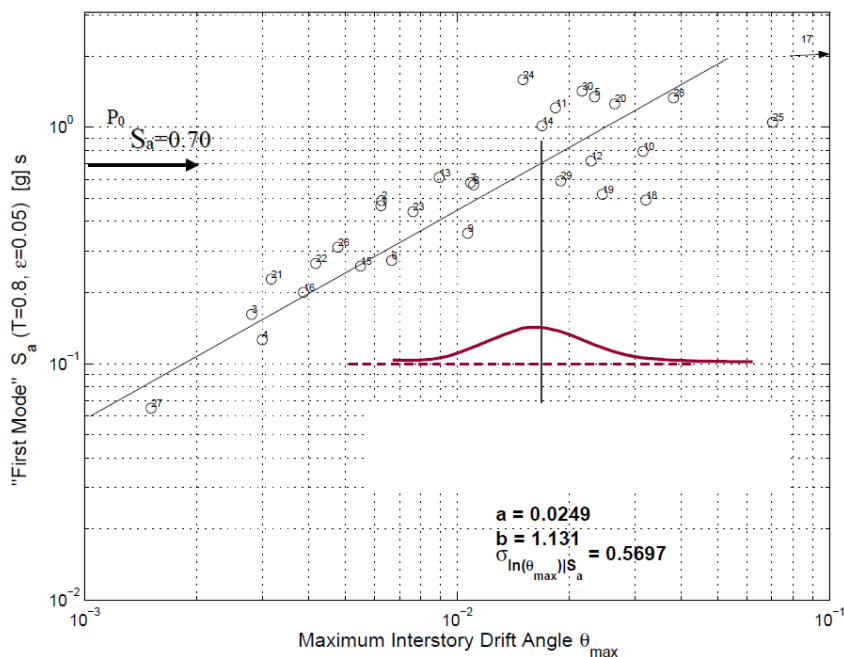
Fig. 4.31 – Definition of statistical parameters, by using cloud analysis with scaled records (Jalayer, 2003)

Regarding to the single stripe analysis, the procedure consists to subject the structure to a set of ground motions, which have the same value of IM. If the IM is the $S_a(T_1)$ the structural response obtained for a certain number of records is constituted by the same number of points with the same $S_a(T_1)$. Being available just a stripe of points, a main parameter to define is the IM to consider, which can well represent the structural response. In (Jalayer, 2003), author selected the IM as the S_a on the Hazard curve approximation (Figure 2.25) correspondent to a given mean annual frequency of exceeding. Once that the IM parameter is chosen, with a certain criterion, the set of

242

records must be scaled for the value selected, in order to display in the graph IM-EDP a stripe of points, such as shown in figure 4.32.
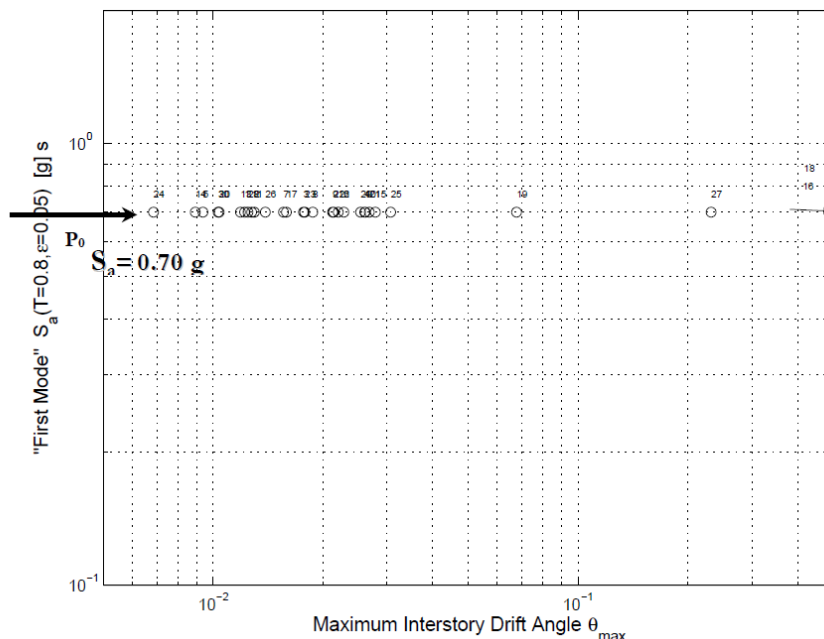
Fig. 4.32 – Single stripe analysis result, for a fixed value of S_a (Jalayer, 2003)

Even in this case, from the single stripe analysis, the statistical parameters can be extracted, such as the $\eta_{DM|Sa}$ and $\beta_{DM|Sa}$ for that level of S_a. In particular, the $\eta_{DM|Sa}$ is provided by the EDP value that subdivide the stripe in two equal parts (in terms of number of points), called also EDP^{50}, while the $\beta_{DM|Sa}$ is computable through the 16 and 84% percentiles values of the data (EDP^{16}, EDP^{84}), as below shown:

$$\beta_{DM|S_a} = \frac{\left(EDP^{84}/EDP^{50}\right) + \left(EDP^{50}/EDP^{16}\right)}{2} \qquad (4.19)$$

Clearly, the response of the single stripe cannot be a linear regression line, except if the values of the probabilistic model are a priori fixed (as the exponential term of the power law), with the risk of obtaining wrong results. As shown in (Jalayer, 2003), by using a double stripe analysis (two single stripe at different IM level), with the second

243

stripe close to the first one, the results were same to the ones obtained from the numerical integration. Despite the results of the above works and the cheap computational efforts for a single or double stripe analysis, the results are strongly influenced from the sensitivity of the analyst. In addition, as for the cloud analysis, there are the problems about the global instability of points (especially in the case in which the IM value is not correctly chosen). In particular, the method provides good results for low seismic intensities (low IM) and significant errors in the cases of high seismic intensities (near to global instability).

Concerning to the wide-range methods, the natural development of the single stripe method is the MSA one. Hence, MSA method consists in the development of a lot of single stripe analyses, for several IM values, in order to cover a large range of IM values. In this case, the procedure can be applied in two different ways. In particular, the set of ground motions can be repetitively scaled, by increasing the IM value selected, such as $S_a(T_1)$, from low values (elastic field) until to have high values of IM (global instability of some points in the stripe). Another possibility can be the change of the records, selecting a new set of ground motions each time that the IM value change, in order to avoid scaling procedures. Furthermore, knowing that at higher IM values, the results are more scattered, it is possible to perform lower analysis at lower IM values (increasing the scaling steps) and increase the number of analysis at higher IM values (reducing the scaling steps). The results of MSA are a lot of stripes, equal to the number of IM imposed with scaling, constituted by a number of points equal to the number of records, which constitute the selected set. The MSA method provides a complete trend of the structural response, as the seismic demand increases. The computation of the statistical parameters for the lognormal probabilistic model are surely correct, as shown in the comparison performed in (Jalayer, 2003) toward the results obtained by numerical integration. In particular, it is possible to compute the $\eta_{DM|Sa}$ and $\beta_{DM|Sa}$ for all S_a levels and compare these parameters with ones obtained from the single stripe analysis. The $\beta_{DM|Sa}$ can be evaluated through the computation of the 16 and 84% percentiles values of the data, at each IM level. Figure 4.33 shows an example of MSA application (same case of figures 4.31 and 4.32) in which is computed the $\eta_{DM|Sa}$ and

$\beta_{DM|Sa}$ for a given value of S_a. Even in this case, for MSA performed at high IM values, some response points can collapse. This can cause the loss of accuracy of statistical parameters. In this case, the collapses points can be considered in the evaluation of the structural response and in the subsequent fragility analyses, by using particular methodologies as the logistic regression (Baker, 2015).
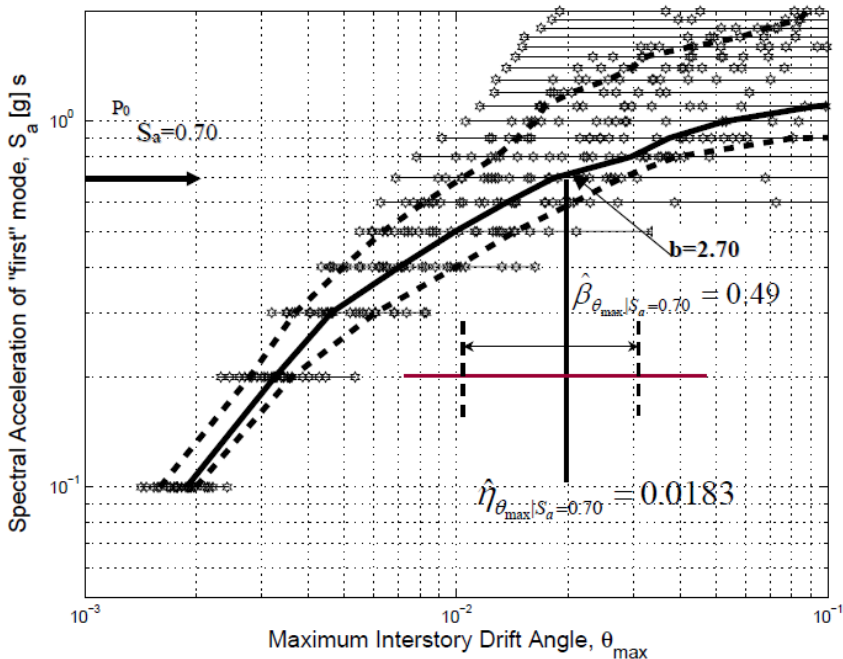
Fig. 4.33 – MSA results, with computation of statistical parameters for a given value of S_a (Jalayer, 2003)

The MSA concept is directly related to the IDA method, which is the most in-volved NLD analysis for investigating the structural response in a probabilistic view. The IDA method (Vamvatsikos, 2002 and Vamvatsikos and Cornell, 2002) consists in the application to the structure of a set of records monotonically scaled to multiple IM levels. The main difference with MSA method is that the results are not provided for some IM values but considering a full response curve for each record, on the graph IM-EDP. This kind of analysis completely covers the range of responses for all IM values (also considering the global instability). The scale factor to apply on accelerograms is

always positive and starts from values near to 0 up to high values. Generally, an IDA curve presents some properties, which is going to listed below:

- The first part of the IDA curve should be linearly elastic up to the end of the elastic field. In particular, the slope of this branch depends from the stiffness of the structure, which is related to the dynamic parameter of building, such as Ts. With this regard, performing more IDAs with several accelerograms, if the system is a SDoF, the first part of each IDA curves should be the same, while if the system is a MDoF, the first parts of IDAs curve can present dispersion, due to the influence of higher modes.

- In the post elastic field, the IDA curves can behave differently. In particular, as shown in figure 4.34, 4 different records on the same structure can cause 4 different results. This is due to the different properties of accelerograms, which justifies the aleatory uncertainties and different properties of the numerical model, as later explained. In the first case, as soon as the accelerogram is scaled up, the curve presents a trend that softens. This is due to a structural response conditioned by initial collapse phenomenon, which does not allow of having strength at greater IM levels. In the second case, the curve presents hardening. The first two cases can be defined as aggressive (Jalayer, 2003) for the collapse at lower IM values. The third and fourth cases present a waving trend around the imaginary line, which extends the elastic branch with the same slope. The two curves present both softening and hardening behaviours and this is one of the most particularity of the IDA method. In fact, in these latter 2 cases, the reversal effect occurs. Graphically, the reversal effect happens when at the increment of the IM level, the EDP of structural response at successive steps is lower than the previous one. Physically, this phenomenon is due to the different timing provided from the accelerograms scaling. In particular, if in the previous step, the yielding occurs at a certain time and the peak response occur in another time, the consequence of scaling the accelerogram can provide that the yielding occurs before of the previous step and the peak response can be in the other verse of the shaking, with a lower value of the previous step. This is typical

of the IDA analysis (in MSA it is impossible to display this phenomenon), which can provide situation of structural resurrection. This can happens also where scaling up the accelerogram, the value of the EDP is lower than the previous one, which was over the global instability, especially in the cases of convergence problems at the previous step. The last two cases can be defined as benign (Jalayer, 2003) for the collapse not displayed at higher IM values.
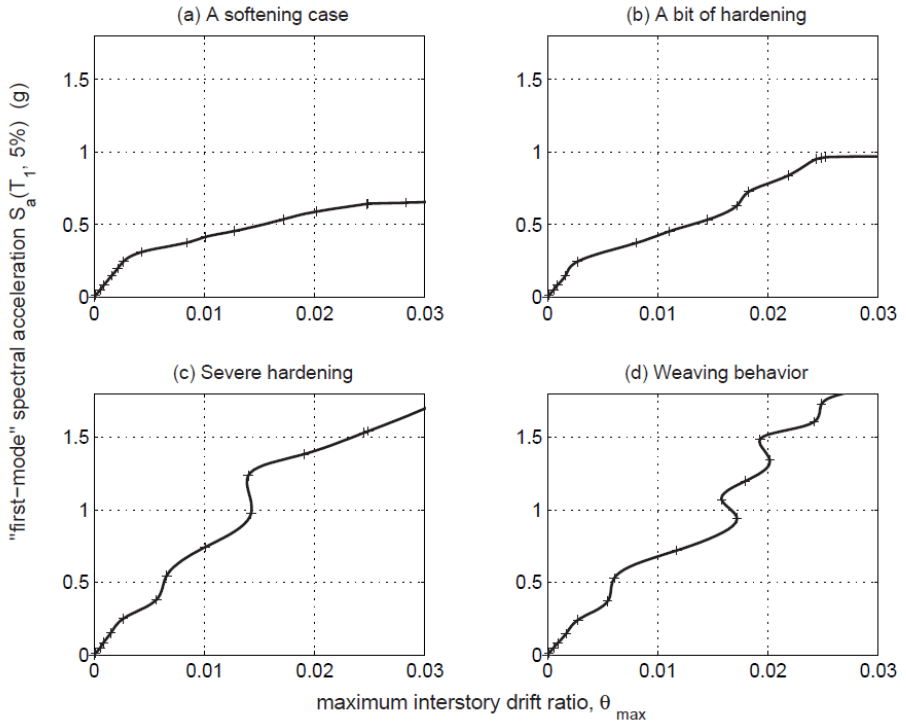
Fig. 4.34 – Possible result of IDA curves, applying different records to the same structure (Vamvatsikos, 2002)

- A result of the IDA curves is the global instability occurrence. In the first two cases of figure 4.34, the curves present at the end, a horizontal branch (flatline), which means that with a little increment of IM, the EDP recorded is strongly higher than the one obtained at the previous step. This is a synonymous of structural lability, such as occur in the pushover curves.

It is worth mentioning that, in the case of IDA curve with reversal effects, the capacity point for a given LS, is the lowest one that reaches the condition imposed for identifying the LS violation. In particular, for reading the IDA curve results (as for MSA method, also if in this case the curve is not displayed), two criteria are available: EDP-based (or DM-based) and IM-based. In the EDP-based criterion, one fixes the EDP value related to the LS and the capacity point is the first that reaches this value of EDP. Less common is the IM-based criterion, where one fixes the IM value related to the LS and the capacity point is the first one that reaches this value of IM. As for the MSA, the IDA method provides the complete trend of the structural response and it is possible to determine the statistical parameters of for the lognormal probabilistic model. Figure 4.35 shows an example of IDA application in which is computed the $\eta_{DM|Sa}$ and $\beta_{DM|Sa}$ (from the percentile curves) for a given value of S_a.
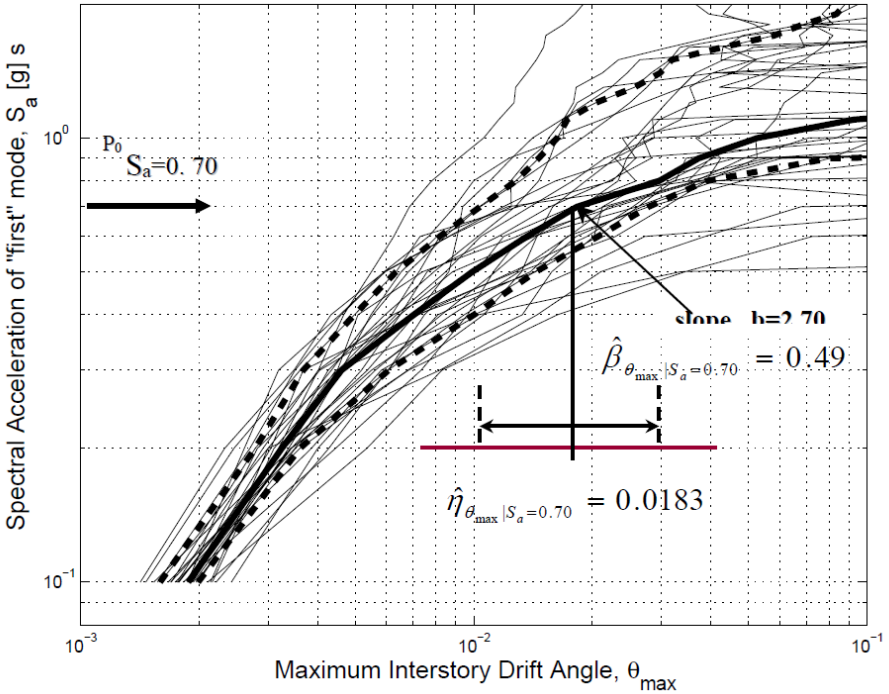
Fig. 4.35 – IDA results, with computation of statistical parameters for a given value of S_a (Jalayer, 2003)

5. Simplified methods for the vulnerability analysis of existing RC buildings

5.1 Overview

The vulnerability analysis of existing RC buildings, as shown in the precedent Chapters, is a composed by several phases, among which modelling and seismic analysis. In this frame, a lot of researchers are trying to simplify the above phases, considering the elevate time and computational efforts that the development of some procedures require. Generally, simplified methods, for both modelling and analysis phases, were proposed in the time, for performing the vulnerability analysis of class of buildings, usually for a regional scale vulnerability analysis. On the other hand, the possibility to have a simplified tool or procedure, able to investigate the seismic behaviour of a single building could represent an advantage for researchers and practitioners, for several reasons. With this regard, the investigation of the response on a simplified model could provide important information about the global behaviour of building, before to perform analysis on the complex numerical model. In addition, a simplified model can be used as support to the complex numerical model, considering the possibility to perform a lot of NLD analysis, in a PBEE view. Finally, the simplified modelling converges in the necessity of investigating the seismic behaviour of the existing building stock. Even from the practitioners' point of view, in the performance of the PBEE procedure for assessing existing RC buildings, the phase of seismic analysis on a FE model can represent a real hitch, especially for who wants investigate the structural behaviour in a wide-range of seismic demand. Besides the number of analyses to perform, it is worth considering the skills of commercial software, which usually are not designed for certain typologies of analysis in addition to require a lot of hard disk space for restoring the results of analysis and for the post-processing phase. Hence, this Chapter proposes, after a presentation of the methods proposed by the scientific literature for simplifying the modelling and analysis phases of the assessment procedure, an application of the MSA method on a sample of 15 real existing RC school buildings, in the province of Foggia, Southern Italy. In particular, the analysis proposed consists in the performance of few stripe analyses (FSA) on full FE models made through commercial software, able to

provide information about the buildings behaviour in both elastic and inelastic fields. Subsequently, the fragility of buildings at different LSs are computed and, subsequently, they have been compared with the same information provided by SPO2FRAG software (Iervolino et al., 2016 and Baltzopoulos et al., 2017). This latter is a computer tool able to compute fragility curves for several LSs, starting from a pushover curve, through the involvement of some procedures proposed by the scientific literature. Considering the nature and the same features of the sample of buildings, regional fragility curves for ultimate LSs are proposed, in order to validate the methodology for a large scale vulnerability analysis. Subsequently, with the aim of investigating the global behaviour of existing RC buildings through simplified models, a new procedure is proposed. In particular, the goal is to provide a way for making simplified 3D reduced-order models, starting from the information about the knowledge of the buildings. The procedure has been tested on the sample of existing RC school buildings previously analysed and the results of some elaborations on the simplified models, such as the computation of structural response, damage states and confidence levels are compared with the same results obtained from the FSA application on the full numerical models. The results of procedure provide interesting observation about the application of PBEE in the practitioners' world, showing some advantages and limitations.

5.2 Simplified methods for the global assessment of existing buildings

Simplified methods applied to seismic engineering can be defined as simplified numerical models or seismic analysis, which lead to estimate more or less accurately the vulnerability of existing RC buildings to seismic actions. When one speak about simplified model, the idea is a numerical model, which can substitute the full FE model of the structure, providing the same response to seismic actions. This concept is implied in the one of equivalent structure. From the mechanic point of view, an equivalent structure is a numerical model, which should be constituted by the same mass and stiffness of the original structure and, if subjected to external action, should exhibit the same global and local response in both elastic and inelastic field of the original structure. In other words, the equivalent structure should behave as the original one, in kinematic (deformation and displacement) and static (stress and strength) terms. The

concept of equivalent structure runs close to the necessity of investigating the structural performance, through NLTH analyses, which have been always considered the point of reference from the scientific community, as just highlighted in the Chapter 4, besides to reduce the uncertainty related to the vulnerability analysis problem. In this frame, the possibility to adopt numerical simplified models has been often taken into account from scientific community, with the aim to simulate and analyse the global seismic behaviour of existing structures and, overall, for reducing the time and computational efforts of NL analyses. In the scientific literature, the first idea of simplified model was the SDoF system, which takes into account the NL properties of the structure. In particular, in (Saiidi and Sozen, 1981), based on the differential equation of dynamic equilibrium of an oscillator, authors provided a way of modelling the NL behaviour of the SDoF system from the features of the full MDoF system, which was able to simulate the displacement history of RC structures under a ground motion excitation. In particular, the SDoF system was modelled as the combination of a spring and a mass, as shown in figure 5.1, through the adoption of a bilinear constitutive law and a hysteretic model for cycling loads. This model was the final proposal, after precedent research works (Gulkan and Sozen, 1974 and Shibata and Sozen, 1976).
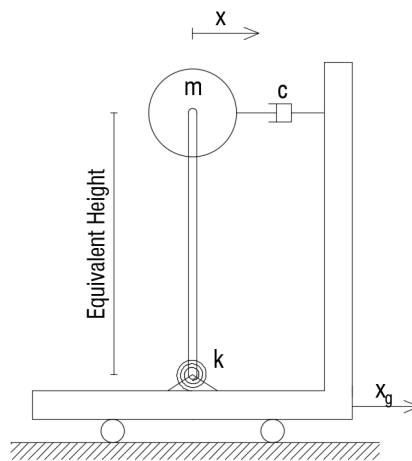
Fig.5.1 – Equivalent SDoF structure, as proposed in (Saiidi and Sozen, 1981)

The use of SDoF models were, for a lot of time, object of research, in order to analyse the seismic behaviour of MDoF models and calibrate some factors useful in

the design and assessment phases of RC buildings and employed in the new generation technical codes. In (Qi and Moehle, 1991) authors elaborated equivalent SDoF models from MDoF inelastic ones, in order to generate a proposal of elastic response spectrum and estimate the maximum response, in terms of displacement (δ_R and θ_i). In (Miranda and Bertero, 1994), authors estimated the value of reduction factor R_μ, based on several design input parameters. Using elastic response spectrum, authors established that R_μ strongly depended from ductility, T and soil typology. In (Miranda and Ruiz-Garcia, 2002) authors reviewed several methods for estimating the inelastic displacement demand, starting from analyses on SDoF models presented in (Miranda, 1991). Based on the previous review, the same authors in a successive work (Miranda and Ruiz-Garcia, 2003), estimated the effects of parameters that influenced the inelastic displacement ratio, which was the ratio between the maximum inelastic displacement and the maximum elastic one in a seismic event. The concept of equivalent SDoF system was subsequently adopted for developing the well-known "N2 method" (Fajfar and Gasperic, 1996), which is actually implemented in the EC8. With this regard, in (Kilar and Fajfar, 1997) authors proposed simplified models, for structural typology, in order to propose an alternative way for providing good results of pushover analysis of buildings, which are not regular. In particular, using macroelements, authors investigated the NL behaviour of structural systems with RC walls, columns and RC walls, coupled RC walls and regular frame. The four models developed in this work are respectively shown in figure 5.2, with indication about the plastic hinges for modelling the nonlinearity of structural elements.
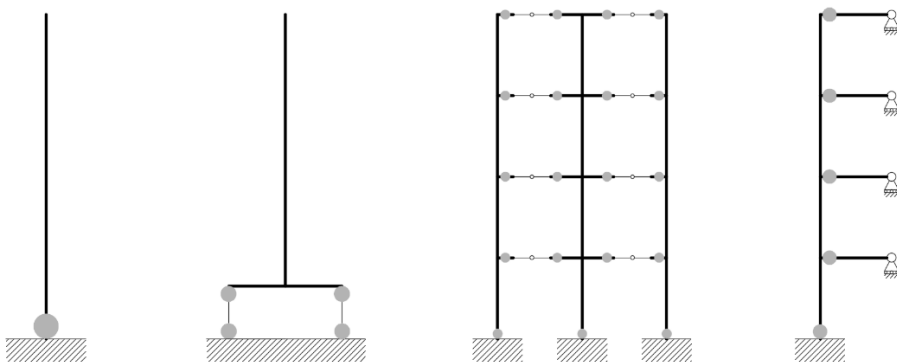
Fig.5.2 – Macroelements model, as proposed in (Kilar and Fajfar, 1979)

The main disadvantage of the SDoF system is the impossibility to monitor all parameters that significantly identify the earthquakes response and damage, such as the θ_i. With this regard, in (Lai et al., 1992), a simplified model was proposed, composed by rigid body assembled and able to simulate a shear type frame. The model, depicted in figure 5.3, allowed of computing the dynamic behaviour of structure, in terms of T and M[%], through the resolution of a matrix system, analogously to the FE software.
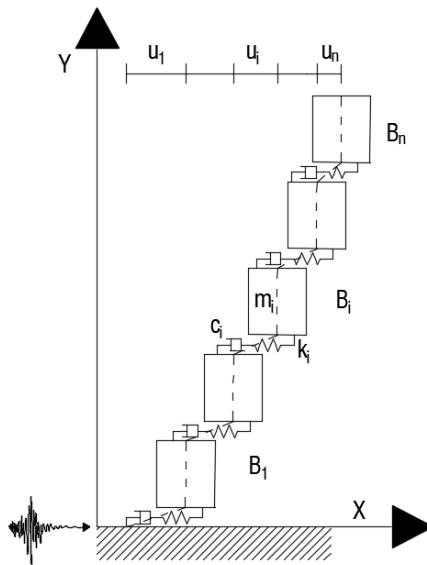
Fig.5.3 – Rigid body model, as proposed in (Lai et al., 1992)

In order to estimate the local parameters of buildings subjected to seismic actions, other kinds of simplified models were proposed, as the "predictor models". These models were proposed because able to match the needs of investigating the buildings with a consistent number of ground motions records, for the probabilistic analysis. The first one was the "generic frame model" (Nakashima et al., 2002), wherein using some commonly assumptions about the congruence and equilibrium concepts, a matrix formulation was provide. The simplified model was composed by a representative column

with rotational springs, linked at each storey with a support, by adding a treat that accounts for the NL features of the beams. In addition, the models were able to predict the panel zone behaviour of steel moment frame. A similar approach to the previous model was adopted for proposing the "fishbone models" (Luco at al. 2003), as depicted in figure 5.4, which was a methodology implemented for estimating the NL response of buildings under earthquake excitations, but also accounting for the elastic properties of the full model. In fact, this kind of predictor was proposed based on the idea of modal superposition, which combined the features of the first two vibration modes. The application to some cases studied showed good precision and bias of results between the models, with the possibility to have wrong results in the case of local yielding in the full model. An improvement of the fishbone models was subsequently proposed (Mori et al. 2004, Mori et al, 2006), by accounting for other modal properties of the full model, such as the consideration of the 3rd mode for the structures with long Ts and the approximation of the post elastic 1st mode to the shape obtained from a NL static analysis.
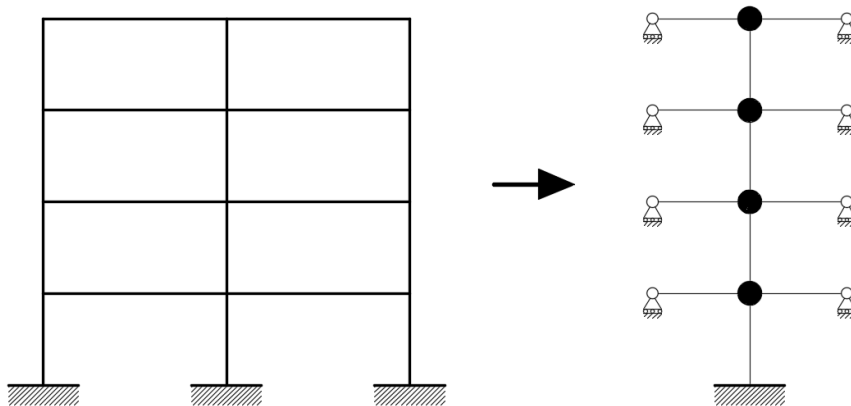
Fig.5.4 – Fishbone model, as proposed in (Luco et al., 2003)

Another simplified model, adopted also in the FEMA440 report (FEMA 440, 2005), was the "stick model", which was able to simulate the behaviour of 2D and 3D full models. In a 3D model view, the stick model is a MDoF model with 3N degrees of

freedom, where N is the number of storeys and the DoFs considered are the two translational and the rotational components of movements, under the hypotheses of rigid floor and storey mass concentrated in the CM of the floor. Figure 5.5 shows the stick models proposed in the above report, considering shear-type models and, respectively, the two limit hypotheses of flexural and shear stiffness's of beams infinitely greater than the one of columns and flexural and shear stiffness's of columns infinitely greater than the one of beams.
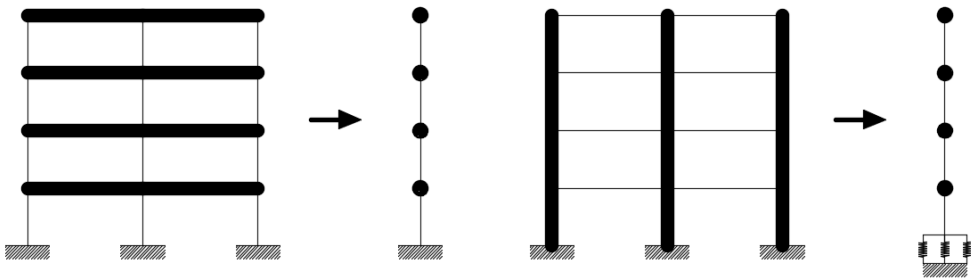
Fig.5.5 – Stick-models, as proposed in FEMA 440 report (2005)

The concept of stick model was accurately investigated in (Bovo, 2013 and Bovo and Savoia, 2015). The procedure proposed was called "equivalent stick model method", where after the performance of the detailed model, the capacity curves of each storey were used for computing the constitutive law of the simplified model. Some full numerical benchmarks were investigated, both regular and irregular, with good estimation of the dynamic behaviour of full models by using the simplified one, as shown from the comparisons of time history analyses. An advantage of the method proposed was the possibility to consider in the stick model the local parameters, thanks to the evaluation of the behaviour of each storey, in terms of V_b and δ_R. With the aim to generalize the procedure for assessing the collapse safety of a class of buildings, in (Haselton et al., 2007) a method for developing simplified "archetype models" was proposed, as shown in figure 5.6, based on a previous work about the RC buildings assessment (Goulet et al. 2007).
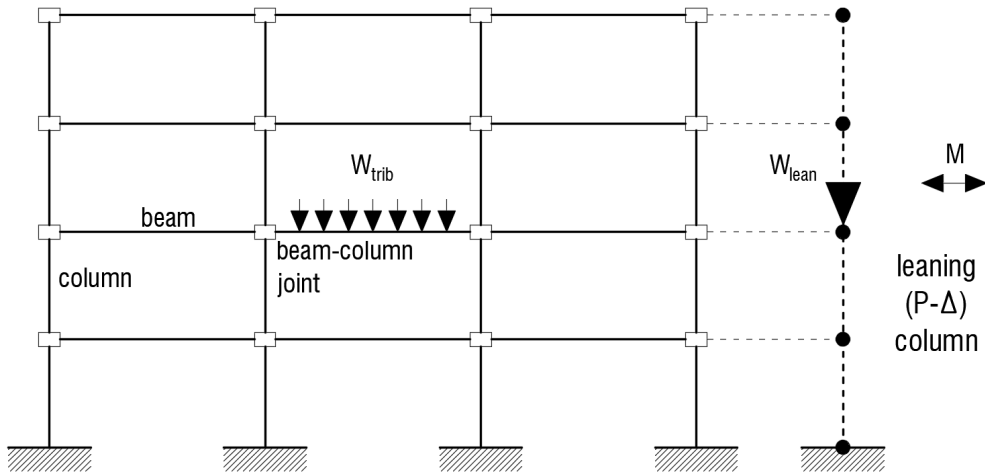
Fig.5.6 – Archetype model, as proposed in (Haselton et al., 2007)

In particular, the archetype model was a 2D frame model, which contains internal and external columns, beams and joints. In addition, it accounts for the P-Δ effects through a leaning column element. The authors, varying the mechanical and geometrical key features of archetype model and considering the additional axial loads due to the other columns elements not considered (overturning effect), studied 30 RC structures in Los Angeles and derived them probability of collapse, through the computation of fragility curves. The method was able to account for the epistemic uncertainties due to the model, besides to lend itself for being analysed by a lot of NLD analyses. The recent scientific literature proposed other kinds of simplified modelling approaches, useful in the risk assessment field. To this scope, some authors proposed the "reduced-order models", which are models with a number of DoFs reduced, but that faithfully represents the salient features of full models. In particular, this modelling provides similar estimation of structural response parameters, like θ_i, but it cannot consider the individual components failing of the full model, such as the rotation of each plastic hinge. One example of reduced-order model is the "parsimonious model" proposed in (Gidaris and Taflanidis, 2013), which is a 2D shear-structure model made using the elastic properties of the full models for computing the elastic stiffness and the information about NL cyclic pushover and sinusoidal dynamic analysis for calibrating the

hysteretic behaviour. The models was used for applying the concepts of PBEE with a great computational efficiency for the NL analyses. The model proposed, depicted in figure 5.7, allowed of estimating with high fidelity, parameters as θ_i, acceleration and velocity of the system and energy dissipation due to cycling loads. Another approach can be provided by the "surrogate models" (Tsompanakis et al., 2008, Taflanidis et al., 2016, Gidaris, 2015, Bakalis et al., 2017), which is a methodology that consist in the establishment of a simple relation between the model parameters (input) and the model performance (output). In particular, the full model and its response at several points of the model parameter space constitute the input, while the output is a model that repro-duce accurately the features of the initial one. Generally, for providing the input/output relations in the earthquake engineering field, where the input space is consistent and the computational efforts become elevated, the surrogate models are usually generated using some resolution methodology. In particular the most used in the recent research studies are the neural networks (Lagaros and Fragiadakis, 2007), response surface models (Gavin and Yau, 2007, Taflanidis and Cheung, 2012) and kriging models (Gidaris at al., 2015, Gidaris and Taflanidis, 2015).
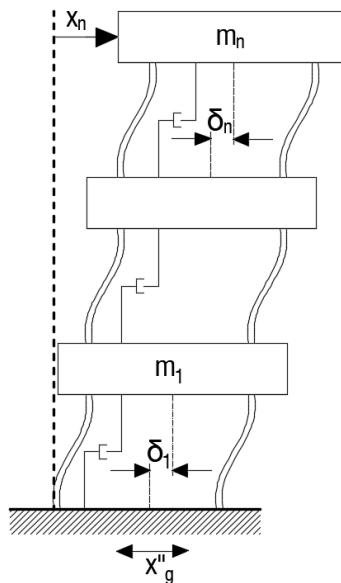
Fig.5.7 – Reduced-order or parsimonious model, as proposed in (Gidaris and Taflanidis, 2015)

As abovementioned, the use of simplified models is widespread in the risk assessment field, above all considering the involvement of the PBEE approach. In order to describe the structural response, the fragility and the vulnerability of a building or a class of buildings, it is necessary to perform NLD analyses as IDAs. In a view of computational inexpensiveness, some researchers proposed tools able to perform IDA analysis in a simplified but faithful way. The main reference is (Vamvatsikos and Cornell, 2006), where authors developed a simple tool, called SPO2IDA, able to provide the IDA curve of whatever SDoF system, with any T and any NL behaviour modelled through a multilinear backbone curve. The tool was developed accounting for the results of a series of IDAs, obtained from the implementation of an extensive set of ground motion, repetitively scaled. In addition, the tool was able to provide the 16% and 84% fractiles IDA curves, besides the median with 50% fractiles. The main aims of SPO2IDA were the estimation of seismic demand capacity and the inelastic displacement ratio of the SDoF system, also accounting for the performance to a certain LS. The results of IDAs showed in figure 4.34 can be related to the result of pushover analysis. As shown in figure 5.8, the equivalence developed for a simple oscillator (SDOF system) between the median curve of IDA and pushover analyses is depicted. The pushover curves are plotted in the graph F-δ_R (where F is equal to V_b if the P-Δ effects are not considered) and the median IDA curves are plotted in the graph $S_a(T_1)$-δ_R. Following the order of figure 4.34, the first case occurs when the NL behaviour of the oscillator is modelled through constitutive laws with an elastic branch and softening behaviour. An evolution of the previous case is the second one, which provide a constitutive law with elastic branch, softening and residual plateau. The last two cases are constituted by bilinear constitutive laws, respectively with elastic-perfectly plastic and elastic-plastic with hardening NL behaviour. A similar application was implemented for MDoF systems (Vamvatsikos and Cornell, 2005), accounting for the fundamental vibration mode of it, starting from the elastic to the inelastic fields. The aims of the tool were the same of the previous cited one. What above shown is one of the computer tools developed from researchers in the time.

IDA curves
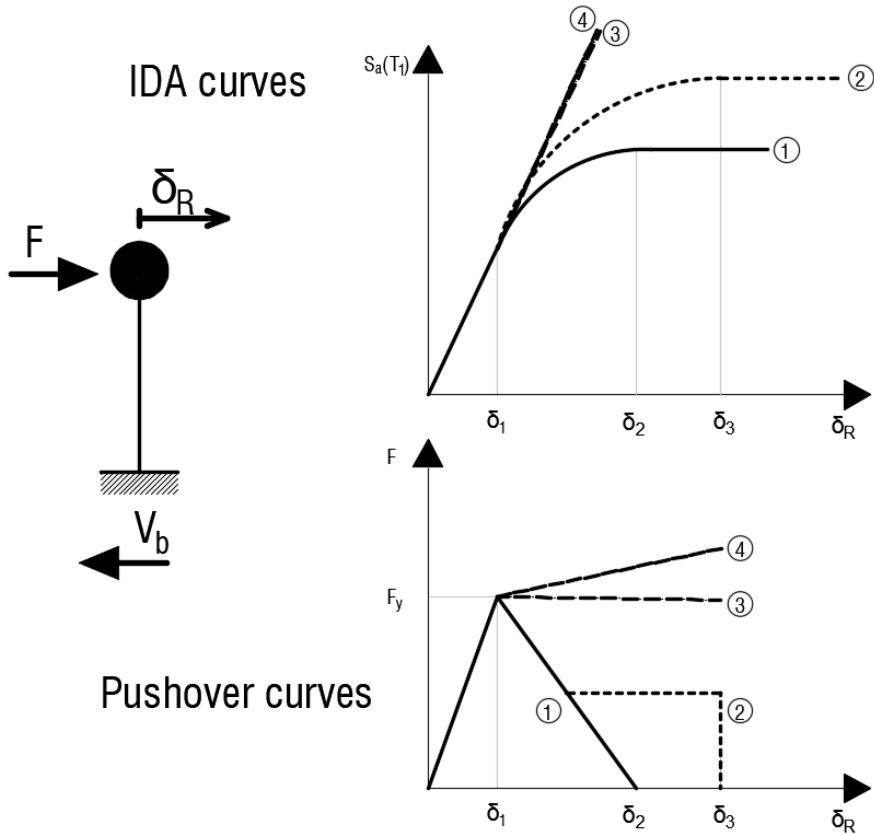
Pushover curves

Fig. 5.8 – Equivalence between pushover and median IDA curves, by using SPO2IDA tool

With the necessity to investigate the fragility of existing buildings and based on the SPO2IDA tool, a new software was proposed the SPO2FRAG software (Iervolino et al., 2016 Baltzoupolos et al., 2017). This latter is a user-friendly tool, able to provide the fragility curves of a new or existing building, for the LSs investigated, starting from the result of a pushover analyses. To this purpose, the software, which is free available online, is characterized by several phases. The input of the procedure is the pushover curve of a building that one can perform as wants. This curve is firstly linearized through a definition of the quadrilinear backbone on the equivalent SDoF oscillator, as proposed in (De Luca et al., 2013). IDA curves are then performed by using the semi-empirical equations proposed in SPO2IDA tool (Vamvatsikos and Cornell, 2006). In particular,

using the 44 records proposed by FEMA P-695 code, the IDA are performed on the equivalent SDoF system and the results are provided in terms of 16, 50 and 84% fractiles curves. Fixing the value of the EDP, for each LS, the Gaussian distribution is computed on the IDA curves, with the definition of the means and the standard deviation (Vamvatsikos and Cornell, 2004). Finally, the SDoF system is transformed in an equivalent MDof one, through the conversion of the numerical curve in the IM-EDP plane and the addition of the contributions given by the MDoF effects: NL behaviour and higher-modes contribute. Finally, the software provides the fragility curves for each LS and it gives, as output, the value of median and standard deviation for each curve. This software will be used later, in the next Sections. Despite the proposal of an equivalent structure or a methodology for making a simplified model could sound interesting, as in all engineering applications, the use of simplified hypothesis corresponds to a certain loss of fidelity, more or less negligible. In particular, despite the inexpensiveness of SDoF and simplified MDoF models, the results of NLD and NLS analysis lose some details that full models provide, which can be called as MDoF effects. For example, some models described are not able to predict the torsional effects, the type of global deformation with loss of the coupling of vibration modes, the distribution of strength and stiffness after that the model come into the inelastic field and local failures related to some structural elements.

5.3 Proposal of a simplified analysis method for the vulnerability analysis via few stripe analyses (FSA)

The use of simplified methods (analysis and modelling) for the vulnerability assessment procedure of existing RC buildings cannot be only a prerogative of the researchers. In fact, simplified methods should be useful for simplifying the work of practitioners, which usually have a different (and practical) background for this kind of application. As just mentioned in the Chapter 2, the application of the PBEE concepts to real cases of existing buildings requires some skills by practitioners, which should be a good knowledge about the seismic vulnerability problem and its probabilistic nature, besides to have time for developing all phases of the PBEE. The method proposed in

this Section can be an useful instrument for practitioners who wish to perform vulnerability analyses of existing buildings. Generally, the main necessity of practitioners is to save time, using friendly software equipped with simple graphical user interface. The modelling job is often limited to development of a single FE numerical model, good enough both for linear and NL analyses. For this latter typology, the choice is most frequently oriented on NLS analysis, considering the computational efforts required by NLD analyses, without any guarantee to achieve a sound and reliable result. In fact, a main problem of commercial software is the poor convergence capacity of the analysis in the inelastic field, as it can be observed by looking at a simple pushover curve, in which one fixes a value of δ_R and the result is usually not attained by the same curve, due to convergence problems of the software used. Moreover, a correct vulnerability analysis should take into account the nature of the seismic demand, which can be simulated through accelerograms properly selected and, in the case, properly scaled. Furthermore, it is important to quantify the performance of the existing buildings for several LSs, with the identification of damage states through the definition of the fragility curves and the vulnerability through the definition of the losses curves, as suggested in PBEE approach. Within the framework of the probabilistic PBEE approach, we are going to propose a practical application of the MSA method (Jalayer, 2003 and Jalayer and Cornell, 2009). The novelty of the proposal, which want be a practical application of the well-known MSA, consists in the performance of few stripe analyses (FSA) on the NL numerical model, with a low number of records. The result obtained from the methodology application, should be able to provide a complete information about the damage states (at the ultimate LSs) of existing RC buildings in elastic and inelastic field, in order to derive practical fragility curves in a "fast manner", particularly suitable for the use by practitioners. It is worth mentioning that the FSA cannot be classified as narrow-range or wide-range method, but it rends to cover a certain band of the structural response, according to the necessity of practitioner. Concerning to our starting point, in (Jalayer, 2003, Jalayer and Cornell, 2009), the stripe analysis method allow of evaluating the seismic behaviour of building, through the performance of NLD analyses, by using a set of ground motions, selected for a same IM level (in that case, the S_a). When

the target S_a varies, the accelerograms used can be changed or scaled, in order to have other levels of stripes. As suggested by the name of the procedure, the output of analysis is given by a number of points, equal to the number of records used, located on the same stripe for one IM level. Performing the analyses for a lot of IMs of increasing levels (MSA), the stripes can provide collapsed and non-collapsed points. The first ones occur when the value of EDP investigated is "high" (beyond the global instability limit) or grows up to a big amount with a little increment of IM level. A "full" MSA provides the trend of the structural response under an increasing seismic action. This trend can be quantified through the regression line of the resultant points, by the computation of the power law approximation, as in eq. 2.39. For each stripe, it is possible to compute the values of $\eta_{DM|Sa}$ and $\beta_{DM|Sa}$, where this latter is computable by using eq. 4.19. FSA method bases its application of what above reported, trying to obtain a similar result of MSA, but with lower expense of time and computational efforts. The first phase of FSA consists in the choice of the seismic input, in a friendly way for practitioners. As many times mentioned, there are several tricky issues and open questions, concerning to the choice, the number and the scaling of accelerograms to involve in NLD analyses. With regard to the ground motions selection phase, it can be very complicated for engineers. Generally, the set of accelerograms can be chosen based on the matching with the site elastic spectrum at LSLS, 5% of damping for RC structures, provided by technical codes. EC8 suggests that all records should be matched with the code spectrum, firstly in terms of PGA*S and secondly in certain parts of the elastic spectrum (with regard to the building property), fixing tolerance limits, as indicated in the Chapter 4. The possibility to perform the records selection through the disaggregation of the site spectrum in one or more earthquake scenarios, simulated with magnitude and distance bins, is far from the practice-oriented applications. Hence, the selection method used in FSA is the friendly method indicated in the Chapter 4. In particular, the records are randomly selected, according to the characterization of the building site in terms of PGA. To this scope, one can search the records on online database, according to the site seismic hazard model. A representative example of hazard model is provided by SHARE project (EFHER association, Giardini et al., 2013), which collects hazard models of Europe,

considering the PGA with 10% in 50 years exceedance probability. Therefore, according to the hazard level of the building site to investigate (low, moderate or high), in terms of PGA, practitioner chooses a random set of accelerograms, knowing that those records must be scaled. Regarding to the number of accelerograms for NLD analysis, it is not immediate and is quite variable among the research works. In practical applications, anyway, performing a large number of NLTH for a single stripe analysis is not feasible. The number of accelerograms to select for a practical application as FSA, should be close to the one proposed by technical codes, which usually provide a good compromise between practitioners' necessities and correctness of the result. EC8 proposes to select a minimum of 3 ground motion records and to evaluate the maximum response effects. If 7 or more accelerograms are employed, the code allows of considering the mean of the structural response instead. We are assuming in the proposed method that it is reasonable to use a number of accelerograms not too different from the one suggested by EC8: the number of real records adopted is equal to 11, considering both horizontal components applied simultaneously for each analysis. In view of a practical application of stripe analysis, it is preferable to select once for all the set of records and scale them, rather than changing the set of data for each different IM levels. Concerning to the scaling of accelerograms, necessary for obtaining more stripes, first of all it is necessary to fix the kind of IM and first desired IM level, commonly for all accelerograms of the set. In fact, whereas the accelerogram are selected based on the PGA level, they are characterized by different IM levels (considering that our IM is not the PGA). With regard of the kind of IM, as suggested by scientific literature, the most common IM used is the S_a. In fact, as shown in (Iervolino et al., 2008), the S_a is an IM sufficient and efficient. In addition, it is also the most used approach suggested in technical codes. Now, the question is: what is the best S_a to consider for scaling the accelerograms? The use of $S_a(T_1)$ is not always the best choice, also considering the request of technical codes, as EC8, which wants the matching of the code spectrum with the one computed by each records, referring to a T range of interest for the building (according to EC8, considering a period ranges from $0.2\ T_1$ and $2\ T_1$). In Chapter 4, based on the research study reported in (Kazantzi and Vamvatsikos, 2015), one of the best

method for obtaining a sufficient and efficient IM is the use of S_{agm}, defined in eq. 4.18, using significant values of T. The method proposed wants investigate the behaviour of existing RC buildings, with application oriented to 3D numerical models, despite can be applied on a 2D FE model. Then, a rational method for computing S_{agm} is to consider the S_a related to the first 3 fundamental vibration modes (as well as the two main translational and the main rotational Ts), as suggested in (Bayer and Bommer, 2007). It is clear that, if the other vibration modes are significant, they can be considered in the computation of S_{agm}. Generally, this method is reliable for low-rise buildings. Hence, the eq. 4.18 can be rewritten as:

$$S_{agm}(T_{1-3}) = \left[\prod_{i=1}^{3} S_a(T_i) \right]^{1/3}$$ (5.1)

Once that the IM to considered has been defined, it is possible to perform the FSA. The application of the method is composed by 3 stripes. This number of stripes is surely low if compared to the indications provided in the scientific literature and MSA method, but can be considered a good compromise between the practitioners' needs (low time and low computational efforts) and a satisfactory identification of the structural response. By adopting a proper approach for the appraisal of the 3 IM levels, it is nevertheless possible to have a "cheap but complete" information about the building behaviour in the elastic and inelastic fields. Then, the missing datum is the first desired IM level. With this regard, the 1st stripe is evaluated to the IM value equal to $S_{agm-code}(T_{1-3})$, which is the geometric mean of the spectral accelerations related to the first three fundamental periods, computed on the code spectrum defined at LSLS, 5% damping. Therefore, one should define the code spectrum of the building site and, knowing the modal parameters of the building to investigate, can define the $S_{agm-code}(T_{1-3})$ as:

$$S_{agm-code}(T_{1-3}) = \left[\prod_{i=1}^{3} S_{a-code}(T_i) \right]^{1/3}$$ (5.2)

The computation of $S_{agm-code}(T_{1-3})$ allow of establishing the desired IM, which is used for scaling all accelerograms, in order to perform the 1st stripe. In particular, it is necessary to define the $S_{agm-records}(T_{1-3})$, which is the geometric mean of the spectral

accelerations related to the first three fundamental periods, computed for both horizontal components of each accelerogram. The value of $S_{agm\text{-}records}(T_{1\text{-}3})$, for each record, can be computed as:

$$S_{agm-records}(T_{1-3}) = \left[\prod_{i\_X=1}^{3} \prod_{i\_Y=1}^{3} S_a(T_{i\_X}) * S_a(T_{i\_Y})\right]^{1/6} \quad (5.3)$$

where X and Y are the directions of application of the two record components, coincident with the two translational directions of the Ts considered. The selected records are then scaled, in order to have the matching of the records with the code spectrum. In particular, the ratio between eqs. 5.2 and 5.3 provides the scale factor (SF) to be applied of each accelerogram component:

$$SF = \frac{S_{agm-code}(T_{1-3})}{S_{agm-records}(T_{1-3})} \quad (5.4)$$

Adopting this method, both horizontal components of accelerograms are scaled for an IM, dependent from a range of Ts defined on the base of the case study. Computing a number of SFs equal to the number of records selected and performing the scaling of the accelerogram components amplitude, the result is a set of accelerograms (each composed by two components) with the same IM level, useful for carrying out the 1st level of stripe. For performing the 2nd level of stripe, the previous IM level must be slightly increased (in accordance with that shown in Jalayer, 2003) and this is done by multiplying each SF for 1.3. The choice of the amplification factor arises from the objective of investigating the structural response in a band of IM levels close to the code target, in terms of S_a. Based on the results obtained, the variation of the structural response can be appraised by observing the number of "collapsed" and "non-collapsed" points for each level of stripe. There are several possibilities, which are propaedeutic for the choice of the next IM level (3rd level of stripe):

- All points of the first 2 levels of stripes are "non-collapsed": the structural response is probably in the elastic field. The 3rd IM level should be much higher than the previous ones;

- Few points of the first 2 levels of stripes are "collapsed": the structural response is in the initial part of inelastic field (such a situation is probably plausible when in the stripe with the high IM level, the number of collapsed points is higher than the ones in the lower stripe). The 3rd IM level should be higher than the previous ones;
- a lot of points of the first 2 levels of stripes are "collapsed": the structural response is in the inelastic field. The 3rd IM level should be lower than the previous ones.

The threshold between "few points" and "a lot of points" collapsed can be quantifiable as the 20% of the total number of points. In the FSA method, the assumption about the amplification factor that multiplies the SF in order to define the 3rd IM level is a subjective point. Generally, it depends on the sensibility of the analyst, who must make a decision, based on the results of the analyses in terms of EDP values and their dispersion. Furthermore, the 3rd IM level depends from the capacity of the commercial software to converge and to provide good results. The main advantage of FSA is that the method provides a definite identification of the elastic and inelastic structural trend, in terms of EDP-IM relation. In fact, the power law shown in eq. 2.39 allows of defining the regression of the stripes and, subsequently, the damage states of the buildings, through the definition of fragility curves for the LSs investigated. The methodology of FSA is summarized in the framework in figure 5.9, wherein is present the methodology for performing the 3 stripes, in order to define the structural response.

5.3.1 Case studies: a sample of 15 real existing RC school buildings in the Province of Foggia, Southern Italy

In order to apply the FSA method and to determine the structural response and the fragility of existing RC buildings, a sample of case studies have been considered. In particular, this latter is constituted by 15 existing RC school buildings in the Province of Foggia (figure 5.10), located as in figure 5.11. These buildings were investigated within an Agreement between "AdB Puglia" and Polytechnic University of Bari, in which the final scope was the development of "Guidelines for the vulnerability assessment of

existing buildings", a document to support the practitioners for carrying out the vulnerability assessment of existing school buildings (Mezzina et al., 2011).
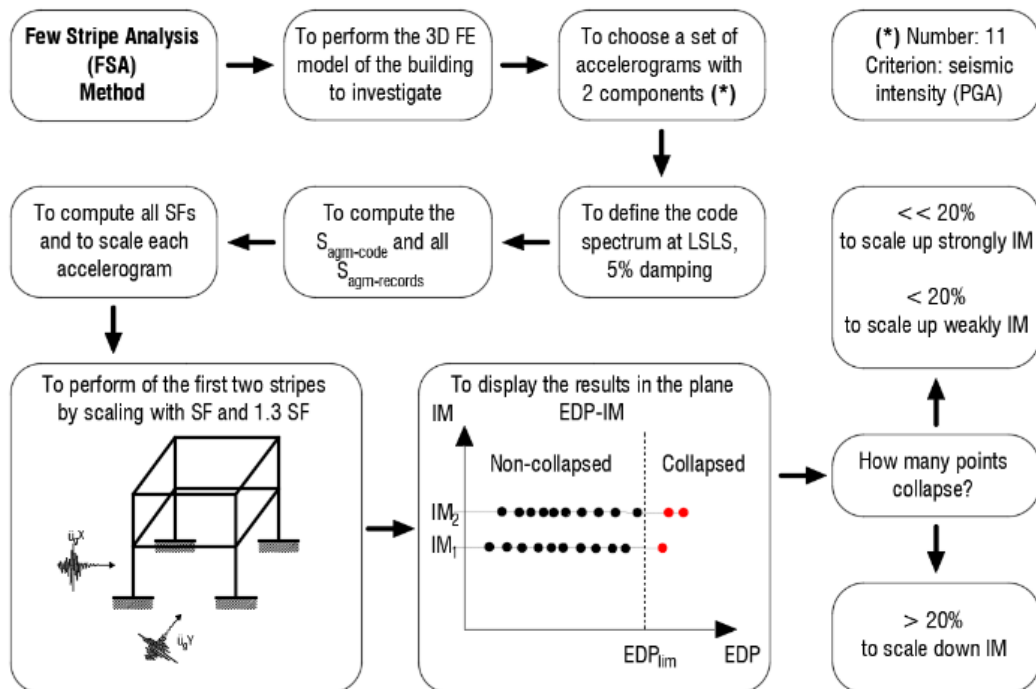
Fig. 5.9 – Framework for performing FSA method

The project was characterized by a continuous information exchange between an expert academic team and the practitioners appointed for the assessment procedures after a public competition. In some cases, there are more independent buildings belonging to a larger complex, which were investigated independently, even if some geometric and mechanical features were similar. For each building, practitioners performed all the phases prescribed by EC8, starting with the retrieval of existing documentation, in-situ surveys and in-situ tests aimed to achieve a "complete" KL (CF equal to 1). Based on the data collected, the practitioners performed the vulnerability assessment for each building through the definition of a NL numerical model (using commercial software) and the execution of NLS analyses (according to EC8). Finally, they performed the final assessment of the structures, with the definition of the CDR value and

they proposed the design of the retrofit solution (in some cases the practicability of the schools were denied).

Fig. 5.10 – Province of Foggia, Southern Italy

It is worth mentioning that the buildings here investigated have already been object of vulnerability analysis from the practitioners involved in the abovementioned project. Hence, the aim of our work is not to assess the results obtained by practitioners, but to use the data collected from them for our research work. In this work, the buildings were numbered as shown in figure 5.11 with a casual tag assignment (B1 – B15) and indication of Foggia province and cities boundaries, wherein are distributed the schools. It is worth mentioning some of the buildings here investigated have been used for other works of this thesis. In particular, building B14 has been used in the section 3.4.2, buildings B10 and B11 have been used in the section 3.6, buildings B4 have been used in the section 4.2.4.

Fig. 5.11 – Spatial distribution of the sample of buildings investigated

Furthermore, for the studies of this Chapter, all structures have been modelled another time, according to the methodology explained later. Several common features characterize the buildings of the sample, as below listed:

- All buildings were built between the 60s' and 80's, and they were designed only for gravity loads. In fact, the old technical laws did not consider seismic actions and consequently, all buildings lack of anti-seismic construction details;

- All buildings have different in-plan shapes, considering that a scholastic complex has usually a large in-plan extension for accommodating more spacious places adapt to the uses of the building. In this case, it is not possible to define that all buildings of the sample investigated are irregular in-plan;

- All buildings are low-rise structures of 2 or 3 storeys above ground. This is a common feature of this building typology in the South Italy, often due to the topography of the sites where they were built. In some cases, the buildings

present on the last floor a pitched roof. The sample of buildings investigated is considered in-elevation regular;

All buildings are RC frame structures with masonry infills. The floor system is usually constituted by a RC ribbed slab of about 25 cm comprising one-way beams and lightweight infills of hollow clay bricks, as typical in Southern Italy. Columns are reinforced by smooth steel rebars. The shear reinforcement is usually composed by smooth stirrups with diameter of 6 mm, with spacing from 10 to 20 cm (it depends from the type of structural element). Occasionally, there are 45° diagonals bars. Foundations are constituted by plinths, which are connected by beams in some cases. General information about the first building of the sample investigated are provided in the figure 5.12. It is worth mentioning that for this Section, where indicated, the major part of the figures are reported in Annex B. Here, only the figures for building B1 are reported. In the Annex B, one can find similar figures for the others buildings. Concerning to figure 5.12 (and figures from B.1 to B.14), it shows the information about one building, among which the schematic plan with total dimensions and the FE model. The picture provides the city of the building with the geographic localization in terms of coordinates (latitude and longitude), the N_L, the U_c, the soil category (Cat) and the topography coefficient (Top), according to the classification in EC8. All these information are necessary for defining the code spectra, for all LSs. In addition, all knowledge path information, collected in the above cited project, are reported, among which the year of construction, the number of storeys, the estimated value of the vertical loads provided by a load analysis (where G are dead loads and Q are live loads), and the drawings of the beam and column sections more representative of the structures. Finally, there are the data provided by investigations about the mechanical parameters of in situ-materials: f'_{cm}, f'_{ym} and E_c. The E_s is assumed equal to 205000 MPa for all numerical models. Concerning to the numerical model depicted in the above figures, using the data collected in the knowledge path performed on each building, the NL numerical models have been implemented in the FE software SAP2000. Beams and columns have been modelled as one-dimensional frame element, with fixed restraints at the base of the columns. The

floor systems have been modelled as rigid, through internal constraints. For each building, geometrical and mechanical parameters and vertical loads have been assumed according to in-situ surveys. Staircases have been implemented in the numerical models only in terms of mass. Where pitched roofs are present, they have been modelled through sloping beams and columns, but neglecting the NL behaviour of this part. The nonlinearity of the frames have been modelled according to a lumped plasticity approach, by introducing plastic hinges at the end sections of structural elements, whose remaining part was elastic. The inelastic mechanisms of plastic hinges have been assumed to be ductile, considering the combination of axial and bending stresses for the columns and simple bending for the beams. In the case of columns, the axial stresses have been derived from the application of the seismic combination of vertical loads, according to formulation proposed by EC8. In the computation of hinges for columns, the variation of axial stress has been not considered. The columns' hinges used take into account the bidirectional behaviour of the sections, useful when the sides of the sections have different dimensions. The plastic hinges have been defined through the evaluation of the chord rotation demand and the corresponding capacity, for each section investigated. In particular, a quadrilinear Moment – Rotation constitutive law were used, representing the backbone with 4 damage levels: first cracking of concrete, yielding of longitudinal bars with hardening behaviour, softening simulating the section's strength degradation and the residual moment, fixed at 20% of the yielding moment. Yielding (θ_y) and ultimate rotation (θ_u) were computed according to the formula proposed in EC8 (part 3.3), as well as indicated in eqs. 3.1 and 3.2. In order to define the chord rotation values at the ultimate LSs, the acceptance criterion, for each section, were fixed equal to ¾ θ_u for the LSLS and θ_u for the NCLS. The cyclic behaviour is governed by the Takeda rule. The shear response has been neglected in the modelling, even if the low amount of transversal reinforcement in the structural elements. This is for avoiding brittle mechanisms in the first steps of the subsequent analyses. It is worth mentioning that the shear capacity should be considered in a structural model and, for this reason, it has been considered in post-processing by using the Biskinis' formulation (eq. 2.3).

B1 - Rocchetta Sant'Antonio
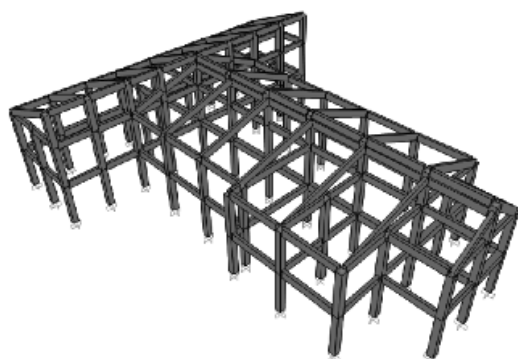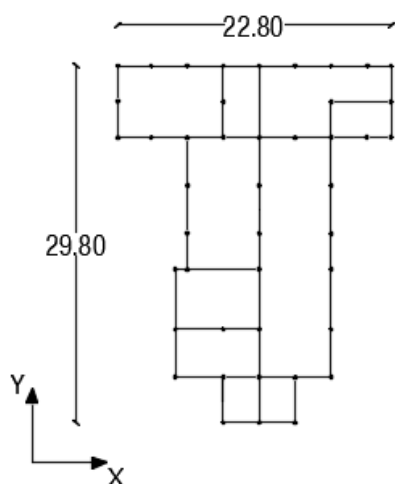
22.80

29,80

Y

X

Structural elements 1° Storey

Columns:
40x40 — $4\emptyset14$

Beams:
40x50 — $4\emptyset14+4\emptyset12$

50x20 — $10\emptyset12$

Structural elements 2° Storey

Columns:
40x40 — $4\emptyset14$

Beams:
40x50 — $4\emptyset14+4\emptyset12$

50x20 — $10\emptyset12$

Information Code Spectra

Building	Coordinates	Soil type
N_L: 50	Lat: 41.104	Cat: B
U_C: 1.5	Lon: 15.462	Top: T2

Knowledge Path Information

Building date: 1960

N. storeys: 2
$H_1 = 3.10\ m$
$H_2 = 3.10\ m$

Loads
$G_1 = 2.5\ kN/m^2$
$G_2 = 1.5\ kN/m^2$
$Q = 3.0\ kN/m^2$

In-situ material
$f_{cm} = 15.00\ MPa$
$f_{ym} = 403.00\ MPa$
$E_c = 25183\ MPa$

Fig. 5.12 – B1 building information

All analyses in this Chapter will be shown without considering the shear mechanisms. In the Annex E and F, there are all results, similar to the ones presented here, accounting for the shear mechanisms. These latter identify the real response of the buildings investigated. On the other hand, we are going to propose some procedures, which are independent from the initial hypotheses about numerical models. Finally, it is worth mentioning that the influence of infill panels have been not considered in the numerical models.

5.3.2 Application of FSA and comparison of the damage states with SPO2FRAG software

The case studies presented in the previous Section have been investigated in order to test the FSA method and to evaluate the seismic response and fragility of the buildings. With this regard, the buildings have been modelled in a FE software, which have a philosophy very close to the commercial software and that needs of a lot of time, computational efforts and hard disk space for the post-processing phase, for performing and solving NLD analyses. Before performing the FSA on the sample of building, other analyses have been performed. First of all, in order to evaluate the dynamic behaviour of the buildings analysed, the first step of the work consisted in the eigenvalue analysis. In particular, the first three periods (T_1, T_2, T_3) and the translational and rotational participating masses ($M_X[\%]$, $M_Y[\%]$, $M_\theta[\%]$) have been evaluated for each building, as shown in table 5.1. The Ts are comprised in a wide range of value: 0.3 s - 0.85 s. This result is consistent with the particular nature of the class of buildings investigated (low-rise; variable in-plan shape and dimensions). In addition, in many cases, the modal shapes are coupled, with low values of the maximum M[%] per direction. Despite this, NLS analyses in the two main directions (X and Y, following the reference systems shown from figures 5.12 and A.1 - A.14) have been performed, by applying only an uniform load pattern and neglecting the eccentricity. The scope of the NLS analyses is twofold: firstly, to use the output of the analyses (pushover curves) as the input data of the SPO2FRAG software; secondly, to appraise the structural response in the inelastic field for defining the EDP values at the relevant LSs, as suggested in (Gunay and Mosalam, 2013).

Tab. 5.1 – First three Ts and M[%]s for the buildings investigated

Building	T_1 (s)	T_2 (s)	T_3 (s)	M_x[%]	M_y[%]	M_θ[%]
B1	0.317	0.310	0.277	79.13	83.42	83.73
B2	0.844	0.828	0.732	46.33	90.88	47.11
B3	0.359	0.320	0.298	90.05	84.05	84.63
B4	0.831	0.539	0.512	86.97	61.58	56.91
B5	0.376	0.301	0.232	76.91	79.18	77.97
B6	0.520	0.412	0.336	99.18	85.53	87.75
B7	0.751	0.590	0.555	53.08	91.5	51.39
B8	0.744	0.591	0.575	89.18	60.83	60.11
B9	0.693	0.668	0.576	99.17	92.44	93.85
B10	0.432	0.396	0.394	58.30	70.65	42.44
B11	0.598	0.445	0.399	90.99	96.52	94.26
B12	0.535	0.461	0.434	92.27	50.26	52.62
B13	0.480	0.409	0.314	69.30	93.47	69.88
B14	0.788	0.776	0.657	84.78	74.54	81.41
B15	0.588	0.572	0.479	83.96	62.89	61.32

In figure 5.13, the results of NLS analyses in X and Y direction are reported, in terms of pushover curves in the plane V_b - δ_R. The values of EDP have been evaluated from the results of NLS analyses, in terms of maximum θ_i for each building and pushing direction, as shown in table 5.2. The criteria established for estimating the EDP values are based on the following definitions of the ultimate LSs violation:

- Violation of LSLS: a certain percentage, 50%, of the structural elements as beams and columns, reach a value of chord rotation equal to ¾ θ_u. In the cases of soft-storey at the first level, the LSLS is violated when the 50% of the columns of the level considered reaches the above mentioned chord rotation;

- Violation of NCLS: the first column reaches a value of chord rotation equal to θ_u;

Considering that the technical laws do not provide clear references about this topic, the authors have established these criteria based on their experience and their sensitivity in the analysis. The values of EDPs in table 5.2 have been then used for computing the fragility curves at the ultimate LSs for each building, both after the application of the FSA method and simultaneously to the application of SPO2FRAG one, as will be highlighted later. Concerning to the shear mechanisms of buildings, after the evaluation of the shear capacity of the structural elements (considered like the achievement of the shear values computed), the criteria established for estimating the EDP values are based on the following definitions of the ultimate LSs violation:

- Violation of LSLS: a certain percentage, 20%, of the structural elements as beams and columns, reach the shear capacity value.
- Violation of NCLS: a certain percentage, 50%, of the structural elements as beams and columns, reach the shear capacity value.

Even in this case, there are not specific criteria to follow, but one should consider that the collapse due to the shear does not allow of separating the serviceability and ultimate LSs, as soon as of separating the LSLS and NCLS. The criteria imposed represent a way for separating the 2 ultimate LSs considered. Analogously to the figure 5.13, in figure E.1 (see Annex E) the results of NLS analyses in X and Y direction are reported, in terms of pushover curves in the plane V_b - δ_R. In this case, there is a specific indication about the achievement of the ultimate LSs. In particular, blue dots represent the achievement of LSLS and red dots represent the achievement of NCLS. In addition, analogously to the table 5.2, table E.1 (see Annex E) shows the values of EDP evaluated from the results of NLS analyses, in terms of maximum θ_i for each building and pushing direction, accounting for the shear mechanisms. It is clear that these values have been used for conditioning in different way the probability of violating the LSs. Furthermore, one can see that the values are lower, but after to the yielding of the backbones, which means that in the major parts of the cases we have ductile shear.
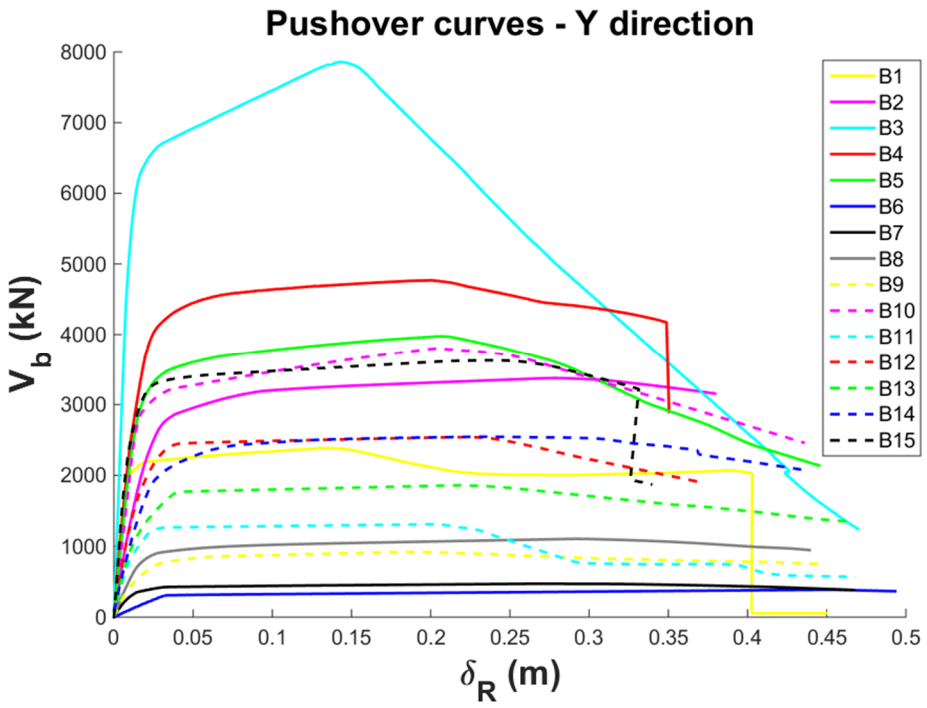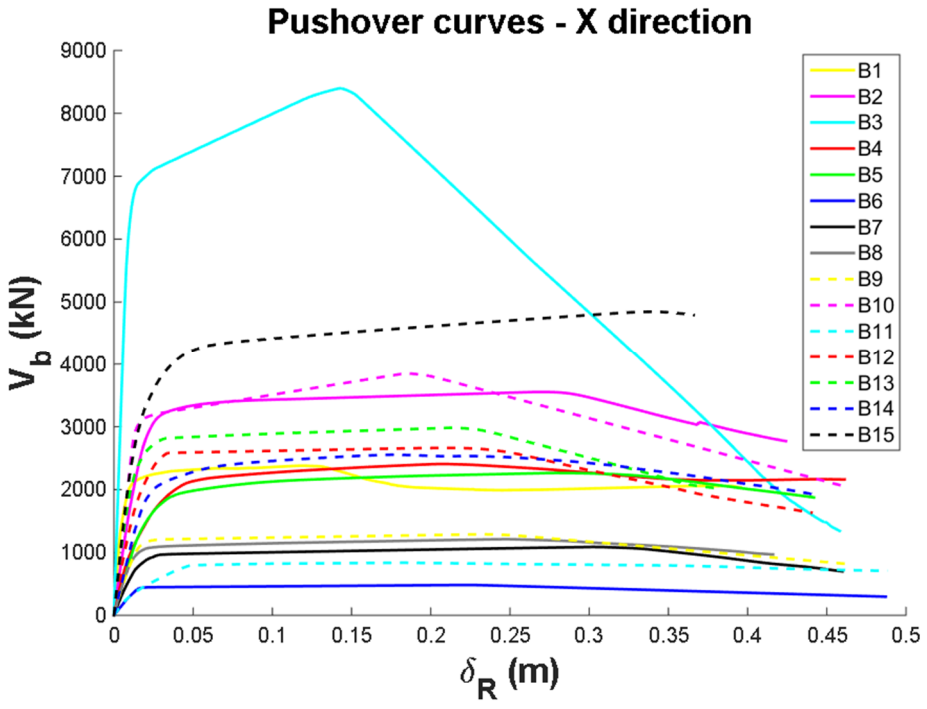
Fig. 5.13 – Pushover curves of all buildings in the two main direction

Tab. 5.2 – Values of EDP, in terms of θ_i estimated from pushover analyses

Building	X direction		Y direction	
	LSLS max θ_i [%]	NCLS max θ_i [%]	LSLS max θ_i [%]	NCLS max θ_i [%]
B1	4.69	6.13	4.71	6.44
B2	3.02	4.23	3.03	4.19
B3	3.39	4.23	3.45	4.43
B4	2.76	3.64	2.35	3.17
B5	2.33	2.90	2.57	3.15
B6	3.87	4.31	4.17	5.00
B7	2.48	3.82	3.55	4.41
B8	2.26	3.93	2.61	4.31
B9	2.52	3.99	2.55	4.42
B10	3.13	3.93	3.22	3.85
B11	3.82	4.75	3.87	4.76
B12	3.50	4.70	3.52	4.51
B13	3.06	4.39	3.59	4.67
B14	2.53	3.36	2.42	3.19
B15	3.45	3.65	2.66	3.56

For applying the FSA method, a set of 11 real accelerograms (each is made up by 2 horizontal components) has been selected from the INNOSEIS project (see the website in the references, 2017), that collects real accelerograms from European seismic events in the last years, classified in high and medium seismicity. Based on the PGA values of the different building sites, the records have been randomly extracted from the set of records available. According to the elastic spectra of buildings at LSLS, 5% damping, the PGAs related to buildings are of medium seismic intensity. The records selected are summarized in table 5.3, where the accelerograms are indicated with tags E1-E11.

Tab. 5.3 – Earthquakes records to medium intensity selected

ID	Earthquake record	Components PEER tag
E1	Chichi aftershock – 20/09/1999	CHY104-N / CHY104-W
E2	Chichi aftershock – 20/09/1999	CHY076-E / CHY076-N
E3	Hector mine – 10/16/1999	0593c090 / 0593c360
E4	Imperial Valley – 15/10/1979	H-CMP015 / H-CMP285
E5	Kocaeli – 17/08/1999	GYN000 / GYN090
E6	Landers – 28/06/1992	BAK050 / BAK140
E7	Lomap – 18/10/1989	SUF090 / SUF180
E8	Manjil – 20/06/1990	ABBAR--L / ABBAR--T
E9	Morgan Hill – 24/04/1984	HD3255 / HD3345
E10	Northridge aftershock – 20/03/1994	TARZA090 / TARZA360
E11	Palm springs – 08/07/1986	NPS210 / NPS300

For all buildings, the values of SFs have been computed: the values of $S_a(T_i)$ have been extracted from the elastic code spectra, 5% damping, at LSLS, for each building, by using the first three Ts reported in table 5.2. Subsequently, from each component of the accelerograms, the values of $S_a(T_i)$ have been computed. Using eqs. 5.2 and 5.3, the values of $S_{agm\text{-}code}(T_{1\text{-}3})$ and $S_{agm\text{-}records}(T_{1\text{-}3})$ have been computed and through eq. 5.4, the values of SFs have been obtained. The SFs values are reported in table 5.4, which are useful for scaling each component of the accelerograms that have been subsequently applied to the numerical models. The first 2 stripes have been performed on 3D numerical models, using the record scaled with SF and 1.3*SF. The results, in terms of maximum θ_i, have been recorded in the 2 main direction for each record ($\theta_{max\_X,Ei}$ and $\theta_{max\_Y,Ei}$). After, for considering a unique response for each building, the value of the EDPs resultant ($\theta_{max\_record,Ei}$) has been computed, by combining the previous terms using the SRSS rule, as provided by the following expression:

$$\theta_{max_{record,Ei}} = \left[\theta_{max\_X,Ei}^{2} + \theta_{max\_Y,Ei}^{2} \right]^{1/2} \qquad (5.5)$$

Tab. 5.4 – Values of SFs for the set of accelerograms selected, via eqs 5.2, 5.3 and 5.4

SF	E1	E2	E3	E4	E5	E6	E7	E8	E9	E10	E11
B1	5,15	10,24	18,42	2,53	2,80	3,24	4,10	0,80	4,82	1,66	0,72
B2	10,40	9,87	12,25	4,36	3,58	4,35	3,92	0,87	3,08	4,67	0,85
B3	3,75	6,63	13,98	1,91	1,95	2,73	3,15	0,54	3,60	1,14	0,51
B4	6,30	9,97	12,69	5,10	3,94	3,79	3,78	2,17	1,69	3,07	1,24
B5	4,38	7,02	13,05	1,94	1,93	2,71	3,22	0,62	3,60	1,03	0,59
B6	5,56	9,04	15,82	2,55	2,83	3,27	4,55	0,74	4,31	1,54	0,83
B7	9,68	11,33	17,72	3,80	4,08	5,09	5,94	1,00	4,87	3,05	1,10
B8	10,01	11,47	17,99	3,91	4,07	5,13	6,05	1,00	4,95	3,25	1,08
B9	10,15	11,61	19,45	3,98	4,42	5,44	5,91	1,05	4,35	3,39	1,07
B10	5,90	10,62	13,90	2,61	2,97	3,40	4,47	0,79	4,86	1,93	0,88
B11	5,91	9,42	12,73	2,49	2,83	3,12	4,26	0,74	4,02	1,81	0,81
B12	6,02	9,76	13,59	2,54	3,14	3,03	4,26	0,82	3,84	1,62	0,92
B13	4,91	8,98	13,50	2,24	2,51	2,77	3,99	0,69	3,84	1,43	0,72
B14	12,87	13,99	21,10	5,21	4,82	6,55	6,49	1,11	4,85	5,69	1,23
B15	5,70	7,75	11,42	2,33	2,64	2,92	4,05	0,69	3,34	1,46	0,76

11 points in the plane IM-EDP represent the result of each stripe analysis. In some cases, some of these points are collapsed. For all the buildings, based on the percentage of collapsed points and on the global trend provided by the first 2 stripes, the values of the 3rd amplification coefficients, of applying to SFs, have been established. Figure 5.14 shows a histogram in which, for each building, there are 3 bars. The first two bars show the number of collapsed and non-collapsed points related to the first two stripes. Instead, the 3rd bar shows such result for the 3rd stripe performed with the multiplying coefficients (and IM levels associated), as reported in table 5.5. As previously explained, the decision about the 3rd IM level (and then of the SF value) depends from the expert opinion of the analyst (in this case the author), which can establish the IM level, on the base of the criteria described in the previous section and in the figure 5.9.
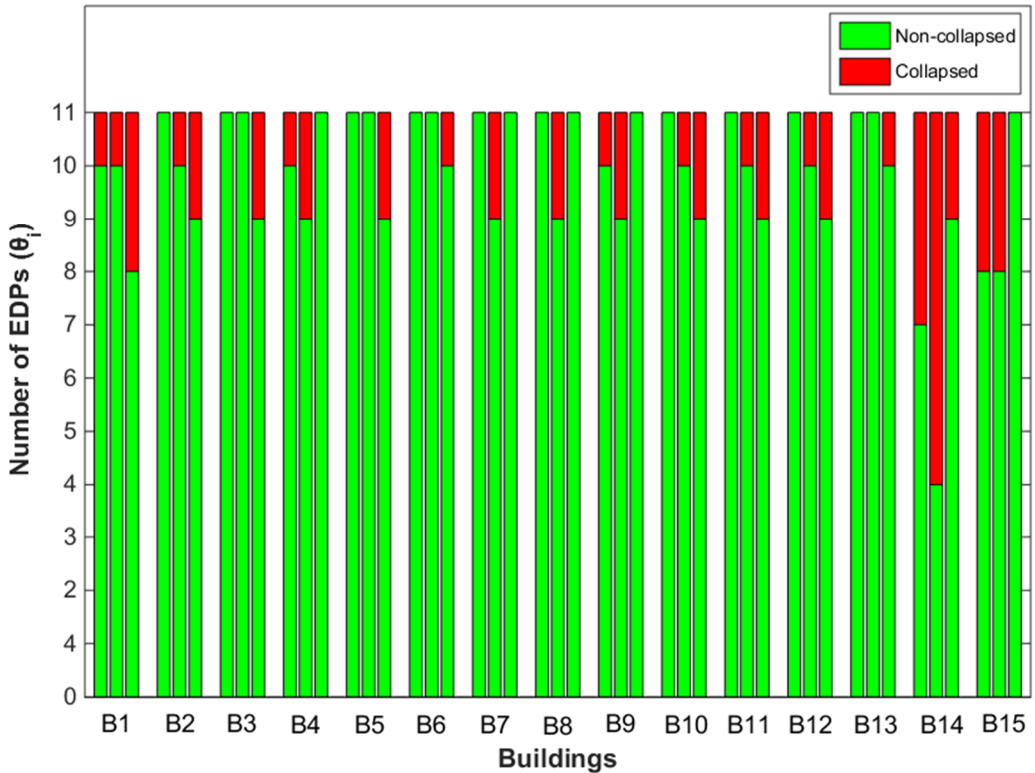
Fig. 5.14 – Number of collapsed and non-collapsed points for each stripe analysis

The 3 stripes analysis provided the trend of the structural behaviour for all buildings, through the computation of the power-law approximation defined in eq. 2.39. In figure 5.15 for B1 (only the figures for building B1 are reported. In the Annex C, it is possible to find similar figures for the others buildings) and figures from C.1 to C.7 for other buildings (see Annex C), the results of FSA for each building are displayed, with the explanation of the power laws in the plane IM-EDP (where EDP is the θ_{max_record}). In these figures, the collapsed points considered in the computation are not shown. It is worth mentioning that for buildings B14 and B15, as also shown in figure A.21, the collapsed points in some stripes are greater than 20% of the total number of points. In these cases, the application of the regression law does not make sense, because the

structural capacity is less than the seismic demand. In other words, to many EDP values correspond a conditioned probability of LS violation equal to 1.

Tab. 5.5 – IM level of the 3rd stripe for each building

Building	3rd SF multiplying coefficient	3rd IM level (per g)
B1	1,77	1.50
B2	1,61	0.70
B3	2,71	1.80
B4	0,81	0.45
B5	2,20	1.50
B6	1,81	1.30
B7	0,92	0.60
B8	0,78	0.50
B9	0,77	0.50
B10	1,68	1.30
B11	1,63	1.00
B12	1,57	1.00
B13	1,51	1.00
B14	0,75	0.50
B15	0,73	0.35

Therefore, for providing the fragility curves in these cases, the maximum likelihood method (Baker, 2015) has been employed: the damage state of the structure has been evaluated as the sum of two distinct functions, one due to collapsed data (logistic regression) and one due to non-collapsed data. Once that the FSA method has been developed and the structural response has been identified, the next step is the performance of fragility curves at the ultimate LSs for each building. In particular, the fragility curves of buildings at ultimate LSs have been computed, through the evaluation of the probability function of violating a certain LS, given a certain IM level.
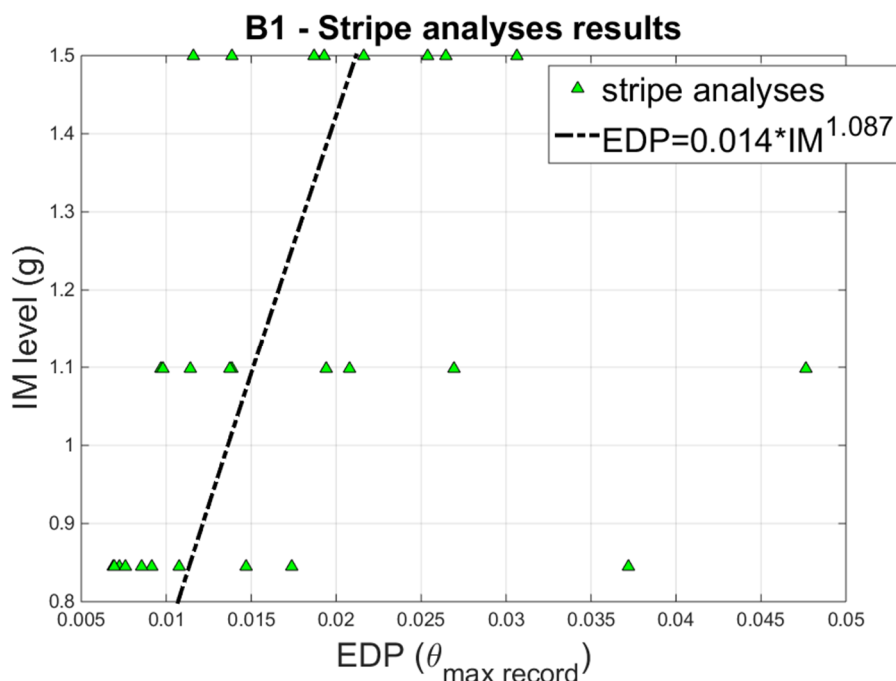
Fig. 5.15 – Stripe analyses' results and related power law for building B1

Based on the EDPs values showed in table 5.2, the criterion adopted for conditioning the damage state, for a given LS, has been the one of considering the minimum value of θ_i between the two directions. Furthermore, other parameter to a-priori fix is the value of epistemic uncertainties, in order to estimate the dispersion of the fragility curves. With this regard, a value of the epistemic uncertainties has been established, taking into account the terms just explained in the eq. 2.30. The choice of this value is based on the suggestions provide by the FEMA P-695 code, in table 7-2. This latter, valid for new buildings, proposes some range of values for all kinds of uncertainties, assigning high values of β when the data quality is poor and vice versa. Considering the nature of the numerical models and the data collected about the buildings knowledge, the value adopted for summarizing the epistemic uncertainties has been assumed equal to 30%. This value has been used in both ultimate LSs considered, even if it is usually suggested just for the NCLS. Therefore, the fragility curves have been computed and they have been directly compared for each building and LS investigated,

one by one, with the results obtained from the SPO2FRAG software. The fragility curves, for the full models, have been computed by using the philosophy of "vertical statistics", such as defined by H. Krawinkler. The concept is explainable as an IM-basis estimation of structural response, given a value of EDP. In other words, a probability level of the fragility curve is computed by the ratio between the number of points, given by the intersection of IDA curves or stripes with the LS threshold in EDP term that are under a fixed IM level and the total number of points considered. By gradually increasing the IM level, it is possible to have all probability levels of fragility curve, for the LS investigated. Still, the fragility curves have been mathematically computed by using a fit of the result obtained by the application of the empirical cumulative distribution function of the points selected as above. Subsequently, in order to find the fragility curves by using SPO2FRAG software, the procedure explained in section 5.2 has been applied to each building. In particular, the input data for the entire sample are the pushover curves depicted in figure 5.13. The LSs thresholds used are the same shown in table 5.2. Moreover, coherently with the precedent procedure, the epistemic uncertainty adopted for the NCLS has been assumed equal to 30%. The first peculiarity is the presence of 2 pushover curves for each building, with subsequent generation of two families of fragility curves for a same case study, which is the consequence of adopting 3D numerical models. For providing a unique solution of the damage state for one building, the procedure has been applied using both pushover curves and, subsequently, the result with the highest MAF of exceeding the LSs investigated, definable as λ_{LS}, has been selected. This choice is surely conservative, but in accordance with the use of practitioners in the CDR definition. Clearly, a highest λ_{LS} corresponds to a lower CDR. The value of λ_{LS} can be evaluated through the definition of the site hazard and the seismic hazard surface, just defined in the Chapter 2. As reported in figure 2.21 (Vamvatsikos and Ascheim, 2016), by vertically cutting the hazard surface, a hazard curve can be obtained, for a selected value of the T. From the hazard curve related to the building analysed, fixing a value of IM and its dispersion, which are function of the LS and the EDP value associated (fragility curve features), it is possible to compute the MAF through the equation 2.28, based on the value of β_{RTR}, definable through eq. 2.29. For each

building of the sample investigated, the hazard surfaces have been derived using the data provided by the SHARE project (see the website in the references). Hazard surfaces have been cut selecting one value of T per building. With this regard, in order to consider one value of T for a 3D structure, the geometric mean of the first three periods (T_{1-3}) have been computed, as provided by the following equation:

$$T_{1-3} = \left[\prod_{i=1}^{3} T_i \right]^{1/3} \tag{5.6}$$

Once that the representative Ts have been selected and, by using the above-mentioned features of the fragility curve, the MAF values have been computed for each direction and for both ultimate LSs, as reported in table 5.6. Figure 5.16 for B1 and figures from C.8 to C.14 for others buildings (see Annex C), show the hazard surfaces of the case studies, plotted in the log-plane MAF-S_a(T). In the same figure, the red curve represents the hazard curve used for the MAF computation, selected for the $S_a(T_{1-3})$. Clearly, the hazard surfaces for buildings B6, B7, B8 and B9, as soon as the ones for B11, B12 and B13 are the same, but the hazard curve is different, cause the assumption of a different value of T. The values of the highest MAFs are displayed in bold in the table 5.6, with the aim of highlighting the directions assumed for identifying the damage state of buildings in SPO2FRAG application. Once that the worst direction of analysis has been identified for each building, fragility curves at ultimate LSs have been computed, by using SPO2FRAG software. Figure 5.16 for B1 and figures from C.15 to C.21 for other buildings (see Annex C) show the one-by-one comparison of the fragility curves obtained from FSA method and SPO2FRAG software. In each graph the fragility curves of one building are reported, for both LSLS (blue curves) and NCLS (red curves). The results show that in some cases, the SPO2FRAG fragility curves are shifted to right, if compared to the ones obtained from FSA application, with a greater dispersion. For explaining these results, one should consider that, firstly, the procedures, even if different, are both simplified. In SPO2FRAG, the information about the seismic demand is more complete than the one used in the FSA

Tab. 5.6 – MAF for ultimate LSs, estimated via SPO2FRAG results

Building	X direction – SPO2FRAG		Y direction – SPO2FRAG	
	LSLS - MAF	NCLS - MAF	LSLS - MAF	NCLS - MAF
B1	0.037	0.023	**0.062**	**0.052**
B2	0.027	0.015	**0.032**	**0.023**
B3	0.0011	0.001	**0.0013**	**0.0011**
B4	**0.005**	**0.0032**	0.0014	0.001
B5	**0.006**	**0.0031**	0.015	0.002
B6	0.0003	0.0002	**0.0004**	**0.0003**
B7	0.0014	0.0008	**0.0025**	**0.0013**
B8	0.0027	0.001	**0.0032**	**0.0014**
B9	0.0019	0.0009	**0.004**	**0.0016**
B10	**0.0011**	**0.0009**	0.0011	0.0009
B11	**0.0037**	**0.0028**	0.0014	0.0012
B12	0.0023	0.0018	**0.0025**	**0.0019**
B13	0.0018	0.0011	**0.0045**	**0.0029**
B14	0.0024	0.0017	**0.0026**	**0.0018**
B15	0.0023	0.0021	**0.0038**	**0.0027**

Moreover, the numerical model investigated in SPO2FRAG was simplified, but it was analysed using IDA analyses, which allow a full investigation of structural response in elastic and inelastic field. Then, the structural response in SPO2FRAG is surely more complete than the one obtained from the other method. In the cases in which fragility curves provided by the two methods are very different, probably this is due to the power law computation. In this case, it is necessary to improve the fragility curves with the addition of another stripe that further investigates the building in the inelastic field. Of course, this would require additional time and computational efforts, which can discourage the use by practitioners, besides the risk to have a lot of collapsed points in a possible new single stripe analysis.
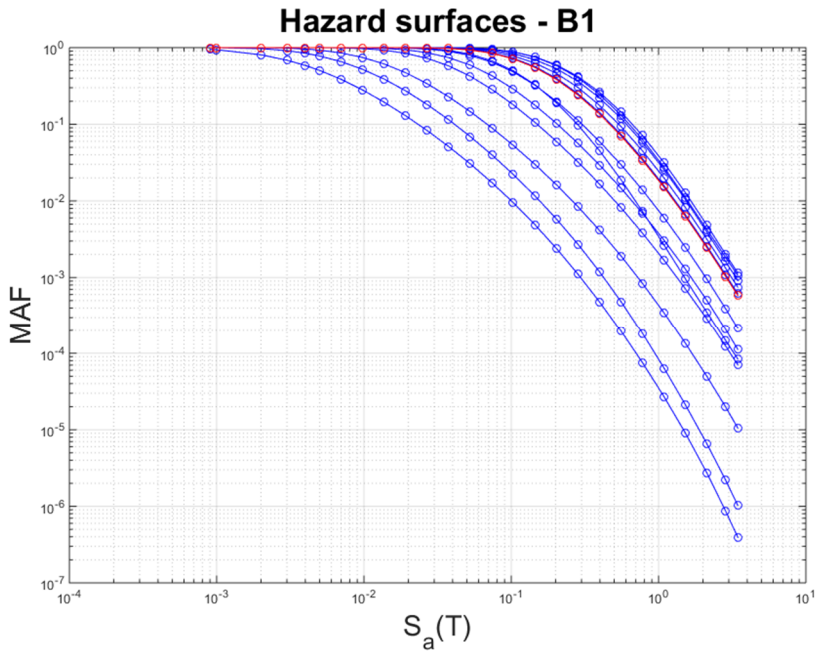
Fig. 5.15 – Hazard surfaces (all curves) and Hazard curve (red curve) for B1
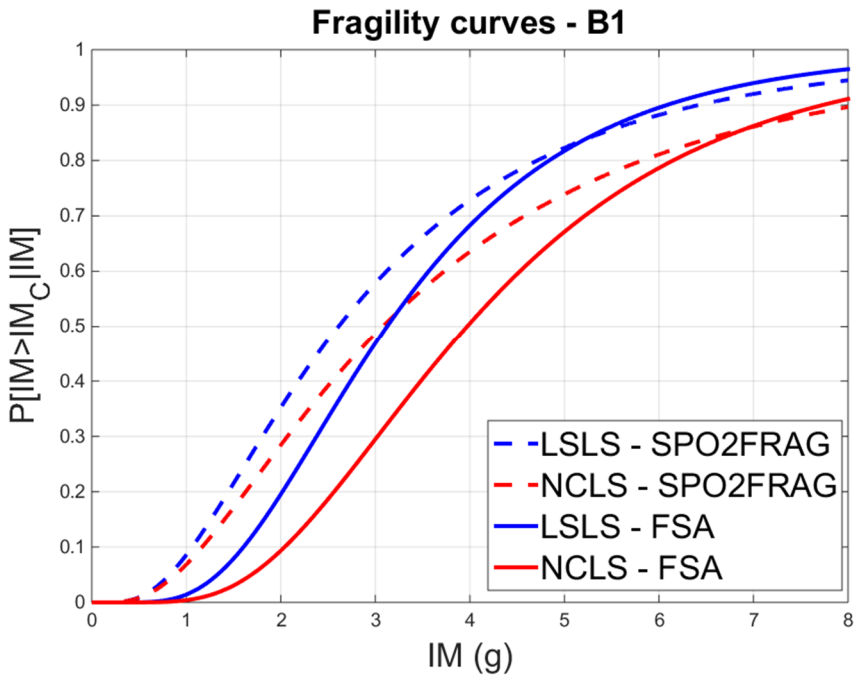
Fig. 5.16 – One-by-one comparison between the fragility curves obtained from the two methodologies adopted, for B1

Generally, we can say that the results obtained are "conservative", which could be a good feature for the design of new buildings, but properly not for the assessment of existing ones. Anyway, this can be a good compromise for the evaluation of damage states by practitioners in a PBEE framework, being sure that results are close enough to the real behaviour. The analogous results, accounting for the shear mechanisms are presented from the figure E.2 to E.9 (see annex E). In these cases, the trend of the comparison is confirmed, but the results are better than the ones without shear mechanisms, due to the achievement of ultimate LSs in the neighbourhood of the yielding.

5.3.3 Regional fragility curve of the sample of buildings

Once that the damage states for the ultimate LSs have been defined, considering the nature of the sample investigated, it is possible to provide an information about the overall behaviour of the entire class of buildings (same geographic area, same typological features: low-rise buildings, existing RC school buildings), by deriving regional fragility curves. To this purpose, one can correlate the results obtained from each building (intra-building), for defining the damage states features of the entire sample (inter-buildings). The scientific literature about the theme is not extensive. In (Baker, 2008), the author provided a correlation among the damage state of the building considered and the damage states of the elements that constitute the same building. In particular, the author provided a simple method for incorporating the influence of the structural components' damage states into the fragility function of the case study. With this regard, using Monte Carlo method for simulating the damage capacity of each element investigated, author correlated the damage capacities of two elements, in order to establishing the total probability of having a certain damage for both components. This kind of correlation can be extended for providing a prediction about the damage state of a class of buildings characterized by common features, like in the case presented. Generally, given a sample of N buildings for which the fragility curves (for a LS investigated) are known, the general damage state of the class of buildings can be defined through by regional fragility function features: median (μ_{reg}) and dispersion (β_{reg}). For predicting the entire probability distribution of the total sample of buildings, the first step is to define the overall median ($S_{aoverall}$) and the overall dispersion ($\beta_{overall}$).

The overall median is the median of all individual medians by fragility curves, while the square of overall dispersion is the sum of the square of the intra-building dispersion (β_{intra}) and inter-building dispersions (β_{inter}). The latter is the expression of the law of total variance. The above concepts are summarized in the following equations:

$$S_{a\,overall} = \left(\frac{N+1}{N}\right)^{th} Sa_i \qquad (5.7)$$

$$\beta_{overall}^2 = \beta_{intra}^2 + \beta_{inter}^2 \qquad (5.8)$$

Subsequently, for computing μ_{reg}, the simple mean of the single fragility median of each building in the sample (S_{ai}^{50}) is simply considered, as shown below:

$$\mu_{reg} = \frac{\sum_{i=1}^{N} Sa_i^{50}}{N} \qquad (5.9)$$

The computation of the regional fragility dispersion is directly linked to the $\beta_{overall}$. In particular, it can be estimated through the SRSS of the β_{intra} and β_{inter}, as here reported:

$$\beta_{reg} = \sqrt{\beta_{intra}^2 + \beta_{inter}^2} \qquad (5.10)$$

β_{intra} is provided by the mean of the all the fragility curves' dispersions ($\beta_{TOT,i}$), computed for each building:

$$\beta_{intra} = \frac{\sum_{i=1}^{N} \beta_{TOT,i}}{N} \qquad (5.11)$$

β_{inter} is computed as the dispersion (standard deviation of the natural logarithm) of all S_{ai}^{50} values:

$$\beta_{inter} = \sqrt{\frac{\sum_{i=1}^{N} [ln(Sa_i^{50} - \mu_{reg})]^2}{N}} \qquad (5.12)$$

For the case studies analysed, μ_{reg} and β_{reg} should be computed, in order to define the regional fragility curves. To this scope, the above parameters should be identified on a sample of buildings with the same T, which means the same $S_a(T)$ and the same IM. This necessity is due to the definition of fragility curves, as defined by eqs. 2.31, 2.32 and 2.33, where the IM is used for conditioning the LS to investigate. Therefore, all fragility curves must have the same IM, in order to carry out the elaborations

presented from the eq. 5.7 to eq. 5.12. In this case, considering that the Ts used for computing the $S_a(T)$ are different among the buildings (they are in a range between 0.3 and 0.85 s), a unique value of the period has been considered, which has been assumed equal to 0.5 s. This implies to scale the abscissa of each fragility curve, previously obtained, of a certain value, given by the ratio between the $S_a(T)$ used for each building and the relative $S_a(T=0.5s)$. Considering that, each fragility curve has been provided by NLD analyses made using several records (44 in the SPO2FRAG case, 11 in the FSA case), the value of $S_a(T=0.5s)$ has been computed as the arithmetic mean of all values of the S_a for a $T=0.5$, extracted record per record. For mathematically expressing the above procedure, the value of $S_a(T=0.5)$ for scaling the abscissa of each fragility curve can be expressed with the following equation:

$$S_a(T = 0.5) = \frac{\sum_{i=1}^{k} S_a(T = 0.5)_{i^{th} record}}{k} \qquad (5.13)$$

where k is the number of records used for each procedure employed and $S_a(T=0.5)_{i^{th} record}$ is the value of the spectral acceleration for the ith record and a $T=0.5s$. Hence, by applying the procedure on the resultant fragility curves obtained with both two methodologies adopted, it is possible to plot the new curves on the same graph. Figures 5.17 and 5.18 show all fragility curves scaled, blue for the LSLS and red for NCLS, while the black curves are the regional fragility curves obtained for each LS, by using the values obtained from eqs. 5.9 and 5.10. These values of μ_{reg} and β_{reg} are summarized in table 5.7.

Tab. 5.7 – Regional fragility curves features, in terms of μ_{reg} and β_{reg}

Regional fragility curves	SPO2FRAG		FSA	
	LSLS	NCLS	LSLS	NCLS
μ_{reg}	2.093	2.498	1.644	2.112
β_{reg}	0.754	0.742	0.845	0.879
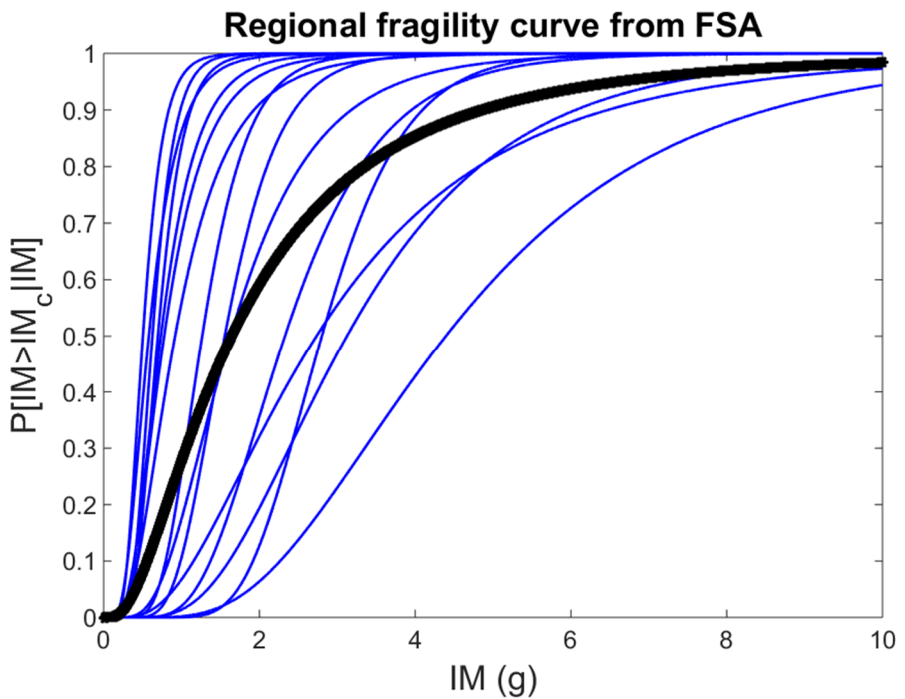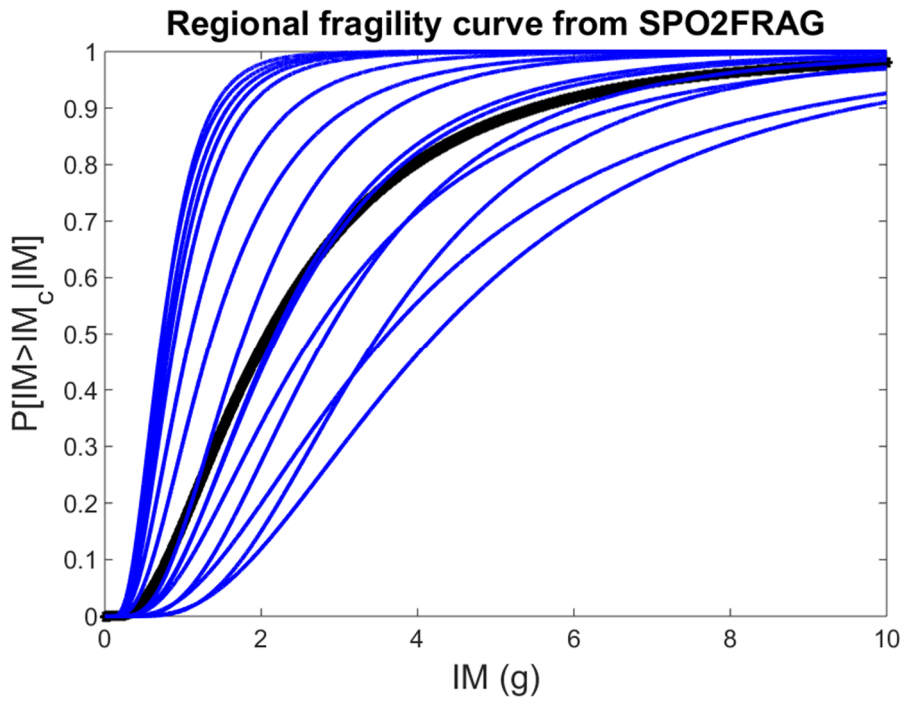
Fig. 5.17 – Regional fragility curves for the LSLS, from FSA and SPO2FRAG
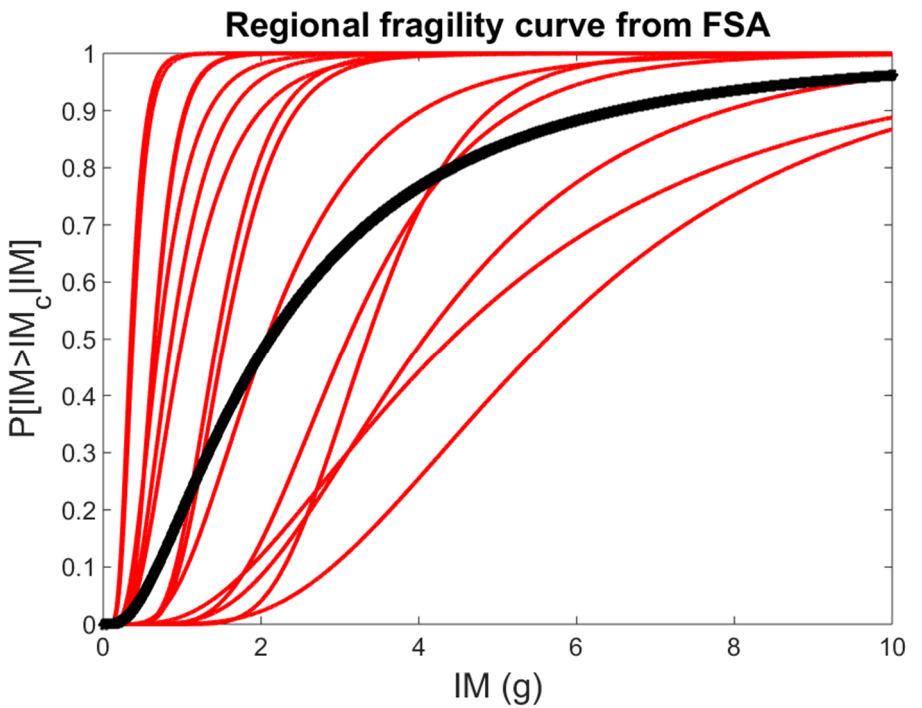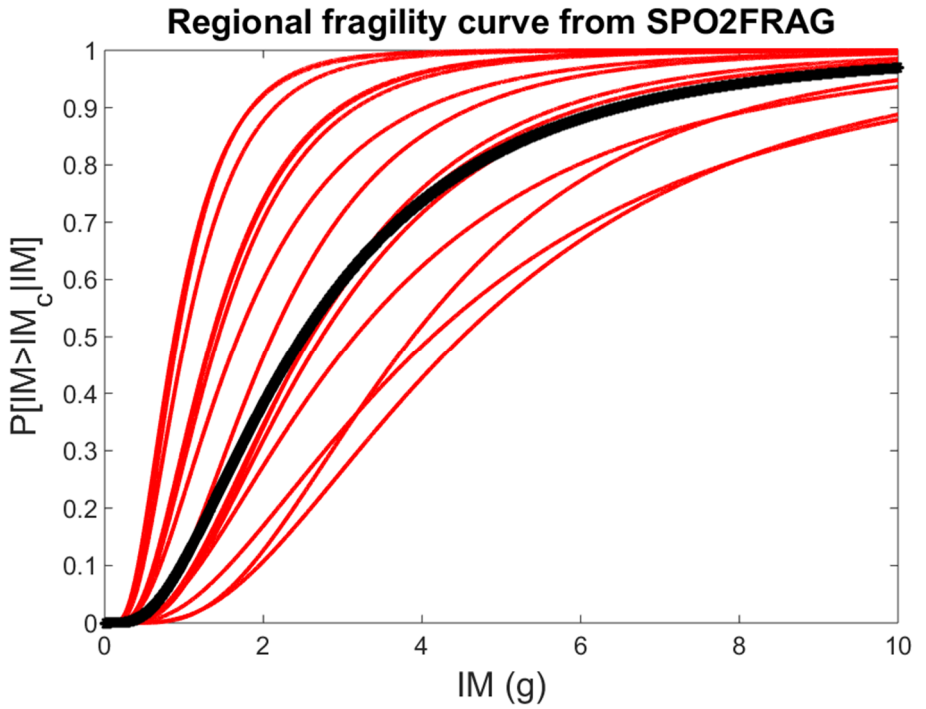
Fig. 5.18 – Regional fragility curves for the NCLS from FSA and SPO2FRAG

The results show a slight difference between the two methods for both LSs investigated. In particular, the regional fragility curves obtained from the FSA method application present a greater dispersion and lower median, evidence maybe due to the different scaling value used in the plotting of fragility curves. The analogous results, accounting for the shear mechanisms are presented from the figure E.10 to E.11 (see annex E). In these cases, the differences between the regional fragility curves are lower, as shown in table E.2.

5.4 Proposal of a parsimonious modelling methodology: 3D reduced-order models

The procedures of simplified modelling of existing RC buildings are usually very attractive among the scientific community, for the skills of reducing computational time and efforts and for the possibility to perform a lot of NLD analyses on the structural modelling. The main aim of simplified models are to provide an adequately characterization of the structural response, equivalent to the one obtained from a full and complex numerical model. In the precedent Sections, a simplified methodology for performing NLD analysis (FSA) has just been presented, which provides an application of the MSA method. The method, as shown from the application on a sample of case studies, is useful for carrying out the assessment of the building fragility in a practical and fast manner, adapt to the use by practitioners, which want to apply the concepts at the base of PBEE approach on FE models made with commercial software. In this Section, the author is going to present a proposal of simplified methodology, which has a similar goal of the previous application. In particular, the method consist in the definition of an analytical path, made of same steps, able to provide simplified models of existing RC buildings that give the same response of full FE models. Even in this case, our scope is to provide a method for matching the real necessity of practitioners with the possibility to assess the existing buildings, by using the PBEE approach. The method here presented is able to provide 3D reduced-order models, which can be feasible for researchers and practitioners. In particular, the present work defines the steps for making a 3D reduce-order numerical model, starting from the linear and NL features of the structural elements of an existing RC building. It is worth mentioning that, as specified in the Section 5.2 for other simplified models, the scope of this methodology is not to

account for all mechanisms of individual components, which is most important for existing buildings without capacity design rules, where local failures may occur. Generally, this latter goal could be captured only indirectly through observing the pushover curve of the full model. Our approach going to investigate the possibility of producing a 3D reduced-order model without knowledge of the capacity curve and other characteristics of the full. In fact, through the development of analytical equations, it is possible to make the 3D reduced-order model of whatever RC building, which here is called "uncalibrated model". On the other hand, a simplified model can be simply calibrated by using the results of full models, in order to obtain the same structural response. In this case, the full models should be available, with them capacity curves, which can be compared with the analogous results obtained from the 3D reduced-order models. Therefore, we are going to provide the possibility of producing the 3D reduced-order models, using the results of the full ones, in order to define a kind of simplified model, here called "calibrated model". Whether this is, a successful endeavour will typically depend on the characteristics of the building under investigation. Still, we can anticipate a certain loss of fidelity especially vis-à-vis the abovementioned effects that a properly calibrated reduced-order model can better account for. The proposed 3D reduced-order model consists in one or more one-bay 3D structures, with same number of storeys of the existing building analysed. In particular, the input data necessary for making the FE model are the ones usually provided from the knowledge path of the building, like the geometrical and mechanical features of the building, the structural elements and the loads applied. As just mentioned, the method proposed, allows of making a simplified model that is independent from the full model (uncalibrated version). In fact, the full model of the structure is not necessary here and it can be unknown. We are going to provide a way for defining the elastic and inelastic 3D reduced-ordered model, through several rules and equations. The aim of the procedure is to ensure, firstly, the equivalence, in terms of stiffness and mass, between the building and the simplified model and secondly, the equivalence of the post-elastic behaviour. The accurateness of the procedure will be assessed subsequently, by using a full model, which is made with the same modelling hypotheses of the 3D reduced-order model. Assuming that all

structural elements are rectangular, such as occur in the existing RC buildings, the geometric features of the ith structural element are the follow:

$$A_i = h_i * b_i \tag{5.14}$$

$$I_i^w = \frac{h_i * b_i^3}{12} \tag{5.15}$$

$$I_i^v = \frac{b_i * h_i^3}{12} \tag{5.16}$$

where A is the section area, b is the section base and h is the section height of the element. I_w and I_v are the inertia moments of the section, considering w and v its local axes. For how to express I_w and I_v, the inertia moment related to the vertical loading is I_v. The reduction is performed per direction. Regarding to the beams, for each storey, the quantities provided by eqs. 5.14, 5.15 and 5.16 are computed for all beams and they are condensed in two new parallel beams, as shown in figure 5.19. In particular, the two beams, for the jth direction, should have the following features:

$$A_{b,j} = \frac{\sum_{i=1}^{N} A_{i,j}}{2} \tag{5.17}$$

$$I_{b,j}^w = \frac{\sum_{i=1}^{N} I_{i,j}^w}{2} \tag{5.18}$$

$$I_{b,j}^v = \frac{\sum_{i=1}^{N} I_{i,j}^v}{2} \tag{5.19}$$

where N represents the number of elements in the jth direction considered, A_b, I_{bw} and I_{bv} are, respectively, the area and the inertia moments of the beams of the 3D reduced-order model. Still, the dimension of the previous beams, which is the dimension of the bay for the direction considered, is provided by a proportion between the inertia moments I_v of the elements and their length ($L_{b,j}$), as shown in the below equation:

$$L_{b,j} = \frac{\sum_{i=1}^{N} (I_{i,j}^v * L_{i,j})}{\sum_{i=1}^{N} I_{i,j}^v} \tag{5.20}$$

Regarding to the columns, the concept is similar to the beams and, for each storey, all elements are computed by using eqs. 5.14, 5.15 and 5.16 and condensed in 4 new columns. For this case, the eqs. 5.18 and 5.19 are rewritten as follow:

$$I_c^w = \frac{\sum_{i=1}^N I_i^w}{4} \tag{5.21}$$

$$I_c^v = \frac{\sum_{i=1}^N I_i^v}{4} \tag{5.22}$$

where I_c^w and I_c^v are the inertia moments of the columns of the 3D reduced-order model. However, the columns area cannot be computed as performed for the beams, because it is necessary to consider the loss of the overturning effect, due to the reduction of the number of columns in the FE model. For accounting this effect, eq. 5.17 can be rewritten in analogous way, but adding the well-known Steiner term. This latter is computable multiplying the area of the ith column (A_i) for the square distance (d_i) between each column considered and the CM of the 3D reduced-order model. In other words, eq. 5.17 became as follow:

$$A_c = \frac{\sum_{i=1}^N \left[A_i + \left(A_i * d_i^2\right)\right]}{4} \tag{5.23}$$

where A_c is the area of the columns of the 3D reduced-order model. The L of the columns is that of the storey considered. In addition, the 3D reduced-order model should consider the total mass of the building, which can be evaluated by computing the total weight (W) of the structure. Generally, one can use the usual formulation provided by the technical codes, such as the one proposed by EC8 and below reported:

$$W = \sum G_k + \sum \Psi_E Q_k \tag{5.24}$$

where G_k are the characteristic dead load, Q_k are the live load and Ψ_E are the seismic combination coefficients of the quasi-permanent values of the live loads. In our case, the evaluation must be made for each storey, where after the evaluation of storey weight (W_s) one can compute the storey mass (M_s), by using the gravity acceleration (g) and, subsequently, can subdivide equally the mass in the four nodes of the storey model, as suggested by the following equation:

$$M_n = \frac{W_s}{4g} = \frac{M_s}{4} \qquad (5.25)$$

where M_n is the mass of each node of the considered storey s. Computationally, M_n is a translational mass and then, it must be applied in the two main horizontal directions. For completing the 3D reduced-order model, the nodes of each storey must consider the rotational effect associated to the structure. To this scope, it is necessary to compute the rotational nodal masses, directly from the rotational mass of the diaphragm. In particular, this quantity is strictly linked to the concept of the floor mass inertia moment (J_s), which in turn depends from the floor inertia radius ($I_{r,s}$), as below reported:

$$J_s = M_s * I_{r,s}^2 \qquad (5.26)$$

where, assuming the total dimensions of the building sides in the two main directions as L_x and L_y, the value of $I_{r,s}$ is provided by:

$$I_{r,s} = \sqrt{\frac{L_x^2 + L_y^2}{12}} \qquad (5.27)$$

Whereas the 3D reduced-order model must have the same behaviour of the building, the rotational mass of the nodes ($J_{r,n}$) is provided by the difference between the J_s of the structure and the floor mass inertia moments of the simplified model, submitted in the 4 nodes of the storey. Mathematically, we have the following equation:

$$J_{r,n} = \frac{J_s - M_s * \left(\dfrac{L_{b,x}^2 + L_{b,y}^2}{12} \right)}{4} \qquad (5.28)$$

where $L_{b,x}$ and $L_{b,y}$ are the expression of $L_{b,j}$ in the two main direction X and Y. One should observe that the 3D reduced-order model built is a regular model, with CM and CS coincident. This means that our simplified model surely loses the property to reproduce the coupled vibration modes, especially when the building to analyse is strongly irregular. On the other hand, it is possible to improve the estimation of irregular buildings, adopting a 3D reduced-order model constituted by more one-bay structures. With this scope, one can subdivide the building in two or more parts and applies the procedure above, respecting all structural elements that fall in the part selected. The

result is given by two or more 3D reduced-order models, which must be linked storey per storey, in order to work together. For having an accurate estimation, one should takes care the position of the simplified models. In fact, their CMs must be coincident with the ones of the building parts selected. Concerning to the NL behaviour of the 3D reduced-order model, the modelling approach adopted is to lumped plastic hinges, placed in the end sections of the elements of the simplified model. The constitutive law of the plastic hinges can be evaluated for all elements, considering the full knowledge of the structure and taking into account the bidirectional behaviour for the columns. The choice of the constitutive law typology is entrusted to the analyst. In this proposal, a quadrilinear Moment – Rotation constitutive law has been assumed, where the back-bone is constituted by 4 damage levels, such as the first cracking of concrete, the yielding of the longitudinal bars with hardening behaviour, a softening part for simulating the strength degradation of the section and a fourth part of residual moment, assumed at 20% of the yielding moment.

Fig. 5.19 – Concept of our 3D reduced-order model, applied on a case studied (B10)

For each element, the values of the yielding ($\theta_{y,i}$) and ultimate rotation ($\theta_{u,i}$) are computed using the formula provided by the EC8 – part 3.3. Once that the constitutive law of each element is defined, the NL behaviour of the 3D reduced-order model elements can be evaluated, with respect of the elements orientation (j^{th} direction), by using the following equations:

for beams:

$$M_{by,j} = \frac{\sum_{i=1}^{N} M_{byi,j}}{2} \tag{5.29}$$

$$M_{bu,j} = \frac{\sum_{i=1}^{N} M_{bui,j}}{2} \tag{5.30}$$

$$\theta_{by,j} = \frac{\sum_{i=1}^{N} \theta_{byi,j}}{N} \tag{5.31}$$

$$\theta_{bu,j} = \frac{\sum_{i=1}^{N} \theta_{bui,j}}{N} \tag{5.32}$$

for columns:

$$M_{cy,j} = \frac{\sum_{i=1}^{N} M_{cyi,j}}{4} \tag{5.33}$$

$$M_{cu,j} = \frac{\sum_{i=1}^{N} M_{cui,j}}{4} \tag{5.34}$$

$$\theta_{cy,j} = \frac{\sum_{i=1}^{N} \theta_{cyi,j}}{N} \tag{5.35}$$

$$\theta_{cu,j} = \frac{\sum_{i=1}^{N} \theta_{cui,j}}{N} \tag{5.36}$$

where the M_{by}, M_{bu}, M_{cy} and M_{cu} are, respectively, the yielding and ultimate moment of the beams and columns and θ_{by}, θ_{bu}, θ_{cy} and θ_{cu} are, respectively, the yielding and ultimate rotation of the beams and columns, all of the simplified model. Figure 5.20 shows graphically what explained from the latter equations, with an example of reduction.

5.4.1 Application to set of real case studies

In order to test the methodology proposed about the 3D reduced-order models, explained in the previous section, the sample of 15 existing RC buildings presented in the Section 5.3.1 has been taken into account. It is worth remembering that all information about the knowledge of buildings are known, such as geometry, materials and

them geometrical and mechanical parameters, loads applied and so on. In addition, the 3D full models made in SAP2000 are available, in order to compare the 3D reduced-order models with the full ones, in terms of linear and NL behaviour. The hypotheses at the base of the full numerical models must be coherent with the ones adopted for the 3D reduced-order models. In particular, the common hypotheses assumed are the rigid floors, the base columns fixed at the ground and the nonlinearity of beams and columns, which are modelled by using a plastic hinges approach.
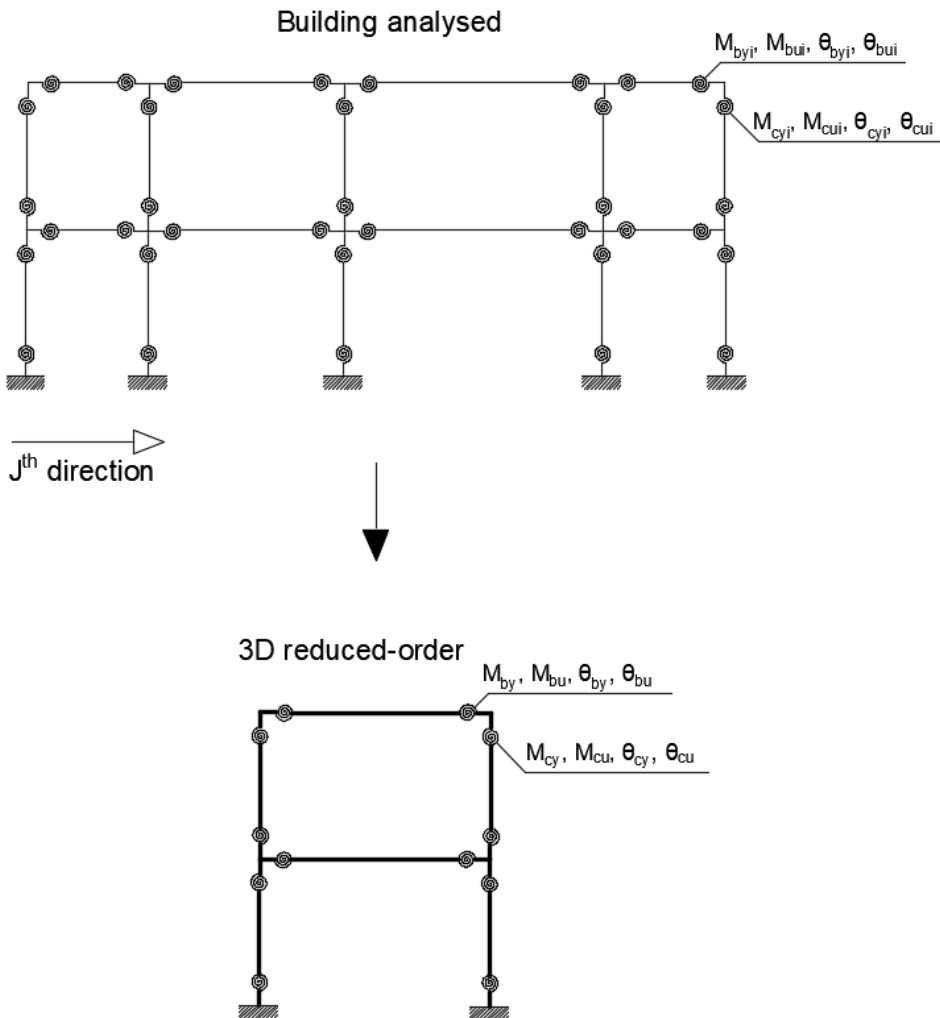
5.20 – Nonlinear behaviour of 3D reduced-order models for the jth direction, by using eqs.5.29 – 5.36

Concerning to the plastic hinges, according to the modelling of full models, the 3D reduced-order models account just for the ductile mechanisms, as the bending and they neglect the brittle mechanisms, as the shear. Even for 3D reduced-order models, the influence of infill panels has been not considered. Regarding to the nonlinearity, for each plastic hinge, the limit states acceptance criteria have been imposed, fixing a chord rotation value equal to θ_y for the DLS, ¾ θ_u for the LSLS and θ_u for the NCLS. The cyclic behaviour of the plastic hinges has been imposed according to the Takeda rule. Therefore, the procedure explained in the previous Section has been performed for all buildings of the sample investigated and numerical 3D reduced-order models have been carried out, by using the Opensees software (McKenna, 2011). The frame members have been modelled by using the element beamWithHinges, in which the constitutive law of plastic hinges is simulated through the Pinching4 material. Each plastic hinge has been defined as soon as made for the full models. In particular, the constitutive law employed, is able to account for the concepts developed by Ibarra (Ibarra et al, 2005) for properly weighting the hinges versus the elastic beam.

B1 - Rocchetta Sant'Antonio	
Full model	**3D reduced-order model**
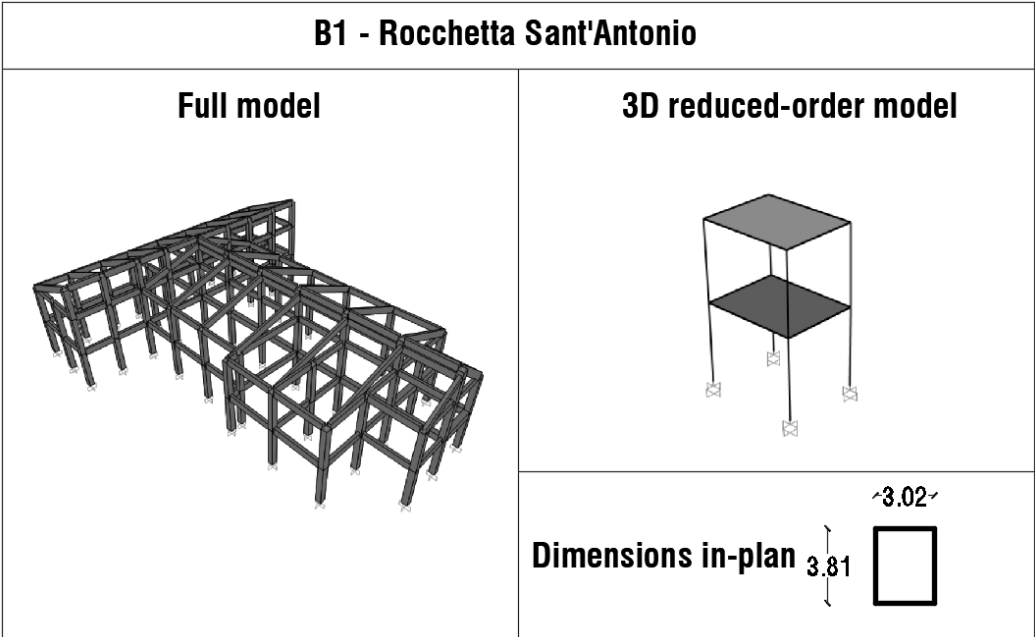
Fig. 5.21 – 3D reduced-order models for the building B1

Concerning to the reduction criterion followed, the main goal has been the one of making a 3D reduced-order by using only a one-bay model for each structure, according to a philosophy of simplified model. Clearly, this is not always applicable, such as in the cases in which the buildings have a particular in-plan shape, like an L. For this eventuality, the 3D reduced-order models have been made by using a double one-bay structure model, where the two structures are rigidly linked storey per storey. Figure 5.21 for B1 and from figures D.1 to D.7 for other buildings (see Annex D), show the numerical model of buildings with the corresponding 3D reduced-order model, with indications about the tag assignment of buildings, the cities and the length sides of the simplified model (in bold). The first comparison performed between full and 3D reduced-order models has been in terms of modal parameters, analogously to table 5.1 (for full models). In particular, for each 3D reduced-order model, T_1, T_2, T_3, $M_X[\%]$, $M_Y[\%]$ and $M_\theta[\%]$ have been evaluated and reported in table 5.8. The results show that the elastic behaviour of models is same in a lot of cases investigated. This means that the 3D reduced-order models take correctly into account the masses and stiffness' of the buildings. Different evaluation can be done regarding the M[%]s where, as just mentioned, the vibration modes are totally uncoupled in the simplified models, which is different from what we have in the full models. In addition, one could take into account the possibility to reduce the building in more one-bay models connected, for better simulating the building dynamic behaviour. As just mentioned, the building can be divided in more parts and the procedure can be applied for each part identified. An example of this application is showed in figure 5.22, where the building B2 has been reduced in a 3D reduced-order made with 4 one-bay structures. In table 5.9 is presented the comparison of Ts and M[%]s among full model, 3D-reduced order model and 3D reduce-order model with 4 one-bay structures.

Tab. 5.8 – First three Ts and M[%]s for the buildings investigated

Building	T_1 (s)	T_2 (s)	T_3 (s)	M_x[%]	M_y[%]	M_θ[%]
B1	0.33	0.32	0.28	92.86	91.71	93.74
B2	0.78	0.73	0.67	95.89	91.47	94.86
B3	0.36	0.34	0.30	89.08	90.93	91.48
B4	0.85	0.57	0.50	89.97	71.35	87.25
B5	0.38	0.33	0.27	74.90	78.12	81.21
B6	0.52	0.41	0.31	93.48	93.05	98.22
B7	0.71	0.55	0.54	97.65	92.27	97.78
B8	0.80	0.62	0.60	92.16	66.69	69.52
B9	0.67	0.62	0.53	98.42	93.26	98.57
B10	0.43	0.42	0.38	98.02	97.77	97.96
B11	0.56	0.47	0.45	92.62	96.98	97.48
B12	0.53	0.47	0.44	82.84	60.57	64.25
B13	0.47	0.41	0.33	94.83	95.36	96.79
B14	0.83	0.74	0.71	93.05	90.00	92.99
B15	0.68	0.65	0.56	86.89	84.25	87.78
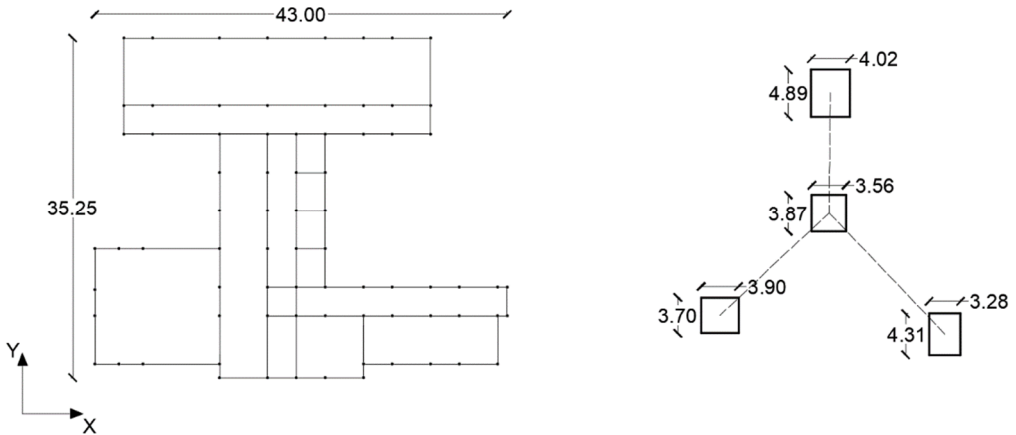
Fig. 5.22 – 3D reduced-order model with 4 one-bay structures for the building B2

Tab. 5.9 – Comparison, in terms of periods and participating masses, among full, 3D reduced-order and 3D reduced-order with 4 one-bay structures models, for the case B2

Building B2	T_1 (s)	T_2 (s)	T_3 (s)	M_x[%]	M_y[%]	M_θ[%]
Full model	0.84	0.83	0.73	46.33	90.88	47.11
3D reduced-order model	0.78	0.73	0.67	95.89	91.47	94.86
3D reduced-order model – 4 one-bay structures	0.83	0.76	0.71	67.35	90.69	62.17

The results show that the last model better approximates the dynamic behaviour of the full model, both for the Ts and M[%]s. On the other hand, the performance of a simplified model like this, can become hardly feasible for practitioners, besides to consider the possible increment of computational mistakes. From this point, all analyses have been performed on the 3D reduced-order models simpler, as in the models shown in figure 5.21 and D.1-D.7. After the modal parameters comparison among the modelling methodologies, the next step has been the check of the NL behaviour between the numerical models (full and 3D reduced-order), for each building analysed. To this scope, NLS analyses have been carried out on the 3D reduced-order models, in the main directions X and Y, according to the reference system reported in figure 5.12 (and figures from A.1 to A.14) and to directions of pushover analyses just performed on the full models. Analogously to these latter, the load pattern adopted for pushover analyses is the uniform one, with each force applied in the CM of each storey and all models have been pushed up to the same displacement of the corresponding full model. The results of NLS analyses has shown that the elastic slope of the elastic branch of the capacity curves, here displayed as V_b-δ_R, of 3D reduced-order models is coincident with the ones obtained from the full models. This is due to the strong closeness among the elastic parameters of the numerical models (in particular in terms of Ts), evidence just shown form the comparison between tables 5.1 and 5.9. With regard to the value of yielding base shear (V_{by}), in some cases there are little differences between the two capacity curves of the same building, such as occur for other properties in post-elastic field. In particular, the pushover curves of the simplified models show some differences

in terms of slope of the hardening part, ultimate V_b and the correspondent δ_R and slope of the softening part. The reasons of this result is of addressing to the nature of the 3D reduced-order, which cannot take into account the continuous stiffness variations of the single elements in the post-elastic field. In addition, the full and simplified models, under the same modelling hypotheses, have been made using two different software, which could be cause of numerical differences in the results. In order to capture the structural response of the full models, especially in the inelastic field, the 3D reduced-order models performed (uncalibrated models) have been calibrated on the base of the pushover curves obtained for the 2 directions considered. To this scope, some parameters of the constitutive law of the plastic hinges involved in the simplified models have been adequately modified and, on these new models (calibrated models), the pushover curves have been newly recalculated. In figures 5.23 for B1 and from figure D.8 to D.21 for other buildings (see Annex D) the pushover curves for each model and each direction are shown, provided by the full models, the calibrated and uncalibrated 3D reduced-order models. The comparison among pushover curves of uncalibrated, calibrated and full models shows that in some cases, the calibrated and uncalibrated curves are similar (figures in which the two curves are superimposed, displayable as sole black dotted curve) and in other cases they are very different. Generally, both calibrated and uncalibrated curves difficulty reproduce the faithful trend of the pushover curve obtained from full model. This is due to the sudden change of stiffness in the full model, which are impossible to reproduce with a simplified model. On the other hand, it is shown how the 3D reduced-order model can reproduce the trend of the structural response (under static loads), with good approximation. Regarding to the calibration of the models, table 5.10 shows the percentage variation made on the hinge parameters, which define the post-elastic behaviour of buildings. In particular, for modifying a curve in a direction, all hinges oriented in that direction have been changed, by applying the same variation for the post-elastic parameters.
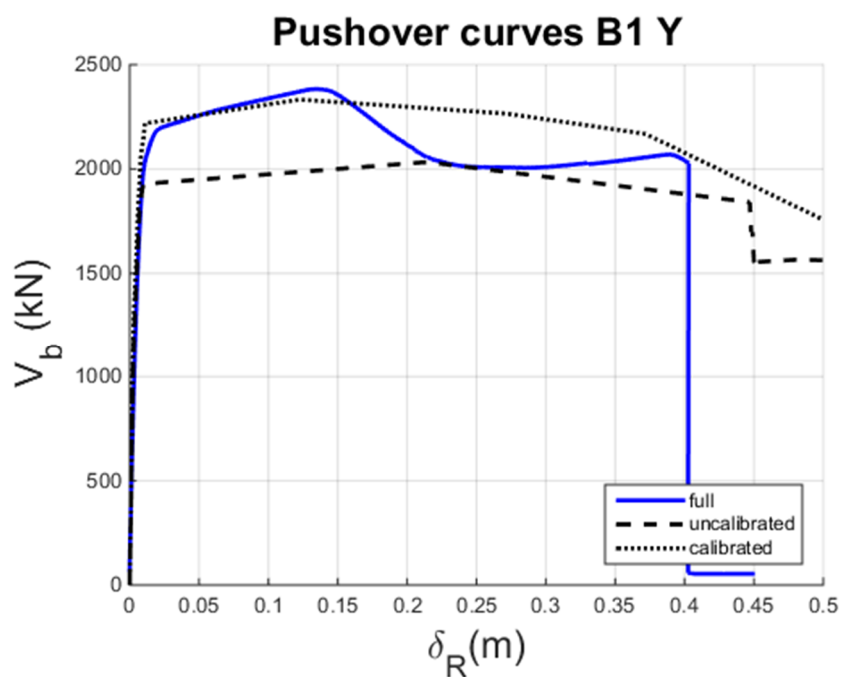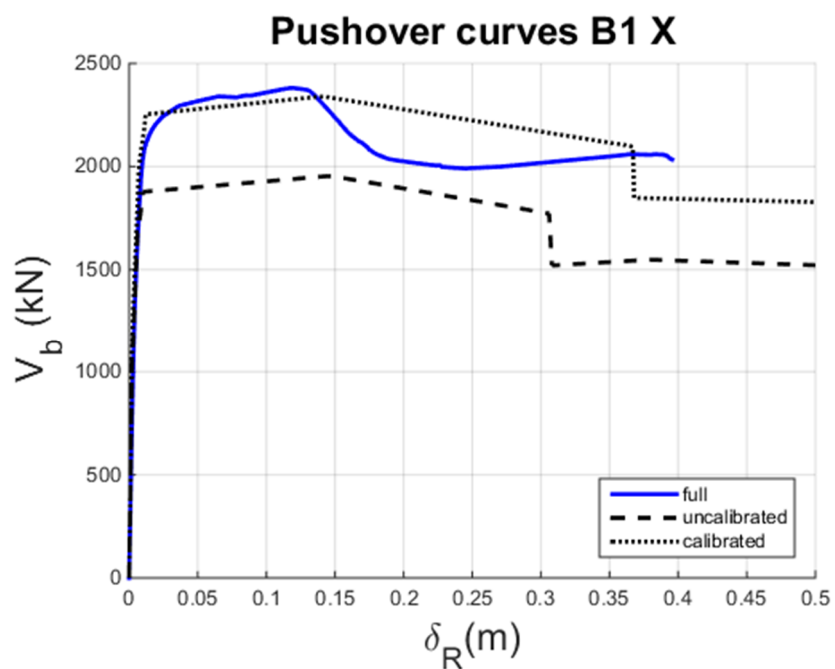
Fig. 5.23 – Pushover curves of full, calibrated and uncalibrated 3D reduced-order models in X and Y direction, for building B1

Tab. 5.10 – First three Ts and M[%]s for the buildings investigated

Building	Calibration X				Calibration Y			
	f_y (%)	a_h (%)	m_c (%)	a_c (%)	f_y (%)	a_h (%)	m_c (%)	a_c (%)
B1	+20	+20	-20	-	+15	+100	-50	-
B2	+8	-	+60	+100	+15	+40	+20	+100
B3	-	+10	-50	-	-	-	-30	+100
B4	-	+100	-10	+100	+5	+10	-30	+80
B5	-	-	+20	+50	+5	+100	-10	+100
B6	-	-	+20	-40	-	+100	+80	-
B7	-	-	-25	+200	-	-	-30	-
B8	-	-	-	-	-	-	-	-
B9	-	-	-	-	-	-	-	-
B10	+5	+70	-55	+100	+5	+50	-50	+100
B11	-	-	-		-	-	-	+200
B12	-	-	+10	+50	-	-	-	+100
B13	-	-	-	+100	-	-20	+25	+50
B14	-	-	-30	-	-	-	-40	+100
B15	-	-	-	-	-10	-	+30	-

Among these, which are defined in the Opensees routine used for defining all hinges, there are f_y, which is the yielding moment (or force, but in this case is a moment for the constitutive law used), a_h, which is the hardening ratio expressed as percentage of the flexural stiffness, m_c, which is ductility expressed in terms of ratio between capping and yielding rotations and a_c, which is the capping slope expressed as percentage of the flexural stiffness. As shown by the percentage values reported in table 5.8, the above parameters are characterized by high sensitivity, which highlights the importance of the FE model definition for having good results. However, our aim is to assess if the proposed procedure, for making the uncalibrated version of 3D reduced-order model, is efficient, provide same results of the calibrated and full models and, above all, can be used in the vulnerability assessment of buildings, by using the PBEE approach. With

this regard, NLTH analyses have been performed on some of the numerical models made. In particular, the aims are firstly, to understand if the uncalibrated models are able to capture the structural response of the buildings investigated under dynamic loads and secondly, to assess the calibration validity, which has been performed through pushover curves. The set of ground motions selected is the one shown in table 5.3. For this analysis, only 5 buildings have been investigated, randomly chosen in the sample, by using just 5 records of the above set. Even in this case, the unscaled accelerograms have been applied on numerical models (full and 3D reduced-order calibrated and uncalibrated) with the two horizontal components simultaneously. Figures 5.24, 5.25, 5.26 and 5.27 show the results of the NLTH analyses performed, with specific reference to the models investigated and records uses. In particular, the figures show the percentage difference in the two main directions, in absolute value, firstly, between full and uncalibrated 3D reduced-order models (figures 5.24 and 5.25) and secondly, between full and calibrated 3D reduced-order models (figure 5.26 and 5.27), in terms of maximum θ_i and δ_R. In some cases, the number of bars is less than the records used, cause the possibility to have the dynamic instability of the structural response, which could also occur only in one of the numerical models performed. Generally, the results of figures 5.24 and 5.25 show that the percentage differences among full models and calibrated and uncalibrated 3D reduced-order, in terms of maximum θ_i and δ_R, are in the order of 20%, results that demonstrate how to simplified models provide a good simulation of the NL behaviour of full models and of the buildings behaviour. In addition, as predictable, the calibrated 3D reduced-order models provide differences lower than the uncalibrated one. Still, in more cases, the differences between the responses of simplified models are negligible, evidence that shows the effectivity of the uncalibrated models and the procedure proposed
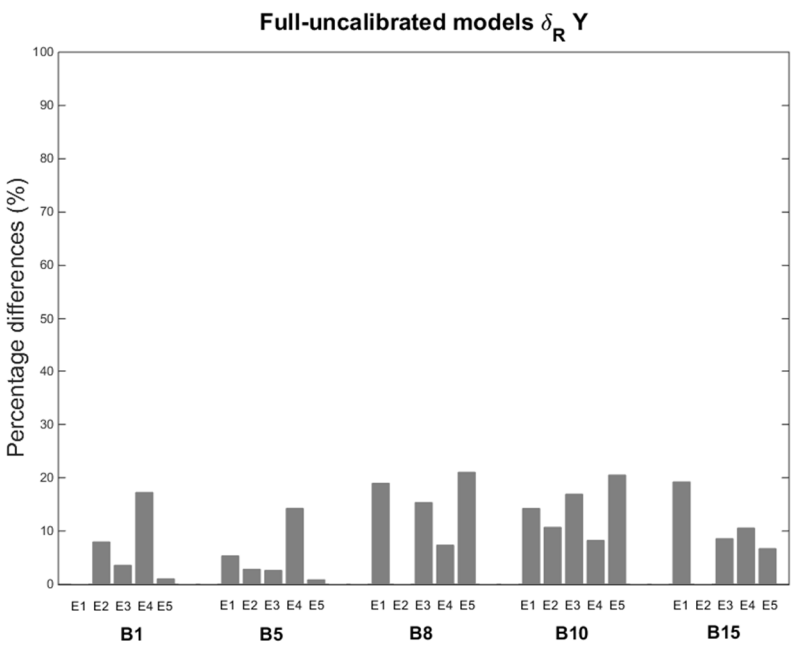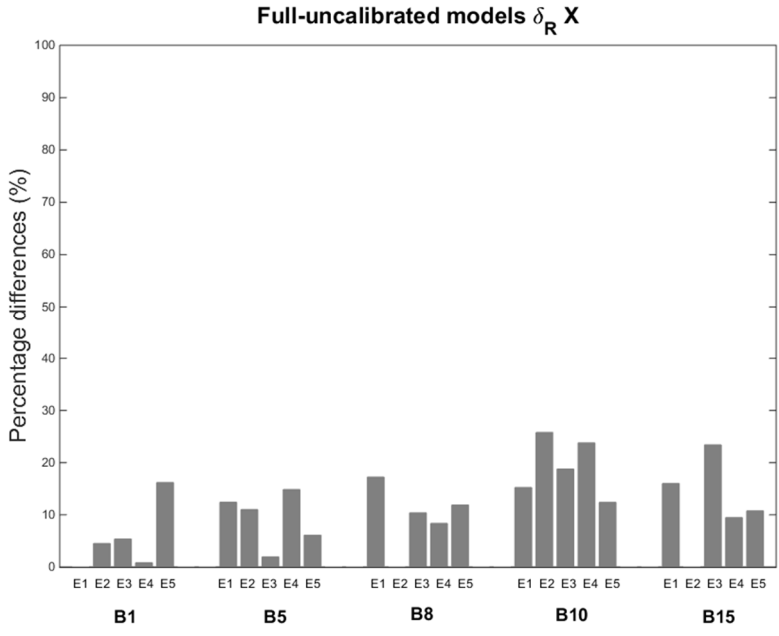
Fig. 5.24 – Percentage differences among full models and uncalibrated 3D reduced-order, in terms of maximum δ_R
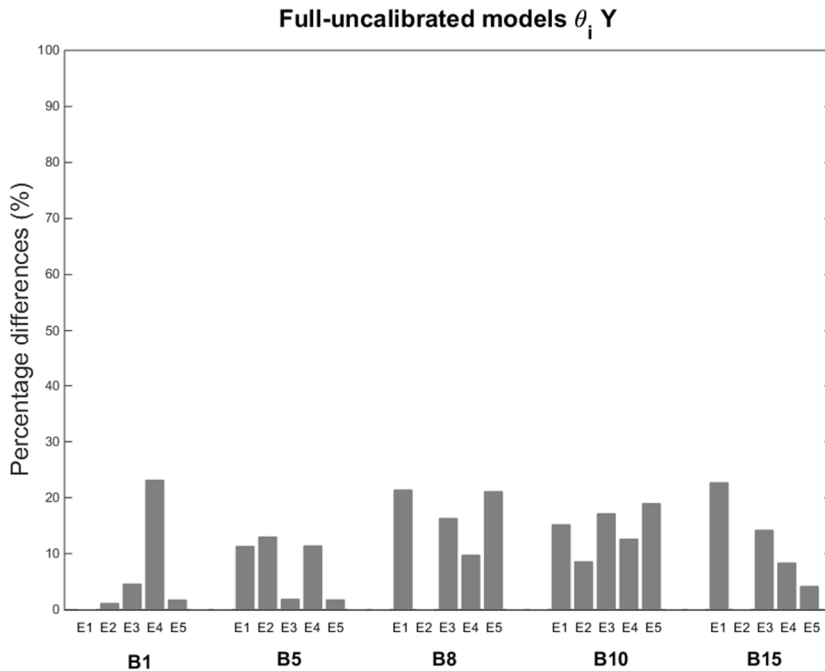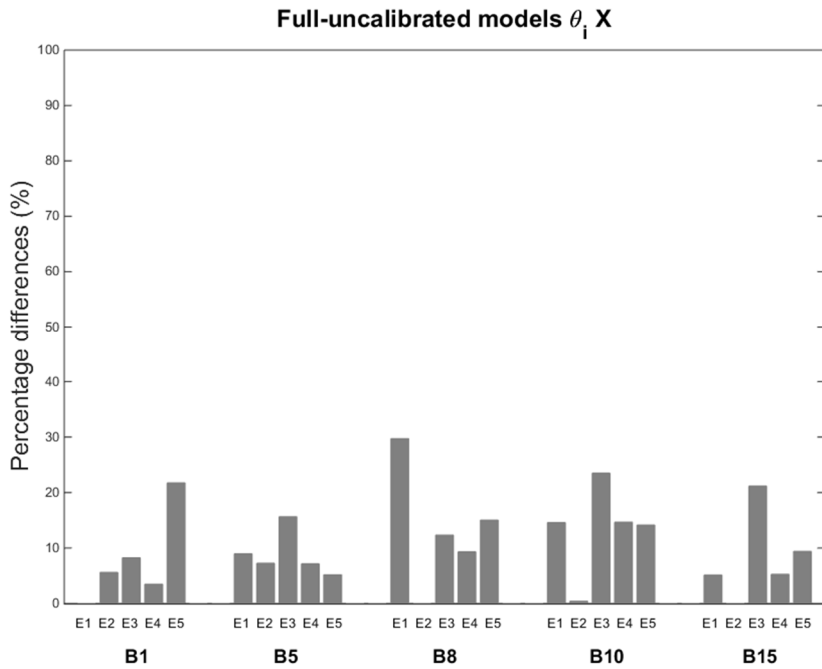
Fig. 5.25 – Percentage differences among full models and uncalibrated 3D reduced-order, in terms of maximum θ_i
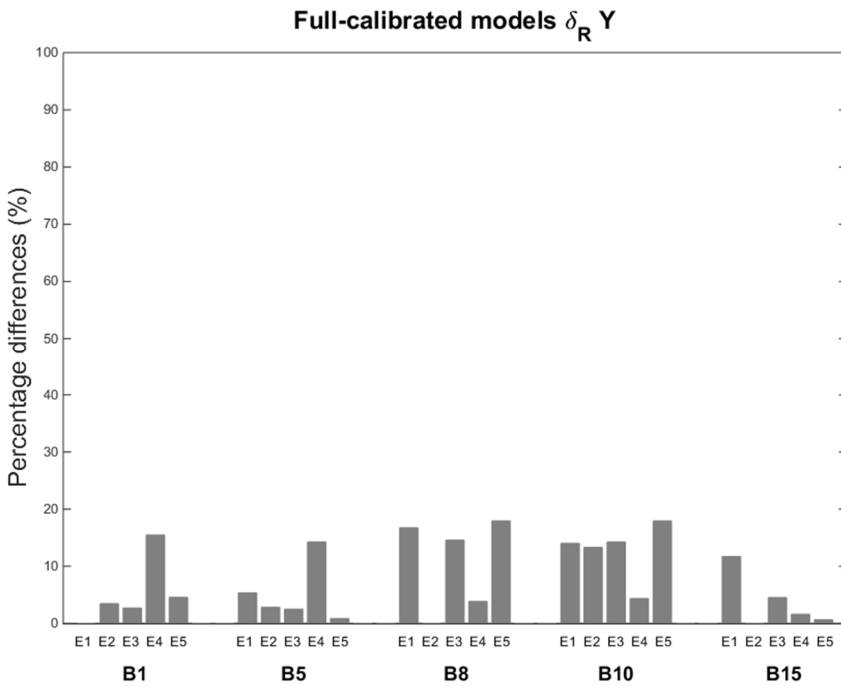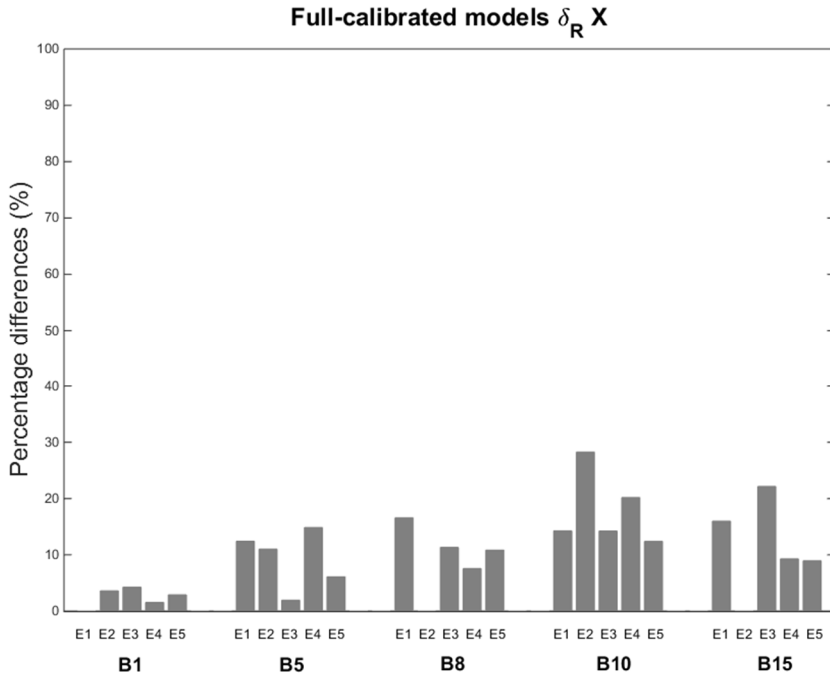
Fig. 5.26 – Percentage differences among full models and calibrated 3D reduced-order, in terms of maximum δ_R
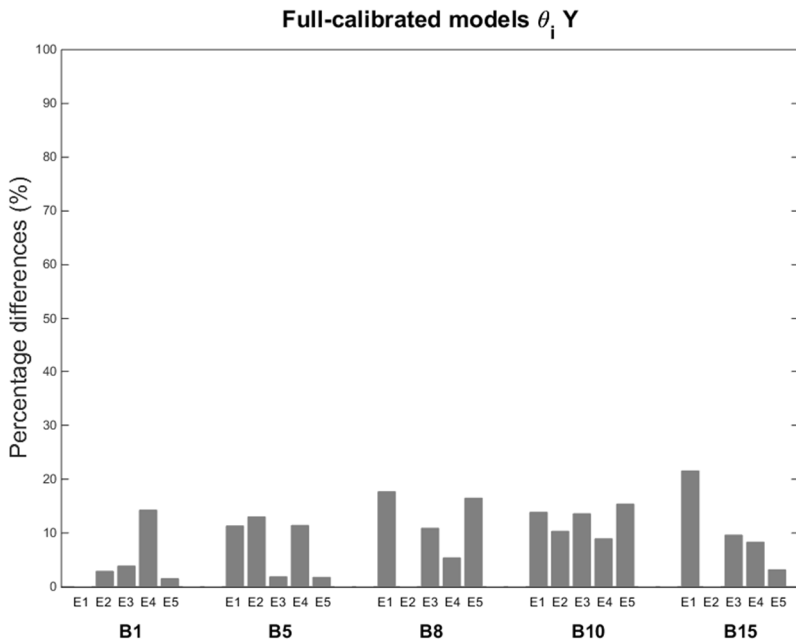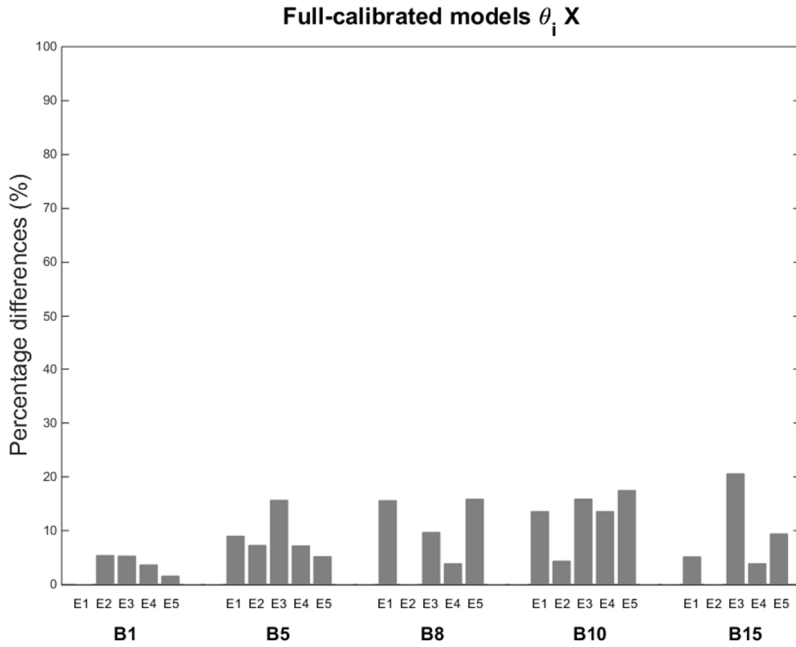
Fig. 5.27 – Percentage differences among full models and uncalibrated 3D reduced-order, in terms of maximum θ_i

5.4.2 Discussion of results: structural responses, damage states and confidence levels

The NLS and NLD analyses results in the previous Section have shown that the 3D reduced-order models are able to catch the global structural response of the buildings and their full models. The next step of the work is the application of the PBEE approach on the sample of buildings, in order to determine the structural responses, the damage states at different LSs and the safety levels. Regarding to the seismic hazard of the buildings sites, the seismic input is represented from the set of accelerogram just used and reported in table 5.3. In addition, the hazard surfaces of the buildings sites have been just defined, as depicted in figures 5.16 and C.8-C.14 (see Annex C). Concerning to the structural analysis phase, the real novelty of this work is the improvement given from the 3D reduced-order models. In particular, in the PBEE approach, one needs to define the structural response of the building analysed in both elastic and inelastic fields, for different IM levels, through several NLD analyses. As just mentioned, for characterizing the structural response from the probabilistic point of view, the numerical model should be investigated through some methodologies of dynamic analysis, such as the IDA, cloud or MSA. On the other hand, the use of these kinds of analysis has an elevated application only in the academic world, related to difficult by practitioners, which needs to reduce the time of analysis and the computational efforts. Therefore, the main skill of the 3D reduced-order model is the possibility to carry out a lot of NLD analyses, useful for fully investigate the structural response, avoiding the above problems, especially for practitioners (without considering the limits of its application for the academic research). With the aim of evaluating the efficiency of our simplified models in the structural response prediction, all models have been investigated by using NLD analyses. In particular, IDA analyses have been performed on the 3D reduced-order models (calibrated and uncalibrated) and compared with the results obtained from the application of FSA method on full models, widely discussed in the Section 5.3.2. Concerning to the IDA analyses on all 3D reduced-order models, the set of records selected has been applied on the FE models and the accelerograms have been scaled up in amplitude sometimes, until to have the convergence of the models. The IDA results are represented by 11 IDA curves. The structural responses obtained from

the application of IDAs on 3D reduced-order models and FSAs on full models can be displayed in the plane EDP – IM, where the values of the EDP has been expressed in terms of maximum interstorey drift ratio ($\theta_{i,max}$) and IM is the $S_{agm}(T_{1-3})$. Figures 5.28 for building B1 and from D.22 to D.35 for other buildings (see Annex D) show the superposition of the IDA curves on the uncalibrated 3D reduced-order models with the points obtained by the FSA application on the full models, plotted for the two main directions (X and Y). Analogously to the uncalibrated model, figures 5.29 for building B1 and from D.36 to D.49 for other buildings (see Annex D) show the superposition of the IDA curves on the calibrated 3D reduced-order models with the points obtained by the FSA application on the full models, plotted for the two main directions (X and Y). Similar results have been obtained by performing IDAs on calibrated and uncalibrated models. The trend of the structural response obtained by the FSA on full models is more or less the same to the one computed with IDAs on the 3D reduced-order models. In particular, one can see that when the stripes are in elastic field, the dispersion of points of the stripes is always the same to the one shows by IDA curves, while in the inelastic field there are some differences. This can be explained considering that, in the inelastic field, some points in the stripes collapse (red points). Furthermore, it is necessary to consider that the full models have been made using a commercial software, as practitioners' use, which is often characterized by convergence problems of analyses in the inelastic fields. Looking the results obtained, the advantages of the 3D reduced-order models are manifold. Firstly, the structural response can be completely investigated in the elastic and inelastic fields, with a simple model implemented in an open source software and, overall, with low computational efforts and analysis time. Secondly, using this simplified model, the input of NL analyses can be increased, by considering a bigger number of accelerograms then the one adopted here, with the consequence to have a consistent definition of the structural response, from the probabilistic point of view. Lastly, comparing the results obtained from IDA and FSA, practitioner is able to increase the number of stripes on the full models, consciously deciding the others IM levels to investigate.
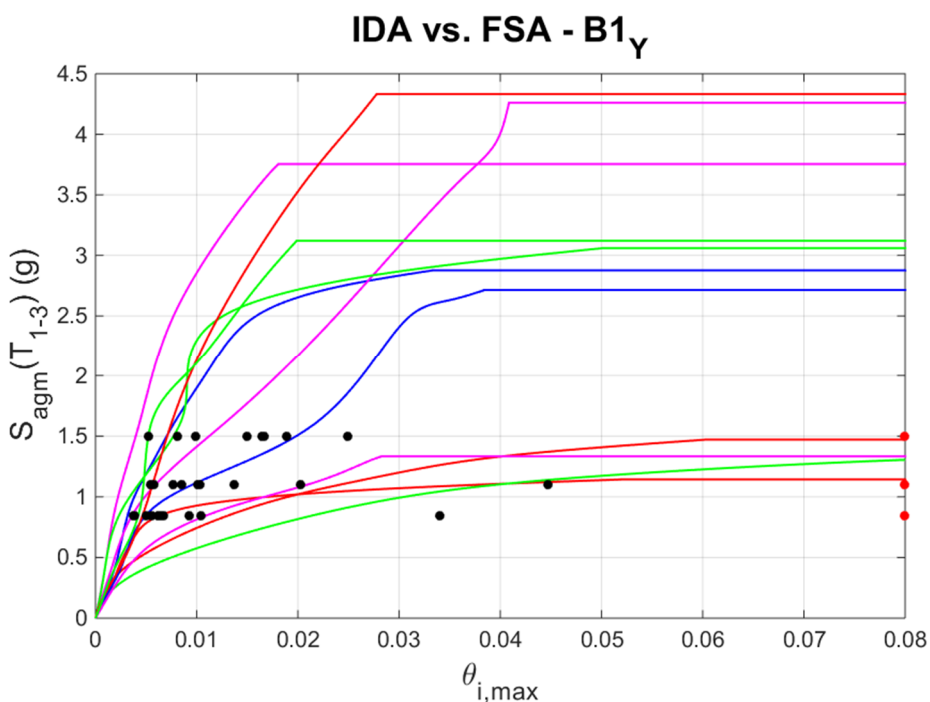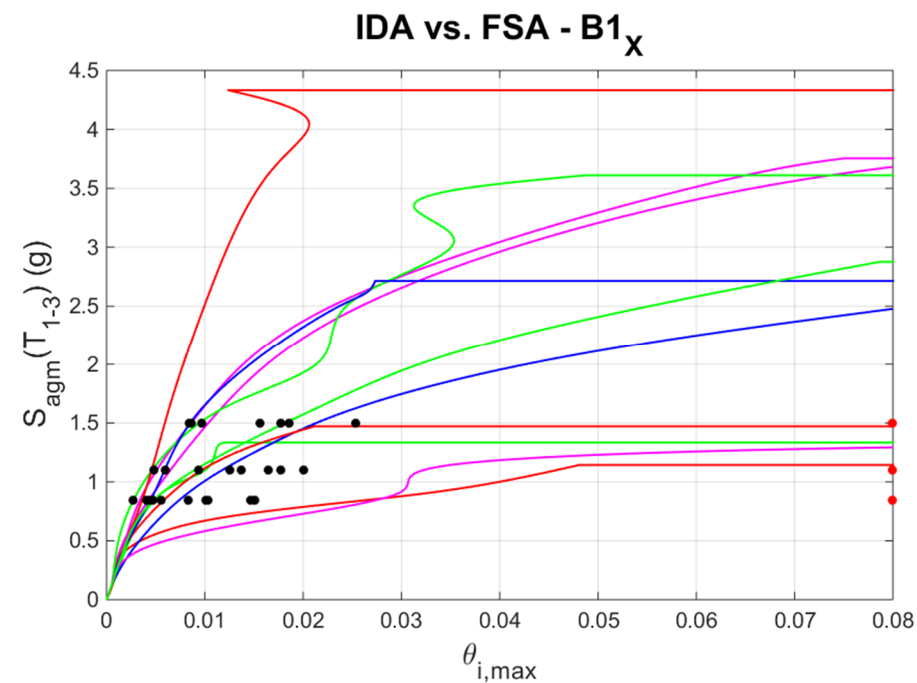
Fig. 5.28 – IDA on 3D reduced-order uncalibrated model vs. FSA on full model, in X and Y direction, for building B1
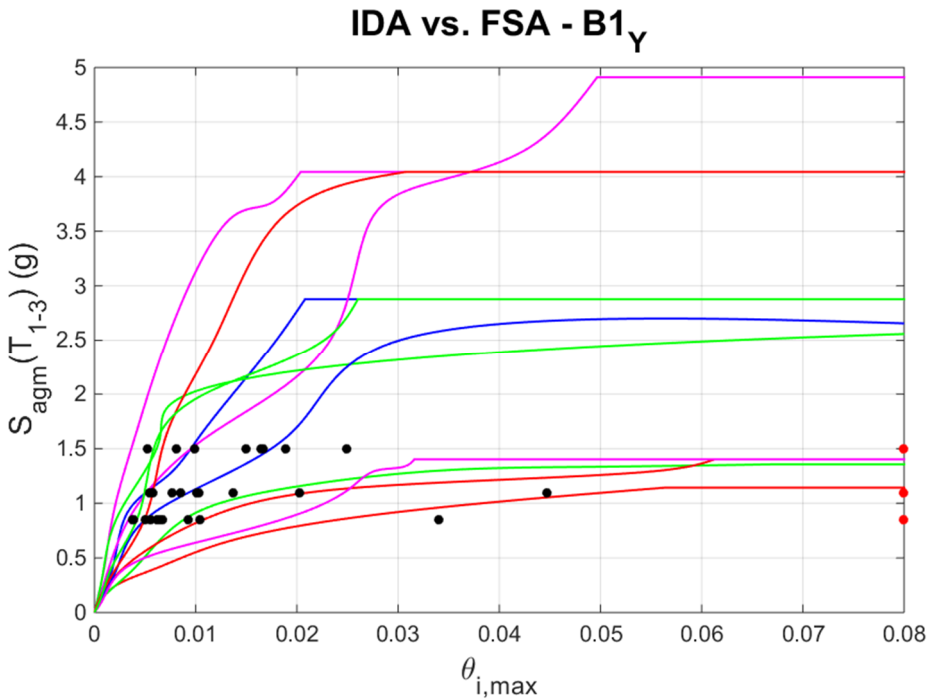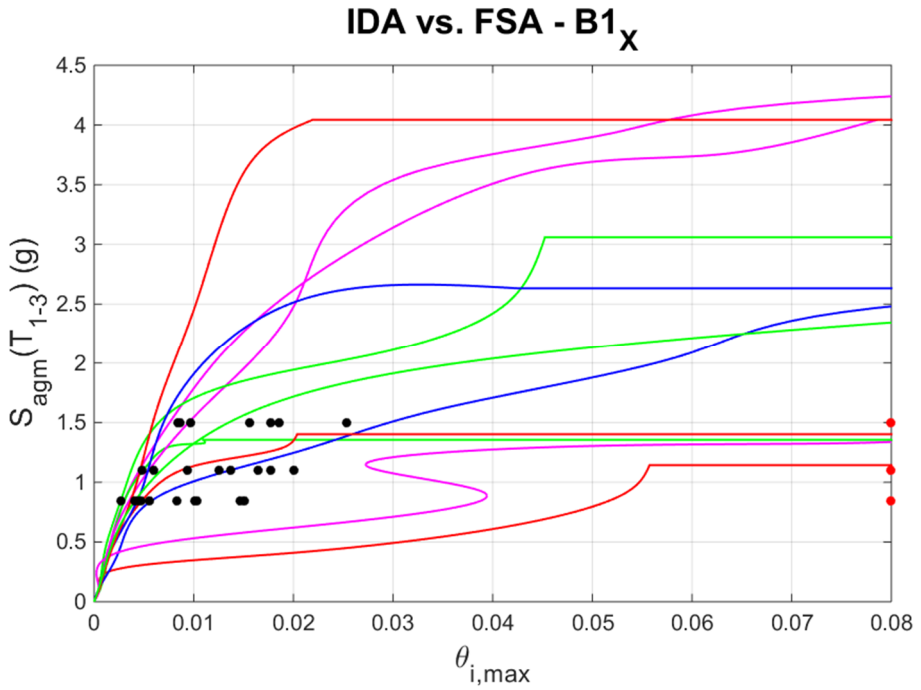
Fig. 5.29 – IDA on 3D reduced-order calibrated model vs. FSA on full model, in X and Y direction, for building B1

Clearly, this can be wasteful, from the computational effort point of view, but one can need to assess the local mechanisms of the structural elements, evidence identifiable only on the full model. Subsequently, the results of the structural analysis have been used for computing the damage states of the sample of buildings investigated. To this scope, fragility curves have been defined, according to the definition reported in Chapter 2. The value of epistemic uncertainties, which depends from the knowledge of buildings and modelling methods adopted, has been fixed for all 3D reduced-order models equal to 30%, according to the evaluation done about the full models. In order to compute the fragility curves from the 3D reduced-order models (calibrated and uncalibrated), the values of EDP have been fixed, for each LS, through the observation of the structural elements status, during the pushover analyses of the full models. In this application, the fragility curves computed from the FSA on full models, account for the DLS, which has been considered and evaluated for all models. In particular, using $\theta_{i,max}$ as EDP, the threshold of DLS has been established equal to 0.5% for each building. For the ultimate LS, the criteria for conditioning the LSs have been assumed equal to the one provided in Section 5.3.2, with the values shown in table 5.2. According to the philosophy used for fragility curves of full models, also in the cases of 3D reduced-order models, the damage states have been evaluated following the IM-basis estimation of structural response, given a value of EDP (vertical statistics). The results of the damage states of the buildings are depicted in figure 5.30 for B1 and from figures D.50 to D.56 for other buildings (see Annex D). In particular, in each graph, there are 9 fragility curves for each building, provided by the combination of 3 LSs (green for DLS, blue for LSLS and red for NCLS) and 3 kinds of models, as indicated in the legend. Results show that, first of all, the fragility curves of the 3D reduced-order models are generally the same for the calibrated and uncalibrated ones. In many cases, the curves of the two simplified models are perfectly fitted, while in the other cases, the calibrated models present fragility curves more close to the ones computed by FSA on full models.
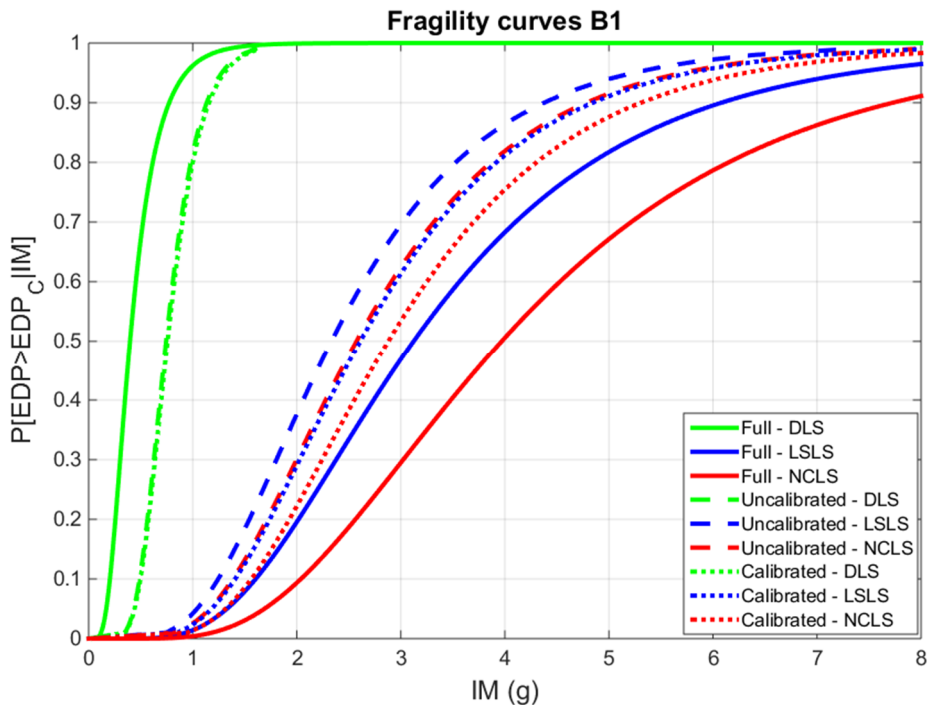
Fig. 5.30 – Comparison of fragility curves, for each model and each LS investigated for B1

Regarding to the comparison among full and simplified models, the results show that for the DLS, the fragility curves are similar, evidence that confirm how the structural response in the elastic field is perfectly captured from all models. On the other hands, for the ultimate LSs, the results show differences in some cases, or anyway, the curves are farther apart than the previous ones. In particular, for the LSLS and NCLS, the fragility curves from full models are usually shifted to right, compared to the ones provided by simplified models. The reason of this effect can be addressed to the definition of the structural response with FSA. In fact, in the inelastic field, the FSA method cannot provide a perfect estimation of the building behaviour, such as in the elastic field, due to the known problem of convergence of NL analyses in a full model. As abovementioned, the FSA results could be improved, increasing the number of stripes (with the usual disadvantage of increasing the computational time and effort). The analogous results, accounting for the shear mechanisms are presented from the figure F.1

to F.8 (see annex F). In these cases, the trend of the comparison is confirmed, but the results are better than the ones without shear mechanisms, due to the achievement of ultimate LSs in the neighbourhood of the yielding. In addition, in these cases, as above-mentioned, to consider the DLS does not make sense, because the ultimate LSs are soon reached. Finally, after the computation of the fragility curves, it has been possible to estimate the assessment of buildings, through the computation of the CLs, associated to the MAF of exceeding a certain LSs. In particular, for each fragility curves, it is possible to estimate the MAF of exceeding its LS ($\lambda_{estimated}$ here or λ_{LS} in the Chapter 2) and to compare this one with the target MAF (λ_{target} here or P_0 in the Chapter 2). If the $\lambda_{estimated}$ is greater than the λ_{target}, the building presents a damage state that has a low probability of exceedance the seismic demand, for the LS investigated and vice versa. In other words, the comparison in terms of λ provides an estimation of the safety level of the building, for the LS used. At the same time, a probabilistic procedure of assessment is aimed to estimate the CL, for a given LS, of a building to exhibit a certain target performance. In this case, we have assessed the CL values, for each case and each LS, quantifying to 100% and 0% the cases in which the building is able or not of satisfying the performance desired. $\lambda_{estimated}$ is computed according to eq. 2.41, while λ_{target} can be computed by using the following formulation:

$$\lambda_{target} = \frac{LN\big(1 - P(LS_{exceedance})\big)}{V_R} \qquad (5.37)$$

where V_R is the reference period. In particular, following the EC8 criteria, the values of probability of exceedance for DLS, LSLS and NCLS are respectively equal to 63%, 10% and 5%, while the V_R for the typologies of buildings investigated is equal to 75 years (provided by a N_L of 50 years and an C_U equal to 1.5). The results about the $\lambda_{estimated}$, λ_{target} and CLs evaluations have been reported in tables 5.11 and 5.12. The results show that the CLs, provided by the comparison of $\lambda_{estimated}$ and λ_{target}, are the same for each kind of model and LS. This, from a global assessment point of view, means that the 3D reduced-order models (calibrated or uncalibrated) provide a good estimation of the safety levels for each LS, coherent with the ones computed from the full models. However, the results of $\lambda_{estimated}$ from the full models show that, in the major

part of cases, the values obtained for DLS are bigger than the ones computed from the simplified models, while for LSLS and NCLS the situation is upside down.

Tab. 5.11 – Computation of $\lambda_{estimated}$ for 3D reduced-order calibrated, uncalibrated and full models, comparison with λ_{target} and computation of confidence levels, for each LS, for buildings B1 – B8

Building	LS	$\lambda_{estimated}$ –Full	$\lambda_{estimated}$ – Calibrated	$\lambda_{estimated}$ – Uncalibrated	λ_{target}	CL (%)
	DLS	0.0637	0.0446	0.0463	0.01325	100
B1	LSLS	0.0018	0.0027	0.0039	0.00140	100
	NCLS	0.0008	0.002	0.0029	0.00068	100
	DLS	0.1966	0.0784	0.079	0.01325	100
B2	LSLS	0.0226	0.0126	0.0141	0.00140	100
	NCLS	0.0141	0.0101	0.0111	0.00068	100
	DLS	0.044	0.0224	0.0284	0.01325	100
B3	LSLS	0.0018	0.0022	0.0022	0.00140	100
	NCLS	0.0008	0.0017	0.0016	0.00068	100
	DLS	0.066	0.117	0.117	0.01325	100
B4	LSLS	0.0093	0.0104	0.011	0.00140	100
	NCLS	0.006	0.0085	0.0082	0.00068	100
	DLS	0.011	0.0043	0.0041	0.01325	0
B5	LSLS	0.0001	0.0008	0.0008	0.00140	0
	NCLS	0.0001	0.0005	0.0005	0.00068	0
	DLS	0.631	0.0347	0.0333	0.01325	100
B6	LSLS	0.0008	0.0008	0.0009	0.00140	0
	NCLS	0.0003	0.0005	0.0006	0.00068	0
	DLS	0.2132	0.0814	0.084	0.01325	100
B7	LSLS	0.0096	0.0139	0.0137	0.00140	100
	NCLS	0.003	0.0112	0.011	0.00068	100
	DLS	0.0717	0.1032	0.1032	0.01325	100
B8	LSLS	0.0076	0.0132	0.0132	0.00140	100
	NCLS	0.0029	0.0085	0.0085	0.00068	100

Tab. 5.11 – Computation of $\lambda_{estimated}$ for 3D reduced-order calibrated, uncalibrated and full models, comparison with λ_{target} and computation of confidence levels, for each LS, for buildings B9 – B15

Building	LS	$\lambda_{estimated}$ –Full	$\lambda_{estimated}$ – Calibrated	$\lambda_{estimated}$ – Uncalibrated	λ_{target}	CL (%)
	DLS	0.235	0.0854	0.0854	0.01325	100
B9	LSLS	0.0161	0.0125	0.0125	0.00140	100
	NCLS	0.006	0.0079	0.0079	0.00068	100
	DLS	0.0645	0.0463	0.0489	0.01325	100
B10	LSLS	0.0028	0.0035	0.005	0.00140	100
	NCLS	0.0018	0.0029	0.0037	0.00068	100
	DLS	0.2356	0.1298	0.1292	0.01325	100
B11	LSLS	0.004	0.0063	0.0058	0.00140	100
	NCLS	0.0022	0.0052	0.0051	0.00068	100
	DLS	0.1259	0.0593	0.06	0.01325	100
B12	LSLS	0.0054	0.0085	0.008	0.00140	100
	NCLS	0.0032	0.0078	0.0069	0.00068	100
	DLS	0.2085	0.0957	0.0962	0.01325	100
B13	LSLS	0.00136	0.0009	0.0009	0.00140	0
	NCLS	0.0008	0.0007	0.0007	0.00068	100
	DLS	0.1626	0.0548	0.0547	0.01325	100
B14	LSLS	0.024	0.0062	0.0065	0.00140	100
	NCLS	0.0123	0.0047	0.005	0.00068	100
	DLS	0.0853	0.0832	0.084	0.01325	100
B15	LSLS	0.0098	0.0095	0.0087	0.00140	100
	NCLS	0.0083	0.0075	0.0069	0.00068	100

This trend is totally consistent with the fragility curves in figures 5.30 and D.50-D.56, where if the curve of one model, to a given LS, is shifted to right towards the same curve for the other kind of model, the $\lambda_{estimated}$ is smaller. In addition, one can see that the values of $\lambda_{estimated}$ obtained from uncalibrated 3D reduced-order models are very similar to the ones estimated from the calibrated models. This evidence confirm the efficiency of the methodology proposed.

6. CONCLUSIONS AND FUTURE DEVELOPMENTS

This dissertation presents a study about some aspects related to the vulnerability analysis of existing RC buildings. Within this framework, the attention is focused on the phases of the assessment process such as the definition of the numerical model and the subsequent seismic analysis. The main objective of the research work is to propose novel procedures and methodologies of modelling and analysis able to provide an extensive structural assessment within a full probabilistic framework guaranteeing, at the same time, easiness of application and effectiveness in terms of computational charges, so to simplify the job of researchers and practitioners. Additionally, an investigation about some common hypotheses assumed in the numerical models, assessing their limitations and possible improvements, has been performed.

After an extensive review of the state of art about the critical issues of existing RC buildings, with the common strategies of modelling and analysis provided by scientific literature, some usual hypotheses at the base of the phases to perform in the seismic assessment have been investigated.

With reference to the secondary structural elements, the validity of the rigid floor assumption in existing RC buildings under horizontal actions has been investigated. A numerical simplified procedure, able to provide a method to simulate the real behaviour of floor system under horizontal actions has been proposed. A preliminary sensitivity analysis has been performed in order to establish which are the most significant parameters that influence the problem, by using micro-models made with FE solid elements. Using the results of all the analyses, the thickness of an equivalent orthotropic shell has been calibrated, providing a macro-model able to explore the effective in-plane floor deformability. In order to test the procedure, a real case study has been investigated and the results of linear analyses have demonstrated that the shell element proposed can be used in the numerical model regardless of any aprioristic assumption about the hypothesis of rigid behaviour of the floor. Subsequently, a retrofit solution consisting in the addition of RC walls at the edges of building has been introduced in the numerical model, performing a linear static analysis. In this case, the results have

shown the different behaviour between the numerical models made by assuming or not the rigid floor assumption, quantifying the differences in terms of stress states.

Moreover, the proposed procedure has been compared with a different modelling approach, based on the schematization of the slab as proper equivalent struts, which is the most commonly adopted to represent the floor deformability into numerical models. The comparison of the models has shown a good convergence of results in terms of modal parameters, such as periods and participating masses and base shear distribution on the frame system and on RC walls. The main advantage to use an equivalent shell instead of the popular "strut model" is the possibility of an accurate characterization of the in-plan stress state of the slab system under horizontal actions, which is a very useful information for the structural verification of the elements constituting the slab. Such a verification, often neglected by practitioners, is fundamental in order to guarantee the consistency of the global model.

The next step has been the analysis of the interaction among structural, secondary structural (slab) and non-structural elements (masonry panels) in the numerical FE model by means of NLS analysis. With this regard, two real existing RC school buildings have been investigated. Each building has been modelled considering first the rigid floor assumption and then considering a flexible floor modelled through equivalent struts. In order to take into account the influence of infill panels, for each building, a group of models including a bare frame model, an infilled model and a reinforced infilled model has been considered. The models respectively simulate the structural behaviour without infill panels, with infill panels and with a seismic retrofit solution. The results of the NLS analyses have shown that the differences between models with and without the rigid floor assumption become greater as long as the infill panels are stronger. In particular, the variation of the V_b for fixed value of δ_R has reached values greater than 10%. Such a result can be appreciated even more by looking at the evolution of the plastic hinges, whose activation follow a completely different sequence, as a consequence of the different stress distribution among the vertical elements. This results demonstrate that the actual deformability of the floor system is an important factor in the evaluation of the seismic capacity of RC buildings and the rigid floor assumption

cannot be always considered a realistic hypothesis. The deformability of the floor system, moreover, can be strongly accentuated when a seismic retrofitting is performed, since practical solutions are usually aimed at reducing the horizontal displacement through an increment of the effective stiffness (RC shear walls, damped braced or infill panels connected with the surrounding frame). With this regard, another existing RC school building has been analysed in order to specifically appraise the contribution of the infill panels and the influence of a retrofit solution consisting in the addition of 2 RC walls on the building's perimeter. NLS analyses have been performed and the results have shown that the deformability of the floor system, in this case plays a fundamental and unneglectable role. In conclusion, the assumption of the rigid floor hypothesis deserves a focus on the presence of frames-walls systems or when the infill panels can be defined as "strong".

The future developments of this part of the research will provide the calibration of the NL behaviour of the equivalent orthotropic shell based on experimental tests, in order to carry out the NLS and NLD analyses on the FE models. This can be powerful in the definition of the post-elastic behaviour of floor system, accounting for the presence of infill panels and possible retrofit solutions.

Another critical issue faced in the dissertation (Chapter 4) has been the use of conventional and non-conventional methods of NLS analysis. With regard to conventional methods, a numerical study has been performed in order to appraise the results of conventional NLS analysis on a group of 92 ideal existing RC buildings characterized by in-plan irregularity, by varying the position of CN. Based on some evaluation about numerical results of NLS analyses, a new simply formulation has been proposed, able to provide the increment or decrement of the performance point (for a LS) of the capacity curves, by using the mathematical equation of a straight line. The method can be used in expeditious estimates of structural behaviour for several RC buildings of urban aggregate (with several in-plan shapes and number of storeys), in order to provide estimation more reliable of structural response and, consequently, fragility and vulnerability.

Concerning non-conventional methods, a multimodal NLS analysis has been proposed. The method can be considered very useful for practical application, because it consists in the computation of a single load pattern, which takes into account the effects due to the higher modes. Then, the procedure has been applied on a case study represented by a building having an irregular in-plan configuration and characterized by a great dispersion of the values of the mechanical parameters of in-situ concrete (as provided by the available information). First of all, the differences between the multimodal and unimodal pushovers have been assessed by comparing the results with those obtained by 3 IDAs performed with 3 design consistent artificial accelerograms. The results have pointed out the presence of appreciable errors in the results provided by the conventional formulation, because of the torsional behaviour of building. Then, in order to consider the influence of mechanical parameters of in-situ materials, the dispersion of concrete compressive strength has been parametrically considered by assuming three different scenarios (10, 20 or 30 MPa), considered as plausible for the case study. For each model, NL analyses (unimodal and multimodal pushover and IDAs) have been carried out. The comparison among the results have shown that an incorrect interpretation of the experimental tests induces an uncertainty about the structural response that is significantly greater than that approximations connected to the analysis method. Furthermore, by varying the concrete strength at each floor, results have shown that, besides the global failure mechanism occurs for soft storey at the 1st floor, the differences obtained in the structural response are much more relevant by varying the concrete strength at the 1st floor than in the other 2 cases. A further development of the research about this aspect will consist in the assessment of the multimodal procedure on additional case studies, characterized by a more severe geometric irregularity both in plan and in elevation.

In Chapter 5, the attention has been focused on the proposal of a novel simplified numerical procedure for performing NL analyses of existing RC structures by exploiting user-friendly FE software with easy graphical interfaces and able to reduce the time and computational efforts, in a view of the application of PBEE. Based on Multi

Stripe Analysis, the procedure proposes the development of a set of "Few Stripe analyses "(FSA), able to investigate the building behaviour both in elastic and inelastic fields. It has been applied on a sample of 15 low-rise existing RC school buildings located in the Province of Foggia, Southern Italy, for which a full knowledge of the geometrical and mechanical properties was available. Damage states at the ultimate LSs have been evaluated, and fragility curves defined. The results have been compared in detail with the ones obtained by the SPO2FRAG software. Some differences between the two methods have emerged, and even if they are quite variable, the trend seems to show a higher dispersion in SPO2FRAG fragility curves, which can be explained by considering that the SPO2FRAG provides a more complete investigation of the structural behaviour in the inelastic field. Furthermore, using again the two methods, the damage states at the ultimate LSs have been computed in a view of regional scale, by evaluating the regional fragility curves and their features, through the law of total variance, of the sample of buildings investigated. Despite the application is limited on a narrow sample of buildings, the application has shown the powerful of the methodology proposed, extensible to more wide classes of building typologies. In addition, a future development of the work will be the evaluation of the damage state of the sample buildings with regard to serviceability LSs, by considering the influence of infill panels or other non-structural elements. Even in this case, the focus will be addressed to practitioners, who strongly require simplified methodologies for carrying out the vulnerability analysis of existing buildings when using the probabilistic approach provided by the PBEE.

The final step of the research has been the proposal of a methodology for making simplified numerical 3D models, here called "3D reduced-order model". The aim is to easily perform a great number of NLD analyses and to provide an extensive probabilistic characterization of the global behaviour of existing RC buildings. The proposed procedure is characterized by a series of rules and equations that involve the knowledge of the geometrical and mechanical properties of the building. The simplified model able to predict the global behaviour both in the elastic and inelastic field is derived through

a DoFs reduction. The models produced in this way are called "uncalibrated 3D reduced-order models". The main novelty of this simplified numerical model, which takes into account the three-dimensionality of problem, is the easiness of application by practitioners without the necessity of implementing a full numerical model.

First of all, the procedure has been applied on the previously cited sample of 15 buildings, deriving the 3D reduced-order models and performing, on each of them, modal analysis and pushover analysis, in order to preliminarily assess the efficiency of the approach. The results of NLS analyses have shown that the pushover curves are similar in the elastic field, while they present differences in the post-elastic branch. The 3D reduced-order models have been then refined, by calibrating the NL parameters of the models for reproducing the same NL behaviour of the full models, based on the pushover analyses results. At this point, a detailed investigation of the NLD response of the 3D reduced-order has been performed (both calibrated and uncalibrated versions), through the application of IDAs (based on the use of real accelerograms). The results have been compared with the ones obtained by applying the FSA approach (developed in the previous part of the research work) on the full models. The damage states of the buildings have been computed at different LSs, providing the fragility curves for each model. Lastly, the safety levels of buildings have been checked, by computing, for each model, the confidence levels related to the MAF of exceeding each LS investigated. The critical discussion of the results has shown that, in each case analysed, the differences between the calibrated and uncalibrated version of the 3D reduced-order models are negligible. This observation supports the conclusion that the methodology proposed is efficient and robust. Furthermore, the comparisons among the results have shown that the structural response of the full and simplified models are similar, with a comparable dispersion in the elastic field and some differences in the inelastic field. This trend is confirmed also by the comparison of the fragility curves. For the Damage LSs, the results are similar for both the methodologies. For the ultimate LSs, instead, for some case studies the results present slight differences. The computation of the MAF of exceeding the investigated LSs has shown that the prediction of

the safety level given by both modelling methods is consistent, with only small some differences.

In conclusion, the proposed 3D reduced-order model presents a number of advantages: the structural response can be exhaustively investigated both in the elastic and inelastic field; it is possible to consider an increasing level of the seismic input via real accelerograms, but with a low amount of time and computational efforts; a good estimation of the damage states and safety levels at serviceable and ultimate LSs is provided.

The future developments of this part of the research work will be the incorporation of the contribution of non-structural elements, such as infills panels, in the 3D reduced-order models. In addition, it is worth denoting the powerful of the methodologies proposed, considering the possibility of using these tools in the context of the probabilistic risk assessment analysis of the existing building stock. In fact, the use of 3D reduced order models combined with FSA, on the one hand, can overcome the limitations about full MDoF models, such as the time analysis and computational efforts and, on the other hand, can provide results more accurate of the SDoF models, without convergence problems, in a seismic analysis at regional scale.

7. REFERENCES

Abrahamson, N. (1998). Non-stationary spectral matching program RSPMATCH. PG&E internal rep., Univ. of California, Los Angeles.

Aktan A. E., Karlsson B. I., Sozen M. A. (1973) "Stress-Strain Relationships of Reinforcing Bars Subjected to Large Strain Reversals". Civil Engineering Studies. Technical Report SRS-397. University of Illinois, Urbana-Champaign.

Alath S, Kunnath SK. (1995) Modeling inelastic shear deformations in RC beam–column joints. Engineering mechanics proceedings of 10th conference, May 21–24, University of Colorado at Boulder, Boulder, Colorado, vol. 2. New York: ASCE: p. 822–5.

American Society of Civil Engineers (2002) Minimum Design Loads for Buildings and Other Structures, ASCE/SEI 7-10, 2nd edn. American Society of Civil Engineers, 1801 Alexander Bell Drive, Reston, pp 20191–24400

Anagnostopoulos SA, Kyrkos MT, Stathopoulos KG (2015) Earthquake induced torsion in buildings: critical review and state of the art. Earthq Struct 8(2):305–377

Antoniou S, Pinho R. (2004a) "Advantages And Limitations Of Adaptive And Non-Adaptive Force-Based Pushover Procedures". Journal of Earthquake Engineering.;08:497-522.

Antoniou S, Pinho R. (2004b) "Development And Verification Of A Displacement-Based Adaptive Pushover Procedure". Journal of Earthquake Engineering.; 8:643-61.

Asteris, P. G., Antoniou, S. T., Sophianopoulos, D. S. & Chrysostomou, C. Z. (2011), 'Mathematical macromodeling of Infilled Frames: State of the Art', Journal of Structural Engineering 137(12), 1508–1517.

Augenti N., Cosenza E., Dolce M., Manfredi G., Masi A., Samela L., (2004) Performance of school buildings during the 2002 Molise, Italy, earthquake, Earthq. Spectra 20 S257–S270

Augenti N., Parisi F. (2010) Learning from construction failures due to the 2009 L'Aquila, Italy, earthquake, J. Perform. Constr. Facil. 24(6) 536–555,

Aziminejad, A. and Moghadam, A.S. (2010) Fragility Based performance evaluation of asymmetric single-storey buildings in near fi eld and Far fi eld earthquakes", Jl. of Earthquake Engg., Vol.14, pp 789–816.

Bakalis K, Fragiadakis M, Vamvatsikos D. (2017) Surrogate modeling for the seismic performance assessment of liquid storage tanks. J Struct Eng,; 143(4):4016199

Bakalis K., Vamvatsikos D. (2018) Seismic Fragility Functions via Nonlinear Response History Analysis. Journal of Structural Engineering, in press DOI: 10.1061/(ASCE)ST.1943-541X.0002141.

Baker J.W. (2008a). "An Introduction to Probabilistic Seismic Hazard Analysis (PSHA)," White Paper, Version 1.3, 72 pp.

Baker J.W. (2008b) Introducing correlation among fragility functions for multiple components, in 14th World Conference on Earthquake Engineering, Beijing, China,

Baker, J. W., (2015) Efficient Analytical Fragility Function Fitting Using Dynamic Structural Analysis." Earthquake Spectra, 31(1), 579–599.

Baker, J.W. (2011) "Conditional Mean Spectrum: Tool for ground motion selection, Journal of Structural Engineering,, 137(3), 322-331.

Baltzopoulos, G., Baraschino, R., Iervolino, I., Vamvatsikos, D. (2017) SPO2FRAG: software for seismic fragility assessment based on static pushover. Bull Earthquake Eng, 15: 4399.

Barron JM, Hueste MBD (2004) Diaphragm effects in rectangular reinforced concrete buildings. ACI Struct J 101(5):615–624

Barros RC, Almeida R. (2005) "Pushover analysis of asymmetric three-dimensional building frames." Journal of Civil Engineering and Management; 11:3-12.

Benedetti D., Petrini V., (1984) Sulla vulnerabilità di edifici in muratura: proposta di un metodo di valutazione. L'industria delle Costruzioni, 149(1), 66-74. (in Italian)

Bertoldi SH, Decanini LD, Gavarini C. (1993) Telai tamponati soggetti ad azioni sismiche, un modello semplificato: confronto sperimentale e numerico. Atti del 6 Convegno Nazionale ANIDIS, vol. 2, Perugia, 13–15 Ottobre 1993 [in Italian]. p. 815–24.

Beyer K., Bommer J. J. (2007) Selection and Scaling of Real Accelerograms for Bi-Directional Loading: A Review of Current Practice and Code Provisions, Journal of Earthquake Engineering, 11:S1, 13-45,

Biskinis, D. E., Roupakias, G. K. and Fardis, M. N. (2004), Degradation of shear strength of reinforced concrete members with inelastic cyclic displacements. ACI Structural Journal, Vol. 101, No. 6, p. 73-783

Blume JA, Sharpe RL, Elsesser E (1961) A structural dynamic investigation of fifteen school buildings subjected to simulated earthquake motion. Division of Agriculture, Sacramento

Bommer JJ., Acevedo A. (2004) The use of real earthquake accelerograms as input to dynamic analysis Journal of Earthquake Engineering, 8 (1), pp. 43-91

Boore D.M. (2003) Simulation of ground motion using the stochastic method, Pure and Applied Geophysics. 160, 635-676

Borzi B., Pinho R., Crowley H., (2008) Simplified pushover based vulnerability analysis for large-scale assessment of RC buildings. Engineering Structures, 30(3), 804-820.

Bovo M., (2013), Valutazione della risposta sismica di edifici mediante modelli anelastici equivalenti, Ph.D. dissertation, Alma Mater Studiorum, Universiy of Bologna (in Italian)

Bovo M., Savoia M. (2015) Evaluation of seismic response of buildings using dynamic analysis on stick models. COMPDYN 2015, 5th ECCOMAS Thematic Conference on Computational Methods in Structural Dynamics and Earthquake Engineering. M. Papadrakakis, V. Papadopoulos, V. Plevris (eds.) Crete Island, Greece, 25–27 May 2015

Bracci JM, Kunnath SK, Reinhorn AM. (1997) "Seismic performance and retrofit evaluation of reinforced concrete structures." J Struct Eng-Asce;123:3-10.

Braga F., Dolce M., Liberatore D., (1982) A statistical study on damaged buildings and an ensuing review of the MSK-76 scale. Proceedings of the 7th European Conference

Bursi O. S., Dusatti T., Pucinotti R., A Reconnaissance report. (2009) The April 6,2009, L'Aquila Earthquake. Italy, ⟨http://www.reluis.it/doc/pdf/Aquila/Rappor to_fo-tografico_V1.2.pdf⟩.

Caliò I, Greco A, Intelisano M. (2010) "Analisi push-over multi-modali: applica-zione ad un edificio irregolare in c.a." XIV convegno Anidis. Bari, 18-22 settembre (in Italian)

Calvi G.M., 1999. A displacement-based approach for vulnerability evaluation of classes of buildings. Journal of Earthquake Engineering, 3(3), 411-438.

Calvi G.M., Pinho R., Magenes G., Bommer J.J., Restrepo-Veléz L.F., Crowley H., (2006) The development of seismic vulnerability assessment methodologies for variable geographical scales over the past 30 years. ISET Journal of Earthquake Tech-nology, 43(3), 75-104.

Calvi, G.M., & Bolognini, D. (2001). Seismic response of reinforced concrete frames infilled with masonry panels weakly reinforced. Journal of Earthquake Engineer-ing, 5, 153–185.

Cavaleri L, Di Trapani F. (2014) Cyclic response of masonry infilled RC frames: experimental results and simplified modeling. Soil Dyn Earthq Eng;65:224–42.

Cavaleri L, Fossetti M, Papia M. (2005) Infilled frames: developments in the evaluation of cyclic behaviour under lateral loads. Struct Eng Mech 21 (4):469–94.

Ceci A. M., Contento A., Fanale L., Galeota D., Gattulli V., Lepidi M., et al. (2010) Structural performance of the historic and modern buildings of the university of L'Aquila during the seismic events of April 2009, Eng. Struct. 32(7) 1899–1924, http://dx.doi.org/10.1016/j.engstruct.2009.12.023.

Celik OC and Ellingwood BR (2008) Modeling Beam-Column Joints in Fragility Assessment of Gravity Load Designed Reinforced Concrete Frames, Journal of Earth-quake Engineering. 12:357-381.

Ceresa P, Petrini L, Pinho R. (2007) Flexure–shear fibre beam-column elements for modelling frame structures under seismic loading—state of the art. Journal of Earth-quake Engineering 2007; 11(1):46–88

Ceresa P., Petrini L., Pinho R., Sousa R. (2009) A fibre flexure-shear model for seismic analysis of RC-framed structures Earthq Eng Struct Dyn, 38, pp. 565-586

Chopra A. K., (2012) Dynamics of Structures (4th Edition) (Prentice-hall International Series in Civil Engineering and Engineering Mechanics)

Chopra AK, Goel RK, Chintanapakdee C. (2004) "Evaluation of a Modified MPA Procedure Assuming Higher Modes as Elastic to Estimate Seismic Demands." Earthquake Spectra;20:757-78.

Chopra AK, Goel RK. (2002) "A modal pushover analysis procedure for estimating seismic demands for buildings." Earthquake Engineering & Structural Dynamics;31:561-82.

Chopra AK, Goel RK. (2004) "A modal pushover analysis procedure to estimate seismic demands for unsymmetric-plan buildings." Earthquake Engineering & Structural Dynamics; 33:903-27.

Chrysostomou, C. Z. (1991). "Effects of degrading infill walls on the nonlinear seismic response of two-dimensional steel frames." Ph.D. thesis, Cornell Univ., Ithaca, NY.

Colajanni, P., Cacciola, P., Potenzone, B., Spinella, N., Testa, G. (2017) Non linear and linearized combination coefficients for modal pushover analysis. Ingegneria Sismica- International Journal of Earthquake Engineering; 34(3-4), 93-112.

Collepardi M. (1992), Scienza e tecnologia del calcestruzzo, Hoepli, (in Italian).

Cornell CA (2004) Hazard, ground-motions and probabilistic assessment for PBSD. In: Fajfar P, Krawinkler H (eds) Performance based seismic design concepts and implementation, PEER report 2004/05. Pacific Earthquake Engineering Research Center University of California, Berkeley, CA, USA

Cornell, C. A. and Krawinkler, H. (2000) "Progress and challenges in seismic performance assessment," PEER News, April.

Cornell, C. A., Jalayer, F., Hamburger, R. O., and Foutch, D. (2002) "Probabilistic Basis for 2000 SAC Federal Emergency Management Agency Steel Moment Frame Guidelines.", Journal of Structural Engineering.

Cosenza E., Manfredi G., Polese M., Verderame G.M., (2005) A multi-level approach to the capacity assessment of existing RC buildings. Journal of Earthquake Engineering, 9(1), 1-22.

Cosenza, E. and Prota, A. (2006) ''Experimental behavior and numerical modeling of smooth steel bars under compression,'' Journal of Earthquake Engineering 10(19), 313–329.

Crisafulli, F. G. (1997). "Seismic behaviour of reinforced concrete structures with masonry infills." Ph.D. thesis, Univ. of Canterbury, Christchurch, New Zealand.

Crisafulli, F. J. & Carr, A. J. (2007), 'Proposed macro-model for the analysis of infilled frame structures', Bulletin of the New Zealand Society for Earthquake Engineering 40(2), 69–77.

Crisafulli, F. J., Carr, A. J., and Park, R. (2000). "Analytical modelling of infilled frame structures—A general review." Bull. New Zealand Soc. Earthquake Eng., 33(1), 30–47.

Cristofaro MT, Pucinotti R, Tanganelli M, De Stefano M. (2015) The dispersion of concrete compressive strength of existing buildings. In: Cimellaro GP, Nagarajaiah S, Kunnath SK, editors. Geotechnical, Geological and Earthquake Engineering, vol. 33, Cham: Springer International Publishing; 2015, p. 275–85. doi:10.1007/978-3-319-06394-2.

Crowley H., Pinho R., Bommer J.J.,(2004) A probabilistic displacement-based vulnerability assessment procedure for earthquake loss estimation. Bulletin of Earthquake Engineering, 2(2), 173-219.

D. Giardini et al. (2013) Seismic Hazard Harmonization in Europe (SHARE): Online Data Resource. SHARE project website: http://www.efehr.org/en/hazard-data-access/hazard-curves/

Dawe JL, Seah CK. Analysis of concrete masonry infilled steel frames subjected to in-plane loads. In: Proceeding of the 5th Canadian Masonry Symposium, Vancouver; 1989. p. 329–40

De Luca F, Verderame GM (2013) A practice-oriented approach for the assessment of brittle failures in existing RC elements. Eng Struct 48:373–388

De Luca F., Vamvatsikos D., Iervolino I. (2013) Near-optimal piecewise linear fits of static pushover capacity curves for equivalent SDOF analysis. Earthq Eng Struct Dyn, 42(4):523–543.

De Risi M.T., Ricci P., Verderame G.M., Manfredi G. (2016) Experimental assessment of unreinforced exterior beam–column joints with deformed bars Eng Struct, 112, pp. 215-232

De Stefano M, Marino EM, Viti S (2005) Evaluation of second order effects on the seismic response of vertically irregular RC framed structures. In: Proceedings of the 4th European workshop on the seismic behaviour of irregular and complex structures, CD ROM. Thessaloniki, August 2005

De Stefano M, Pintucchi B (2002) A model for analyzing inelastic seismic response of plan-irregular building structures. In: Proceedings of the 15th ASCE engineering mechanics conference, CD ROM. New York, June 2002

De Stefano M, Pintucchi B. (2008) A review of research on seismic behaviour of irregular building structures since 2002. Bull Earthq Eng 6:285–308.

De Stefano M, Tanganelli M, Viti S. (2012)Effect of the variability in plan of concrete mechanical properties on the seismic response of existing RC framed structures. Bulletin of Earthquake Engineering;11:1049–60. doi:10.1007/s10518-012-9412-5.

De Stefano M, Tanganelli M, Viti S. (2013) On the variability of concrete strength as a source of irregularity in elevation for existing RC buildings: A case study. Bulletin of Earthquake Engineering;11:1711–26. doi:10.1007/s10518-013-9463-2.

Decanini L. D., De Sortis A., Goretti A., Liberatore L., Mollaioli F., Bazzurro P., (2004) Performance of reinforced concrete buildings during the 2002 Molise, Italy, earthquake, Earthq. Spectra 20(2004)S221–S255

Del Gaudio C, Ricci P, Verderame GM, Manfredi G (2015) Development and urban-scale application of a simplified method for seismic fragility assessment of RC buildings. Eng Struct 91:40–57

Del Gaudio C. (2015) Seismic fragility assessment of RC buildings at large scale, Ph.D. thesis, University of Naples Federico II

Del Vecchio C., Gentile R., Di Ludovico M., Uva G., Pampanin S. (2018): Implementation and Validation of the Simple Lateral Mechanism Analysis (SLaMA) for the Seismic Performance Assessment of a Damaged Case Study Building, Journal of Earthquake Engineering, in press

De-la-Colina J (2003) Assessment of design recommendations for torsionally unbalanced multistorey buildings. Earthq Spectra 19:47–66

De-La-Colina J. In-plane floor flexibility effects on torsionally unbalanced systems. Journal of Earthquake Engineering and Structural Dynamics 1999; 28:1705–1715.

Di Pasquale G., Orsini G., Romero R.W., (2005) New developments in seismic risk assessment in Italy. Bulletin of Earthquake Engineering, 3(1), 101-128.

Dolce M., Lorusso V.D., Masi A. (1994) Seismic response of building structures with flexible inelastic diaphragm, Struct. Des. Tall Build. 3 87–106

Dolce M., Masi A., Marino M., Vona M., (2003) Earthquake damage scenarios of the building stock of Potenza (southern Italy) including site effects. Bulletin of Earthquake Engineering, 1(1), 115-140.

Dolce, M. & Di Bucci, D. (2017) Comparing recent Italian earthquakes. Bull Earthquake Eng 15: 497.

Dolce, M. & Goretti, A. (2015) Building damage assessment after the 2009 Abruzzi earthquake. Bull Earthquake Eng 13: 2241.

Dolšek, M., Fajfar, P. (2001). Soft storey effects in uniformly infilled reinforced concrete frames. Earthquake Engineering, 5(1), 1-12.

Dolšek, M., Fajfar, P. (2004). Inelastic spectra for infilled reinforced concrete frames. Earthquake Engineering and Structural Dynamics, 33(15), 1395-1416.

Dolšek, M., Fajfar, P. (2008a). The effect of masonry infills on the seismic response of a fourstorey reinforced concrete frame – a deterministic assessment. Engineering Structures, 30(7), 1991-2001.

Dolšek, M., Fajfar, P. (2008b). The effect of masonry infills on the seismic response of a fourstorey reinforced concrete frame – a probabilistic assessment. Engineering Structures, 30(11), 3186-3192

Doudoumis IN, Athanatopoulou AM (2001) Code provisions and analytical modelling for the in-plane flexibility of floor diaphragms in building structures. J Earthq Eng 5:565–594

Dutta SC, Das PK (2002a) Inelastic seismic response of code-designed reinforced concrete asymmetric buildings with strength degradation. Eng Struct 24:1295–1314

Dutta SC, Das PK (2002b) Validity and applicability of two simple hysteresis models to assess progressive seismic damage in R/C asymmetric buildings. J Sound Vibrat 257:753–777

Eivani H, Moghadam AS, Aziminejad A, Nekooei M, Seismic Response of Plan-Asymmetric Structures with Diaphragm Flexibility, Shock and Vibration Volume 2018, Article ID 4149212, 18 pages

El-Dakhakhni, W. W., Elgaaly, M., and Hamid, A. A. (2003). "Three-strut model for concrete masonry-infilled frames." J. Struct. Eng., 129(2), 177–185.

Elnashai AS. (2001) "Advanced inelastic static (pushover) analysis for earthquake applications." Structural Engineering and Mechanics;12:51-69.

Elwood K.J., Moehle J.P. (2005) Axial capacity model for shear-damaged columns ACI Structural Journal, 102 (4), pp. 578-587

Elwood, K. J. (2004): Modelling failures in existing reinforced concrete columns. Canadian Journal of Civil Engineering 31.5 846-859.

Elwood, K.J. and Moehle, J.P. (2005) Drift capacity of reinforced concrete columns with light transverse reinforcement, Earthquake Spectra, Vol. 12, No. 1, pp. 71–89.

EN 1998-3 (2005) Eurocode 8: Design of structures for earthquake resistance - Part 3: Assessment and retrofitting of buildings.

Faccioli E., Pessina V., Calvi G.M., Borzi B., (1999) A study on damage scenarios for residential buildings in Catania city. Journal of Seismology, 3(3), 327-343.

Fajfar P, Gaspersic P. (1996) The N2 method for the seismic damage analysis of RC buildings. Earthq Eng Struct Dyn ; 25(1):31–46.

Fajfar P, Marusic D, Perus I. (2005) The extension of N2 method to asymmetric buildings. Proceedings of the 4th European workshop on the seismic behaviour of irregular and complex structures, Thessaloniki. 2005.

Fajfar P. (2000) A nonlinear analysis method for performance-based seismic design. Earthquake Spectra, 16:573–92.

Fardis MN (2007) LESSLOSS—risk mitigation for earthquakes and landslides. Guidelines for displacement-based design of buildings and bridges. Report No. 5/2007. IUSS Press, Pavia

Fardis, M. N., and Panagiotakos, T. B. (1997). "Seismic design and response of bare and masonry-infilled reinforced concrete buildings. Part II: Infilled structures." J. Earthquake Eng., 1(3), 475–503.

Fayfar P., Fischinger M. (1989) "N2 - A method for non-linear seismic analysis of regular buildings". Proc. 9th World Conference on Earthquake Engineering. Tokyo-Kyoto, Japan. Vol. 5, pp. 111-116.

FEMA 356 (2000) FEMA 356 Prestandard and Commentary for the Seismic Rehabilitation of Building.

FEMA 440 "Improvement of Nonlinear Static Seismic Analysis Procedures" Federal Emergency Management Agency. Washington, D.C., June 2005.

FEMA P695 (2009) Quantification of building seismic performance factors.

FEMA, (2001) HAZUS99 Technical Manual. Service Release 2. Federal Emergency Management Agency, Washington, D.C., USA.

Ferraioli, M. (2017) Multi-mode pushover procedure for deformation demand estimates of steel moment-resisting frames. International Journal of Steel Structures; 17(2), 653-676.

Ferraioli, M., Lavino, A. and Mandara, A. (2016) An adaptive capacity spectrum method for estimating seismic response of steel moment-resisting frames, Ingegneria Sismica - International Journal of Earthquake Engineering; 1-2, 47-60.

Fiore A, Porco F, Uva G, Mezzina M. (2013) On the dispersion of data collected by in situ diagnostic of the existing concrete. Construction and Building Materials;47:208–17. doi:10.1016/j.conbuildmat.2013.05.001.

Fiore, A., Uva, G. (2013). Effects of "reinforced" infilled frames on existing RC buildings. ECCOMAS Thematic Conference - COMPDYN 2013: 4th International Conference on Computational Methods in Structural Dynamics and Earthquake Engineering, Proceedings - An IACM Special Interest Conference, pp. 4213-4225.

Flanagan, R. D., and Bennett, R. M. (2001). "In-plane analysis of masonry infill materials." Pract. Period. Struct. Des. Constr., 6(4), 176–182.

Fleischman RB, Farrow KT (2001) Dynamic behavior of perimeter lateral-system structures with flexible diaphragms. J Earthq Eng Struct Dyn 30:745–763

Fleischman RB, Farrow KT, Eastman K (2001) Seismic performance of perimeter lateral system structures with highly flexible diaphragms. Earthq Spectra 18:251–286

Fragiadakis M, Vamvatsikos D, Papadrakakis M (2005) Evaluation of the influence of vertical stiffness irregularities on the seismic response of a 9-story steel frame. In: Proceedings of the 4th European workshop on the seismic behaviour of irregular and complex structures, CD ROM. Thessaloniki, August 2005

Franchin P., Pinto P.E., Rajeev P., (2010) Confidence factor? J Earthquake Eng, 14 (7), pp. 989-1007

Gasparini D. A., Vanmarcke E. H. (1976) Simulated earthquake motions compatible with prescribed response spectra, Dept of Civil Engineering, Research Report R76-4, Massachusetts Institute of Technology, Cambridge, Massachusetts.

Gavin, H. P. and Yau, S. C. (2008) "High-order limit state functions in the response surface method for structural reliability analysis," Structural Safety, 30(2): 162-179

Gentile R., Uva G., Pampanin S. (2018) Mechanical Interpretation of Infills-to-Frame Interaction: Contributions to the Global Base Shear for Strut-Based Models, 16th European Conference on Earthquake Engineering (16ECEE), Thessaloniki, Greece, in June 18-21, 2018.

Gentile, R. (2017) "Extension, refinement and validation of the Simple Lateral Mechanism Analysis (SLaMA) for the seismic assessment of RC structures, Ph.D. thesis, Polytechnic University of Bari, Bari, Italy.

Giannini R, Sguerri L, Paolacci F, Alessandri S. (2014) Assessment of concrete strength combining direct and NDT measures via Bayesian inference. Engineering Structures 2014;64:68–77. doi:10.1016/j.engstruct..01.036.

Gidaris I, Taflanidis A. A. (2013) Parsimonious modeling of hysteretic structural response in earthquake engineering: calibration/validation and implementation in probabilistic risk assessment. Eng Struct 49:1017–1033

Gidaris I. (2015) Risk assessment and optimal design of seismic protective systems through surrogate and reduced ordered modelling" Ph.D. dissertation, Graduate School of the University of Notre Dame

Gidaris I., Taflanidis A.A., (2015) Optimal Design of Floor Isolation Systems subject to Multiple Reliability Criteria utilizing Kriging Surrogate Modeling", in Y. Tsompanakis, J. Kruis, B.H.V. Topping, (Editors), "Proceedings of the Fourth International Conference on Soft Computing Technology in Civil, Structural and Environmental Engineering", Civil-Comp Press, Stirlingshire, UK, Paper 25

Gidaris I., Taflanidis A.A., Mavroeidis G.P. (2015) Kriging metamodeling in seismic risk assessment based on stochastic ground motion Earthq. Eng. Struct. Dyn, 44(14): 2377-2399

Giordano F., Rasulo A., Zambrano A., (2009). Rapporto dei danni osservati su alcuni edifici industriali a seguito del terremoto abruzzese del 6/04/2009 (inItalian), ⟨http://www.reluis.it/doc/pdf/Aquila/Rapporto_edifici_prefab-GRVZ.pdf⟩.

Giovinazzi S., (2005) The vulnerability assessment and the damage scenario in seismic risk analysis. PhD thesis, Technical University Carolo-Wilhelmina, Braunschweig and University of Florence, Italy

Giuffre`, A. and Pinto, P. E. (1970) ''Il comportamento del cemento armato per sollecitazioni cicliche di forte intensità, Giornale del Genio Civile

Goel RK, Chopra AK. (2005) "Role of Higher-"Mode" Pushover Analyses in Seismic Analysis of Buildings." Earthquake Spectra;21:1027-41.

Goldberg JE (1967) Analysis of multi-story buildings considering shear wall and floor deformations Tall buildings. Pergamon Press Long, Island City, pp 349–373

Goulet, C. A., Haselton, C. B., et al. (2007) "Evaluation of the seismic performance of code-conforming reinforced-concrete frame building-From seismic hazard to collapse safety and economic losses," Earthquake Engineering and Structural Dynamics, 36(13): 1973-1997.

Greek Seismic Code (2000) Earthquake resistant design of structures. Earthquake Planning and Protection Organization, Athens

Grünthal G., (1998) Cahiers du Centre Européen de Géodynamique et de Séismologie: Volume 15 – European Macroseismic Scale 1998. European Center for Geodynamics and Seismology, Luxembourg.

Gulkan P., Sozen M. A. (1974) "Inelastic responses of reinforced concrete structure to earthquake motions". ACI Structural Journal. Vol. 71, No. 12, pp. 604-610.

Günay S. & Mosalam K. M. (2013) PEER Performance-Based Earthquake Engineering Methodology, Revisited, Journal of Earthquake Engineering, 17:6, 829-858

Gupta B, Kunnath S. K. (2000) "Adaptive spectra-based pushover procedure for seismic evaluation of structures". Earthquake Spectra. Vol. 16, No. 2, pp. 367-392.

H. Sezen, J.P. Moehle (2004) Shear strength model for lightly reinforced concrete columns ASCE J Struct Eng, 130 (11), pp. 1692-1703

Hanckock j., Bommer J. J., Stafford P. J. (2008) Numbers of scaled and matched accelerograms required for inelastic dynamic analyses Earthquake Engng Struct. Dyn.; 37:1585–1607

Haselton, C. B., and Deierlein, G. G., (2007). Assessing Seismic Collapse Safety of Modern Reinforced Concrete Moment Frame Buildings, Pacific Earthquake Engineering Research Center Technical Report 2007/08, Berkeley, CA

Hassan A.F., Sozen M.A., (1997) Seismic vulnerability assessment of low-rise buildings in regions with infrequent earthquakes. ACI Structural Journal, 94(1), 31-39.

Hassan WM (2011) Analytical and Experimental Assessment of Seismic Vulnerability of Beam-Column Joints without Transverse Reinforcement in Concrete Buildings, PhD Dissertation, University of California, Berkeley, California, USA.

Hernández-Montes E, Kwon O-S, Aschheim Ma. (2004) "An Energy-Based Formulation For First- And Multiple-Mode Nonlinear Static (Pushover) Analyses." Journal of Earthquake Engineering; 08:69-88.

Holmes, M. (1961). Steel frames with brickwork and concrete infilling. ICE Proc., 19(4), 473–478. Stafford Smith B. Behaviour of square infilled frames. J Struct Div 1966;92(1):381–403.

Ibarra, L.F., Medina, R.A., and Krawinkler, H. (2005). "Hysteretic models that incorporate strength and stiffness deterioration," Earthquake Engineering and Structural Dynamics, Vol. 34, pp. 1489-1511.

Iervolino I, Cornell CA (2005) Record selection for nonlinear seismic analysis of structures. Earthq Spectra 21(3):685–713

Iervolino I, Maddaloni G, Cosenza E (2008) Eurocode 8 compliant real record sets for seismic analysis of structures. J Earthq Eng 12(1):54–90

Iervolino, I. , Baltzopoulos, G. , Vamvatsikos, D. (2016) SPO2FRAG V1.0: Software for pushover-based derivation of seismic fragility curves; ECCOMAS Congress 2016 - Proceedings of the 7th European Congress on Computational Methods in Applied Sciences and Engineering

Iervolino, I., Galasso, C. and Cosenza (2010) E. REXEL: computer aided record selection for code-based seismic structural analysis. Bulletin of Earthquake Engineering, 8: 339–362.

INNOSEIS Project (2017) Valorization of innovative anti-seismic devices. Recommended procedure for EN1998-compatible behaviour factor evaluation of new structural systems. INNOSEIS project website: http://innoseis.ntua.gr/deliverables.php?deliverable=records

International Building Code (IBC) (2009) International Code Council, Country Club Hills

Iranian Code of Practice for Seismic Resistant Design of Buildings (2007) Standard no 2800-05 3rd Edition

ISTAT (2001) 14° Censimento generale della popolazione e delle abitazioni. dawincilstat.it.

ISTAT (2011) 15° Censimento generale della popolazione e delle abitazioni. da-winciIstat.it.

Jalayer, F. (2003) Direct Probabilistic Seismic Analysis: Implementing Non-linear Dynamic Assessments. Ph.D. dissertation, Dept. of Civil and Environmental Engineering, Stanford Univ., Stanford, CA.

Jalayer, F., and Cornell, C. A. (2009). "Alternative non-linear demand estimation methods for probability-based seismic assessments." Earthquake Engineering & Structural Dynamics, 38(8), 951–972.

Jalayer, F., Cornell, C.A. (2003): «A Technical Framework for Probability-Based Demand and Capacity Factor Design (DCFD) Seismic Formats», PEER Report.

Jalayer, F., Iervolino, I. and Manfredi, G. (2008) Structural modeling uncertainties and their influence on seismic assessment of existing RC structures. Structural Safety, 32(3): 220–228.

JBDPA, (1990) Standard for seismic capacity assessment of existing reinforced concrete buildings. Japanese Building Disaster Prevention Association, Ministry of Construction, Tokyo, Japan.

Ju SH, Lin MC (1999) Comparison of building analyses assuming rigid or flexible floors. J Struct Eng ASCE 125:25–39

Kaatsız, K. and Sucuoğlu, H. (2014) Generalized force vectors for multi-mode pushover analysis of torsionally coupled systems, Earthquake Engng Struct. Dyn.; 43: 2015–2033.

Kadir MRA. (1974) The structural behaviour of masonry infill panels in framed structures. PhD Thesis, University of Edinburgh;

Kappos, A. (2000). Feasibility of using advanced analytical tools in the seismic design of R/C structures. Penelis International Symposium on Concrete and Masonry Structures October, Thessaloniki, Greece.

Kappos, A.J., Stylianidis, K.C. and Michailidis, C.N. (1998). Analytical models for brick masonry infilled r/c frames under lateral loading. Journal of Earthquake Engineering, 2(1), pp. 59–87.

Kazantzi, A. K., and Vamvatsikos, D., (2015) Intensity measure selection for vulnerability studies of building classes. Earthquake engineering and structural dynamics; 44:2677–2694

Kent D. C., Park, R. (1973). "Cyclic load behavior of reinforcing steel". Strain. An International Journal for Experimental Mechanics. Vol. 9, No. 3, 98-103.

Khajehdehi R, Panahshahi N (2016) Effect of openings on in-plane structural behavior of reinforced concrete floor slabs. J Build Eng 7:1–11

Kilar V., Fajfar P. (1997) "Simple push-over analysis of asymmetric buildings". Earthquake Engineering and Structural Dynamics. Vol. 26, No. 2, pp. 233-249.

Kim S., D'Amore E. (1999) "Push-over Analysis Procedure in Earthquake Engineering". Earthquake Spectra. Vol. 15, No. 3, pp. 417-434.

Kim, J., and LaFave, J. M.(2007). Key influence parameters for the joint shear behavior of reinforced concrete (RC) beam-column connections, Engineering Structures 29, 2523–2539.

Kim, J., LaFave, J. M., and Song, J. (2007) A new statistical approach for joint shear strength determination of RC beam-column connections subjected to lateral earthquake loading, Structural Engineering and Mechanics 27, 439–456.

King, D. J., Priestley, M. J. N. & Park, R. (1986), Computer programs for concrete column design, Research Report 86/12, Technical report, University of Canterbury, New Zealand, Department of Civil Engineering.

Klingner RE, Bertero VV. (1976) Infilled frames in earthquake-resistant construction. Report EERC 76-32. Earthquake Engineering Research Center;

Krawinkler H., Seneviratna G. D. P. K. (1998) "Pros and cons of a pushover analysis of seismic performance evaluation". Engineering Structures. Vol. 20, No. 4-6, pp. 452-464.

Kreslin, M. and Fajfar, P. (2012) The extended N2 method considering higher mode effects in both plan and elevation, Bulletin of Earthquake Engineering; 10(2), 695–715.

Kunnath S, Panahshahi N, Reinhorn A (1991) Seismic response of RC buildings with inelastic floor diaphragms. J Struct Eng ASCE 117:1218–1237

Kunnath SK. (2004) "Identification of Modal Combinations for Nonlinear Static Analysis of Building Structures." Computer-Aided Civil and Infrastructure Engineering; 19:246-59.

Lagaros ND, Fragiadakis M. (2007) Fragility assessment of steel frames using neural networks. Earthq Spectra; 23:735–52.

Lai M., Zhang Y. L., Zhang C. (1992) "Analysis method of multi-rigid-body model for earthquake responses of shear-type structure". Proc. 10th World Conference on Earthquake Engineering. Madrid, Spain

LeBorgne M. R., Ghannoum W. M. (2014) Analytical Element for Simulating Lateral-Strength Degradation in Reinforced Concrete Columns and Other Frame Members. Journal of Structural Engineering. Vol. 140, Issue 7 (July 2014)

Lee HJ, Aschheim MA, Kuchma D. (2007) Interstorey drift estimates for low-rise diaphragm structures. Journal of Engineering Structures; 29:1375–1397.

Lee, D.H. and Elnashai, A.S. (2001) Seismic analysis of RC bridge columns with flexure-shear interaction, ASCE Journal of Structural Engineering, Vol. 127, No. 5, pp. 546–553.

Liberatore L., Sorrentino L., Liberatore D., Decanini L. D. (2013) Failure of industrial structures induced by the Emilia (Italy) 2012 earthquakes, Eng. Fail. Anal. 34 629–647, http://dx.doi.org/10.1016/j.engfailanal.2013.02.009.

Lowes LN and Altoontash A. (2003) Modeling Reinforced-Concrete Beam-Column Joints Subjected to Cyclic Loading, Journal of Structural Engineering. 129:1686-1697.

Luco N, Cornell CA. (2007) Structure-specific scalar intensity measures for near-source and ordinary earthquake ground motions. Earthquake Spectra; 23(2): 357–392.

Luco N, Mori Y, Funahashi Y, Cornell CA, Nakashima M. Evaluation of predictors of nonlinear seismic demands using 'fishbone' models of SMRF buildings. Earthquake Engineering and Structural Dynamics 2003; 32(14): 2267–2288.

Mackie, K., and Stojadinovic, B. (2001). "Probabilistic Seismic Demand Model for California Highway Bridges." Journal of Bridge Engineering, 6(6), 468–481.

Maffei J., Bazzurro P. (Eds.), Special Issue on the 2002 Molise, Italy earthquake, Earthq. Spectra, 20 (S1) (2004) 358

Magliulo G, Ramasco R (2008) Seismic performance of R/C frameswith regular and irregular strength vertical distributions. In: Proceedings of the 14th world conference on earthquake engineering, Bejing, China, Mira Digital Publishing, St. Louis, USA, paper No. 08-02-0079

Magliulo G, Ramasco R, Capozzi V (2012) Seismic performance of R/C frames with overstrength discontinuities in elevation. Bull Earthq Eng 10:679–694

Magliulo G, Ramasco R, Realfonzo R (2002) A critical review of seismic code provisions for vertically irregular frames. In: Proceedings of the third European workshop on the seismic behaviour of irregular and complex structures, CD ROM. Florence, September 2002

Mainstone RJ. On the stiffness and strength of infilled frames. Proc Inst Civil Eng, Suppl (IV) – Lond 1971;Paper 7360S:57–89.

Manfredi G., Masi A., Pinho R., Verderame G., Vona M. (2007) Valutazione degli edifici esistenti in Cemento Armato (in Italian), IUSSPress, Pavia.

Masi A, Chiauzzi L. (2013) An experimental study on the within-member variability of in situ concrete strength in RC building structures. Construction and Building Materials;47:951–61. doi:10.1016/j.conbuildmat.2013.05.102.

Masi A, Digrisolo A, Santarsiero G. (2014) Concrete Strength Variability in Italian RC Buildings: Analysis of a Large DataBase of Core Tests. Applied Mechanics and Materials;597:283–90.

Masi A. (2005) The estimation of in situ concrete strength through destructive and non-destructive tests (in Italian). Il Giornale Delle Prove Non Distruttive Monitoraggio Diagnostica (In Italian);1:1–9.

Masi A. (2003) Seismic vulnerability assessment of Gravity Load Designed R/C frames. Bulletin of Earthquake Engineering, 1(3), 371-395.

Masi A., Santarsiero G., Nigro D. (2013) Cyclic Tests on External RC Beam-Column Joints: Role of Seismic Design Level and Axial Load Value on the Ultimate Capacity, Journal of Earthquake Engineering, 17:1, 110-136

Masi A., Chiauzzi L., Manfredi V. (2016) Criteria for identifying concrete homogeneous areas for the estimation of in-situ strength in RC buildings Constr. Build. Mater., 121, pp. 576-587

Masi, A., Chiauzzi, L., Santarsiero, G. et al. (2017) Seismic response of RC buildings during the Mw 6.0 August 24, 2016 Central Italy earthquake: the Amatrice case study. Bull Earthquake Eng.

McKenna F. (2011) OpenSees: a framework for earthquake engineering simulation. Comput Sci Eng;13:58–66.

Melo J, Fernandes C, Varum H, Rodrigues H, Costa A, Are'de A (2011) Numerical modelling of the cyclic behaviour of RC elements built with plain reinforcing bars. Eng Struct 33(2):273–286. doi:10.1016/j.engstruct.2010.11.005

Melo, J.; Rossetto, T.; Varum, H. (2015) Experimental study of bond–slip in RC structural elements with plain bars. Mater. Struct. 2015, 48, 2367–2381.

Menegotto M., Pinto P.E. (1973) "Method of analysis for cyclically loaded R.C. plane frames including changes in geometry and non-elastic behavior of element under combined normal force and bending". Proc. IABSE Symp. of Resistance and Ultimate Deformability of Structures Acted on by Well-Defined Repeated Loads. International Association of Bridge and Structural Engineering. pp.15-22. Lisbon, Portugal.

Menegotto, M. and Pinto, P. E. (1973) ''Method of analysis for cyclically loaded reinforced concrete frames including changes in geometry and non-elastic behaviour of elements under combined normal forces and bending moment,'' IASBE Proceedings, Lisbon

Mergos PE, Kappos AJ (2008) A distributed shear and flexural flexibility model with shear-flexure interaction for R/C members subjected to seismic loading. Earthq Eng Struct Dyn 37: 1349–1370

Miano A, Jalayer F, Ebrahimian H, Prota A. (2017) Cloud to IDA: Efficient fragility assessment with limited scaling. Earthquake Engng Struct Dyn; 1-24

Miranda E. (1991) "Seismic Evaluation and Upgrading of Existing Buildings". Ph. D. Thesis. University of California. Berkeley, California.

Miranda E., Bertero V. V. (1994) "Evaluation of Strength Reduction Factors for Earthquake-Resistant Design". Earthquake Spectra. Vol. 10, No. 2, pp. 357-379.

Miranda E., Ruiz-Garcia J. (2002) "Evaluation of approximate methods to estimate maximum inelastic displacement demands". Earthquake Engineering and Structural Dynamics. Vol. 31, No. 3, pp. 539-560.

Miranda, E. (2001). Estimation of inelastic deformation demands of SDOF systems, ASCE Journal of Structural Engineering, 127(9): 1005–1012.

Moehle, J., and Deierlein, G.G. (2004). 'A framework methodology for performance based earthquake engineering.' Proc., 13th World Conf. on Earthquake Engineering CD-ROM, Canadian Association for Earthquake Engineering, Vancouver, Canada.

Moeni M., Rafezy B. (2011) Investigation into the floor diaphragms flexibility in reinforced concrete structures and code provision, Glob. J. Res. Eng. 11 (1) 25–35

Moghadham S.A., Tso W. K., (2002) "A pushover procedure for tall buildings." In: Ltd. ES, editor. 12thEuropean Conference on Earthquake Engineering: Paper 395.

Mola, E., Negro, P. and Pinto, A., (2004), "Evaluation of current approaches for the analysis and design of multi-story torsionally unbalanced frames", Proceedings of the 13th World Conference, Earthq. Eng.

Monti, G. and Nuti, C. (1992) ''Nonlinear Cyclic behaviour of reinforcing bars Including buckling,'' Journal of Structural Engineering 118(12), 3268–3285

Mori Y, Yamanaka T, Luco N, Nakashima M, Cornell CA. Predictors of seismic demand of SMRF buildings considering post-elastic mode shape. 13th World Conference on Earthquake Engineering. 2004a. Vancouver, Canada, 15.

Mori Y., Yamanaka T., Luco N., Allin Cornell C., A static predictor of seismic demand on frames based on a post-elastic deflected shape. Earthquake Engineering and Structural Dynamics 2006b; 35:1295–1318

Mouroux P., Le Brun B., (2006) Presentation of RISK-UE project. Bulletin of Earthquake Engineering, 4(4), 323-339.

Mwafy A.M. and Elnashai S.A. (2000) Static pushover versus dynamic-to-collapse analysis of RC buildings, Engineering Seismology and Earthquake Engineering

Section, Imperial College of Science, Technology and Medicine. Report No. 00/1, January.

Mwafy AM and Elnashai AM (2008) Importance of shear assessment of concrete structures detailed to different capacity design requirements. Engineering Structures 30(6): 1590–1604.

Myslimaj B, Tso WK (2005) A design-oriented approach to strength distribution in single story asymmetric systems with elements having strength-dependent stiffness. Earthq Spectra 21:197–212

Nakashima M, Ogawa K, Inoue K. (2002) Generic frame model for simulation of earthquake responses of steel moment frames. Earthquake Engineering and Structural Dynamics; 31(3):671– 692.

Negro, P., Colombo, A. (1997). Irregularities induced by nonstructural masonry panels in framed buildings. Engineering Structures, 19(7), 576-85.

New Zealand Standard (NZS) 1170.5 Supp 1:2004 (2004) Structural Design Actions. Part 5: Earthquake actions New Zealand—Commentary, Standards New Zealand, Wellington

NTC08 (2008) Nuove norme tecniche per le costruzioni. D.M. Infrastrutture

Ozdemir P., Boduroglu M.H., Ilki A., (2005) Seismic safety screening method. Proceedings of the International Workshop on Seismic Performance Assessment and Rehabilitation of Existing Buildings (SPEAR), Ispra, Italy, April 4-5. Paper No. 23.

Padgett, J. E., and DesRoches, R. (2008). "Methodology for the development of analytical fragility curves for retrofitted bridges." Earthquake Engineering & Structural Dynamics, 37(8), 1157–1174.

Pampanin, S., Calvi, G. M. & Moratti, M. (2002), Seismic behaviour of R.C. Beam-column joints designed for gravity loads, in '12th European Conference on Earthquake Engineering', Vol. 726.

Pampanin, S., Magenes, G., and Carr, A. (2003). "Modelling of shear hinge mechanism in poorly detailed RC beam-column joints." Proc. FIB Symp. Concrete Structures in Seismic Regions, Federation International du Beton, Athens, Paper No. 171

Panagiotakos TB, Fardis MN. (1996)Seismic response of infilled RC frames structures. In: Proceedings of 11th world conference on earthquake engineering. Acapulco; 1996 [Paper No. 225]

Panagiotakos, T. B. & Fardis, M. N. (2001), 'Deformation of RC members at yielding and ultimate', ACI Structural Journal 2(98), 135–148.

Panagiotakos, T. B. and Fardis, M. N. (1994) "Proposed nonlinear strut models for infill panels," 1st year progress report of PREC8 project. Univ. of Patras, Patras

Papanikolaou V.K., Elnashai A.S. and Pareja J.F. (2006) Evaluation of conventional and adaptive pushover analysis, Journal of Earthquake Engineering, Vol. 10, No. 1, pp. 127-132.

Papia M, Cavaleri L, Fossetti M. (2003) Infilled frames: developments in the evaluation of the stiffening effect of infills. Structural engineering and mechanics, vol. 16. Korea: Techno Press;

Paret T.F., Sasaki, K.K., Elibeck, D.H., Freeman, S.A. (1996) "Approximate inelastic procedures to identify failure mechanism from higer mode effects." Proceedings of the 11thWorld Conference on Earthquake Engineering. Acapulco, Mexico.

Park R, Priestley MJN, Gill WD (1982) Ductility of square-confined concrete columns. J Struct Div ASCE 108(ST4):929–950

Park S and Mosalam KM (2013) Simulation of Reinforced Concrete Frames with Non ductile Beam-Column Joints, Earthquake Spectra, 29(1), 233-257.

Park S and Mosalam KM, (2012) Parameters for shear strength prediction of exterior beam–column joints without transverse reinforcement. Engineering Structures, 36, 198–209.

Paulay T (2002) An estimation of displacement limits for ductile systems. Earthq Eng Struct Dyn 31:583–599

Paulay T, Priestley MJN (1992) Seismic design of reinforced concrete and masonry buildings. Wiley, New York

Paulay, T. (1998), 'Torsional mechanisms in ductile building systems', Earthquake Engineering & Structural Dynamics 27(May 1998), 1101–1121.

Paulay, T. (2001), 'Some design principles relevant to torsional phenomena in ductile buildings', Journal of Earthquake Engineering 5(3), 273–308.

Pecce M., Ceroni F., Maddaloni G., Innuzzella V. (2017) Assessment of the in-plane deformability of RC floors with traditional and innovative lightening elements in RC framed and wall structures, Bull. Earthq. Eng., 15: 3125-3149

Penelis GG, Kappos AJ. (1997) Earthquake-resistant concrete structures. London: E & FN Spon.

Peruš I, Fajfar P (2005) On the inelastic torsional response of single-storey structures under bi-axial excitation. Earthq Eng Struct Dyn 34:931–941

Perus I, Poljansek K, Fajfar P (2006) Flexural deformation capacity of rectangular RC columns determined by the CAE method. Earthq Eng Struct Dyn 35(12):1453–1470

Petrini L., Pinho R., Calvi G.M. (2007) Criteri di Progettazione Antisismica degli Edifici, IUSS Press, ISBN: 88-7358-039-4

Pettinga D, Pampanin S, Christopoulos C, Priestley MJN (2005) Effects of irregularities on the residual displacements of structures subjected to inelastic torsional response. In: Proceedings of the 4th European workshop on the seismic behaviour of irregular and complex structures, CD ROM. Thessaloniki, August 2005

Pincheira, J.A., Dotwiala, F.S., and D'Souza J.T. (1999) Seismic analysis of older reinforced concrete columns, Earthquake Spectra, Vol. 15, No. 2, pp. 245–272.

Polyakov, S. V. (1960). On the interaction between masonry filler walls and enclosing frame when loading in the plane of the wall. Translation in earthquake engineering, Earthquake Engineering Research Institute (EERI), San Francisco, 36–42.

Porco F, Uva G, Fiore A, Mezzina M. (2014) Assessment of concrete degradation in existing structures: a practical procedure. Struct Eng Mech;52(4):701–21.

Porco F., Ruggieri S., Raffaele D. (2017) Influence of rigid floor assumption in seismic analysis of RC existing buildings, COMPDYN 2017 - Proceedings of the 6th International Conference on Computational Methods in Structural Dynamics and Earthquake Engineering, 2, pp. 3439–3449.

Porco F., Ruggieri S., Uva G., (2018) Seismic assessment of irregular existing building: appraisal of the influence of compressive strength variation by means of non-linear conventional and multimodal static analysis, Ingegneria Sismica, 35(3), pp. 64-86

Porco, F., Fiore, A., Uva, G., Raffaele, D. (2014). The influence of infilled panels in retrofitting interventions of existing reinforced concrete buildings: a case study. Structure and Infrastructure Engineering, 11 (2), pp.162-175

Porter KA. (2003) An Overview of PEER's Performance-Based Earthquake Engineering Methodology. 9th International Conference on Applications of Statistics and Probability in Civil Engineering; 273: 973-980.

Porter, K., (2018). A Beginner's Guide to Fragility, Vulnerability, and Risk. University of Colorado Boulder, 110 pp., http://spot.colorado.edu/~porterka/Porter-beginnersguide.pdf

Poursha M, Khoshnoudian F, Moghadam AS. (2009) A consecutive modal pushover procedure for estimating the seismic demands of tall buildings. Engineering Structures.31:591-9.

Priestley M.J.N., Verma R., Xiao Y. (1994) Seismic shear strength of reinforced concrete columns J Struct Div ASCE, 120 (8) , pp. 2310-2329

Priestley MJN, Park R (1987) Strength and ductility of concrete bridge columns under seismic loading. ACI Struct J 84(1):61–76

Priestley, M. (1997), 'Displacement-based seismic assessment of reinforced concrete buildings', Journal of Earthquake Engineering 1(1), 157–192.

Prota A., de Cicco F., Cosenza E. (2009) Cyclic behavior of smooth steel reinforcing bars: experimental analysis and modeling issues, Journal of Earthquake Engineering, 13:4, 500-519, DOI: 10.1080/13632460902837686

Pucinotti R. (2013) Assessment of in situ characteristic concrete strength. Construction and Building Materials;44:63–73. doi:10.1016/j.conbuildmat.2013.02.041.

Pujol, S., Ramirez, J.A., and Sozen, M.A. (1999) Drift capacity of reinforced concrete columns subjected to cyclic shear reversals, Seismic Response of Concrete Bridges, SP-187, American Concrete Institute, Farmington Hills, MI, pp. 255–274.

Qi X., Moehle J. P. (1991) "Displacement design approach for reinforced concrete structures subjected to earthquakes". UCB/EERC Report 91/02. Earthquake Engineering Research Center, University of California. Berkeley, California.

Quagliarini E, Clementi F, Maracchini G, Monni F. (2016) Experimental assessment of concrete compressive strength in old existing RC buildings: A possible way to reduce the dispersion of DT results. Journal of Building Engineering;8:162–71. doi:10.1016/j.jobe.2016.10.008.

R.K. Dowell, F. Seible, E.L. Wilson (1998) Pivot Hysteresis model for reinforced concrete members Struct J (ACI), 95 (5) , pp. 607-617

Reinhorn AM, Kusumastuti D, Rutenberg A (2005) Seismic response of irregular frame structures near collapse: experimental and analytical investigation. In: Proceedings of the 4th European workshop on the seismic behaviour of irregular and complex structures, CD ROM. Thessaloniki, August 2005

Requena M, Ayala G. (2000) "Evaluation of a simplified method for the determination of the non-linear seismic response of RC frames." World Conference on Earthquake Engineering. Auckland.

Ricci P., De Luca F., Verderame G. M. (2011) 6th April 2009 L'Aquila earthquake, Italy: reinforced concrete building performance, Bull. Earthq. Eng. 9(1) 285–305, http://dx.doi.org/10.1007/s10518-010-9204-8.

Ricci P., De Risi M.T., Verderame G.M., Manfredi G. (2016) Experimental tests of unreinforced exterior beam–column joints with plain bars Eng Struct, 118 , pp. 178-194

Ritter W. (1899) Die Bauweise Hennebique Schweizerische Bauzeitung (Zurich), 33 (7), pp. 59-61

Romão X, Costa A, Delgado R (2004) Seismic behaviour of reinforced concrete frames with setbacks. In: Proceedings of the 13th World conference on earthquake engineering, CD ROM. Vancouver, August 2004

Rossetto T (2002) Prediction of deformation capacity of non-seismically designed reinforced concrete members. In: Proceedings of the 7th U.S. national conference on earthquake engineering, Boston, July 21–25

Rossetto T., Elnashai A., (2005) A new analytical procedure for the derivation of displacement-based vulnerability curves for populations of RC structures. Engineering Structures, 7(3), 397-409.

Rossetto, T. and Elnashai, A. (2003) Derivation of Vulnerability Functions for European-Type RC Structures Based on Observational Data. Journal of Engineering Structures, 25, 1241-1263.

Rota, M., Penna, A. and Strobbia, C. L. (2008) Processing Italian damage data to derive typological fragility curves. Soil Dynamics and Earthquake Engineering, 28(10-11), 933-947.

Ruggieri S., Porco F., Raffaele D., Uva G. (2018b) Seismic analysis of RC buildings by modeling floor deformability and infill walls, SP-326 Durability and Sustainability of Concrete Structures - 2nd Workshop Proceedings, Moscow, 6-7 June 2018.

Ruggieri S., Porco F., Raffaele D., Uva G.,(2017) Rigid floor assumption in nonlinear static analysis of reinforced concrete existing buildings, XVII Convegno Anidis, Pistoia, 2017/17-21/9, pp. 462–473.

Ruggieri S., Porco F., Uva G., (2018a) A numerical procedure for modeling the floor deformability in seismic analysis of existing RC buildings, Journal of Building Engineering, 19, pp. 273-284

Rutenberg A (2002) EAEE Task Group (TG) 8: behaviour and irregular and complex structures—progress since 1998. In: Proceedings of the 12th European conference on earthquake engineering, CD ROM. London, September 2002

Sabetta F., Goretti A., Lucantoni A., (1998) Empirical fragility curves from damage surveys and estimated strong ground motion. Proceedings of the 11th European Conference on Earthquake Engineering, Paris, France, September 6-11.

Sadashiva VK, MacRae GA, Deam BL, Spooner MS (2012) Quantifying the seismic response of structures with flexible diaphragms. Earthquake Engng Struct. Dyn. 41, 10:1365-1389

Saffarini H, Qudaimat M (1992) In-plane floor deformations in RC Structures. J Struct Eng 118:3089–3102

Saiidi M., Sozen M.A. (1981) Simple nonlinear seismic analysis of RC structures. Journal of the Structural Division-ASCE, 107 (5) , pp. 937-952

Salvatore W., Caprilli S., Barberi V., (2009). Rapporto dei danni provocati dall'evento sismico del 6 Aprile sugli edifici scolastici del centro storico dell'Aquila (in Italian), ⟨http://www.reluis.it/doc/pdf/Aquila/Rapporto_danni_scuole_ Aquila.pdf⟩.

Saneinejad, A., and Hobbs, B. (1995). "Inelastic design of infilled frames." J. Struct. Eng., 121(4), 634–650.

Santarsiero G, Chiauzzi L, Masi A (2016) Analisi del danneggiamento di edifici situati nella zona Sud del comune di Amatrice: confronto pre e post sisma del 24/08/2016 V2. http://www.reluis.it

SAP 2000 (2018) Linear and nonlinear static and dynamic analysis of three dimensional structures. Computers and Structures, Inc., Berkeley

Sarkar, P., Prasad, A.M., and Menon, D. (2010) "Vertical geometric irregularity in stepped building frames", Engg. Structs., Vol. 32, No., pp 2175-2182.

Sasaki K. K. FSA, Paret T.F. (1998) "Multi-Mode pushover procedure (MMP) - A method to identify the effects of higer modes in a pushover analysis." Proceedings of the 6thUS National Conference on Earthquake Engineering. Seattle, Washington.

Savoia M., Buratti N., Vincenzi L. (2017), Damage and collapses in industrial precast buildings after the 2012 Emilia earthquake. Eng. Struct., 137(162-180).

Sezen, H. (2008) Shear deformation model for reinforced concrete columns Structural Engineering and Mechanics 28, (1), pp.39-52

Sezen, H. and Chowdhury, T. (2009) Hysteretic model for the lateral behavior of reinforced concrete columns including shear deformation, ASCE Journal of Structural Engineering, Vol. 135, No. 2, pp. 139–146.

Sezen, H., Moehle, J.P. (2006) Seismic tests of concrete columns with light transverse reinforcement. ACI Structural Journal, 103 (6), pp. 842-849.

Sharma A, Eligehausen R, Reddy GR (2011) ―A new model to simulate joint shear behavior of poorly detailed beam–column connections in RC structures under seismic loads, part I: exterior joints‖. Engineering Structures, 33(3), 1034-1051.

Shibata A. Sozen M. A. (1976) "Substitute-Structures Method for Seismic Design in R/C". Journal of the Structural Division, ASCE. Vol. 102, No. 1, pp. 1-18.

Shin M and LaFave JM (2004) ―Testing and modelling for cyclic joint shear deformations in RC beam–column connections‖. Proceedings of the thirteenth world conference on earthquake engineering. Paper no. 0301.

Shome, N., Cornell, C. A., Bazzurro, P., and Carballo, J. E. (1998) Earthquakes, Records, and Nonlinear Responses." Earthquake Spectra, 14(3), 469–500.

Singhal A., Kiremidjian A.S., (1996) Method for probabilistic evaluation of seismic structural damage. ASCE Journal of Structural Engineering, 122(12), 1459-1467.

Sommer A, Bachmann H (2005) Seismic behaviour of asymmetric RC wall buildings: principles and new deformation-based design methods. Earthq Eng Struct Dyn 34:101–124

Structural Engineers Association of California (SEAOC) (1999) Recommended Lateral Force Requirements and Commentary, Seismology Committee Structural Engineers Association of California, Seventh Edition, Sacramento, California

Sucuoğlu H., Günay M.S. (2011) Generalized force vectors for multi-mode pushover analysis Earthq Eng Struct Dynam, 40 , pp. 55-74

Surmeli M., Yuksel E. (2015) A variant of modal pushover analyses (VMPA) based on a non-incremental procedure, Bulletin of Earthquake Engineering 13(11)

Syrmakezis, C.A., Vratsanou, V.Y., 1986. Influence of infill walls to RC frames Response, in: Proc., 8th European Conf. on Earthquake Engineering, European Association for Earthquake Engineering (EAEE). Istanbul, Turkey, pp. 47–53.

Taflanidis A. A., Jia G., Gidaris I. (2016) Natural Hazard Probabilistic Risk Assessment Through Surrogate Modeling., Multi-hazard Approaches to Civil Infrastructure Engineering, P. Gardoni, J.M. LaFave (eds.)

Taflanidis A.A., Cheung S. H. (2012) Stochastic sampling using moving least squares response surface approximations. Probab. Engrg. Mech., 28, pp. 216-224

Takeda T., Sozen M. A., Nielsen N. (1970) "Reinforced Concrete Response to Simulate Earthquakes". Journal of Structural Engineering, ASCE. Vol. 96, No. 12, pp 2557-2573.

Tena-Colunga A (2004) Evaluation of the seismic response of slender, setback RC moment-resisting frame buildings designed according to the seismic guidelines of a modern building code. In: Proceedings of the 13th World conference on earthquake engineering, CD ROM. Vancouver, August 2004

Tena-Colunga A, Chinchilla-Portillo KL, Juarez-Luna G (2015) Assessment of the diaphragm condition for floor systems used in urban buildings. Eng Struct 93:70–84

Tena-Colunga A., Abrams D.P. (1995) Simplified 3-D dynamic analysis of structures with flexible diaphragms, Earthq. Eng. Struct. Dyn. 24 (2) 221–232.

Toniolo G., Colombo A., Precast concrete structures: the lessons learned from the L'Aquila earthquake (2012) Struct. Concr. 13(2) 73–83, http://dx.doi.org/10.1002/suco.201100052.

Tso WK, Myslimaj B (2003) A yield displacement distribution-based approach for strength assignment to lateral force-resisting elements having strength dependent stiffness. Earthq Eng Struct Dyn 32:2319–2351

Tsompanakis, Y., Lagaros, N. D., et al. (2008) "Soft computing techniques in parameter identification and probabilistic seismic analysis of structures," Advances in Engineering Software, 39(7): 612-624.

Uva G, Porco F, Fiore A, Mezzina M. (2014) The assessment of structural concretes during construction phase. Struct Surv;32(3):2–22.

Uva G., Porco F., Fiore A., Mezzina M., (2013) "Proposal of a methodology for assessing the reliability of in situ concrete tests and improving the estimate of the compressive strength." Construction and Building Materials, 38:72-83.

Uva G., Porco F., Fiore A., Ruggieri S. (2017) Effects in conventional nonlinear static analysis: evaluation of control node position, Structures, 13:178–192.

Uva, G., Raffaele, D., Porco, F., Fiore, A., (2012). On the role of equivalent strut models in the seismic assessment of infilled RC buildings. Engineering Structures, 42, pp. 83-94.

Uva, G., Sanjust, C.A., Casolo, S., Mezzina, M. (2016) ANTAEUS Project for the Regional Vulnerability Assessment of the Current Building Stock in Historical Centres. International Journal of Architectural Heritage 10(1):20-43.

Vamvatsikos D, Aschheim M. (2016) Performance-based seismic design via yield frequency spectra. Earthquake Engineering and Structural Dynamics; 45(11):1759–1778.

Vamvatsikos D, Cornell CA. (2002) "Incremental Dynamic Analysis." Earthquake Engineering and Structural Dynamics; 31:491-514.

Vamvatsikos D., Cornell C.A. (2004) Applied incremental dynamic analysis. Earthq Spectra, 20(2):523–553

Vamvatsikos D., Cornell C.A. (2005). Direct estimation of the seismic demand and capacity of MDOF systems through Incremental Dynamic Analysis of an SDOF Approximation. ASCE Journal of Structural Engineering, 131(4): 589-599.

Vamvatsikos D., Cornell C.A. (2006) Direct estimation of the seismic demand and capacity of oscillators with multi-linear static pushovers through IDA. Earthq Eng Struct Dyn, 35:1097–1117

Vamvatsikos, D. (2002) Seismic performance, capacity and reliability of structures as seen through incremental dynamic analysis. Ph.D. dissertation, Dept. of Civil and Environmental Engineering, Stanford Univ., Stanford, CA.

Vamvatsikos, D., Cornell, C. A. (2002). "Incremental dynamic analysis." Earthquake Engineering & Structural Dynamics, 31(3), 491–514.

Vardharajan S., Sehgal V.K., Babita Saini (2012), Review of different structural irregularities in buildings, Journal of Structural Engineering 39 (5) 393–418

Vecchio, F.J. and Collins, M.P. (1986) The modified compression field theory for reinforced concrete elements subjected to shear, ACI Structural Journal, Vol. 83, No. 2, pp. 219–231.

Vecchio, F.J. and Collins, M.P. (1986) The modified compression field theory for reinforced concrete elements subjected to shear, ACI Structural Journal, Vol. 83, No. 2, pp. 219–231.

Verderame G. M., De Luca F., Ricci P., Manfredi G. (2011a) Preliminary analysis of a soft-storey mechanism after the 2009 L'Aquila earthquake, Earthq. Eng. Struct. Dyn. 40(8) 925–944.

Verderame G. M., Iervolino I., Ricci P. (2009). Report on the damages on buildings following the seismic event of 6th of april 2009, V1.20, ⟨http://www. reluis.it/doc/pdf/Aquila/Rapporto_fotografico_V1.2.pdf⟩.

Verderame G.M., Ricci P., Esposito M., Sansiviero F.C. (2011b) Le caratteristiche meccaniche degli acciai impiegati nelle strutture in c.a. realizzate dal 1950 al 1980, 26° convegno nazionale aicap, padova: 19 – 21 maggio 2011

Verderame G.M., Stella A., Cosenza E. (2001), Le proprietà meccaniche degli acciai impiegati nelle strutture in cemento armato realizzate negli anni '60, X Convegno Nazionale "L'Ingegneria Sismica in Italia", Potenza e Matera 9-13 Settembre 2001.

Verderame GM, Ricci P, Manfredi G, Cozenza E. (2010) Ultimate chord rotation of RC columns with smooth bars: some considerations about EC8 prescriptions. Bulletin of Earthquake Engineering. (6) 8,1573-1456

Vona M, Nigro D. (2013) Evaluation of the predictive ability of the in situ concrete strength through core drilling and its effects on the capacity of the RC columns. Materials and Structures ;48:1043–59. doi:10.1617/s11527-013-0214-2.

Yakut A., (2004) Preliminary seismic performance assessment procedure for existing RC buildings. Engineering Structures, 26(10), 1447-1461.

Yang, T.Y. (2009). Performance-based Earthquake Engineering. Pacific Earthquake Engineering Research Center (PEER), University of California, Berkeley. http://peer.berkeley.edu/~yang/ATC58website/

Youssef M, Ghobarah A (2001). ―Modelling of RC beam–column joints and structural walls‖. Journal Earthquake Engineering;5(1):93–111.

Zarnic, R. and M. Tomazevic, (1988) An experimentally obtained method for evaluation of the behavior of masonry infilled R/C frames. Proceedings of the 9th World Conference on Earthquake Engineering, Aug. 7-9, Japan, pp: 163-168.

Zarnic, R., Gostic, S. (1997). Masonry infilled frames as an effective structural sub-assemblage, Seismic design Methodologies for the Next Generation of Codes: Proceedings of the International Workshop. Bled, Slovenia

Zhu L., Elwood K. & Haukaas T. (2007) Classification and seismic safety evaluation of existing reinforced concrete columns. Journal of Structural Engineering, (September), 1316–1330.

8. Annex A: Extended results of conventional pushover application
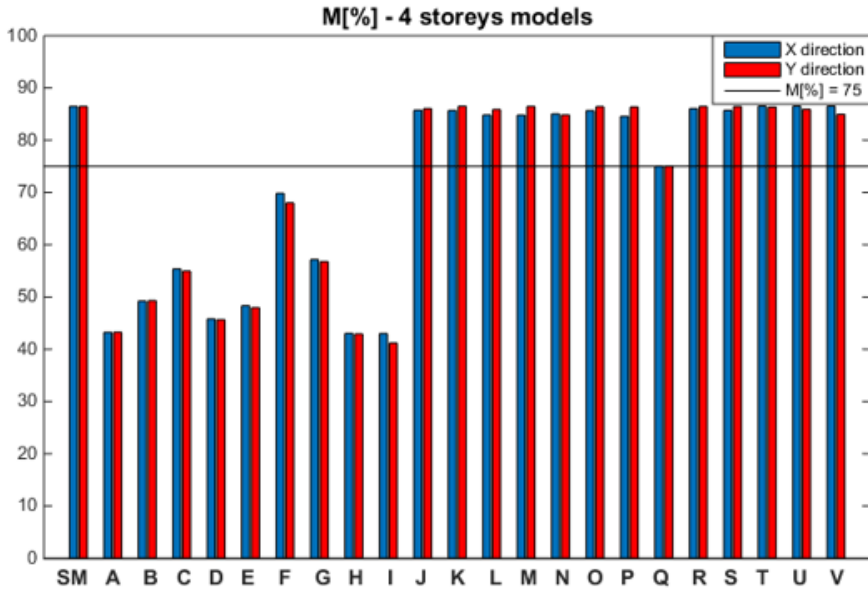
Fig. A.1 – M[%]s of fundamental modes in both directions (X and Y) for models with 4 storeys.
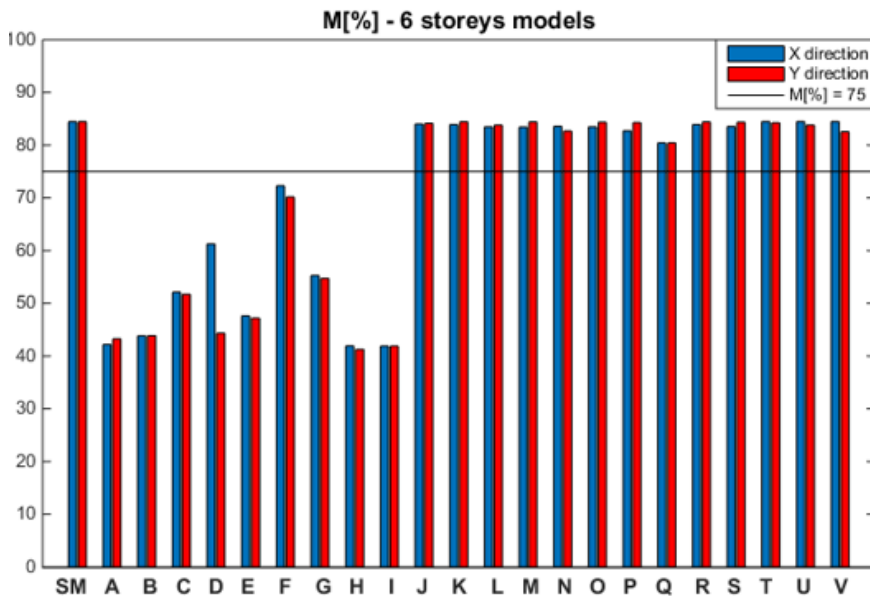
Fig. A.2 – M[%]s of fundamental modes in both directions (X and Y) for models with 6 storeys.
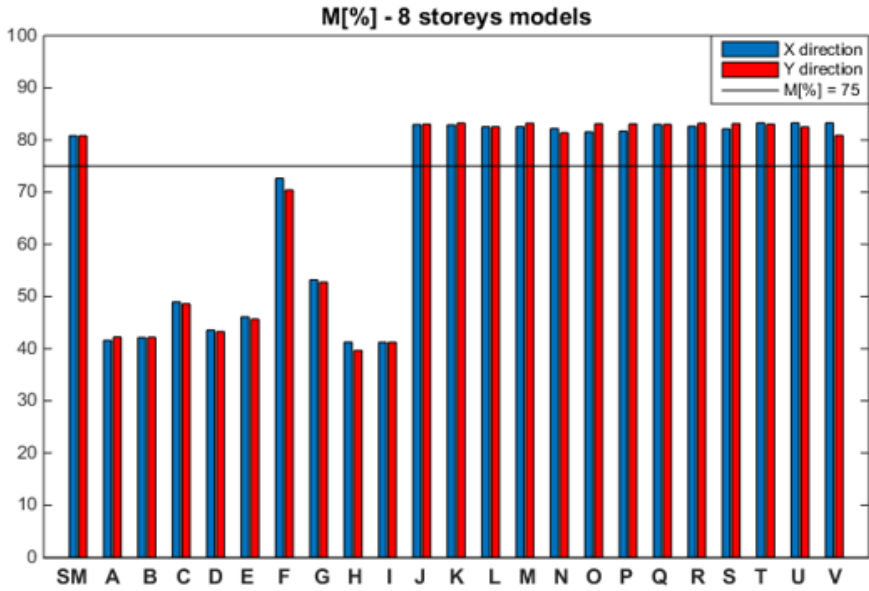
Fig. A.3 – M[%]s of fundamental modes in both directions (X and Y) for models with 8 storeys.
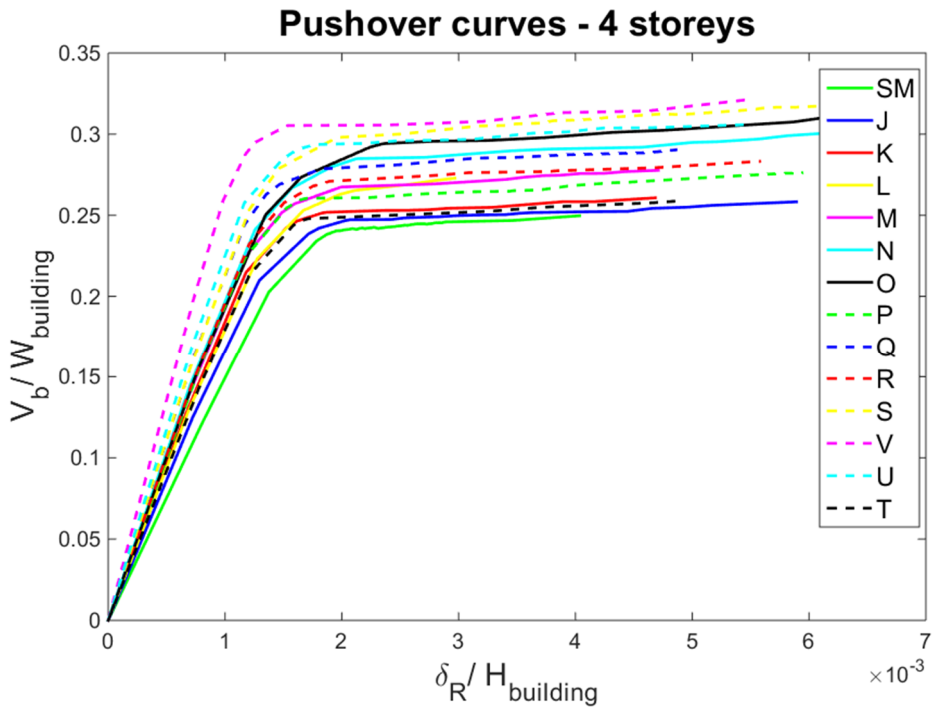
Fig. A.4 – A-dimensional pushover curves of 4-storeys models selected, assuming CM =CN.
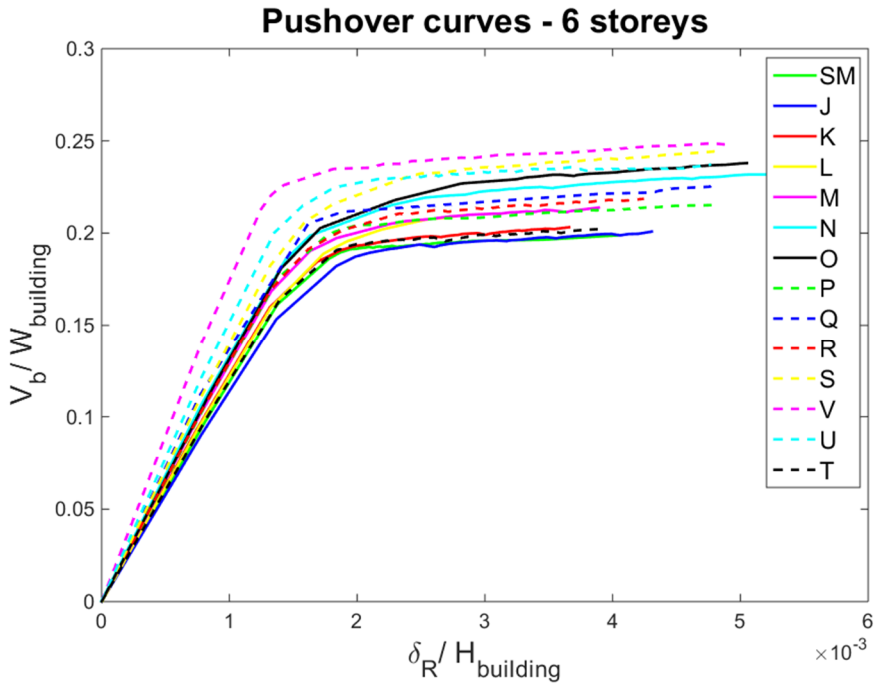
Fig. A.5 – A-dimensional pushover curves of 6-storeys models selected, assuming CM =CN.
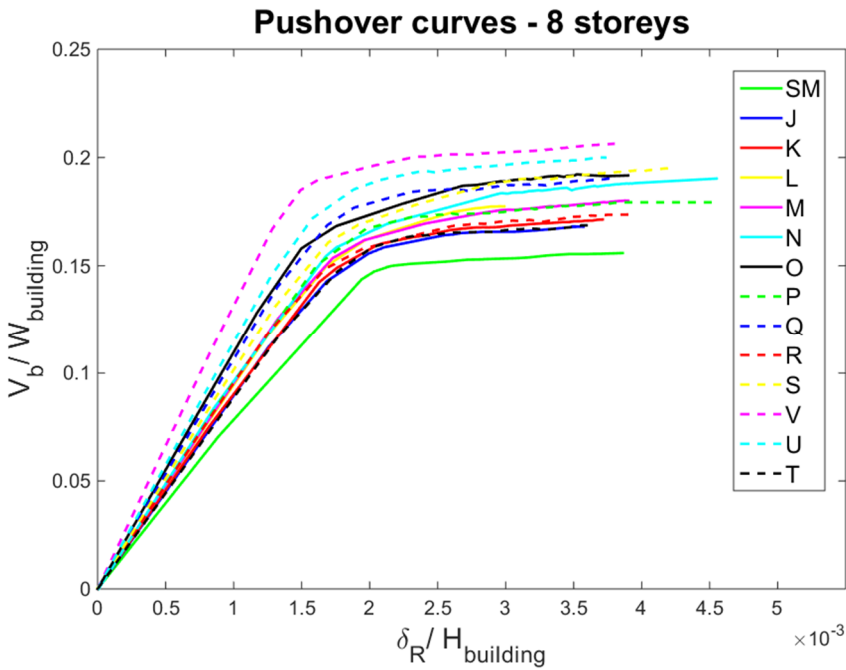
Fig. A.6 – A-dimensional pushover curves of 8-storeys models selected, assuming CM =CN.

362

Pushover curves - 4 storeys
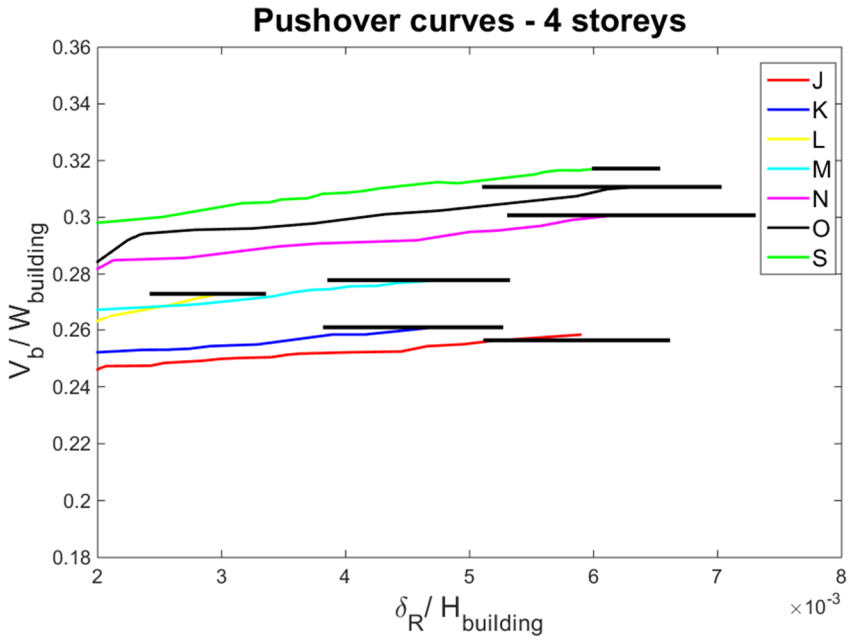
Fig. A.7 – Zoom view of a-dimensional pushover curves of models selected and reported in tab. 4.2, considering the variation of δ_{LS} for each model to 4 storeys

Pushover curves - 6 storeys
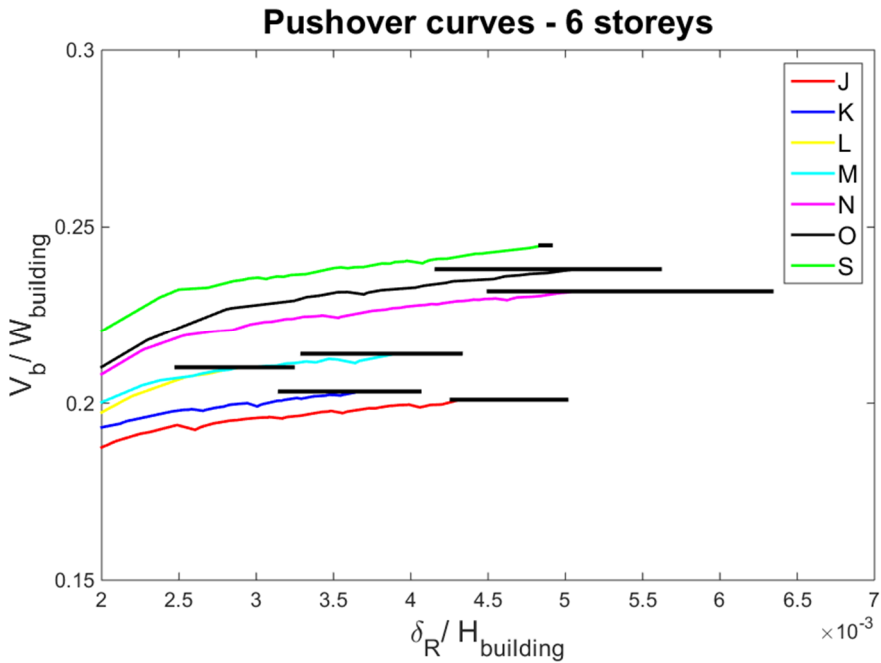
Fig. A.8 – Zoom view of a-dimensional pushover curves of models selected and reported in tab. 4.2, considering the variation of δ_{LS} for each model to 6 storeys
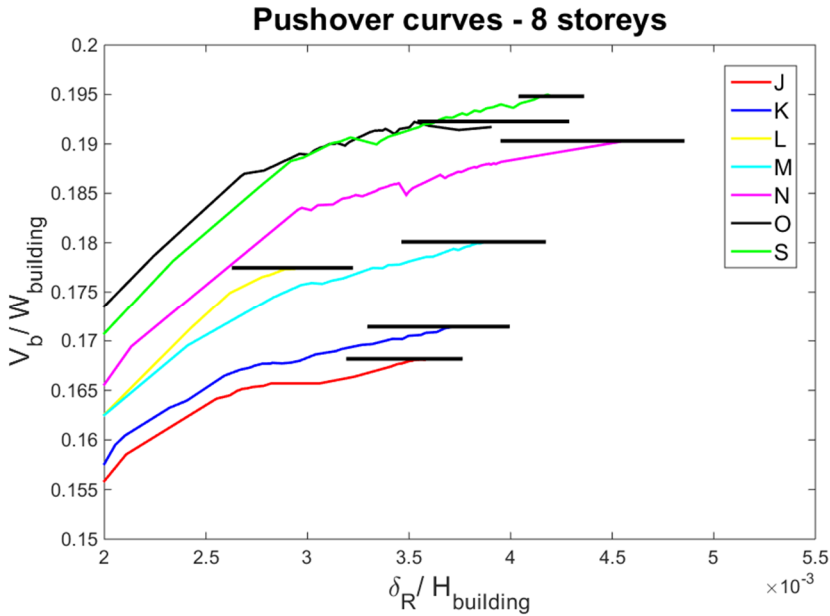
Fig. A.9 – Zoom view of a-dimensional pushover curves of models selected and reported in tab. 4.2, considering the variation of δ_{LS} for each model to 8 storeys
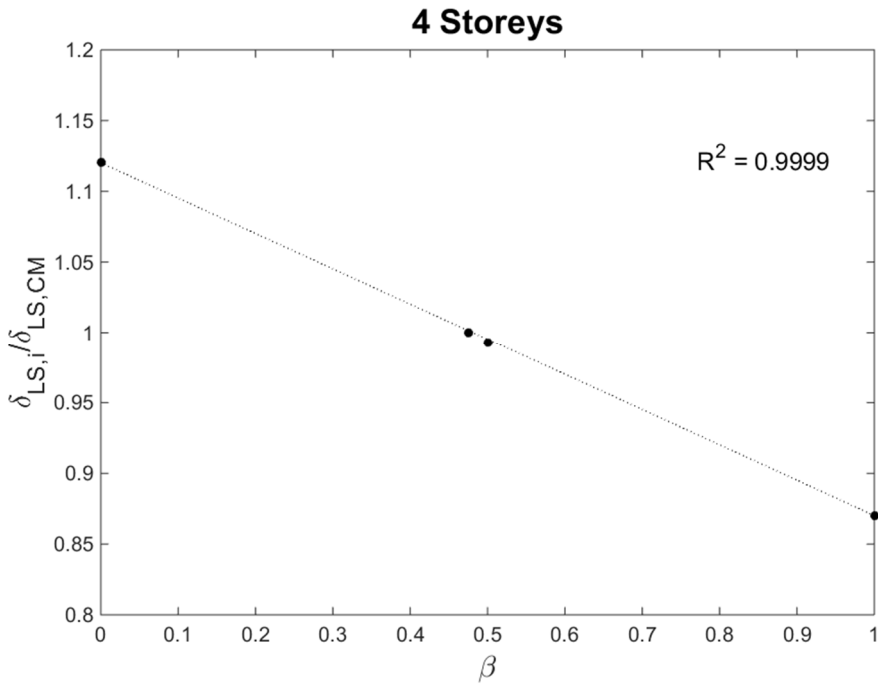
Fig. A.10 – Distribution of $\delta_{LS,i}/\delta_{LS,CM}$, varying β for 4-storeys models for J.
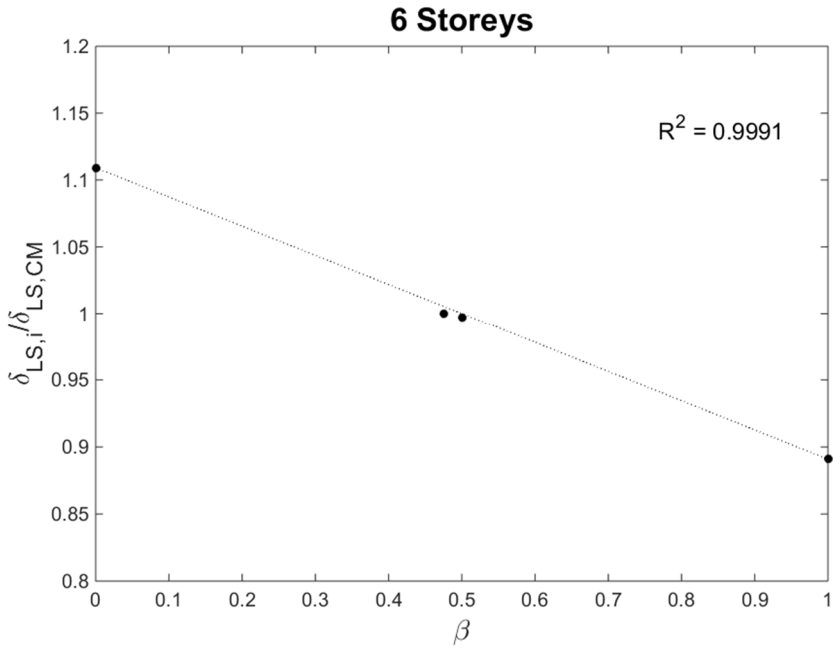
Fig. A.11 – Distribution of $\delta_{LS,i}/\delta_{LS,CM}$, varying β for 6-storeys models for J.
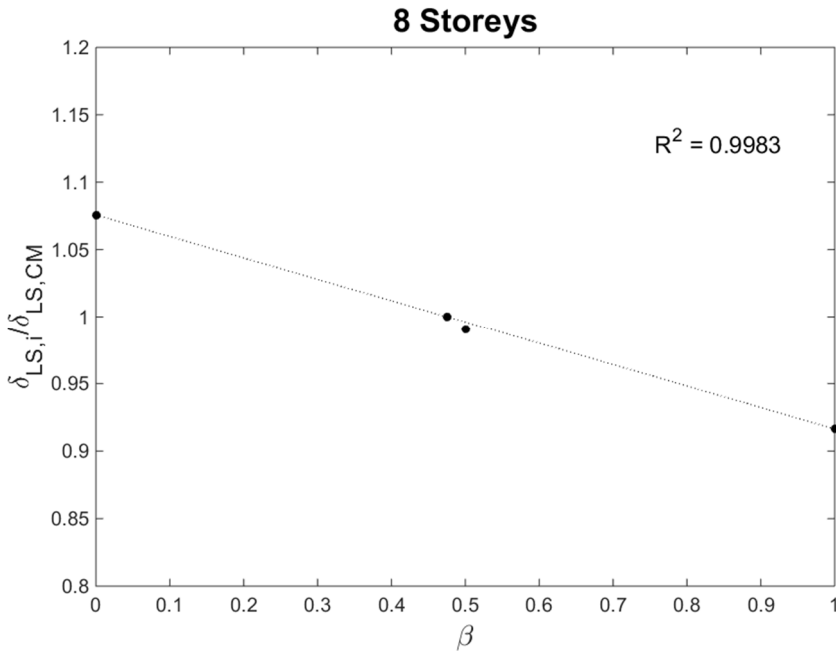
Fig. A.12 – Distribution of $\delta_{LS,i}/\delta_{LS,CM}$, varying β for 8-storeys models for J.
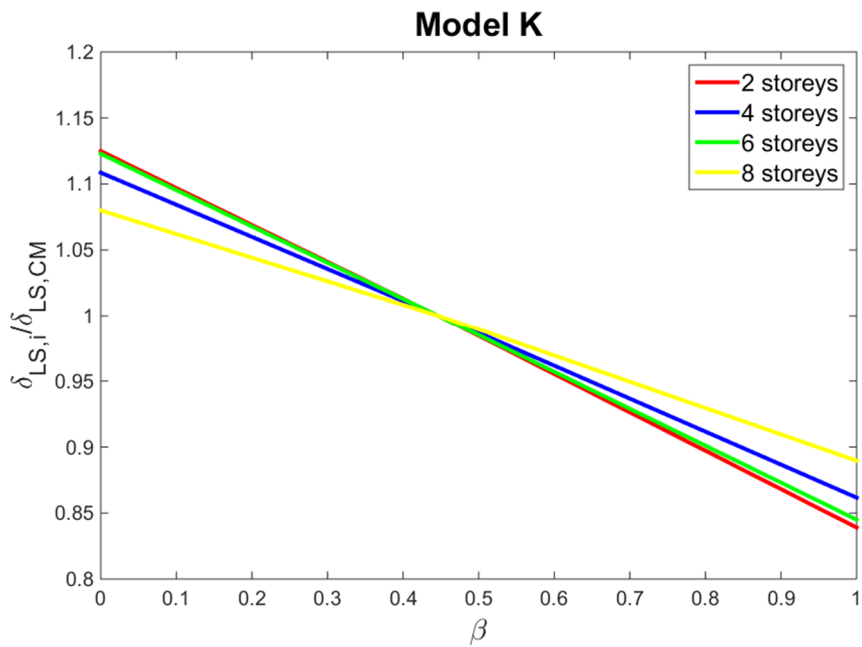
Fig. A.13 – Distribution of $\delta_{LS,i}/\delta_{LS,CM}$, varying number of storeys, for models K
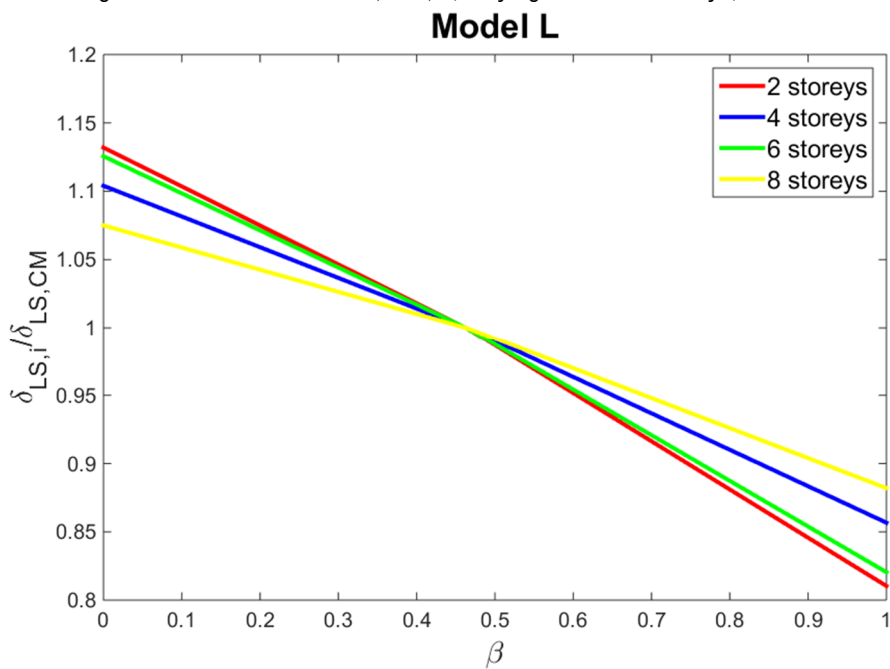
Fig. A.14 – Distribution of $\delta_{LS,i}/\delta_{LS,CM}$, varying number of storeys, for models L
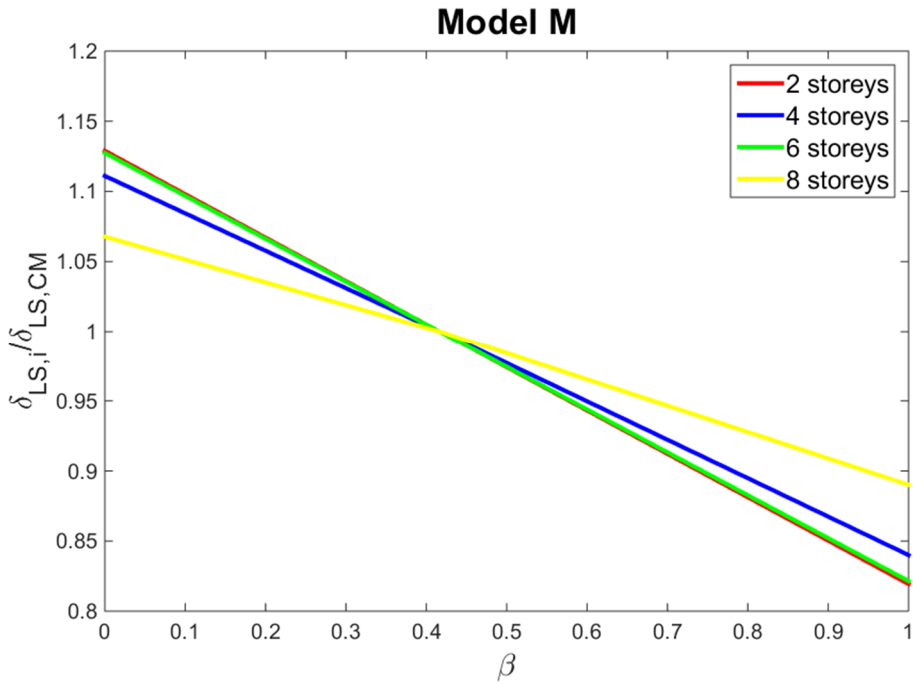
Fig. A.15 – Distribution of $\delta_{LS,i}/\delta_{LS,CM}$, varying number of storeys, for models M
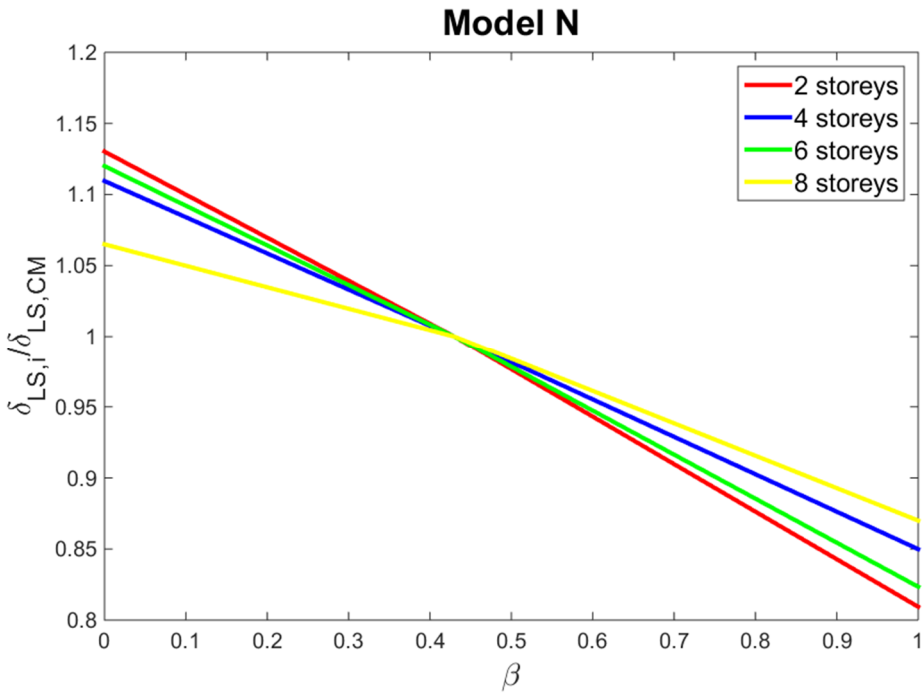
Fig. A.16 – Distribution of $\delta_{LS,i}/\delta_{LS,CM}$, varying number of storeys, for models N
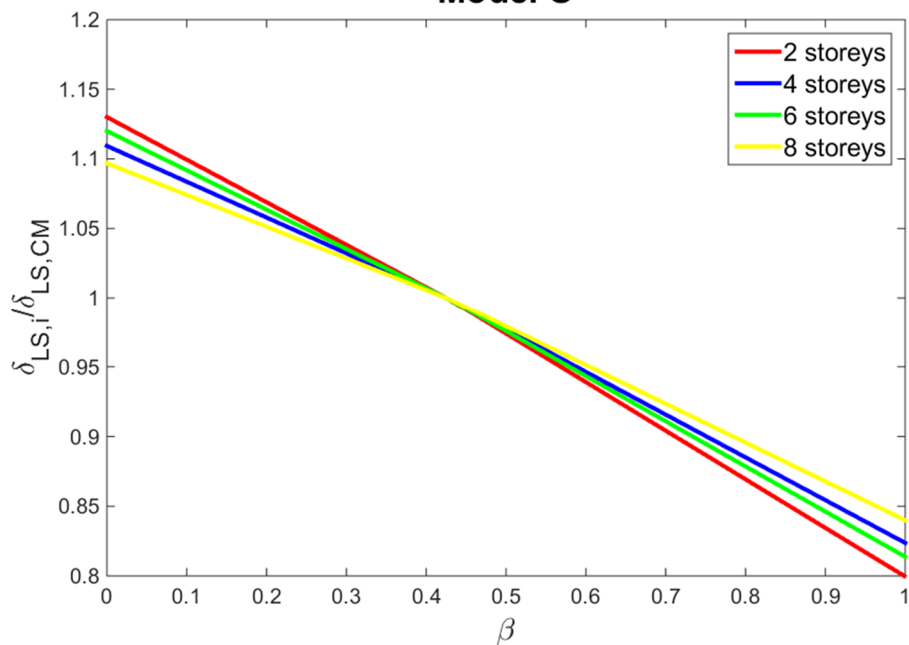
Fig. A.17 – Distribution of $\delta_{LS,i}/\delta_{LS,CM}$, varying number of storeys, for models O
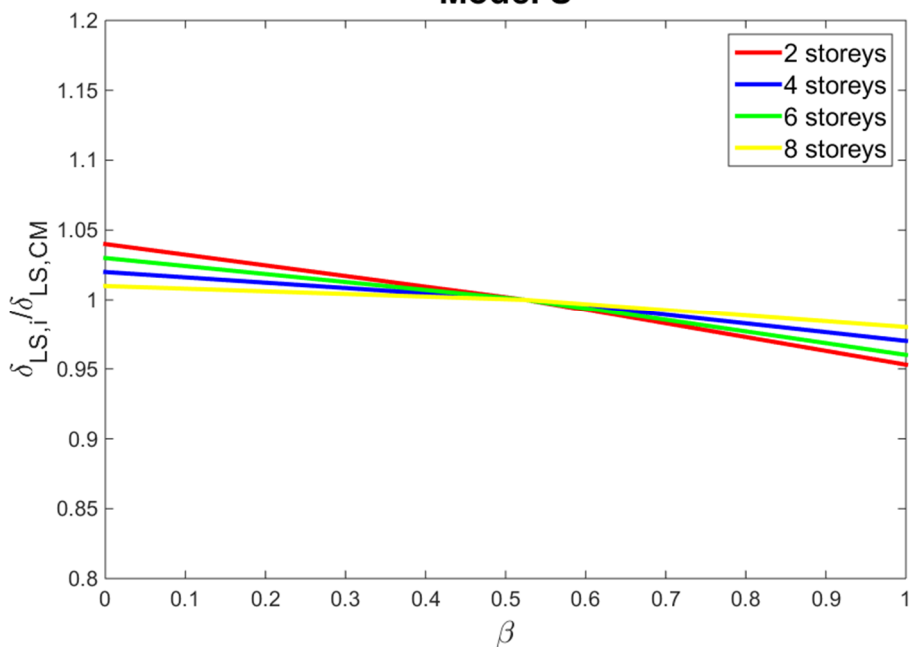
Fig. A.17 – Distribution of $\delta_{LS,i}/\delta_{LS,CM}$, varying number of storeys, for models S
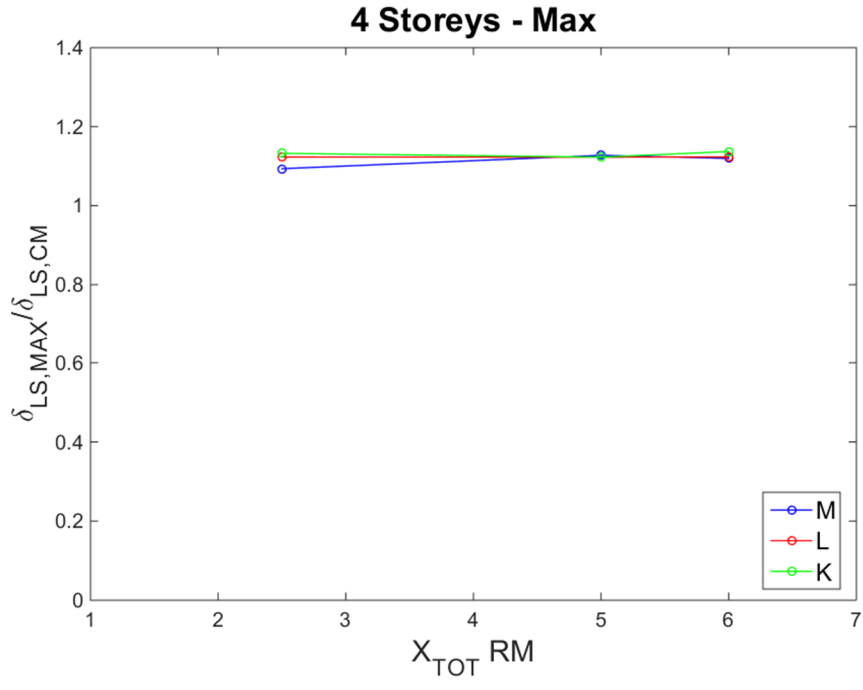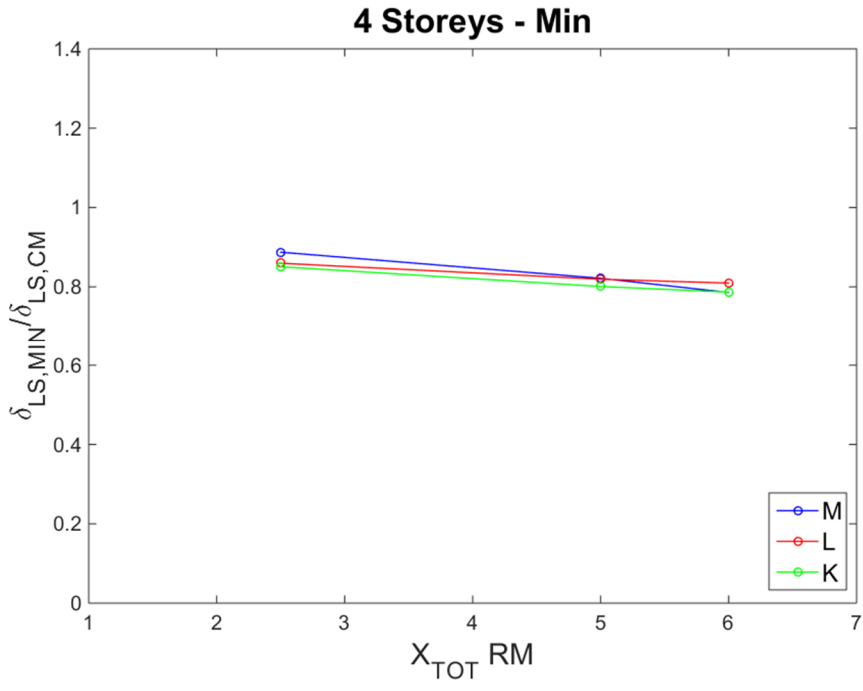
Fig. A.18 –Trend of $\delta_{LS,i\,MIN}/\delta_{LS,CM}$ and $\delta_{LS,i\,MAX}/\delta_{LS,CM}$, varying X_{TOT} for models M,L and K, with 4 storeys.
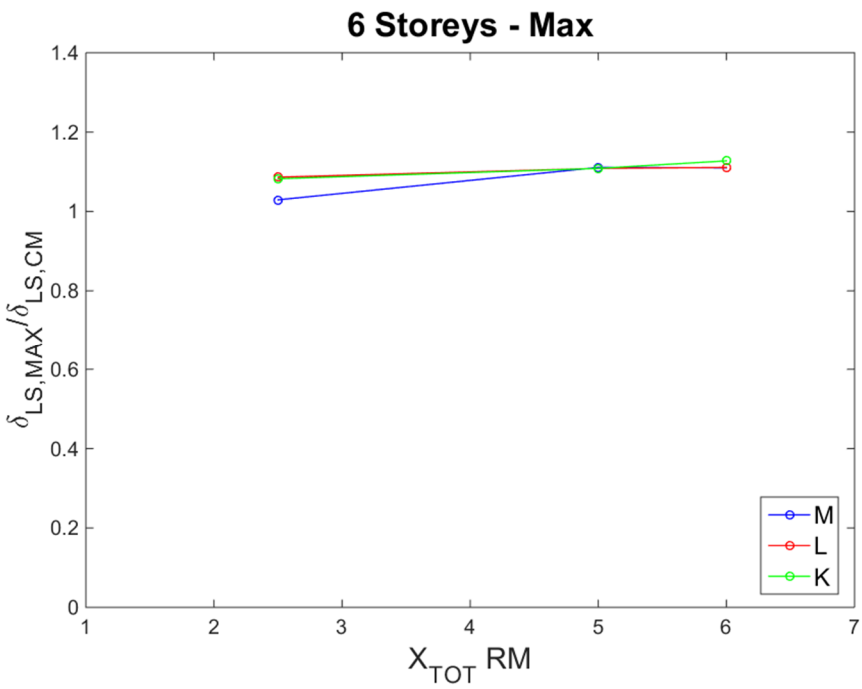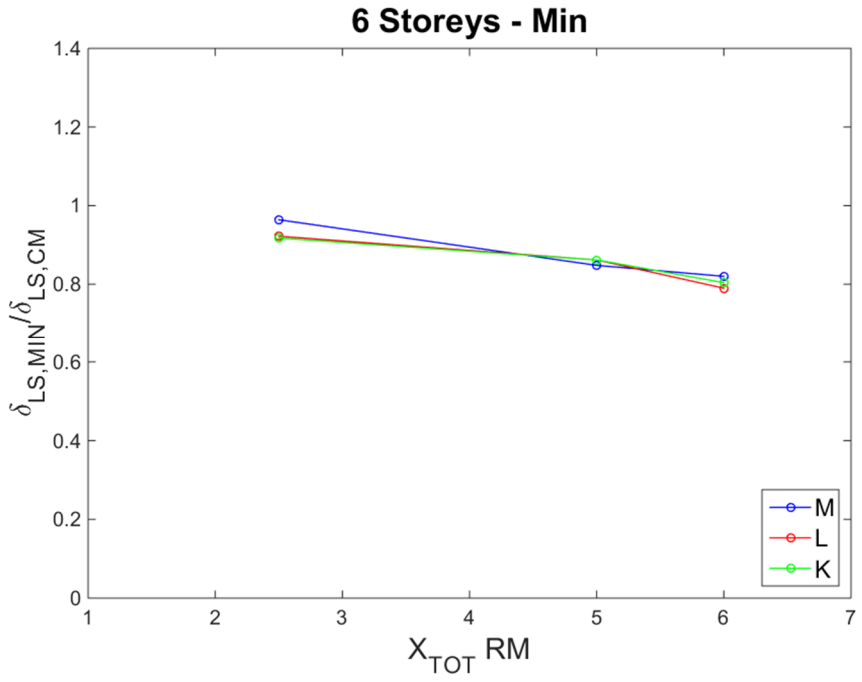
Fig. A.19 –Trend of $\delta_{LS,i\,MIN}/\delta_{LS,CM}$ and $\delta_{LS,i\,MAX}/\delta_{LS,CM}$, varying X_{TOT} for models M,L and K, with 6 storeys.
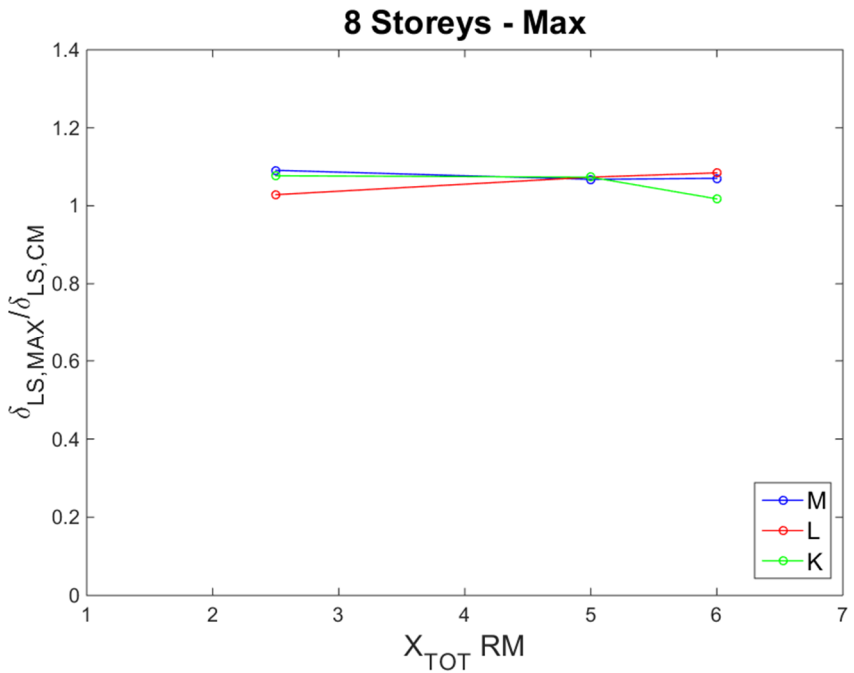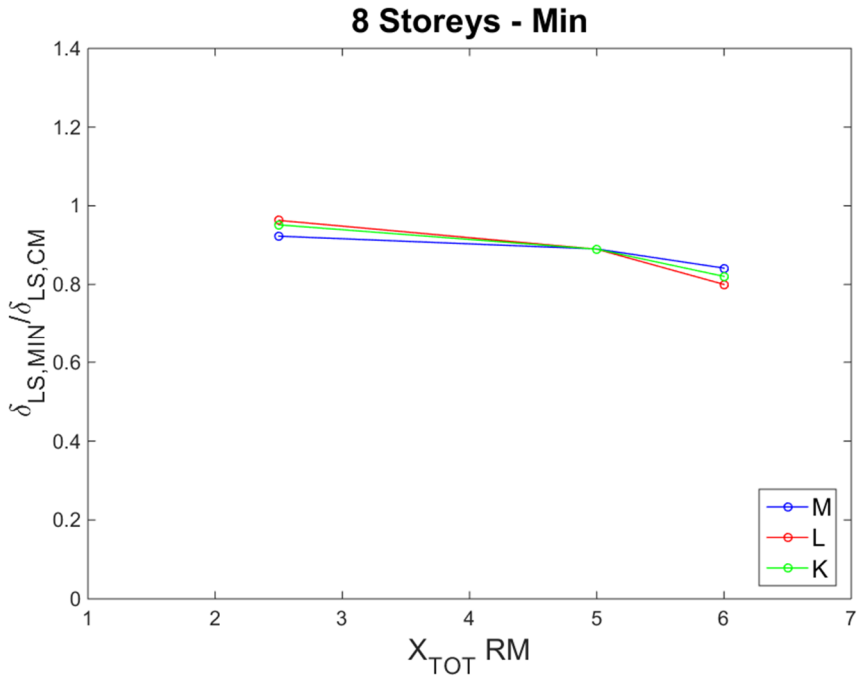
Fig. A.20 –Trend of $\delta_{LS,i\,MIN}/\delta_{LS,CM}$ and $\delta_{LS,i\,MAX}/\delta_{LS,CM}$, varying X_{TOT} for models M,L and K, with 8 storeys.

Tab. A.1 – Results of methods validation; percentage differences between FE models and formulation in terms of δ_{LS}, for 4 storeys buildings

Model	β	$\delta_{LS,i}/\delta_{LS,CM}$ Model	$\delta_{LS,i}/\delta_{LS,CM}$ (eq.4.8)	Variation (%)
J	1	0,869	0,832	8,779
	0.5	0,994	0,992	0,339
	β_{CM}	1,000	1,000	0,000
	0	1,119	1,152	9,009
K	1	0,814	0,823	19,646
	0.5	0,967	0,973	3,909
	β_{CM}	1,000	1,000	0,000
	0	1,120	1,143	9,995
L	1	0,820	0,828	18,895
	0.5	0,971	0,988	4,693
	β_{CM}	1,000	1,000	0,000
	0	1,126	1,148	10,556
M	1	0,822	0,813	16,849
	0.5	0,975	0,973	2,425
	β_{CM}	1,000	1,000	0,000
	0	1,128	1,133	12,237
N	1	0,823	0,818	16,945
	0.5	0,962	0,978	5,517
	β_{CM}	1,000	1,000	0,000
	0	1,129	1,152	10,844
O	1	0,827	0,816	15,970
	0.5	0,978	0,976	1,996
	β_{CM}	1,000	1,000	0,000
	0	1,129	1,136	12,280
S	1	0,894	0,832	3,714
	0.5	0,958	0,992	7,852
	β_{CM}	1,000	1,000	0,000
	0	1,071	1,152	0,489

Tab. A.2 – Results of methods validation; percentage differences between FE models and formulation in terms of δ_{LS}, for 6 storeys buildings

Model	β	$\delta_{LS,i}/\delta_{LS,CM}$ Model	$\delta_{LS,i}/\delta_{LS,CM}$ (eq.4.8)	Variation (%)
J	1	0,889	0,853	7,030
	0.5	0,998	0,993	0,321
	$β_{CM}$	1,000	1,000	0,000
	0	1,107	1,133	8,371
K	1	0,863	0,845	11,617
	0.5	0,986	0,977	0,449
	$β_{CM}$	1,000	1,000	0,000
	0	1,109	1,125	9,455
L	1	0,857	0,850	13,506
	0.5	0,952	0,990	8,674
	$β_{CM}$	1,000	1,000	0,000
	0	1,116	1,130	10,378
M	1	0,849	0,837	13,663
	0.5	0,980	0,977	1,675
	$β_{CM}$	1,000	1,000	0,000
	0	1,111	1,117	10,575
N	1	0,850	0,840	13,892
	0.5	0,946	0,980	9,021
	$β_{CM}$	1,000	1,000	0,000
	0	1,195	1,220	17,412
O	1	0,830	0,839	18,107
	0.5	0,973	0,979	3,337
	$β_{CM}$	1,000	1,000	0,000
	0	1,116	1,119	11,312
S	1	0,916	0,853	1,443
	0.5	0,975	0,993	4,295
	$β_{CM}$	1,000	1,000	0,000
	0	1,077	1,133	2,454

Tab. A.3 – Results of methods validation; percentage differences between FE models and formulation in terms of δ_{LS}, for 8 storeys buildings

Model	β	$\delta_{LS,i}/\delta_{LS,CM}$ Model	$\delta_{LS,i}/\delta_{LS,CM}$ (eq.4.8)	Variation (%)
J	1	0,914	0,874	4,142
	0.5	0,994	0,994	0,520
	β_{CM}	1,000	1,000	0,000
	0	1,074	1,114	3,754
K	1	0,896	0,867	7,140
	0.5	0,988	0,980	0,346
	β_{CM}	1,000	1,000	0,000
	0	1,080	1,107	5,524
L	1	0,882	0,871	10,566
	0.5	0,926	0,991	14,448
	β_{CM}	1,000	1,000	0,000
	0	1,075	1,111	4,140
M	1	0,893	0,860	7,042
	0.5	0,982	0,980	1,633
	β_{CM}	1,000	1,000	0,000
	0	1,071	1,100	4,357
N	1	0,870	0,863	12,218
	0.5	0,921	0,983	14,694
	β_{CM}	1,000	1,000	0,000
	0	1,065	1,103	2,913
O	1	0,903	0,862	5,262
	0.5	0,996	0,982	0,906
	β_{CM}	1,000	1,000	0,000
	0	1,089	1,102	7,610
S	1	0,970	0,874	6,903
	0.5	0,997	0,994	0,002
	β_{CM}	1,000	1,000	0,000
	0	1,036	1,114	3,936

9. Annex B: Data sheets of the case studies
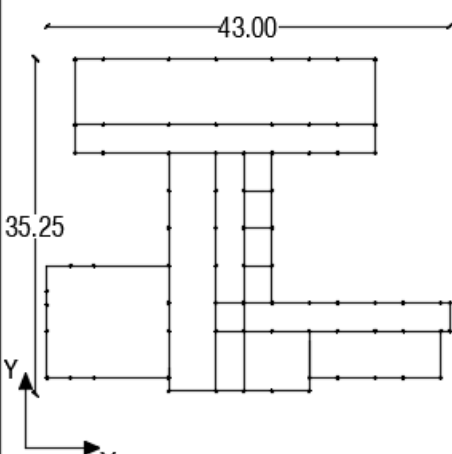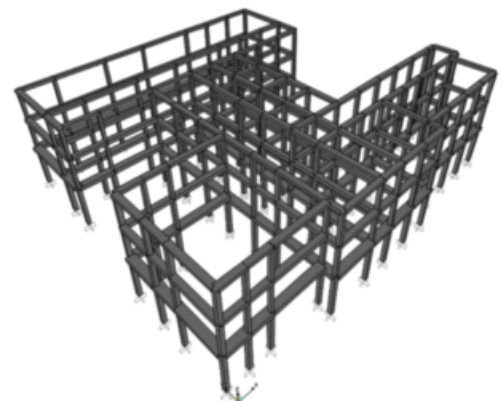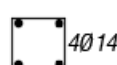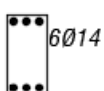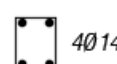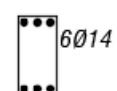
B2 - Carpino

Structural elements 1° Storey

Columns:

40x40   4Ø14

Beams:

30x60   6Ø14

90x40   12Ø14

Structural elements 2°-3° Storeys

Columns:

30x40   4Ø14

Beams:

30x60   6Ø14

60x40   10Ø14

Information Code Spectra

Building	Coordinates	Soil type
N_L: 50	Lat: 41.845	Cat: B
U_C: 1.5	Lon: 15.857	Top: T1

Knowledge Path Information

Building date: 1970

N. storeys: 2   Loads

$H_1 = 5.05\ m$ $G_1 = 2.4\ kN/m^2$

$H_2 = 3.75\ m$ $G_2 = 1.8\ kN/m^2$

$H_3 = 3.65\ m$ $Q = 3.0\ kN/m^2$

In-situ material

$f'_{cm} = 15.60\ MPa$

$f'_{ym} = 405.00\ MPa$

$E_c = 25515\ MPa$

Fig. B.1 – B2 building information

B3 - Manfredonia
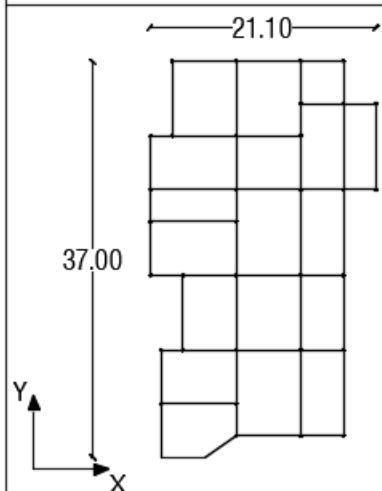
Structural elements 1° Storey

Columns:
35x65   10Ø16

Beams:
30x70   6Ø16

90x30   12Ø16

Structural elements 2° Storey

Columns:
35x65   10Ø16

Beams:
30x70   6Ø16

90x30   12Ø16

Information Code Spectra

Building	Coordinates	Soil type
N_L: 50	Lat: 41.627	Cat: B
U_C: 1.5	Lon: 15.91	Top: T1

Knowledge Path Information

Building date: 1982

N. storeys: 2
$H_1 = 3.40\ m$
$H_2 = 3.40\ m$

Loads
$G_1 = 3.6\ kN/m^2$
$G_2 = 2.4\ kN/m^2$
$Q = 3.0\ kN/m^2$

In-situ material
$f'_{cm} = 24.60\ MPa$
$f'_{ym} = 440.00\ MPa$
$E_c = 29610\ MPa$

Fig. B.2 – B3 building information
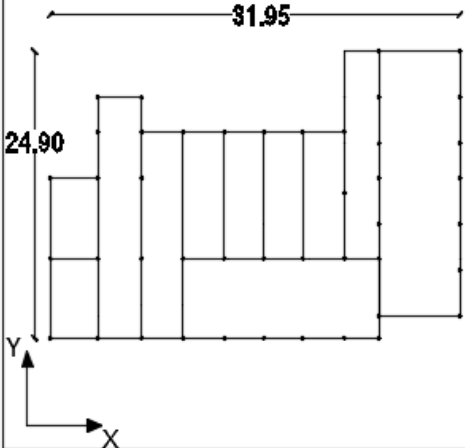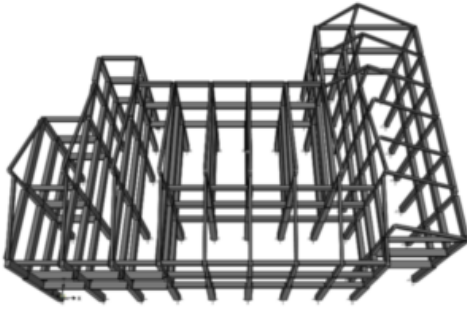
B4 - Bovino

Structural elements 1° Storey

Columns: 40x40   Beams: 80x20
         50x60   40x60
         55x70

Structural elements 2° Storey

Columns: 40x60   Beams: 80x20
         50x65   40x60

Structural elements 3° Storey

Columns: 40x60   Beams: 70x20
         35x50   35x50

Information Code Spectra

Building	Coordinates	Soil type
N_L: 50	Lat: 41.251	Cat: B
U_C: 1.5	Lon: 15.342	Top: T1

Knowledge Path Information

Building date: 1959

N. storeys: 2   Loads

$H_1 = 5.30\ m$ $G_1 = 2.6\ kN/m^2$

$H_2 = 3.50\ m$ $G_2 = 1.7\ kN/m^2$

$H_3 = 3.50\ m$ $Q = 3.0\ kN/m^2$

In-situ material

$f^t_{cm} = 14.87\ MPa$

$f^t_{ym} = 401.00\ MPa$

$E_c = 25078\ MPa$

Fig. B.3 – B4 building information

B5 - Cerignola (1)
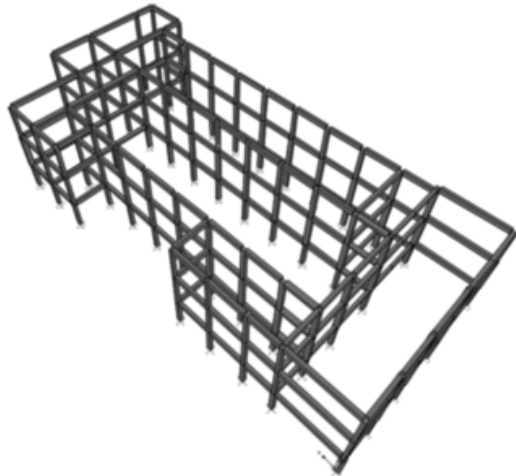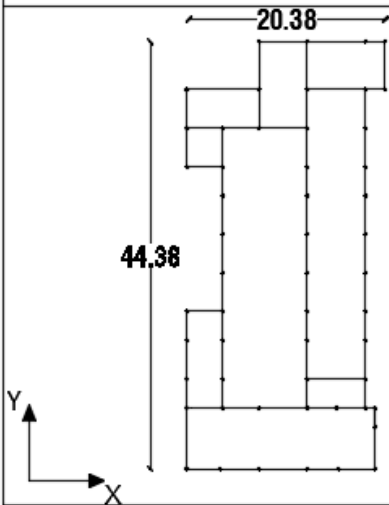
Structural elements 1° Storey
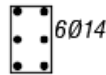
Columns:
40x40   4Ø16
30x50   6Ø14

Beams:
30x50   6Ø14
50x25   8Ø12

Structural elements 2°-3° Storeys

Columns:
30x30   4Ø16
30x40   6Ø14
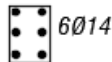
Beams:
30x50   6Ø14
30x25   6Ø12
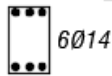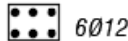
Information Code Spectra

Building   Coordinates   Soil type
N_L: 50   Lat: 41.265   Cat: C
U_C: 1.5   Lon: 15.901   Top: T1

Knowledge Path Information

Building date: 1970

N. storeys: 2   Loads
H_1 = 3.00 m G_1 = 3.2 kN/m^2
H_2 = 3.80 m G_2 = 2.2 kN/m^2
H_3 = 3.75 m Q = 3.0 kN/m^2

In-situ material
f'_{cm} = 15.77 MPa
f'_{ym} = 415.00 MPa
E_c = 25608 MPa

Fig. B.4 – B5 building information

B6 - Cerignola (2)

Structural elements 1° Storey

Columns:
30x50   6Ø14

Beams:
30x50   6Ø14

Structural elements 2° Storey

Columns:
30x50   6Ø14

Beams:
30x50   6Ø14

Information Code Spectra

Building	Coordinates	Soil type
N_L: 50	Lat: 41.252	Cat: C
U_C: 1.5	Lon: 15.891	Top: T1

Knowledge Path Information

Building date: 1968

N. storeys: 2
$H_1 = 5.55\ m$
$H_2 = 3.77\ m$

Loads
$G_1 = 2.7\ kN/m^2$
$G_2 = 2.0\ kN/m^2$
$Q = 3.0\ kN/m^2$

In-situ material
$f^t_{cm} = 18.30\ MPa$
$f^t_{ym} = 422.00\ MPa$
$E_c = 26910\ MPa$

Fig. B.5 – B6 building information

B7 - Cerignola (2)

Structural elements 1° Storey

Columns:
40x40 — 4Ø16
30x50 — 6Ø14

Beams:
30x50 — 6Ø14
30x60 — 6Ø14

Structural elements 2° Storey

Columns:
30x30 — 4Ø16
30x40 — 6Ø14

Beams:
30x50 — 6Ø14
30x60 — 6Ø14

Information Code Spectra

Building	Coordinates	Soil type
N_L: 50	Lat: 41.252	Cat: C
U_C: 1.5	Lon: 15.891	Top: T1

Knowledge Path Information

Building date: 1968

N. storeys: 2
$H_1 = 5.55\ m$
$H_2 = 3.77\ m$

Loads
$G_1 = 2.7\ kN/m^2$
$G_2 = 2.0\ kN/m^2$
$Q = 3.0\ kN/m^2$

In-situ material
$f'_{cm} = 18.30\ MPa$
$f'_{ym} = 422.00\ MPa$
$E_c = 26910\ MPa$

Fig. B.6 – B7 building information

B8 - Cerignola (2)
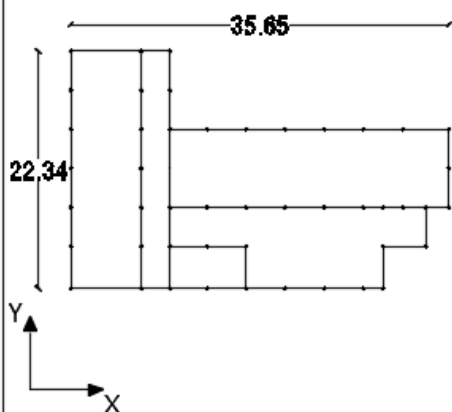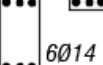
35.65

22.34

Y
X

Structural elements 1° Storey

Columns:
40x40   4Ø16
30x50   6Ø14

Beams:
30x50   6Ø14
30x60   6Ø14

Structural elements 2° Storey

Columns:
30x30   4Ø16
30x40   6Ø14

Beams:
30x50   6Ø14
30x60   6Ø14

Information Code Spectra

Building	Coordinates	Soil type
N_L: 50	Lat: 41.252	Cat: C
U_C: 1.5	Lon: 15.891	Top: T1

Knowledge Path Information

Building date: 1968

N. storeys: 2   Loads
$H_1 = 5.55\ m$ $G_1 = 2.7\ kN/m^2$
$H_2 = 3.77\ m$ $G_2 = 2.0\ kN/m^2$
$Q = 3.0\ kN/m^2$

In-situ material
$f'_{cm} = 18.30\ MPa$
$f'_{ym} = 422.00\ MPa$
$E_c = 26910\ MPa$

Fig. B.7 – B8 building information

381

B9 - Cerignola (2)
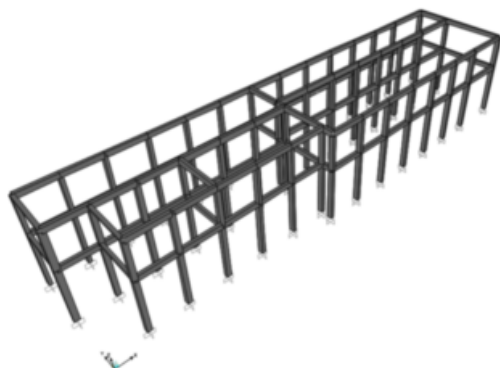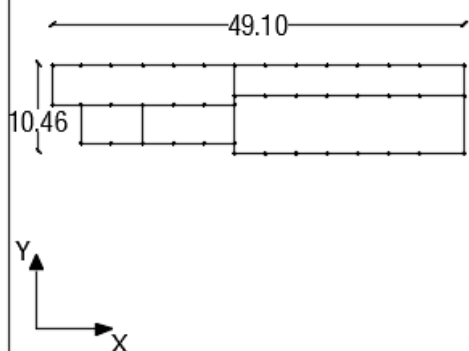
Structural elements 1° Storey

Columns:
40x40
30x50 — 4Ø16
6Ø14
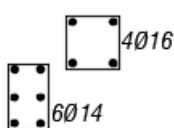
Beams:
30x50 — 6Ø14
30x60 — 6Ø14
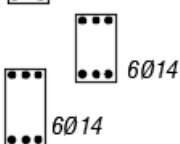
Structural elements 2° Storey

Columns:
30x30
30x40 — 4Ø16
6Ø14
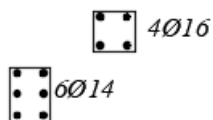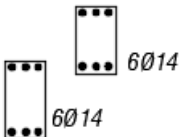
Beams:
30x50 — 6Ø14
30x60 — 6Ø14

Information Code Spectra

Building	Coordinates	Soil type
N_L: 50	Lat: 41.252	Cat: C
U_C: 1.5	Lon: 15.891	Top: T1

Knowledge Path Information

Building date: 1968

N. storeys: 2
$H_1 = 5.55$ m
$H_2 = 3.77$ m

Loads
$G_1 = 2.7$ kN/m^2
$G_2 = 2.0$ kN/m^2
$Q = 3.0$ kN/m^2

In-situ material
$f_{cm} = 18.30$ MPa
$f_{ym} = 422.00$ MPa
$E_c = 26910$ MPa

Fig. B.8 – B9 building information

B10 - Lesina (1)
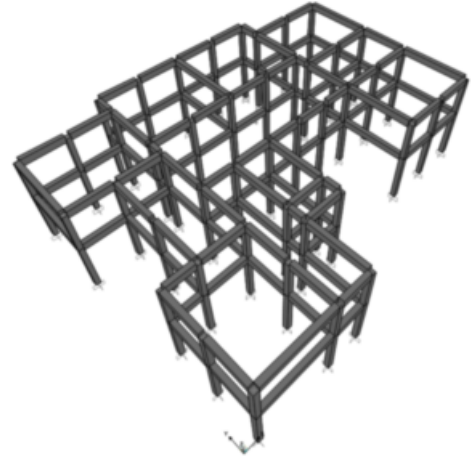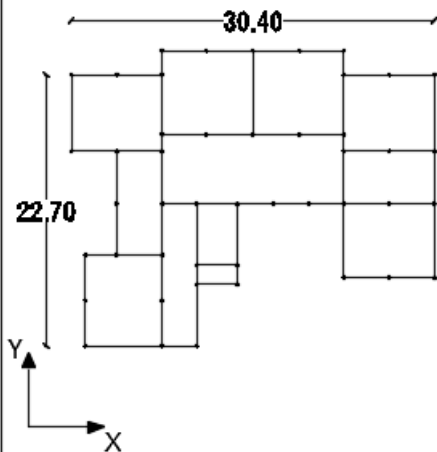
Structural elements 1° Storey

Columns:
40x40   8Ø12

Beams:
40x60   8Ø14

Structural elements 2° Storey

Columns:
40x40   8Ø12
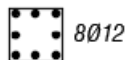
Beams:
40x60   8Ø14
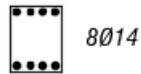
Information Code Spectra

Building	Coordinates	Soil type
N_L: 50	Lat: 41.860	Cat: C
U_C: 1.5	Lon: 15.3536	Top: T1

Knowledge Path Information

Building date: 1987

N. storeys: 2
$H_1 = 4.60$ m
$H_2 = 3.60$ m

Loads
$G_1 = 3.5$ kN/m^2
$G_2 = 2.5$ kN/m^2
$Q = 3.0$ kN/m^2

In-situ material
$f^t_{cm} = 20.00$ MPa
$f^t_{ym} = 437.00$ MPa
$E_c = 27655$ MPa

Fig. B.9 – B10 building information

B11 - Lesina (2)	
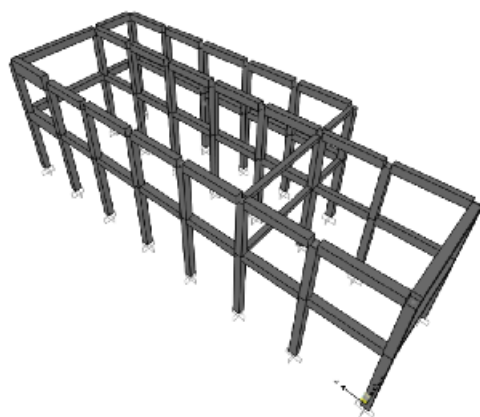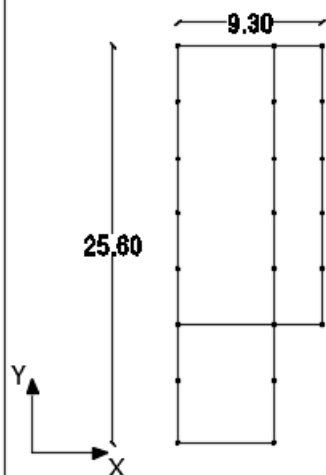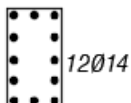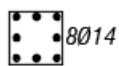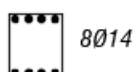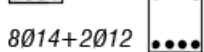
9.30

25.60

Y

X

Structural elements 1° Storey

Columns:

40x40   8Ø14

40x75   12Ø14

Beams: 8Ø14

40x60

40x90   8Ø14+2Ø12

Structural elements 2° Storey

Columns:

30x40   6Ø14

40x75   12Ø14

Beams:

40x60   8Ø14

Information Code Spectra

Building	Coordinates	Soil type
N_L: 50	Lat: 41.842	Cat: B
U_C: 1.5	Lon: 15.342	Top: T1

Knowledge Path Information

Building date: 1979

N. storeys: 2

$H_1 = 4.75$ m

$H_2 = 3.50$ m

Loads

$G_1 = 3.0$ kN/m^2

$G_2 = 2.0$ kN/m^2

$Q = 3.0$ kN/m^2

In-situ material

$f^t_{cm} = 24.00$ MPa

$f^t_{ym} = 450.00$ MPa

$E_c = 29369$ MPa

Fig. B.10 – B11 building information

B12 - Lesina (2)
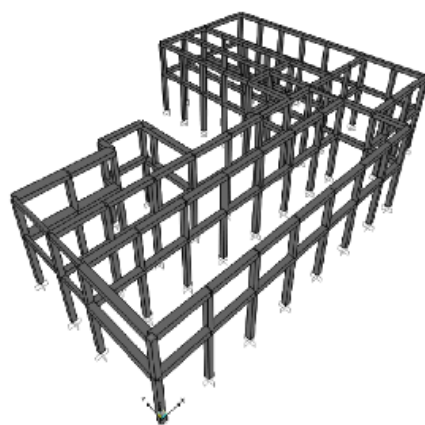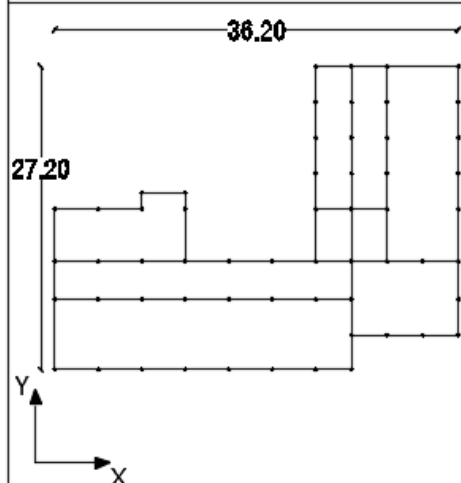
36.20

27.20

Y

X

Structural elements 1° Storey

Columns:
40x40   8Ø14   12Ø14
40x75

Beams: 8Ø14
40x60
40x90   8Ø14+2Ø12

Structural elements 2° Storey

Columns:
30x40   6Ø14
40x75   12Ø14

Beams:
40x60   8Ø14

Information Code Spectra

Building	Coordinates	Soil type
N_L: 50	Lat: 41.842	Cat: B
U_C: 1.5	Lon: 15.342	Top: T1

Knowledge Path Information

Building date: 1979

N. storeys: 2   Loads
$H_1 = 4.75 \, m$ $G_1 = 3.0 \, kN/m^2$
$H_2 = 3.50 \, m$ $G_2 = 2.0 \, kN/m^2$
                            $Q = 3.0 \, kN/m^2$

In-situ material
$f'_{cm} = 24.00 \, MPa$
$f'_{ym} = 450.00 \, MPa$
$E_c = 29369 \, MPa$

Fig. B.11 – B12 building information

B13 - Lesina (2)

Structural elements 1° Storey

Columns:
40x40   8Ø14
40x75   12Ø14

Beams:
40x60   8Ø14
40x90   8Ø14+2Ø12

Structural elements 2° Storey

Columns:
30x40   6Ø14
40x75   12Ø14

Beams:
40x60   8Ø14

Information Code Spectra

Building	Coordinates	Soil type
N_L: 50	Lat: 41.842	Cat: B
U_C: 1.5	Lon: 15.342	Top: T1

Knowledge Path Information

Building date: 1979

N. storeys: 2
$H_1 = 4.75\ m$
$H_2 = 3.50\ m$

Loads
$G_1 = 3.0\ kN/m^2$
$G_2 = 2.0\ kN/m^2$
$Q = 3.0\ kN/m^2$

In-situ material
$f^i_{cm} = 24.00\ MPa$
$f^i_{ym} = 450.00\ MPa$
$E_c = 29369\ MPa$

Fig. B.12 – B13 building information

B14 - Castelluccio Valmaggiore

Structural elements 1° Storey

Columns: 50x50   Beams: 40x60
　　　　40x40　　　　　 40x50
　　　　45x60

Structural elements 2° Storey

Columns: 50x50   Beams: 40x40
　　　　40x40　　　　　 40x50
　　　　45x60　　　　　 40x60
　　　　　　　　　　　　40x80

Structural elements 3° Storey

Columns: 50x50   Beams: 40x80
　　　　40x40　　　　　 40x50
　　　　45x60

Information Code Spectra

Building	Coordinates	Soil type
N_L: 50	Lat: 41.343	Cat: C
U_C: 1.5	Lon: 15.199	Top: T2

Knowledge Path Information

Building date: 1966

N. storeys: 2   Loads
H_1 = 4.70 m G_1 = 3.5 kN/m²
H_2 = 4.00 m G_2 = 2.5 kN/m²
H_3 = 3.75 m Q = 3.0 kN/m²

In-situ material
f^*_{cm} = 9.30 MPa
f^*_{ym} = 430.00 MPa
E_c = 21479 MPa

Fig. B.13 – B14 building information

387

B15 - Foggia

Structural elements 1° Storey
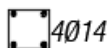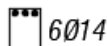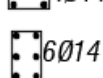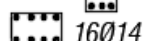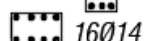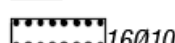
Columns:
40x40   4Ø14
50x30   6Ø14   6Ø14

Beams: 6Ø14
30x50 - 50x25   16Ø14
30x75 - 120x25   16Ø10

Structural elements 2°-3° Storeys

Columns:
30x30   4Ø14
40x30   6Ø14   6Ø14

Beams: 6Ø14
30x50 - 50x25   16Ø14
30x75 - 120x25   16Ø10
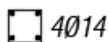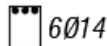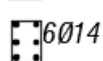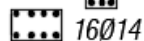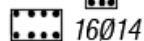
Information Code Spectra

Building	Coordinates	Soil type
N_L: 50	Lat: 41.462	Cat: B
U_C: 1.5	Lon: 15.55	Top: T1

Knowledge Path Information

Building date: 1970

N. storeys: 2   Loads
$H_1 = 3.50\ m$ $G_1 = 3.0\ kN/m^2$
$H_2 = 3.50\ m$ $G_2 = 2.8\ kN/m^2$
$H_3 = 3.50\ m$ $Q = 3.0\ kN/m^2$

In-situ material
$f'_{cm} = 24.74\ MPa$
$f'_{ym} = 405.00\ MPa$
$E_c = 29754\ MPa$

Fig. B.14 – B15 building information

388

10. Annex C: Extended results of FSA and SPO2FRAF application
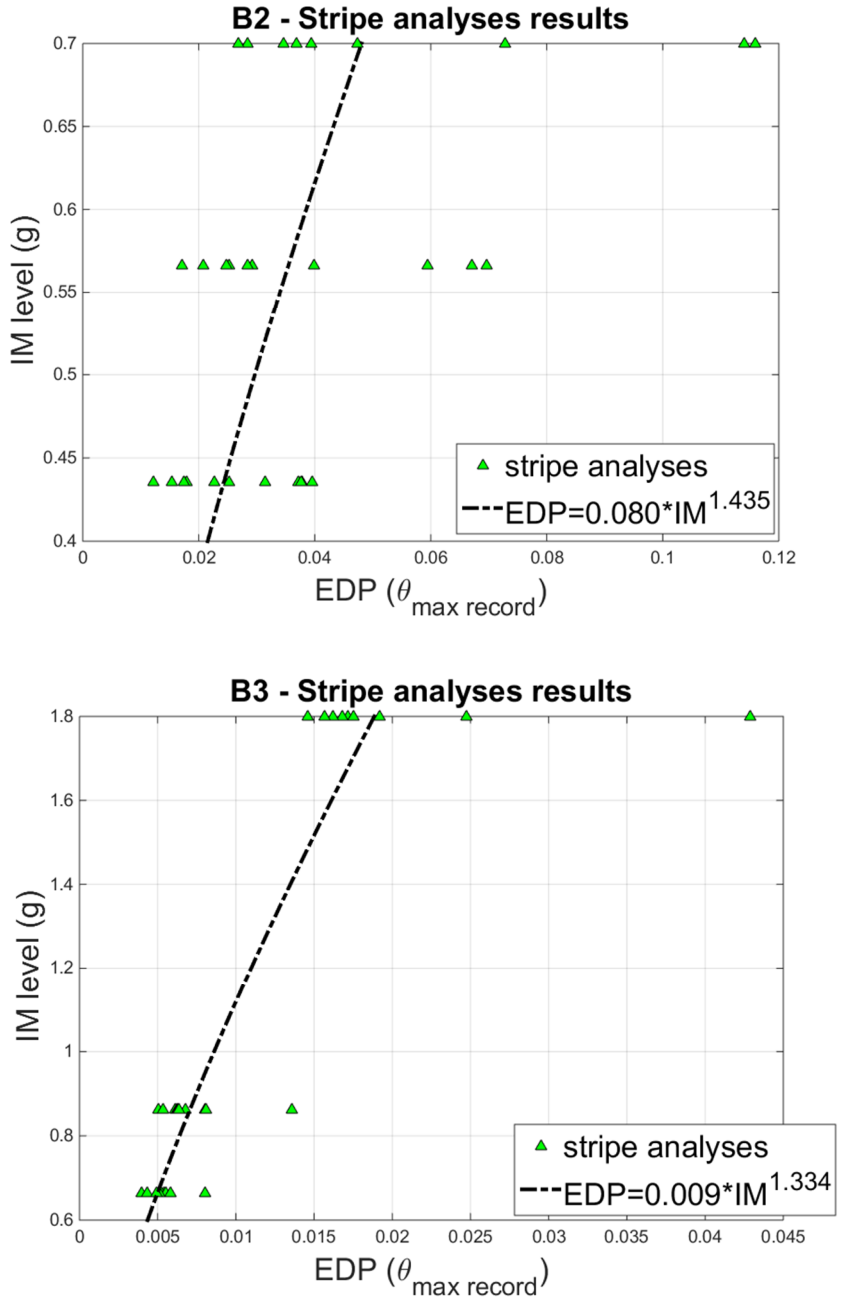
Fig. C.1 – Stripe analyses' results and related power laws for buildings B2 and B3

B4 - Stripe analyses results

legend:
△ stripe analyses
--- EDP=0.044*IM$^{1.713}$

B5 - Stripe analyses results

legend:
△ stripe analyses
--- EDP=0.005*IM$^{1.036}$
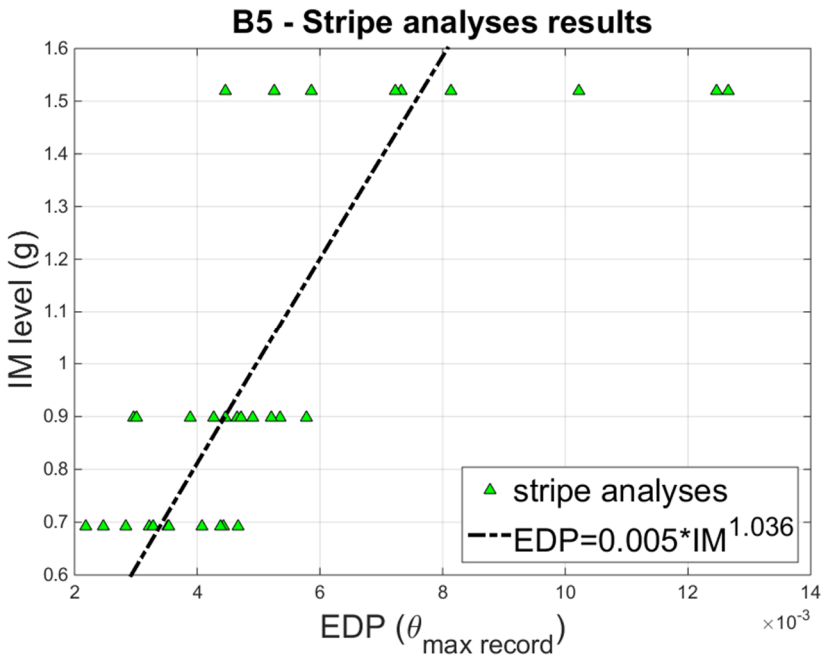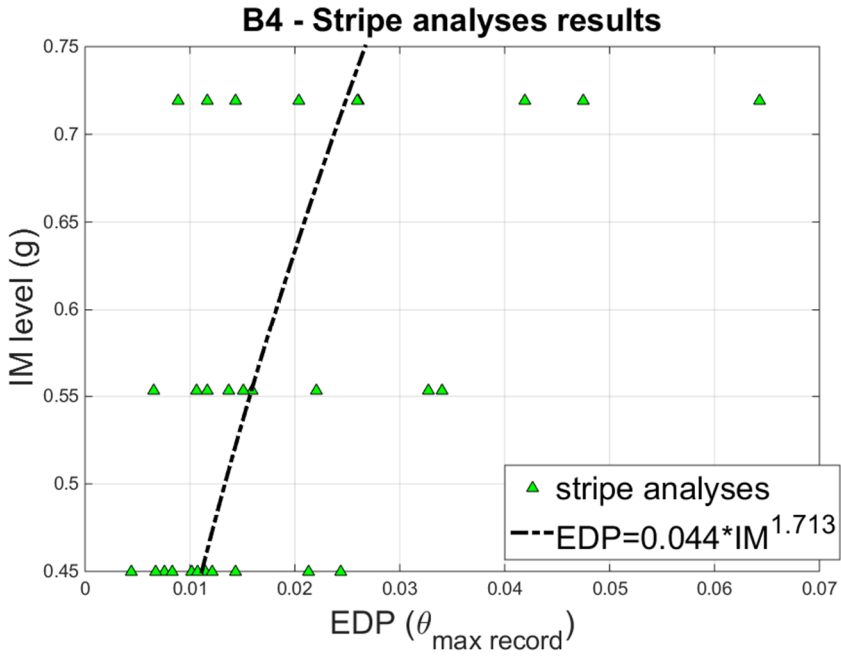
Fig. C.2 – Stripe analyses' results and related power laws for buildings B4 and B5
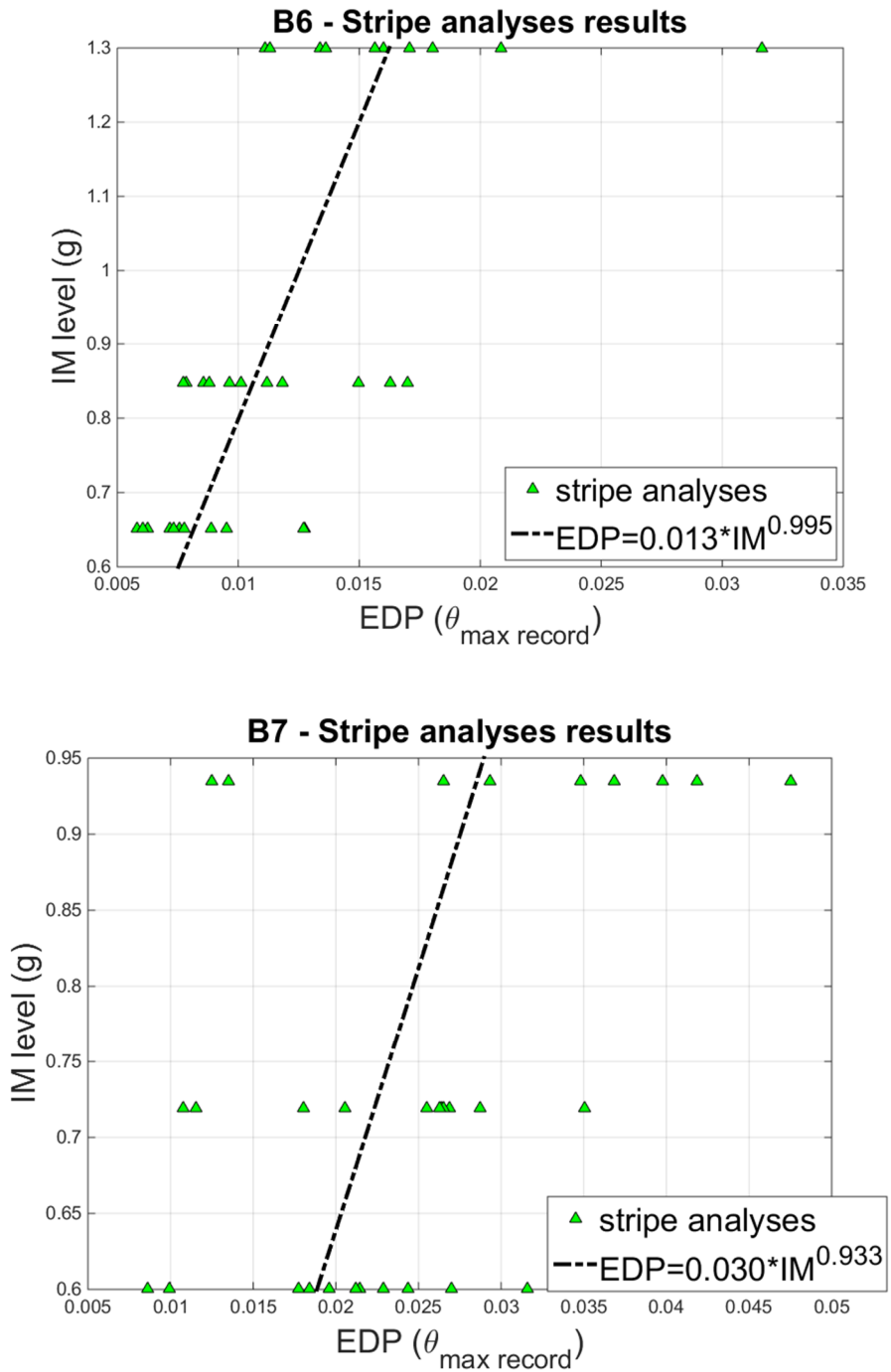
Fig. C.3 – Stripe analyses' results and related power laws for buildings B6 and B7
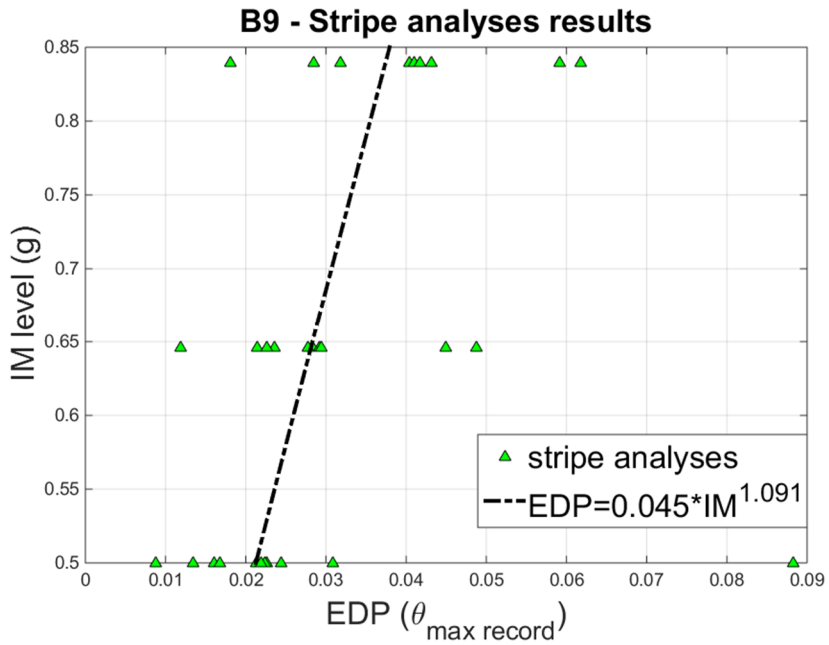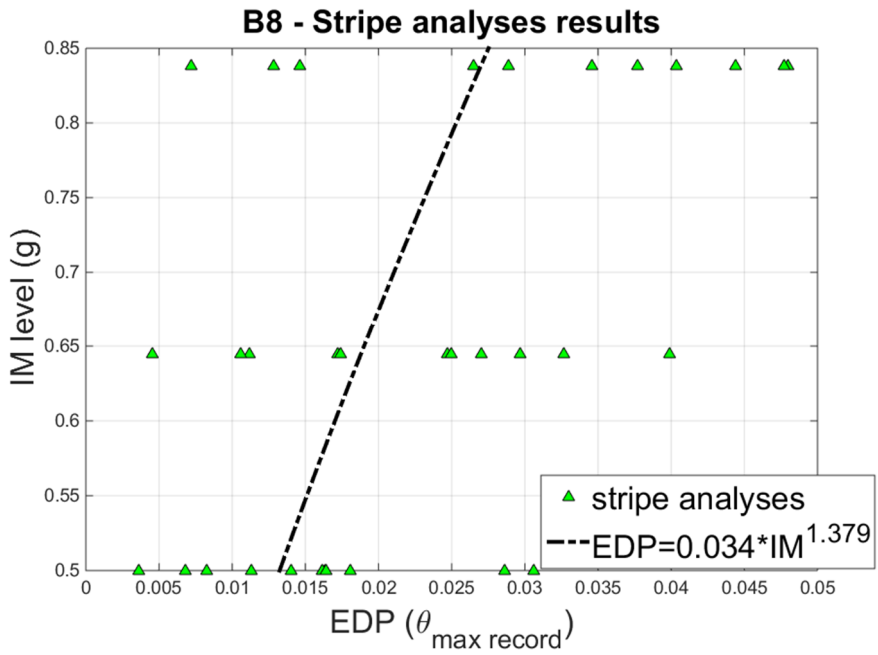
Fig. C.4 – Stripe analyses' results and related power laws for buildings B8 and B9
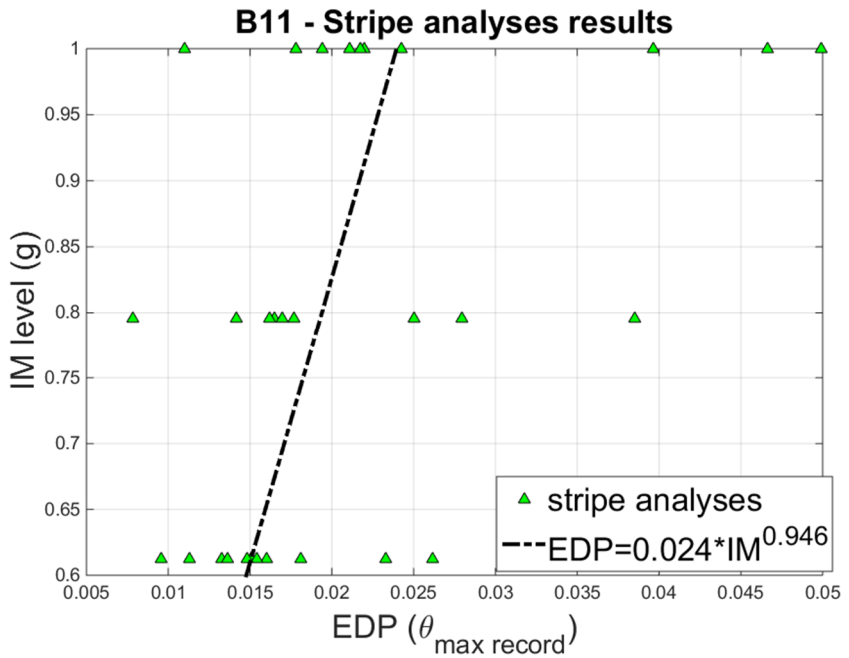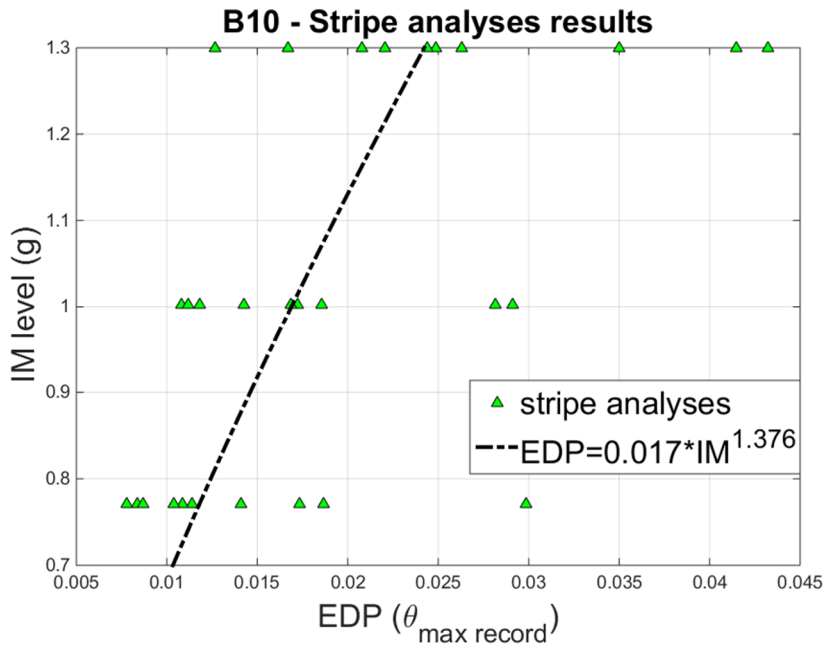
Fig. C.5 – Stripe analyses' results and related power laws for buildings B10 and B11
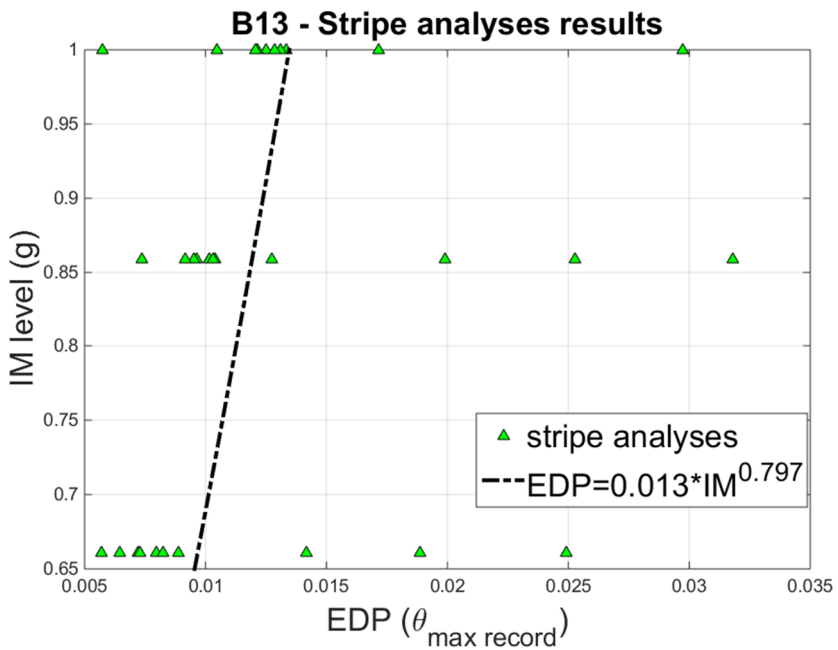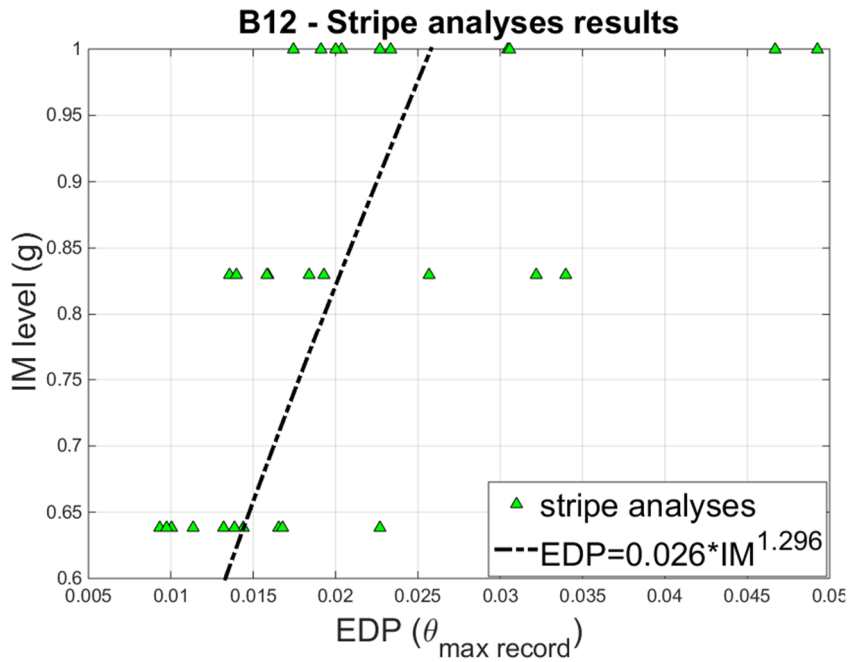
Fig. C.6 – Stripe analyses' results and related power laws for buildings B12 and B13
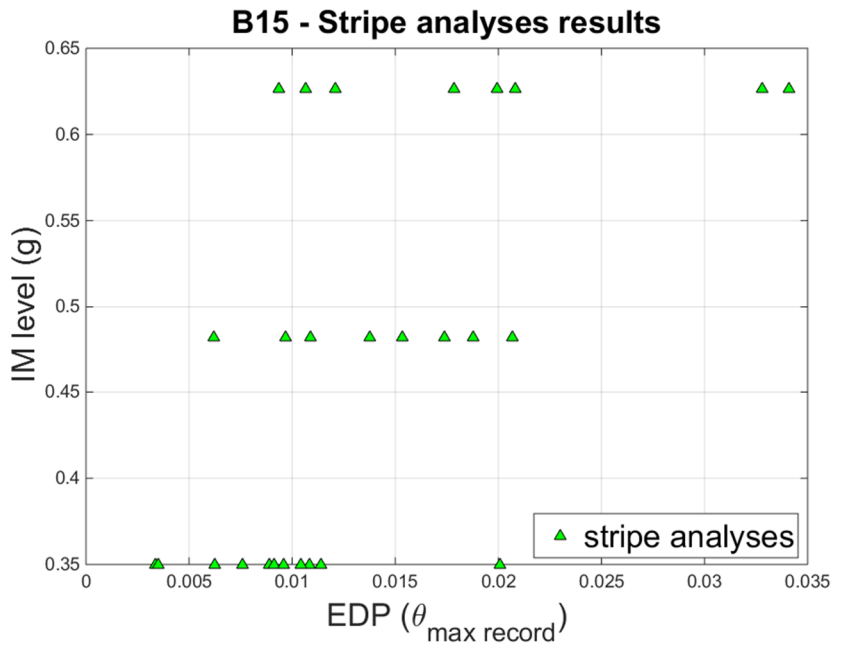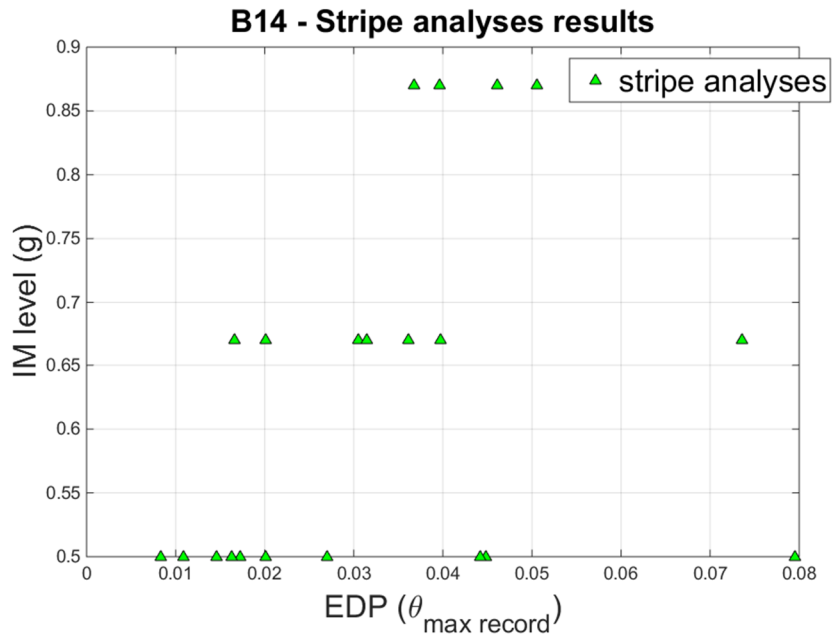
Fig. C.7 – Stripe analyses' results and related power laws for buildings B4 and B15
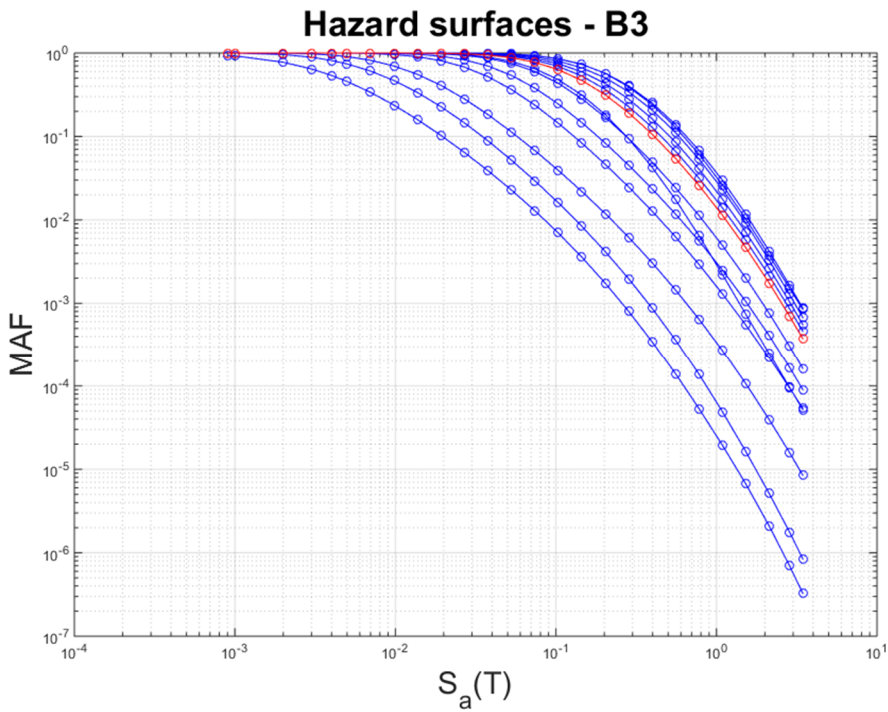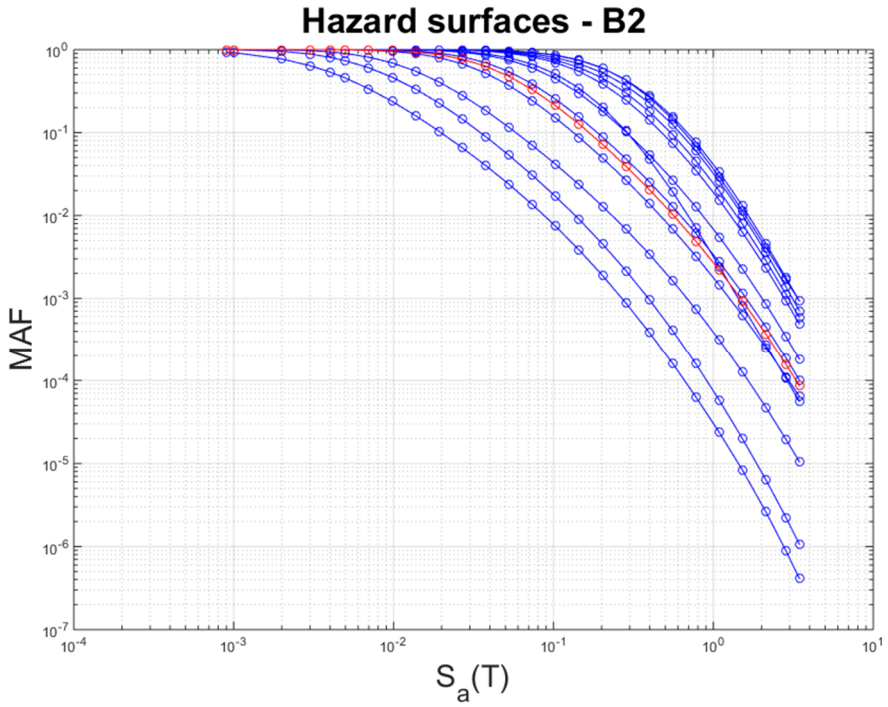
Fig. C.8 – Hazard surfaces (all curves) and Hazard curve (red curve) for B2 and B3
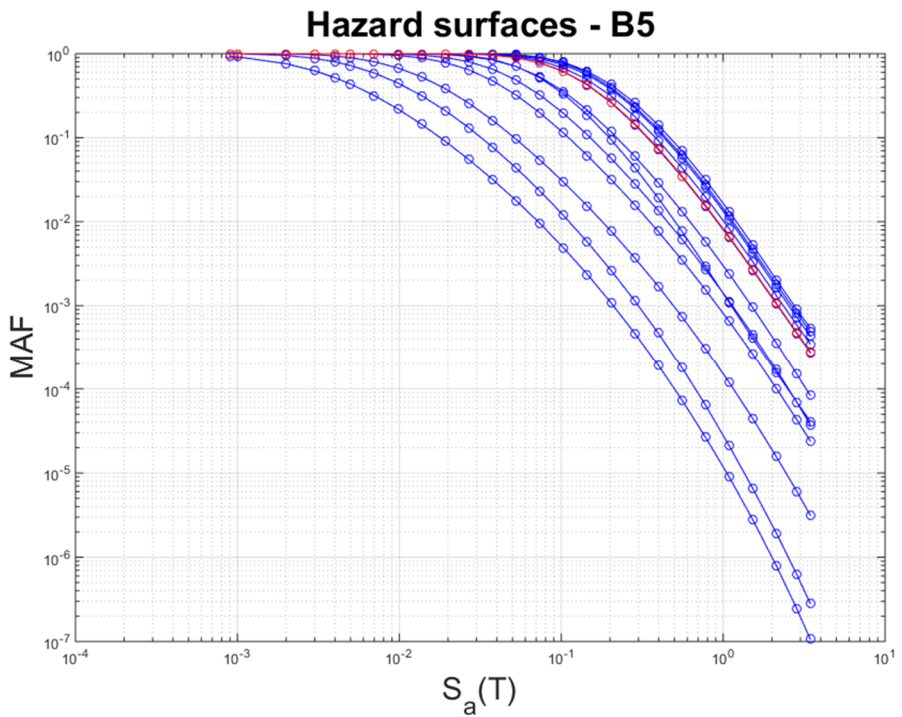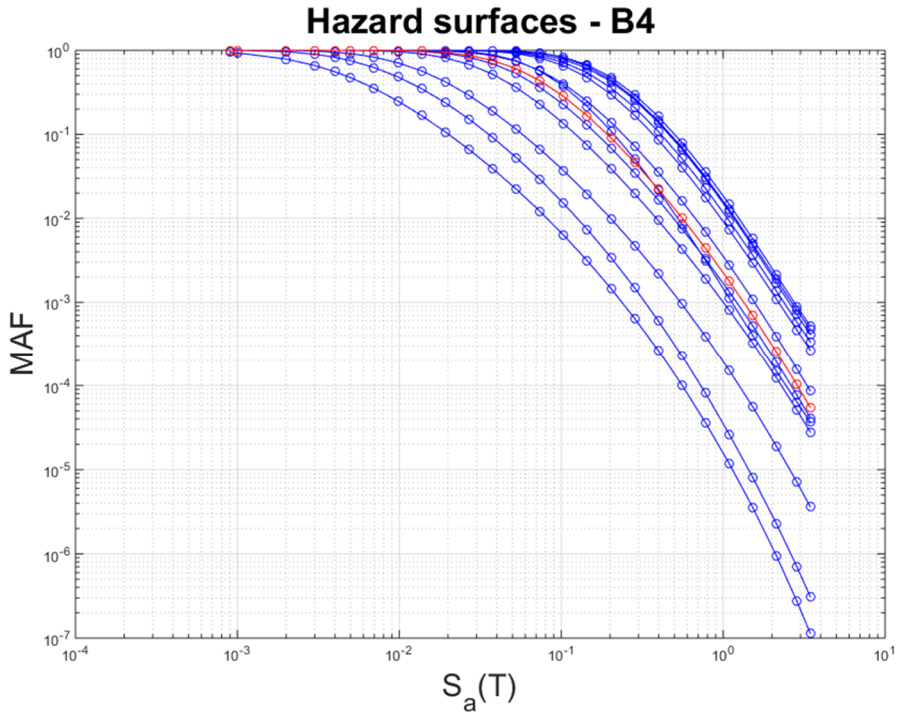
Fig. C.9 – Hazard surfaces (all curves) and Hazard curve (red curve) for B4 and B5
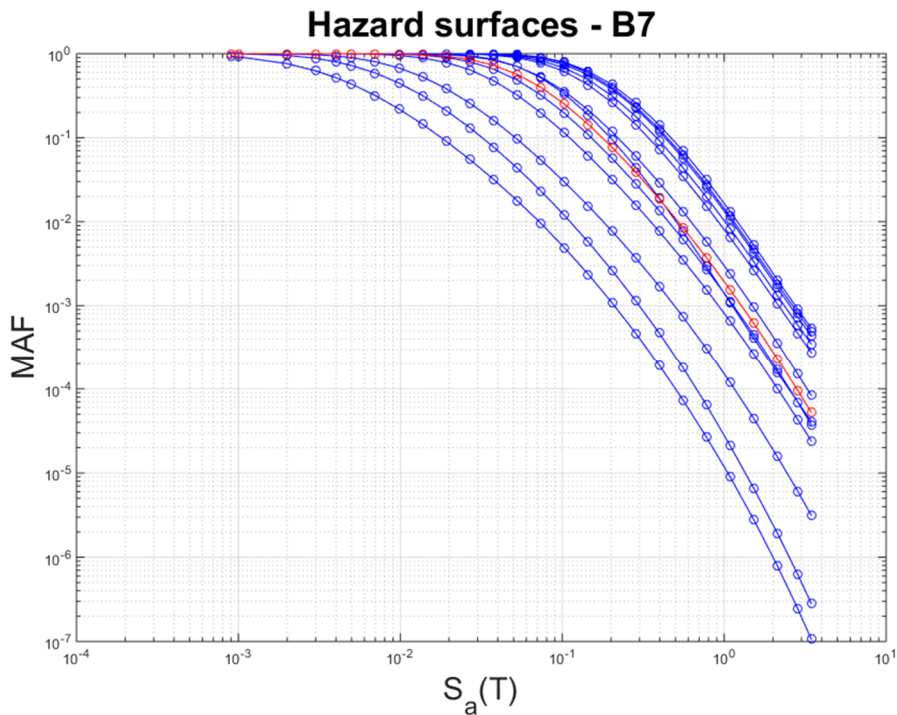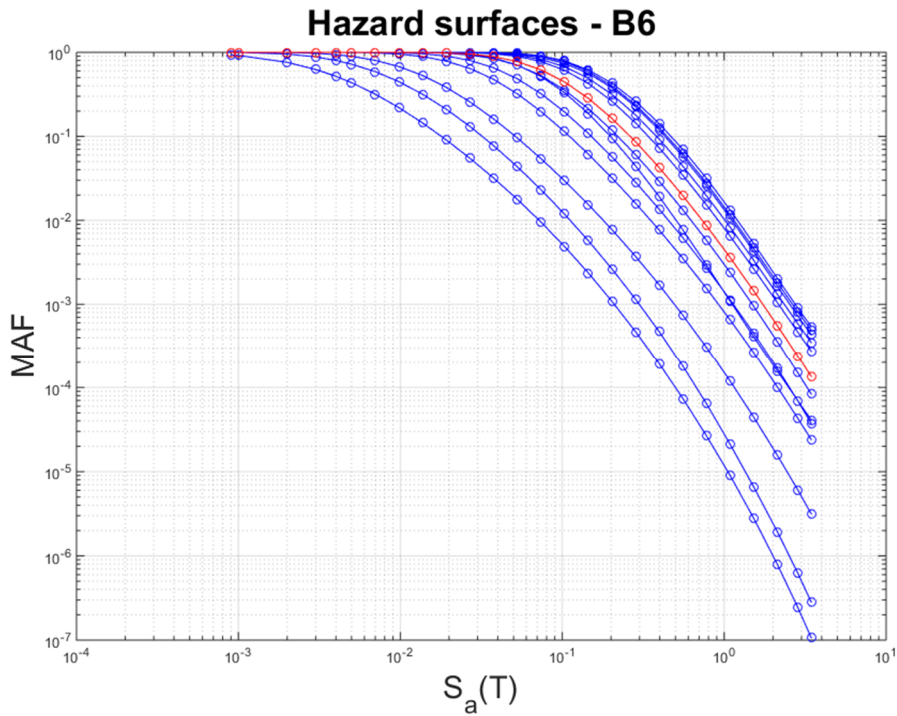
Fig. C.10 – Hazard surfaces (all curves) and Hazard curve (red curve) for B6 and B7
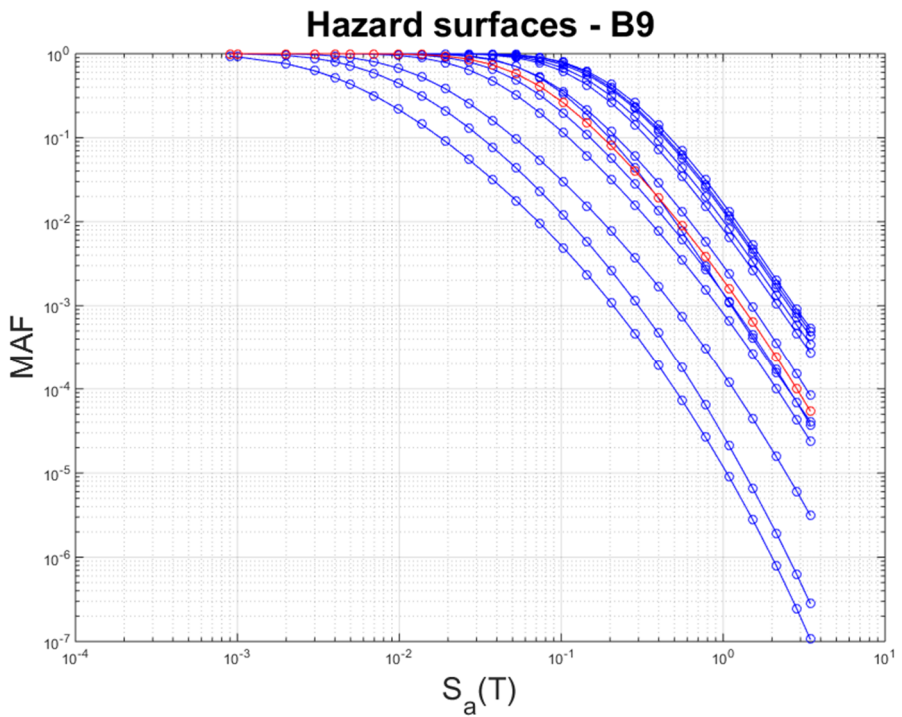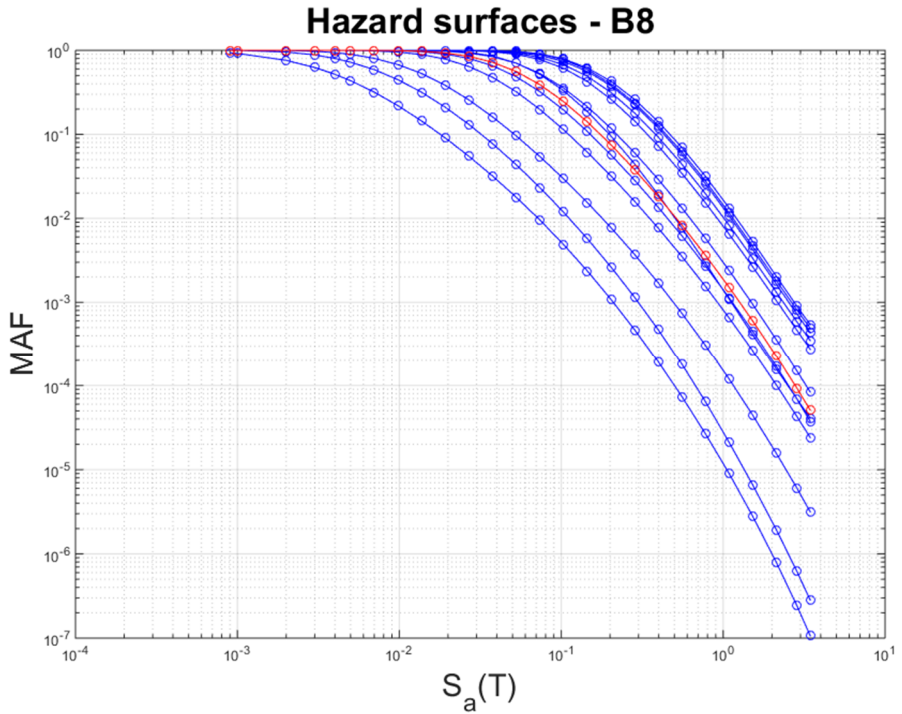
Fig. C.11 – Hazard surfaces (all curves) and Hazard curve (red curve) for B8 and B9
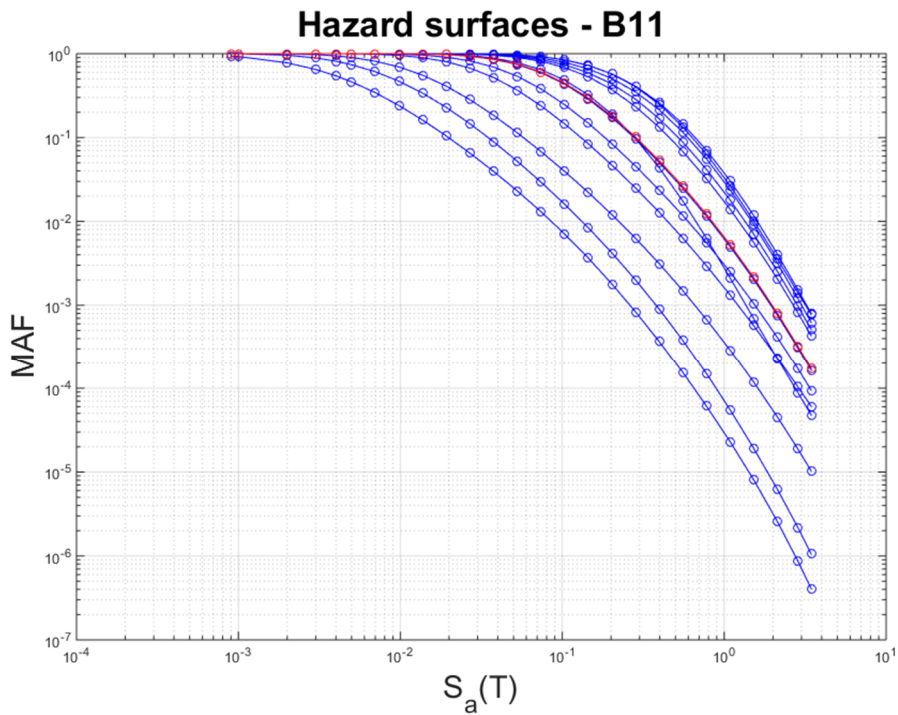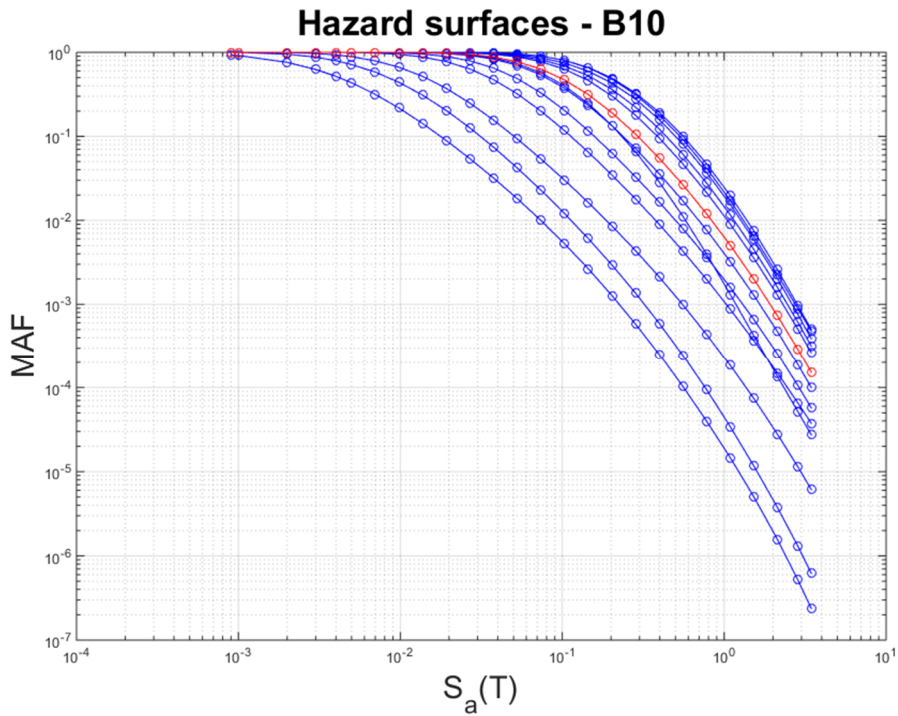
Fig. C.12 – Hazard surfaces (all curves) and Hazard curve (red curve) for B10 and B11
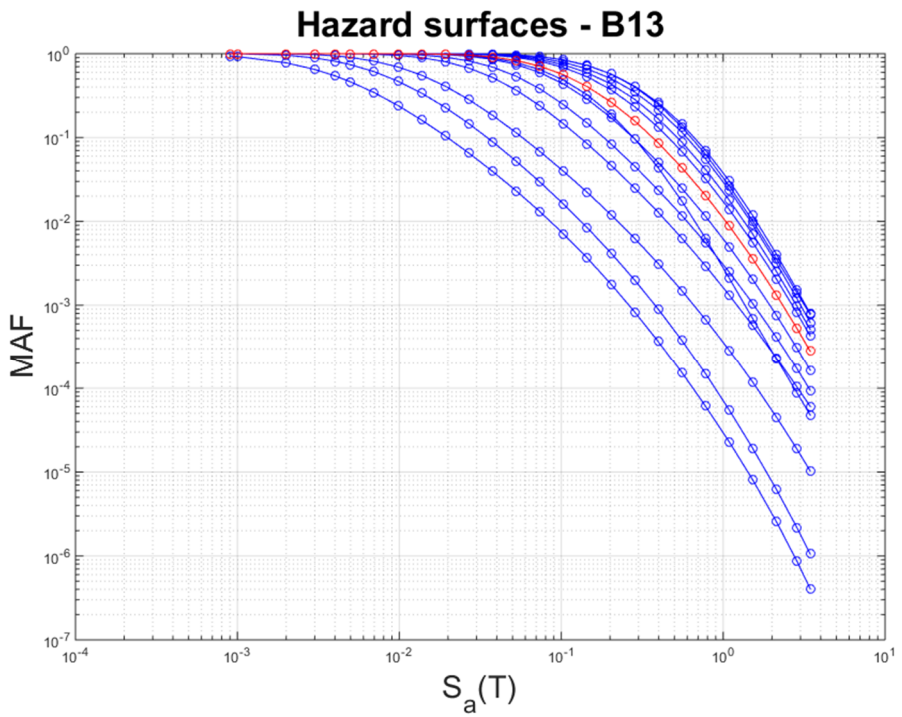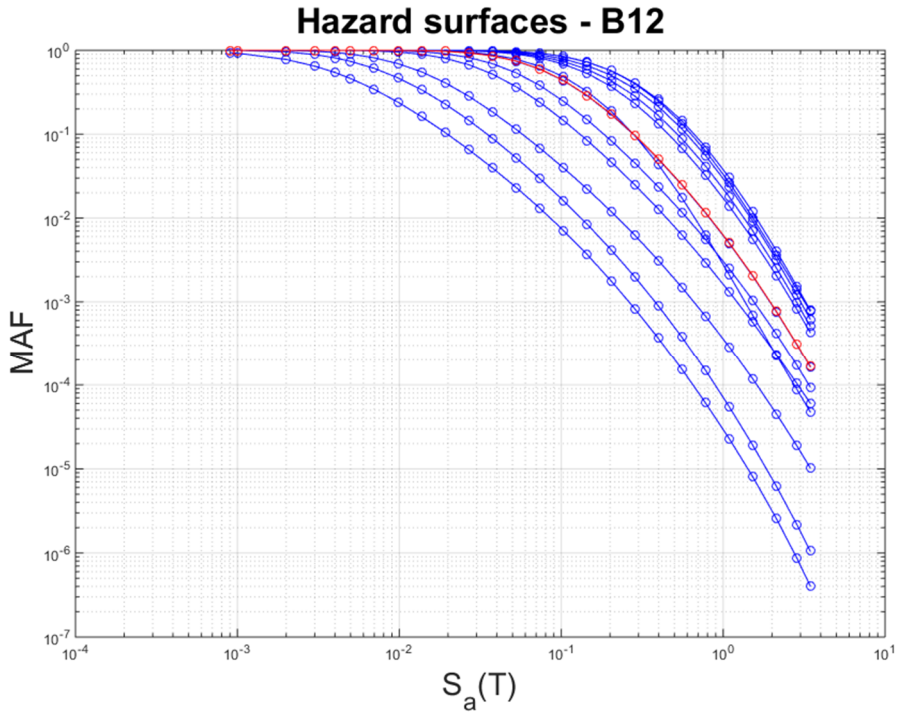
Fig. C.13 – Hazard surfaces (all curves) and Hazard curve (red curve) for B12 and B13
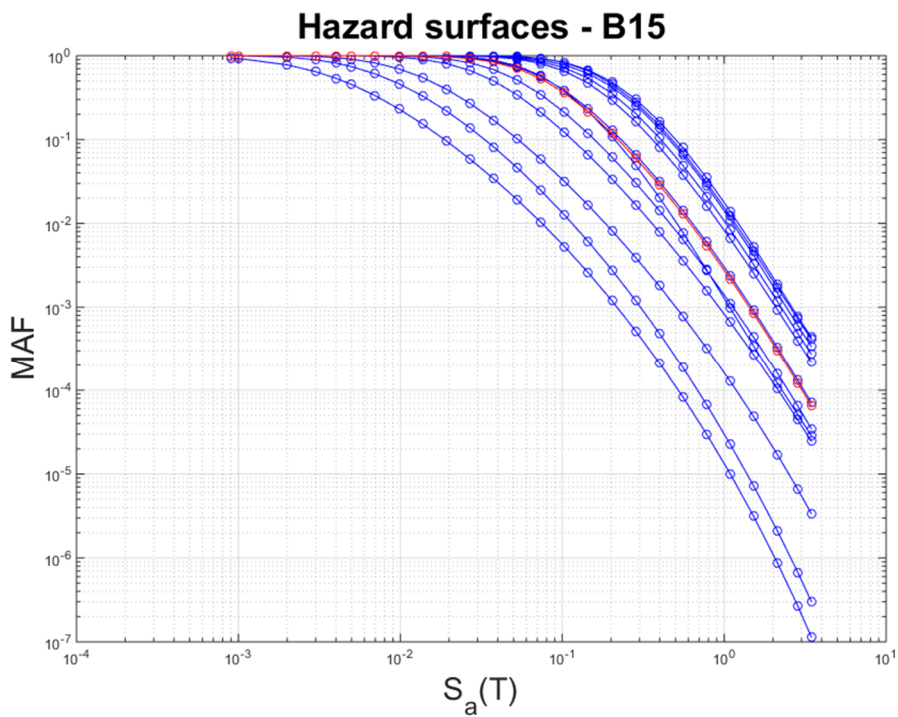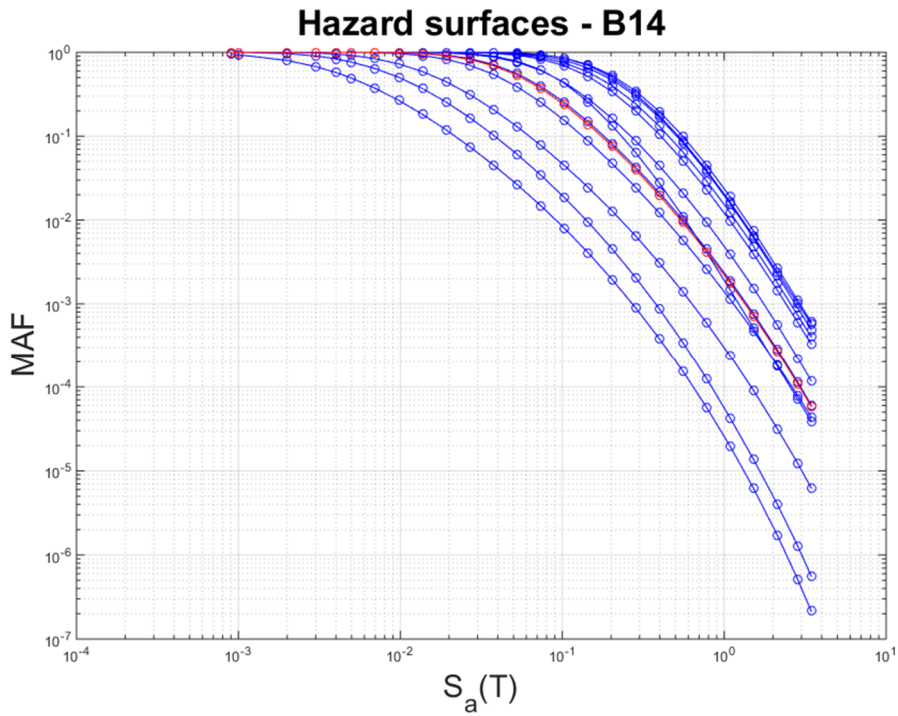
Fig. C.14 – Hazard surfaces (all curves) and Hazard curve (red curve) for B14 and B15
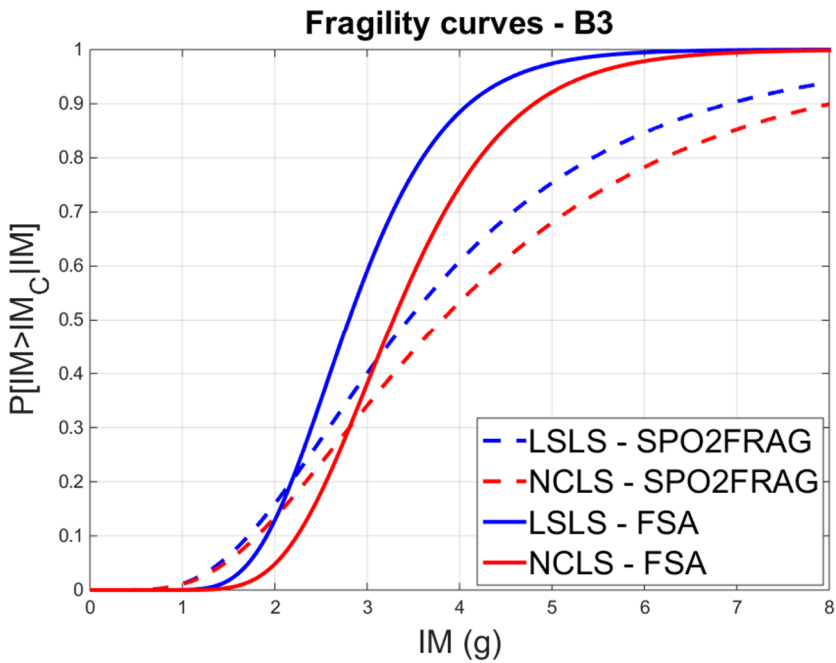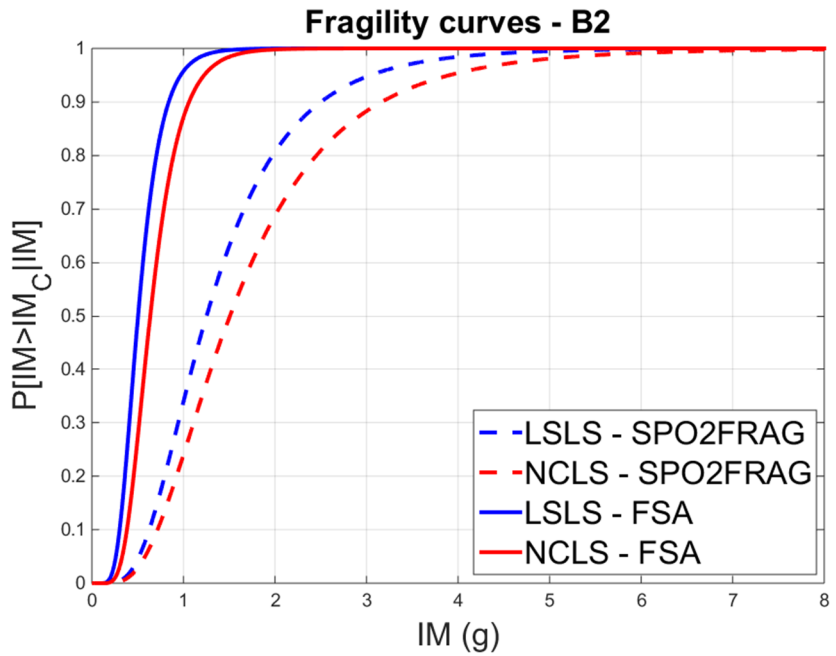
Fig. C.15 – One-by-one comparison between the fragility curves obtained from the two methodologies adopted, for B2 and B3
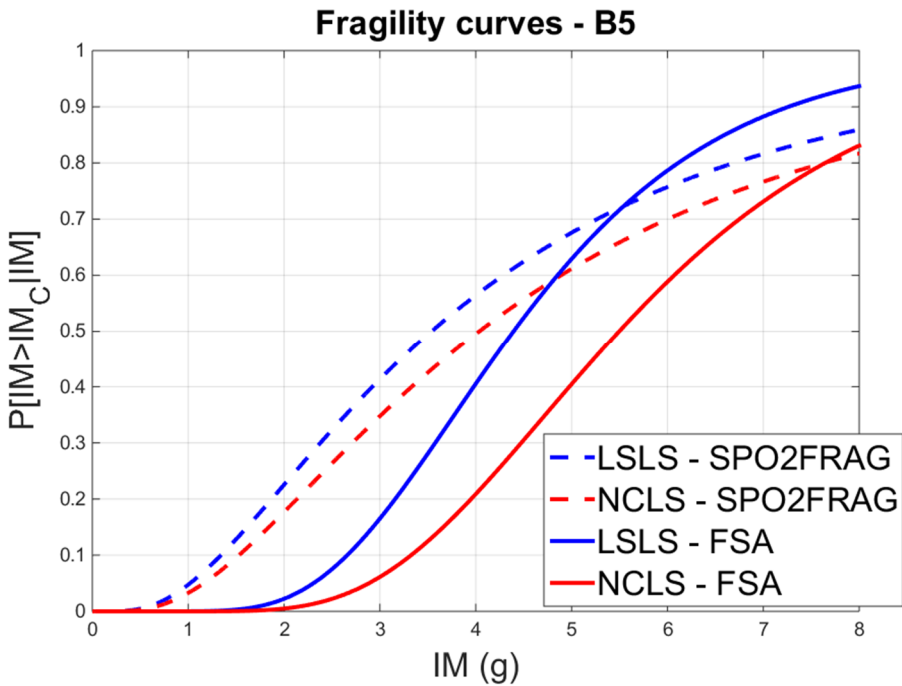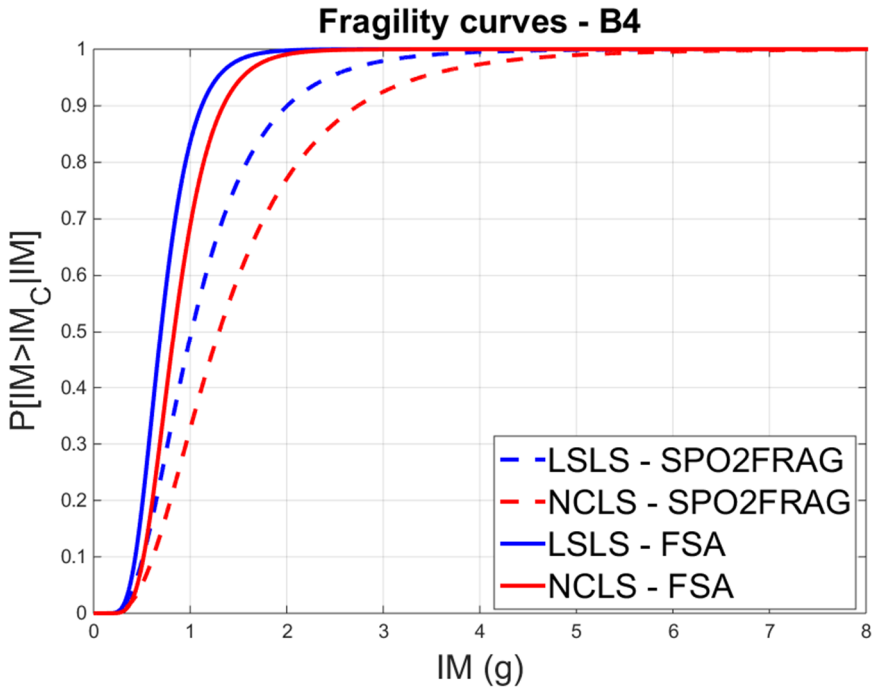
Fig. C.16 – One-by-one comparison between the fragility curves obtained from the two methodologies adopted, for B4 and B5
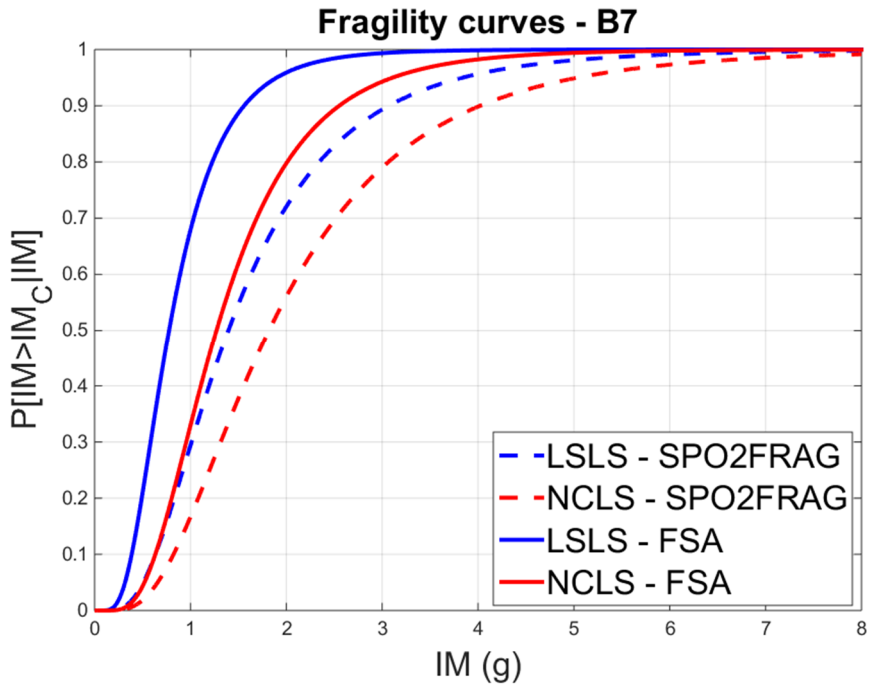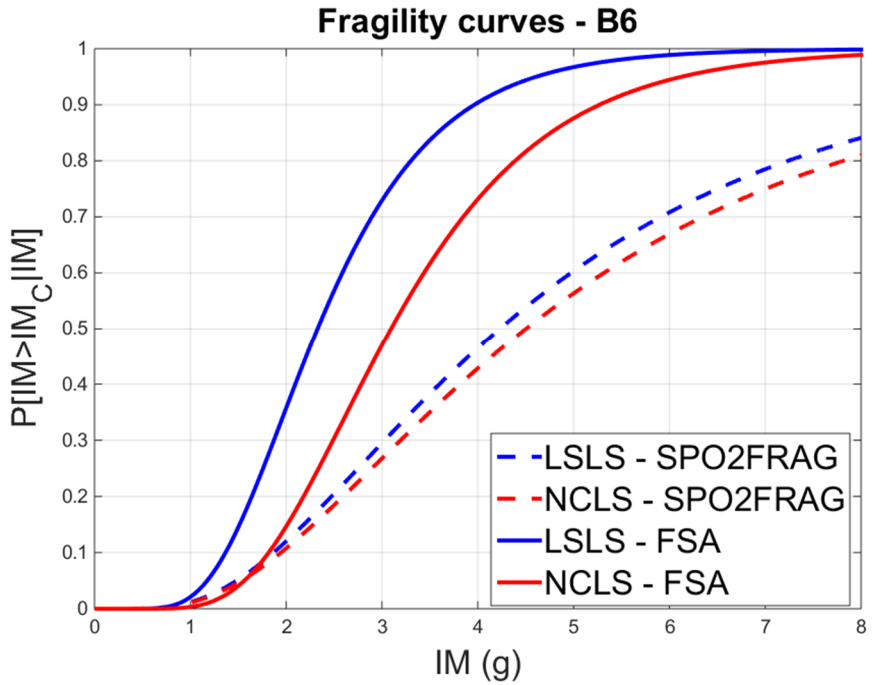
Fig. C.17 – One-by-one comparison between the fragility curves obtained from the two methodologies adopted, for B6 and B7
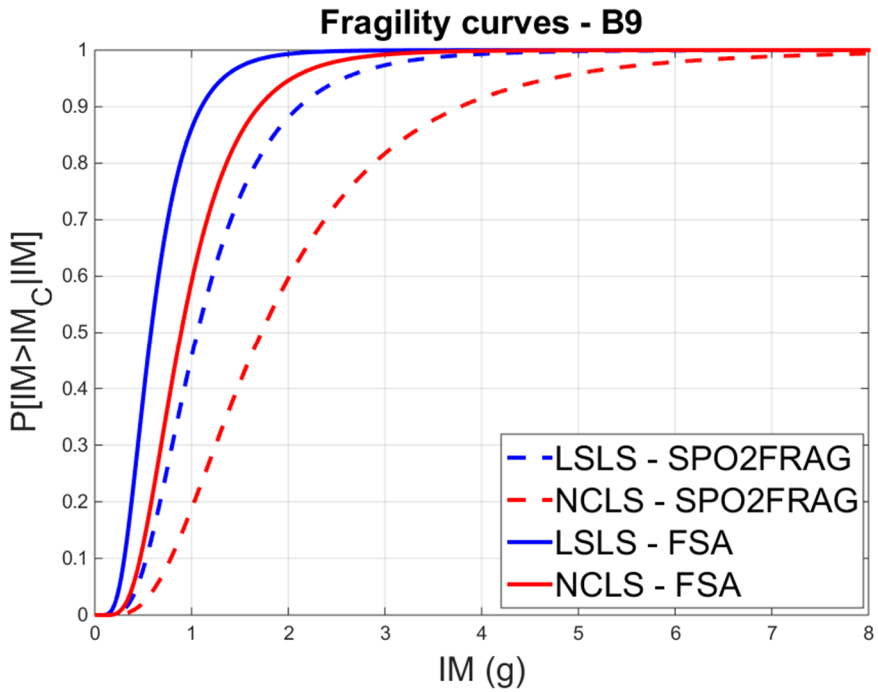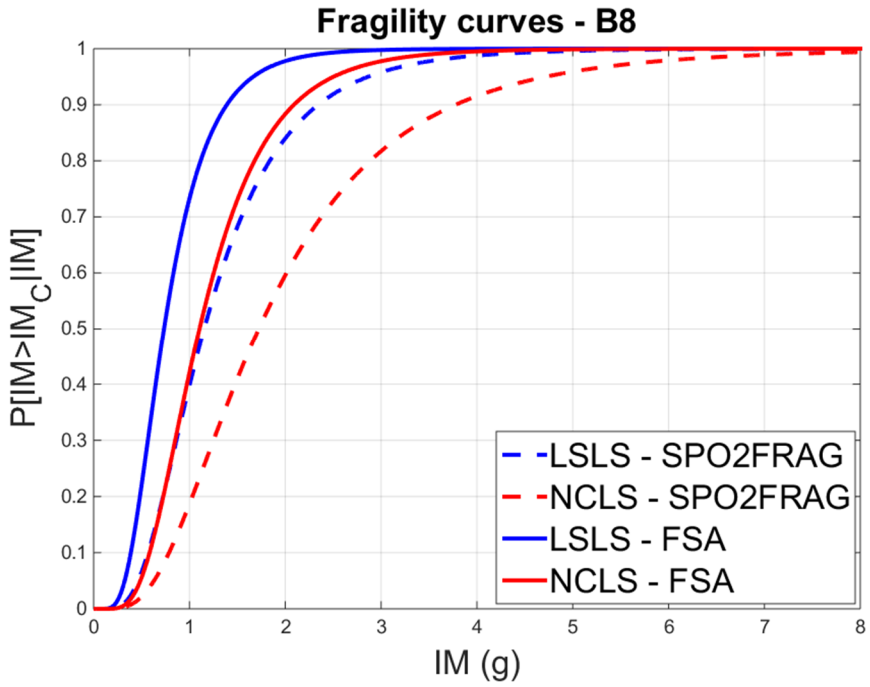
Fig. C.18 – One-by-one comparison between the fragility curves obtained from the two methodologies adopted, for B8 and B9
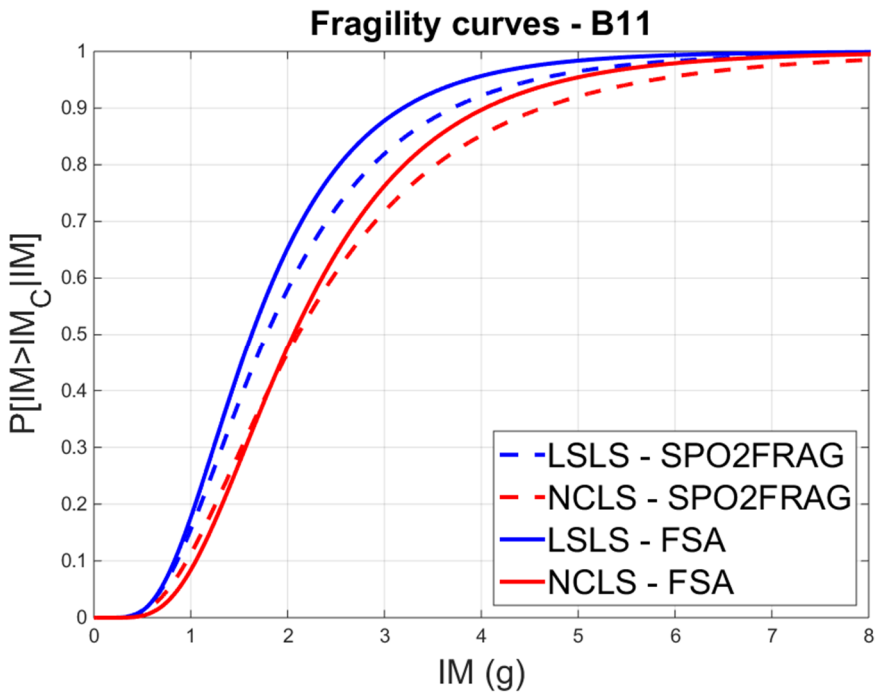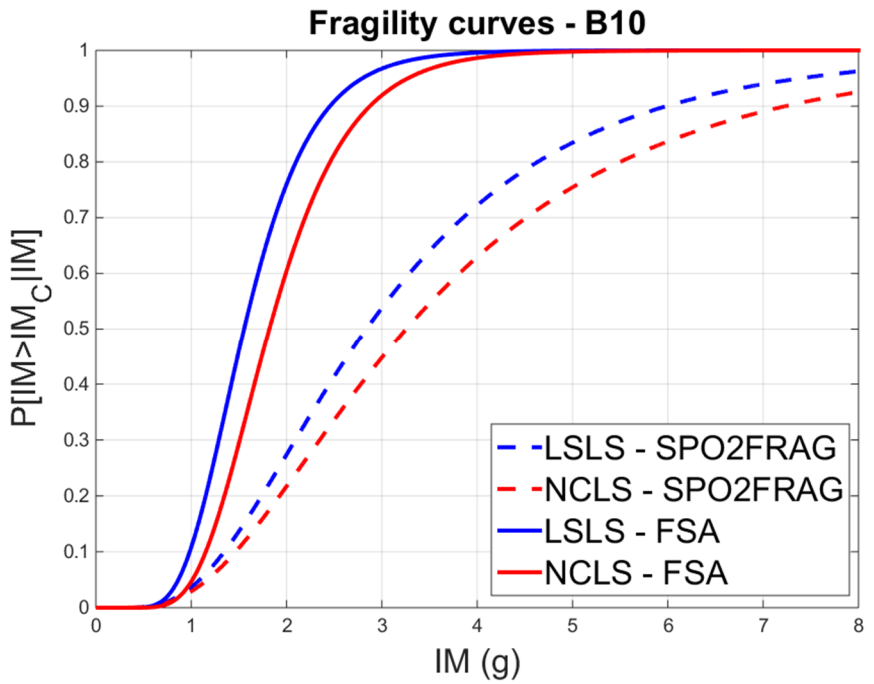
Fig. C.19 – One-by-one comparison between the fragility curves obtained from the two methodologies adopted, for B10 and B11
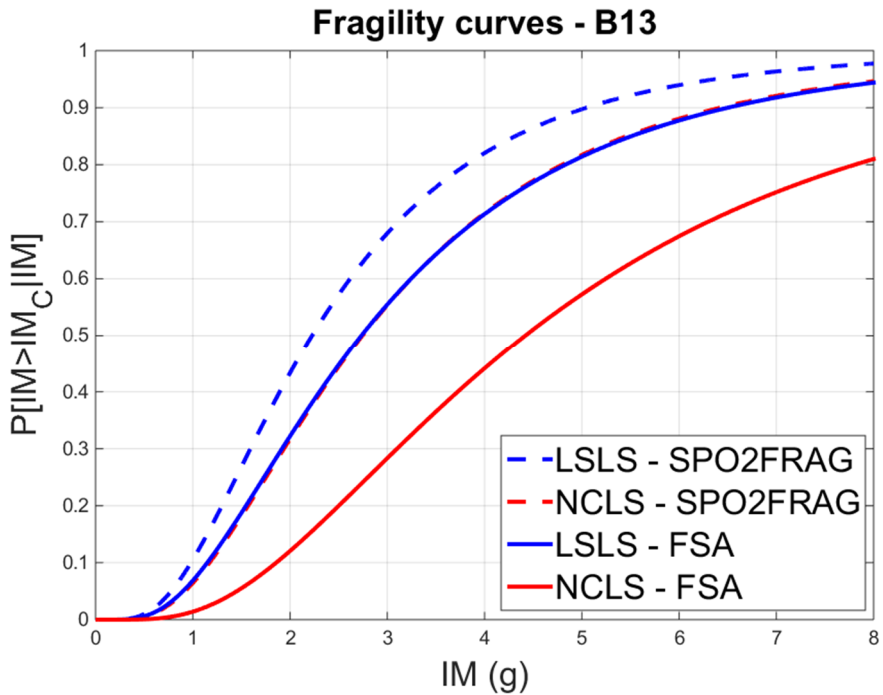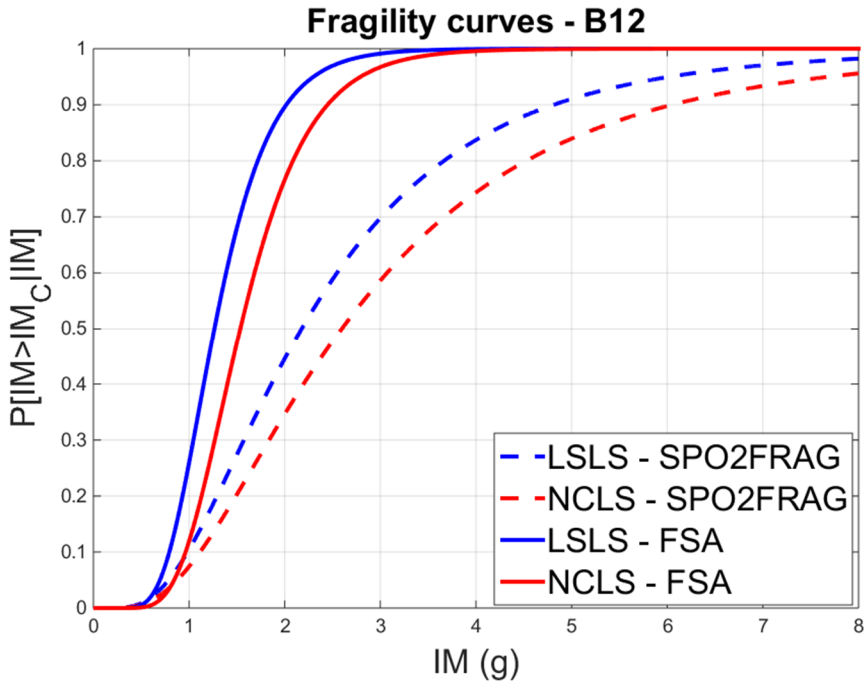
Fig. C.20 – One-by-one comparison between the fragility curves obtained from the two methodologies adopted, for B12 and B13
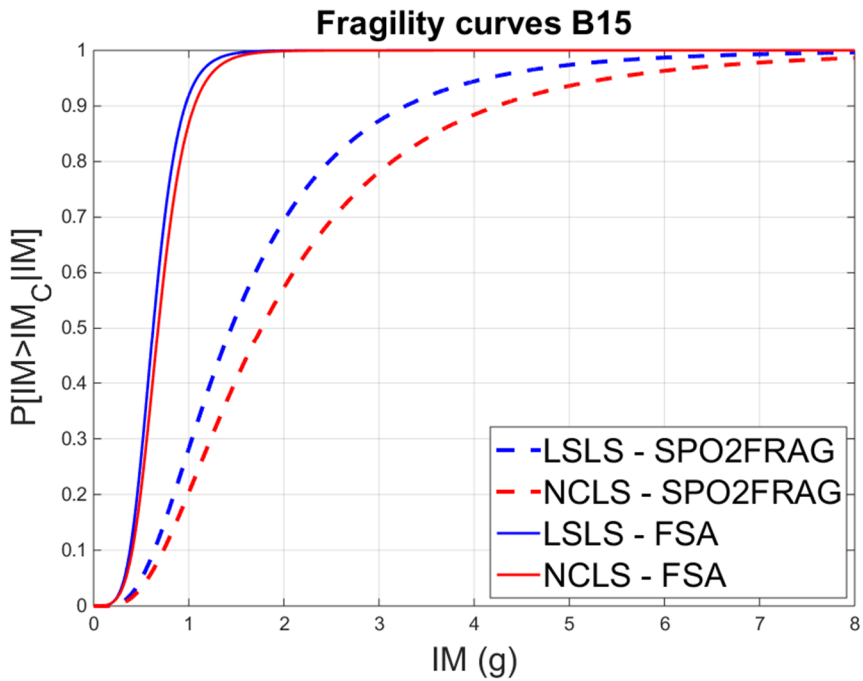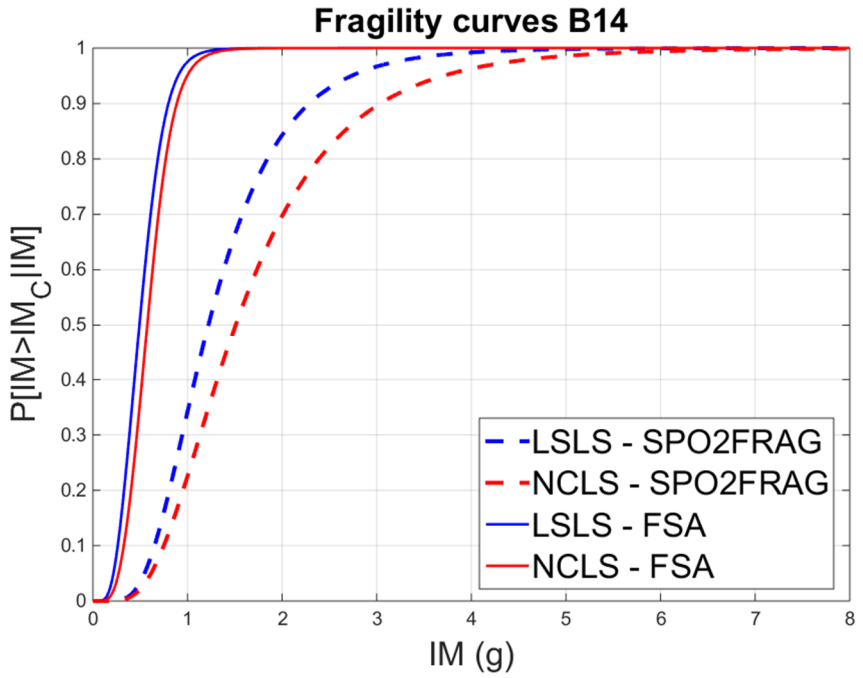
Fig. C.21 – One-by-one comparison between the fragility curves obtained from the two methodologies adopted, for B14 and B15

11. Annex D: Extended results of 3D reduced-order models application

B2 - Carpino	
Full model	**3D reduced-order model**
	Dimensions in-plan 3.69 / 4.06

B3 - Manfredonia	
Full model	**3D reduced-order model**
	Dimensions in-plan 4.61 / 5.59
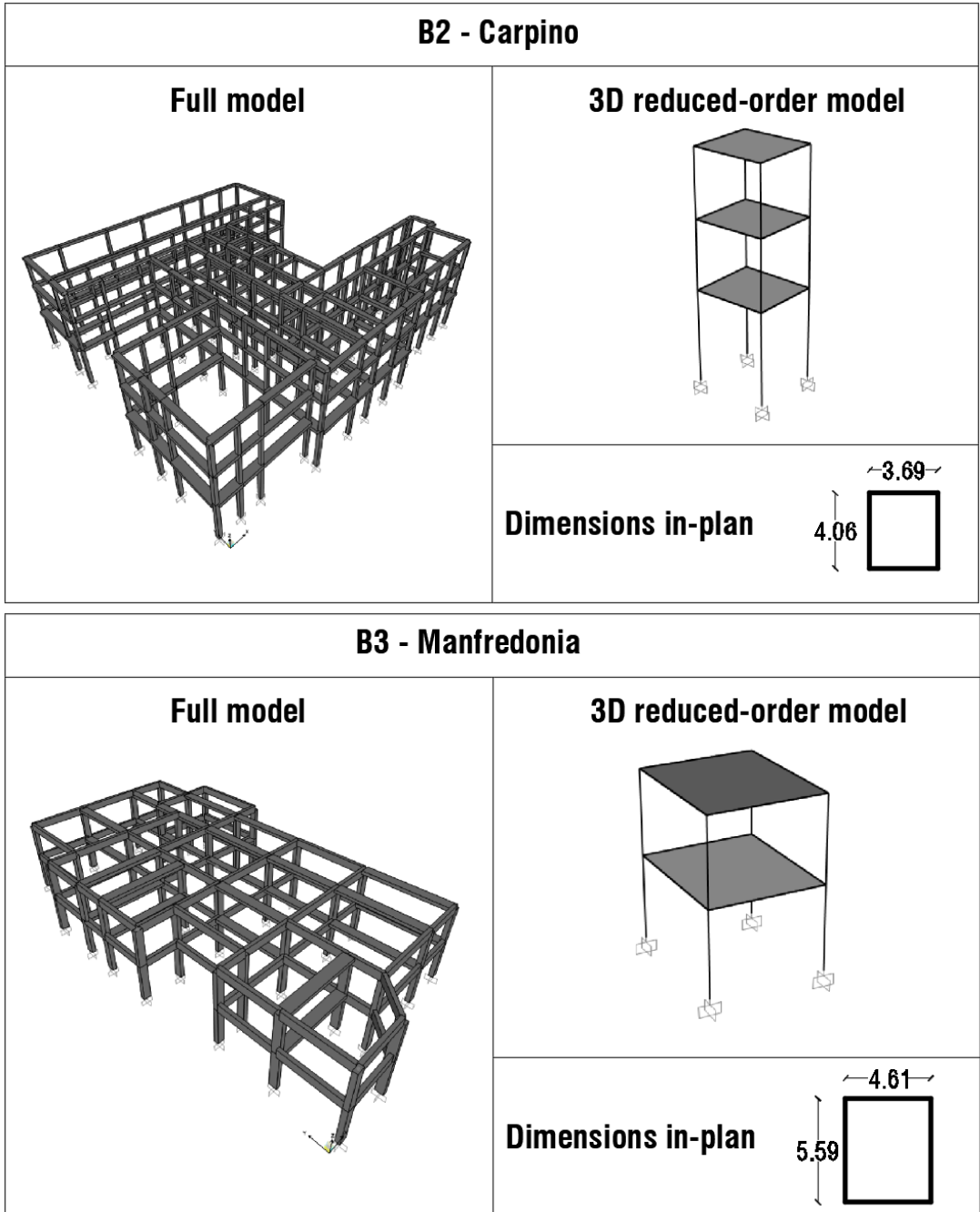
Fig. D.1 – 3D reduced-order models for the buildings B2 and B3

B4 - Bovino	
Full model	**3D reduced-order model**
	Dimensions in-plan
	3.54 / 6.98

B5 - Cerignola (1)	
Full model	**3D reduced-order model**
	Dimensions in-plan
	4.89 / 3.93
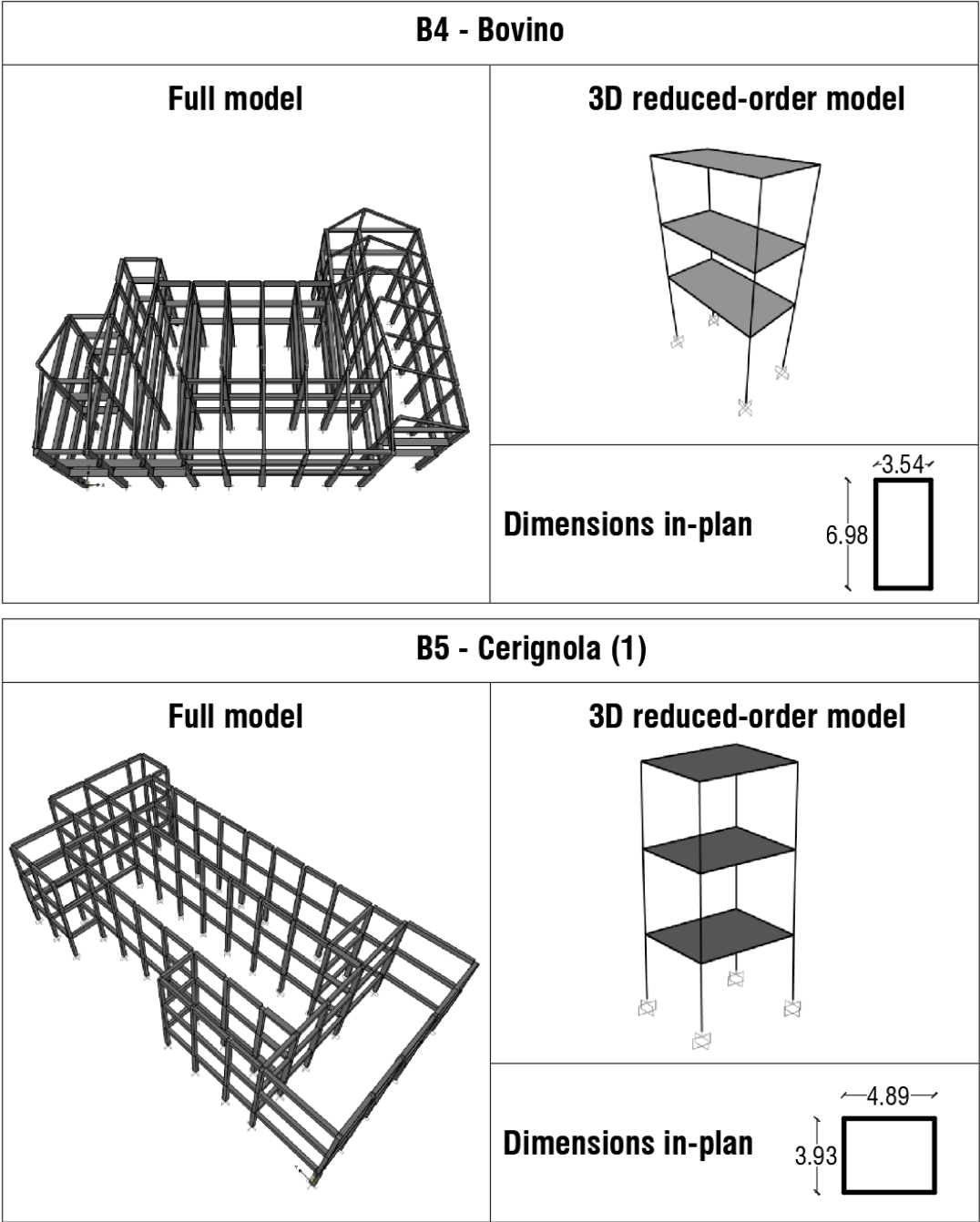
Fig. D.2 – 3D reduced-order models for the buildings B4 and B5

B6 - Cerignola (2)	
Full model	**3D reduced-order model**
	Dimensions in-plan — 5.54, 3.63
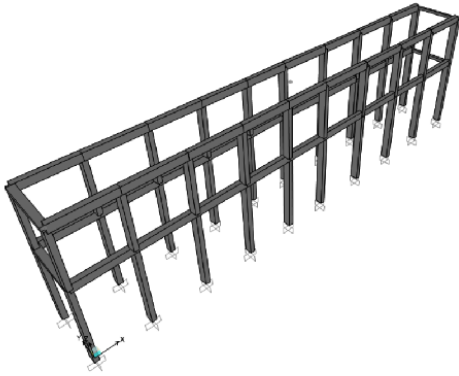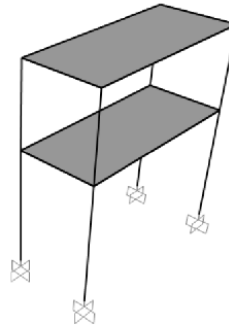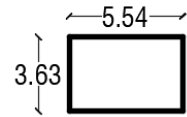
B7 - Cerignola (2)	
Full model	**3D reduced-order model**
	Dimensions in-plan — 3.71, 3.38
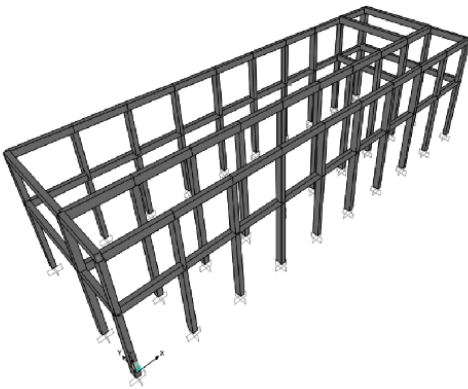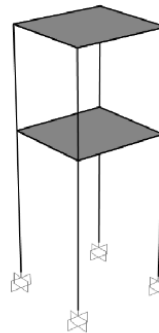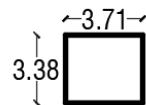
Fig. D.3 – 3D reduced-order models for the buildings B6 and B7

| B8 - Cerignola (2) | |
| Full model | 3D reduced-order model |

Dimensions in-plan

4.00
3.73
3.14
3.77

| B9 - Cerignola (2) | |
| Full model | 3D reduced-order model |

Dimensions in-plan

3.79
3.74
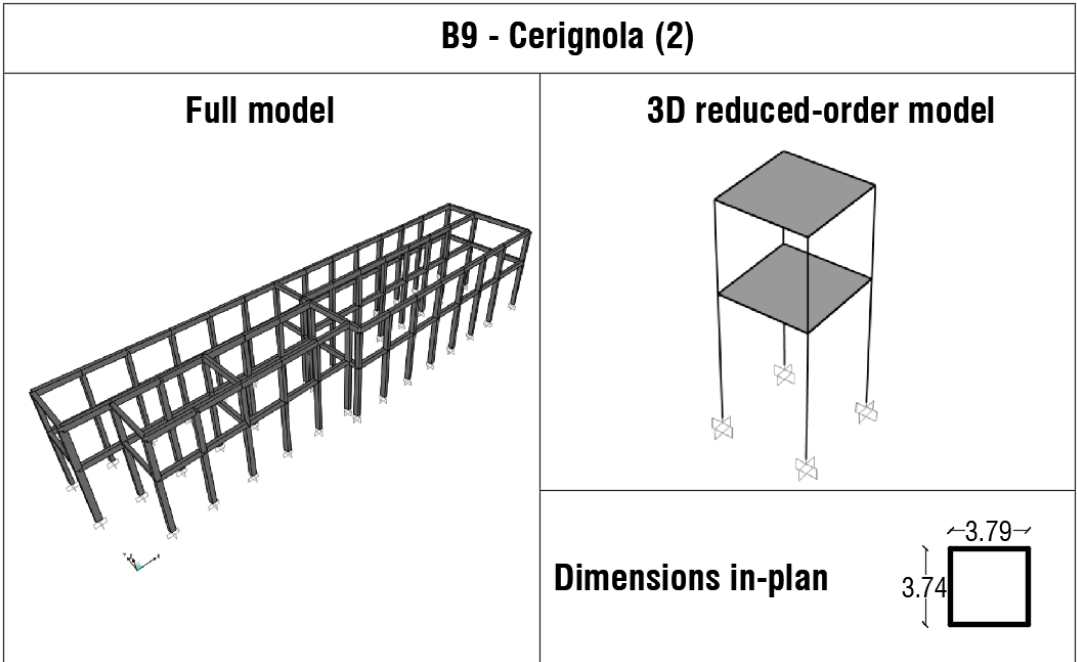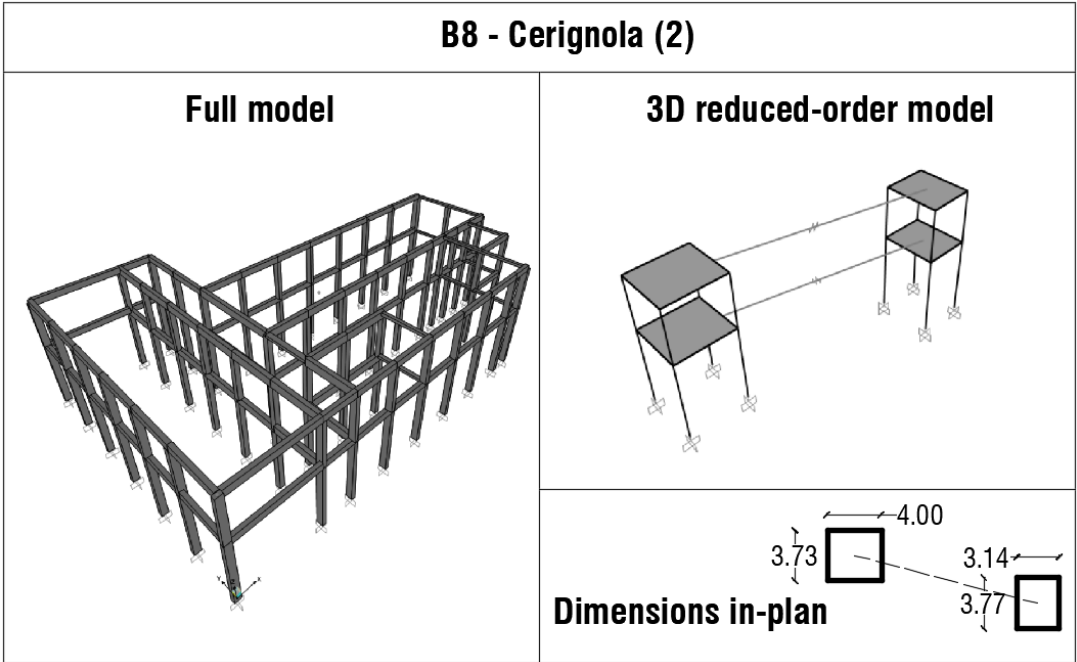
Fig. D.4 – 3D reduced-order models for the buildings B8 and B9

B10 - Lesina (1)	
Full model	**3D reduced-order model**
	Dimensions in-plan
	3.67 / 4.21
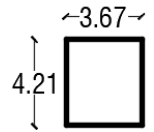
B11 - Lesina (2)	
Full model	**3D reduced-order model**
	Dimensions in-plan
	3.20 / 4.30
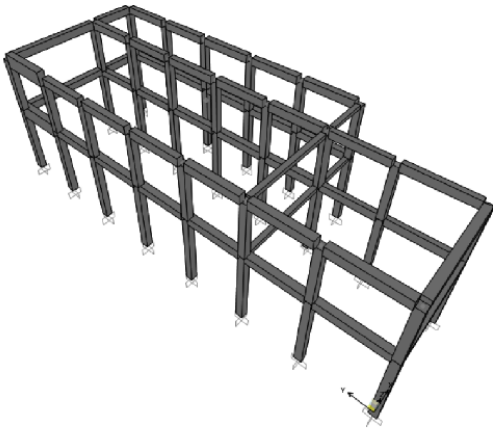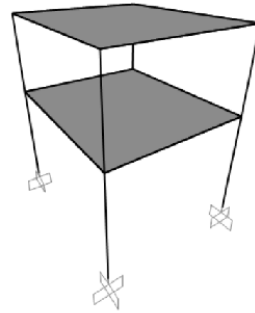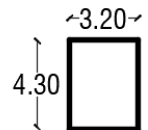
Fig. D.5 – 3D reduced-order models for the buildings B10 and B11

B12 - Lesina (2)	
Full model	**3D reduced-order model**
	Dimensions in-plan
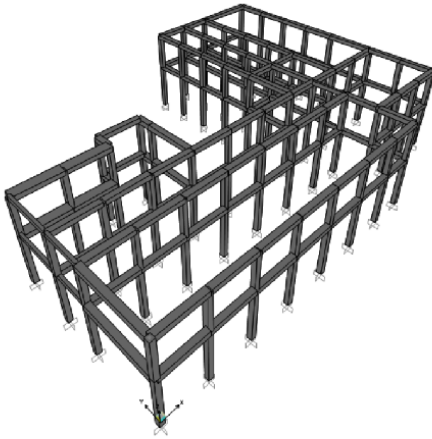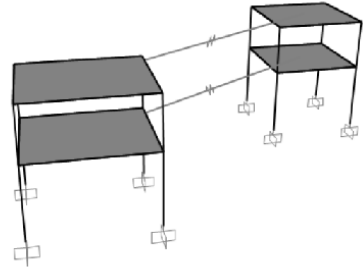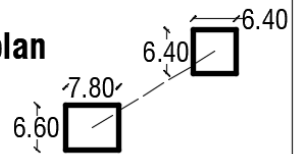
B13 - Lesina (2)	
Full model	**3D reduced-order model**
	Dimensions in-plan
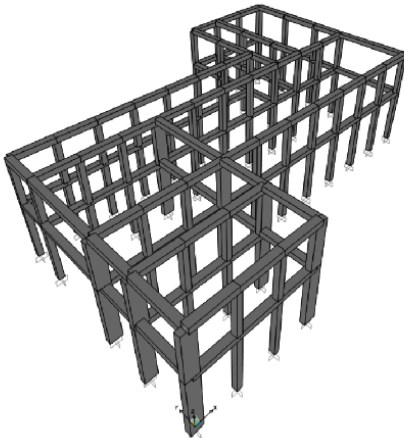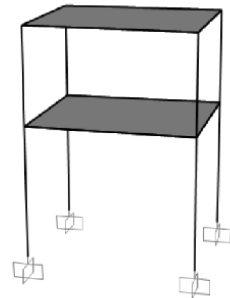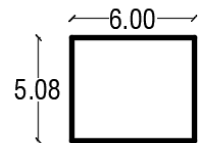
Fig. D.6 – 3D reduced-order models for the buildings B12 and B13

B14 - Castelluccio Valmaggiore

Full model

3D reduced-order model

Dimensions in-plan

3.56

6.66
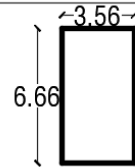
B15 - Foggia

Full model

3D reduced-order model

5.06

5.50

Dimensions in-plan

4.41

4.51
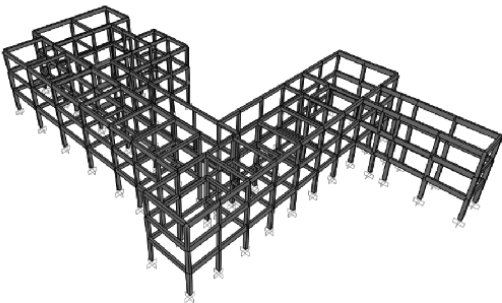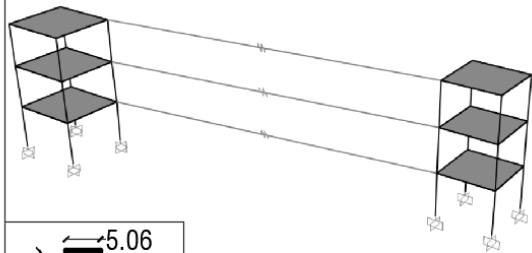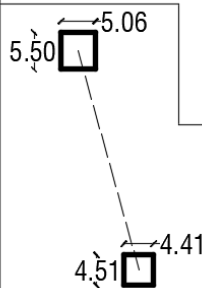
Fig. D.7 – 3D reduced-order models for the buildings B14 and B15
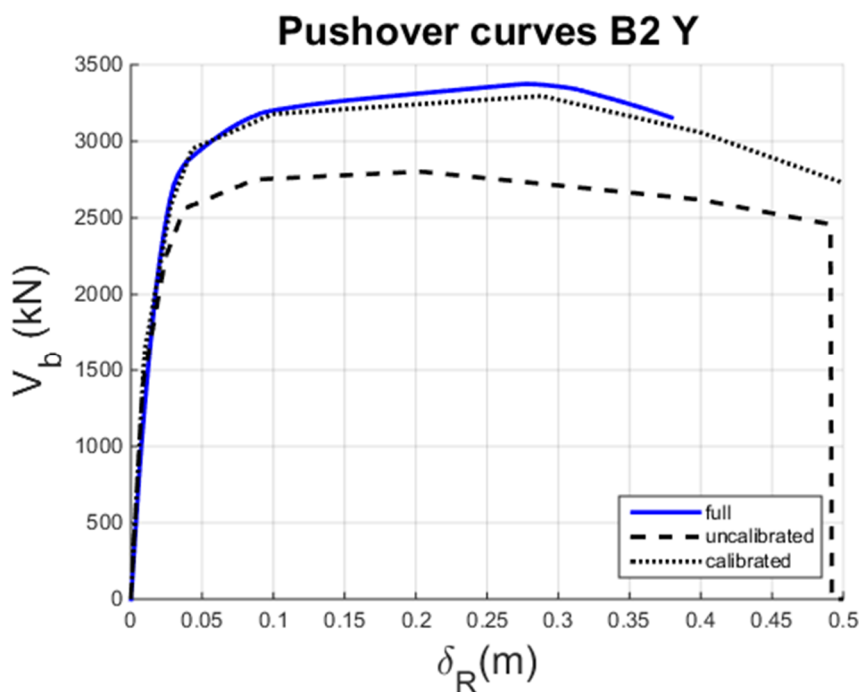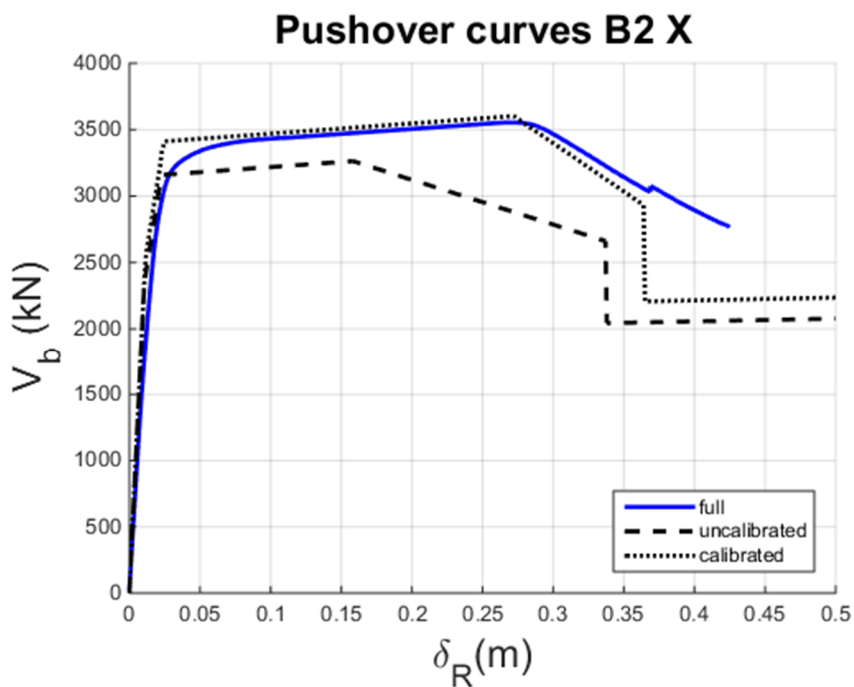
Fig. D.8 – Pushover curves of full, calibrated and uncalibrated 3D reduced-order models in X and Y direction, for building B2

Pushover curves B3 X

Pushover curves B3 Y
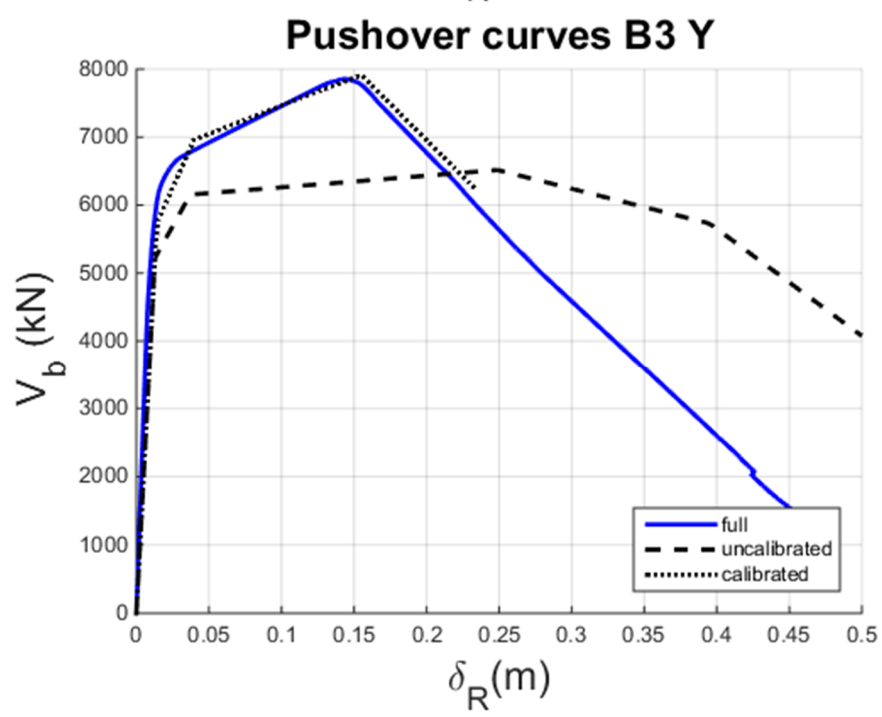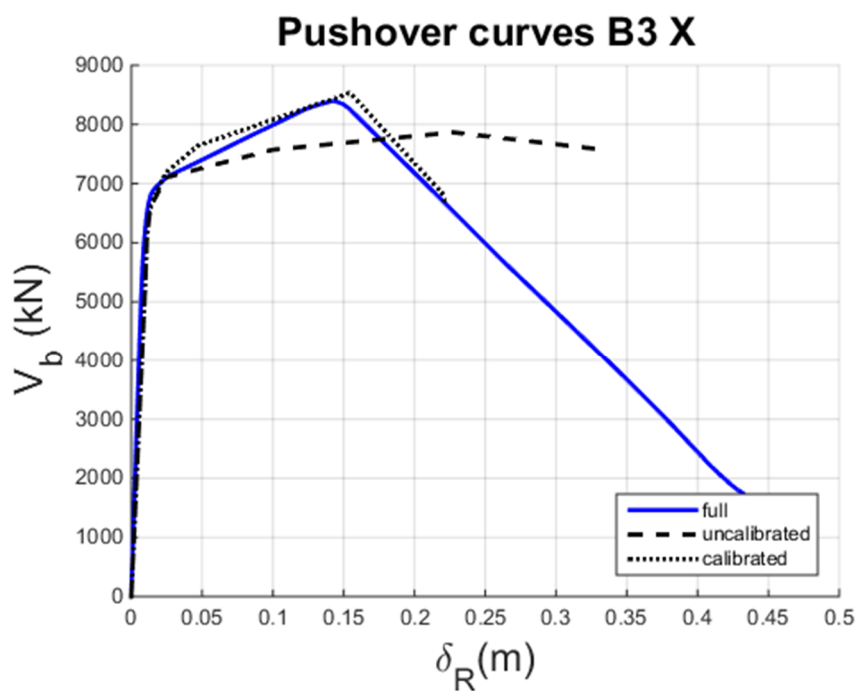
Fig. D.9 – Pushover curves of full, calibrated and uncalibrated 3D reduced-order models in X and Y direction, for building B3
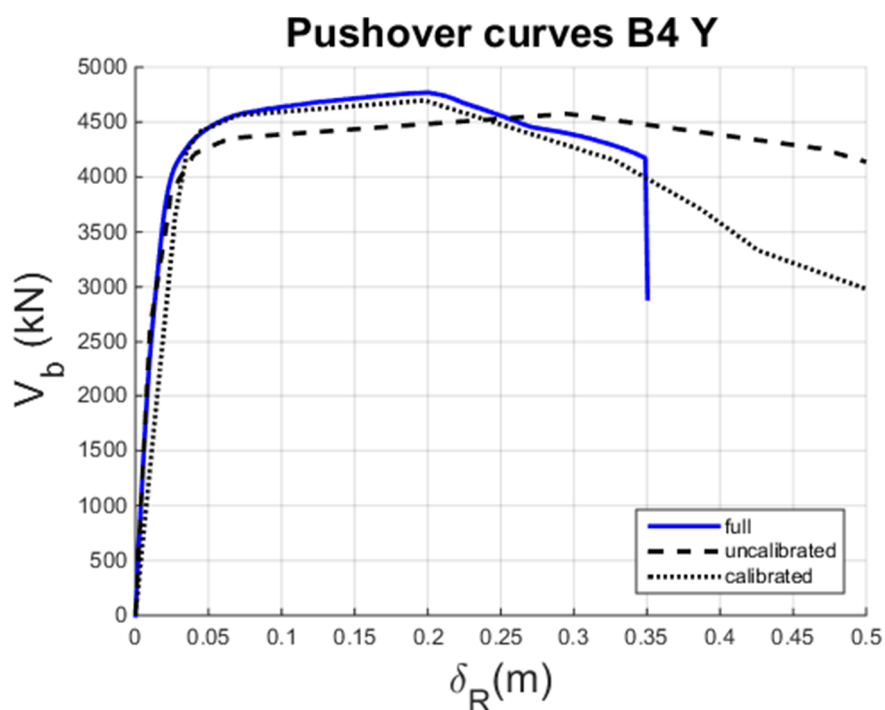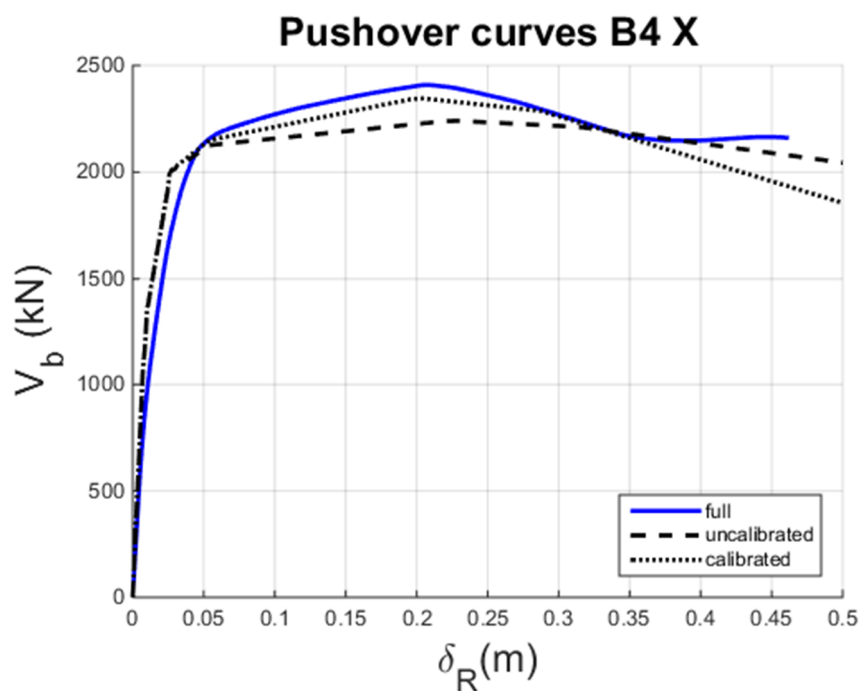
Fig. D.10 – Pushover curves of full, calibrated and uncalibrated 3D reduced-order models in X and Y direction, for building B4
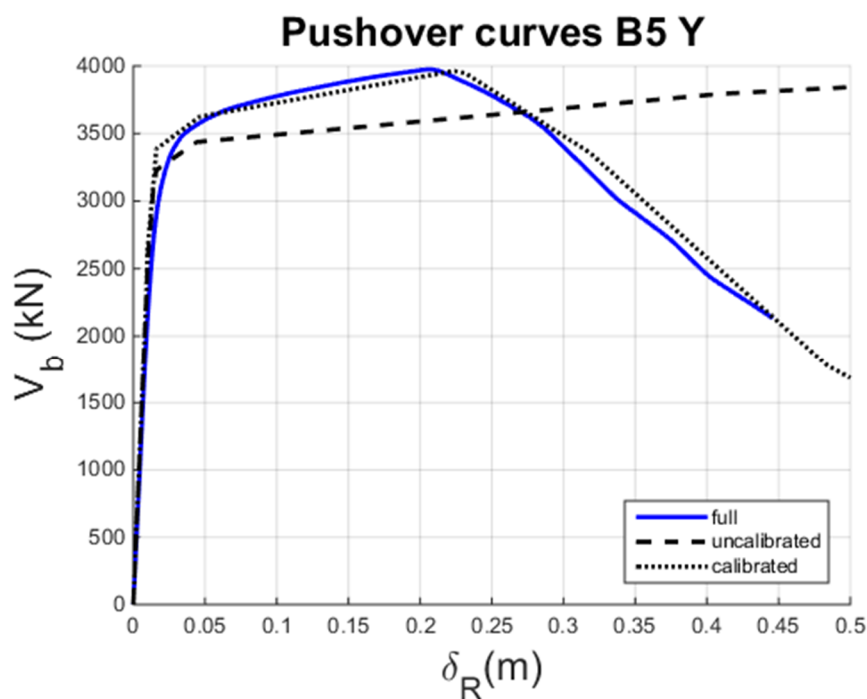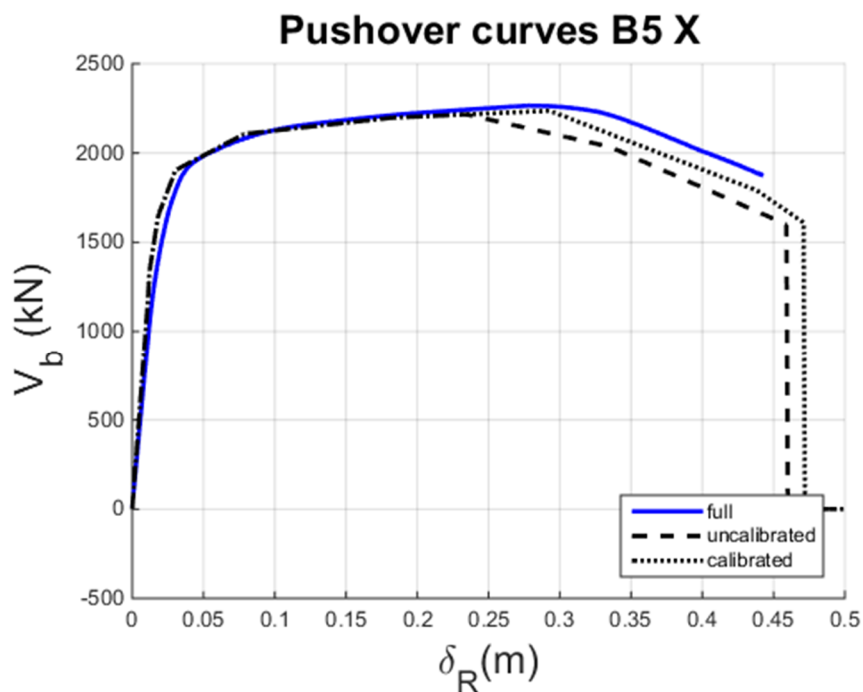
Fig. D.11 – Pushover curves of full, calibrated and uncalibrated 3D reduced-order models in X and Y direction, for building B5
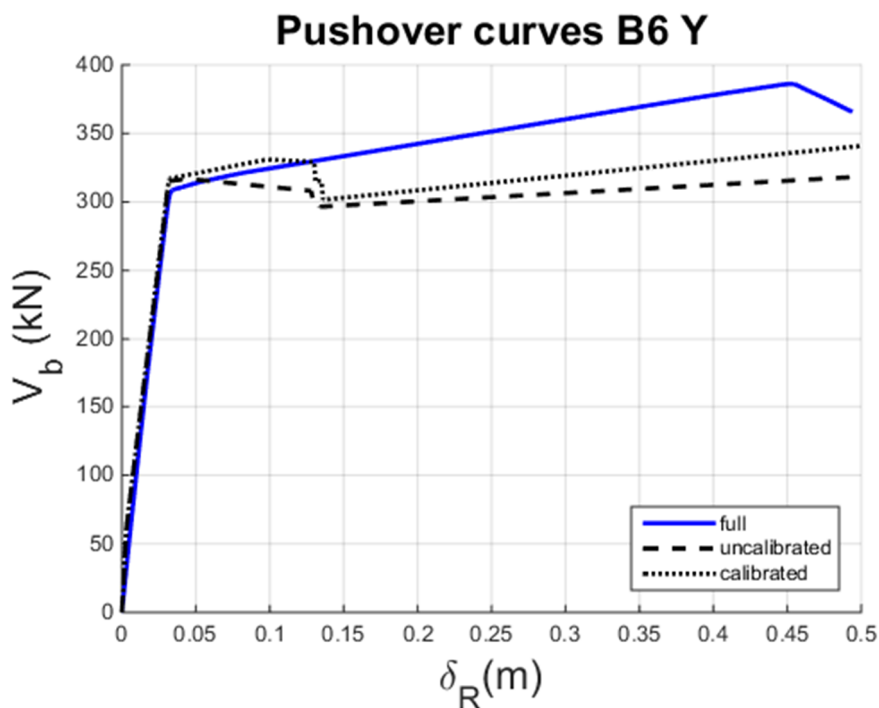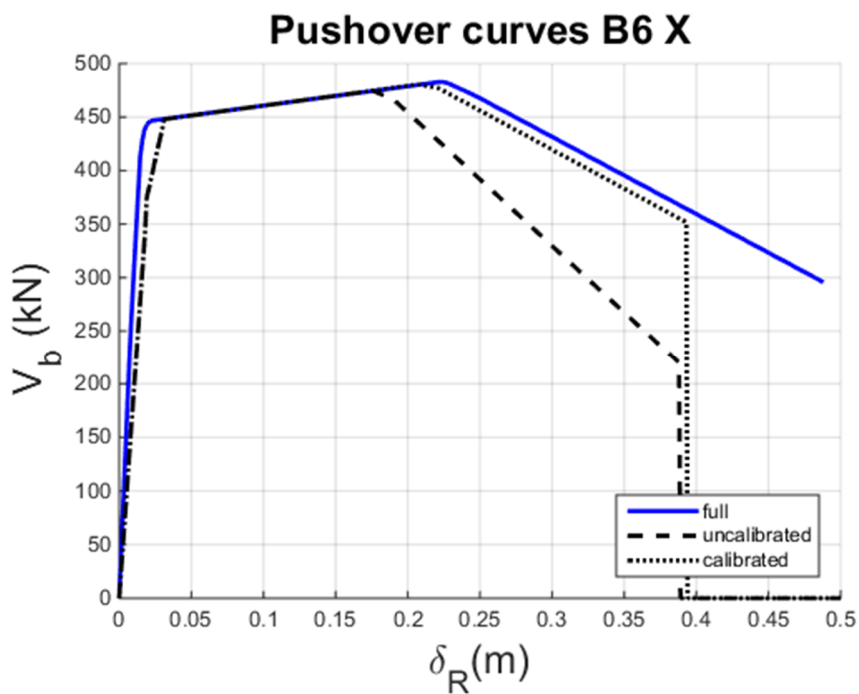
Fig. D.12 – Pushover curves of full, calibrated and uncalibrated 3D reduced-order models in X and Y direction, for building B6
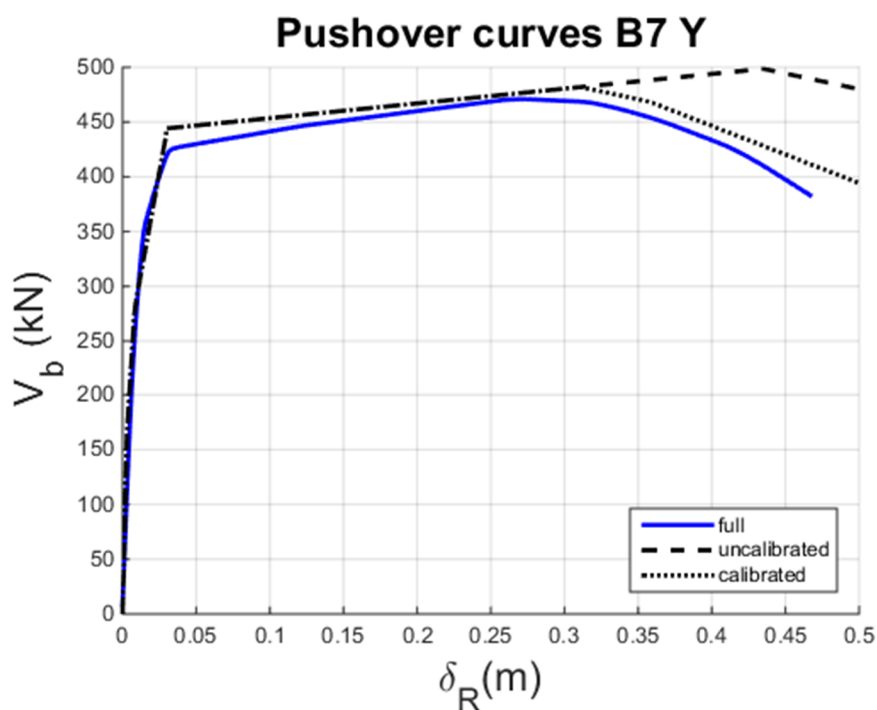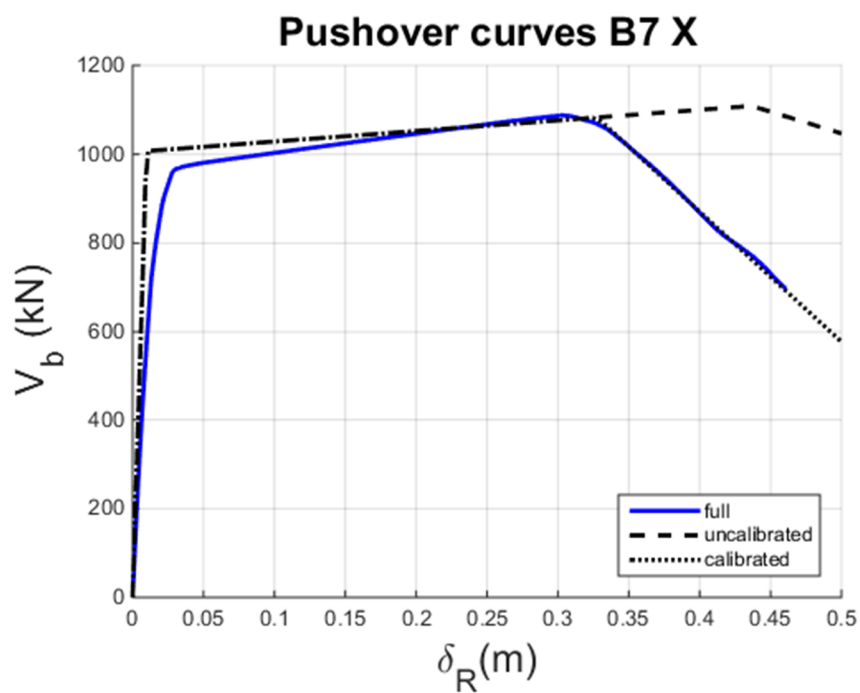
Fig. D.13 – Pushover curves of full, calibrated and uncalibrated 3D reduced-order models in X and Y direction, for building B7
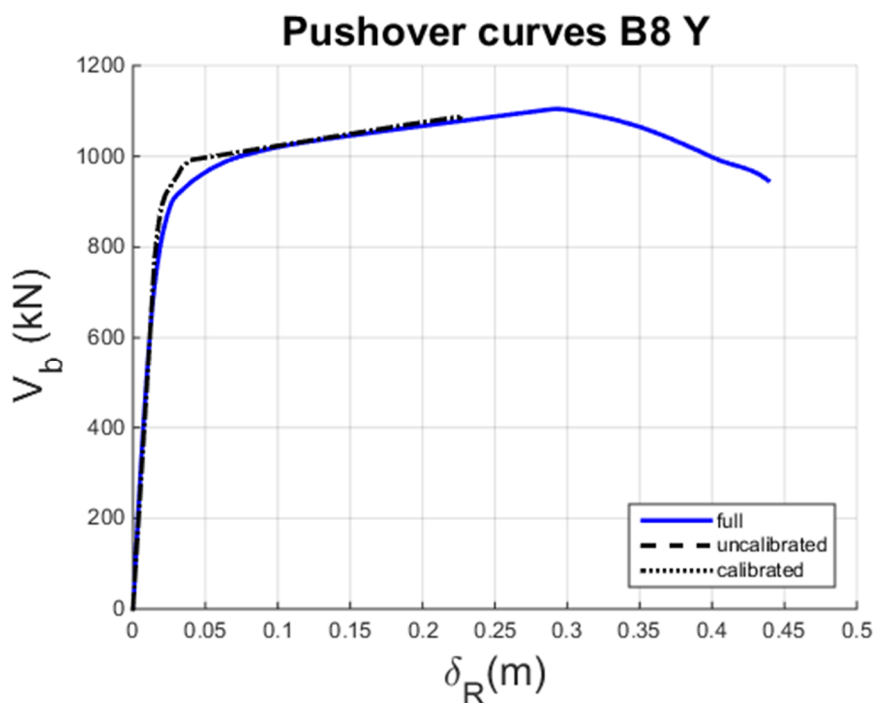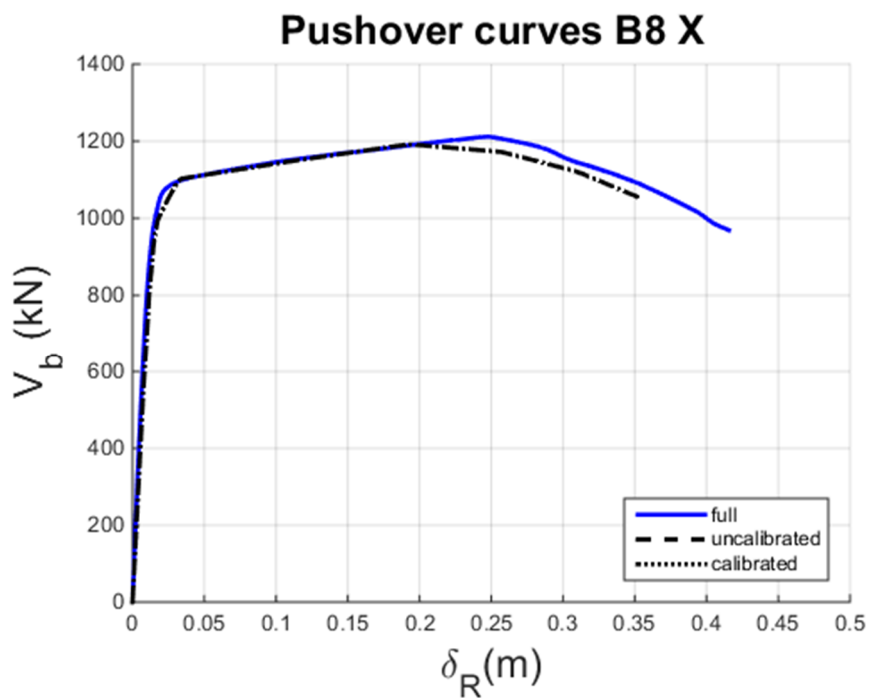
Fig. D.14 – Pushover curves of full, calibrated and uncalibrated 3D reduced-order models in X and Y direction, for building B8
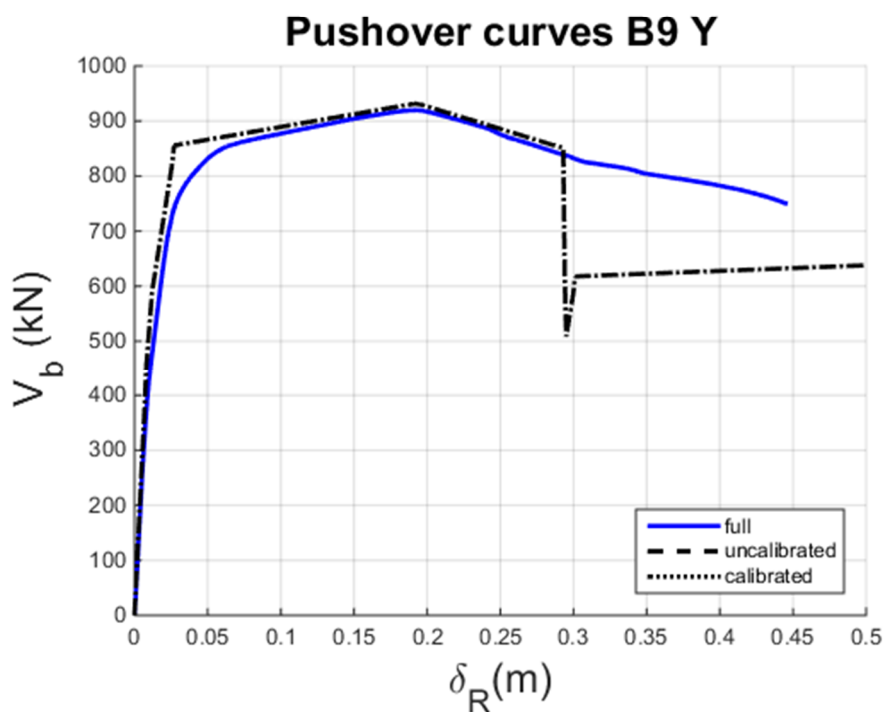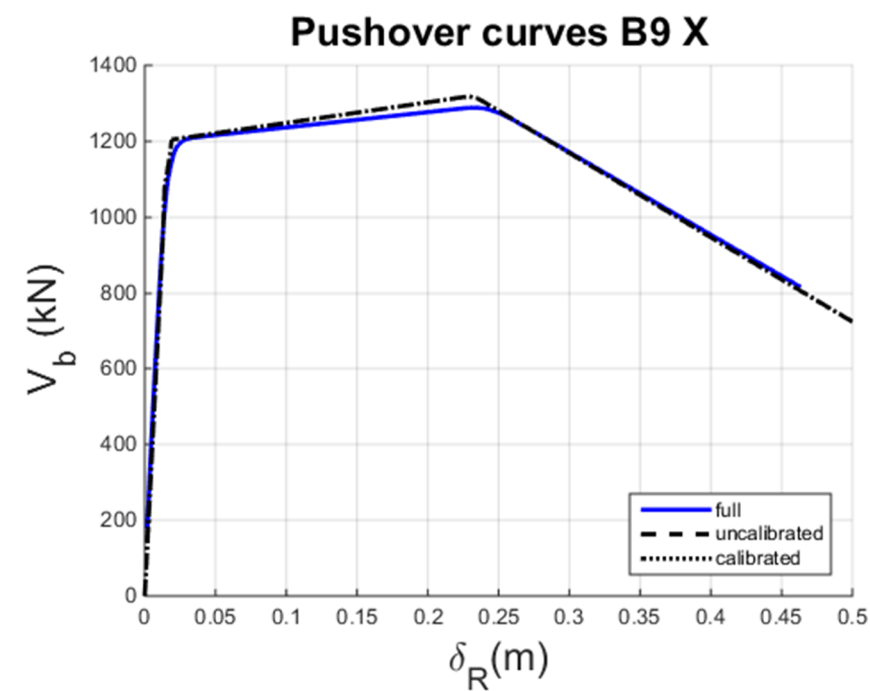
Fig. D.15 – Pushover curves of full, calibrated and uncalibrated 3D reduced-order models in X and Y direction, for building B9
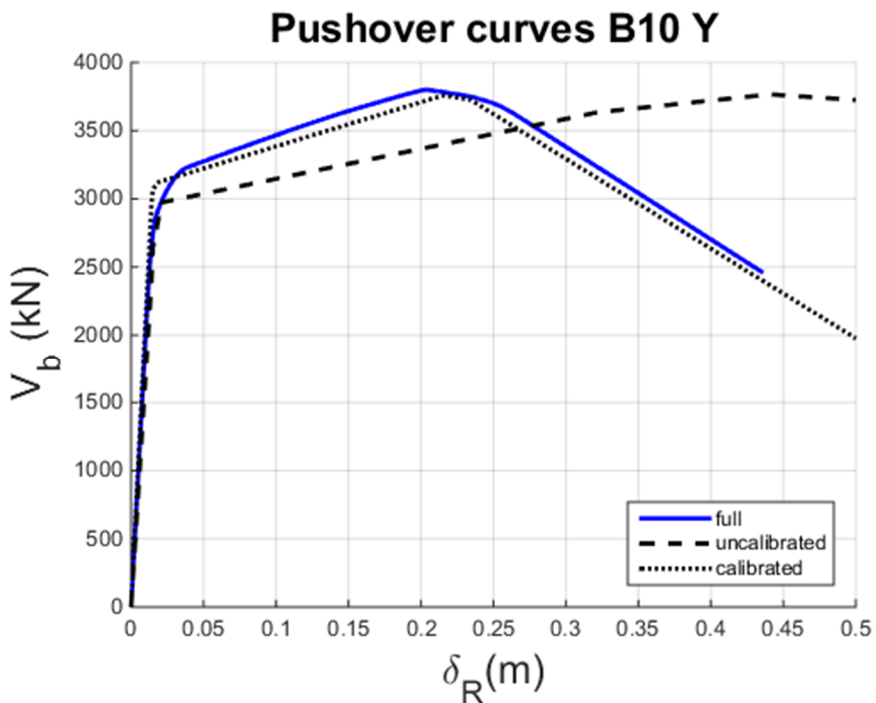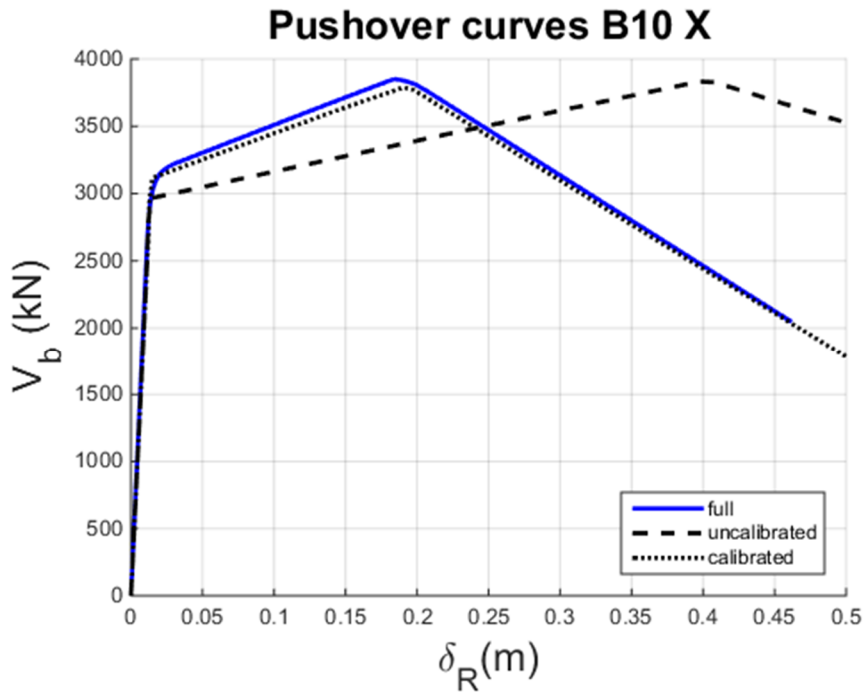
Fig. D.16 – Pushover curves of full, calibrated and uncalibrated 3D reduced-order models in X and Y direction, for building B10
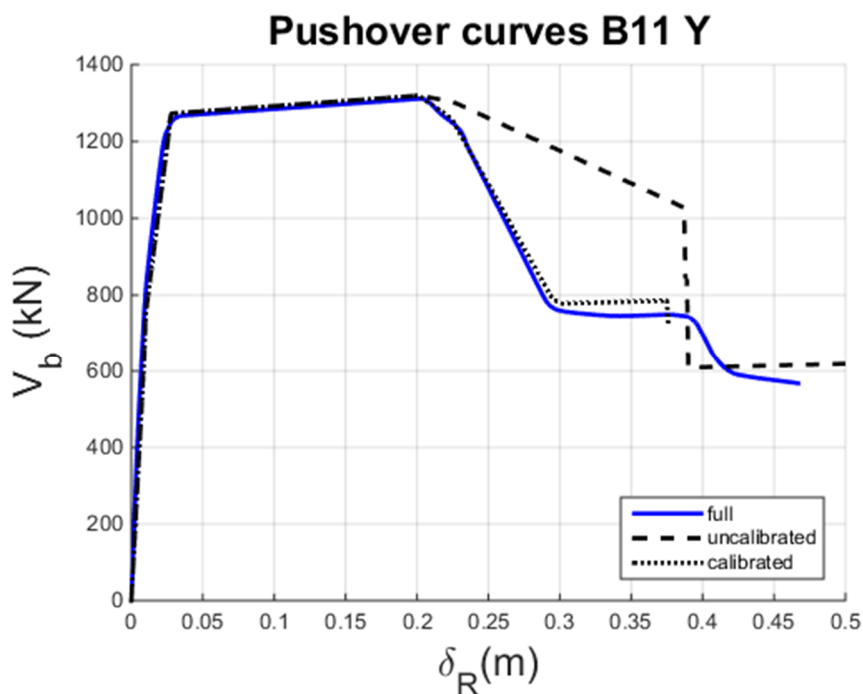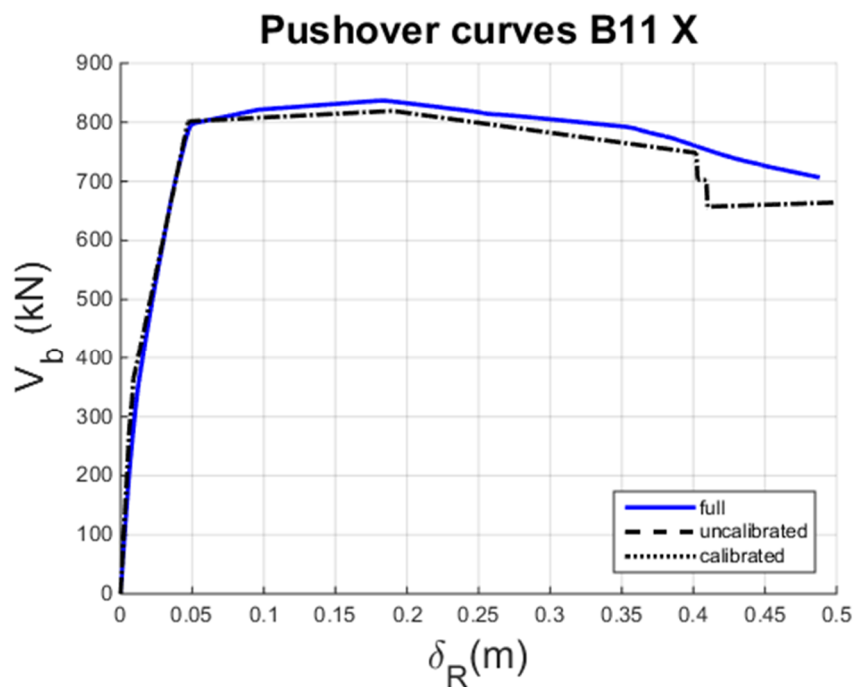
Fig. D.17 – Pushover curves of full, calibrated and uncalibrated 3D reduced-order models in X and Y direction, for building B11
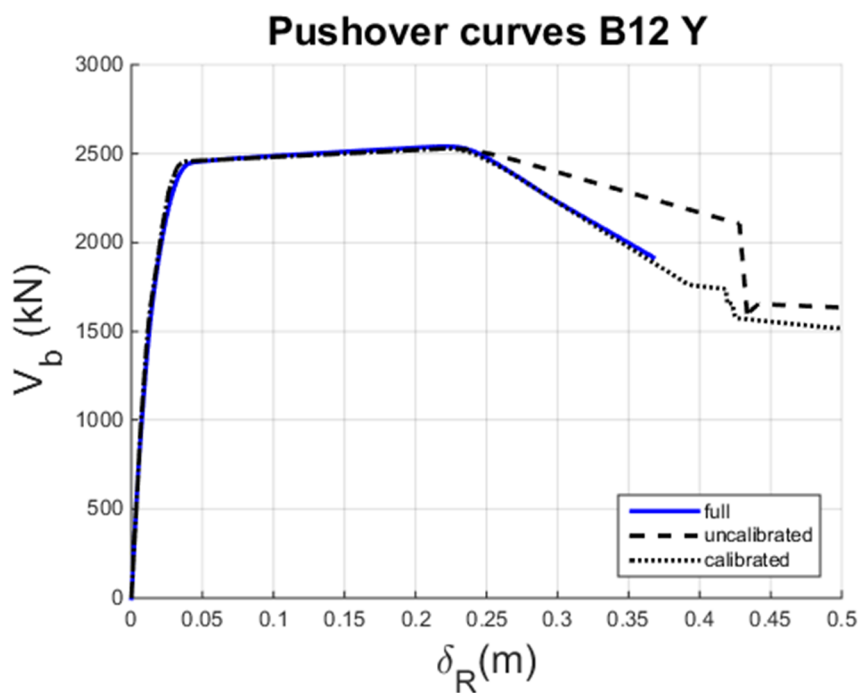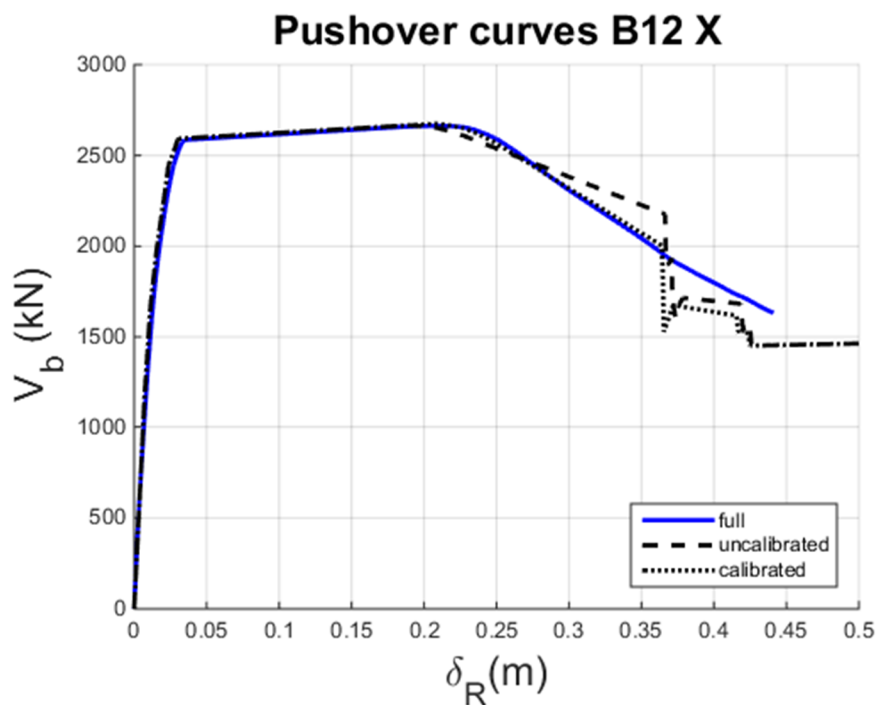
Fig. D.18 – Pushover curves of full, calibrated and uncalibrated 3D reduced-order models in X and Y direction, for building B12
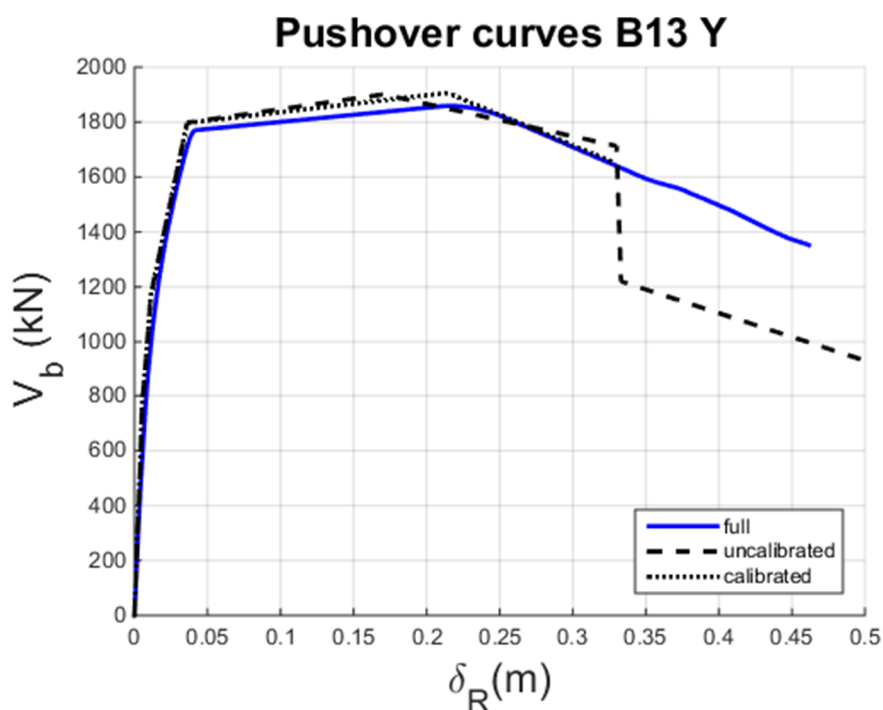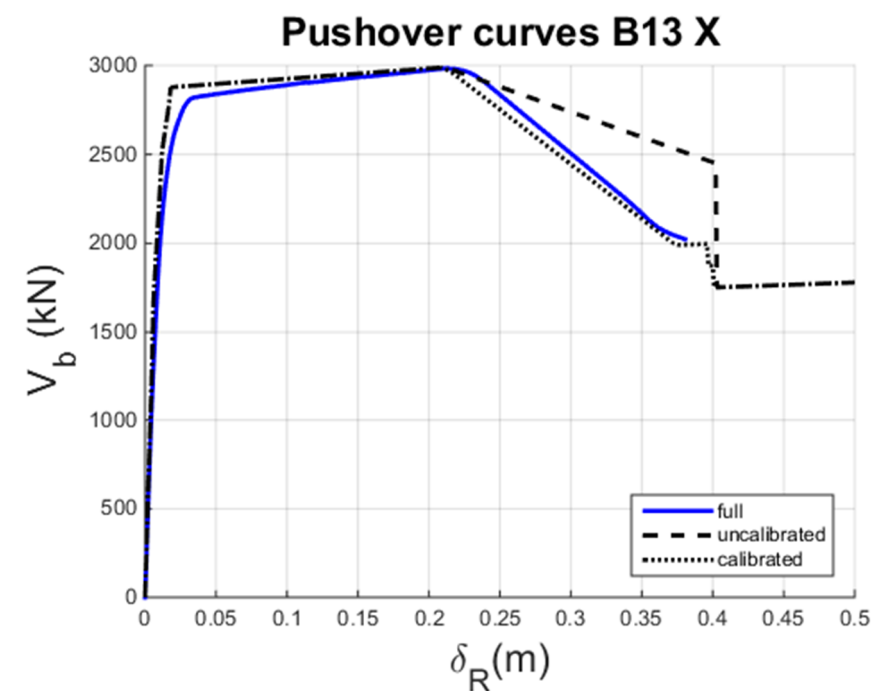
Fig. D.19 – Pushover curves of full, calibrated and uncalibrated 3D reduced-order models in X and Y direction, for building B13
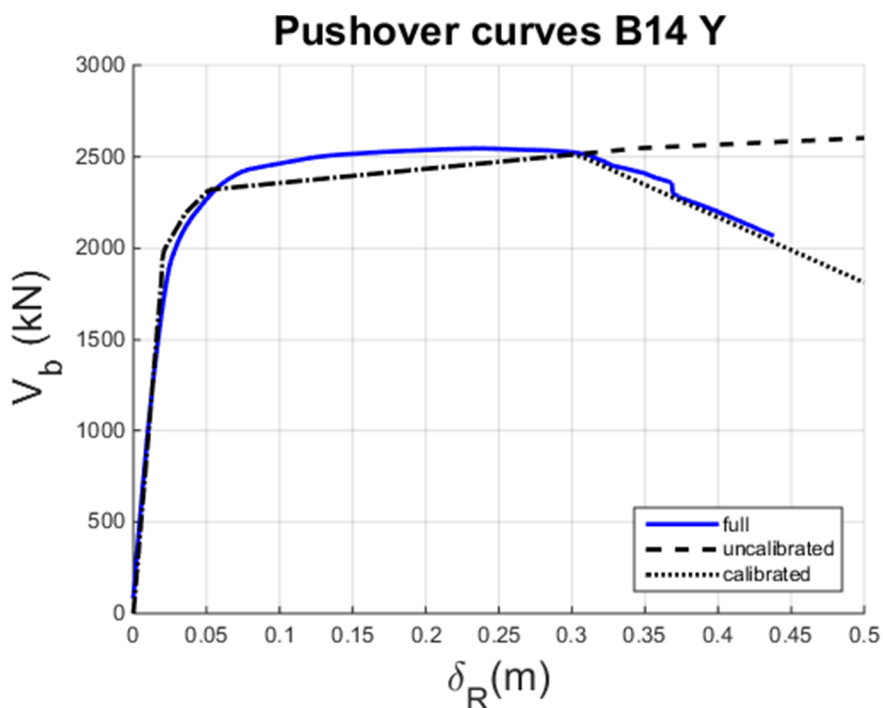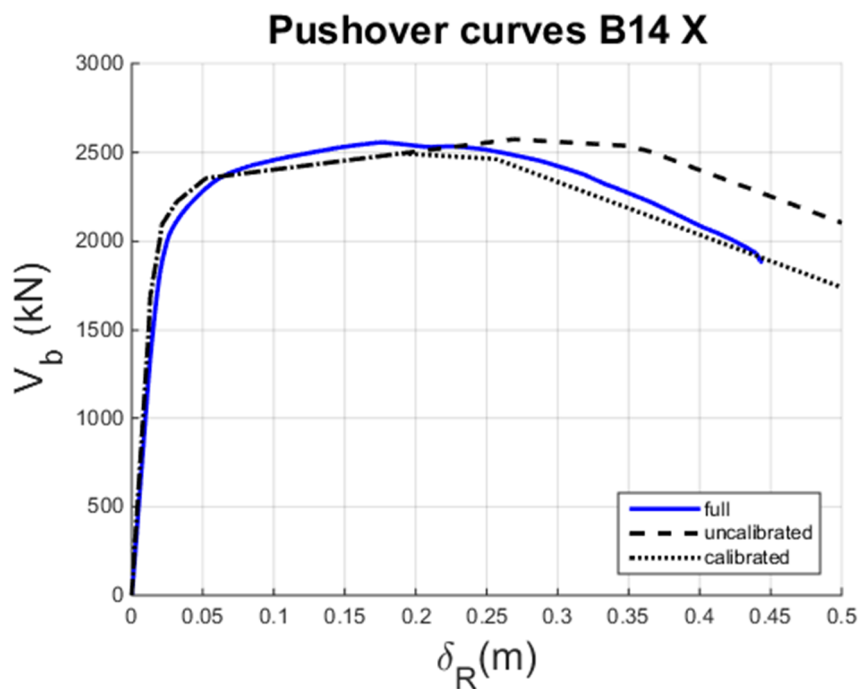
Fig. D.20 – Pushover curves of full, calibrated and uncalibrated 3D reduced-order models in X and Y direction, for building B14
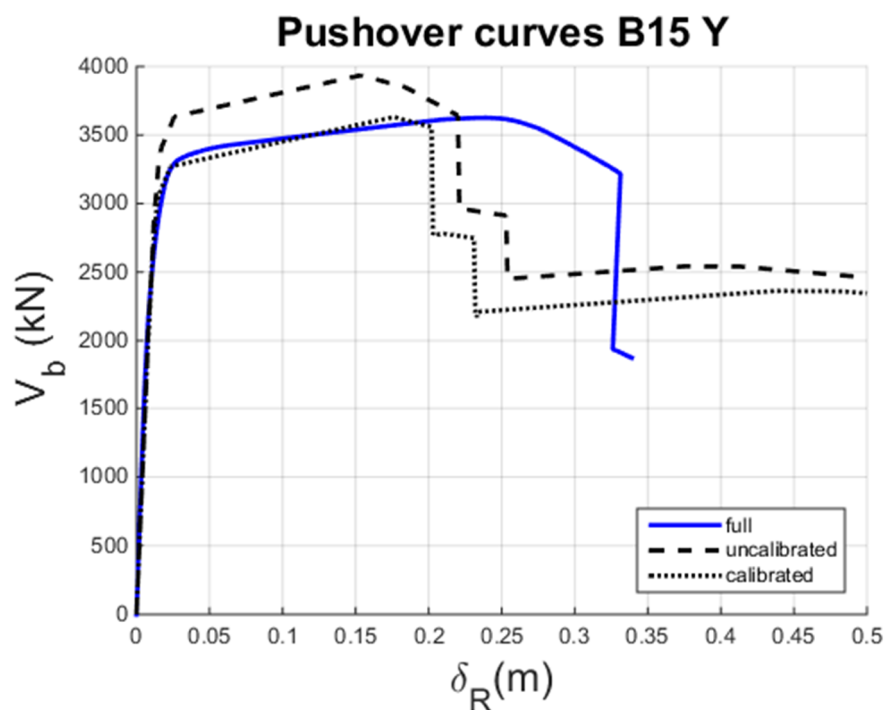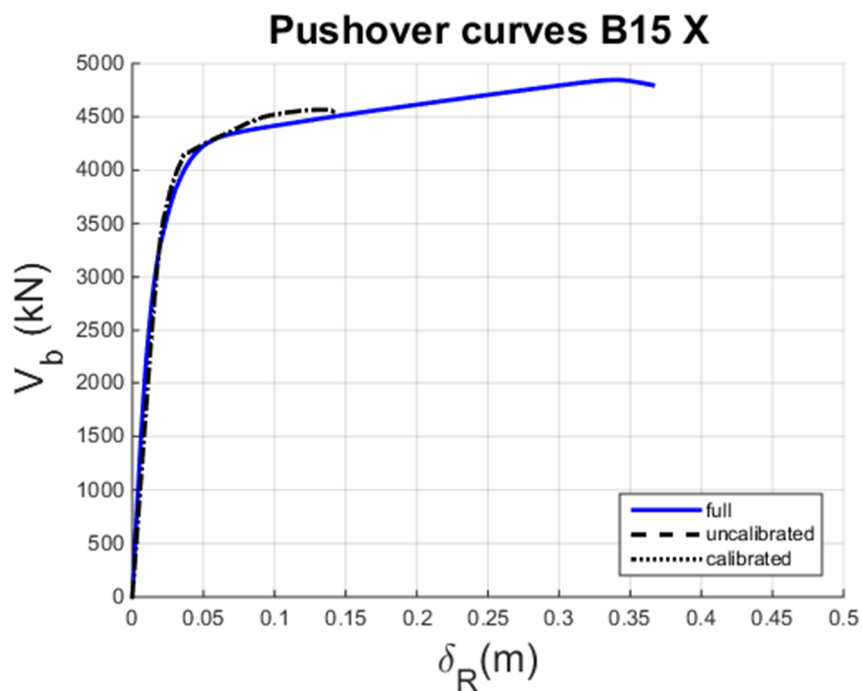
Fig. D.21 – Pushover curves of full, calibrated and uncalibrated 3D reduced-order models in X and Y direction, for building B15
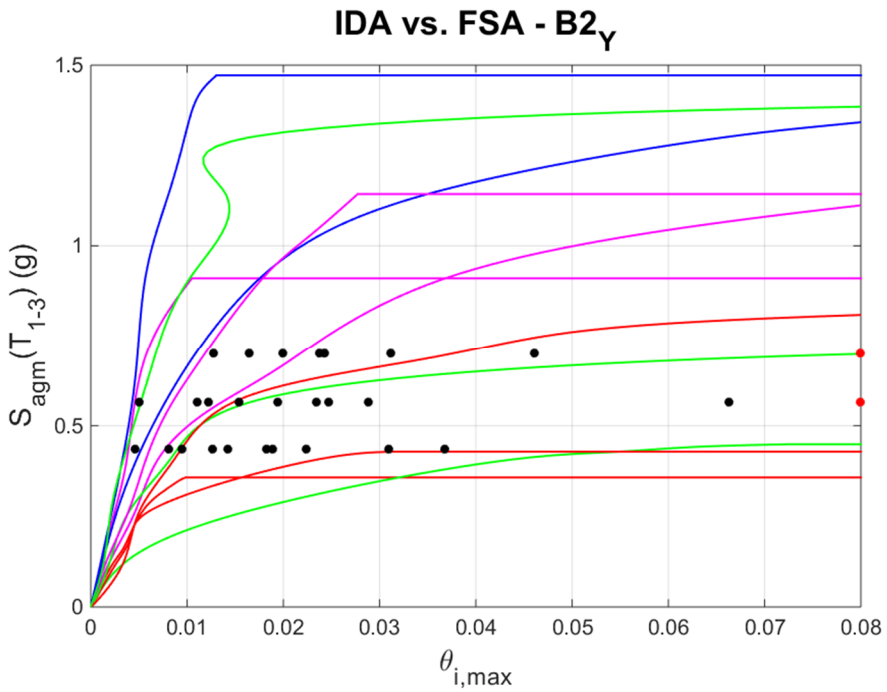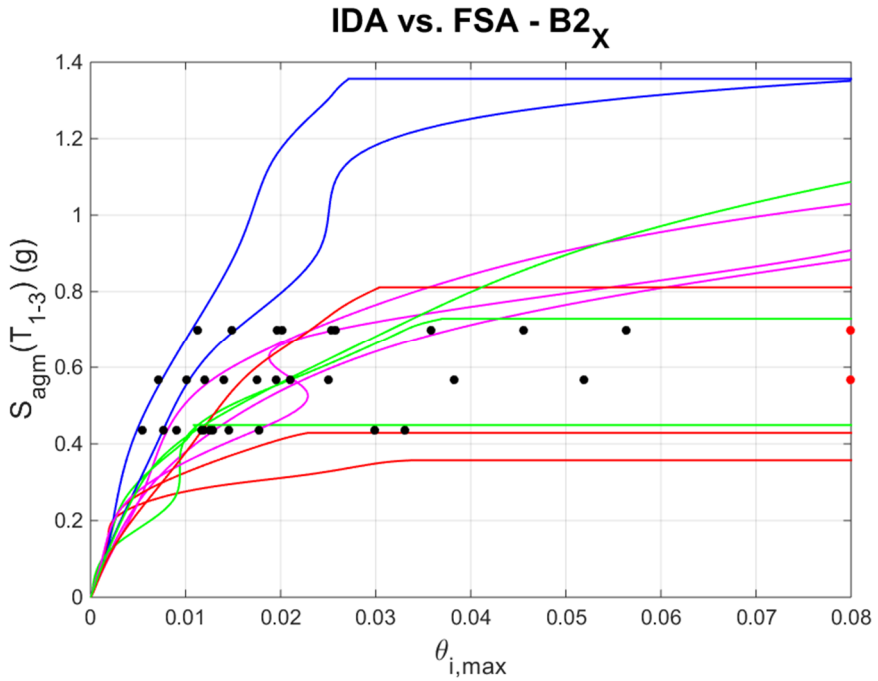
Fig. D.22 – IDA on 3D reduced-order uncalibrated model vs. FSA on full model, in X and Y direction, for building B2
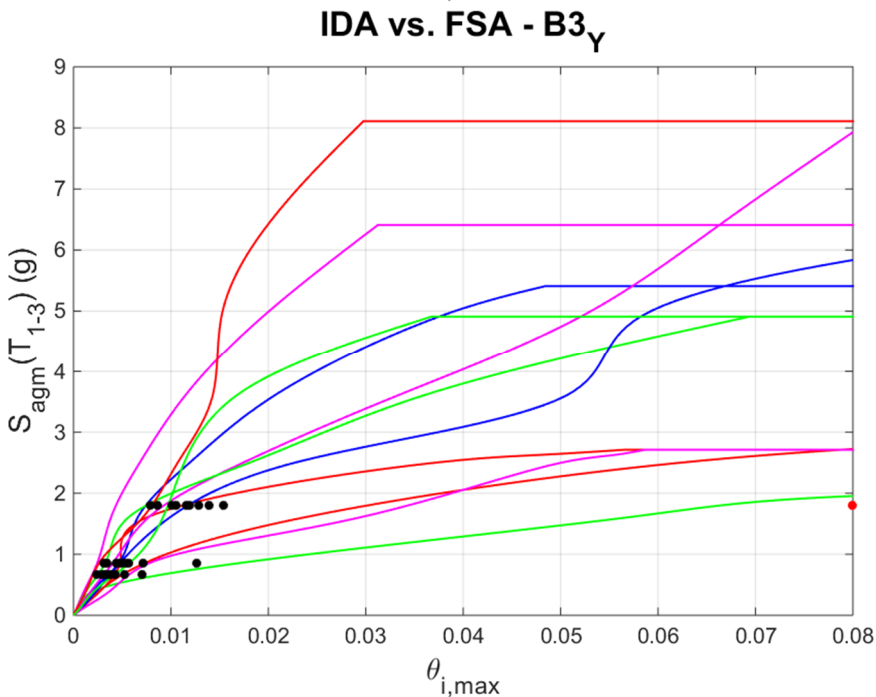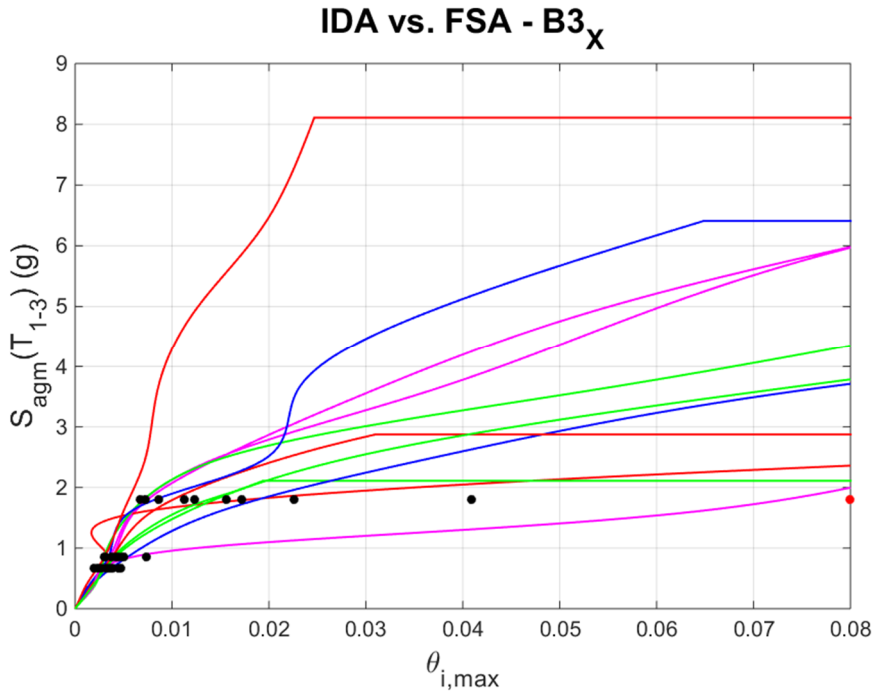
Fig. D.23 – IDA on 3D reduced-order uncalibrated model vs. FSA on full model, in X and Y direction, for building B3
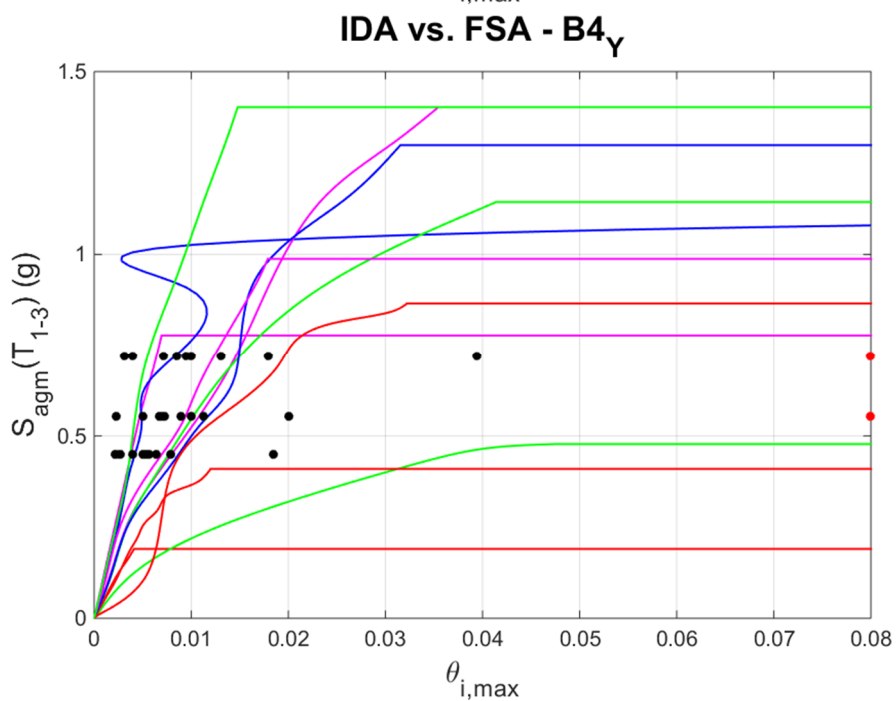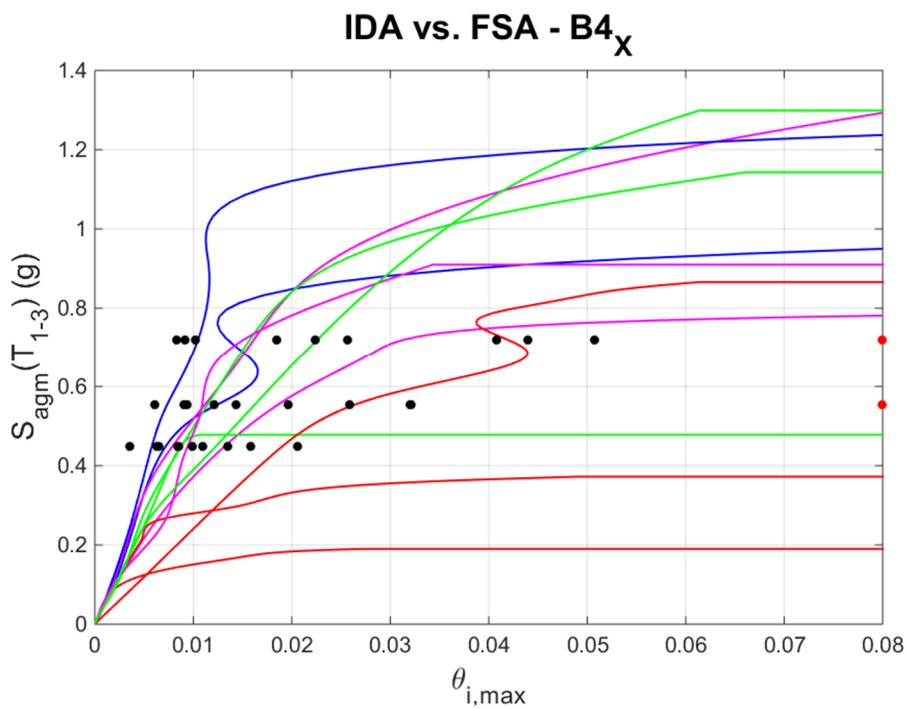
Fig. D.24 – IDA on 3D reduced-order uncalibrated model vs. FSA on full model, in X and Y direction, for building B4
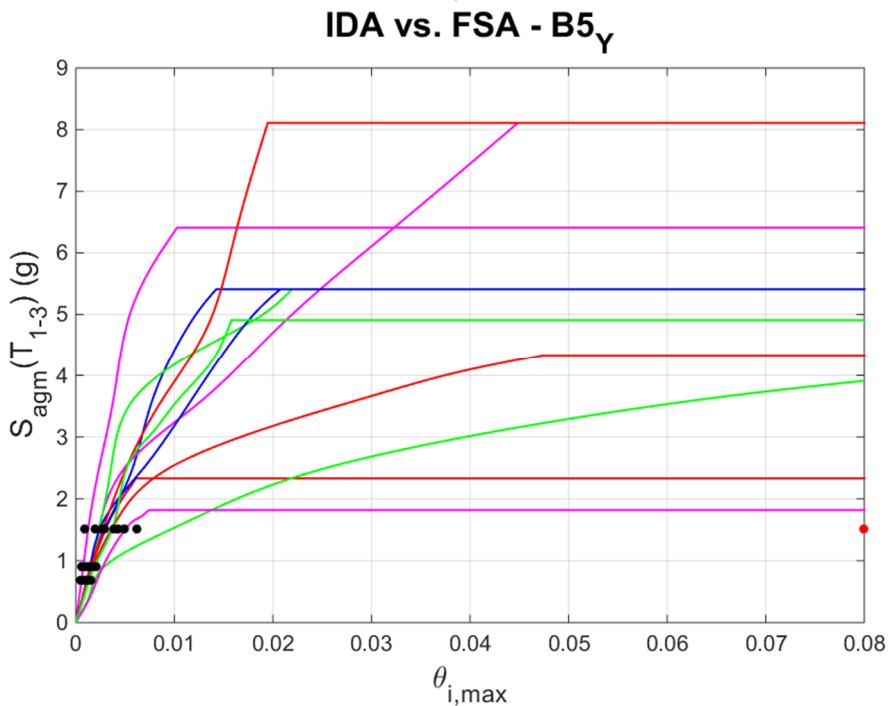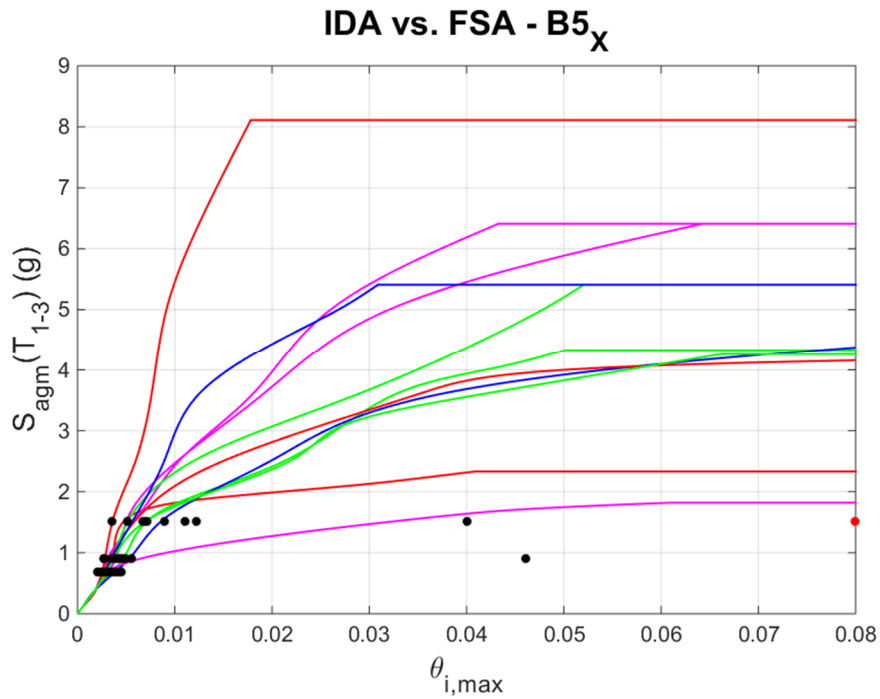
Fig. D.25 – IDA on 3D reduced-order uncalibrated model vs. FSA on full model, in X and Y direction, for building B5
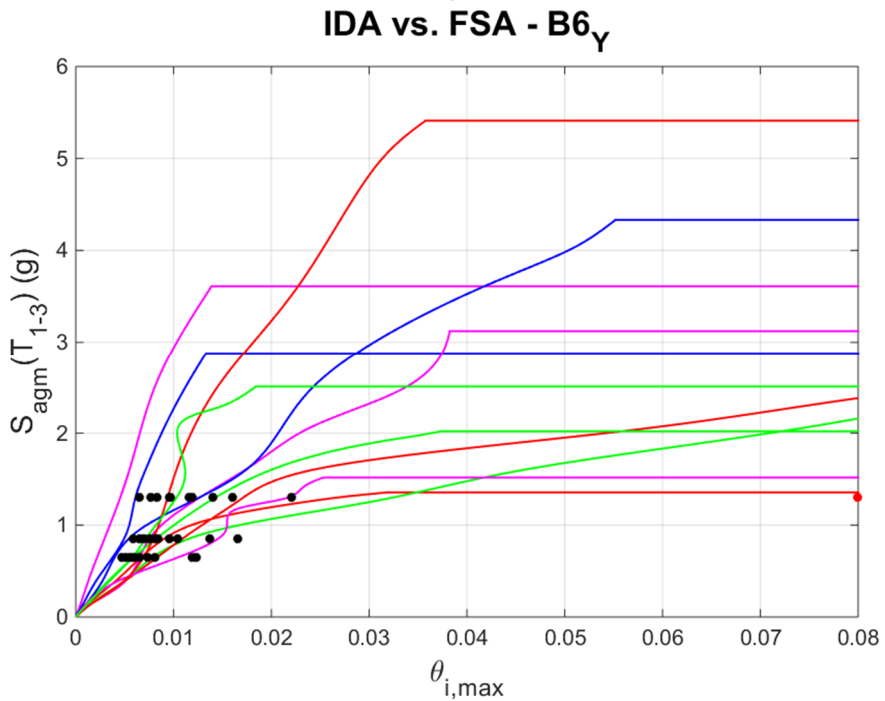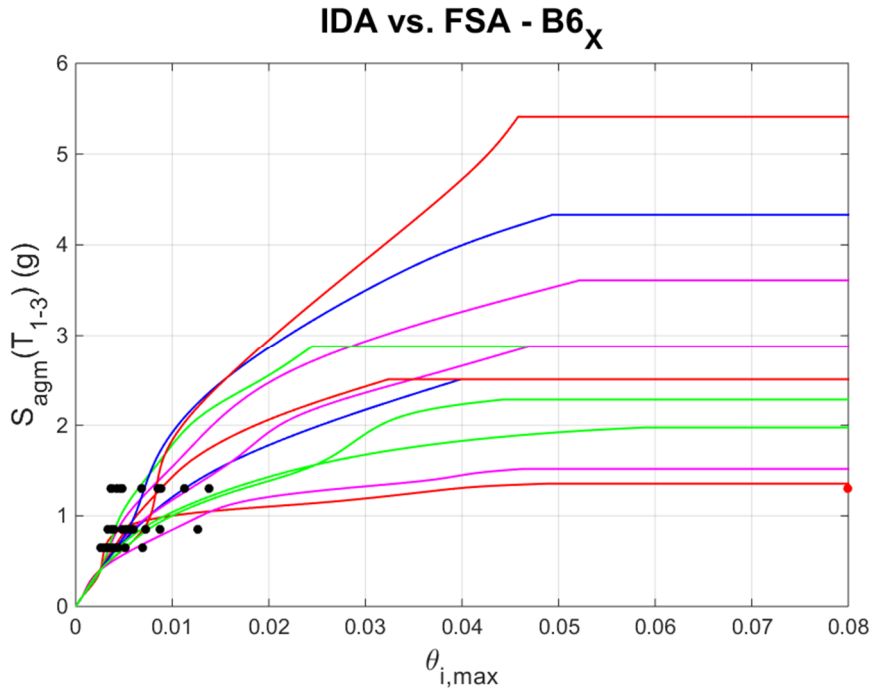
Fig. D.26 – IDA on 3D reduced-order uncalibrated model vs. FSA on full model, in X and Y direction, for building B6
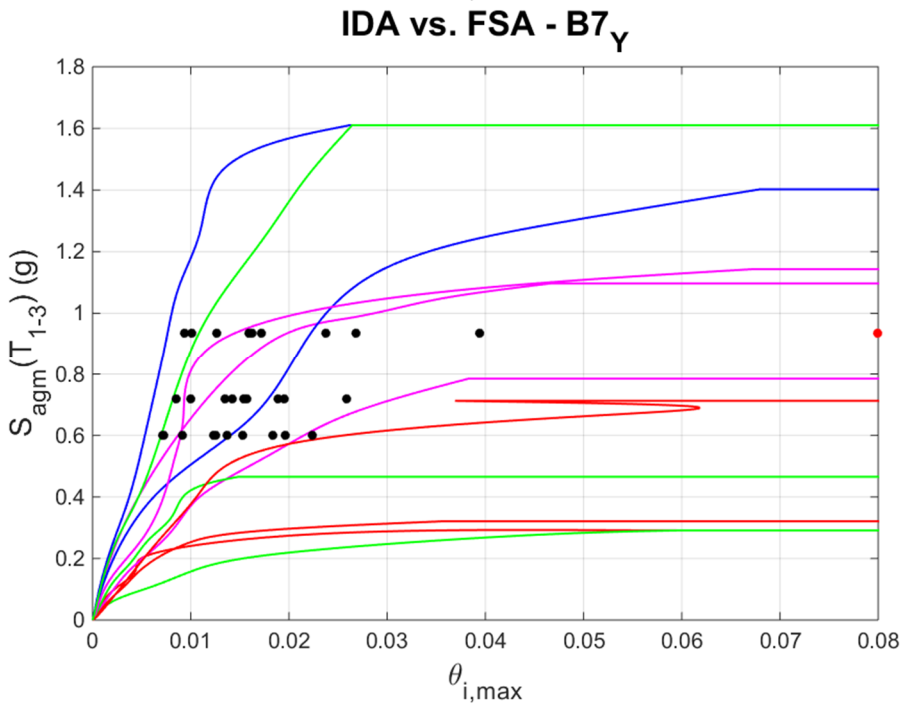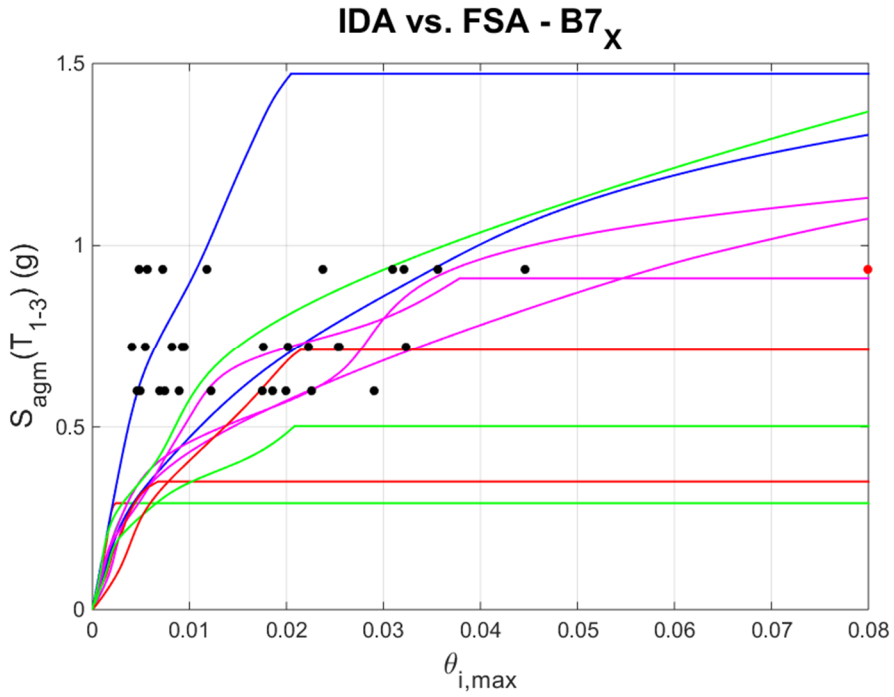
Fig. D.27 – IDA on 3D reduced-order uncalibrated model vs. FSA on full model, in X and Y direction, for building B7
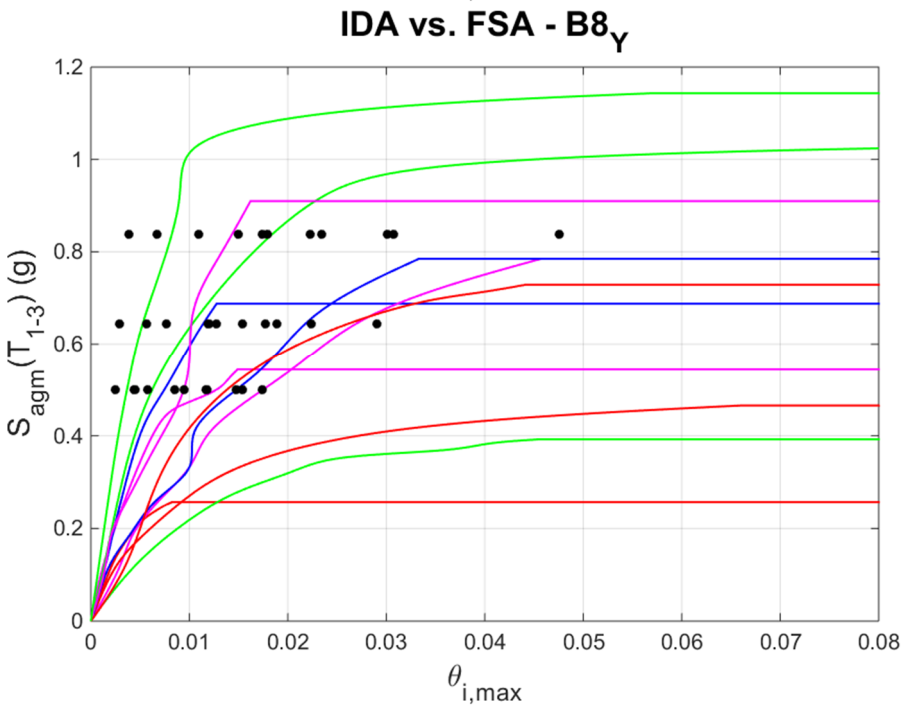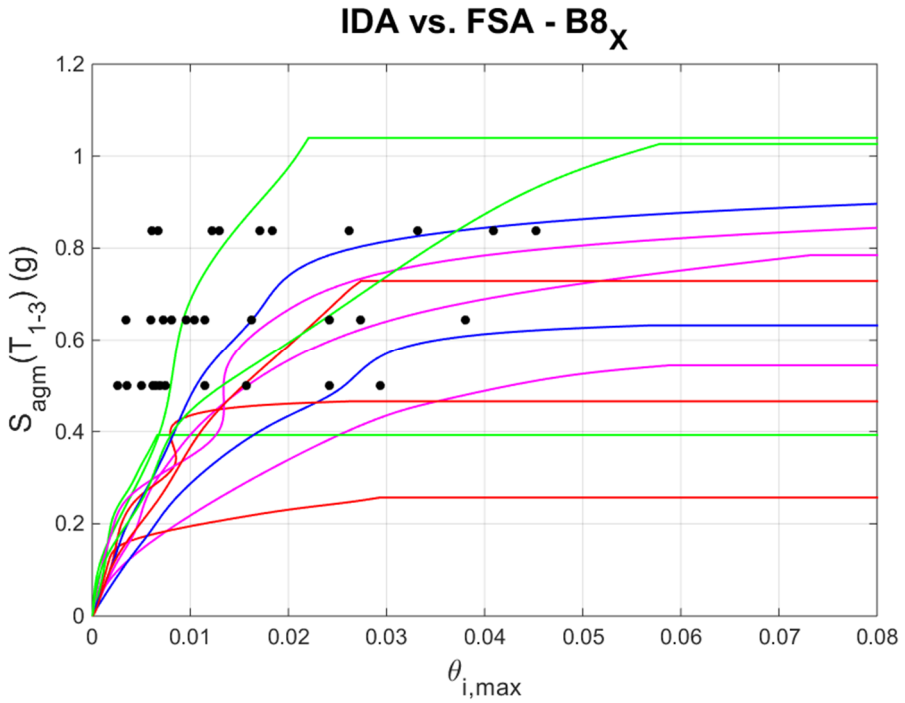
Fig. D.28 – IDA on 3D reduced-order uncalibrated model vs. FSA on full model, in X and Y direction, for building B8
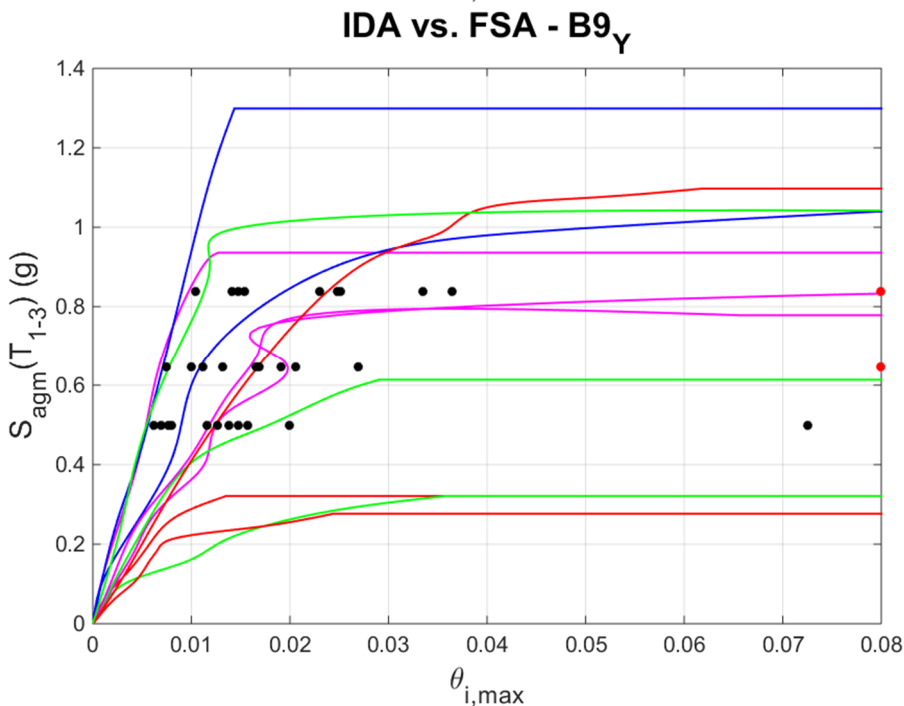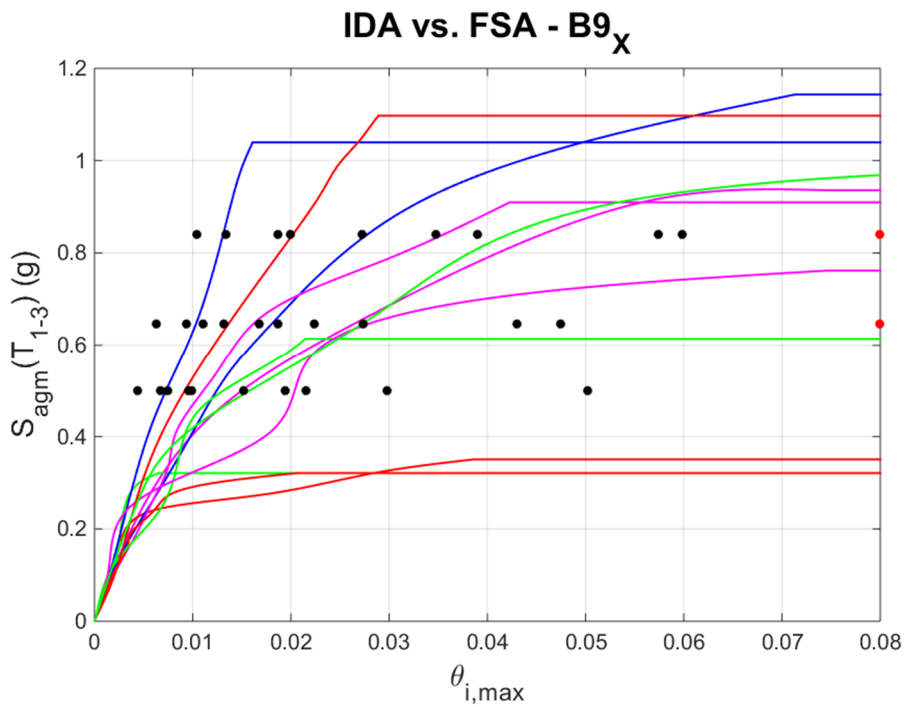
Fig. D.29 – IDA on 3D reduced-order uncalibrated model vs. FSA on full model, in X and Y direction, for building B9
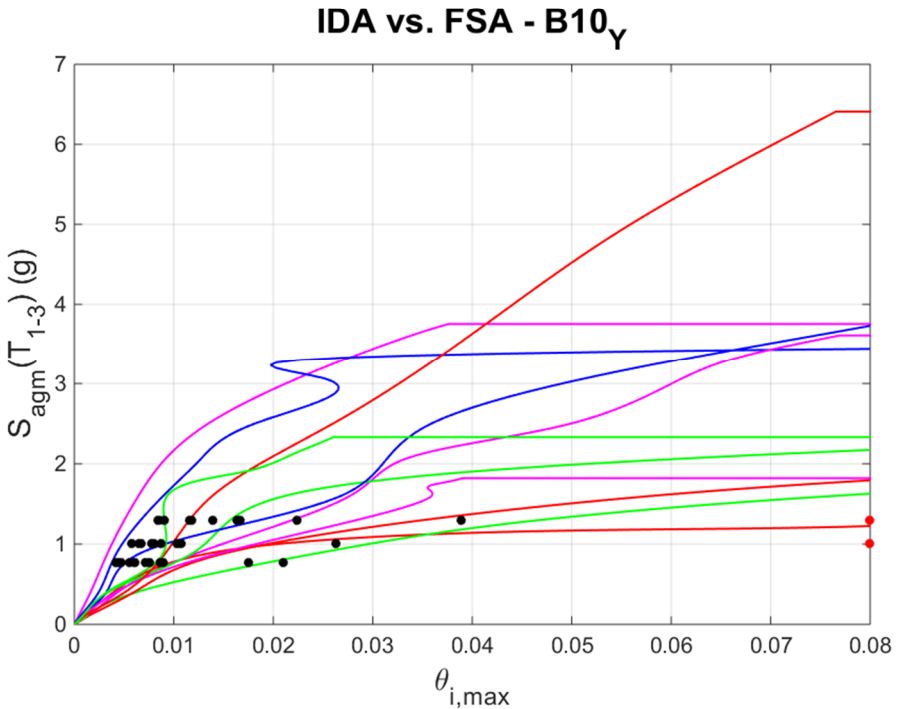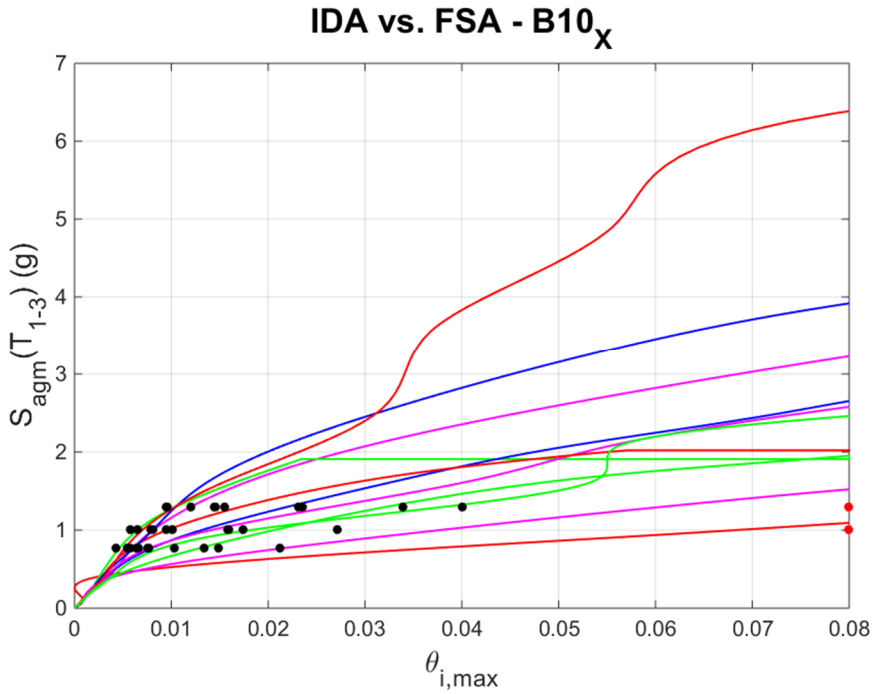
Fig. D.30 – IDA on 3D reduced-order uncalibrated model vs. FSA on full model, in X and Y direction, for building B10
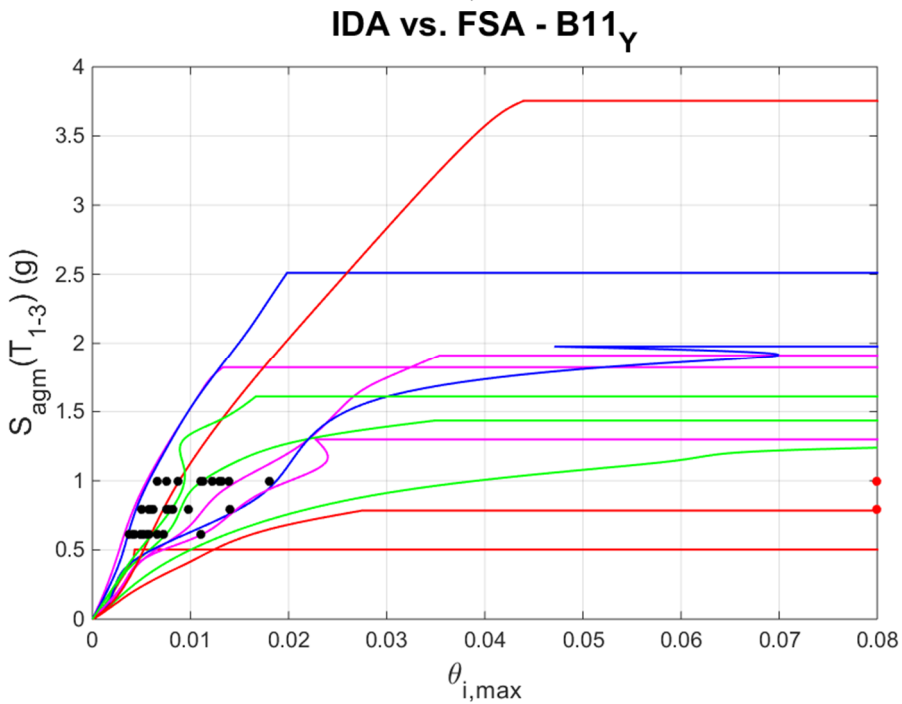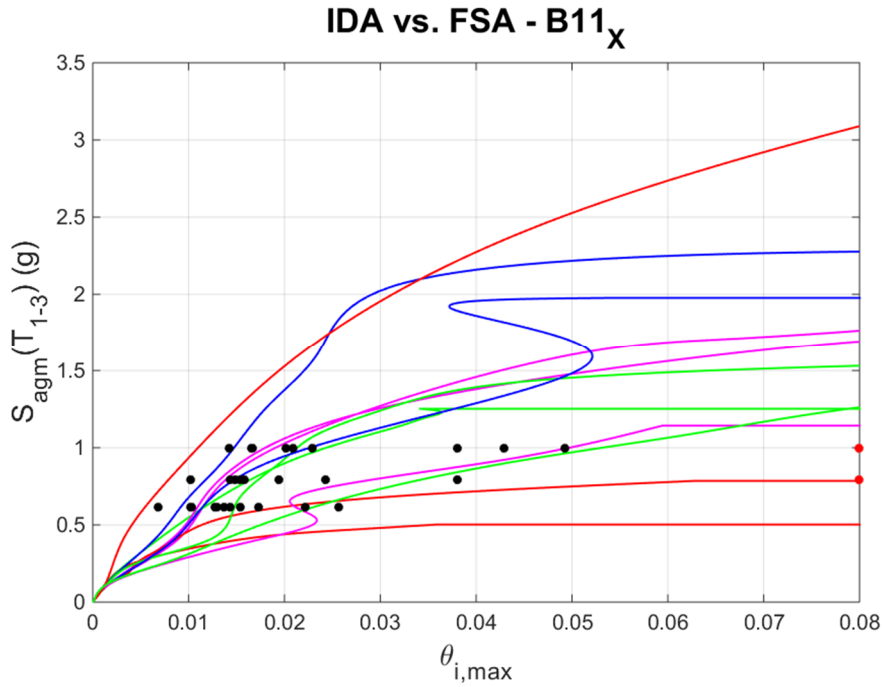
Fig. D.31 – IDA on 3D reduced-order uncalibrated model vs. FSA on full model, in X and Y direction, for building B11
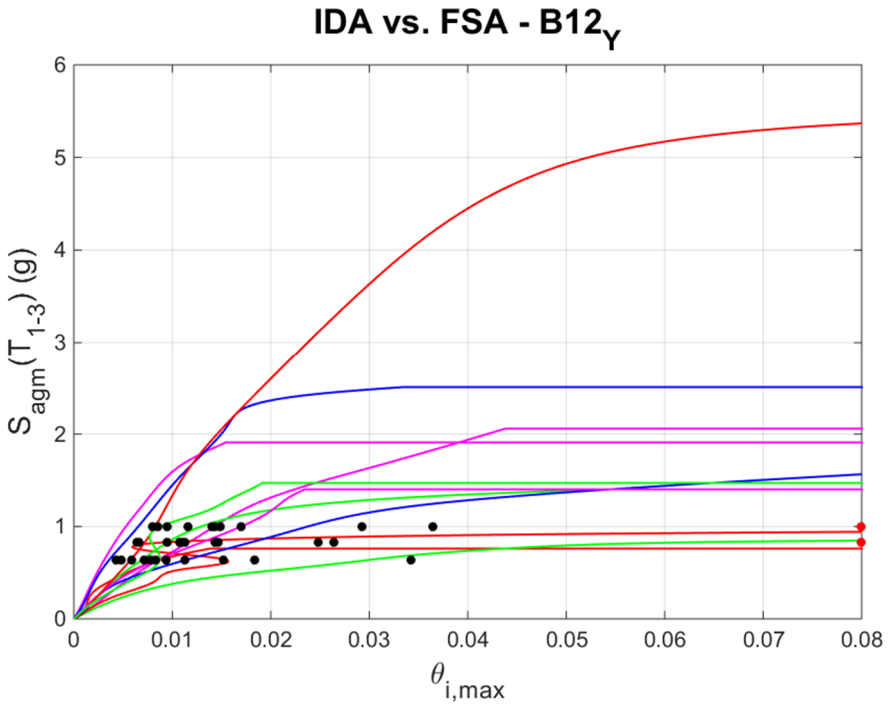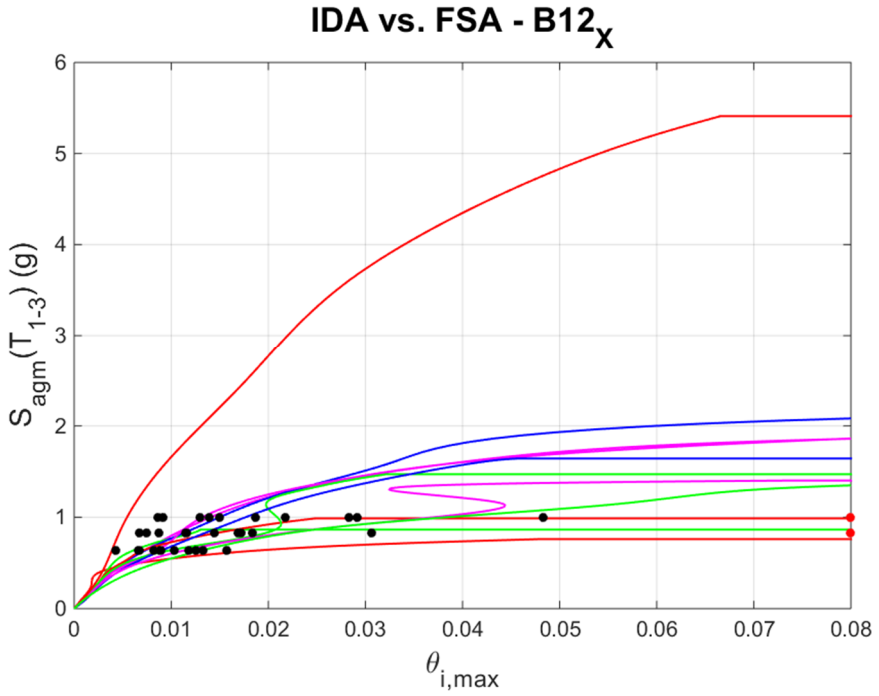
Fig. D.32 – IDA on 3D reduced-order uncalibrated model vs. FSA on full model, in X and Y direction, for building B12
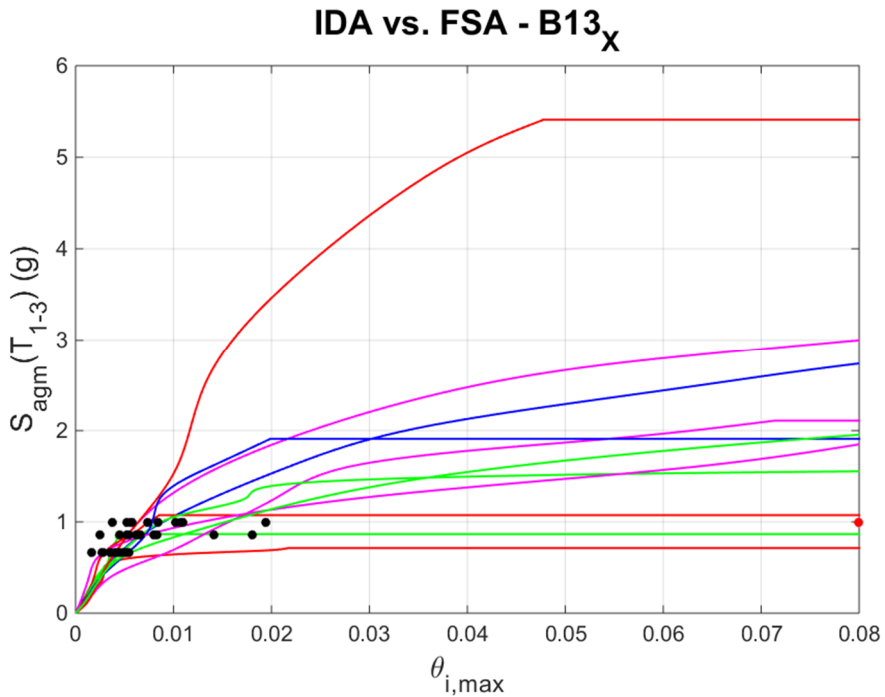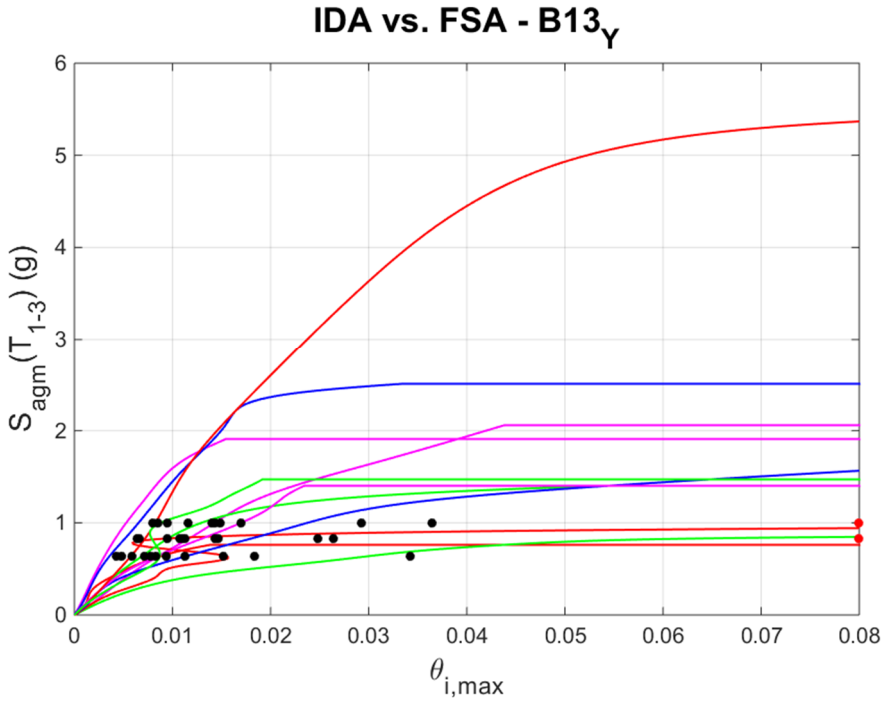
Fig. D.33 – IDA on 3D reduced-order uncalibrated model vs. FSA on full model, in X and Y direction, for building B13

442
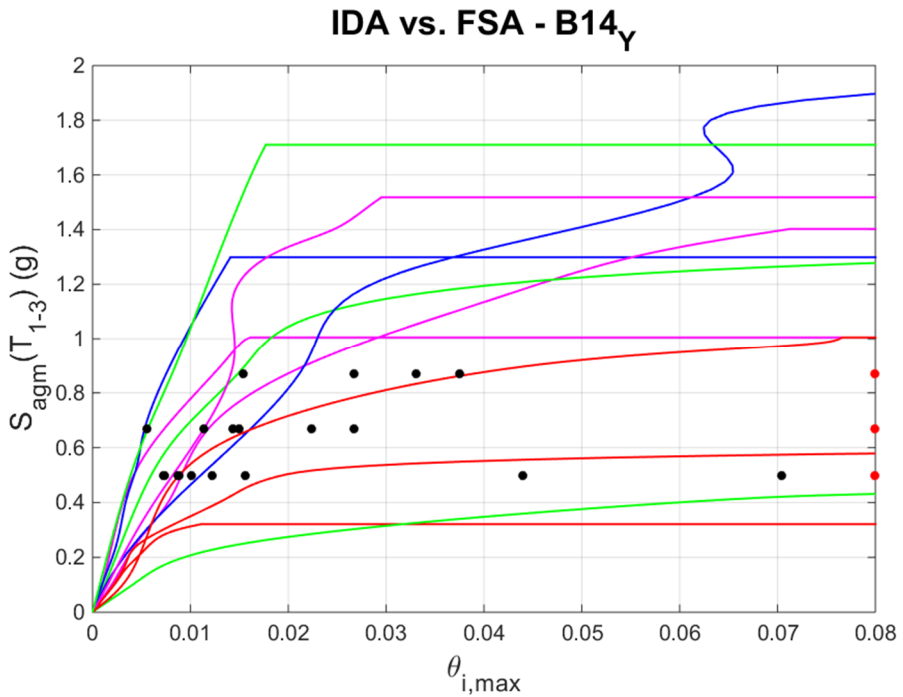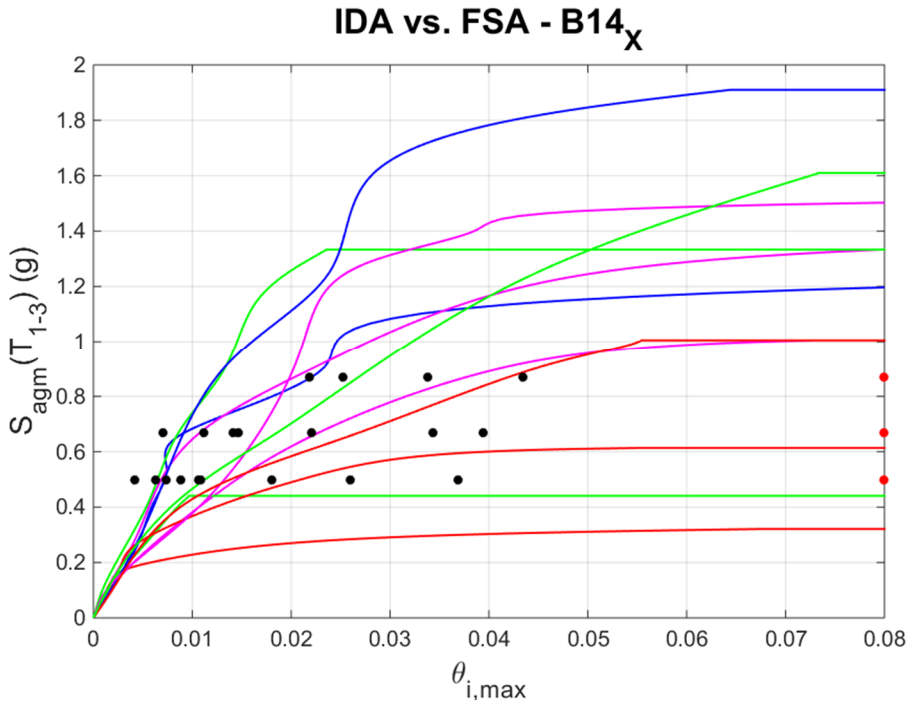
Fig. D.34 – IDA on 3D reduced-order uncalibrated model vs. FSA on full model, in X and Y direction, for building B14
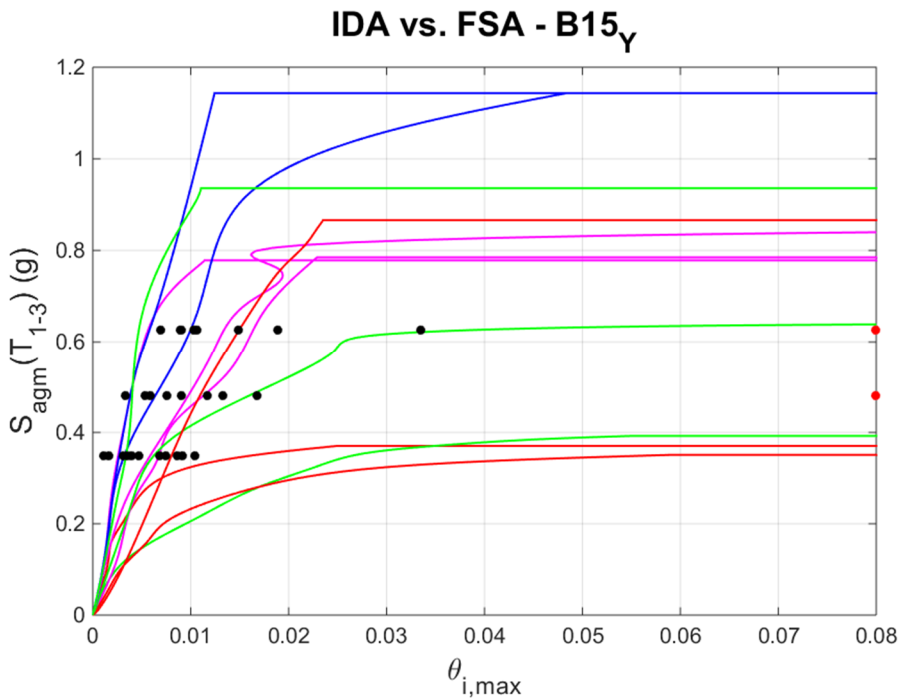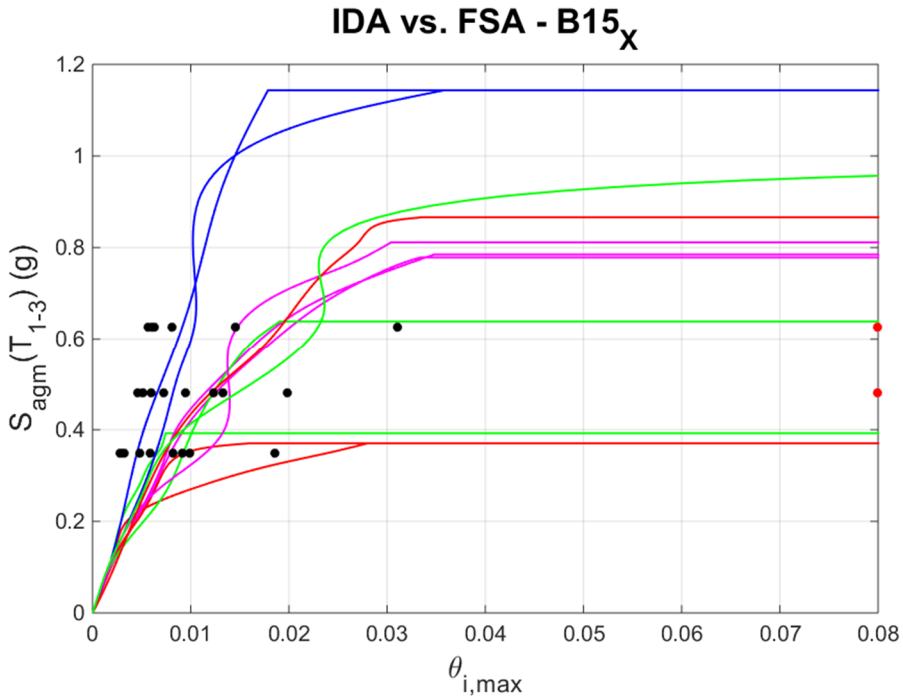
Fig. D.35 – IDA on 3D reduced-order uncalibrated model vs. FSA on full model, in X and Y direction, for building B15
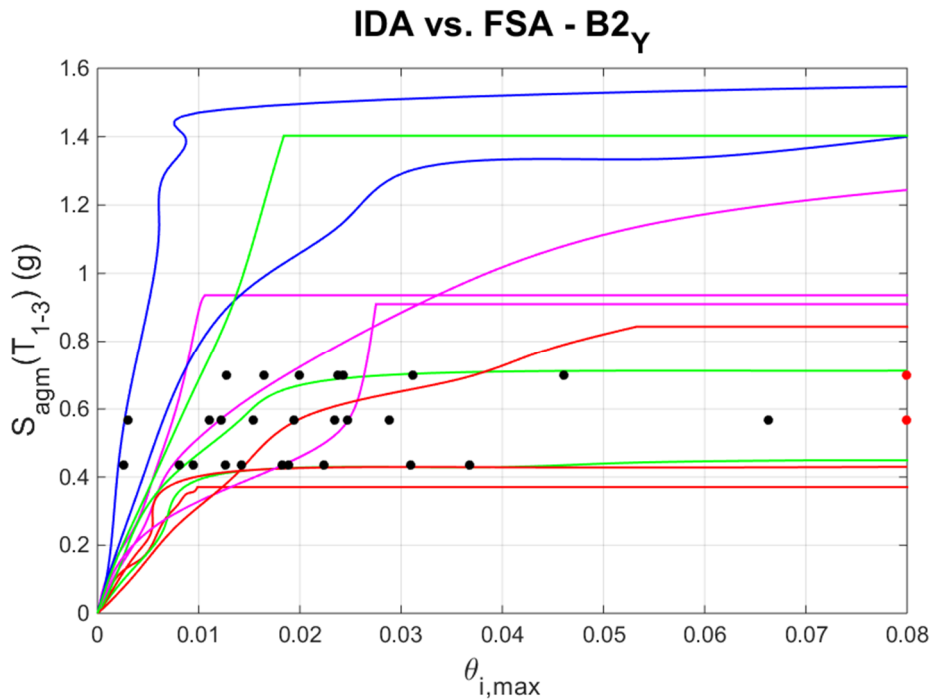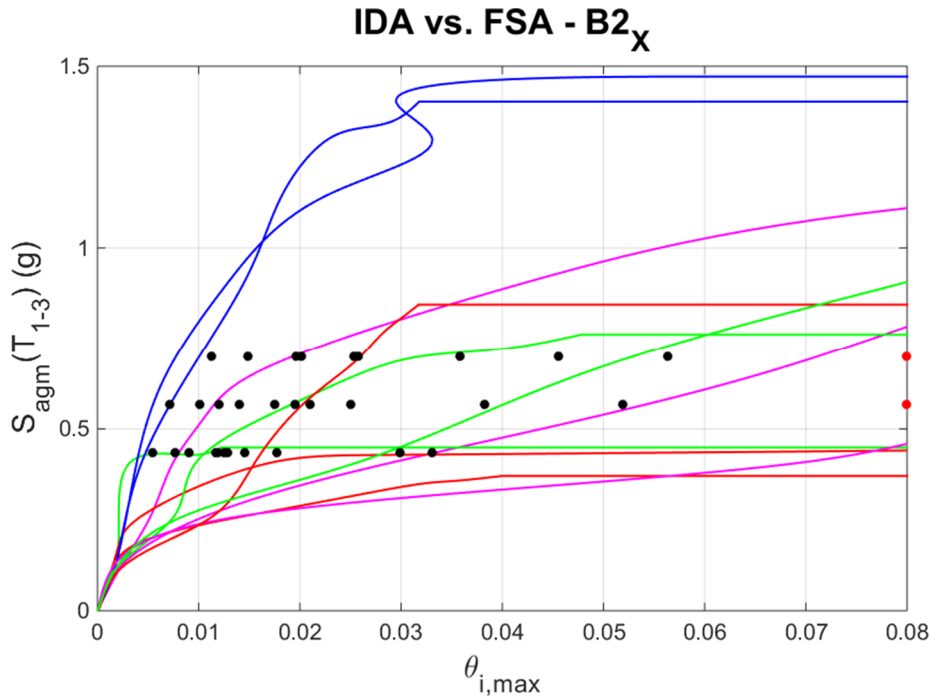
Fig. D.36 – IDA on 3D reduced-order calibrated model vs. FSA on full model, in X and Y direction, for building B2
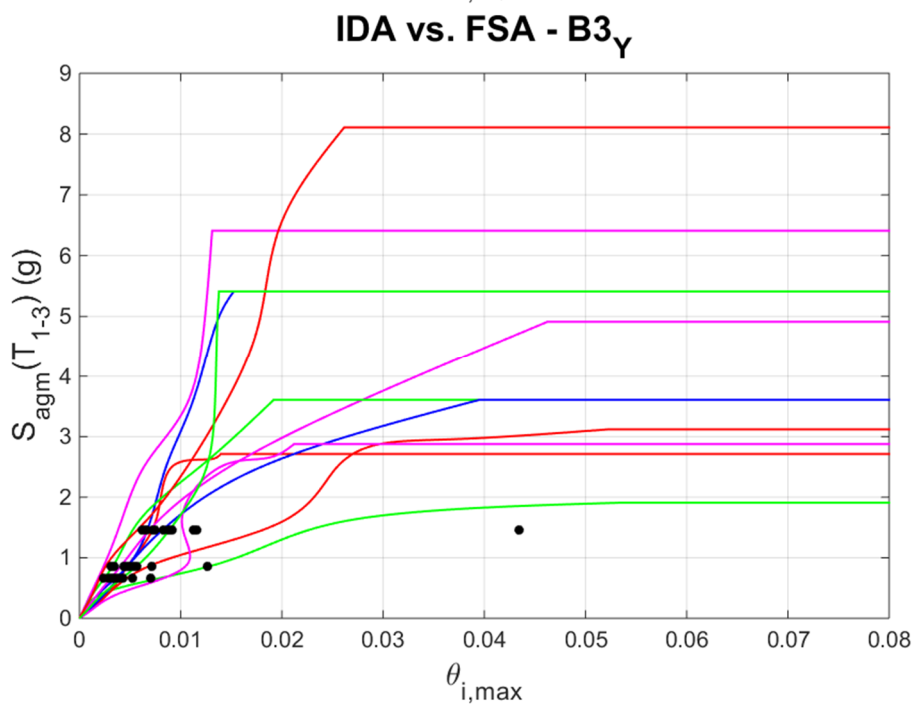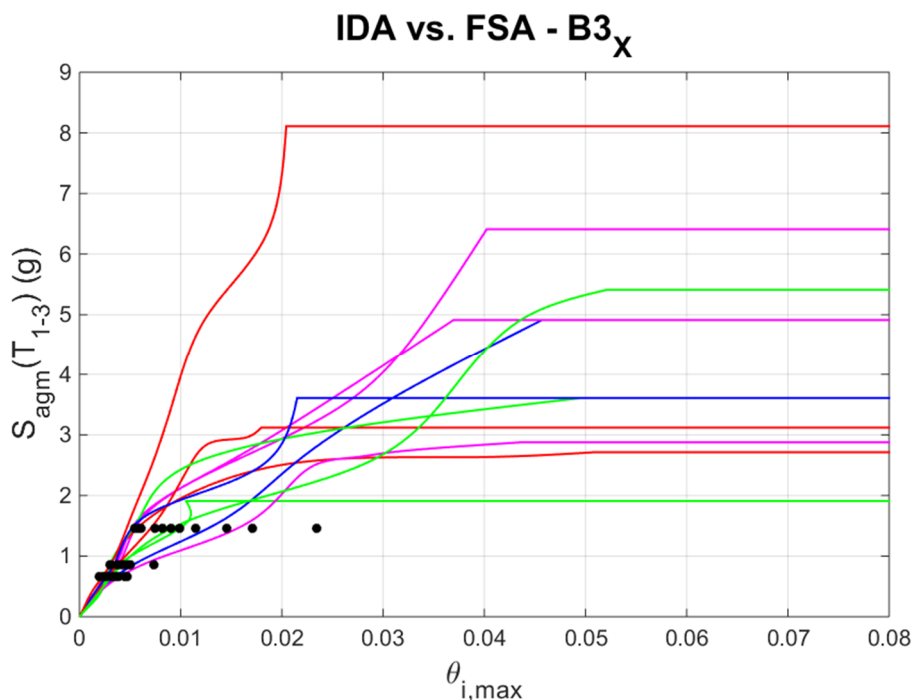
Fig. D.37 – IDA on 3D reduced-order calibrated model vs. FSA on full model, in X and Y direction, for building B3
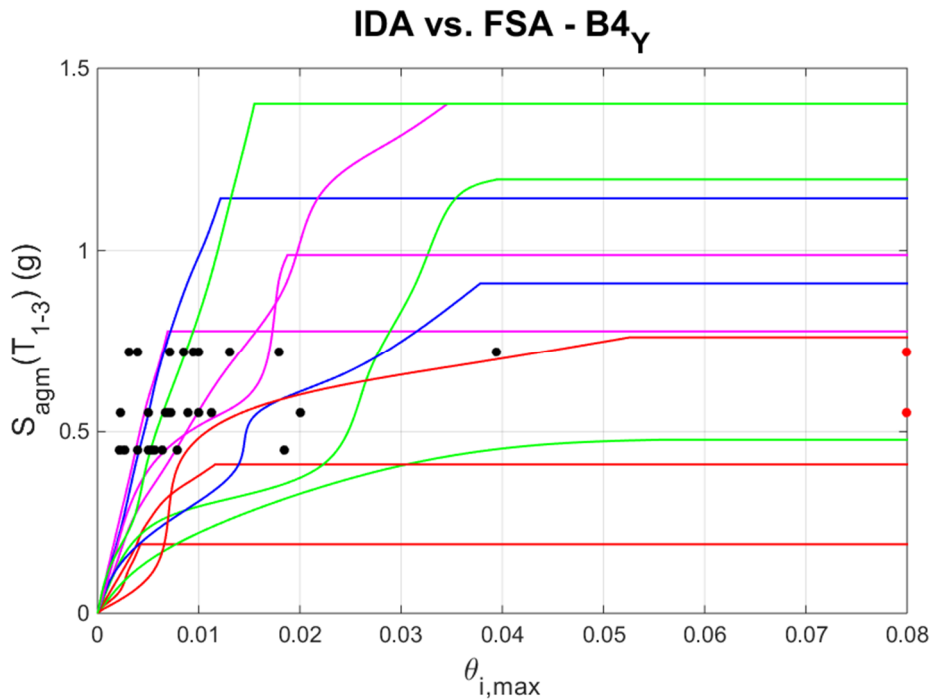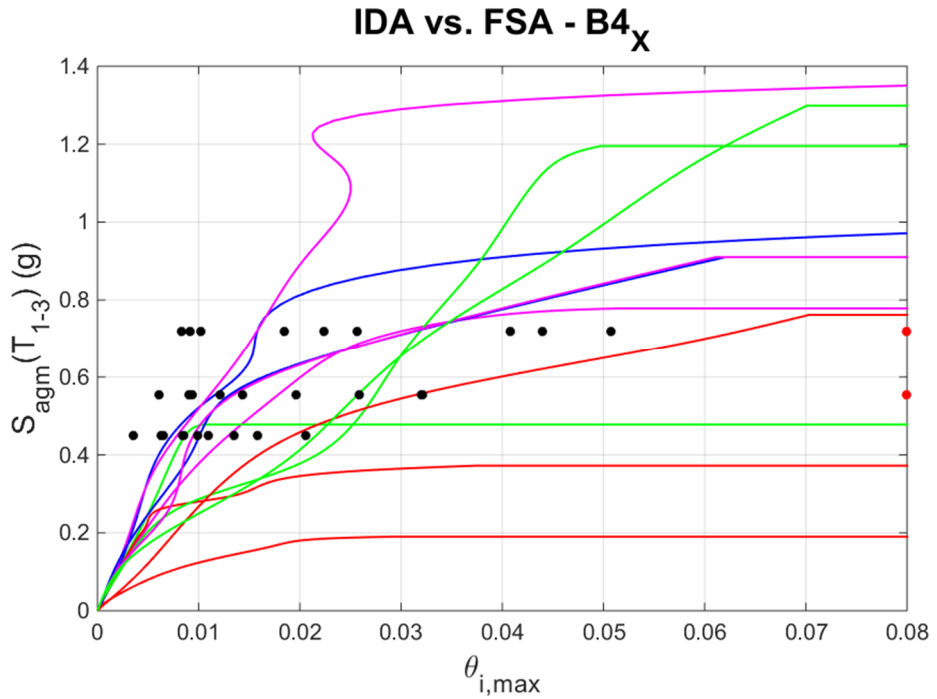
Fig. D.38 – IDA on 3D reduced-order calibrated model vs. FSA on full model, in X and Y direction, for building B4
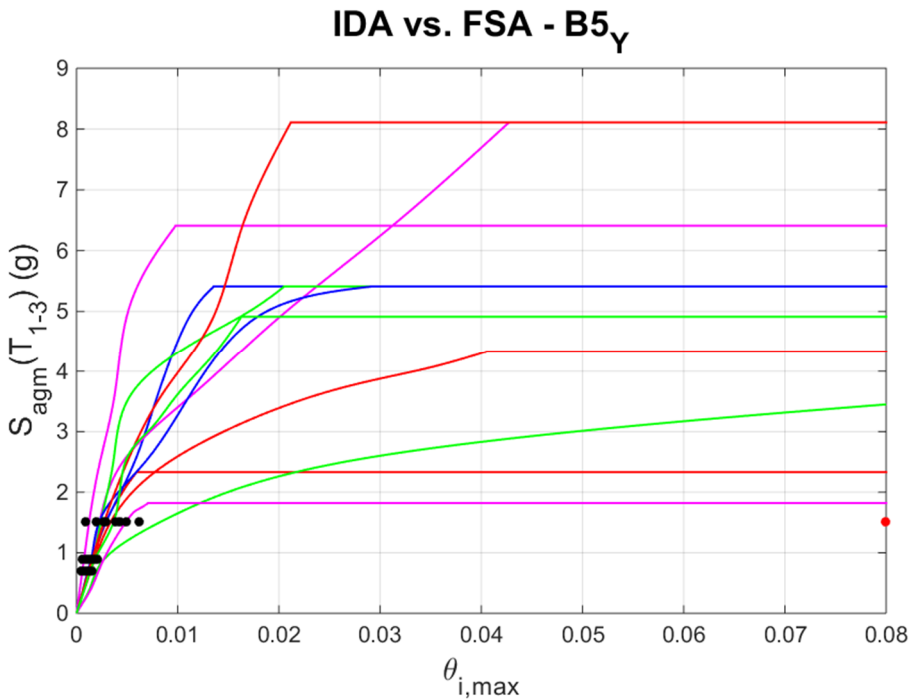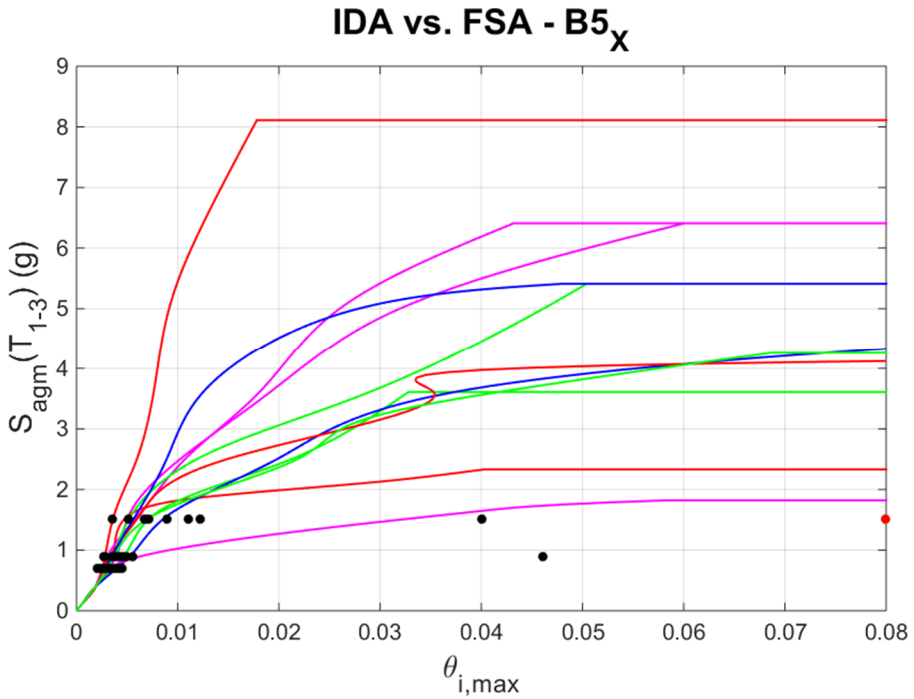
Fig. D.39 – IDA on 3D reduced-order calibrated model vs. FSA on full model, in X and Y direction, for building B5
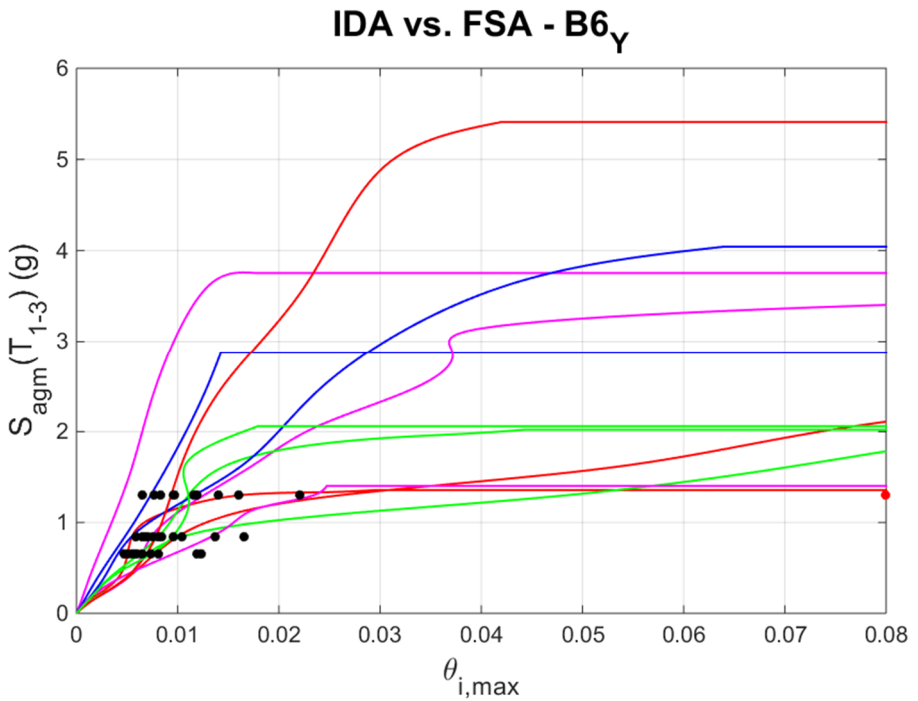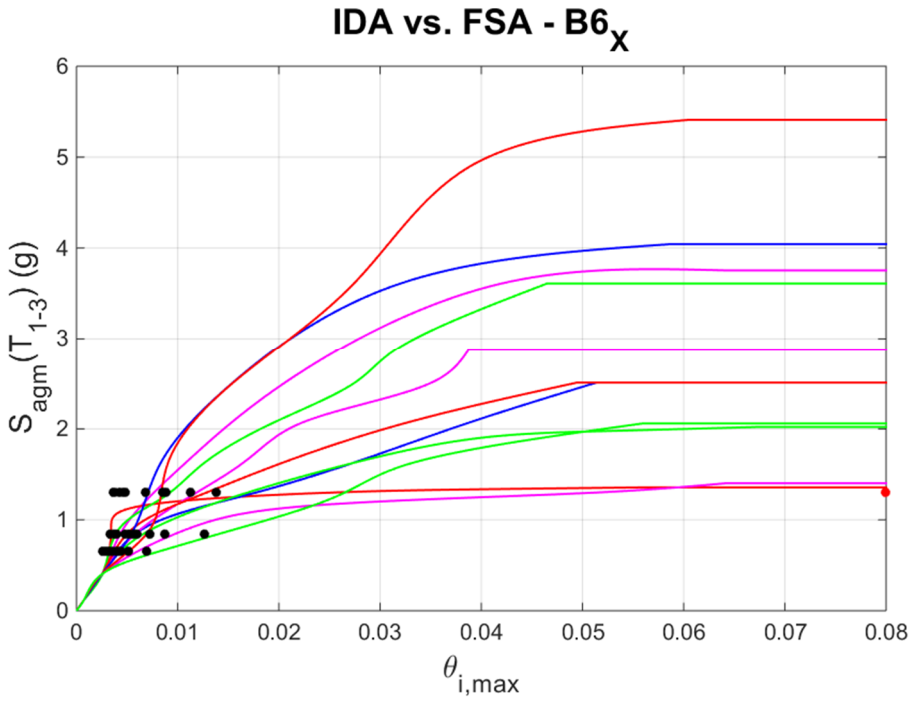
Fig. D.40 – IDA on 3D reduced-order calibrated model vs. FSA on full model, in X and Y direction, for building B6
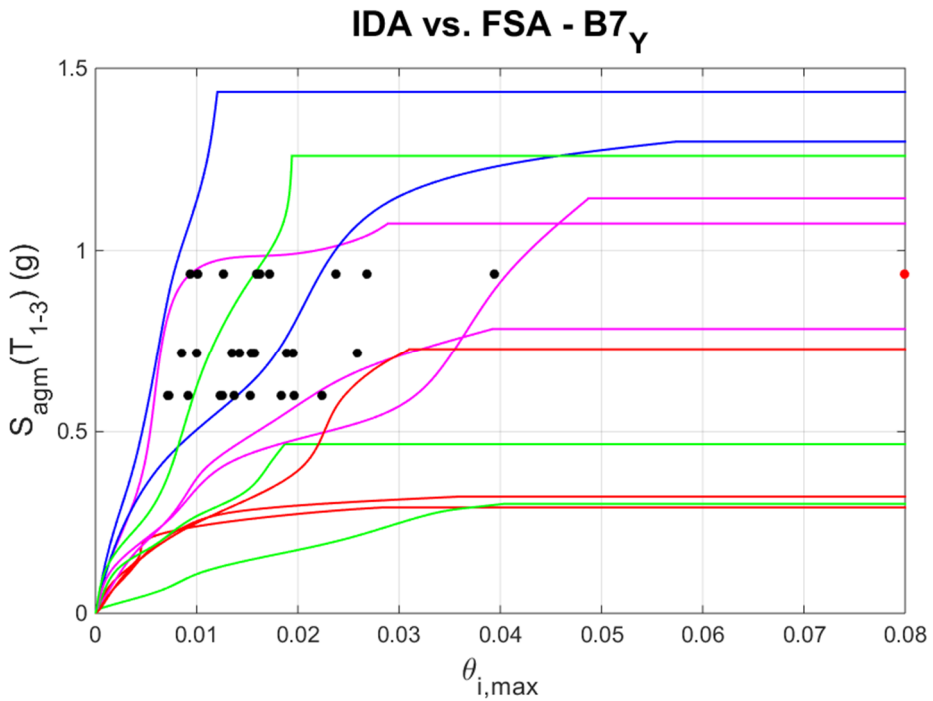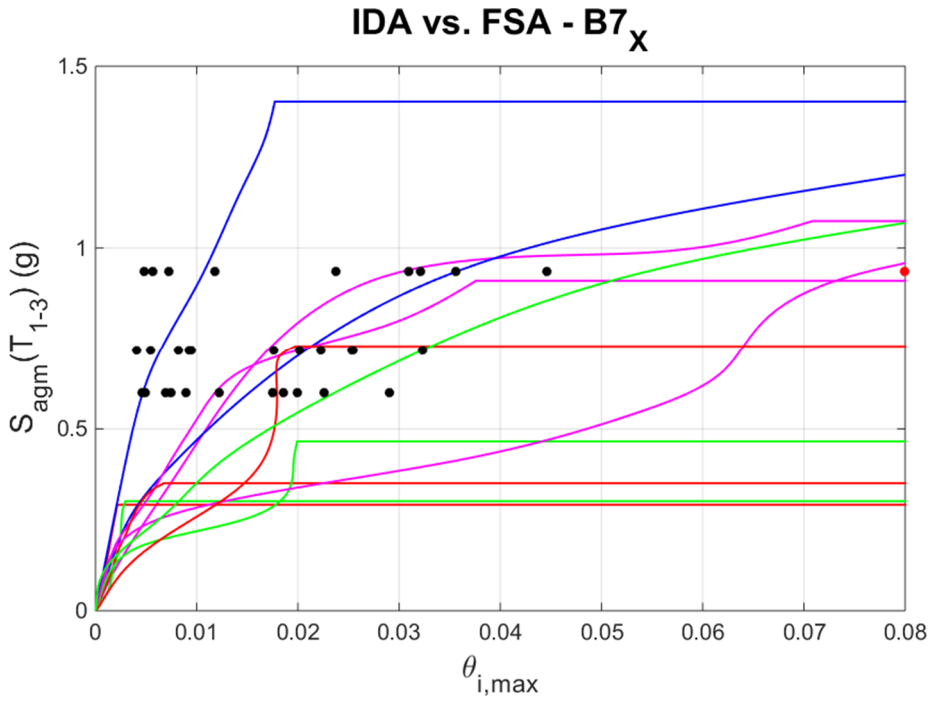
Fig. D.41 – IDA on 3D reduced-order calibrated model vs. FSA on full model, in X and Y direction, for building B7
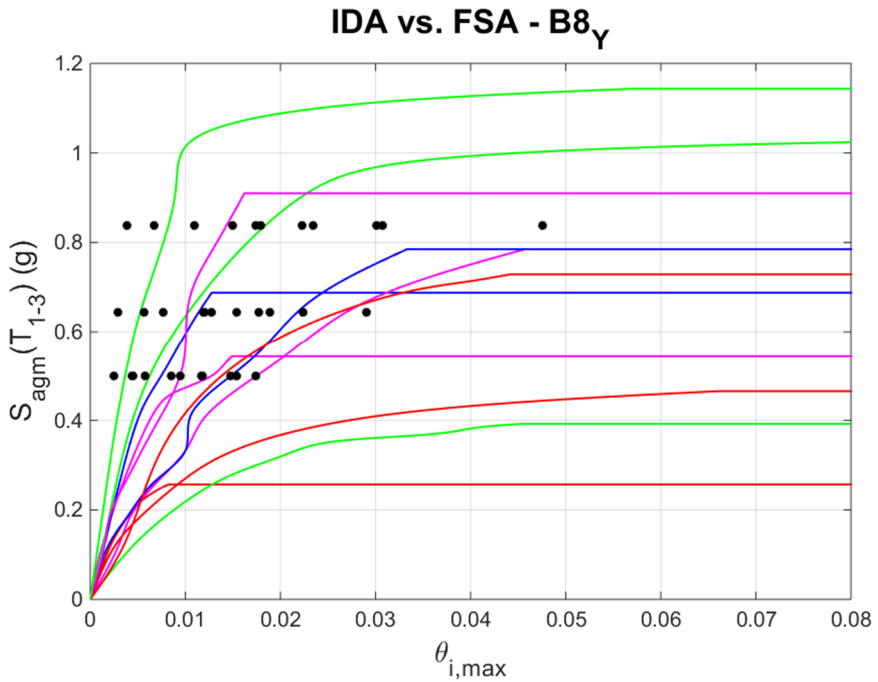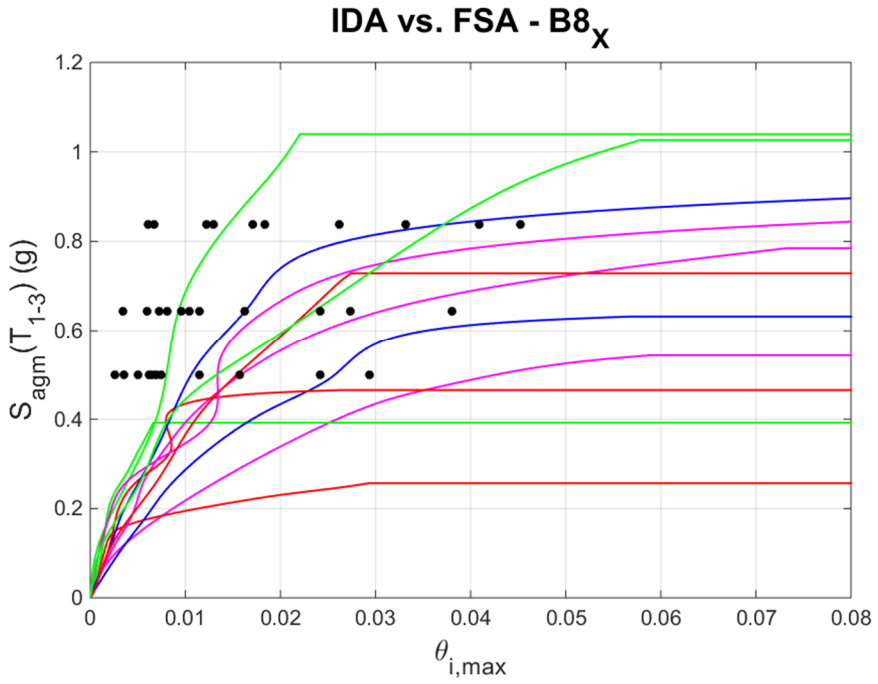
Fig. D.42 – IDA on 3D reduced-order calibrated model vs. FSA on full model, in X and Y direction, for building B8
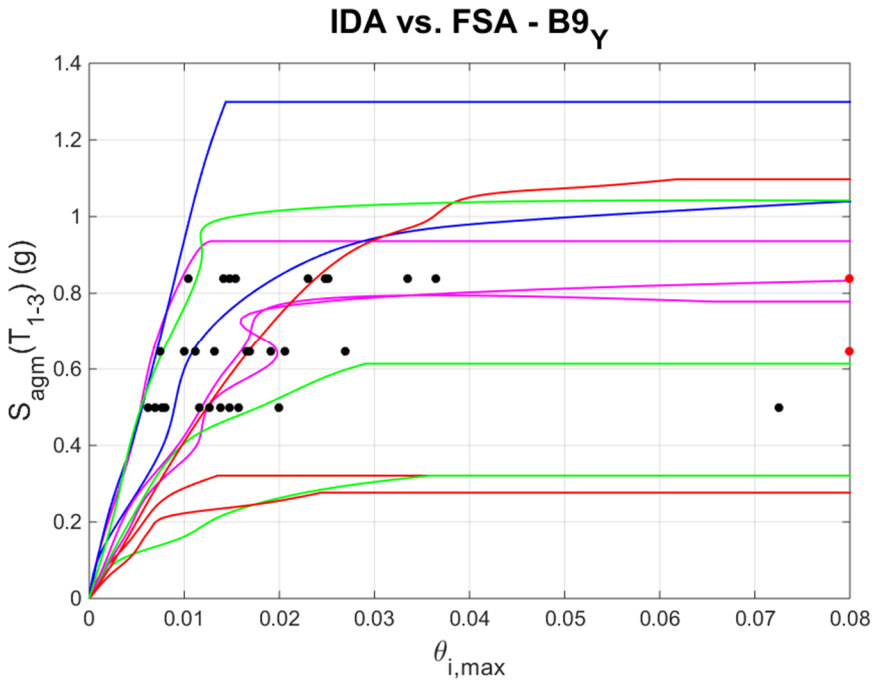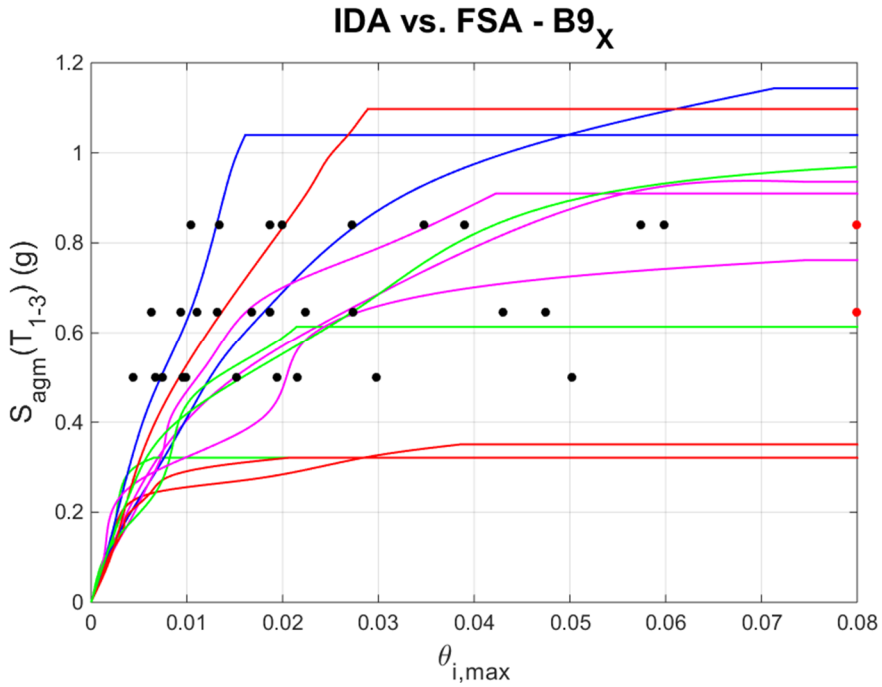
Fig. D.43 – IDA on 3D reduced-order calibrated model vs. FSA on full model, in X and Y direction, for building B9
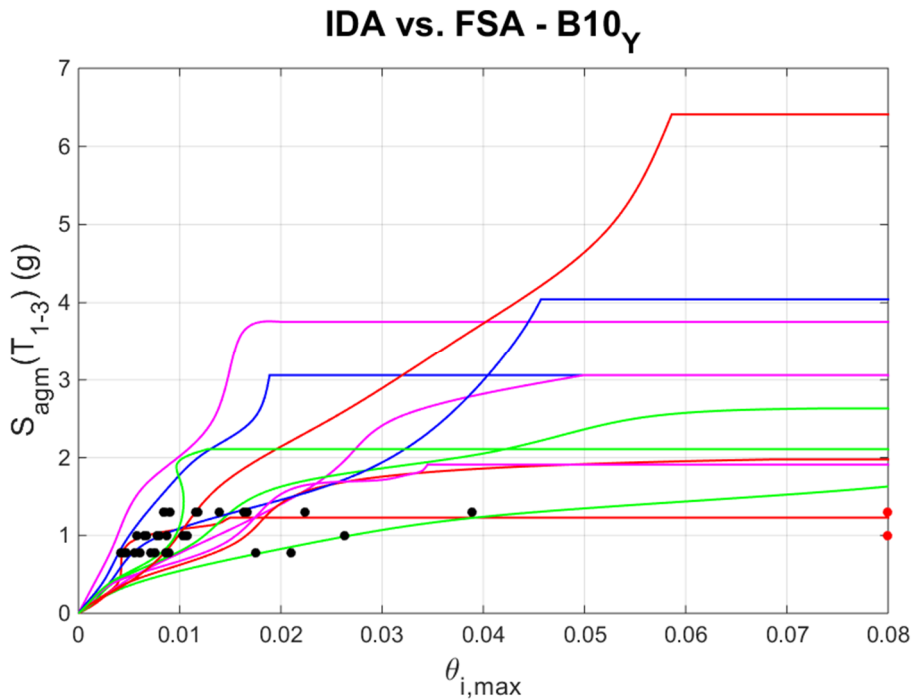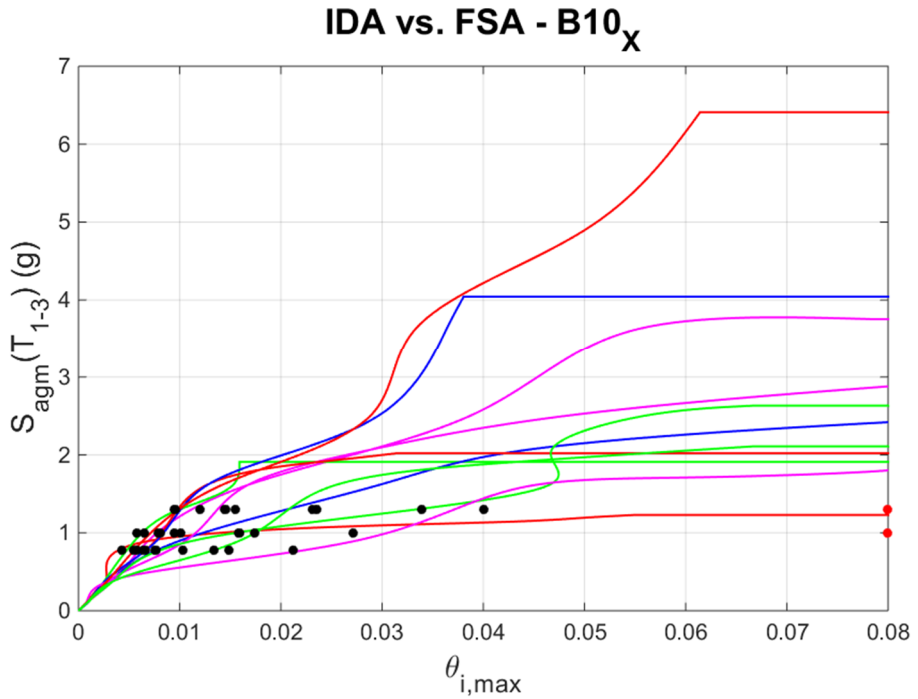
Fig. D.44 – IDA on 3D reduced-order calibrated model vs. FSA on full model, in X and Y direction, for building B10
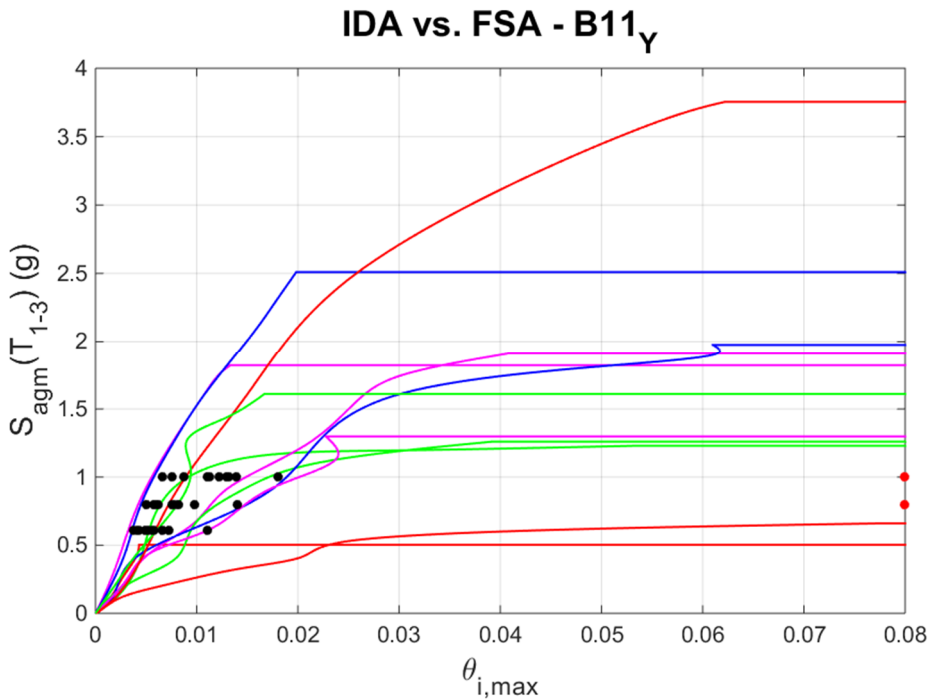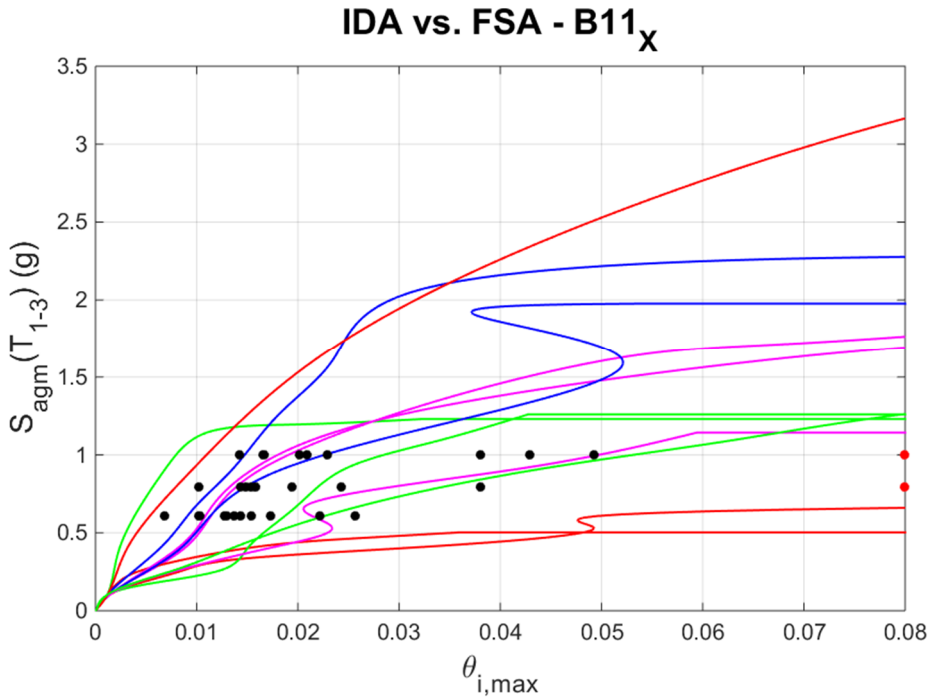
Fig. D.45 – IDA on 3D reduced-order calibrated model vs. FSA on full model, in X and Y direction, for building B11
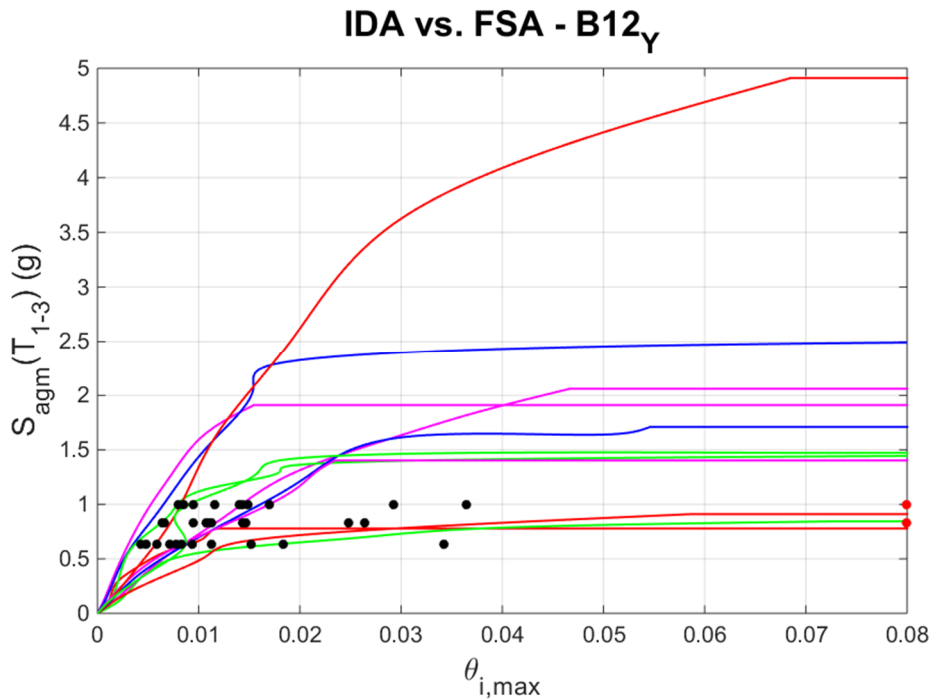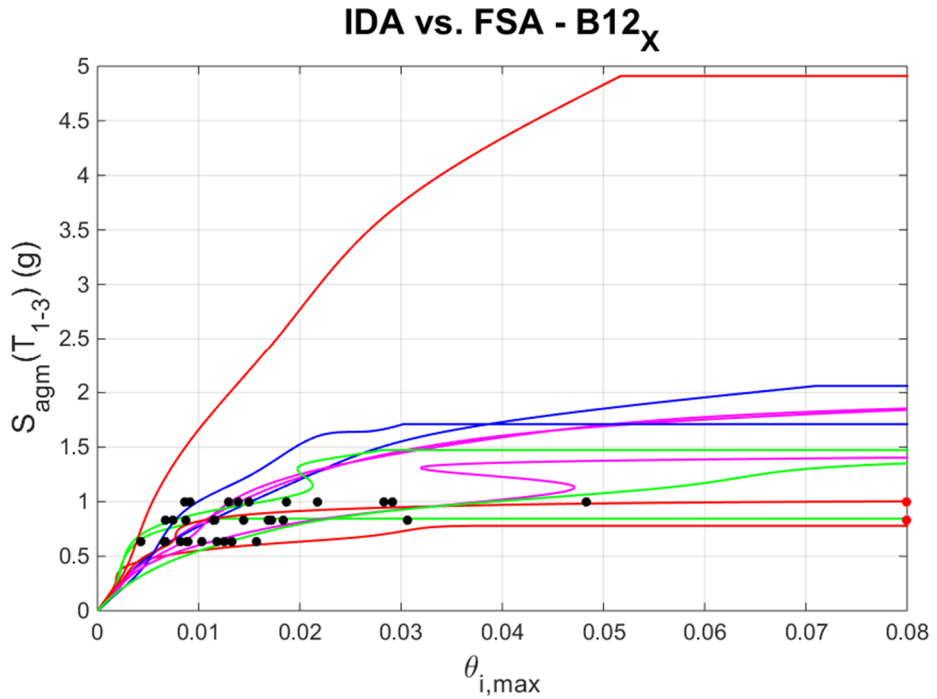
Fig. D.46 – IDA on 3D reduced-order calibrated model vs. FSA on full model, in X and Y direction, for building B12
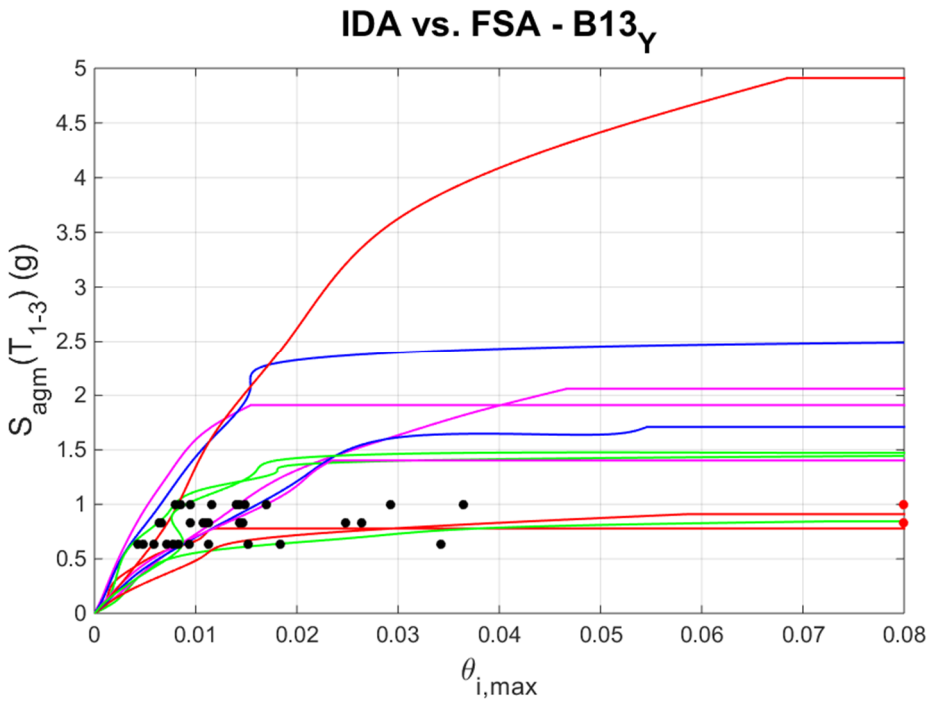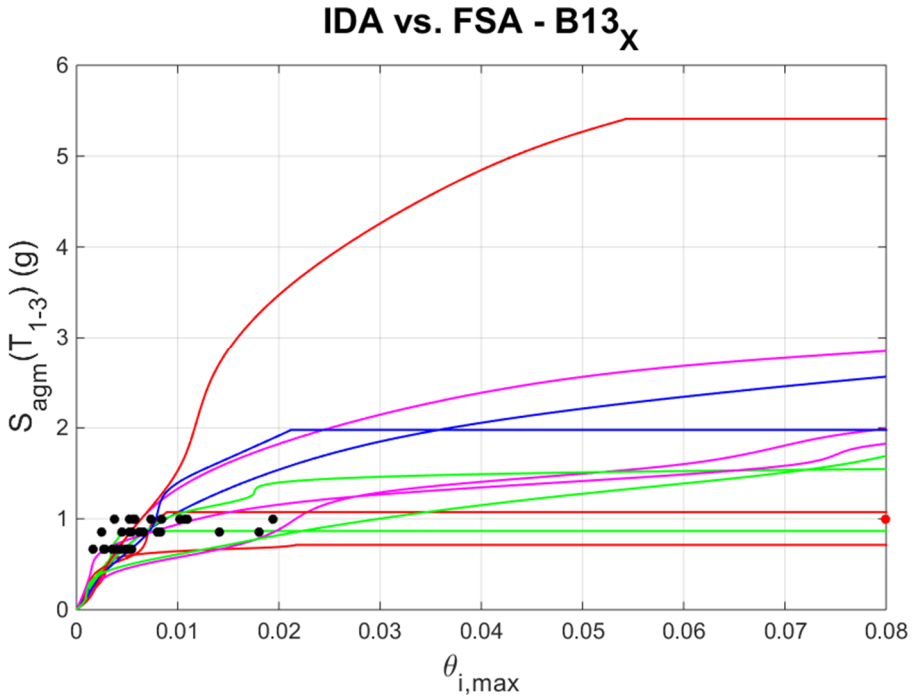
Fig. D.47 – IDA on 3D reduced-order calibrated model vs. FSA on full model, in X and Y direction, for building B13
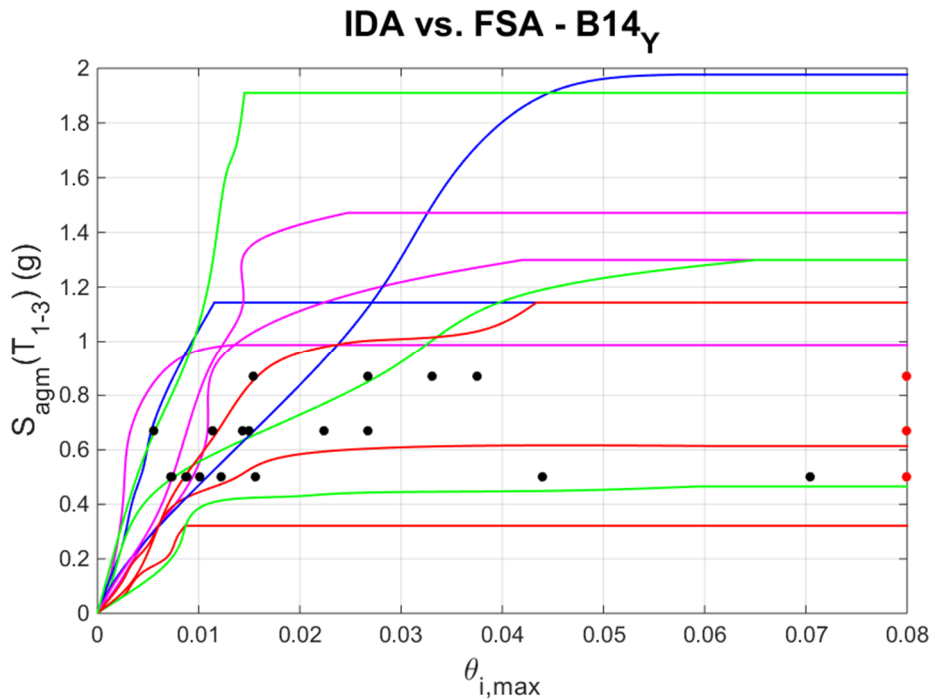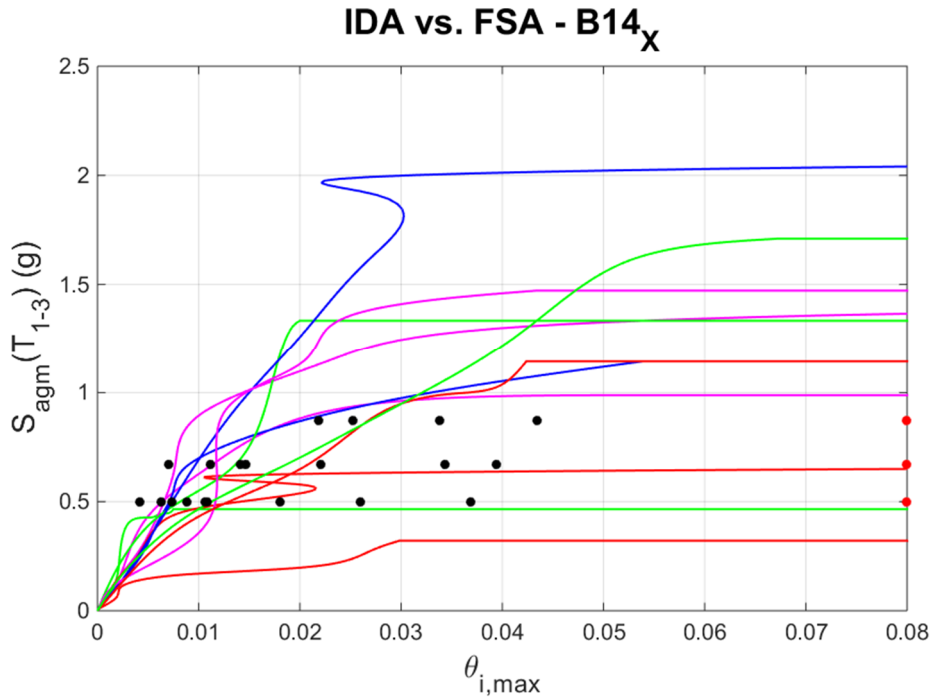
Fig. D.48 – IDA on 3D reduced-order calibrated model vs. FSA on full model, in X and Y direction, for building B14
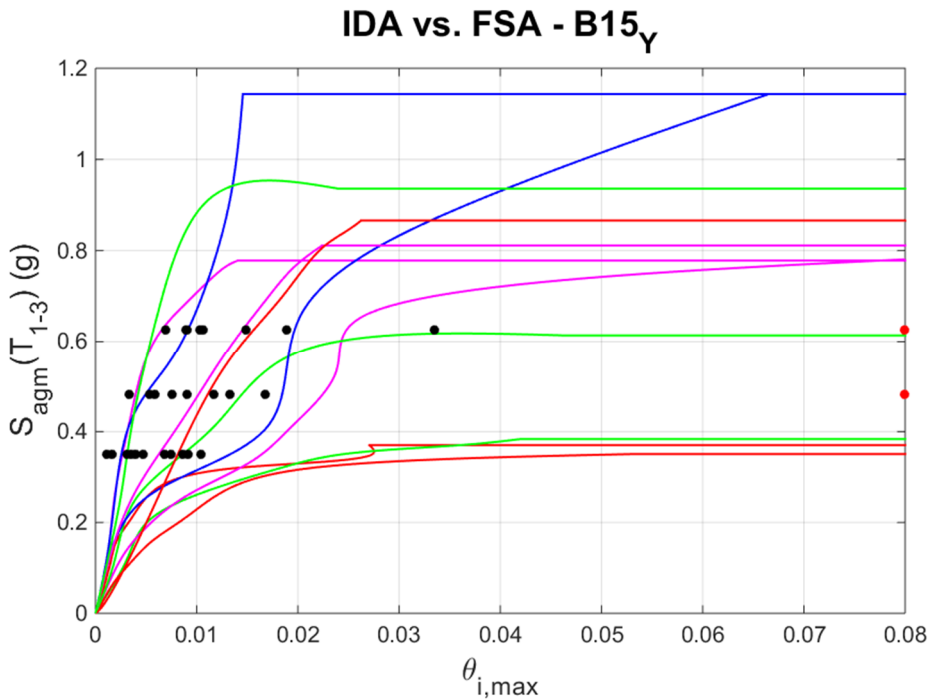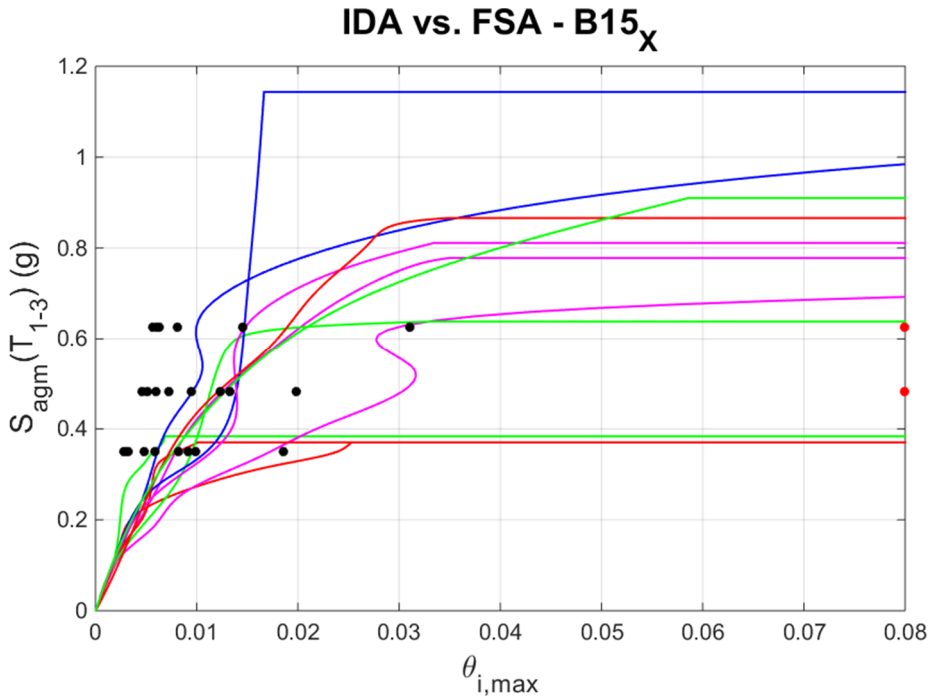
Fig. D.49 – IDA on 3D reduced-order calibrated model vs. FSA on full model, in X and Y direction, for building B15
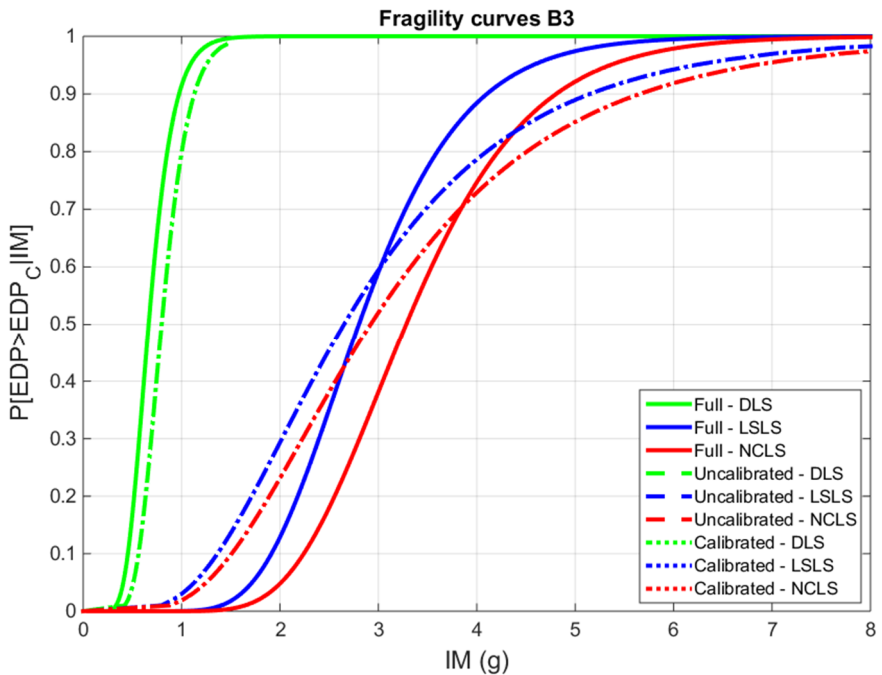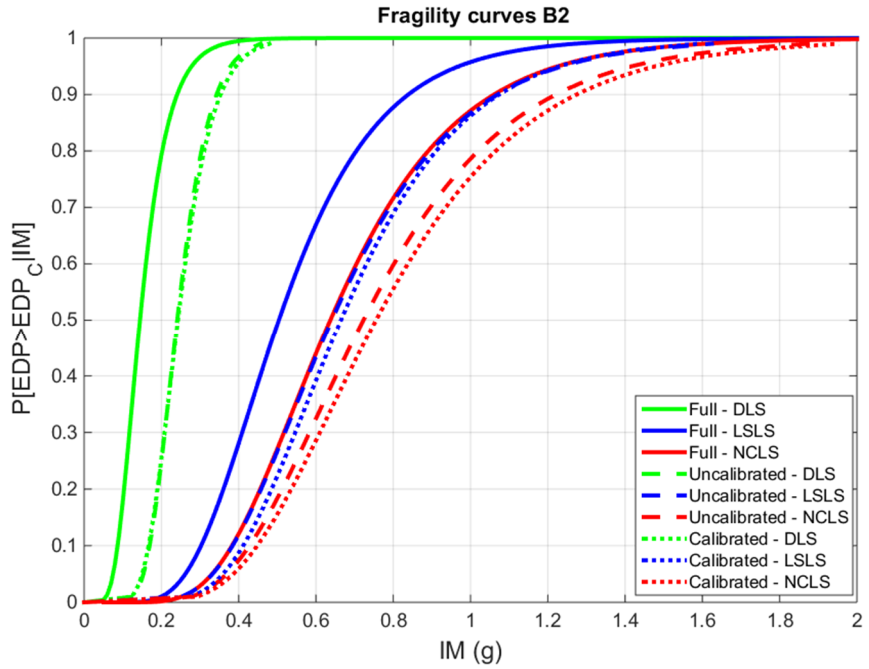
Fig. D.50 – Comparison of fragility curves, for each model and each LS investigated for building B2 and B3
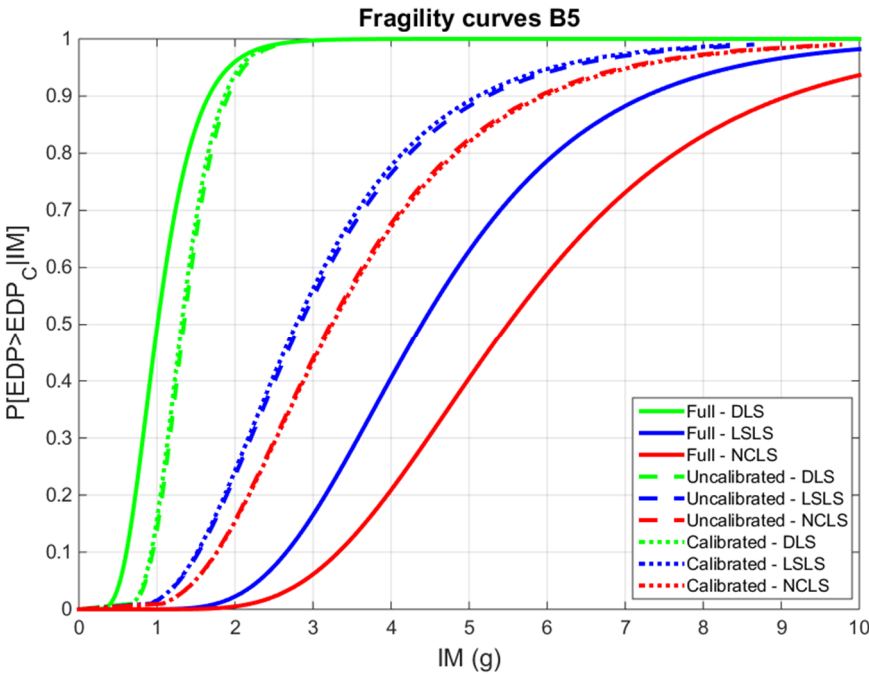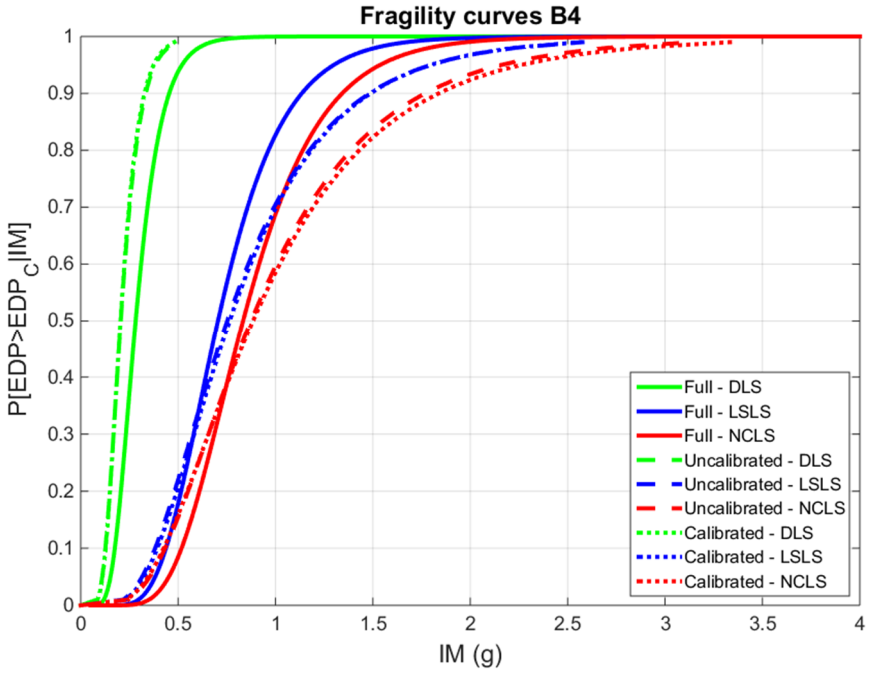
Fig. D.51 – Comparison of fragility curves, for each model and each LS investigated for building B4 and B5
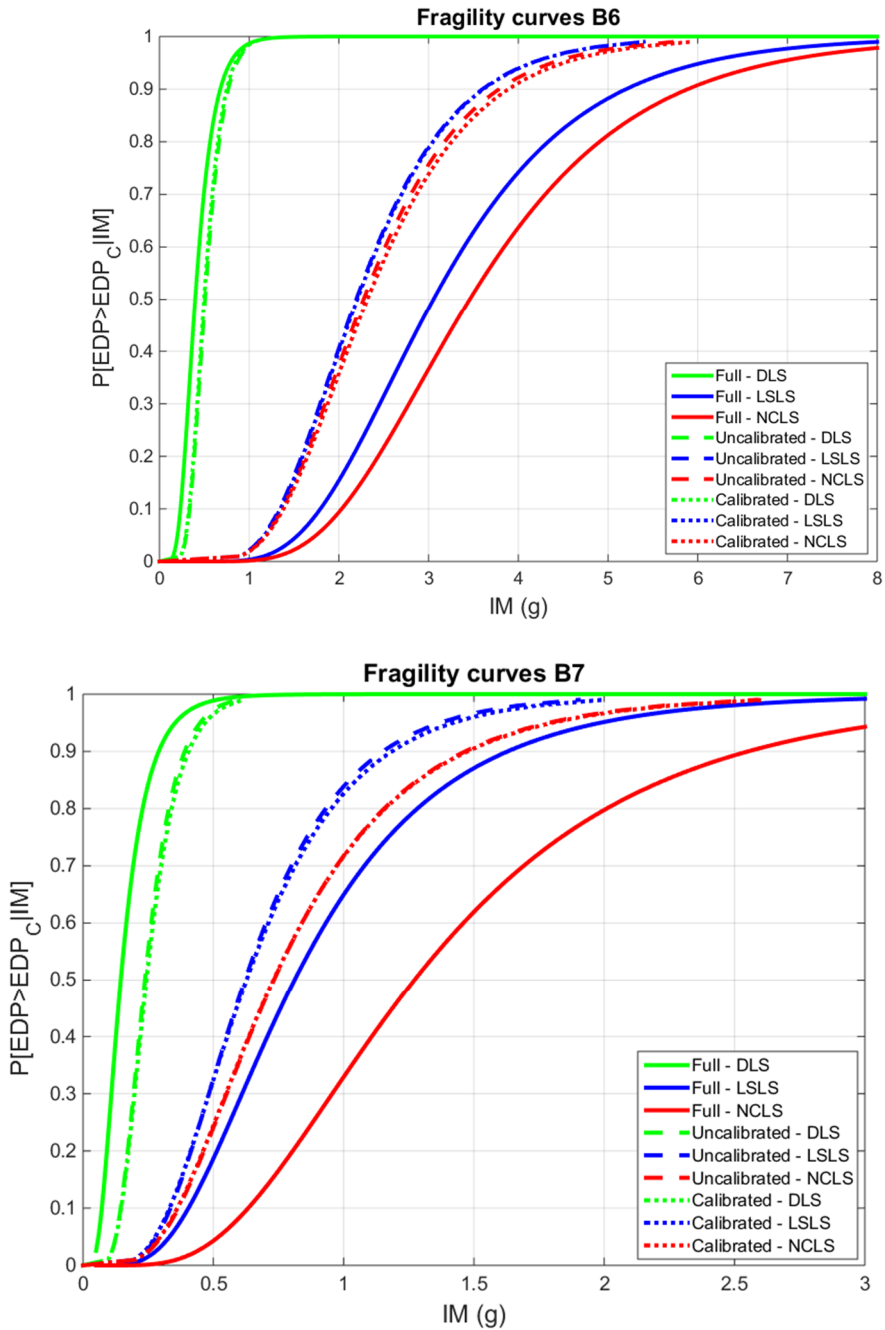
Fig. D.52 – Comparison of fragility curves, for each model and each LS investigated for build-ing B6 and B7
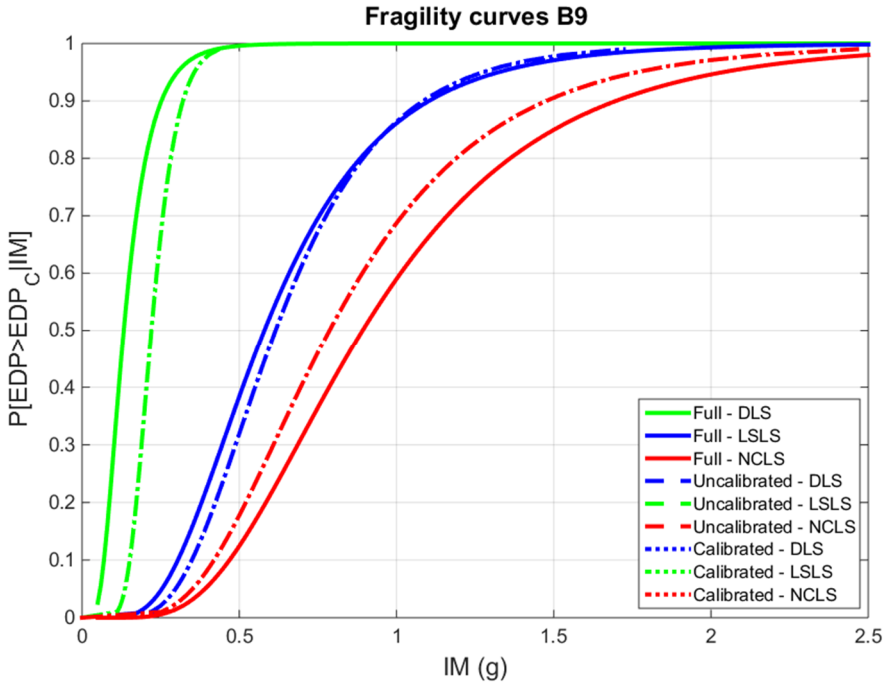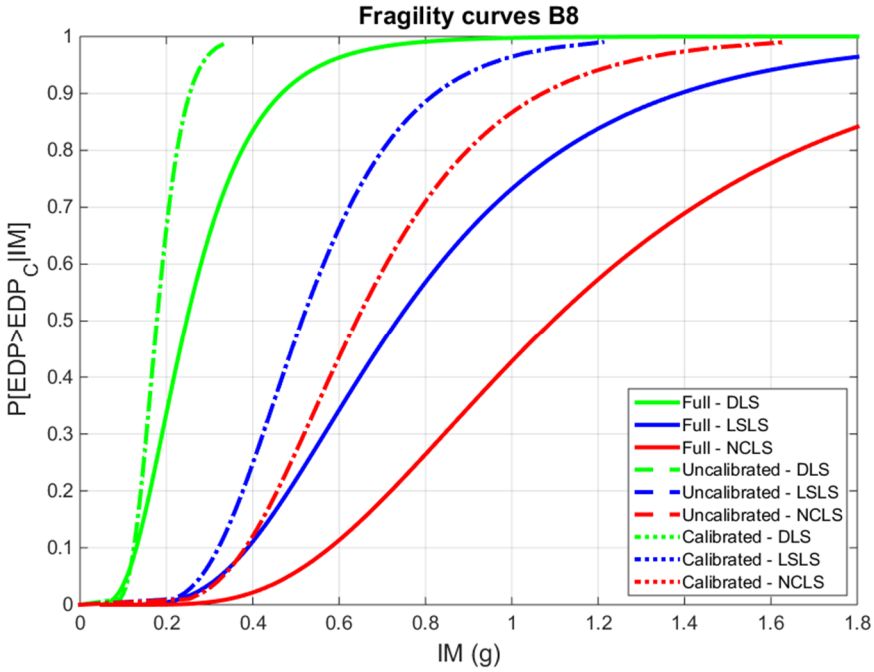
Fig. D.53 – Comparison of fragility curves, for each model and each LS investigated for building B8 and B9
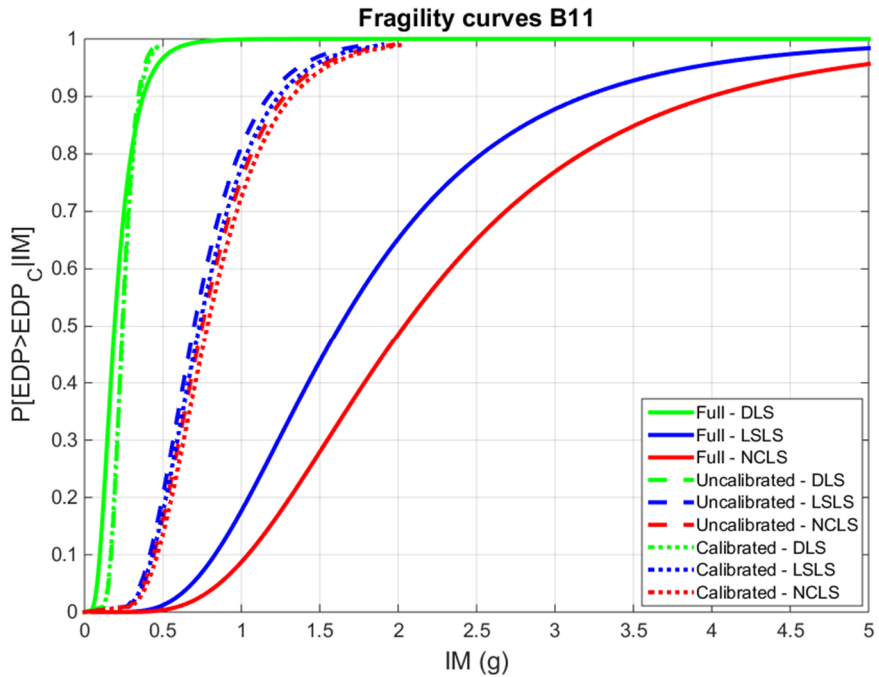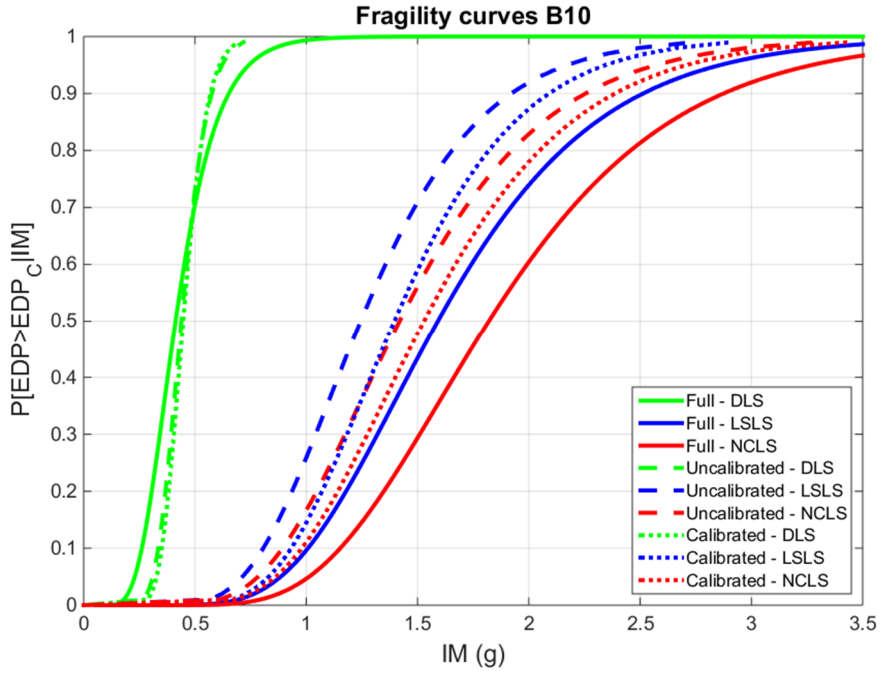
Fig. D.54 – Comparison of fragility curves, for each model and each LS investigated for building B10 and B11
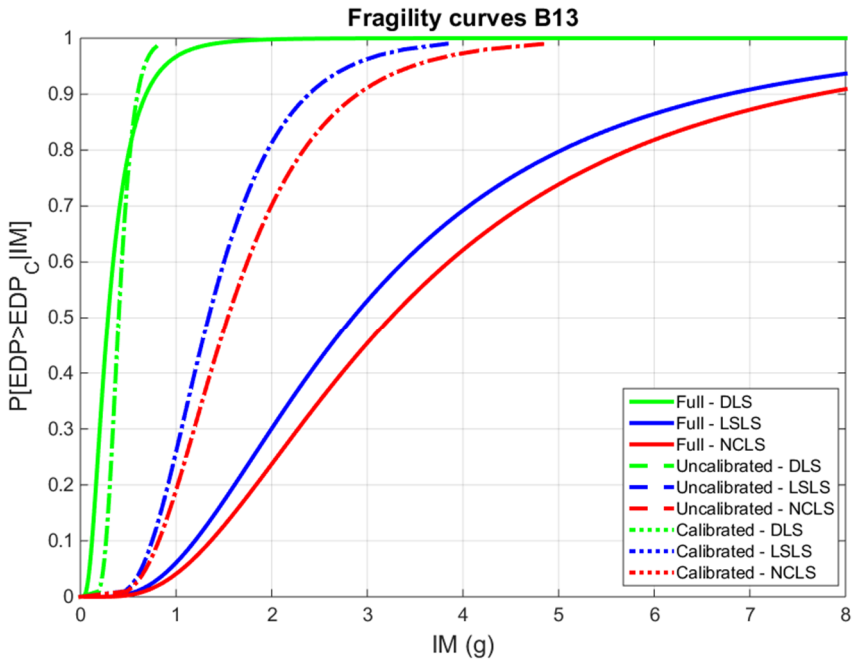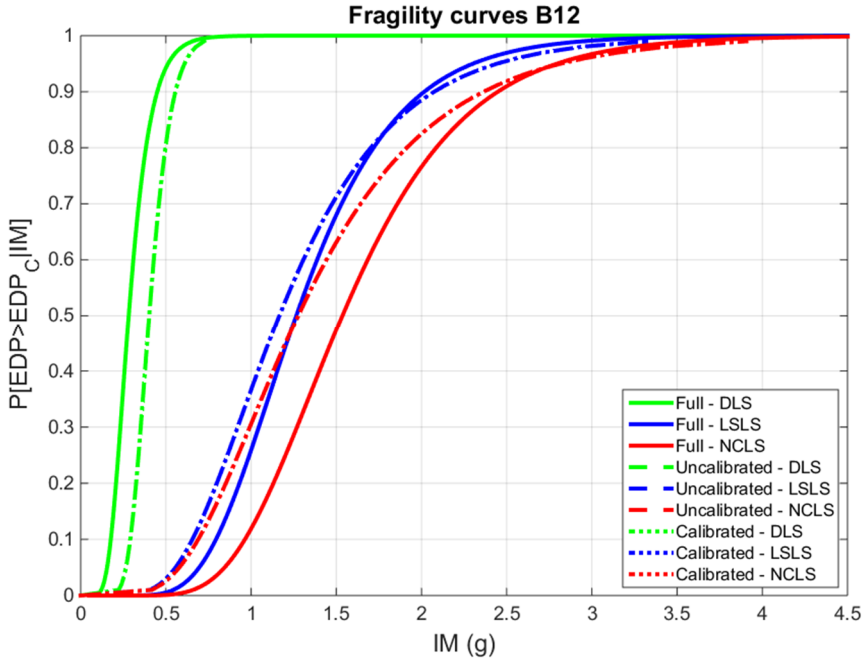
Fig. D.55 – Comparison of fragility curves, for each model and each LS investigated for building B12 and B13
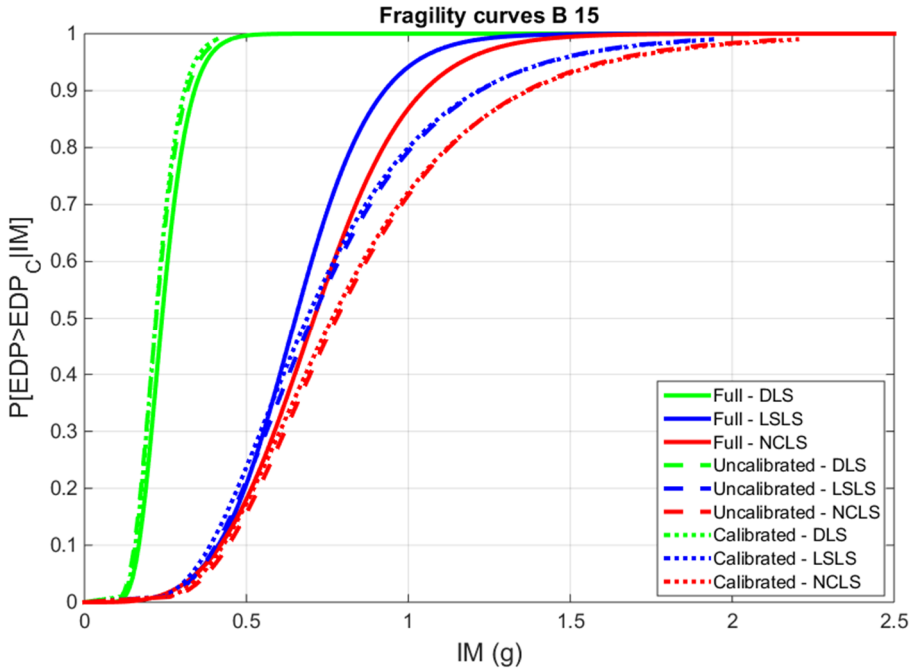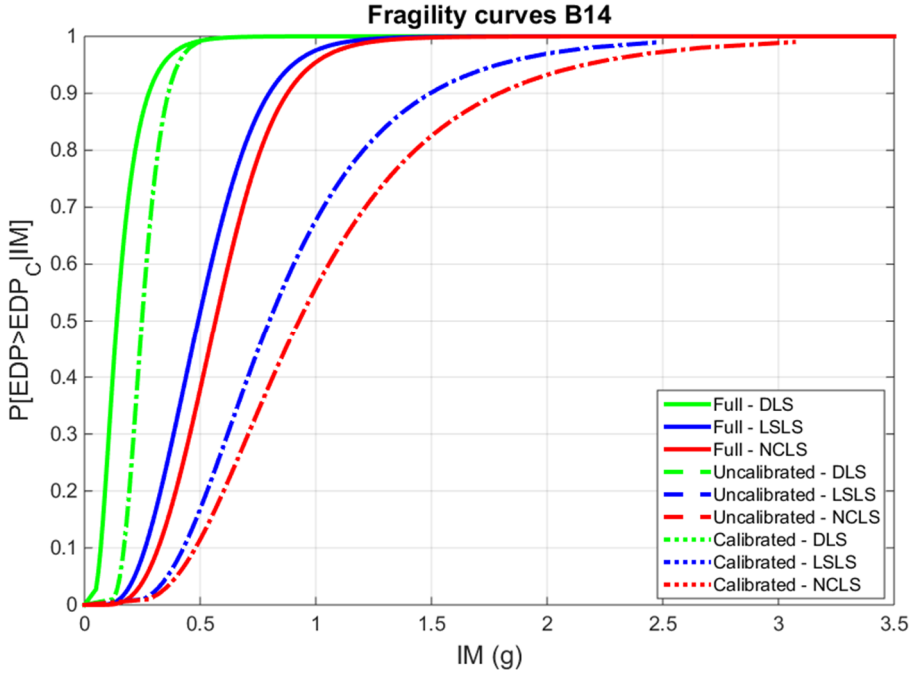
Fig. D.56 – Comparison of fragility curves, for each model and each LS investigated for building B14 and B15

12. Annex E: Extended results of FSA and SPO2FRAG methods, accounting for shear mechanisms
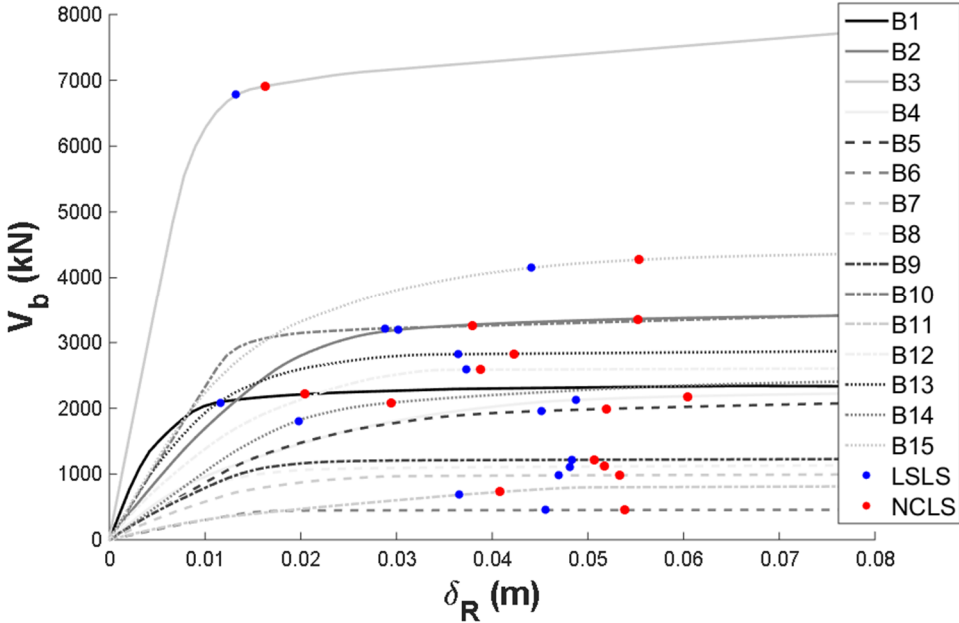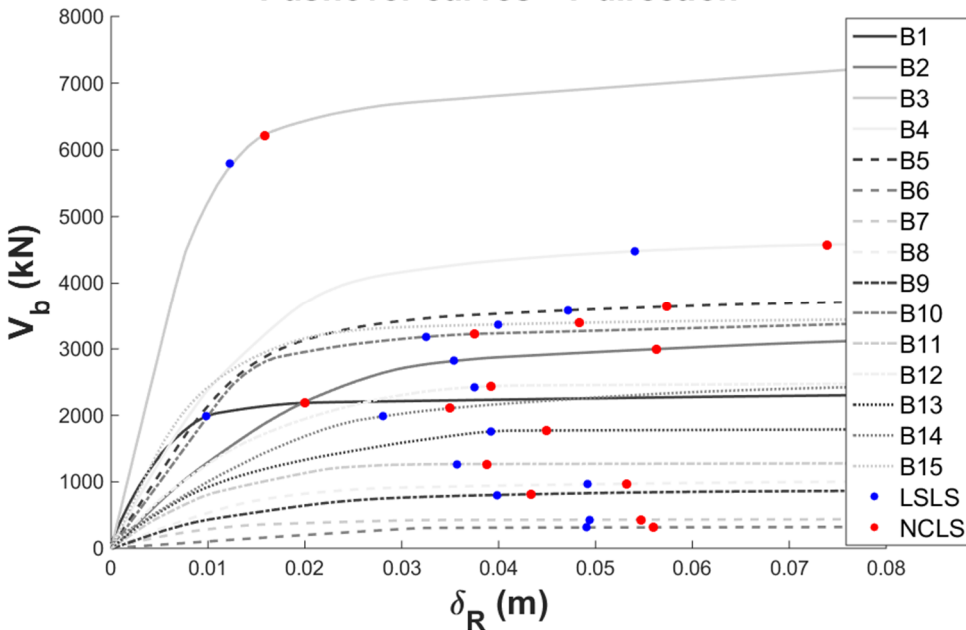
Fig E.1 - Pushover curves of all buildings in the two main direction, with shear indication

Tab. E.1 – Values of EDP, in terms of θ_i estimated from pushover analyses, accounting for shear mechanisms

Building	X direction		Y direction	
	LSLS max θ_i [%]	NCLS max θ_i [%]	LSLS max θ_i [%]	NCLS max θ_i [%]
B1	0.25	0.440	0.210	0.430
B2	0.299	0.547	0.350	0.557
B3	0.26	0.320	0.240	0.310
B4	0.46	0.570	0.510	0.697
B5	0.594	0.684	0.620	0.754
B6	0.548	0.647	0.590	0.672
B7	0.564	0.641	0.593	0.657
B8	0.578	0.621	0.591	0.639
B9	0.581	0.609	0.478	0.521
B10	0.417	0.550	0.472	0.543
B11	0.513	0.573	0.501	0.545
B12	0.524	0.545	0.526	0.550
B13	0.512	0.593	0.550	0.631
B14	0.210	0.313	0.298	0.372
B15	0.630	0.790	0.570	0.690
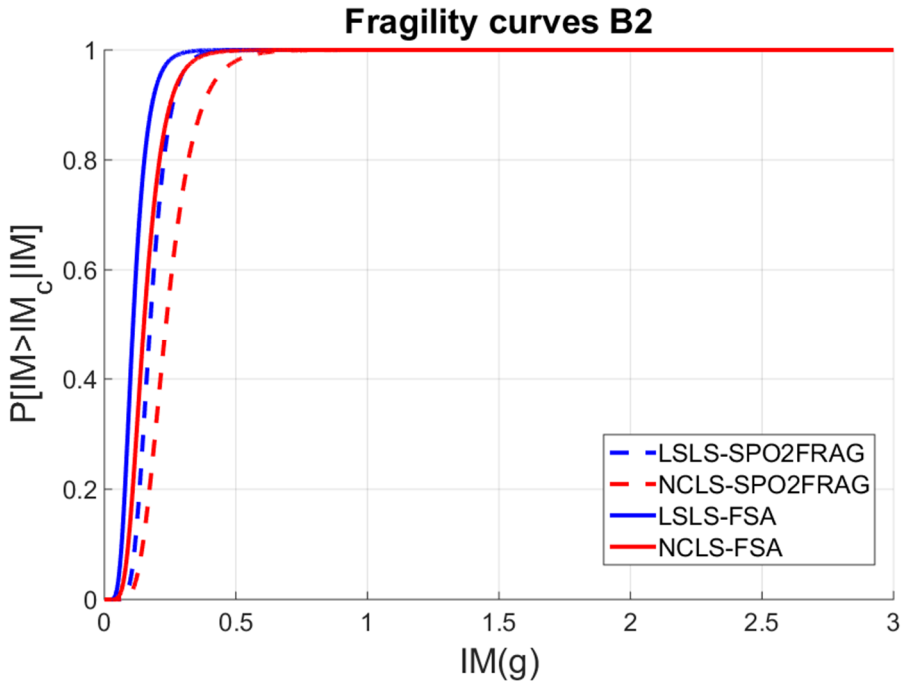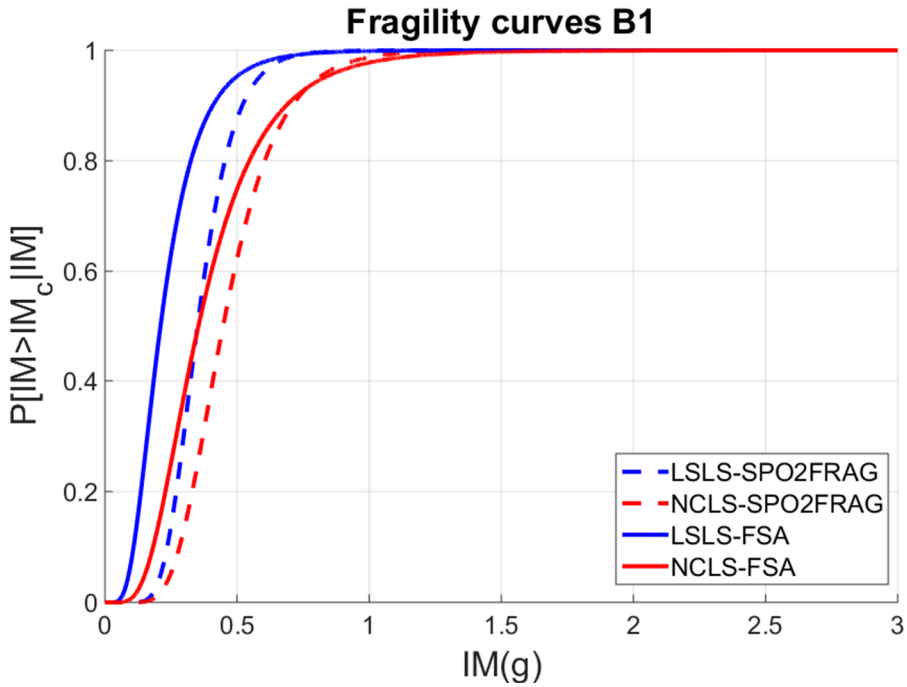
Fig. E.2 – One-by-one comparison between the fragility curves obtained from the two methodologies adopted, for B1 and B2, accounting for the shear mechanisms
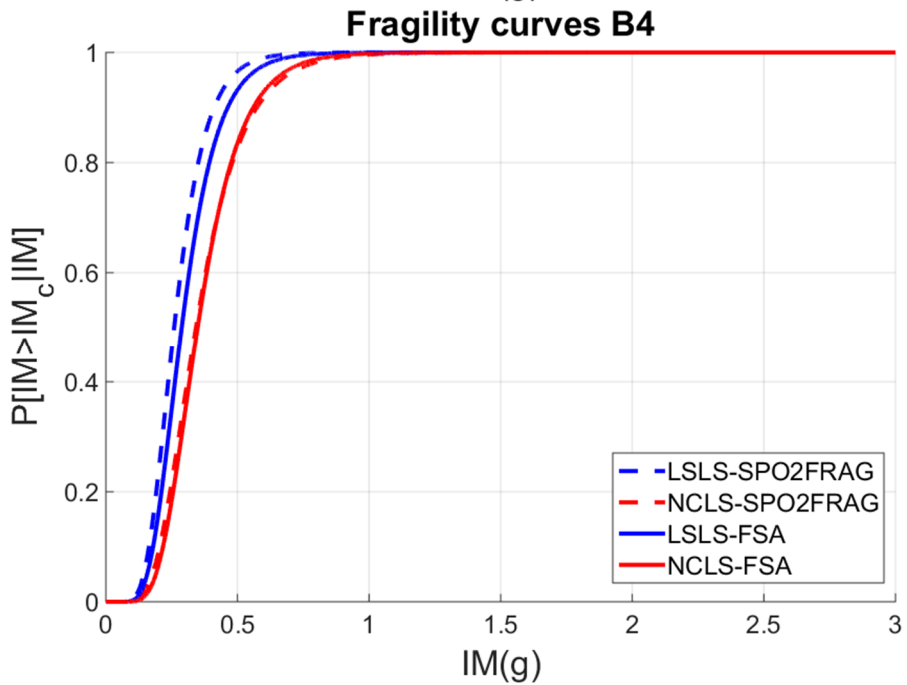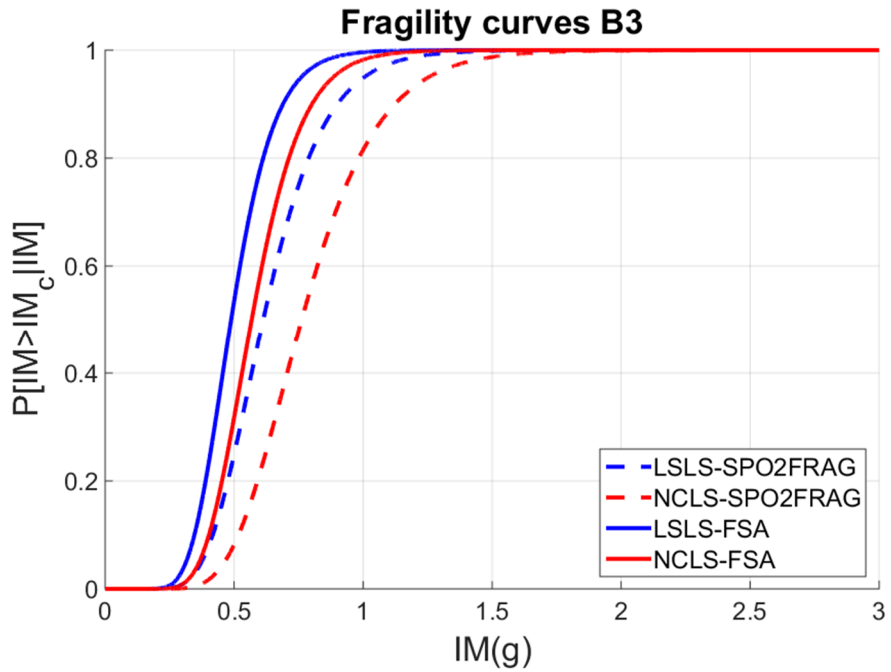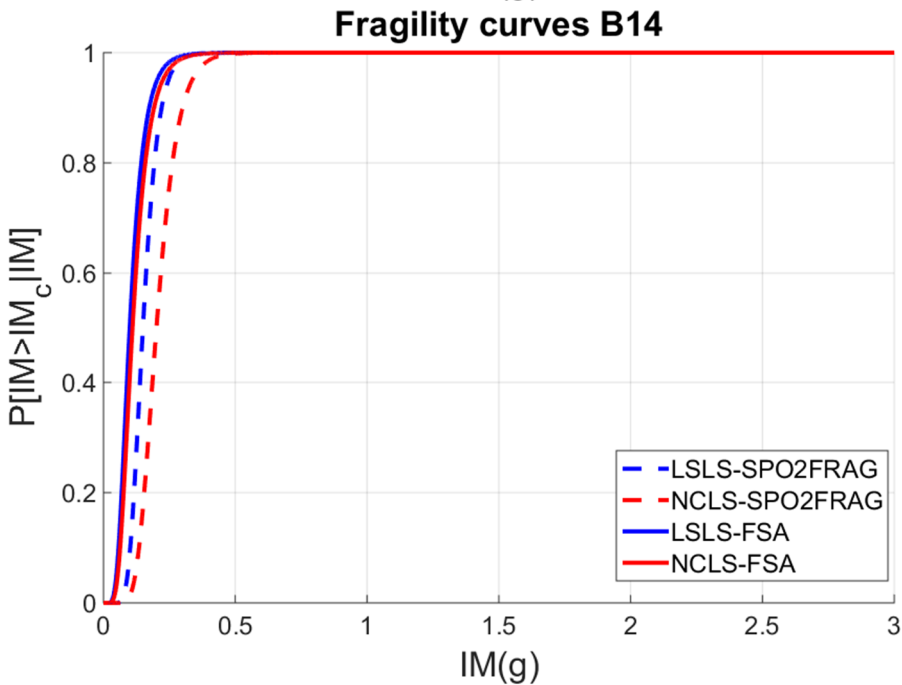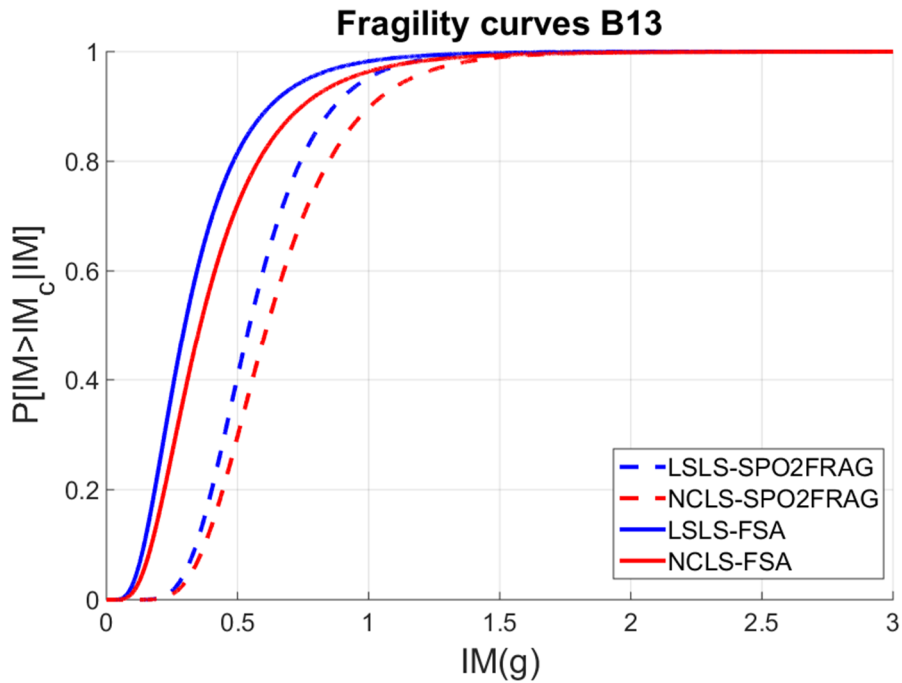
Fig. E.3 – One-by-one comparison between the fragility curves obtained from the two methodologies adopted, for B3 and B4, accounting for the shear mechanisms
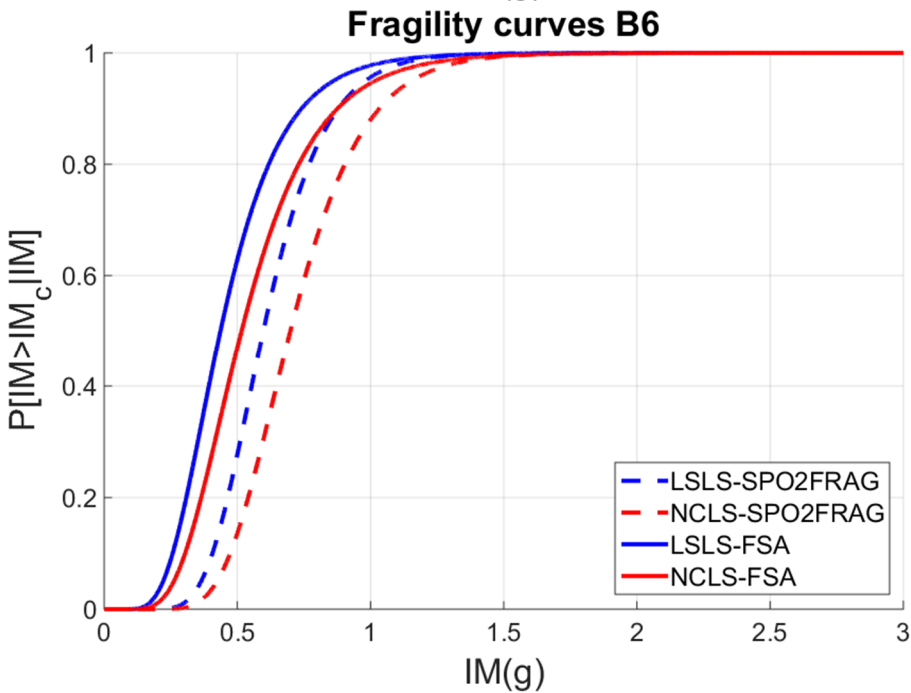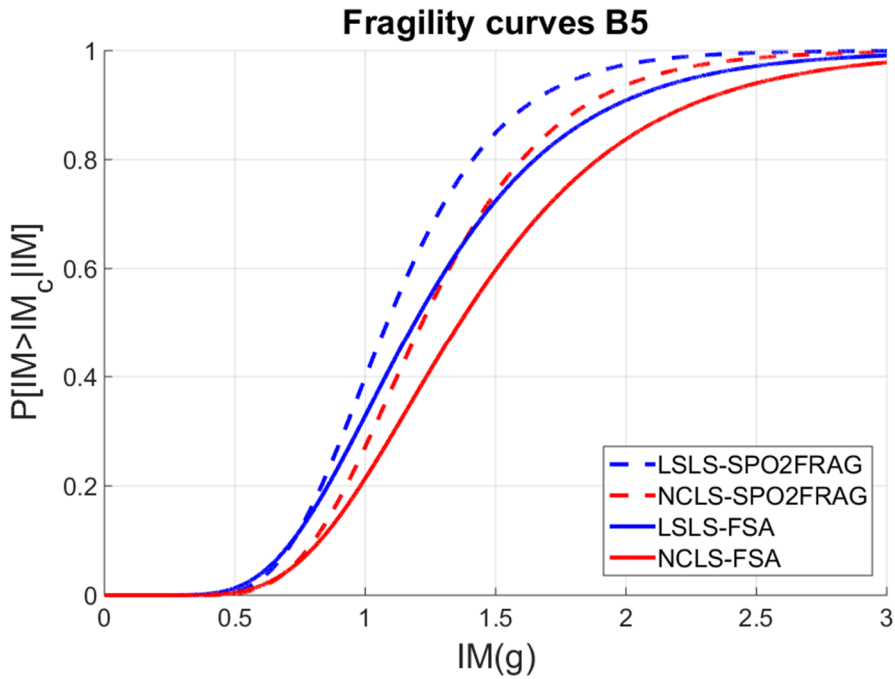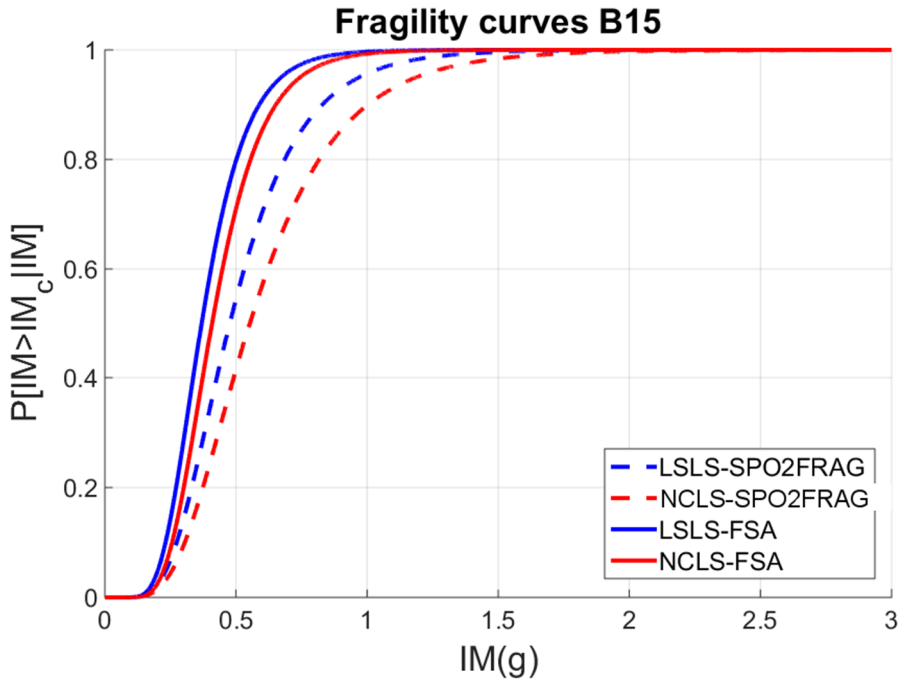
Fig. E.4 – One-by-one comparison between the fragility curves obtained from the two methodologies adopted, for B5 and B6, accounting for the shear mechanisms
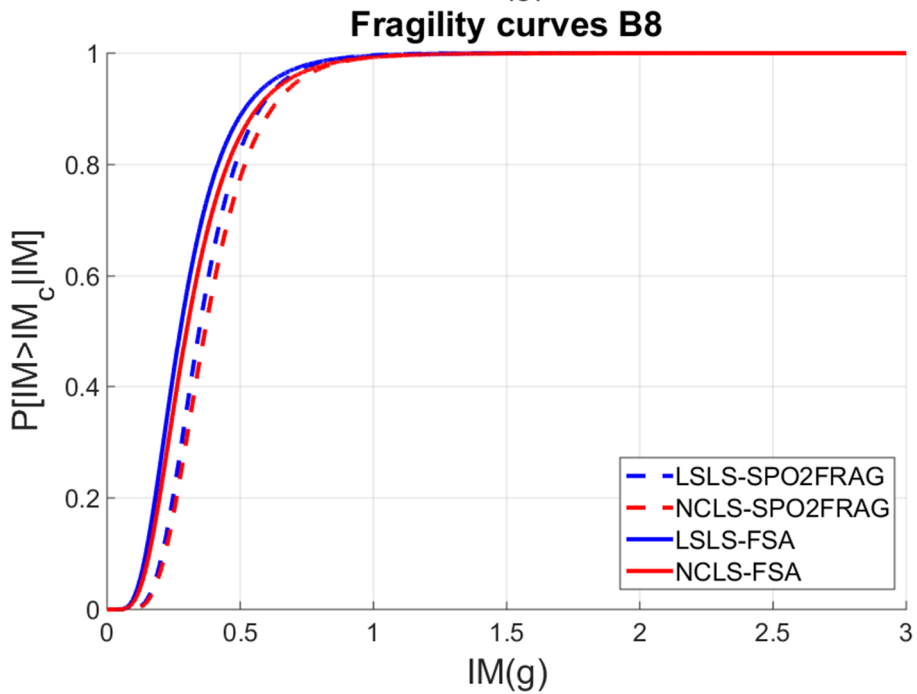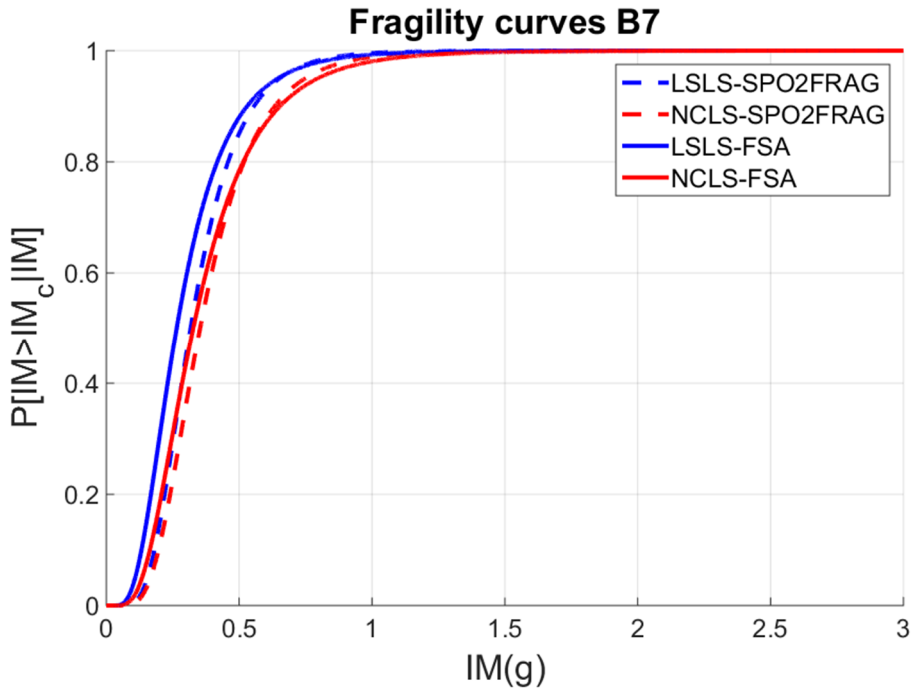
Fig. E.5 – One-by-one comparison between the fragility curves obtained from the two methodologies adopted, for B7 and B8, accounting for the shear mechanisms
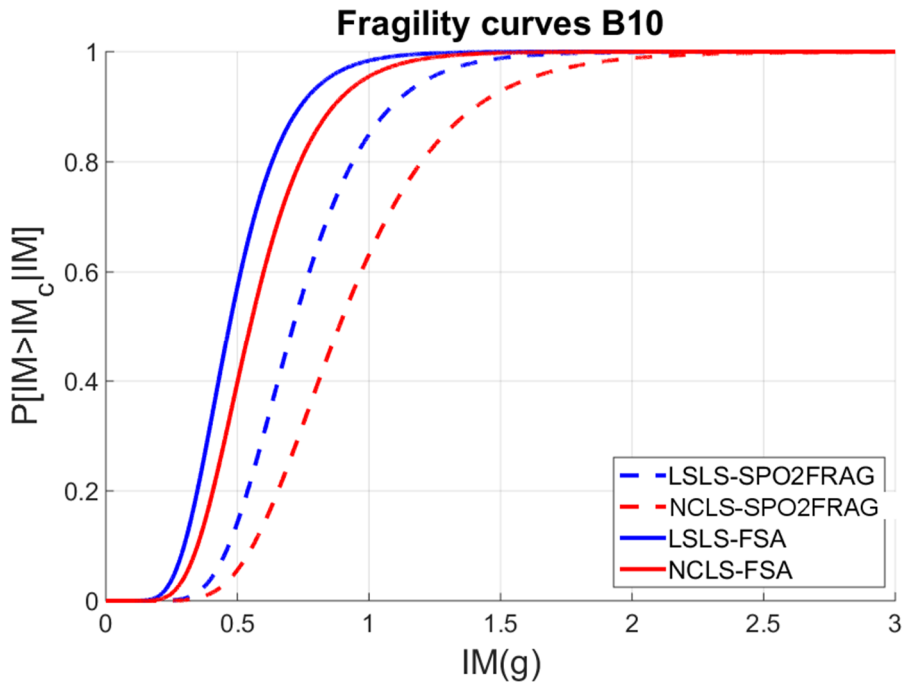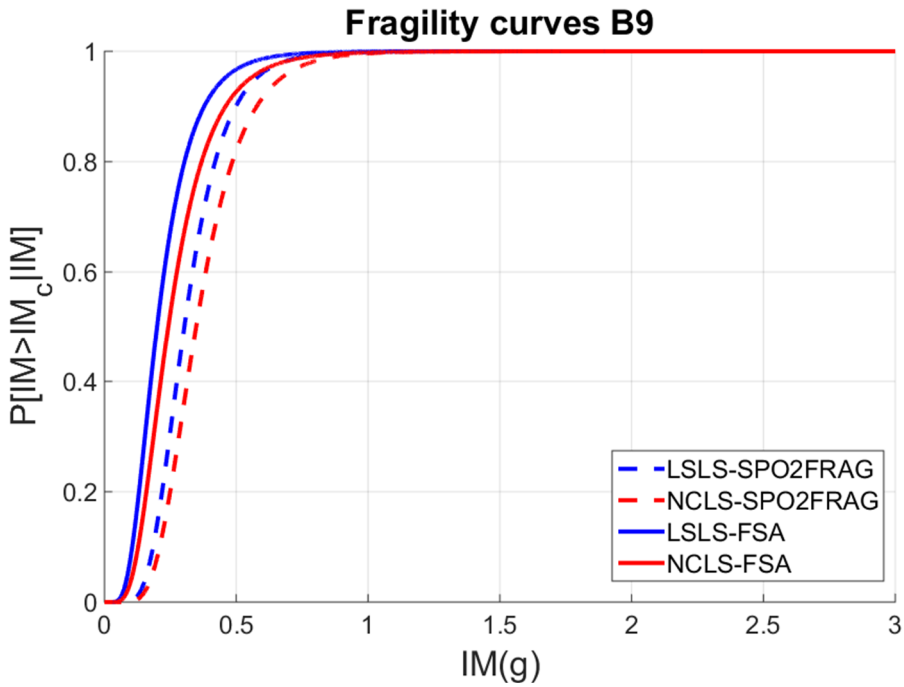
Fig. E.6 – One-by-one comparison between the fragility curves obtained from the two methodologies adopted, for B9 and B10, accounting for the shear mechanisms
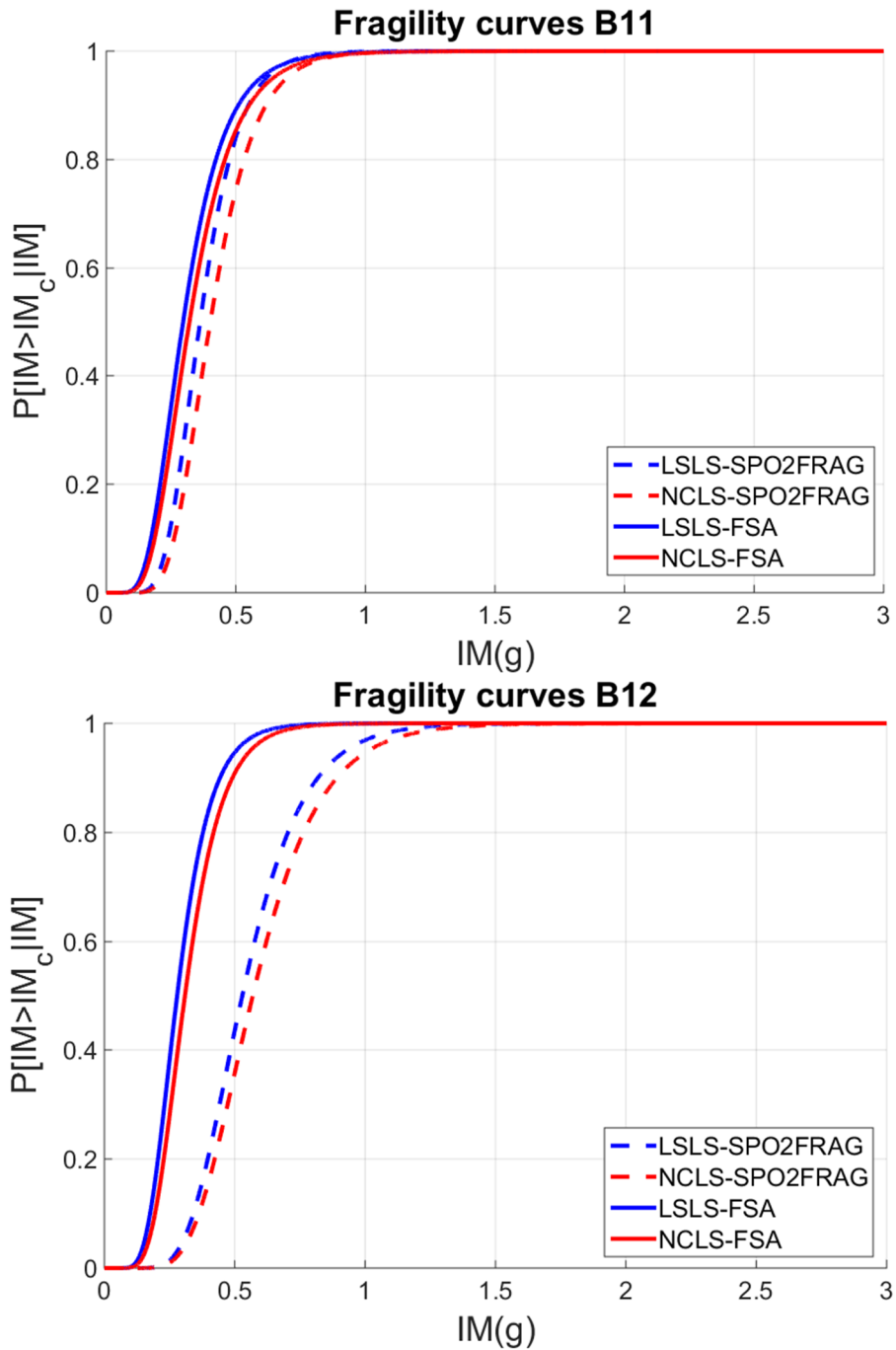
Fig. E.7 – One-by-one comparison between the fragility curves obtained from the two methodologies adopted, for B11 and B12, accounting for the shear mechanisms

Fig. E.8 – One-by-one comparison between the fragility curves obtained from the two methodologies adopted, for B13 and B14, accounting for the shear mechanisms

Fig. E.9 – One-by-one comparison between the fragility curves obtained from the two methodologies adopted, for B15, accounting for the shear mechanisms

Tab. E.2 – Regional fragility curves features, in terms of μ_{reg} and β_{reg}, accounting for shear mechanisms

Regional fragility curves	SPO2FRAG		FSA	
	LSLS	NCLS	LSLS	NCLS
μ_{reg}	0.4543	0.5328	0.3513	0.4146
β_{reg}	0.3504	0.372	0.4341	0.434
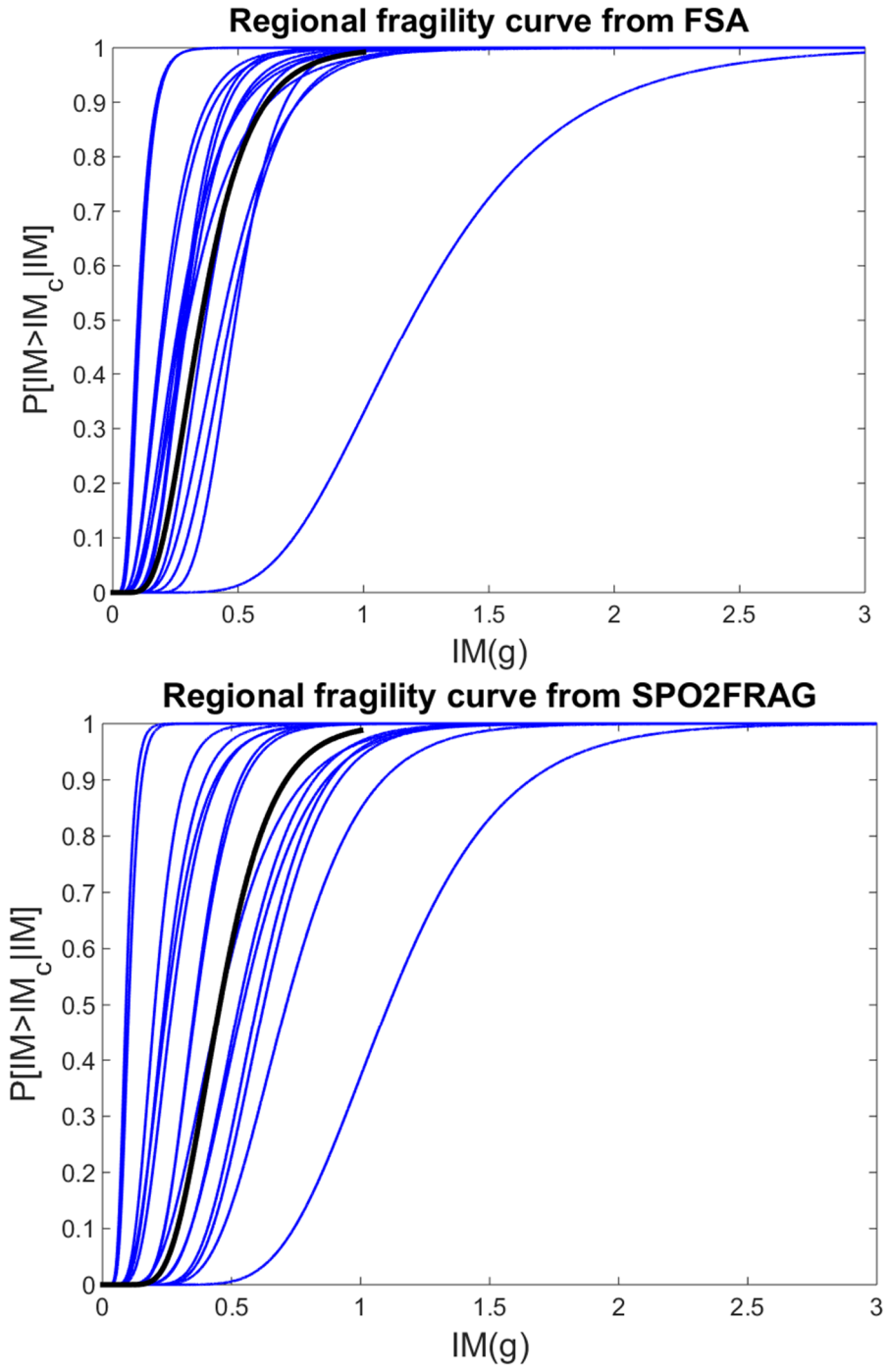
Fig. E.10 - Regional fragility curves for the LSLS, from FSA and SPO2FRAG, accounting for shear mechanisms
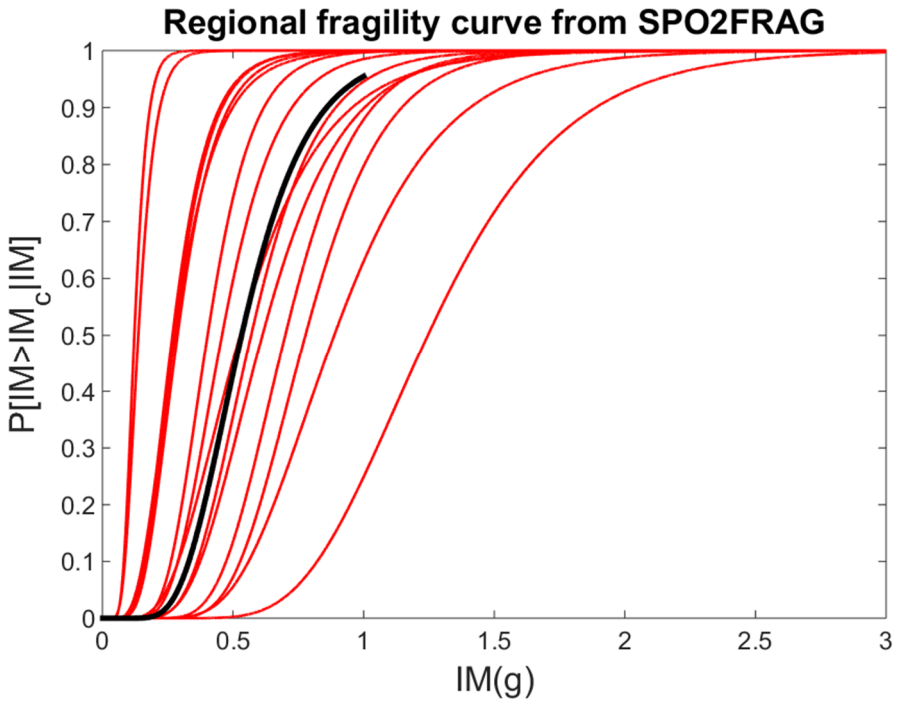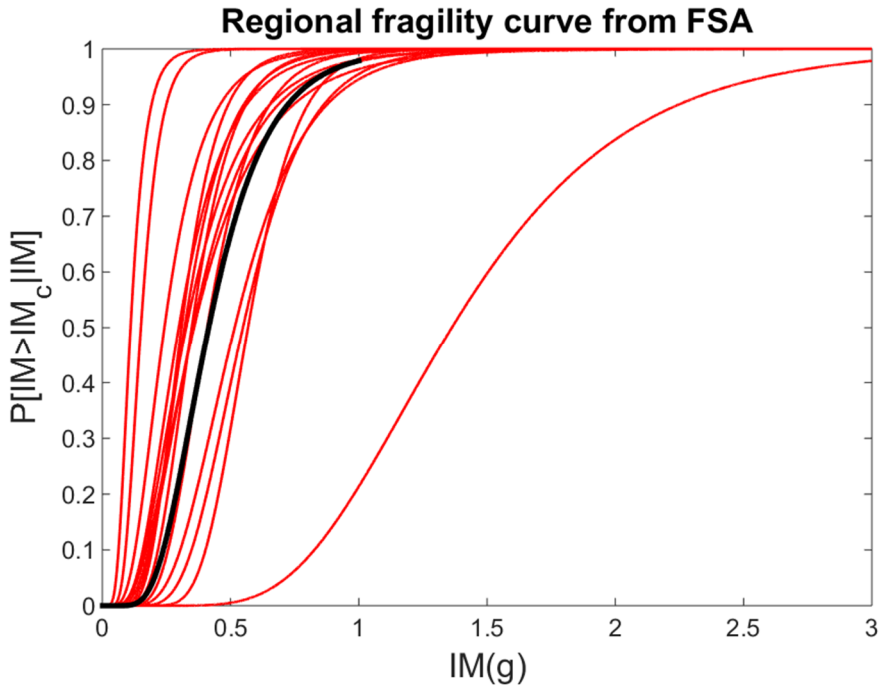
Fig. E.11 - Regional fragility curves for the NCLS, from FSA and SPO2FRAG, accounting for shear mechanisms

13. Annex F: Extended results of 3D reduced-order models methods, accounting for shear mechanisms
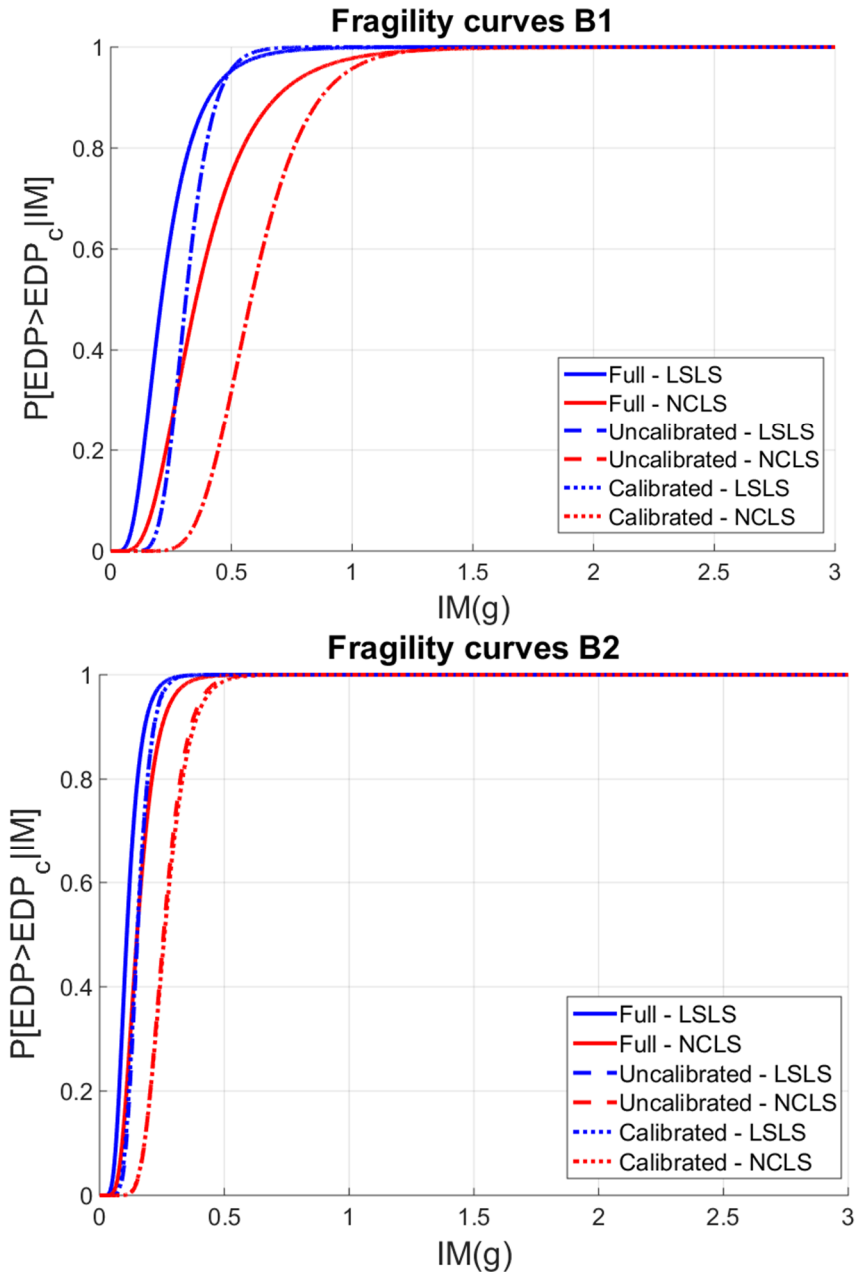
Fig. F.1 – Comparison of fragility curves, for each model and each LS investigated for B1 and B2, accounting for shear mechanisms
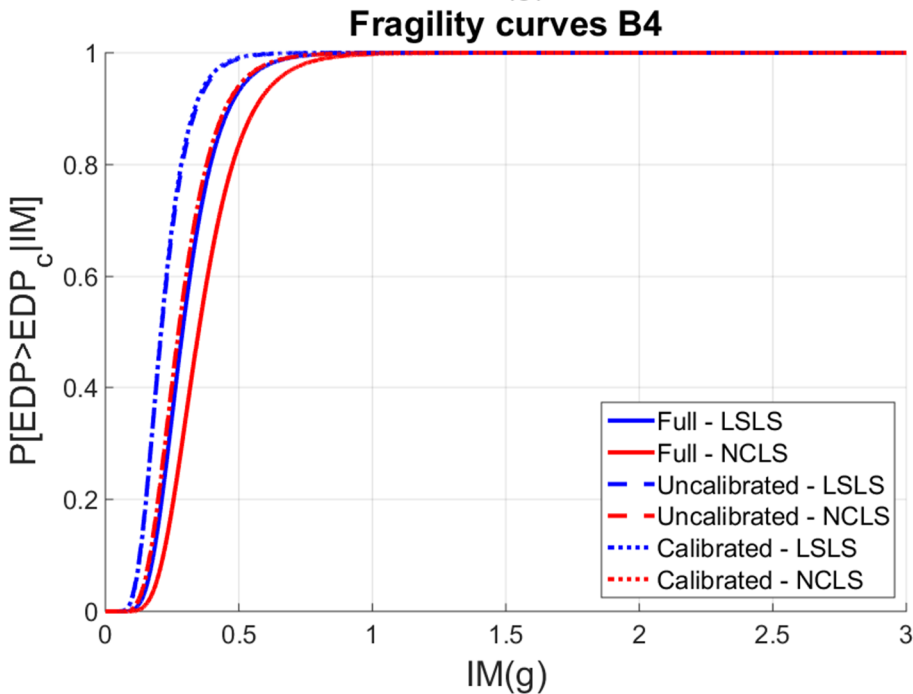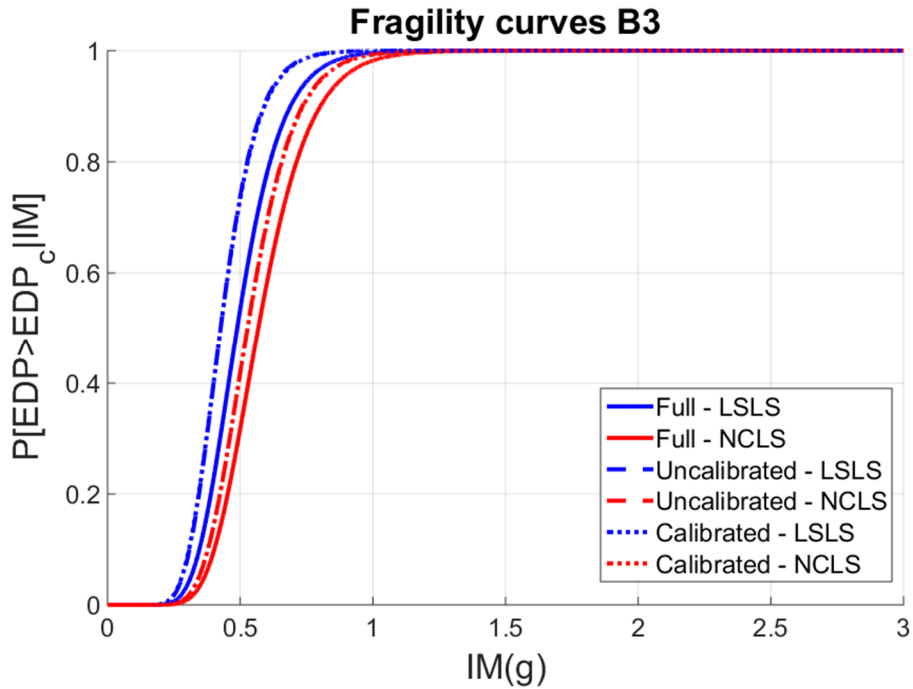
Fig. F.2 – Comparison of fragility curves, for each model and each LS investigated for B3 and B4, accounting for shear mechanisms
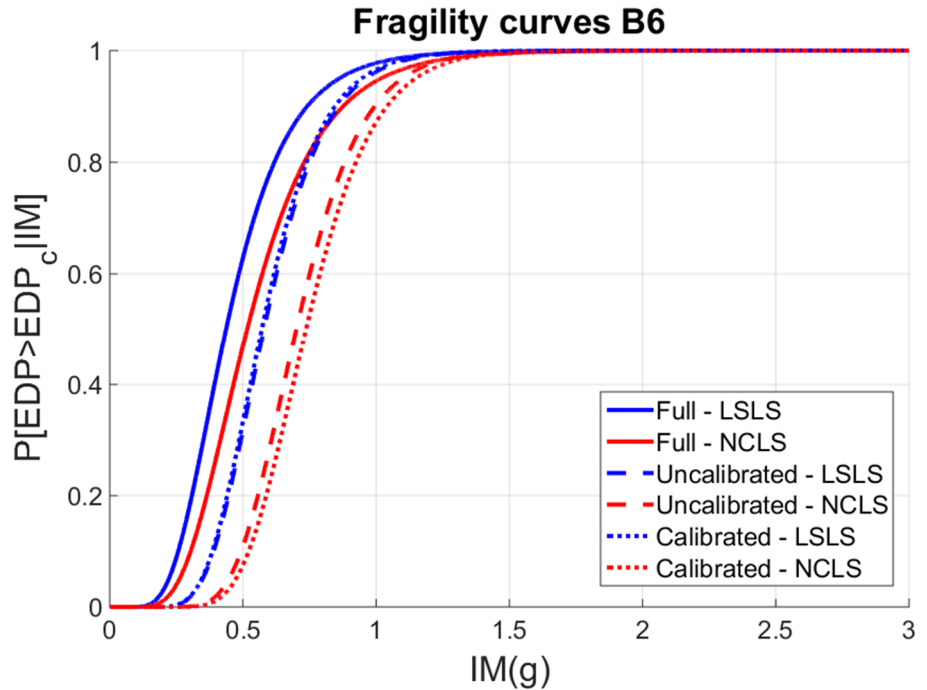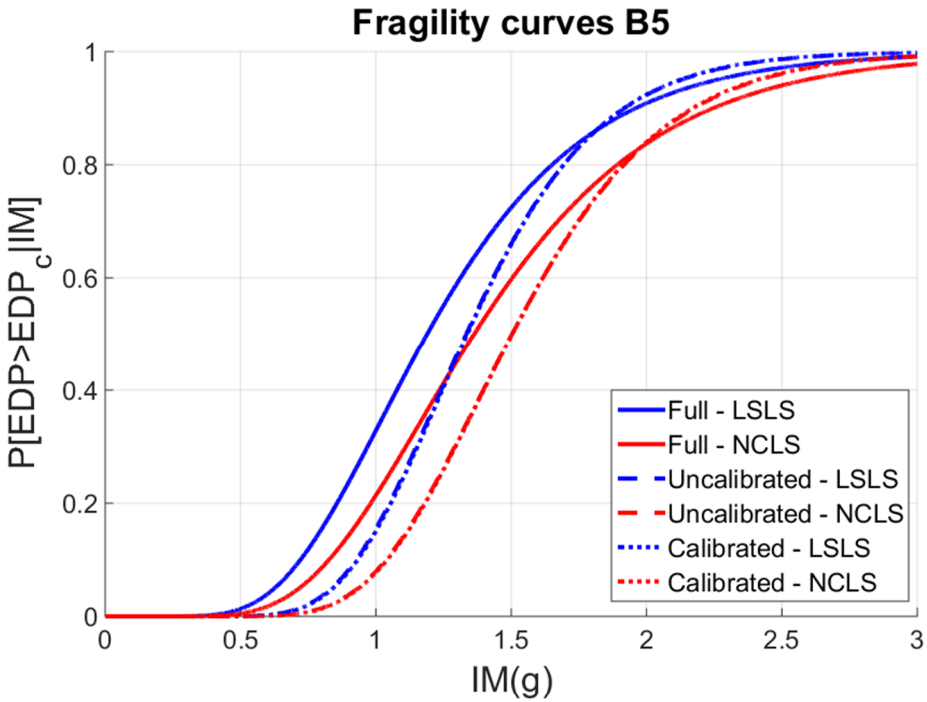
Fig. F.3 – Comparison of fragility curves, for each model and each LS investigated for B5 and B6, accounting for shear mechanisms
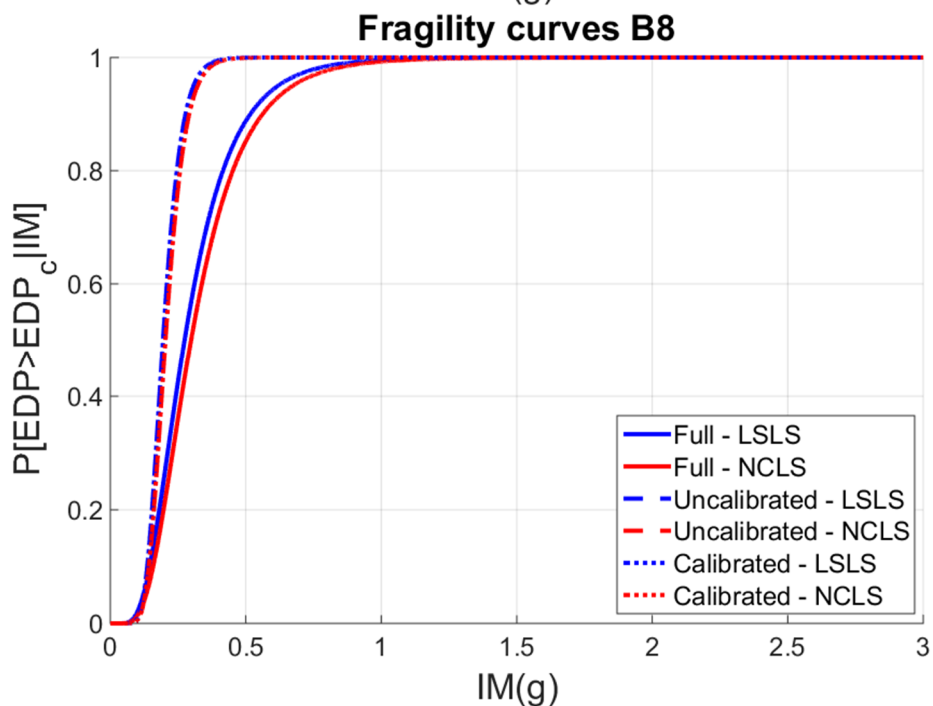
Fig. F.4 – Comparison of fragility curves, for each model and each LS investigated for B7 and B8, accounting for shear mechanisms

Fig. F.5 – Comparison of fragility curves, for each model and each LS investigated for B9 and B10, accounting for shear mechanisms
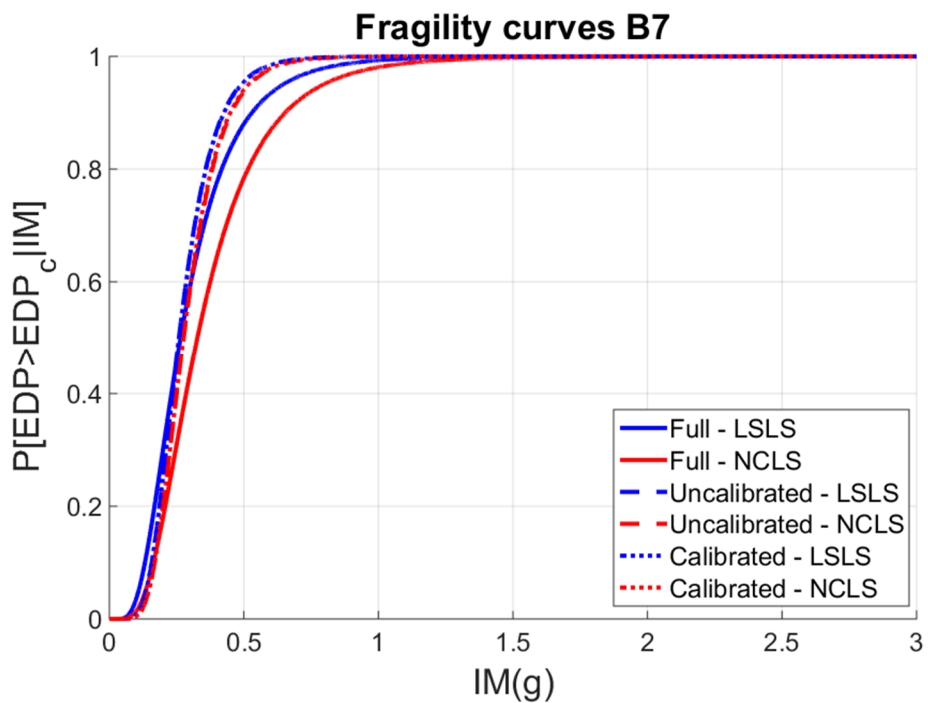
Fig. F.6 – Comparison of fragility curves, for each model and each LS investigated for B11 and B12, accounting for shear mechanisms
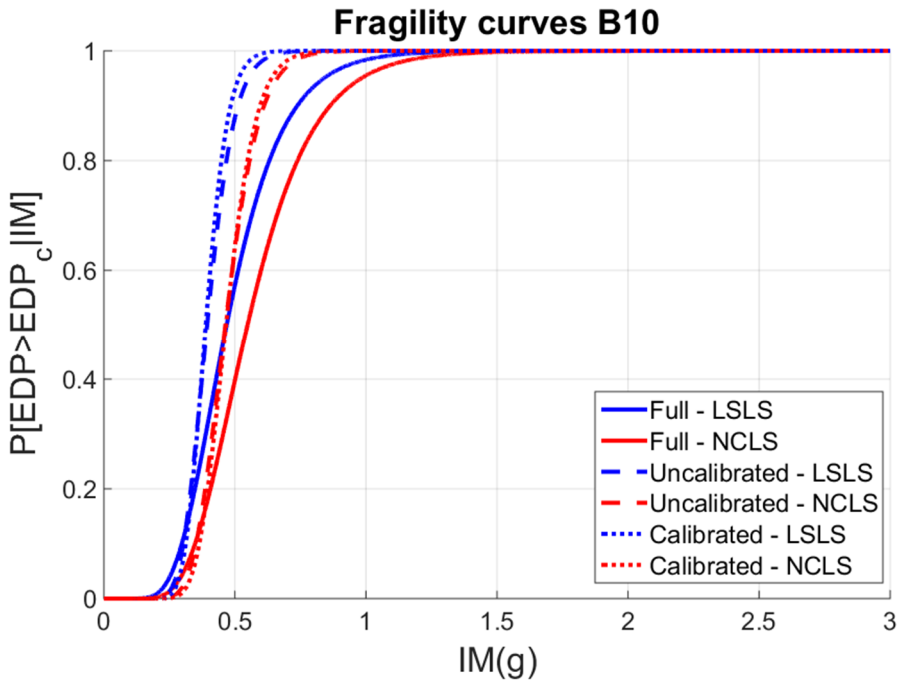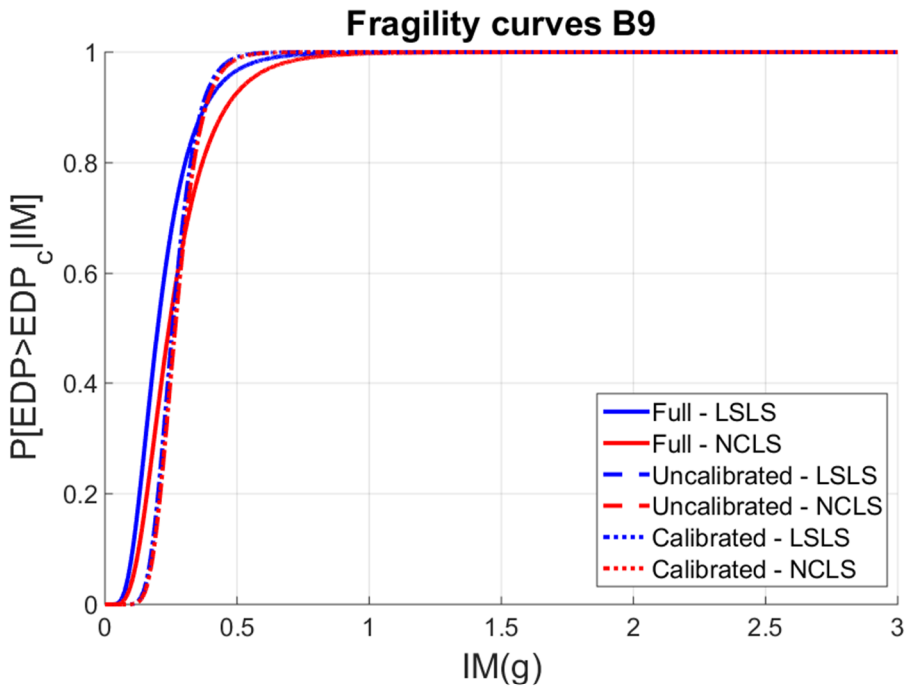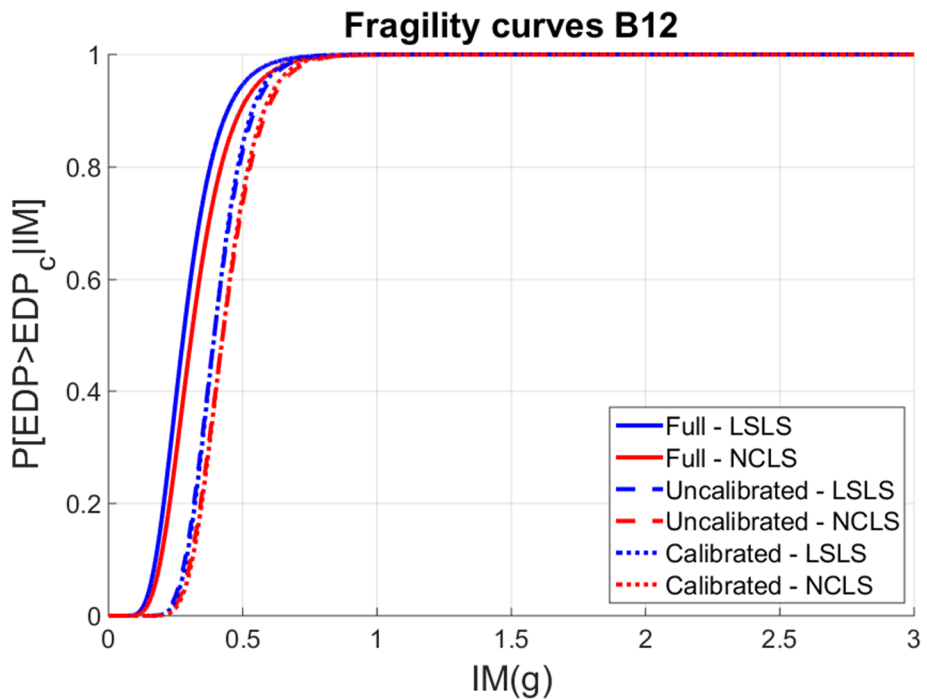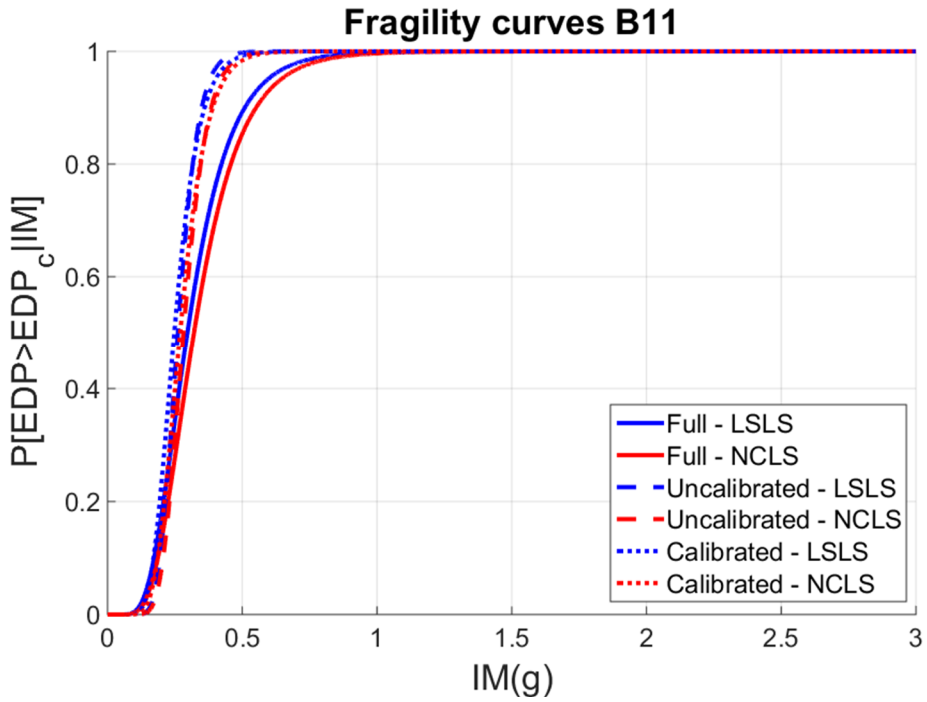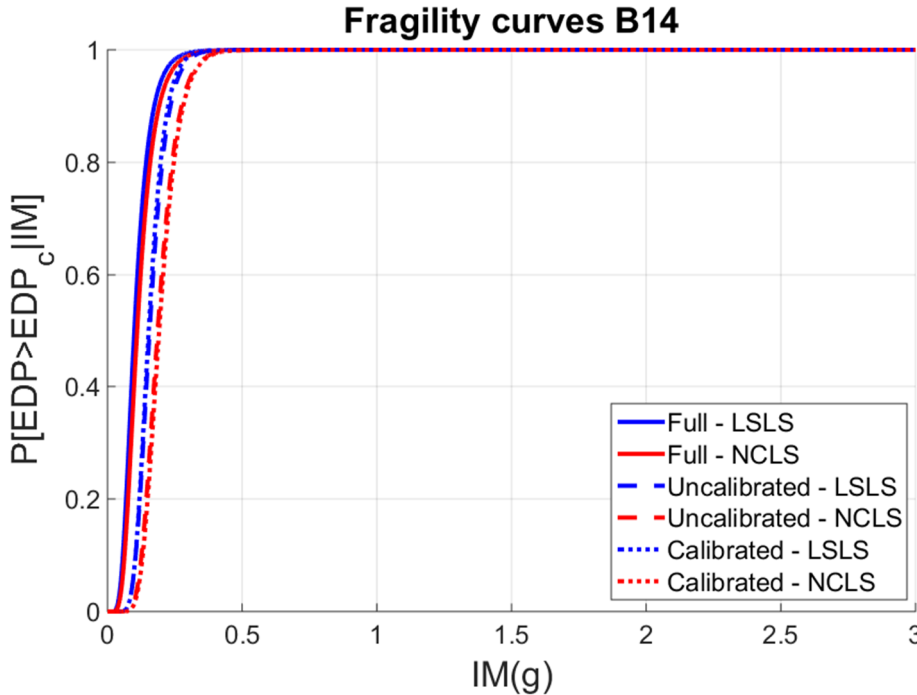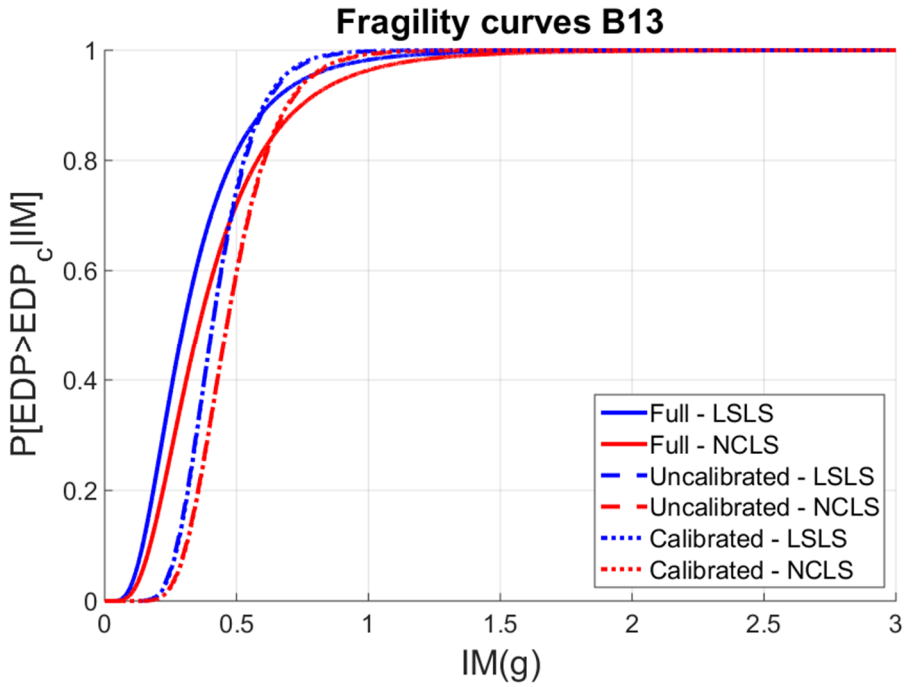
Fig. F.7 – Comparison of fragility curves, for each model and each LS investigated for B13 and B14, accounting for shear mechanisms
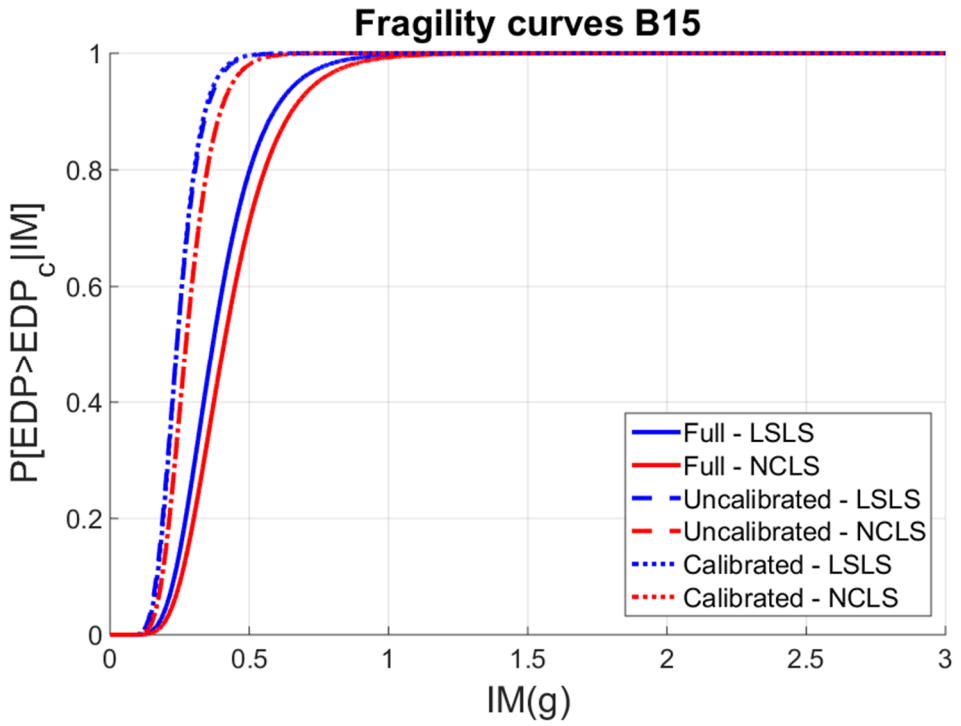
Fig. F.8 – Comparison of fragility curves, for each model and each LS investigated for B15, accounting for shear mechanisms

14. ACKNOWLEDGEMENTS

With these few lines, I want to express the dutiful acknowledgments to the people that marked this part of my life path, called PhD.

First of all, I would like thank the Prof. Eng. Giuseppina Uva, for the possibility that she gave me and with the word "possibility" I mean all things related to the PhD, such as the researches, the conferences, the period abroad and so on. Thanks for the valuable drive in my research, with your critic and open eye to new topics. Finally, thanks for the kindness, as few people can feel in the academic world.

I would to thank Eng. Francesco Porco, which has been the practical mind and engine of my works, with the developments of ideas and proposals. Thank you for being the most important point of reference for these 3 years, for shearing your competences in our debates, with continuous exchanges of feedbacks and reports. I cannot forget the phone calls, typical of our Saturdays, Sundays or other holidays (Sorry!!).

I would like thank Prof. Eng. Domenico Raffaele, for the fundamental knowledge and intellect shared with all members of the "Uva staff". You face your work with such an accuracy, which should be an example for all researchers and practitioners. As we told, just now I can recognize the value of the culture and, above all, the things that I know and the ones that I don't know.

My special thanks to Prof. Eng. Dimitrios Vamvatsikos, for the possibility to experience the period abroad of my PhD in Athens, at NTUA. It has been one of the most important and exciting experiences of my life. Thank you for the ideas and for showing me a new way to make research, teaching me a lot about unknown topics (for me) in the field of seismic engineering. I believe that the achievements that I set up, before facing this challenge, have been amply satisfied. Then, I thank you for making me feel the famous "Greek hospitality", for the suggestions about the Greek food, for the big heater and so on. (PS. sorry for the English!!). If for you it's only work, maybe you do it very well. In addition, I feel of mentioning the guys of "Vamva staff", as Akrivi

Dinos and Billionis. Beautiful the pictures in the presentations of your Greek dissertations! You have been true friends and despite it was not up to me, I believe that you did it.

I would to thanks the colleagues and the people met in the "Poliba world". Starting from my mate, Eng. Roberto Gentile (I will miss our discussions, the conferences together and what happened after the "X hour"), Eng. Andrea Fiore (point of reference for a lot of things) and last but not least the researchers and PhD students that I've known (How many coffees I drunk in this three years?). You are beautiful people.

It's time to thank my family. Thank you dad for the patience and the sapience (maybe, one day, I will explain you what I did in my PhD) and thank you mum for the words and the silences, at the right places in the right moments. However, my family is also composed by a band of friends. Now, it's the time to explain them that my work doesn't consist in the research of things on Wikipedia (I used it just for something). Thanks to all, for all (I can't be prosaic about the word "all", because I've not space. Hence, let you image).

Finally, thanks to whom left my life (luckily), who entered, who has been always part of it. Thanks to you, I'm no more the same Sergio. Just for summarizing this experience (I promised Angelica to do it), I leave here an expression that few will understand: "not for the head, not for the body…".

15. SERGIO RUGGIERI'S CURRICULUM VITAE

SERGIO RUGGIERI   December 2018

Contact Information	Sergio Ruggieri, Civil and Structural Engineer, birthday: 31/10/1989, Nationality: Italian E-mail: sergio.ruggieri@poliba.it; ingsergio.ruggieri@gmail.com Phone: +39-3473128082 Linkedin url: Sergio Ruggieri
Current job	PhD Candidate, Doctor of Philosophy in Risk and Environmental, Territorial and Building Development, XXXI Cycle, SSD: ICAR/09, Structural Engineering DICATECh Department, Polytechnic University of Bari, Via Edoardo Orabona, 4, 70126, Bari, Italy
Main Interests	Seismic assessment and design of structures Structural engineering FE modelling Seismic engineering
Education Nov.2015 - Oct.2018	Doctor of Philosophy studies, Course of Civil, Environmental and Building Risk and Development, XXXI° cycle, Polytechnic University of Bari. Thesis Title: *"Advanced strategies for the seismic assessment of existing RC moment-frame buildings: appraisal of modelling assumptions and development of parsimonious PBEE-based methods of analysis"*. Tutors: Prof. Eng. Giuseppina Uva, Prof. Eng. Domenico Raffaele, Prof. Eng. Francesco Porco, Prof. Eng. Dimitrios Vamvatsikos. Main studies: FE modelling, seismic analysis, nonlinear behaviour of structures.

Jan.2018 - Mar.2018	PhD visiting, Institute of Steel Structure – National Technical University of Athens. Tutor: Prof. Eng. Dimitrios Vamvatsikos. Main Studies: probability theory applied to seismic engineering, FE modelling, seismic analysis.
Sep.2012 - Apr.2015	Master's degree of Civil Engineering, curriculum Structural engineering Polytechnic University of Bari, grade 110/110 cum laude. Thesis Title: *"Strategie di adeguamento sismico di edifici scolastici con strutture dissipative esterne"* (In Italian), Seismic engineering. Tutors: Prof. Eng. Giuseppina Uva, Prof. Eng. Domenico Raffaele. Main studies: Seismic engineering, mechanic of structures, design of bridge, design and assessment of foundations, design of hydraulic systems, design of transportation system.
Sep.2008 - Apr.2012	Bachelor's degree of Civil Engineering, Polytechnic University of Bari, grade 98/110. Thesis Title: *"Verifica delle coordinate dei vertici della rete trigonometrica GNSS, regione Puglia"* (In Italian), Topography. Tutor: Prof. Eng. Mauro Caprioli.
July 2008	<u>High school degree</u>, Surveyor, grade 100/100.

Professional qualification

Nov. 2015	Civil engineer qualifying examination.

Professional Experiences

2015 - ongoing	Assistant Technical Consultant of the "Court of Trani", Eng. Vincenzo Lopopolo .
Oct.2018 – Dec.2018	Census surveyor for Istat, *"Censimenti permanenti abitazioni e popolazione, 2018"*, City of Bisceglie, Bat, Italy.
2012 – 2017	Private lessons of maths, geometry, physic.
Oct.2011 – Mar.2012	Census surveyor for Istat, *"15° Censimento generale della popolazione e delle abitazioni"*, City of Bisceglie, Bat, Italy.

Teaching and Tutoring	
2015-2016	"Anti-seismic structures design and assessment" course (150 students), 40 hours, Tutor: Prof. Eng. Giuseppina Uva. "Fundamental of structural engineering" course (50 students), 40 hours Tutor: Prof. Eng. Francesco Porco.
2016-2017	"Anti-seismic structures design and assessment" course (150 students), 40 hours, Tutor: Prof. Eng. Giuseppina Uva. "Fundamental of structural engineering" course (50 students), 20 hours, Tutor: Prof. Eng. Francesco Porco.
2017-2018	"Bridge theory and design" course (50 students), 40 hours, Tutor: Prof. Eng. Domenico Raffaele.
2015-2018	Co-tutor of 12 MSc theses in the field of Seismic assessment of RC buildings, FE modelling, seismic analysis and analysis to regional scale.
Technical skills	
Spoken languages	Italian (Mother), English (Operational proficiency).
Programming languages	Matlab, Tcl/tk
Structural analysis software	Sap2000, Etabs, CSIbridge, OpenSees, Strauss, Edilus, Seismostruct, 3Muri, 3DMacro, Abaqus, MidasGen.
CAD and Graphic	Autocad, Archicad, Photoshop.
Soft skills	Curiosity, self-motivation, rapid learning, problem solving, teamwork, leadership propensity.
Other interests	Volunteering: jointed to ACI association since 2004, President of the association, parochial level, 2014-2017, Bursar of the association, parochial level, 2017-2018. Librarian at the library "Don Michele Cafagna", City of Bisceglie, Bat, Italy, 2010-2014 Team Sports: Soccer. Music: Rock, Indie, Electronic, play guitar.

Publications

<u>Journal Papers</u>

- Uva G., Porco F., Fiore A., Ruggieri S. (2017) Effects in conventional nonlinear static analysis: evaluation of control node position, Structures, 13:178–192.
- Porco F., Ruggieri S., Uva G., (2018) Seismic assessment of irregular existing building: appraisal of the influence of compressive strength variation by means of nonlinear conventional and multimodal static analysis, Ingegneria Sismica, Issue 3, 2018.
- Ruggieri S., Porco F., Uva G., (2018) A numerical procedure for modeling the floor deformability in seismic analysis of existing RC buildings, Journal of Building Engineering, 19, pp. 273-284
- Uva G., Sangiorgio V., Ruggieri S., Fatiguso F. (2019) Structural vulnerability assessment of masonry churches supported by user-reported data and modern Internet of Things (IoT) Measurement: Journal of the International Measurement Confederation 131, pp. 183-192
- Ruggieri S., Uva G., Porco F., Vamvatsikos D., Practical class fragility and seismic safety assessment for low-rise reinforced concrete school buildings in Southern Italy, under preparation;
- Ruggieri S., Vamvatsikos D., Uva G., Reduced-order models for the seismic assessment of complex 3D reinforced concrete moment-frame buildings, under preparation.

<u>Conference Papers</u>

- Uva G., Raffaele D., Ruggieri S., (2016) Influence of materials mechanical properties for the RC buildings assessment. IV Workshop on New Boundaries of Structural Concrete - Sept. 29 – Oct. 1, 2016
- Porco F., Ruggieri S., Raffaele D. (2017) Influence of rigid floor assumption in seismic analysis of RC existing buildings, COMPDYN 2017 - Proceedings of the 6th International Conference on Computational Methods in Structural Dynamics and Earthquake Engineering, 2, pp. 3439–3449.
- Ruggieri S., Porco F., Raffaele D., Uva G.,(2017) Rigid floor assumption in nonlinear static analysis of reinforced concrete existing buildings, XVII Convegno Anidis, Pistoia, 2017/17-21/9, pp. 462–473.
- Uva G., Ruggieri S., Sangiorgio V., Fatiguso F., (2017) Structural vulnerability assessment of masonry churches supported by user-reported data. IMEKO INTERNATIONAL CONFERENCE ON Metrology for Archaeology and Cultural Heritage, 23-25 Ottobre, 2017
- Ruggieri S., Sangiorgio V. (2017) Information system for supporting of the assessment of masonry churches vulnerability PhDays 2017, Polytechnic University of Bari, 11-12 December 2017
- Ruggieri S., Porco F., Raffaele D., Uva G. (2018) Seismic analysis of RC buildings by modeling floor deformability and infill walls, SP-326

Durability and Sustainability of Concrete Structures - 2nd Workshop Proceedings, Moscow, 6-7 June 2018.

- Lima C., Angiolilli M., Barbagallo F., Belletti B., Bergami A. V., Camata G., Cantagallo C., Di Domenico M., Fiorentino G., Ghersi A., Gregori A., Lavorato D., Luciano R., Marino E.M., Martinelli E., Nuti C., Ricci P., Rosati L., Ruggieri S., Sessa S., Spacone E., Terrenzi M., Uva G., Vecchi F., Verderame G.M. (2018) Nonlinear modeling approaches for existing reinforced concrete buildings: the case study of De Gasperi-Battaglia school building in Norcia. Italian concrete Days 2018, 13-15 June, 2018